



Universidade de Aveiro
2021

**EMANUEL DE
ALMEIDA CRESPO**

**DESENVOLVIMENTO DE MODELOS
MOLECULARES TRANSFERÍVEIS PARA A
INDÚSTRIA PETROLÍFERA**

**DEVELOPMENT OF TRANSFERABLE MOLECULAR
MODELS FOR THE OIL & GAS INDUSTRY**



Universidade de Aveiro
2021

**EMANUEL DE
ALMEIDA CRESPO**

**DESENVOLVIMENTO DE MODELOS MOLECULARES
TRANSFERÍVEIS PARA A INDÚSTRIA PETROLÍFERA**

**DEVELOPMENT OF TRANSFERABLE MOLECULAR
MODELS FOR THE OIL & GAS INDUSTRY**

Tese apresentada à Universidade de Aveiro para cumprimento dos requisitos necessários à obtenção do grau de Doutor em Engenharia Química, realizada sob a orientação científica do Professor Doutor João Manuel da Costa e Araújo Pereira Coutinho, Professor Catedrático do Departamento de Química da Universidade de Aveiro, do Dr. Germán Pérez-Sánchez, investigador doutorado do CICECO – Aveiro Institute of Materials, e da Professora Doutora Lourdes Vega Fernández, Professora Catedrática do Departamento de Engenharia Química da Khalifa University of Science and Technology.

Apoio financeiro do POCTI no âmbito do III Quadro Comunitário de Apoio. Co-financiamento do POPH/FSE.

O doutorando agradece o apoio financeiro da FCT no âmbito do III Quadro Comunitário de Apoio (SFRH/BD/130870/2017)



Aos meus pais.

o júri

presidente

Doutor João Manuel Nunes Torrão
Professor Catedrático, Universidade de Aveiro

vogais

Doutor João Manuel da Costa e Araújo Pereira Coutinho
Professor Catedrático, Universidade de Aveiro

Doutora Amparo Galindo
Professora Catedrática, Imperial College of London

Doutor Manuel Martinez Piñeiro
Professor Catedrático, Universidade de Vigo

Doutor Felix Lluis Llovell Ferret
Professor Agregado, Universidade de Rovira i Virgili

Doutor Eduardo Jorge Morilla Filipe
Professor Associado, Universidade de Lisboa

agradecimentos

Ao Prof. João Coutinho por me ter dado a oportunidade de trabalhar sob a sua orientação ao longo de todos estes anos. Obrigado pela sua honestidade e confiança. Por me deixar falhar, e por me fazer sempre procurar por alternativas quando nada parece funcionar. Obrigado por, mais do que um supervisor, ter sido um verdadeiro mentor para mim, desde que me enganou com a velocidade das moléculas na 1ª aula de TPQ.

À Profª Lourdes Vega pela oportunidade de trabalhar com ela e o seu grupo, de poder aprender sobre SAFT de uma maneira que seria impossível se apenas recorresse a softwares comerciais. Pelo sempre pertinente e enriquecedor feedback, e pela oportunidade de ter conhecido uma cultura totalmente diferente durante as estadias nos UAE, onde tão bem me recebeu. Não há dúvidas de que é este o tipo de experiências que nos fazem crescer, bem para lá do aspeto profissional.

Ao Germán pela paciência e disponibilidade incessante para me ajudar em tudo o que sempre precisei, e por ter tornado simples aprender uma técnica tão importante como simulações de dinâmica molecular. Não o teria feito sem ti.

Quero também agradecer ao Prof. Eduardo Filipe e ao Dr. Pedro Morgado do IST, pela disponibilidade e ajuda prestadas durante os cálculos efetuados com a SAFT- γ -Mie.

Tenho também de agradecer à Fundação para a Ciência e Tecnologia e à PARTEX – Oil & Gas pelo financiamento que tornou esta jornada possível.

Um agradecimento especial ao Pedro Carvalho pelas inúmeras colaborações, pela ajuda em tudo o que precisei ao longo destes anos com bugs, ideias, críticas, ou muitas vezes simplesmente por ouvir os meus desabaços.

Um obrigado sincero a todos os colegas com quem partilhei gabinete ao longo dos quatro anos: Helena, Tânia, Mónia, Catarina, Ana Maria, André Palma, Luís Pereira, Nicolas, e Pedro Madeira pelo companheirismo e pelo ambiente de trabalho, aprendizagem e ambição. Um agradecimento a todos os restantes membros do PATH pelos inúmeros convívios e espírito familiar único do nosso grupo!

Aos meus amigos, por estarem sempre lá para um momento de descontração, uma conversa, um café, ou simplesmente um joguinho de computador ao fim do dia para desanuviar.

Ele não fala, e muito menos lê, mas ainda assim comunica. Ao meu Brownie, por ter sido a minha companhia durante mais de um ano de trabalho pós-Covid. Por perceber quando algo não está bem, por me deixar trabalhar sem perturbações, e pelos passeios para descontrair na hora de almoço.

Aos meus pais, por acreditarem no meu potencial e pelo esforço que fizeram para que eu pudesse ser o primeiro da família a frequentar o ensino superior. Pelo vosso amor eterno e incondicional, e porque eu posso até saber agora um pouco mais sobre termodinâmica do que o que sabia há uns anos atrás, mas o que sei sobre a vida e amor, é em grande parte a vocês que o devo.

Por fim, tenho de agradecer à Liliana, pela bela equipa formada para enfrentar as adversidades do dia-a-dia. Pelo amor e apoio sem limites. Por acreditar em mim, mesmo quando eu não quero acreditar. Por fazer com que haja muito mais para lá da vida profissional, e por me ter feito crescer como pessoa.

palavras-chave

Termodinâmica, modelação, equações de estado, SAFT, simulações de dinâmica molecular, petroquímica, captura de CO₂, solventes alternativos.

resumo

Dado o aumento da população mundial e das conseqüentes necessidades energéticas, a indústria petrolífera desempenha um papel vital na sociedade. Não só porque o petróleo e o gás natural continuam a ser as principais fontes de energia no nosso planeta, mas também porque são matérias-primas fundamentais para a produção industrial de um grande número de bens e produtos. Por outro lado, os impactos ambientais resultantes das suas atividades estabelecem uma busca incessante pelo desenvolvimento de novas tecnologias que sejam mais limpas, sustentáveis, e eficientes do que as atuais.

Além disso, considerando a depleção dos reservatórios e a diminuição do custo de fontes de energia alternativas, processos de recuperação avançada tornam-se cada vez mais importantes, com a injeção de surfactantes ou de CO₂ sendo duas das técnicas mais promissoras. Esta última tem tido como principal limitação a escassez de fontes económicas de CO₂, o que reforça também a importância de se desenvolverem tecnologias alternativas para a sua captura e armazenamento em larga escala.

Tendo tudo isto em consideração, compostos contendo óxido de etileno são de um interesse acrescido para a indústria petrolífera: glicóis são comumente usados como agentes de desidratação, glimas ou éteres de glicol são frequentemente apontados como solventes físicos promissores para a captura de CO₂, ou para a remoção de gases ácidos no processamento de gás natural, e surfactantes do tipo Brij, também conhecidos como C_iE_j, são usados para recuperação avançada de petróleo. Recentemente, solventes verdes alternativos como os solventes eutécticos profundos e os líquidos iónicos próticos têm sido sugeridos para melhorar a sustentabilidade de diferentes processos de separação na indústria petrolífera, como por exemplo a separação de CO₂, dessulfurização e desaromatização do petróleo, entre outros.

Contudo, antes da aplicação industrial destes sistemas, é necessário possuir modelos capazes de providenciar uma descrição precisa das suas propriedades termofísicas e do equilíbrio de fases, conhecimentos fundamentais para efetuar o desenho, simulação, controlo e avaliação económica de novos projetos de forma rigorosa. Contudo, a maior parte dos modelos termodinâmicos disponíveis atualmente para descrever o comportamento destes sistemas possuem uma precisão insatisfatória, bem como uma capacidade preditiva e extrapolativa muito limitada.

Como tal, este projeto tem como principal objetivo o desenvolvimento, melhoria e análise de modelos termodinâmicos de base molecular com alta transferibilidade, capazes de descrever sistemas complexos de interesse para a indústria petrolífera, como os acima mencionados. É expectável que o aumento da capacidade extrapolativa, e em alguns casos preditiva, das ferramentas de modelação aqui discutidas constitua uma vantagem sobre os modelos usados atualmente, permitindo uma diminuição significativa do trabalho experimental (mais caro e demorado) tipicamente necessário durante as fases iniciais do desenvolvimento de novos processos e tecnologias.

keywords

Thermodynamics, modelling, equations of state, SAFT, molecular dynamics simulations, oil & gas, CO₂ capture, alternative solvents.

abstract

Given the world's population growth and the consequent increase on the global energy demand, the Oil & Gas industry plays a vital role in today's society. Not only because oil and gas are the main energy sources in our planet, but also because they serve as important feedstocks to produce a huge diversity of commodities and goods. Conversely, the huge environmental impact driven by their activities establishes an endless demand for the development of novel technologies desired to be cleaner, more sustainable, and efficient than their state-of-art homologous.

Moreover, considering the depletion of oil reserves and the decrease in cost of alternative energy sources, enhanced oil recovery (EOR) is also becoming increasingly important with the use of surfactant flooding or CO₂ injection being two of the most promising techniques. The latter has mainly been hindered by the scarcity of economical supplies of CO₂, reinforcing the importance of developing alternative technologies for CO₂ capture and storage at large scale.

Taking this into account, compounds containing ethylene oxide groups are of a special and increasing interest for the Oil & Gas industry: glycols are commonly used as dehydration agents, glymes have been suggested as promising physical solvents for CO₂ capture and natural gas processing, and C_iE_j surfactants can be used for surfactant flooding. Recently, alternative greener solvents such as protic ionic liquids and deep eutectic solvents have also been suggested to improve the sustainability of different separation processes such as CO₂ separation, fuel desulfurization, among others.

Prior to the industrial application of these systems, an accurate description of their thermophysical properties and phase equilibria is necessary for the rigorous design, simulation, control, and economical evaluation of new technologies or process configurations. However, most of the thermodynamic approaches and molecular models currently available to describe these compounds have a limited predictive/extrapolative ability or accuracy.

Therefore, this work aims at the development, improvement, and analysis of transferable molecular models able to correctly describe complex systems of interest to the Oil & Gas industry, such as those mentioned above. The enhanced extrapolative, and in some cases predictive, ability of the modelling approaches proposed in this work are expected to constitute an advantage over current thermodynamic models, by allowing for a significant decrease on the experimental efforts required during initial solvent screenings or the initial stages of new processes and technologies development.

Contents

CONTENTS	XIII
LIST OF FIGURES	XV
LIST OF TABLES	XXIII
NOMENCLATURE	XXV
LIST OF SYMBOLS	XXV
GREEK	XXVI
LIST OF ABBREVIATIONS	XXVII
LIST OF COMPOUNDS.....	XXVIII
SUPERSCRIPTS	XXIX
SUBSCRIPTS	XXIX
1- INTRODUCTION	1
1.1- GENERAL CONTEXT	3
1.2- SCOPE AND OBJECTIVES	10
2- THERMODYNAMIC BACKGROUND	13
2.1- SAFT-TYPE EOSs.....	15
2.1.1- <i>soft-SAFT EoS</i>	19
2.1.2- <i>PC-SAFT EoS</i>	25
2.1.3- <i>SAFT-γ-Mie EoS</i>	28
2.1.4- <i>Development of a Thermodynamic Modelling Package in MATLAB®</i>	30
2.2- MOLECULAR DYNAMICS SIMULATIONS.....	34
2.2.1- <i>MARTINI Forcefield</i>	36
3- THERMODYNAMIC MODELLING OF GLYCOLS AND GLYMES	41
3.1- A SIMPLE, YET ROBUST, SOFT-SAFT MODEL FOR GLYCOLS	43
3.2- EXTENDING THE MODEL TO GLYMES	58
3.3- GLYCOLS AND GLYMES AS PHYSICAL SOLVENTS FOR CO ₂ SEPARATION	75
3.4- AQUEOUS SOLUTIONS OF GLYCOLS AND GLYMES.....	87
4- EOS MODELLING OF C_iE_j SURFACTANTS: THE FALLACY OF HETERONUCLEAR SAFT VARIANTS	101
4.1- INTRODUCTION.....	103
4.2- SAFT MODELLING OF C _i E _j SURFACTANTS AND THE CASE FOR A PREDICTIVE TOOL.....	105
4.3- RESULTS.....	107
4.4- CONCLUSIONS	141
5- MOLECULAR DYNAMICS SIMULATIONS OF SURFACTANT SYSTEMS	143
5.1- UNVEILING THE PHASE BEHAVIOUR OF C _i E _j SURFACTANTS IN WATER THROUGH CG-MD SIMULATIONS	145
5.2- THE IMPACT OF OIL ON THE PHASE BEHAVIOUR OF C _i E _j /H ₂ O SYSTEMS.....	169
5.3- PERSPECTIVES ON THE USE OF CG-MD SIMULATIONS FOR EOR APPLICATIONS.....	178

6-	A DISCUSSION ON THE THERMODYNAMIC MODELLING OF ALTERNATIVE SOLVENTS	189
6.1-	ON THE PARAMETERIZATION OF SAFT MODELS FOR DEEP EUTECTIC SOLVENTS.....	191
6.2-	REMARKS ON THE THERMODYNAMIC MODELLING OF PROTIC ILS	217
7-	FINAL REMARKS	229
7.1-	CONCLUSIONS	231
7.2-	FUTURE WORK.....	234
	LIST OF PUBLICATIONS	237
	REFERENCES.....	243
	SUPPLEMENTARY MATERIAL	285
A.	ADDITIONAL EXPRESSIONS FOR THE MATHEMATICAL DESCRIPTION OF THE SOFT-SAFT EOS.....	287
B.	SAFT MODELLING OF GLYCOLS AND GLYMES.....	290
C.	SAFT- τ -MIE EOS CALCULATIONS	294
D.	CG-MD SIMULATIONS OF C ₆ E ₆ + H ₂ O SYSTEMS.....	302
E.	CG-MD SIMULATIONS OF SURFACTANT FLOODING PROCESSES	307
F.	THERMODYNAMIC MODELLING OF DESS	309
G.	FREE VOLUME THEORY (FVT) - DESCRIPTION	312
H.	EXCESS MOLAR VOLUMES OF PILS AND DES	314

List of Figures

FIGURE 1.1. PRIMARY ENERGY CONSUMPTION WORLDWIDE BY FUEL TYPE.[6].....	5
FIGURE 2.1. A "SMALL" SAMPLE OF THERMODYNAMIC MODELS AVAILABLE IN THE LITERATURE.....	15
FIGURE 2.2. SCHEMATIC REPRESENTATION OF THE PHYSICAL FOUNDATION OF SAFT. YELLOW AND GREY COLOURS ARE USED TO REPRESENT TWO DIFFERENT SEGMENTS/COMPONENTS, WHILE GREEN, BLUE, AND ORANGE ARE USED TO DISTINGUISH THREE DIFFERENT ASSOCIATION SITE TYPES.	16
FIGURE 2.3. HOMONUCLEAR AND HETERONUCLEAR APPROACHES OF SAFT-TYPE EOSS, ILLUSTRATED FOR PROPANOIC ACID.....	18
FIGURE 2.4. ORGANIZATION OF THE SOURCE CODE DEVELOPED IN THIS WORK.....	31
FIGURE 2.5. DEPENDENCY GRAPH OF THE SOURCE CODE DEVELOPED IN THIS WORK.....	32
FIGURE 2.6. MOLECULAR MODELLING AT DIFFERENT RESOLUTIONS.....	36
FIGURE 2.7. SKETCH OF THE CG MAPPING FOR THE 1-TETRADECYL-3-METHYLIMIDAZOLIUM CATION AND CORRESPONDING BEAD TYPES UNDER THE MARTINI FORCEFIELD.[52]	39
FIGURE 3.1. ASSOCIATION SCHEMES (C.F. TABLE 3.1) USED TO DESCRIBE THE HYDROGEN-BONDING CHARACTER OF GLYCOLS IN THE FRAMEWORK OF ASSOCIATION MODELS.....	45
FIGURE 3.2. NUMBER OF MODELLING WORKS (C.F. TABLE B.1.) USING SAFT OR CPA AS A FUNCTION OF THE GLYCOLS <i>MW</i> . THE POINTS 300 AND 500 REPRESENT THE WORKS WITH A <i>MW</i> IN THE RANGE OF 200-400 G/MOL AND HIGHER THAN 400 G/MOL, RESPECTIVELY.	46
FIGURE 3.3. SKETCH OF THE MOLECULAR MODEL PROPOSED FOR GLYCOLS, ILLUSTRATED FOR TRIEG.	48
FIGURE 3.4. SATURATED LIQUID AND VAPOR DENSITIES AS A FUNCTION OF TEMPERATURE FOR THE EG, DEG, TEG, AND TEEG. THE SOLID LINES REPRESENT THE SOFT-SAFT EOS FIT TO THE EXPERIMENTAL DATA,[118] FOR EG, DEG, TEG, AND TEEG, WHILE FOR PEEG AND HEEG, PREDICTIONS ARE PROVIDED.....	50
FIGURE 3.5. LOGARITHM OF THE VAPOR PRESSURE, AS A FUNCTION OF TEMPERATURE FOR GLYCOL OLIGOMERS. THE SOLID LINES REPRESENT THE SOFT-SAFT EOS FIT TO THE EXPERIMENTAL DATA.[118] ...	50
FIGURE 3.6. DENSITY AS A FUNCTION OF PRESSURE AND TEMPERATURE FOR DIFFERENT GLYCOLS. THE SYMBOLS REPRESENT EXPERIMENTAL DATA,[119] WHILE THE SOLID LINES REPRESENT THE SOFT-SAFT RESULTS.	52
FIGURE 3.7. SOFT-SAFT MOLECULAR PARAMETERS AS A FUNCTION OF THE GLYCOLS MOLECULAR WEIGHT.	53
FIGURE 3.8. DENSITY AS A FUNCTION OF PRESSURE AND TEMPERATURE FOR THE PEG400. SYMBOLS REPRESENT EXPERIMENTAL DATA,[119] WHILE THE SOLID LINES DEPICT THE SOFT-SAFT EOS PREDICTIONS.	54
FIGURE 3.9. ISOTHERMAL COMPRESSIBILITY OF PURE GLYCOLS AS A FUNCTION OF PRESSURE AND TEMPERATURE. SYMBOLS REPRESENT ESTIMATES FROM THE EXPERIMENTAL <i>PPT</i> DATA,[119] WHILE THE SOLID LINES REPRESENT THE SOFT-SAFT PREDICTIONS.	55
FIGURE 3.10. ISOTHERMAL EXPANSIVITY OF PURE GLYCOLS AS A FUNCTION OF PRESSURE AND TEMPERATURE. SYMBOLS REPRESENT ESTIMATES FROM THE EXPERIMENTAL DATA,[119] WHILE THE SOLID LINES REPRESENT THE SOFT-SAFT PREDICTIONS.....	56
FIGURE 3.11. SKETCH OF THE PROPOSED MOLECULAR MODELS FOR MONO- AND DI-ALKYL GLYCOL ETHERS.....	61
FIGURE 3.12. SATURATED LIQUID AND VAPOR DENSITIES AS A FUNCTION OF TEMPERATURE FOR DIFFERENT GLYMES. SYMBOLS REPRESENT EXPERIMENTAL DATA,[118] WHILE THE SOLID LINES DEPICT THE SOFT-SAFT EOS FITTING TO THE DATA.	63
FIGURE 3.13. LOGARITHM OF THE VAPOR PRESSURE, P^* , AS FUNCTION OF THE INVERSE OF TEMPERATURE FOR THE STUDIED GLYMES. SYMBOLS REPRESENT EXPERIMENTAL DATA,[118] WHILE THE SOLID LINES REPRESENT THE SOFT-SAFT EOS FITTING TO THE DATA.....	63
FIGURE 3.14. DENSITY AS A FUNCTION OF P AND T OF THE STUDIED GLYMES. SYMBOLS REPRESENT THE EXPERIMENTAL DATA,[120] WHILE THE SOLID LINES REPRESENT THE SOFT-SAFT RESULTS.	65

FIGURE 3.15. ISOTHERMAL COMPRESSIBILITY, K_T , AS FUNCTION OF PRESSURE AND TEMPERATURE FOR THE STUDIED GLYMES. SYMBOLS REPRESENT EXPERIMENTAL DATA,[120] WHILE THE SOLID LINES REPRESENT THE SOFT-SAFT PREDICTIONS.	67
FIGURE 3.16. ISOBARIC THERMAL EXPANSIVITY, A_p , AS FUNCTION OF PRESSURE AND TEMPERATURE FOR THE STUDIED GLYMES. SYMBOLS REPRESENT EXPERIMENTAL DATA, WHILE THE SOLID LINES DEPICT THE SOFT-SAFT PREDICTIONS.	68
FIGURE 3.17. TRENDS OF THE SOFT-SAFT PURE-COMPONENT PARAMETERS FOR DIFFERENT FAMILIES OF COMPOUNDS, AS A FUNCTION OF THEIR MOLECULAR WEIGHT.[120]	70
FIGURE 3.18. LIQUID DENSITY DATA FOR PEGDME250. SYMBOLS REPRESENT THE EXPERIMENTAL DATA,[129] WHILE THE SOLID LINE DEPICTS THE SOFT-SAFT PREDICTIONS.	72
FIGURE 3.19. SOFT-SAFT ASSOCIATION PARAMETERS FOR THREE FAMILIES OF COMPOUNDS.	73
FIGURE 3.20. A) VLE FOR THE SYSTEM DEG + CO ₂ . SYMBOLS REPRESENT EXPERIMENTAL DATA, WHILE THE SOLID LINES DEPICT THE SOFT-SAFT RESULTS.[132] B) TEMPERATURE-DEPENDENT BINARY INTERACTION PARAMETER USED IN THE CALCULATIONS.	77
FIGURE 3.21. SOLUBILITY OF CO ₂ IN DIFFERENT GLYMES AND DEG AT 313.15 K.[11,16,17,19,132] THE SOLID LINE DEPICTS THE CORRELATION PROPOSED BY CARVALHO AND COUTINHO[133] FOR THE CO ₂ SOLUBILITY IN IDEAL LOW-VOLATILITY PHYSICAL SOLVENTS.	78
FIGURE 3.22. CO ₂ SOLUBILITIES IN DI-ALKYL ETHERS AT 313.15 K. SYMBOLS REPRESENT THE EXPERIMENTAL DATA,[17] WHILE THE DASHED AND SOLID LINES DEPICT THE SOFT-SAFT PREDICTIONS AND FITTING TO THE EXPERIMENTAL DATA, RESPECTIVELY.	80
FIGURE 3.23. SATURATED LIQUID AND VAPOR DENSITIES AT EQUILIBRIUM FOR THE DEGDM + CO ₂ SYSTEM. SYMBOLS REPRESENT EXPERIMENTAL DATA,[17] WHILE THE LINES DEPICT THE SOFT-SAFT RESULTS.	80
FIGURE 3.24. CO ₂ SOLUBILITIES AS A FUNCTION OF TEMPERATURE FOR TRIEGME AND PEGDME250. SYMBOLS REPRESENT EXPERIMENTAL DATA,[11,16] WHILE THE SOLID LINES DEPICT THE SOFT-SAFT RESULTS.	81
FIGURE 3.25. PRESSURE-COMPOSITION DIAGRAMS AT DIFFERENT TEMPERATURES FOR THE BINARY SYSTEMS: CO ₂ + DEGREE, DEGME, DEGDM, AND DEGD. SYMBOLS REPRESENT EXPERIMENTAL DATA,[19] WHILE THE SOLID LINES REPRESENT THE SOFT-SAFT RESULTS, USING THE TEMPERATURE-DEPENDENT BINARY INTERACTION PARAMETERS FROM TABLE 3.8.	83
FIGURE 3.26. CH ₄ SOLUBILITIES IN TRIEGDM AND DEGREE. SYMBOLS REPRESENT EXPERIMENTAL MEASUREMENTS, WHILE THE SOLID LINES DEPICT THE SOFT-SAFT FITTING TO THE EXPERIMENTAL DATA.	85
FIGURE 3.27. SELECTIVITY CO ₂ /CH ₄ IN DEGREE, AS PREDICTED BY THE SOFT-SAFT EOS.	86
FIGURE 3.28. ISOBARIC TEMPERATURE-COMPOSITION DIAGRAMS OF THE GLYCOLS + WATER BINARY SYSTEMS. THE SYMBOLS REPRESENT EXPERIMENTAL DATA,[138] WHILE THE DASHED AND SOLID LINES REPRESENT THE SOFT-SAFT EOS PREDICTIONS AND FITTING TO THE DATA.	89
FIGURE 3.29. WATER ACTIVITY COEFFICIENTS FOR THE BINARY SYSTEMS WATER + GLYCOLS AT THREE DIFFERENT PRESSURES. SYMBOLS REPRESENT ESTIMATES FROM THE EXPERIMENTAL BOILING TEMPERATURES,[138] WHILE THE SOLID LINES REPRESENT THE SOFT-SAFT CALCULATIONS.	91
FIGURE 3.30. WATER ACTIVITY FOR THE BINARY SYSTEM WATER + PEGS. SYMBOLS REPRESENT EXPERIMENTAL DATA,[139–141] WHILE THE SOLID LINES REPRESENT THE SOFT-SAFT RESULTS, USING $\xi = 1.22$	93
FIGURE 3.31. ISOBARIC TEMPERATURE-COMPOSITION PHASE DIAGRAMS OF THE BINARY GLYME+ WATER MIXTURES. SYMBOLS REPRESENT EXPERIMENTAL DATA,[142] WHILE THE SOLID LINES REPRESENT THE SOFT-SAFT RESULTS, USING THE BINARY INTERACTION PARAMETERS FROM TABLE 3.11.	95
FIGURE 3.32. BOILING TEMPERATURES (@1ATM) OF THE PURE GLYMES AND THEIR AQUEOUS SOLUTIONS AT DIFFERENT CONCENTRATIONS AS CALCULATED WITH SOFT-SAFT EOS.	97

FIGURE 3.33. WATER ACTIVITY COEFFICIENTS FOR GLYME + WATER BINARY MIXTURES. SYMBOLS REPRESENT ESTIMATES OBTAINED FROM THE EXPERIMENTAL BOILING TEMPERATURES,[142] WHILE THE SOLID LINES DEPICT THE SOFT-SOFT PREDICTIONS.	99
FIGURE 4.1. SOLUBILITY OF <i>N</i> -ALKANES IN WATER. SYMBOLS REPRESENT EXPERIMENTAL DATA,[169–174] WHILE THE SOLID LINES AND DASHED LINES REPRESENT THE SAFT- Γ -MIE RESULTS USING THE UNLIKE INTERACTION PARAMETERS WITH ALKYL GROUPS PROPOSED BY HUTACHAROEN ET AL.[168] AND DUFAL ET AL.[153], RESPECTIVELY.	112
FIGURE 4.2. VLE OF PENTAN-1-OL (1) + WATER (2) AT ATMOSPHERIC PRESSURE. SYMBOLS REPRESENT EXPERIMENTAL DATA, [191–194] WHILE THE SOLID LINES DEPICT THE SAFT- Γ -MIE EOS PREDICTIONS USING THE NEW OH GROUP PARAMETERS.	116
FIGURE 4.3. LLE OF ALKAN-1-OL (1) + WATER MIXTURES. (LEFT) ALCOHOL RICH PHASE (RIGHT) AQUEOUS PHASE. SYMBOLS REPRESENT EXPERIMENTAL DATA (C.F. TABLE 4.6) WHILE THE SOLID AND DASHED LINES REPRESENT THE SAFT- Γ -MIE RESULTS USING AN OH OR A CH ₂ OH GROUP, RESPECTIVELY.	117
FIGURE 4.4. DENSITIES AND VAPOR PRESSURES FOR α , Ω -ALKANEDIOLS. SYMBOLS REPRESENT EXPERIMENTAL DATA[118] WHILE THE SOLID AND DASHED LINES REPRESENT THE SAFT- Γ -MIE EOS RESULTS USING AN OH OR A CH ₂ OH TO DESCRIBE THE ALCOHOL GROUPS, RESPECTIVELY.	118
FIGURE 4.5. APPROACHES CONSIDERED TO SUBDIVIDE THE GLYCOL MOLECULES IN THE FRAMEWORK OF A HETERONUCLEAR MODEL.	120
FIGURE 4.6. SATURATION LIQUID DENSITIES AND VAPOR PRESSURES OF PURE GLYCOL OLIGOMERS. SYMBOLS REPRESENT EXPERIMENTAL DATA,[118] WHILE THE LINES DEPICT THE SAFT- Γ -MIE RESULTS, USING TWO DIFFERENT APPROACHES.	123
FIGURE 4.7. LLE OF GLYCOL + <i>N</i> -HEPTANE SYSTEMS. SYMBOLS REPRESENT EXPERIMENTAL DATA[205] WHILE THE DASHED AND SOLID LINES REPRESENT THE SAFT- Γ -MIE RESULTS USING APPROACH A AND APPROACH B, RESPECTIVELY.	124
FIGURE 4.8. <i>PPT</i> OF PURE GLYCOLS. SYMBOLS REPRESENT EXPERIMENTAL DATA,[119] WHILE THE SOLID LINES DEPICT THE SAFT- Γ -MIE RESULTS FOLLOWING APPROACH B.	125
FIGURE 4.9. VLE OF GLYCOL + WATER SYSTEMS. SYMBOLS REPRESENT EXPERIMENTAL DATA,[138] WHILE THE SOLID AND DASHED LINES REPRESENT THE SAFT- Γ -MIE RESULTS USING APPROACH A AND APPROACH B, RESPECTIVELY.	127
FIGURE 4.10. WATER ACTIVITY FOR BINARY SYSTEMS PEG + WATER. SYMBOLS REPRESENT EXPERIMENTAL DATA,[139–141] WHILE THE SOLID AND DASHED LINES REPRESENT THE SAFT- Γ -MIE PREDICTIONS USING APPROACH A AND B, RESPECTIVELY.	129
FIGURE 4.11. VAPOR PRESSURES OF PURE GLYMES. SYMBOLS REPRESENT EXPERIMENTAL DATA[118], WHILE THE SOLID LINES DEPICT THE SAFT- Γ -MIE RESULTS USING A) APPROACH A; B) APPROACH G.	131
FIGURE 4.12. SATURATION LIQUID DENSITIES OF PURE GLYMES. SYMBOLS REPRESENT EXPERIMENTAL DATA, WHILE THE SOLID LINES DEPICT THE SAFT- Γ -MIE RESULTS USING A) APPROACH A; B) APPROACH G.	131
FIGURE 4.13. BOILING TEMPERATURES OF GLYMES + WATER MIXTURES AT DIFFERENT PRESSURES. SYMBOLS REPRESENT EXPERIMENTAL DATA[142] WHILE THE SOLID AND DASHED LINES REPRESENT THE SAFT- Γ -MIE RESULTS USING APPROACH A AND APPROACH G, RESPECTIVELY.	134
FIGURE 4.14. VAPOR PRESSURES AND LIQUID DENSITIES OF PURE C ₄ E ₁ . SYMBOLS REPRESENT EXPERIMENTAL DATA[118] WHILE THE DASHED LINES REPRESENT THE MODELLING PREDICTIONS USING DIFFERENT APPROACHES IN SAFT- Γ -MIE.	136
FIGURE 4.15. LLE OF C ₆ E ₁ + WATER SYSTEMS. SYMBOLS REPRESENT EXPERIMENTAL DATA,[209–213] WHILE THE DASHED LINES REPRESENT THE MODELLING PREDICTIONS USING THE DIFFERENT MODELLING APPROACHES.	137
FIGURE 4.16. LLE OF C ₆ E ₁ (1) + WATER (2) SYSTEMS. SYMBOLS REPRESENT EXPERIMENTAL DATA[209–213] WHILE THE RED AND BLUE LINES REPRESENT THE SAFT- Γ -MIE RESULTS WHEN THE EO-H ₂ O UNLIKE	

INTERACTION PARAMETERS WERE FITTED TO THE EXPERIMENTAL DATA FOR THE C ₄ E ₁ AND C ₁₀ E ₄ SYSTEMS, RESPECTIVELY.	140
FIGURE 5.1. SCHEMATIC REPRESENTATION OF THE CG MAPPING CONSIDERED FOR THE C ₁₂ E ₆ SURFACTANT. .	148
FIGURE 5.2. CG-MD SIMULATIONS OF C ₈ E ₆ IN WATER AT DIFFERENT SURFACTANT CONCENTRATIONS. GREEN REPRESENTS THE ALKYL TAIL BEADS, WHILE PURPLE IS USED TO REPRESENT THE BEADS OF THE HYDROPHILIC MOIETY. WATER MOLECULES ARE OMITTED FOR A CLEARER VISUALIZATION.	153
FIGURE 5.3. CG-MD SIMULATIONS FOR C ₁₂ E ₂ IN WATER AT DIFFERENT SURFACTANT CONCENTRATIONS. COLOURS AS IN FIGURE 5.2.	155
FIGURE 5.4. CG-MD SIMULATIONS FOR C ₁₂ E ₆ IN WATER AT DIFFERENT SURFACTANT CONCENTRATIONS. COLOURS AS IN FIGURE 5.2.	157
FIGURE 5.5. SPATIAL ORGANIZATION OF THE ALKYL TAILS IN THE H ₁ PHASE OBSERVED IN THE C ₁₂ E ₁₀ /H ₂ O SYSTEM AT 70 WT% CONCENTRATION.....	158
FIGURE 5.6. CG-MD SIMULATIONS FOR C ₁₂ E ₁₂ /H ₂ O AT DIFFERENT SURFACTANT CONCENTRATIONS. COLOURS AS IN FIGURE 5.2. BLACK REPRESENTS THE DIRECTION OF PLANE IN WHICH THE CONTENT OF THE BOX WAS CUT TO ALLOW FOR A CLEARER VISUALIZATION.....	159
FIGURE 5.7. CG-MD SIMULATIONS FOR C ₁₆ E ₄ /H ₂ O AT DIFFERENT SURFACTANT CONCENTRATIONS. COLOURS AS IN FIGURE 5.2.....	161
FIGURE 5.8. ARRANGEMENT OF THE ALKYL TAILS IN THE C ₁₆ E ₆ /H ₂ O SYSTEM AT DIFFERENT SURFACTANT CONCENTRATIONS.....	162
FIGURE 5.9. CG-MD SIMULATIONS FOR C ₁₆ E ₈ /H ₂ O AT DIFFERENT SURFACTANT CONCENTRATIONS. COLOURS AS IN FIGURE 5.2.....	163
FIGURE 5.10. MICELLE DENSITY PROFILE FOR THE C ₁₂ E ₆ IN WATER AS OBTAINED FROM THE CG-MD SIMULATION AT 15 WT%.....	167
FIGURE 5.11. FINAL SNAPSHOTS OF THE CG-MD SIMULATIONS FOR C ₁₀ E ₄ + H ₂ O + N-DODECANE MIXTURES AT 313 K. YELLOW REPRESENTS THE OIL MOLECULES, WHILE GREEN IS USED TO REPRESENT THE SURFACTANT ALKYL TAILS. WATER AND THE POLAR SECTION OF THE SURFACTANTS ARE REMOVED FOR A CLEARER VIEW OF THE SYSTEM BUT OCCUPY THE REST OF THE SIMULATION BOX.....	170
FIGURE 5.12. FINAL SNAPSHOTS OF THE CG-MD SIMULATIONS FOR C ₁₀ E ₄ + H ₂ O + N-EICOSANE MIXTURES. COLOURS AS IN FIGURE 5.11.	171
FIGURE 5.13. FINAL SNAPSHOTS OF THE CG-MD SIMULATIONS FOR C ₁₂ E ₆ + H ₂ O + N-DODECANE MIXTURES AT 313 K. THE SIMULATIONS START FROM AN AQUEOUS SOLUTION OF C ₁₂ E ₆ WITH 80 WT% OF SURFACTANT TO WHICH OIL MOLECULES WERE ADDED UNTIL THE TOTAL OIL AMOUNTS TO 10, 20, 30 AND 40 WT% OF THE TOTAL SYSTEM'S WEIGHT. COLOURS AS IN FIGURE 5.11.....	172
FIGURE 5.14. FINAL SNAPSHOTS OF THE CG-MD SIMULATIONS FOR C ₁₂ E ₆ + H ₂ O + N-DODECANE MIXTURES AT 313 K. THE SIMULATIONS START FROM AN AQUEOUS SOLUTION OF C ₁₂ E ₆ WITH 70 WT% OF SURFACTANT TO WHICH OIL MOLECULES WERE ADDED UNTIL THE OIL AMOUNTS TO 10, 30, AND 40 WT% OF THE TOTAL SYSTEM'S WEIGHT. COLOURS AS IN FIGURE 5.11.	173
FIGURE 5.15. FINAL SNAPSHOTS OF THE CG-MD SIMULATIONS FOR C ₁₂ E ₆ + H ₂ O + N-DODECANE MIXTURES AT 313 K. THE SIMULATIONS START FROM AN AQUEOUS SOLUTION OF C ₁₂ E ₆ WITH 50 WT% OF SURFACTANT TO WHICH OIL MOLECULES WERE ADDED UNTIL THE OIL AMOUNTS TO 10, 20, AND 30 WT% OF THE TOTAL SYSTEM'S WEIGHT. YELLOW REPRESENTS THE OIL MOLECULES, GREEN AND PURPLE ARE USED TO REPRESENT THE SURFACTANT HYDROPHOBIC AND HYDROPHILIC PARTS, RESPECTIVELY, AND BLUE REPRESENTS THE WATER MOLECULES.	175
FIGURE 5.16. CG-MD SIMULATIONS FOR C ₁₂ E ₆ + H ₂ O + N-DODECANE. OIL MOLECULES AMOUNTING TO A TOTAL OF 5 WT% WERE ADDED TO AN AQUEOUS SOLUTION OF C ₁₂ E ₆ AT 15 WT%. COLOURS AS IN FIGURE 5.15.	176

FIGURE 5.17. MICELLAR GROWTH IN $C_{12}E_6 + H_2O + N$ -DODECANE MIXTURES AS THE AMOUNT OF OIL IN THE MIXTURE INCREASES. COLOURS AS IN FIGURE 5.15.	176
FIGURE 5.18. NUMBER DENSITY OF N -DODECANE MOLECULES AS A FUNCTION OF THE Z-COORDINATE OF THE SIMULATION BOX. THE FINAL SNAPSHOT OF THE CG-MD SIMULATION OF 1664 N -DODECANE (REPRESENTED IN GREY) NEAR A SILICA SURFACE (YELLOW COLOUR) IS SHOWN AS AN INSET.	181
FIGURE 5.19. CG-MD SIMULATION SNAPSHOTS AFTER 100 AND 1000 NS OF A SYSTEM CONTAINING A SILICA SURFACE (YELLOW), 1664 N -DODECANE MOLECULES (GREY), AND 100000 WATER MOLECULES (BLUE).	182
FIGURE 5.20. FINAL SNAPSHOT OF THE CG-MD SIMULATION CARRIED OUT FOR THE SYSTEM SILICA + N -DODECANE + WATER USING THE MARTINI 3.0 FF. YELLOW REPRESENTS THE SILICA SURFACE, GREY AND BLUE REPRESENTS THE OIL AND WATER MOLECULES, RESPECTIVELY.	184
FIGURE 5.21. FINAL SNAPSHOTS OF THE CG-MD SIMULATIONS (1 NS OF SIMULATION TIME) OF SILICA + N -DODECANE + WATER + $C_{12}E_6$ SYSTEMS USING THE MARTINI 3.0 FF. YELLOW REPRESENTS THE SILICA SURFACE, GREY REPRESENTS THE N -DODECANE, GREEN, PURPLE, AND ORANGE REPRESENT THE ALKYL TAILS, EO GROUPS AND ALCOHOL GROUP OF THE SURFACTANTS, AND BLUE REPRESENTS THE WATER MOLECULES. A) 500 MOLECULES OF $C_{12}E_6$ B) 1664 MOLECULES OF $C_{12}E_6$	185
FIGURE 5.22. FINAL SNAPSHOT OF THE CG-MD SIMULATIONS (300 NS OF SIMULATION TIME) OF SILICA + N -DODECANE + WATER + $C_{12}E_6$ SYSTEMS USING THE MARTINI 3.0 FF, USING AN INCREASED ENERGY VALUE FOR THE 'SN1DQ' – 'TW' INTERACTIONS. COLOURS AS IN FIGURE 5.21.	186
FIGURE 6.1. HIGH-PRESSURE DENSITIES OF [CH]CL-BASED DESS WITH A) EG; B) GLYCEROL; C) UREA AS HBD. SYMBOLS REPRESENT EXPERIMENTAL DATA,[322] WHILE LINES REPRESENT THE PC-SAFT RESULTS WITH (LEFT) AND WITHOUT (RIGHT) USING A TEMPERATURE-DEPENDENT BINARY INTERACTION PARAMETER FITTED TO THE DATA.	196
FIGURE 6.2. VISCOSITIES OF [CH]CL-BASED DES WITH DIFFERENT HBDS. A) EG; B) GLYCEROL; C) UREA. SYMBOLS REPRESENT EXPERIMENTAL DATA,[322] WHILE THE SOLID LINES DEPICT THE RESULTS OBTAINED WITH PC-SAFT + FVT.	199
FIGURE 6.3. SKETCH OF THE ASSOCIATING SITES PROPOSED IN THIS WORK FOR [CH]CL. BLUE IS USED FOR H-BOND DONOR SITES WHILE RED IS USED FOR H-BOND ACCEPTOR SITES.	201
FIGURE 6.4. A) HIGH-PRESSURE LIQUID DENSITIES AND B) SLE PHASE DIAGRAM FOR THE MIXTURE [CH]CL + EG (1:2). SYMBOLS REPRESENT EXPERIMENTAL DATA[322,329] WHILE THE SOLID LINES DEPICT THE SOFT-SAFT RESULTS AND IDEAL SOLUBILITY CURVES. IN B), THE DASHED LINES REPRESENT THE SLE RESULTS WITHOUT ACCOUNTING FOR THE SOLID-SOLID TRANSITION OF [CH]CL.	204
FIGURE 6.5. VLE FOR [CH]CL + EG MIXTURES. SYMBOLS REPRESENT EXPERIMENTAL DATA,[334] WHILE THE SOLID LINES DEPICT THE SOFT-SAFT PREDICTIONS.	207
FIGURE 6.6. A) DENSITIES AT 0.10 MPA FOR [CH]CL + TRIEG (1:2). B) DENSITIES AT 0.10 MPA FOR [CH]CL + PHENOL. SYMBOLS REPRESENT EXPERIMENTAL DATA[335,336] WHILE THE SOLID LINES DEPICT THE SOFT-SAFT PREDICTIONS.	208
FIGURE 6.7. PPT DATA FOR THE [CH]CL + GLYCEROL (1:2) DES. SYMBOLS REPRESENT THE EXPERIMENTAL DATA, WHILE THE LINES DEPICT THE SOFT-SAFT RESULTS USING A) $\bar{\epsilon}_{ij}=1$ (PURE PREDICTIONS); B) $\bar{\epsilon}_{ij}=1.022$	209
FIGURE 6.8. SOLUBILITY OF [CH]CL IN GLYCEROL. SYMBOLS REPRESENT EXPERIMENTAL DATA,[313,329,337] WHILE THE DASHED AND SOLID LINES REPRESENT THE SOFT-SAFT RESULTS ($\bar{\epsilon}_{ij}=1.022$) AND IDEAL SOLUBILITY CURVES, WITH AND WITHOUT ACCOUNTING FOR THE SOLID-SOLID TRANSITION OF [CH]CL, RESPECTIVELY.	210
FIGURE 6.9. A) DENSITIES AND B) BOILING TEMPERATURES OF AQUEOUS SOLUTIONS OF [CH]CL. SYMBOLS REPRESENT EXPERIMENTAL DATA,[338,339] WHILE THE SOLID AND DASHED LINES REPRESENT THE SOFT-SAFT RESULTS USING $\bar{\epsilon}=1.25$ AND $\bar{\epsilon}=1$, RESPECTIVELY.	211

FIGURE 6.10. A) BOILING TEMPERATURES FOR [CH]CL + ETOH; B) WATER ACTIVITIES AT 298.2 K IN AQUEOUS SOLUTION OF [CH]CL. SYMBOLS REPRESENT EXPERIMENTAL DATA,[338,340] WHILE THE LINES DEPICT THE SOFT-SAFT PREDICTIONS.	211
FIGURE 6.11. A) DENSITY OF PURE [CH]CL AS PREDICTED BY SOFT-SAFT. B) DENSITY OF [CH]CL AQUEOUS SOLUTIONS AT 303.15 K. BLUE CIRCLES REPRESENT EXPERIMENTAL DATA FROM LITERATURE,[339] WHILE THE RED TRIANGLE REPRESENT THE HYPOTHETICAL DENSITY OF PURE [CH]CL PREDICTED BY SOFT-SAFT AT 303.15 K.	212
FIGURE 6.12. DENSITIES OF AQUEOUS SOLUTIONS OF DES. A) [CH]CL + EG (1:2); B) [CH]CL + GLYCEROL (1:2). SYMBOLS REPRESENT EXPERIMENTAL DATA,[322] WHILE THE SOLID LINES DEPICT THE SOFT-SAFT PREDICTIONS.	213
FIGURE 6.13. CO ₂ SOLUBILITIES IN TWO DIFFERENT DES: A) [CH]CL + EG (1:2); B) [CH]CL + GLYCEROL (1:2). SYMBOLS REPRESENT THE EXPERIMENTAL DATA,[347,348] WHILE THE SOLID LINES DEPICT THE SOFT-SAFT RESULTS.	214
FIGURE 6.14. A) SLE PHASE DIAGRAM FOR [CH]CL + LACTIC ACID. B) DENSITIES OF [CH]CL + LACTIC ACID AT DIFFERENT HBA TO HBD MOLAR RATIOS. SYMBOLS REPRESENT EXPERIMENTAL DATA,[310,349] WHILE THE SOLID LINES DEPICT THE SOFT-SAFT RESULTS USING $\Xi=1.04$	215
FIGURE 6.15. LIQUID DENSITIES, AT ATMOSPHERIC PRESSURE, OF CARBOXYLATE-BASED PILS WITH A 1:1 ACID:BASE RATIO, WITH THE FOLLOWING BASE PRECURSORS: A) DEEA, B) MEA, C) MEEA, AND D) DEA/DBA. SYMBOLS REPRESENT EXPERIMENTAL DATA,[43,361,382–385] WHILE THE DASHED LINES DEPICT THE PC-SAFT PREDICTIONS.	221
FIGURE 6.16. A) EXCESS MOLAR VOLUMES, V^E . B) MOLAR VOLUME DEVIATION FROM THE IDEAL MOLAR VOLUME, (V^{ID}), FOR DIFFERENT PILS AND DESS.	222
FIGURE 6.17. DENSITIES AT ATMOSPHERIC PRESSURE OF DIFFERENT PILS. SYMBOLS REPRESENT EXPERIMENTAL DATA,[43,361,382–385] WHILE THE SOLID LINES DEPICT THE PC-SAFT EOS MODELLING RESULTS, CORRECTED TO ACCOUNT FOR THE EFFECT OF PROTON TRANSFER.	225
FIGURE 6.18. PERCENTAGE RELATIVE EXCESS MOLAR VOLUMES OF CARBOXYLATE BASED PILS WITH DIFFERENT AMINES AS BASE PRECURSORS.	226
FIGURE 6.19. DENSITY OF PILS BASED ON THE DEEA CATION. SYMBOLS REPRESENT EXPERIMENTAL DATA,[364] WHILE THE SOLID AND DASHED LINES REPRESENT THE PC-SAFT PREDICTIONS WITH AND WITHOUT CORRECTION OF THE MOLAR VOLUMES.	227
FIGURE. B.1. SOFT-SAFT MODELLING OF THE <i>PPT</i> DATA AND SECOND-ORDER DERIVATIVE PROPERTIES OF DEG. SYMBOLS REPRESENT EXPERIMENTAL DATA,[119] WHILE THE SOLID LINES DEPICT THE SOFT-SAFT RESULTS USING THE PARAMETERS PROPOSED BY PEDROSA ET AL.[75].	292
FIGURE. B.2. ISOBARIC TEMPERATURE-COMPOSITION PHASE DIAGRAMS OF THE BINARY GLYME+ WATER MIXTURES. SYMBOLS REPRESENT EXPERIMENTAL DATA,[142] WHILE THE SOLID AND DASHED LINES REPRESENT THE SOFT-SAFT RESULTS, WITH AND WITHOUT USING THE BINARY INTERACTION PARAMETERS FROM TABLE 3.11, RESPECTIVELY.	293
FIGURE. C.1. SATURATED LIQUID DENSITY OF LINEAR ALKANES. A) FROM ETHANE TO N-DECANE (FITTING) B) FROM N-DODECANE TO N-EICOSANE (PREDICTED). SYMBOLS REPRESENT EXPERIMENTAL DATA FROM THE DIPPR DATABASE,[118] WHILE THE SOLID LINES DEPICT THE SAFT- Γ -MIE RESULTS.	294
FIGURE. C.2. VAPOR PRESSURES OF LINEAR ALKANES. A) FROM ETHANE TO N-DECANE (FITTING) B) FROM N-DODECANE TO N-EICOSANE (PREDICTED). SYMBOLS REPRESENT EXPERIMENTAL DATA FROM THE DIPPR DATABASE,[118] WHILE THE SOLID LINES DEPICT THE SAFT- Γ -MIE RESULTS.	294

FIGURE. C.3. VAPOR PRESSURES OF LINEAR ALKANES. A) FROM ETHANE TO N-DECANE (FITTING) B) FROM N-DODECANE TO N-EICOSANE (PREDICTED). SYMBOLS REPRESENT EXPERIMENTAL DATA FROM THE DIPPR DATABASE,[117] WHILE THE SOLID LINES DEPICT THE SAFT- Γ -MIE RESULTS.....	295
FIGURE. C.4. A) ISOBARIC VLE OF N-HEXANE + N-HEXADECANE; B) ISOTHERMAL VLE OF ETHANE + N-DECANE; C) ATMOSPHERIC PRESSURE LIQUID DENSITIES OF N-DECANE + N-C22; D) HIGH-PRESSURE LIQUID DENSITIES OF N-OCTANE + N-DODECANE. SYMBOLS REPRESENT THE EXPERIMENTAL DATA,[406–409] WHILE THE SOLID LINES DEPICT THE SAFT- Γ -MIE PREDICTIONS.	295
FIGURE. C.5. SATURATION LIQUID DENSITIES AND VAPOR PRESSURES OF PURE EG. SYMBOLS REPRESENT EXPERIMENTAL DATA,[118] WHILE THE DASHED AND SOLID LINES REPRESENT THE SAFT- Γ -MIE RESULTS FOLLOWING APPROACH A AND APPROACH B, RESPECTIVELY.	296
FIGURE. C.6. HIGH-PRESSURE LIQUID DENSITIES OF PURE GLYCOLS. SYMBOLS REPRESENT THE EXPERIMENTAL DATA,[119] WHILE THE SOLID LINES REPRESENT THE SAFT- Γ -MIE RESULTS FOLLOWING APPROACH A....	297
FIGURE. C.7. HIGH-PRESSURE LIQUID DENSITIES OF PURE GLYMES. SYMBOLS REPRESENT EXPERIMENTAL DATA,[120] WHILE THE SOLID LINES DEPICT THE SAFT- Γ -MIE RESULTS, FOLLOWING APPROACH A.	299
FIGURE. C.8. HIGH-PRESSURE LIQUID DENSITIES OF PURE GLYMES. SYMBOLS REPRESENT EXPERIMENTAL DATA,[120] WHILE THE SOLID LINES DEPICT THE SAFT- Γ -MIE RESULTS FOLLOWING APPROACH G.....	301
FIGURE. D.1. FINAL SNAPSHOT OF THE CG-MD SIMULATION OF C ₈ E ₆ /H ₂ O AT 60 WT%, SHOWING THE ALKYL TAILS DISPOSITION IN THE H ₁ PHASE OBSERVED.	302
FIGURE. D.2. FINAL SNAPSHOTS OF THE CG-MD SIMULATIONS CARRIED OUT FOR THE SYSTEM C ₈ E ₆ /H ₂ O AT 15 AND 30 WT%. GREEN IS USED TO REPRESENT THE ALKYL TAIL BEADS, WHILE PURPLE REPRESENTS THE BEADS FROM THE HYDROPHILIC MOIETY. WATER MOLECULES ARE OMITTED TO ALLOW FOR AN EASIER VISUALIZATION.	302
FIGURE. D.3. FINAL SNAPSHOTS OF THE CG-MD SIMULATIONS CARRIED OUT FOR THE SYSTEM C ₈ E ₁₂ /H ₂ O AT DIFFERENT CONCENTRATIONS. COLOURS AS IN FIGURE D.2.	303
FIGURE. D.4. FINAL SNAPSHOTS OF THE CG-MD SIMULATIONS CARRIED OUT FOR THE SYSTEM C ₁₂ E ₄ /H ₂ O AT DIFFERENT CONCENTRATIONS. FOR AN EASIER VISUALIZATION OF THE LIQUID STRUCTURAL ORGANIZATION ONLY THE ALKYL CHAINS ARE REPRESENTED.	304
FIGURE. D.5. FINAL SNAPSHOTS OF THE CG-MD SIMULATIONS CARRIED OUT FOR THE SYSTEM C ₁₂ E ₁₀ /H ₂ O AT DIFFERENT CONCENTRATIONS. COLOURS AS IN FIGURE D.2.	305
FIGURE. D.6. FINAL SNAPSHOTS OF THE CG-MD SIMULATIONS CARRIED OUT FOR THE SYSTEM C ₁₂ E ₂₃ /H ₂ O AT DIFFERENT CONCENTRATIONS. FOR AN EASIER VISUALIZATION ONLY THE ALKYL CHAINS ARE REPRESENTED.	305
FIGURE. D.7. PORE DEFECT IN THE C ₁₆ E ₆ /H ₂ O SYSTEM AT 70 WT%.	306
FIGURE. D.8. FINAL SNAPSHOTS OF THE CG-MD SIMULATIONS FOR THE C ₁₆ E ₁₂ /H ₂ O SYSTEM AT DIFFERENT CONCENTRATIONS. COLOURS AS IN FIGURE D.2.....	306
FIGURE. E.1. FINAL SNAPSHOT OF THE CG-MD SIMULATION CARRIED OUT FOR A SIMULATION BOX CONTAINING A FIXED SILICA SURFACE (YELLOW), 1664 N-DODECANE MOLECULES (GREY), AND 400000 WATER MOLECULES (BLUE).....	307
FIGURE. E.2. FINAL SNAPSHOT OF THE CG-MD SIMULATION CARRIED OUT FOR A SIMULATION BOX CONTAINING A FIXED SILICA SURFACE (YELLOW), 1664 N-DODECANE MOLECULES (GREY), AND 100000 WATER MOLECULES (BLUE) IN THE PRESENCE OF 90 MOLECULES OF C ₁₂ E ₆	307
FIGURE. E.3. CG-MD SIMULATIONS OF WATER IN CONTACT WITH A SILICA OR GRAPHENE SURFACE USING THE MARTINI 2.0 FF.	308
FIGURE. E.4. NUMBER DENSITY OF DODECANE MOLECULES AS A FUNCTION OF THE Z-COORDINATE OF THE SIMULATION BOX. THE FINAL SNAPSHOT OF THE CG-MD SIMULATION OF 1664 N-DODECANE MOLECULES (REPRESENTED IN GREY) NEAR A SILICA SURFACE (YELLOW) USING THE MARTINI 3.0 FF IS SHOWN AS AN INSET.....	308

FIGURE. F.1. PREDICTION OF HIGH-PRESSURE DENSITIES OF PURE ETHYLENE GLYCOL. SYMBOLS REPRESENT EXPERIMENTAL DATA FROM CRESPO ET AL.[119] WHILE THE SOLID LINES DEPICT THE PC-SAFT PREDICTIONS USING THE PARAMETERS FROM: A) ATILHAN ET AL.[319] B) RESCHKE ET AL.[320] C) LIANG ET AL.[321].....	309
FIGURE. F.2. VISCOSITIES OF PURE A) EG; B) GLYCEROL. SYMBOLS REPRESENT EXPERIMENTAL DATA,[118,323] WHILE THE SOLID LINES DEPICT THE FVT FITTING TO THE EXPERIMENTAL DATA.	310
FIGURE. F.3. A) VISCOSITIES OF [CH]CL-BASED DESS AT A 1:2 HBA:HBD RATIO, AT ATMOSPHERIC PRESSURE. B) VISCOSITIES OF [CH]CL + UREA (1:2), AT ATMOSPHERIC PRESSURE. SYMBOLS REPRESENT THE EXPERIMENTAL DATA,[410] WHILE THE SOLID LINES DEPICT THE PC-SAFT + FVT RESULTS.	310
FIGURE. F.4. SATURATED LIQUID DENSITIES AND VAPOR PRESSURES OF PHENOL. SYMBOLS REPRESENT EXPERIMENTAL DATA FROM THE DIPPR DATABASE,[118] WHILE THE SOLID LINES DEPICT THE SOFT-SAFT FITTING TO THE DATA.....	311
FIGURE. F.5. SATURATED LIQUID DENSITIES AND VAPOR PRESSURES OF GLYCEROL. SYMBOLS REPRESENT EXPERIMENTAL DATA FROM THE DIPPR DATABASE,[118] WHILE THE SOLID LINES DEPICT THE SOFT-SAFT FITTING TO THE DATA.....	311

List of Tables

TABLE 1.1. COMPOUNDS OF INTEREST TO THE OIL & GAS INDUSTRY CONTAINING EO REPEATING UNITS.	6
TABLE 2.1. OUTLINE OF SOFT-SAFT AND PC-SAFT EOSS FOR NON-ASSOCIATING COMPONENTS.....	26
TABLE 3.1. ASSOCIATION SCHEMES EMPLOYED IN THE MODELLING OF GLYCOLS USING EITHER SAFT OR CPA. BLUE AND RED COLOURS ARE USED TO DEFINE POSITIVE AND NEGATIVE SITES THAT CAN ONLY INTERACT WITH THE OPPOSITE SIGN, WHILE GREEN REPRESENTS BINARY SITES THAT CAN INTERACT WITH BOTH POSITIVE AND NEGATIVE SITES.....	45
TABLE 3.2. SOFT-SAFT PURE-COMPONENT PARAMETERS FOR GLYCOLS.	51
TABLE 3.3. NAME, CHEMICAL STRUCTURE, AND MOLECULAR WEIGHT OF THE STUDIED GLYMES.	60
TABLE 3.4. SOFT-SAFT PURE-COMPONENT PARAMETERS FOR THE STUDIED GLYMES AND DEVIATIONS FROM THE EXPERIMENTAL DATA.	62
TABLE 3.5. SOFT-SAFT MOLECULAR PARAMETERS FOR GLYMES AS A FUNCTION OF THE MOLECULAR WEIGHT.	71
TABLE 3.6. SOFT-SAFT PURE-COMPONENT PARAMETERS USED IN THIS WORK.....	76
TABLE 3.7. THERMAL CYCLE CAPACITIES PREDICTED BY SOFT-SAFT FOR THE DIFFERENT SOLVENTS AT 5 MPA.	82
TABLE 3.8. BINARY INTERACTION PARAMETERS USED IN THE SOFT-SAFT CALCULATIONS AND DEVIATIONS FROM THE EXPERIMENTAL DATA REPORTED BY AMARAL ET AL.[19].....	84
TABLE 3.9. SOFT-SAFT PURE-COMPONENT PARAMETERS FOR WATER AND DIFFERENT PEGS.	88
TABLE 3.10. BINARY INTERACTION PARAMETERS AND DEVIATIONS FROM THE EXPERIMENTAL DATA FOR GLYCOLS + WATER SYSTEMS.....	90
TABLE 3.11. BINARY INTERACTION PARAMETERS FOR THE SYSTEM GLYMES + WATER, AND THE DEVIATIONS BETWEEN THE MODEL CALCULATIONS AND THE EXPERIMENTAL DATA.	96
TABLE 4.1. GROUP SPECIFIC PARAMETERS USED IN THE SAFT- Γ -MIE EOS CALCULATIONS.	108
TABLE 4.2. UNLIKE PHYSICAL INTERACTION PARAMETERS USED IN THE SAFT- Γ -MIE EOS CALCULATIONS.....	109
TABLE 4.3. SITE-SITE HYDROGEN-BONDING PARAMETERS USED IN THE ASSOCIATION TERM.	111
TABLE 4.4. DEVIATIONS BETWEEN THE SAFT- Γ -MIE EOS RESULTS AND THE EXPERIMENTAL DATA[118] FOR THE VAPOR PRESSURE, SATURATION LIQUID DENSITY AND VAPORIZATION ENTHALPY OF PURE ALKAN-1-OLS, USING THE ALCOHOL GROUP PARAMETERIZED AS AN OH (THIS WORK) OR AS A CH ₂ OH[168].	114
TABLE 4.5. BINARY ALKAN-1-OLS + N-ALKANES SYSTEMS STUDIED IN THIS WORK, USING THE SAFT- Γ -MIE EOS AND THE CORRESPONDENT DEVIATIONS FROM THE EXPERIMENTAL DATA MODELLING THE HYDROXYL GROUPS AS AN OH (THIS WORK) OR AS A CH ₂ OH GROUP[168].....	114
TABLE 4.6. BINARY ALKAN-1-OLS + WATER SYSTEMS STUDIED IN THIS WORK, USING THE SAFT- Γ -MIE EOS AND THE CORRESPONDENT DEVIATIONS FROM THE EXPERIMENTAL DATA MODELLING THE HYDROXYL GROUPS AS AN OH (THIS WORK) OR A CH ₂ OH GROUP.[168]	117
TABLE 4.7. DEVIATIONS BETWEEN SAFT- Γ -MIE RESULTS AND THE EXPERIMENTAL DATA FOR PURE A, Ω – ALKANEDIOLS WITH HETERONUCLEAR SAFT- Γ -MIE.	119
TABLE 4.8. REFINED PARAMETERS FOR THE OH GROUP TO ACCURATELY DESCRIBE THE PROPERTIES OF A, Ω - ALKANEDIOLS.....	119
TABLE 4.9. DEVIATIONS BETWEEN THE EXPERIMENTAL DATA FOR PURE GLYCOLS[49] AND THE SAFT- Γ -MIE RESULTS, EXPRESSED IN %ARD.	124
TABLE 4.10. DEVIATIONS BETWEEN THE MODELLING RESULTS AND THE VLE EXPERIMENTAL DATA FOR GLYCOL + WATER SYSTEMS.[138–140]	127
TABLE 4.11. GLYMES INVESTIGATED IN THIS WORK AND ITS DECOMPOSITION INTO FUNCTIONAL GROUPS FOR THEIR MODELLING WITH HETERONUCLEAR SAFT- Γ -MIE.....	130
TABLE 5.1. NON-IONIC SURFACTANTS STUDIED IN THIS WORK.....	151

TABLE 5.2. MICELLE AGGREGATION NUMBERS DETERMINED FROM THE CG-MD SIMULATIONS AT 15 WT% OF SURFACTANT CONCENTRATION AND LITERATURE VALUES FOR N_{AGG} AND CMC .	165
TABLE 6.1. PC-SAFT PARAMETERS USED IN THIS WORK (2B ASSOCIATION SCHEME).	195
TABLE 6.2. BINARY INTERACTION PARAMETERS USED IN THE PC-SAFT CORRELATIONS OF THE <i>PPT</i> DATA OF [CH]CL-BASED DES.	197
TABLE 6.3. FVT PARAMETERS USED IN THIS WORK.	198
TABLE 6.4. SELF AND CROSS-ASSOCIATION INTERACTIONS PRESENT IN A [CH]CL-BASED DES.	202
TABLE 6.5. SOFT-SAFT PURE-COMPONENT PARAMETERS USED IN THIS WORK.	204
TABLE 6.6. BINARY INTERACTION PARAMETERS USED IN THIS WORK. $\bar{\epsilon}_{ij}=1.000$ MEANS PREDICTION FORM PURE-COMPONENT PARAMETERS.	205
TABLE 6.7. MELTING PROPERTIES USED IN THIS WORK.	206
TABLE 6.8. PC-SAFT EOS PARAMETERS USED IN THIS WORK AND VOLUME-SHIFT TYPE CORRECTIONS EMPLOYED.	220
TABLE. B.1. LITERATURE SURVEY ON THE MODELLING OF GLYCOLS USING SAFT-BASED EOSS.	290
TABLE. C.1. DEVIATIONS BETWEEN THE SAFT- Γ -MIE RESULTS AND THE EXPERIMENTAL DATA FOR THE LLE OF GLYCOL (1) + N-HEPTANE (2) SYSTEMS [81] EXPRESSED IN %ARD. X_2'' REPRESENTS THE MOLAR FRACTION OF GLYCOL IN THE ALKANE-RICH PHASE, WHILE X_2' REPRESENTS THE WATER MOLE FRACTION IN THE GLYCOL RICH-PHASE.	296
TABLE. C.2. DEVIATIONS FROM THE EXPERIMENTAL VLE AND <i>PPT</i> DATA OF PURE GLYMES,[120] REPORTED IN %ARD.	298
TABLE. C.3. DEVIATIONS BETWEEN THE SAFT- Γ -MIE MODELLING RESULTS AND THE VLE EXPERIMENTAL DATA FOR GLYME + WATER SYSTEMS.[138]	301
TABLE. H.1. AVERAGE EXCESS MOLAR VOLUMES OF DIFFERENT DES CALCULATED USING EXPERIMENTAL DENSITY DATA AVAILABLE IN THE LITERATURE.	314
TABLE. H.2. AVERAGE EXCESS MOLAR VOLUMES OF DIFFERENT PILS CALCULATED USING EXPERIMENTAL DENSITY DATA AVAILABLE IN THE LITERATURE.	315

Nomenclature

List of Symbols

A	Helmholtz free energy	$J \cdot \text{mol}^{-1}$
C_p	isobaric heat capacity	$J \cdot \text{mol}^{-1} \cdot K^{-1}$
C_v	isochoric heat capacity	$J \cdot \text{mol}^{-1} \cdot K^{-1}$
G	Gibbs energy	$J \cdot \text{mol}^{-1}$
G^E	excess Gibbs energy	$J \cdot \text{mol}^{-1}$
g_{LJ}	radial distribution function for the LJ fluid	
H	enthalpy	$J \cdot \text{mol}^{-1}$
k_B	Boltzmann constant	$\text{m}^2 \cdot \text{kg} \cdot \text{s}^{-2} \cdot \text{K}^{-1}$
k_{ij}	energy binary interaction parameter	
k_T	isothermal compressibility	Pa^{-1}
l_{ij}	size binary interaction parameter	
m_i	chain length parameter of component i	
M_w	molecular weight	$\text{kg} \cdot \text{mol}^{-1}$
N_A	Avogadro's number	molecules/mol
N_{agg}	average aggregation number	
NS	Total number of different site types	
$NS_{k,e1}$	Number of sites type 'e1' in a group type k in SAFT- γ -Mie	
p	pressure	Pa
$p\rho T$	pressure-density-temperature	
Q_i	quadrupolar moment of component i	$\text{C} \cdot \text{m}^2$
S	entropy	$J \cdot \text{mol}^{-1} \cdot K^{-1}$
S_i^α	number of sites of type α in component i	
T	temperature	K
U	internal energy	$J \cdot \text{mol}^{-1}$
$x_{c,i}$	molar fraction of monomeric segments of component i	
x_i	molar fraction of component i in the liquid phase	
y_i	molar fraction of component i in the vapor phase	
X_i^α	fraction of molecules of component i not bonded at site α	
xm	effective chain length of the hypothetical fluid	

Greek

α_{ij}^{HB}	parameter correcting the cross-association energy	
α_p	isobaric thermal expansivity	K^{-1}
$\Delta_{i,j}^{\alpha,\beta}$	association strength between site α in component i and site β in component j	
γ_i	activity coefficient of component i	
δ	coupling factor	
ϵ_0	vacuum permittivity	$F \cdot m^{-1}$
ϵ_{ii}	dispersive energy parameter of component i	J
$\epsilon^{A_i B_j}$	energy of association between a site type A in component i and a site type B in component j	J
$\epsilon_{kl,ab}^{HB}$	energy of association between a site type a in group k and a site type b in group l	J
η_{ij}	size binary interaction parameter used in soft-SAFT EoS	
$\kappa^{A_i B_j}$	volume of association between a site type A in component i and a site type B in component j	m^3
$\kappa_{kl,ab}^{HB}$	volume of association between a site type a in group k and a site type b in group l	m^3
λ_{kl}^a	attractive exponent of the Mie potential	
λ_{kl}^r	repulsive exponent of the Mie potential	
μ_i	chemical potential of component i	J/mol
$\nu_{k,i}$	number of group type k in component i	
ρ	molar density	$mol \cdot m^{-3}$
ρ_c	monomeric density	$segments \cdot m^{-3}$
σ_{ii}	segment diameter of component i	m
ξ_{ij}	energy binary interaction parameter used in soft-SAFT EoS	
φ_i^α	fugacity coefficient of component i in phase α	
$\Phi_{k,l}^{Mie}$	Mie potential	

List of Abbreviations

AA	all-atom
CCS	carbon capture and storage
CG	coarse-grain
CMC	critical micellar concentration
CPA	Cubic plus association EoS
CR	combining rule
DES	deep eutectic solvent
DGT	density gradient theory
DFT	density functional theory
EO	ethylene oxide
EOR	enhanced oil recovery
EoS	equation of state
FF	forcefield
FVT	free volume theory
GC	group-contribution
GHG	greenhouse gases
GUI	graphical user interface
HBA	hydrogen bond acceptor
HBD	hydrogen bond donor
HLB	hydrophilic-lipophilic balance
IFT	interfacial tension
IL	ionic liquid
LC	liquid crystal
LJ	Lennard-Jones
LLE	liquid-liquid equilibria
MBWR	Modified Benedict-Webb-Rubin equation
MD	molecular dynamics
OF	objective function
PIL	protic ionic liquid
POM	polarizing optical microscopy
PR	Peng-Robinson

rdf	radial distribution function
SAFT	Statistical Associating Fluid Theory
SANS	small-angle neutron scattering
SAXS	small-angle X-ray scattering
SRK	Soave-Redlich-Kwong
TCC	thermal cycle capacity of a solvent
TPT1	first-order thermodynamic perturbation theory
VLE	vapor-liquid equilibria
VLLE	vapor-liquid-liquid equilibria

List of Compounds

CH₄	methane
C_iE_j	Alkyl polyoxyethylene glycols, where <i>i</i> and <i>j</i> are the numbers of methyl groups in the alkyl residue and the number of ethylene oxide groups, respectively.
CO	carbon monoxide
CO₂	carbon dioxide
DEG	diethylene glycol
DEGDDE	diethylene glycol diethyl ether
DEGDME	diethylene glycol dimethyl ether
DEGEE	diethylene glycol ethyl ether
DEGME	diethylene glycol methyl ether
EG	ethylene glycol
EGDME	ethylene glycol dimethyl ether
EGEE	ethylene glycol ethyl ether
H₂O	water
H₂S	hydrogen sulfide
HeEG	hexaethylene glycol
MEG	ethylene glycol
N₂	nitrogen
NO_x	nitrogen oxides
PEG	polyethylene glycol
PeEG	pentaethylene glycol
PEGDME	polyethylene glycol dimethyl ethers (blend)

TEG	triethylene glycol
TriEG	triethylene glycol
TriEGDME	triethylene glycol dimethyl ether
TeEG	tetraethylene glycol
TeEGDME	tetraethylene glycol dimethyl ether
TeEGME	tetraethylene glycol methyl ether

Superscripts

<i>res</i>	residual term
<i>seg</i>	segment term
<i>ref</i>	reference term
<i>chain</i>	chain term
<i>assoc</i>	association term
<i>id</i>	ideal term
<i>polar</i>	polar term
*	properties of the reference fluid
α, β	association site types
a, b	association site types
<i>exp</i>	experimental values
<i>calc</i>	values calculated from a model

Subscripts

<i>i</i>	data point number
<i>m</i>	mixture parameters for the hypothetical fluid
<i>i, j</i>	components
<i>k, l</i>	groups
<i>m</i>	mixture parameters for the hypothetical fluid
<i>R</i>	reference component

1- Introduction

“Thermodynamics is a funny subject. The first time you go through it, you don’t understand it at all. The second time you go through it, you think you understand it, except for one or two points. The third time you go through it, you know you don’t understand it, but by that time you are so used to it, it doesn’t bother you anymore.”

Arnold Sommerfeld

1.1- General Context

The Oil & Gas industry is considered to be the largest economical sector in the world, actively contributing to the employment of hundreds of thousands of people and generating huge revenues every year. Given the world's population growth and the consequent increase of the global energy demand, the Oil & Gas industry plays a vital role in today's society. Firstly, because oil and gas are the main energy sources in the planet, satisfying around 50% of the world's energy needs with more than 90 million barrels of crude oil being consumed daily.[1] Secondly, because oil and gas are widely used in modern life: as fuel for transports, burned for heating and electricity generation, but also as a source of important raw materials for the industrial production of several bulk chemicals and consumer goods such as fertilizers, toys, cosmetics, detergents, gums, plastics, textiles and dyes, among countless others.

Crude oil production is usually carried out in three phases: first, the primary oil recovery that consists in the natural rise of hydrocarbons to the surface, or in those artificially lifted. Then, in the second phase, water and/or gas are commonly injected into the reservoirs, allowing for a displacement of additional oil, forcing it to move towards the surface. However, as a given reservoir is explored and the oil is being extracted from deep underground, the pressure inside the reservoir decreases, hampering the removal of additional oil. On average, up to 2/3 of the crude oil remains trapped in the reservoir after the primary and secondary phases of oil recover took place, which is particularly problematic considering the projected prevalence of oil and gas as main energy sources and the emergent oil reserves depletion.[2,3] Nonetheless, a further increase on the oil production can be achieved through tertiary recovery methods, the enhanced oil recovery (EOR). EOR can be distinguished from the previous phases as it consists in changing the properties of the reservoir's fluid and restoring the reservoir's pressure. Three main types of EOR technologies exist[4]:

- 1) Thermal recovery – consisting in the heating of the reservoir fluids through steam injection to reduce the oil's viscosity and consequently enhance its flow behaviour.
- 2) Chemical injection – the injection of chemicals (e.g., alkali, polymers, surfactants, or a combination of them) that facilitate the release of additional oil from the rock formation, by effectively decreasing the interfacial tension (IFT) between oil and water, resulting in an increased capillarity.
- 3) Gas injection – involves the injection of a gas into the reservoir. Once in the reservoir, the gas mixes with the oil, swelling it and making it lighter and less viscous, which along with the

increased pressure within the reservoir allows the displacement of additional oil to the nearby production well.

Carbon dioxide-EOR (CO_2 – EOR) is often suggested as one of the most promising techniques as, in theory, it allows for both the production of additional oil and a decrease on the greenhouse gases (GHG) emissions, given that much of the CO_2 injected remains trapped in the reservoir rock. Thus, not only additional revenues are generated from the additional oil produced, but also the CO_2 is stored in well-characterized sites, allowing to partly offset the current high cost of CO_2 capture and storage (CCS). Despite this win-win solution, and the fact that the Oil & Gas industry already possesses the required know-how, CO_2 -EOR has been hindered due to the scarcity of economically viable supplies of CO_2 . Much of the CO_2 currently used for EOR is obtained from naturally occurring reservoirs, instead of derived from anthropogenic sources, highlighting the need for the development of novel CCS technologies at large scale.[5] Moreover, the discovery of oil and gas reservoirs rich in CO_2 , initiated a new era of oil exploration with striking challenges for the oil companies involved in their exploration that are committed not to vent the naturally produced CO_2 .[5]

Alternatively, surfactant flooding techniques allow the design of reservoir operations with an increased displacement efficiency. Surfactants are injected in the reservoir to decrease the IFT between the aqueous and organic phases, normally blended with co-surfactants that allow the tailoring of the injection fluid properties. The injection fluid should remain stable under the reservoir conditions, so the knowledge on the sensitivity of surface-active agents toward high temperatures/pressures and salinities must be known. Moreover, the use of multi-component injection fluids may be problematic if phase separation occurs within the reservoir, changing the surfactant concentration, and consequently, its thermodynamic behaviour. Clearly, the phase behaviour of the injection fluid (that contains surfactant, water, and other co-surfactants) is the most crucial factor governing the success of a surfactant flooding process. Therefore, accurate models able to describe the macroscopic and mesophasic behaviour of these systems are necessary to provide a quick screening of the most appropriate fluids to apply in a given reservoir, or to the initial design of new and efficient surfactant flooding processes.

Natural gas is often praised as a cleaner energy source, if compared with oil or coal because, when natural gas is burned, lower emissions of harmful gases such as carbon monoxide (CO), CO_2 , and nitrogen oxides (NO_x) are observed, and ashes or particulates are greatly avoided. Moreover, its relative abundance and low cost have contributed to the increase on its global production and consumption as highlighted in **Figure 1.1**. Considering the production of natural gas, raw natural gas is much different than end-use natural gas which is almost pure methane (CH_4), mainly due to the presence of several impurities that include hydrocarbons (mainly C2 to C5), water (H_2O), nitrogen (N_2), and acid gases such

as CO₂, hydrogen sulfide (H₂S), and mercaptans. Therefore, prior to its distribution, natural gas must be processed, aiming at the removal of the different impurities to meet the required pipeline and final use specifications.

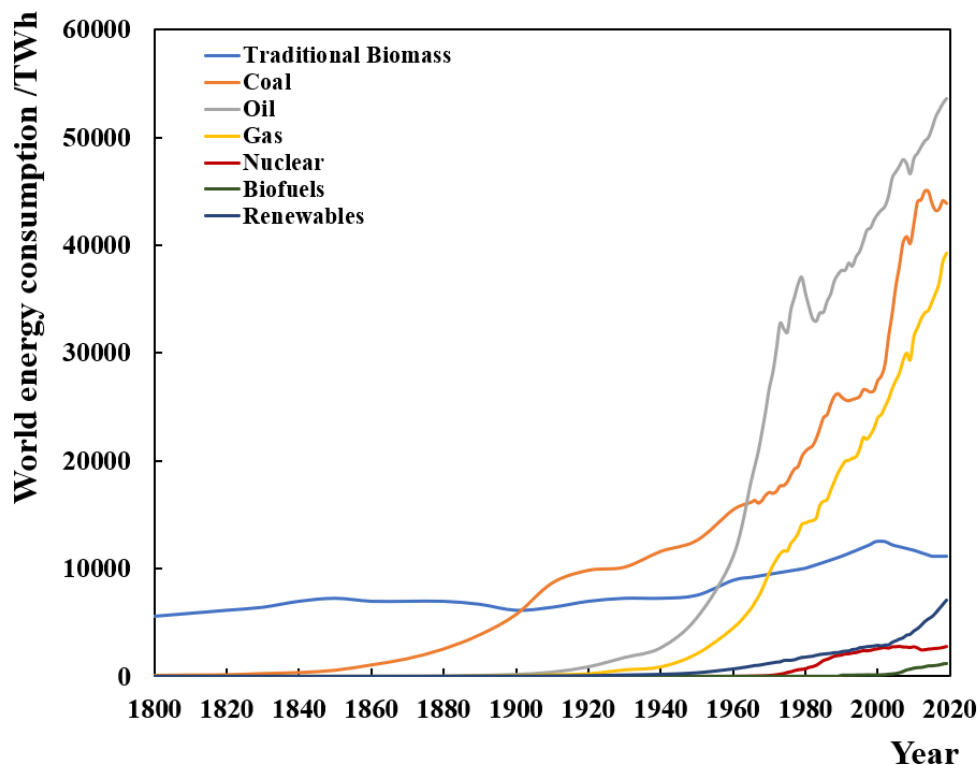



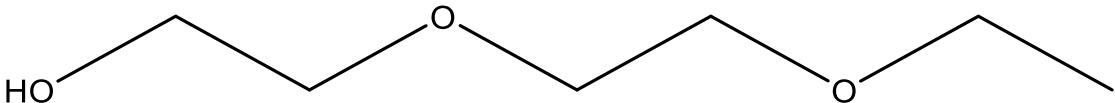
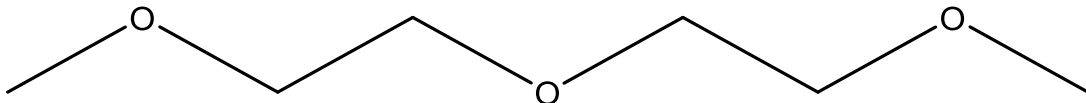
Figure 1.1. Primary energy consumption worldwide by fuel type.[6]

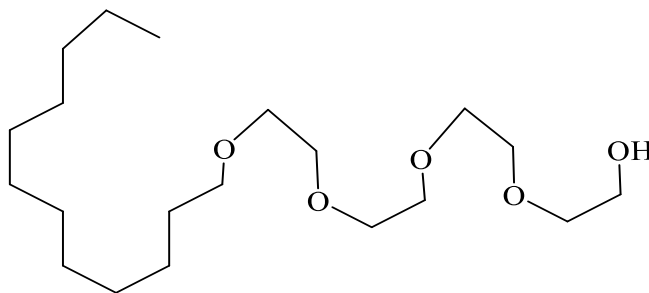
In this context, the Oil & Gas industry continuously demands for the development of novel low-cost, cleaner, and more efficient technologies in the framework of EOR, CCS and gas processing that would allow them to increase their revenues, while mitigating the environmental impact driven by their activities and their share in the world's GHG emissions.

Because of this, compounds containing ethylene oxide (EO) groups (summarized in **Table 1.1**) have become of special interest for the oil and gas industry. Glycols, whose general chemical formula is given by $H-(OCH_2CH_2)_n-OH$ are polyethers with two hydroxyl end-groups having EO as a repeating unit. They are characterized by interesting properties such as their high boiling point, hygroscopicity, non-corrosiveness, freezing point depression, lubricating and plasticizing character, being used for several operation purposes. Ethylene glycol (EG) is commonly used as a gas hydrate inhibitor or added to water for a further decrease of its melting point. Diethylene glycol (DEG) and triethylene glycol (TriEG) have been used as dehydration agents in natural gas streams, as otherwise, if water is present in

the natural gas it could cause hydrate formation at high pressure and low temperatures, corroding and blocking the transportation pipelines.[7] Tetraethylene glycol (TeEG) is also used as a solvent in the purification of aromatic hydrocarbons, while 1,2 – propylene glycol is used in the production of resins.[8]

Table 1.1. Compounds of interest to the Oil & Gas industry containing EO repeating units.

Glycols: e.g. triethylene glycol

Mono-alkyl glymes: e.g. diethylene glycol methyl ether

Di-alkyl glymes: e.g. diethylene glycol dimethyl ether

C_iE_j non-ionic surfactants: Brij-30 ($C_{11}E_4$)



Glymes or glycol ethers, where one (mono-alkyl glymes) or both (di-alkyl glymes) hydroxyl end-groups were replaced by a small ether group are known by their high affinity towards acid gases such as H_2S and CO_2 , due to the strong interactions that can be established between the gas and the solvent's oxygenated/sulfur groups.[9] Hence, a number of studies in literature report the larger solubilities of acid gases in glymes or blends of glymes, suggesting them as very attractive physical solvents for acid gas removal or CO_2 separation.[10–19] In fact, the UOP Selexol™ process, which is the state-of-the-art process for high-pressure gas sweetening, typically uses a blend of polyethylene glycol dimethyl ethers (PEGDME) as a physical solvent (chemical formula: $CH_3O(C_2H_4O)_nCH_3$, where n has a specific

distribution).[20,21] The main characteristics contributing to the Selexol process success are a low vapor pressure preventing solvent losses, a good selectivity of H₂S over CO₂ allowing for the selective absorption of H₂S in an absorber and an enhanced recovery of CO₂ in the flash drum in a dual stage configuration, low corrosion rates, generation of minimal waste and low energy requirements for the solvent regeneration. However, despite their affinity towards CO₂, glymes are seldomly reported as physical solvents for high-pressure CO₂ capture applications from sources other than natural gas.

Finally, alkyl polyoxyethylene glycols constitute a family of substances which behave as surfactants (surface active agents) in aqueous solutions. They are represented by the general chemical formula: H(CH₂)_i(OCH₂CH₂)_jOH, or simply C_iE_j, where *i* refers to the number of methylene groups in the alkyl residue and *j* refers to the number of EO groups in the hydrophilic part of the molecule that contains an hydroxyl group as end group. They can be viewed as a particular case of mono-alkyl glymes, where the length of the alkyl residue can considerably vary. These compounds have numerous applications in different fields ranging from cosmetics, detergents, refrigerants and obviously in EOR applications, through surfactant flooding.[22,23] Their use in EOR is based on their ability to increase the capillary displacement of an aqueous flooding medium along with other useful properties such as their high thermal stability (related to their cloud points), its biodegradability and its stability under high salinity media.

Moreover, as result of continuous scientific and technological developments, several new fluids/solvents with potential interesting applications appear every day, with deep eutectic solvents (DES) and protic ionic liquids (PILs) being some of the most relevant for the Oil & Gas industry, in a new wave of 'green' and more sustainable solvents with interesting properties such as a low vapor pressure, wide liquid range, thermal stability, and their designer solvent character that allows the tailoring of their thermophysical properties aiming at a specific task. DESs consist of mixtures of weak Lewis or Brønsted acids and bases that although usually solid at room temperature, present a eutectic temperature much lower than that predicted assuming an ideal behaviour of the liquid phase, mostly due to the presence of strong hydrogen bonding between the two molecular precursors, yielding solvents with interesting properties in a wide liquidus temperature range.[24,25] Their properties can be tuned depending on the choice of different hydrogen bond donor (HBD) and hydrogen bond acceptor (HBA) combinations and molar ratios between the molecular precursors. As such their potential for several applications of interest such as gas separations including CO₂ capture,[26–29] enhanced oil recovery,[30,31] dearomatization, denitrogenation, and desulfurization of fuels,[27,32–35] mercury removal from petroleum,[36] and hydrate formation inhibition[37,38] has been reported. PILs are also mixtures of Lewis or Brønsted acids and bases, but with a considerable ΔpK_a , prepared through the

stoichiometric neutralization reaction of acids and bases where, contrarily to DES, a proton transfer occurs from the acid to the base. Depending on the acid/base pair selected, the proton transfer may or may not be complete so that neutral molecular precursors will coexist in solution with ion pairs and ionic species. Due to their low cost, easy preparation, high CO₂ sorption capacity, mild regeneration, and variable proton activity, PILs have also been gathering an increasing interest from both industry and academia as potential solvents for CO₂ absorption,[39–43] oil desulfurization,[44,45] methane hydration inhibition,[46] asphaltenes extraction or stabilization,[47,48] among others.

Prior to the development or optimization of new or existing technologies or reservoir operations involving these systems, an accurate knowledge of the thermophysical properties and phase equilibria of the fluids involved is required for a rigorous design, simulation, or economical evaluation of different process configurations and conditions. Although much of the required data could be obtained from experiments, except for those at extreme temperature and pressure conditions impossible to achieve under common experimental setups, the cost and time required to perform all the necessary measurements quickly becomes prohibitive, urging the development of thermodynamic models able to describe this type of fluids with ease and that can be used for the prediction/extrapolation of the required information from limited amounts of experimental data.

Equations of State (EoSs) are the most versatile methods to provide fast calculations of thermophysical properties and phase equilibrium data as required by process simulators. However, contrarily to what happens in most petroleum refining processes, the presence of strongly polar compounds or fluids exhibiting strong associative interactions (e.g. hydrogen bonding), such as those mentioned before, increases the complexity of the fluids thermodynamic behaviour, resulting in a decreased performance of classical thermodynamic models commonly used by the Oil & Gas industry, namely cubic EoSs like Peng-Robinson (PR) and Soave-Redlich-Kwong (SRK) or even activity coefficient models like UNIQUAC, UNIFAC and NRTL.[49] For this reason, the development, analysis, and improvement of thermodynamic modelling approaches in the framework of EoSs that can explicitly account for such phenomena, such as those derived from the Statistical Associating Fluid Theory (SAFT),[50,51] are extremely relevant towards decreasing the dependency on experimental data, and accelerating the development of new processes using EO-containing compounds or novel alternative greener solvents.

Furthermore, the poly(oxyethylene) alkyl ethers surfactants presented in **Table 1.1** owe much of their success to their ability to, in aqueous solution, self-assemble to form a variety of 3-D structures with a controllable morphology, ranging from simple spherical, rod, disk or worm-like micelles at low surfactant loadings, to the formation of more complex liquid crystalline (LC) phases at higher

concentrations. As structural and dynamical properties cannot be directly obtained from EoSs, Molecular Dynamics (MD) simulations stand out as an appropriate method to investigate the nanostructure of the liquid phase, while providing a clear picture of the system at the microscopic level and contributing to a better understanding of the system's behaviour at the molecular level. All-atom (AA) models, those more widely applied in MD simulations, although able to provide detailed and precise information about initial stages of micellization in diluted systems, are unable to address the time and size scales relevant for self-assembling and mesophase transition processes. Conversely, coarse-grain (CG) models, significantly reduce the computational demand, being a suitable tool to investigate the mesophase behaviour of C_iE_j surfactants in water but, unfortunately, there is a lack of methods properly validated with a good transferability and predictive ability, for efficient screening purposes and to tackle the design of new surfactant systems for EOR injection.

This work addresses the thermodynamic modelling of different systems of interest to the Oil & Gas industry, namely those containing EO-based compounds or promising alternative solvents, using appropriate modelling techniques, that are SAFT-type EoSs and CG-MD simulations. Novel modelling approaches and parameterization methodologies, aimed at enhancing the predictive and extrapolative ability of current state of art models are proposed, while retaining or improving its overall accuracy. The limitations of the different models are also discussed.

1.2- Scope and Objectives

As mentioned before, the Oil & Gas industry plays a major role in our society. Clearly, there is an on-going transition towards the development of novel technologies aiming at improving the sustainability of their operations, partially solving several environmental, economic, and political problems related to the conventional petrochemical processes. Knowledge about the phase equilibria, and thermophysical properties of relevant systems and a proper understanding of their microscopic behaviour are thus of ubiquitous importance for the adequate design, operation and optimization of new processes and reservoir operations. Therefore, being able to quickly predict or extrapolate some of the necessary data with accuracy, from a limited number of experiments, can considerably expedite the task and lower its cost.

Even though most thermodynamic modelling approaches have been around for decades, the development/improvement of the different models remains a very active research topic, with most efforts being devoted to improving one or more of the following characteristics:

- Accuracy/Applicability – There is an increasing demand for models that can deal not only with simple, common fluids, but also with complex systems that have recently found widespread application in industry, and for which the performance of the current models is still not optimal. This can include strong associating and polar fluids (bio-based solvents, ionic liquids, deep eutectic solvents), or electrolyte systems, to name just a few.
- Extrapolative ability – The amount of experimental data available to parameterize EoS models or forcefields is often limited in terms of temperature, pressure, and/or composition range. Therefore, thermodynamic models should be able to successfully extrapolate results for thermodynamic conditions other than those used in the parameterization procedure, without a significant loss of performance.
- Predictive ability – One of the advantages of using EoSs over excess Gibbs energy (G^E) models is their versatility and potential to provide a wide range of thermodynamic properties. Hence, a good thermodynamic model should be able to provide reliable predictions for properties other than those used in the model's parameterization.
- Parameterization methods – The parameterization method (amount and type of experimental data used in the fitting; weights of the different properties considered, existence of transferable/fixed parameters, etc.) can have a profound effect on the performance and applicability of any given model. Moreover, in the case of SAFT-type EoSs, alternative

parameterization methodologies are often required when the pure compounds are solid, have negligible vapor pressures, and no densities nor critical properties are available, hindering the use of traditional parameterization approaches.

- Parameters' transferability – Related to the predictive ability of the model, there have been several attempts to transfer model parameters between different compounds of a given homologous series, or between different families.
- Computational efficiency – Models should be complex enough to capture most of the physical features of the system but remain simple enough so that the computational cost of the calculations does not become problematic for the desired application. One of the disadvantages of SAFT over cubic EoSs is its increased computational cost due to the implicit-iterative nature of the association term that can become problematic when a large number of flash calculations is required in a small-time frame (e.g., in dynamic state simulations or optimizations). Therefore, unless considerable improvements in terms of accuracy can be achieved, the association models should remain simple and accessible.

With all these aspects in mind, this work aims at the development, improvement and discussion of modelling approaches and parameterization methodologies, in the framework of SAFT-type EoSs and MD simulations, to be applied for the description of EO-based compounds and promising alternative solvents of interest to the Oil & Gas industry. Most of the work presented in this thesis is object of publication at different international peer-reviewed journals in the areas of chemical engineering, applied thermodynamics, and physical chemistry, whose detailed bibliographic information is provided in the “**List of Publications**” at the end of the manuscript.

The next sections are organized as follow:

Chapter 2 - Thermodynamic Background: In this section, the different modelling techniques applied in this work are outlined. It starts with an overall description of SAFT-type EoSs and the different variants of the SAFT theory applied in this work. Then, the development of a thermodynamic package for phase equilibrium and thermophysical properties calculations using EoSs in MATLAB® is reported, presenting its main features and code organization. Finally, a brief introduction to MD simulations and the MARTINI forcefield[52] used to investigate the mesophase behaviour of C_iE_j systems is provided.

Chapter 3 - Thermodynamic modelling of glycols and glymes: In this chapter, through an appropriate parameterization and relating the values of the model parameters to the differences in the compounds' chemical structure, a transferable soft-SAFT model is proposed for both glycols and glymes. Built on top of low molecular weight oligomers, the model is applicable to higher chain length homologues, even in the absence of experimental data. Then, having in mind that glycols and glymes are

mainly used for gas dehydration and CO₂ capture, the model is successfully applied to mixtures of both glycols and glymes with water and other gases (mainly CO₂), to evaluate its performance.

Chapter 4 – EoS Modelling of C_iE_j/H₂O systems: Given the absence of experimental data for pure surfactants, the suitability of SAFT- γ -Mie, the most acknowledged heteronuclear SAFT-type EoS, to describe C_iE_j surfactants, using the knowledge acquired from studying simpler compounds (e.g., alkanes, alkan-1-ols, glycols, and glymes), is assessed in this chapter.

Chapter 5 – MD simulations of surfactant systems: In this chapter, an extensive validation of the MARTINI FF to describe the mesophase behaviour of aqueous solutions of C_iE_j surfactants is provided, spanning a wide range of hydrophilic-lipophilic balance (HLB) values and surfactant concentrations, in both the micellar and the LC regimes. Once the model is adequately validated, it is further applied to investigate the behaviour of ternary systems oil + water + surfactant in order to analyse the impact that the presence of an oil has in the behaviour of the aqueous solution. The chapter is then concluded with a few remarks on the study of silica + water + oil + surfactant systems relevant for EOR applications, highlighting the suitability of the MARTINI FF to model the oil detachment process from a surface.

Chapter 6 – A discussion on the modelling of alternative solvents using SAFT-type EoSs: The widespread of applications for DESs and PILs over the last decade has not been followed by the development of robust thermodynamic modelling approaches that can reliably provide or describe their thermophysical properties and phase behaviour. One of the reasons is that the specific features of these systems usually prevent the use of common modelling strategies and parameterization methodologies applied with other molecular compounds. Thus, this chapter aims to discuss the modelling of both DESs and PILs using SAFT-type EoSs, while commenting on the most adequate parameterization methodologies.

Chapter 7 – Final remarks: Conclusions and future perspectives in the field.

2- Thermodynamic Background

“It is fine to work on any problem, so long as it generates interesting mathematics along the way – even if you don’t solve it at the end of the day.”

Andrew Wiles

2.1- SAFT-type EoSs

As illustrated in **Figure 2.1**, a large number of thermodynamics models is available with dozens of different activity coefficient models and EoSs reported in the literature,[53] the choice of the most adequate representing a cumbersome challenge for the design engineer not specifically trained in applied thermodynamics. Despite the simplicity, ease of application, and accuracy of G^E models, EoSs have been the industry preferred tool to model phase equilibria and thermophysical properties, mainly due to their ability to provide a global description of the thermodynamic behaviour of a fluid (and not just the phase equilibria as occurs with activity coefficient models) and their better performance at high-pressure high-temperature conditions.

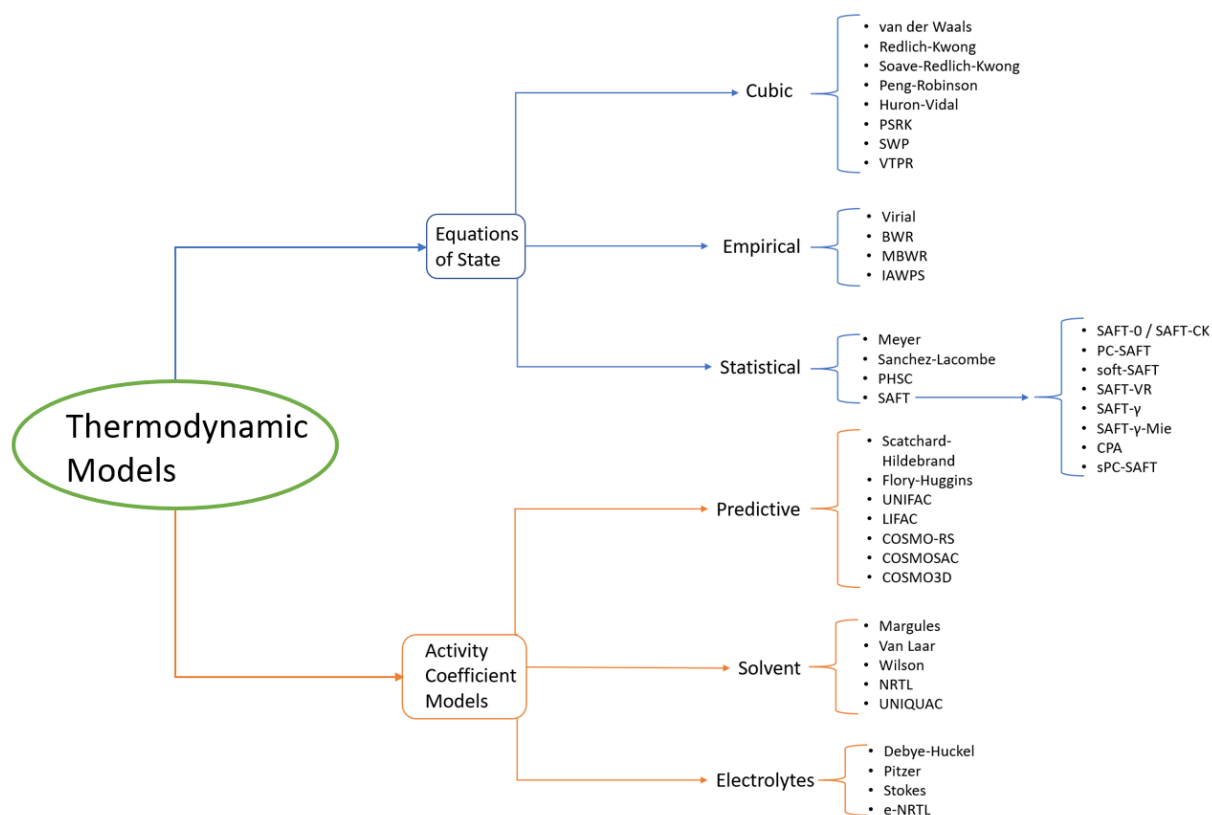


Figure 2.1. A "small" sample of thermodynamic models available in the literature.

Classical EoSs, such as PR and SRK, have been the gold standard in a variety of industrial areas ranging from Oil & Gas to bulk and specialty chemicals. By combining a mean-field attractive term with a hard-sphere repulsive term, although appropriate for small, simple, and spherical molecules, they have several limitations as the hard-sphere reference exhibits considerable deviations for chainlike fluids. Furthermore, due to their semiempirical character, the physical meaning of their parameters is fuzzy,

resulting in a poor predictive or extrapolative ability of such models, requiring large amounts of experimental data for an extensive characterization of a new solvent or fluid mixture.

Moreover, it is undeniable that the systems of interest for industry have become increasingly complex, and cubic EoSs, despite being very simple and easy to implement, are not able to model molecular level behaviour explicitly, failing when applied to describe polar (e.g. CO₂) or associating compounds (e.g. water, glycols, glymes, C_iE_j surfactants, DESs, PILs, etc), making the case for the development of thermodynamic models that can explicitly account for different structural and energetic effects. Clearly, the most apparent progress toward EoSs with such capabilities was achieved by applying statistical mechanics concepts. Wertheim's work on a first order thermodynamic perturbation theory (TPT1)[54–57] and its later implementation in the form of an engineering EoS, the Statistical Associating Fluid Theory – SAFT – by Chapman and co-workers[50,51] (original SAFT) and Huang and Radosz[58] (CK-SAFT) represent the major advances toward such an advanced molecular-based EoS. These equations, contrarily to cubic EoSs, explicitly account for the contribution of different effects including the non-spherical shape of the molecules, chain length, polar interactions, and hydrogen bonding to the thermodynamic behaviour of the system, providing a more rigorous perception of the fluids physics.

As represented in **Figure 2.2**, in the framework of SAFT, molecules are generally represented as homonuclear chainlike fluids composed of a number of spherical segments of equal size and energy, exhibiting both dispersive and repulsive interactions, tangentially bonded to each other forming chains that might associate at specific bonding sites present in some of the chain's segments (if it represents an associating compound).

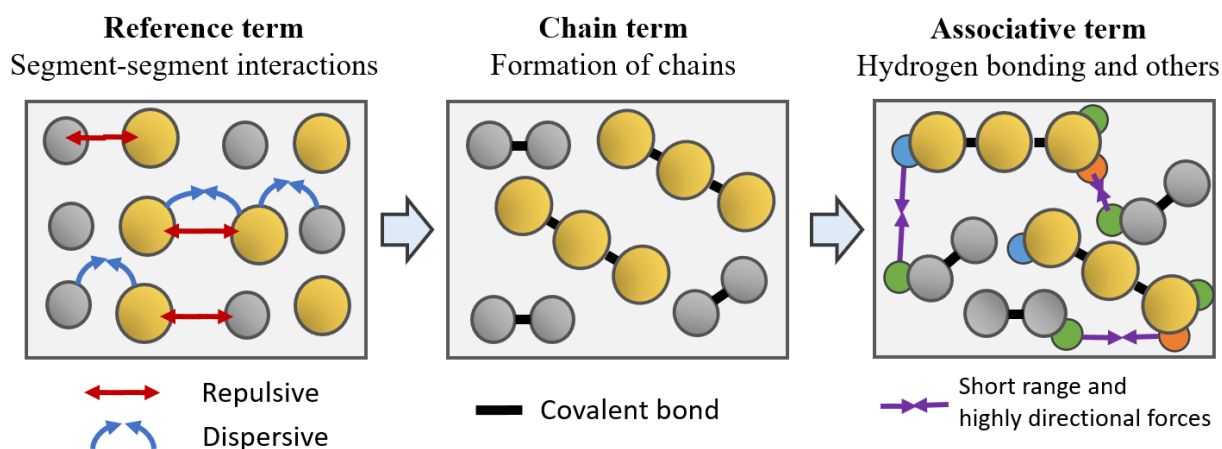


Figure 2.2. Schematic representation of the physical foundation of SAFT. Yellow and grey colours are used to represent two different segments/components, while green, blue, and orange are used to distinguish three different association site types.

From the SAFT theory, the residual Helmholtz energy of the system (A^{res}) is obtained as a sum of the different contributions, each of them accounting for a specific effect, according to **eq. 2.1**: a segment term, A^{seg} , accounting for the monomer-monomer physical interactions, including both the repulsive and attractive terms; a chain term, A^{chain} , accounting for the formation of chains from the individual segments, and an association term, A^{assoc} , that takes into account the presence of strong and highly directional forces, such as hydrogen-bonding. A^{id} is the ideal term required to determine the system's total free energy.

$$A^{res} = A - A^{id} = A^{seg} + A^{chain} + A^{assoc} + A^{polar} + \dots \quad (2.1)$$

Wertheim's contributions[54–57] present a theoretically derived model for anisotropic interactions like hydrogen-bonding, in the form of a perturbation term to the Helmholtz free energy of the system as a function of the monomer density, which is related to the so-called association strength.[51] This theory presents the basis for both the chain and association terms of SAFT, the former being obtained from the theory in the limit of infinite association, by imposing the condition of total bonding between two adjacent chain segments.

By considering different segment terms, mainly in the attractive contribution, several SAFT variants have been proposed over the last decades by different research groups. Among the most well-known SAFT-type EoSs one could include original SAFT,[50,51] CK-SAFT,[58] sSAFT,[59] LJ-SAFT,[60] soft-SAFT,[61] SAFT-VR,[62] and PC-SAFT, in both its original[63,64] and simplified version.[65] More recently, heteronuclear versions of SAFT-type EoSs (refer to **Figure 2.3**), using a group contribution (GC) approach such as the GC-SAFT-VR,[66] SAFT- γ ,[67] and SAFT- γ -Mie[68] have also received a great deal of attention.

An EoS written in terms of the residual Helmholtz energy of the system has the key advantage that many thermodynamic properties can be readily obtained using only derivatives and ideal-gas integrals. The most striking example being the direct calculation of derivative properties that are key for the design of many processes such as heat capacities, speed of sound, isothermal compressibility, among others. Furthermore, the theory underlying SAFT, makes it possible its systematic improvement and extension in a sound manner, allowing the inclusion of additional terms, depending on the systems' nature such as the addition of a polar term (A^{polar}) to account for polar interactions. The ease with which SAFT-type EoSs can be coupled to other theories, such as the density gradient theory[69,70] (DGT) or the Free Volume Theory[71] (FVT) for the calculation of interfacial or transport properties is another key advantage of this type of models.

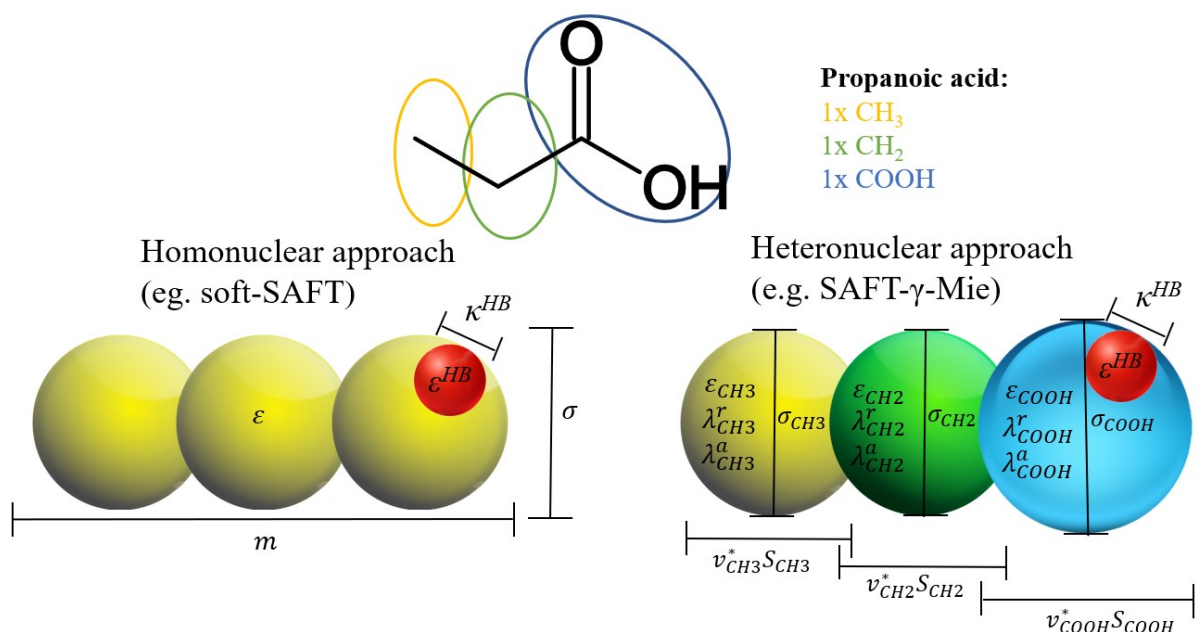


Figure 2.3. Homonuclear and heteronuclear approaches of SAFT-type EoSs, illustrated for propanoic acid.

Because of the strong theoretical foundation of SAFT, the model parameters have a well-defined physical meaning that obviously enhance the predictive and extrapolative capabilities of the model. In the majority of homonuclear SAFT variants, each pure component i is characterized by its chain length, m_i , i.e., the number of individual segments constituting the molecule, the segments' size diameter, σ_{ii} , and the segment-segment dispersive energy, ϵ_{ii} . If the molecule is self-associating, an association scheme specifying the number and type of association sites, and interactions allowed in the system, needs to be specified a priori and the values of association energy ($\epsilon^{A_i B_i}$ or ϵ^{HB}) and volume ($\kappa^{A_i B_i}$ or κ^{HB}) defined pairwise for each site-site interaction. However, in most cases, the energy and volume of the association sites within a given molecule are considered equivalent, resulting in a total of five unknown parameters for a self-associating component like propanoic acid illustrated in **Figure 2.3**. While defining an appropriate association scheme for a given molecule, Table VII and VIII of Huang and Radosz[58] present some of the most common association schemes and hence represent a good starting point.

Among the several modifications to the original model, soft-SAFT[61] stands out given its demonstrated ability to accurately describe the thermophysical properties and phase behaviour of a wide variety of compounds (e.g. n -alkanes,[72] perfluoroalkanes,[73] alkan-1-ols,[74] glycols,[75] nitriles,[76] ILs,[77] refrigerants,[78] and polymers[79]). Hence, in this work, the soft-SAFT EoS was successfully implemented in a thermodynamic modelling package coded in MATLAB® for the calculation of phase equilibria and thermophysical properties (cf. **Chapter 2.1.4**). A detailed description

of the different terms of the soft-SAFT EoS is thus provided in **Chapter 2.1.1**. In some cases, the Perturbed-Chain-SAFT (PC-SAFT) was applied, so the main differences between the two variants are presented in **Chapter 2.1.2**. For the thermodynamic modelling of the aqueous solutions of C_iE_j surfactants, as experimental data is not available for the pure surfactants, the performance of a heteronuclear SAFT variant, namely SAFT- γ -Mie (described in **Chapter 2.1.3**), was evaluated.

2.1.1- soft-SAFT EoS

Dimensionless variables, parameters, and properties

For the sake of consistency, all the equations of soft-SAFT must be solved using dimensionless variables in respect to a reference component. Therefore, i_R may be defined as the reference component, characterized by its corresponding parameters (σ_R and ε_R). These parameters are then used to obtain the dimensionless thermodynamic variables and parameters required for the soft-SAFT implementation. Those dimensionless variables (identified by an upper tilde) are summarized as follow:

$$\tilde{T} = \frac{T}{\varepsilon_R/k_B} \quad (2.2) \quad \tilde{\rho} = \rho N_A \sigma_R^3 \quad (2.3) \quad \tilde{p} = p \frac{\sigma_R^3}{\varepsilon_R} \quad (2.4)$$

$$\tilde{A} = \frac{A}{N_A \varepsilon_R} \quad (2.5) \quad \tilde{G} = \frac{G}{N_A \varepsilon_R} \quad (2.6) \quad \tilde{U} = \frac{U}{N_A \varepsilon_R} \quad (2.7)$$

$$\tilde{H} = \frac{H}{N_A \varepsilon_R} \quad (2.8) \quad \tilde{S} = \frac{S}{N_A \varepsilon_R} \quad (2.9) \quad \tilde{\mu}_i = \frac{\mu_i}{N_A \varepsilon_R} \quad (2.10)$$

$$\tilde{C}_p = \frac{C_p}{R} \quad (2.11) \quad \tilde{C}_v = \frac{C_v}{R} \quad (2.12) \quad \tilde{\alpha}_p = \alpha_p \varepsilon_R/k_B \quad (2.13)$$

$$\tilde{k}_T = k_T \frac{\varepsilon_R}{\sigma_R^3} \quad (2.14) \quad \tilde{Q} = \frac{Q}{4\pi \times \varepsilon_R \times \sigma_R^5 \times \varepsilon_0} \quad (2.15) \quad \tilde{\sigma} = \frac{\sigma}{\sigma_R} \quad (2.16)$$

$$\tilde{\varepsilon} = \frac{\varepsilon}{\varepsilon_R} \quad (2.17) \quad \tilde{\kappa}^{\alpha_i B_j} = \frac{\kappa^{\alpha_i B_j}}{\sigma_R^3} \quad (2.18) \quad \tilde{\varepsilon}^{\alpha_i B_j} = \frac{\varepsilon^{\alpha_i B_j}}{\varepsilon_R} \quad (2.19)$$

In **eqs. 2.2-2.19**, T , p , and ρ are the system's temperature, pressure and density. N_A , k_B , and ε_0 represent the Avogadro number, Boltzmann constant, and vacuum permittivity, respectively. G , U , H , and S stand for Gibbs energy, internal energy, enthalpy and entropy of the system, while μ_i is the chemical potential of component i . C_p and C_v are the isobaric and isochoric heat capacities of the fluid, k_T is the isothermal compressibility and α_p the isobaric thermal expansivity. Q is the quadrupolar moment parameter used in the polar term of soft-SAFT EoS.

Extension to mixtures

Fluid mixtures usually consist of chains with a different number of segments, which in turn may have a different size and/or energy of interaction. Therefore, to apply SAFT models to mixtures, one must make use of “mixture parameters” that are able to represent a hypothetical fluid having the same physical features and thermodynamic properties of the mixture. This is usually done by means of appropriate mixing rules, with those derived from the van der Waals’ one fluid theory being the most used. Denoting the ‘mixture parameters’ by the subscript m , they can be expressed as a function of the individual monomers present in the mixture as follow:

$$\sigma_m^3 = \frac{\sum_{i=1}^{NC} \sum_{j=1}^{NC} x_i x_j m_i m_j \tilde{\sigma}_{ij}^3}{\left(\sum_{i=1}^{NC} x_i m_i\right)^2} \quad (2.20)$$

$$\varepsilon_m \sigma_m^3 = \frac{\sum_{i=1}^{NC} \sum_{j=1}^{NC} x_i x_j m_i m_j \tilde{\sigma}_{ij}^3 \tilde{\varepsilon}_{ij}}{\left(\sum_{i=1}^{NC} x_i m_i\right)^2} \quad (2.21)$$

The effective chain length for the hypothetical fluid, xm , and the molar fraction of monomeric segments of component i , $x_{c,i}$, are given by **eqs. 2.22** and **2.23**, respectively:

$$xm = \sum_{i=1}^{NC} x_i m_i \quad (2.22)$$

$$x_{c,i} = \frac{x_i m_i}{xm} \quad (2.23)$$

The equations presented before require the knowledge of the unlike interaction parameters between the monomeric segments of different components ($i \neq j$) which are determined using the conventional Lorentz-Berthelot combining rules (CR):

$$\sigma_{ij} = \eta_{ij} \frac{\sigma_{ii} + \sigma_{jj}}{2} \quad (2.24)$$

$$\varepsilon_{ij} = \xi_{ij} \sqrt{\varepsilon_{ii} \varepsilon_{jj}} \quad (2.25)$$

Here, adjustable binary interaction parameters, correcting significant differences in size (η_{ij}/l_{ij}) or energy (ξ_{ij}/k_{ij}) of the molecules may be applied when required for an accurate description of the experimental data. In **eqs. 2.24-2.25**, η_{ij} and ξ_{ij} are equivalent to the $(1 - l_{ij})$ and $(1 - k_{ij})$ commonly applied in classical cubic EoSs and other SAFT variants. These parameters are usually adjusted by fitting the model to the correspondent binary data and used along with the pure-component parameters to perform ternary and multicomponent calculations in a predictive manner, without any additional fittings or fine tunings. When both parameters are equal to one, the model is used in a fully predictive approach where mixture calculations are carried using solely the pure-component parameters.

When cross-association between different compounds exists, the evaluation of the association term requires the knowledge of the correspondent cross-association energies and volumes, which are typically obtained from appropriate CR, using the self-associating values. Different CR have been applied with different association models but results show that there is not a universally best choice. As an example, the CR employed in soft-SAFT for the interactions between a site of type ‘A’ in component i and a site of type ‘B’ in component j are given below:

$$\varepsilon^{A_i B_j} = \alpha_{ij}^{HB} \sqrt{\varepsilon^{A_i B_i} \varepsilon^{A_j B_j}} \quad (2.26)$$

$$\kappa^{A_i B_j} = \left(\frac{\sqrt[3]{\kappa^{A_i B_i}} + \sqrt[3]{\kappa^{A_j B_j}}}{2} \right)^3 \quad (2.27)$$

Reference term

The original SAFT model employs in the reference term a perturbation approach in which a hard-sphere fluid is taken as a reference for the repulsive interactions and the attractive interactions are added as a perturbation term. Instead, soft-SAFT considers the Lennard-Jones (LJ) potential for the reference fluid, accounting for both the repulsive and attractive interactions between the monomers in a single term. Therefore, this segment term should correspond to the residual Helmholtz free energy of a LJ fluid of spheres, for which two accurate EoSs are available in the literature: the Modified Benedict-Webb-Rubin (MBWR) EoS presented by Johnson et al.[80] and an EoS based on a perturbed virial expansion reported by Kolafa and Nezbeda.[81] Both equations have 32 parameters fitted to computer simulation data for the LJ fluid, with the choice between them representing a compromise between accuracy and robustness. In fact, the choice between one of these equations represents the main difference between soft-SAFT[61] and the LJ-SAFT variant[60].

soft-SAFT makes use of the LJ EoS by Johnson et al.[80] which proposed the following expression for the residual Helmholtz energy of the LJ reference fluid:

$$\tilde{A}^{seg} = xm \times \varepsilon_m \left(\sum_{i=1}^8 \frac{a_i}{i} (\rho_c^*)^i + \sum_{i=1}^6 b_i G_i \right) \quad (2.28)$$

where the coefficients a_i and b_i are functions of the reference fluid temperature, T^* , and contain the 32 linear parameters of the MBWR equation. The G_i functions contain exponentials of the monomeric density of the reference fluid, ρ_c^* , and one non-linear parameter. Variables that refer to the reference fluid are denoted by the superscript “*” and are obtained from the following expressions:

$$T^* = \frac{\tilde{T}}{\varepsilon_m} \quad (2.29) \quad \rho^* = \tilde{\rho} \times \sigma_m^3 \quad (2.30) \quad \rho_c^* = xm \times \tilde{\rho} \times \sigma_m^3 \quad (2.31)$$

The contribution to pressure due to the segment term can be easily obtained through the derivative of the residual Helmholtz energy in respect to the monomeric density of the reference fluid as follow:

$$\tilde{p}^{seg} = (\rho_c^*)^2 \left(\frac{\partial \tilde{A}^{seg}}{\partial \rho_c^*} \right)_{T^*, N} = \frac{\varepsilon_m}{\sigma_m^3} \left(\sum_{i=1}^8 a_i (\rho_c^*)^{i+1} + F \sum_{i=1}^6 b_i (\rho_c^*)^{2i+1} \right) \quad (2.32)$$

In the same paper, Johnson et al.[80] also provided the coefficients c_i and d_i required for the calculation of the residual (configurational) internal energy using the following expression:

$$\tilde{U}^{seg} = -(T^*)^2 \left(\frac{\partial \tilde{A}^{seg}}{\partial T^*} \right)_{\rho_c^*, N} = xm \times \varepsilon_m \left(\sum_{i=1}^8 \frac{c_i}{i} (\rho_c^*)^i + \sum_{i=1}^6 d_i G_i \right) \quad (2.33)$$

Finally, the contribution of the segment term to the residual chemical potential of component i can be obtained from the values of \tilde{A}^{seg} , \tilde{p}^{seg} , and \tilde{U}^{seg} as given below:

$$\frac{\tilde{\mu}_i^{seg}}{xm \times m_i} = \frac{\tilde{A}^{seg}}{xm \times \varepsilon_m} + \left(\frac{(\tilde{p}T + \tilde{p}^{seg})\sigma_m^3}{\varepsilon_m \times \rho_c^*} - T^* \right) \left(\frac{\partial \sigma_m^3}{\partial x_{c,i}} \frac{1}{\sigma_m^3} - 1 \right) + \frac{\tilde{U}^{seg}}{xm \times \varepsilon_m} \frac{\partial \varepsilon_m}{\partial x_{c,i}} \frac{1}{\varepsilon_m} \quad (2.34)$$

Eq. 2.34, whose derivation is outlined in **Appendix A**, requires the evaluation of the derivatives of the ‘mixture parameters’ in respect to the fraction of cores of component i , whose expressions are also detailed in **Appendix A**.

Chain term

The chain term is derived from the TPT1 theory by Wertheim,[54–57] in the limit of infinite association by imposing the condition of total bonding between the m segments forming the chain and the correct number of bonding sites in each segment (either one or two association sites being required in the end or inner segments of the chain, respectively).

The expression for the residual Helmholtz energy of the system due to the formation of chains is given by **eq. 2.35** below:

$$\tilde{A}^{chain} = \sum_{i=1}^{NC} x_i \tilde{A}_i^{chain} = \sum_{i=1}^{NC} x_i \tilde{T} (1 - m_i) \ln g_{LJ}(\sigma_m) \quad (2.35)$$

where $g_{LJ}(\sigma_m)$ is the pair correlation function of the reference fluid for the interaction between two monomeric segments in the mixture, evaluated at the mixture’s segment diameter. Johnson et al.[82] proposed the following empirical function for the radial distribution function (rdf) of the LJ fluid:

$$g_{LJ}(\sigma_m) = 1 + \sum_{p=1}^5 \sum_{q=1}^5 a_{pq} (\rho_c^*)^p (T^*)^{1-q} \quad (2.36)$$

where the parameters a_{pq} were fitted to MD simulation data of LJ chain fluids with different numbers of segments, over the entire fluid density range, at several temperatures.

The contribution to pressure, residual chemical potential, and internal energy due to the formation of chains can then be obtained from the appropriate derivatives:

$$\tilde{p}^{chain} = \tilde{\rho}^2 \left(\frac{\partial \tilde{A}^{chain}}{\partial \tilde{\rho}} \right)_{\tilde{T},x} = \tilde{\rho}^2 \sum_{i=1}^{NC} x_i \left(\frac{\partial \tilde{A}_i^{chain}}{\partial \tilde{\rho}} \right)_{\tilde{T},x} = \tilde{\rho}^2 \tilde{T} (1 - xm) \left(\frac{\partial g_{LJ}(\sigma_m)}{\partial \tilde{\rho}} \right)_{\tilde{T},x} \frac{1}{g_{LJ}(\sigma_m)} \quad (2.37)$$

$$\begin{aligned} \tilde{\mu}_i^{chain} &= \left(\frac{\partial \tilde{A}^{chain}}{\partial x_i} \right)_{\tilde{\rho},\tilde{T},x_{k \neq i}} = \tilde{A}_i^{chain} + \sum_{j=1}^{NC} x_j \left(\frac{\partial \tilde{A}_j^{chain}}{\partial x_i} \right)_{\tilde{\rho},\tilde{T},x_{k \neq i}} \\ &= \tilde{T} \left[(1 - m_i) \ln g_{LJ}(\sigma_m) + \frac{(1 - xm)}{g_{LJ}(\sigma_m)} \left(\frac{\partial g_{LJ}(\sigma_m)}{\partial x_i} \right)_{\tilde{\rho},\tilde{T},x_{k \neq i}} \right] \end{aligned} \quad (2.38)$$

$$\tilde{U}^{chain} = -\tilde{T}^2 \left(\frac{\partial \tilde{A}^{chain}}{\partial \tilde{T}} \right)_{\tilde{\rho},x} = \tilde{T} (xm - 1) \tilde{T} \left(\frac{\partial g_{LJ}(\sigma_m)}{\partial \tilde{T}} \right)_{\tilde{\rho},x} \frac{1}{g_{LJ}(\sigma_m)} \quad (2.39)$$

Eqs. 2.37-2.39 require the knowledge of the derivatives of the rdf in respect to the molar density of the fluid, temperature, and molar fraction. The mathematical expressions to determine those derivatives are provided in **Appendix A**.

Association term

The association term for the different SAFT variants, including soft-SAFT is expressed by **eq.40**:

$$\tilde{A}^{assoc} = \tilde{T} \sum_{i=1}^{NC} x_i \tilde{A}_i^{assoc} = \tilde{T} \sum_{i=1}^{NC} x_i \sum_{\alpha=1}^{NS} S_i^\alpha (\ln(X_i^\alpha) - 0.5X_i^\alpha + 0.5) \quad (2.40)$$

where NS is the total number of different site types in the system, S_i^α is the number of sites type α in component I , and X_i^α is the fraction of molecules of component i not bonded at site α which is a key property in association theories. Such information can be used for example to compute the fraction of molecules present as clusters of size N , N -mers, present in the system.[83] From the solution of the mass action equations, such fractions can be obtained as:

$$X_i^\alpha = \frac{1}{1 + \tilde{\rho} \sum_{j=1}^{NC} x_j \sum_{\beta=1}^{NS} S_j^\beta X_j^\beta \Delta_{j,i}^{\beta,\alpha}} \quad (2.41)$$

Eq. 2.41 involves a double summation over all components and site types considering both self and cross association interactions. $\Delta_{j,i}^{\beta,\alpha}$ is the association strength between a site type β on component j and a site type α in component I and is given by the following expression:

$$\Delta_{j,i}^{\beta,\alpha} = 4\pi \left[\exp\left(\frac{\tilde{\epsilon}^{\alpha_i B_j}/k_B}{\tilde{T}}\right) - 1 \right] \tilde{\kappa}^{\alpha_i B_j} \tilde{I} \quad (2.42)$$

\tilde{I} is a dimensionless integral for which an empirical function proposed by Müller and Gubbins,[84] assuming a particular position of the association sites within the segments is used.

By appropriate derivation, the contribution of the association term to pressure, chemical potential and internal energy of the system can then be obtained:

$$\tilde{p}^{assoc} = \tilde{\rho}^2 \left(\frac{\partial \tilde{A}^{assoc}}{\partial \tilde{\rho}} \right)_{\tilde{T},x} = \tilde{\rho}^2 \tilde{T} \sum_{i=1}^{NC} x_i \sum_{\alpha=1}^{NS} S_i^\alpha \left(\frac{1}{X_i^\alpha} - 0.5 \right) \left(\frac{\partial X_i^\alpha}{\partial \tilde{\rho}} \right)_{\tilde{T},x} \quad (2.43)$$

$$\begin{aligned} \tilde{\mu}_i^{assoc} &= \left(\frac{\partial \tilde{A}^{assoc}}{\partial x_i} \right)_{\tilde{\rho},\tilde{T},x_{k \neq i}} = \tilde{A}_i^{assoc} + \sum_{j=1}^{NC} x_j \left(\frac{\partial \tilde{A}_j^{assoc}}{\partial x_i} \right)_{\tilde{\rho},\tilde{T},x_{k \neq i}} \\ &= \tilde{T} \sum_{\alpha=1}^{NS} S_i^\alpha (\ln(X_i^\alpha) - 0.5X_i^\alpha + 0.5) + \sum_{j=1}^{NC} x_j \sum_{\beta=1}^{NS} S_j^\beta \left(\frac{1}{X_j^\beta} - 0.5 \right) \left(\frac{\partial X_j^\beta}{\partial x_i} \right)_{\tilde{\rho},\tilde{T},x_{k \neq i}} \end{aligned} \quad (2.44)$$

$$\tilde{U}^{assoc} = -\tilde{T}^2 \left(\frac{\partial \tilde{A}^{assoc}}{\partial \tilde{T}} \right)_{\tilde{\rho},x} = -\tilde{T}^2 \sum_{i=1}^{NC} x_i \sum_{\alpha=1}^{NS} S_i^\alpha \left(\frac{1}{X_i^\alpha} - 0.5 \right) \left(\frac{\partial X_i^\alpha}{\partial \tilde{T}} \right)_{\tilde{\rho},x} \quad (2.45)$$

Eq. 2.41 shows that the fraction of nonbonded molecules at site α in component i depends on the number of molecules not bonded at sites of type β in component j suggesting the need for an iterative procedure to solve for X_i^α . For detailed information on how to solve such equations and to obtain not only the values of X_i^α but also of their first and second-order derivatives required in further calculations (e.g., **eqs. 2.43-2.45**), the reader is referred to two excellent works by Tan et al.[85] and Michelsen et al.[86], where robust solution procedures for any association scheme were provided.

Polar term

To be able to deal with the quadrupolar moment of CO₂, a polar term is also considered in the calculations carried out with the soft-SAFT EoS. The inclusion of this term requires the value of an effective quadrupole moment, Q , that is related to the experimental quadrupolar moment, Q_{exp} , and the fraction of segments in the chain that effectively contains the polar moment, x_p , that is usually fixed a priori:

$$Q = Q_{exp} \times x_p \quad (2.46)$$

The contribution of the quadrupole-quadrupole interactions to the Helmholtz free energy of the system is obtained as an expansion up to the third order of the quadrupole-quadrupole potential, using the Padé approximation proposed by Stell et al.[87]:

$$\tilde{A}^{polar} = \frac{(A_2^{qq})^2}{A_2^{qq} - A_3^{qq}} = \frac{(A_2^{qq})^2}{A_2^{qq} - (A_{3A}^{qq} + A_{3B}^{qq})} \quad (2.47)$$

Expressions for A_2^{qq} , A_{3A}^{qq} , and A_{3B}^{qq} were provided by Gubbins and Twu[88]:

$$A_2^{qq} = -\frac{14\pi\tilde{\rho}}{5\tilde{T}} J_{10} \sum_{i=1}^{NC} \sum_{j=1}^{NC} x_i x_j m_i m_j \tilde{Q}_i^2 \tilde{Q}_j^2 \frac{1}{\tilde{\sigma}_{ij}^7} \quad (2.48)$$

$$A_{3A}^{qq} = \frac{144\pi\tilde{\rho}}{245\tilde{T}^2} J_{15} \sum_{i=1}^{NC} \sum_{j=1}^{NC} x_i x_j m_i m_j \tilde{Q}_i^3 \tilde{Q}_j^3 \frac{1}{\tilde{\sigma}_{ij}^{12}} \quad (2.49)$$

$$A_{3B}^{qq} = \frac{32\pi^3\tilde{\rho}^2}{2025\tilde{T}^2} \sqrt{2002\pi} k_{444,555} \sum_{i=1}^{NC} \sum_{j=1}^{NC} \sum_{k=1}^{NC} x_i x_j x_k m_i m_j m_k \tilde{Q}_i^2 \tilde{Q}_j^2 \tilde{Q}_k^2 \frac{1}{\tilde{\sigma}_{ij}^3 \tilde{\sigma}_{ik}^3 \tilde{\sigma}_{jk}^3} \quad (2.50)$$

In eqs. 2.48-2.50, J_{10} , J_{15} , and $k_{444,555}$ are the integrals over pair- and triplet- correlation functions for the reference LJ fluid. These integrals have been evaluated numerically using results from molecular simulation and have been fitted to functions of the reduced density and pressure, over an extended range of conditions. Such correlations have been reported by different authors, the most used being those reported by Gubbins and Twu[88] and Luckas et al.[89].

2.1.2- PC-SAFT EoS

There are two general forms to present the residual Helmholtz energy for associating molecules according to SAFT models:

$$\begin{cases} \text{Form 1: } A^{res} = A^{HS} + A^{disp,seg} + A^{chain,seg} + A^{assoc} \\ \text{Form 2: } A^{res} = A^{HS} + A^{chain,HS} + A^{disp,chain} + A^{assoc} \end{cases} \quad (2.51)$$

In both forms A^{HS} accounts for the repulsive interactions in a spherical segment fluid of hard-spheres but they consider a different reference fluid. In ‘‘Form 1’’, employed in the original SAFT, $A^{disp,seg}$ represents the contribution to add to the repulsive hard-sphere segments to obtain the Helmholtz energy of real segments (or monomers). The reference fluid is thus made up of real monomers not bonded together to which the term $A^{chain,seg}$, describing the formation of covalent bonds between real segments, is added. soft-SAFT uses a particular case of ‘‘Form 1’’, in which $A^{HS} + A^{disp,seg}$ are replaced by the A^{seg} term discussed in the previous section, which accounts for both the repulsive and dispersive

contributions in a single term. Alternatively, PC-SAFT EoS relies on Form 2 of **eq. 2.51** and considers a hard-chain fluid composed of freely jointed spherical segments (exhibiting only repulsive interactions) as a reference fluid. Therefore, it starts from A^{HS} and adds $A^{chain,HS}$ to account for the formation of chains between hard-sphere segments. The attractive dispersive interactions between the hard-chain reference fluid are then described by $A^{disp,chain}$.

A detailed description of the PC-SAFT EoS would be redundant with that of soft-SAFT EoS so the main differences between the two EoSs are instead summarized in **Table 2.1**. In this work all the PC-SAFT calculations were carried out using commercial software for advanced thermodynamics calculations, namely Multiflash™ from KBC and VLXE|Blend® from VLXE – Advanced PVT Simplified.

Table 2.1. Outline of soft-SAFT and PC-SAFT EoSs for non-associating components.

SAFT EoS	soft-SAFT	PC-SAFT
References	[61,80,82,90]	[63,64]
A^{seg} (replaces $A^{HS} + A^{disp,seg}$) in “Form 1”	See eq.2.28 $\sum_{i=1}^8 \frac{a_i}{i} (\rho_c^*)^i + \sum_{i=1}^6 b_i (T^*) G_i$	Expression derived by Carnahan and Starling[91] and extended to mixtures by Boublik[92] and Mansoori[93]. $\frac{xm}{\zeta_0} \left[\frac{3\zeta_1\zeta_2}{1-\zeta_3} + \frac{\zeta_2^3}{\zeta_3(1-\zeta_3)^2} + \left(\frac{\zeta_2^3}{\zeta_3^2} - \zeta_0 \right) \ln(1 - \zeta_3) \right]$ with $\zeta_n = \frac{\pi}{6} \sum_{i=1}^{NC} \rho x_i m_i d_i^n$ and $d_i(T) = \sigma_i \left[1 - 0.12 \exp\left(\frac{-3\epsilon_i}{k_B T}\right) \right]$
$A^{chain,seg}$	(1 - m) ln $y_R(\sigma)$ with: $\begin{cases} y_R = g_R^{LJ} \exp[\phi_{LJ}(\sigma)/(k_B T)] = g_R^{LJ} \\ \phi_{LJ}(r = \sigma) = 0 \\ g_R^{LJ} = 1 + \sum_{p=1}^5 \sum_{q=1}^5 a_{pq} (\rho_c^*)^p (T^*)^{1-q} \end{cases}$	-

Table 2.1. (continued)

SAFT EoS	soft-SAFT	PC-SAFT
$A^{chain,HS}$	-	$-\sum_{i=1}^{NC} x_i (m_i - 1) \ln g_{ii}^{hs}(d_{ii})$ $g_{ij}^{hs}(d_{ij}) = \frac{1}{1 - \zeta_3} + \frac{d_i d_j}{d_i + d_j} \frac{3\zeta_2}{(1 - \zeta_3)^2}$ $+ \left(\frac{d_i d_j}{d_i + d_j} \right)^2 \frac{2\zeta_2^2}{(1 - \zeta_3)^2}$
$A^{disp,chain}$	-	$-2\pi\rho I_1(\eta, xm) \sum_{i=1}^{NC} \sum_{j=1}^{NC} x_i x_j m_i m_j \frac{\varepsilon_{ij}}{k_B T} \sigma_{ij}^3$ $- \pi\rho C_1 x m I_2(\eta, xm) \sum_{i=1}^{NC} \sum_{j=1}^{NC} x_i x_j m_i m_j \left(\frac{\varepsilon_{ij}}{k_B T} \right)^2 \sigma_{ij}^3$ <p style="text-align: center;">where $\eta = \zeta_3$ and</p> $C_1 = \left(\begin{array}{l} 1 + xm \frac{8\eta - 2\eta^2}{(1 - \eta)^4} + \\ (1 - xm) \frac{20\eta - 27\eta^2 + 12\eta^3 - 2\eta^4}{[(1 - \eta)(2 - \eta)]^2} \end{array} \right)^{-1}$ $I_1(\eta, xm) = \sum_{i=0}^6 a_i(xm) \eta^i$ $I_2(\eta, xm) = \sum_{i=0}^6 b_i(xm) \eta^i$
CR for A^{assoc}	$\varepsilon^{A_i B_j} = \alpha_{ij}^{HB} \sqrt{\varepsilon^{A_i B_i} \varepsilon^{A_j B_j}}$ $\kappa^{A_i B_j} = \left(\frac{\sqrt[3]{\kappa^{A_i B_i}} + \sqrt[3]{\kappa^{A_j B_j}}}{2} \right)^3$	$\varepsilon^{A_i B_j} = \alpha_{ij}^{HB} \frac{\varepsilon^{A_i B_i} + \varepsilon^{A_j B_j}}{2}$ $\kappa^{A_i B_j} = \sqrt{\kappa^{A_i B_i} \kappa^{A_j B_j}} \left[\frac{\sqrt{\sigma_{ii} \sigma_{jj}}}{(\sigma_{ii} + \sigma_{jj})/2} \right]^3$

2.1.3- SAFT- γ -Mie EoS

As discussed before, most SAFT variants apply a homonuclear approach to treat molecules as homo-segmented chains. Since all the beads constituting the molecule are equal, i.e., have the same energy and size, each compound has its own individual set of molecular parameters, representing “averaged” mean values that are used to capture most physical features of the compound being described, not explicitly accounting for the heterogeneity of the molecules, or the different functional groups making up the molecule.

Aiming at the development of more physically realistic models, of enhanced predictive ability and transferability, heteronuclear treatments of the SAFT-theory, coupled with GC methods, have been proposed in the framework of some SAFT-type EoSs. As depicted in **Figure 2.3**, where homonuclear and heteronuclear CG models for propanoic acid are schematically represented, heteronuclear variants of SAFT allow the study of chainlike molecules built with beads having different characteristics that can thus be assigned to represent key functional groups present in the molecule’s chemical structure. The clear advantage of these approaches is that, as in most GC-based methods, once parameters have been determined for a wide range of functional groups, one can easily predict the thermodynamic behaviour of a virtually unlimited number of compounds containing those same groups without further fitting.

Another clear advantage is that, in this way, the model’s parameterization can be carried out using a broader range of experimental data that is not necessarily limited to the fluid of interest. This is particularly relevant for molecules like the C_iE_j surfactants to be investigated in this work since they are usually found together with water and, consequently, no experimental data for the pure component is available. One of the most prominent heteronuclear SAFT-type EoSs is the SAFT- γ -Mie variant[68], where molecules are represented as associating heteronuclear chains of fused spherical segments. Within the SAFT- γ -Mie framework, each functional group k is represented as a number of spherical segments, v_k^* , (note that in the example provided in **Figure 2.3**, all groups are composed of only one segment, i.e. $v_k^* = 1$), and every pair of segments in the mixture (k, l) are assumed to interact according to a Mie potential of variable range, according to **eq. 2.52**, where r_{kl} is the distance between the centers of the two segments, σ_{kl} is the segment diameter, ϵ_{kl} is the depth of the potential well, and λ_{kl}^r and λ_{kl}^a are the repulsive and attractive exponents of the segment-segment potential.

$$\Phi_{k,l}^{Mie} = \frac{\lambda_{kl}^r}{\lambda_{kl}^r - \lambda_{kl}^a} \left(\frac{\lambda_{kl}^r}{\lambda_{kl}^a} \right)^{\frac{\lambda_{kl}^a}{\lambda_{kl}^r - \lambda_{kl}^a}} \epsilon_{kl} \left[\left(\frac{\sigma_{kl}}{r_{kl}} \right)^{\lambda_{kl}^r} - \left(\frac{\sigma_{kl}}{r_{kl}} \right)^{\lambda_{kl}^a} \right] \quad (2.52)$$

Considering that the model contemplates the use of fused segments, instead of tangentially bonded ones, an additional parameter, known as the shape factor, S_k , is required to reflect the fraction of the

segment that effectively contributes to the system's free energy. Furthermore, as in the more classical homonuclear approaches, associating forces are modelled by incorporating a number of short-range square-well association sites, which are, in this case, placed in any segment of the functional group exhibiting the interactions. Hence, for each 'associating group' the number and type of association sites must be specified, and any interaction allowed to occur between an associating site type a in group k and a site type b in group l has to be characterized by two additional parameters: the association energy, $\varepsilon_{kl,ab}^{HB}$, and the bonding volume, $\kappa_{kl,ab}^{HB}$. The number of sites type 'e1' in a group k is denoted by $NS_{k,e1}$.

In summary, any non-associating functional group k becomes fully defined once the values for v_k^* , S_k , σ_{kk} , ε_{kk} , λ_{kk}^r and λ_{kk}^a are known. If the compound is associating, the number of association sites of each type has to be defined along with the energy, $\varepsilon_{kk,ab}^{HB}$, and volume, $\kappa_{kk,ab}^{HB}$, characterizing each type of site-site interaction. From these parameters, v_k^* can usually be defined a priori based on the size/structure of the functional group being considered, and λ_{kk}^a is usually kept constant to its default value of 6, being usually excluded from the parameterization procedure.

Within a heteronuclear approach such as SAFT- γ -Mie, the unlike interaction parameters are required not only to treat mixtures, as occurs in classical SAFT models, but also for pure component calculations, unless the compound of interest is made up of only one functional group, as it is the case for water or methanol. For the unlike interactions, the values of σ_{kl} , ε_{kl} , λ_{kl}^r , λ_{kk}^a , $\varepsilon_{kl,ab}^{HB}$, and $\kappa_{kl,ab}^{HB}$ must be specified. The values for the unlike parameters can be obtained from CR employing the group-specific parameters, namely:

$$\sigma_{kl} = \frac{\sigma_{kk} + \sigma_{ll}}{2} \quad (2.53)$$

$$\varepsilon_{kl} = \frac{\sqrt{\sigma_{kk}^3 \sigma_{ll}^3}}{\sigma_{kl}^3} \sqrt{\varepsilon_{kk} \varepsilon_{ll}} \quad (2.54)$$

$$\lambda_{kl} = 3 + \sqrt{(\lambda_{kk} - 3)(\lambda_{ll} - 3)} \quad (2.55)$$

$$\varepsilon_{kl,ab}^{HB} = \sqrt{\varepsilon_{kk,aa}^{HB} \varepsilon_{ll,bb}^{HB}} \quad (2.56)$$

$$\kappa_{kl,ab}^{HB} = \left(\frac{{}^3\sqrt{\kappa_{kk,aa}^{HB}} + {}^3\sqrt{\kappa_{ll,bb}^{HB}}}{2} \right)^3 \quad (2.57)$$

These CR are known to provide a good initial estimate. Nonetheless, for a higher accuracy of the model when used to describe real experimental systems, available experimental data is typically used to refine the values obtained using eqs. 2.53-2.57, especially those characterizing the unlike dispersive and

associative energies (ε_{kl} and $\varepsilon_{kl,ab}^{HB}$). The unlike interaction parameters can be obtained from fitting to the experimental data along with the group-specific parameters and, contrarily to what occurs in homonuclear models, they can be obtained from pure-component data alone, assuming the selected compounds contain all the necessary functional groups.

The detailed expressions for each of the terms required for the calculation of the residual Helmholtz energy of the system are not presented here for sake of simplicity, but can be found in the original publication of the SAFT- γ -Mie EoS.[68] The calculations shown in this work using this model were carried out using the gSAFT® advanced thermodynamics software by Process Systems Enterprise™.

2.1.4- Development of a Thermodynamic Modelling Package in MATLAB®

A set of MATLAB® programs for the calculation of phase equilibrium and thermophysical properties, using the soft-SAFT EoS, was developed in the framework of this thesis. The original proprietary soft-SAFT FORTRAN code by Vega and co-workers was used as reference.[94] The motivation behind this task was the following:

- Acquire a better understanding of the SAFT theory and how SAFT-type EoSs are implemented.
- Partially avoid the use of black box type software. This allows to infer the reason behind error calculations and convergence issues more easily.
- Easier coupling with other theories, or extension to different types of calculations, if desired. As an example, the original soft-SAFT code by Vega and co-workers[94] solves the phase equilibrium problem through the equality of chemical potentials in the different phases. Here, additional methods for phase equilibrium calculations based on fugacity coefficients ($\varphi - \varphi$ approaches) were implemented. An extension for solid-liquid equilibrium (SLE) calculations was also included.
- Tailoring the parameterization routines depending on the available experimental data (particularly relevant for alternative solvents such as DES and PILs).
- Simultaneous data analysis and visualization within the same software.

As depicted in **Figure 2.4**, the source code developed in this work is adequately organized in different folders:

- a) **Parent folder**: contains the files responsible for the user interface (UI) and those that store physical and model constants.
- b) **Theory folder**: contains the mathematical expressions related to the SAFT theory.

- c) **\SAFT_solvers** folder: contains the necessary solvers for the EoSs. Even in its non-associating form, SAFT-type EoSs cannot be solved analytically for density, hence a density solver has to be implemented. In its current version, the robust volume iteration procedure proposed by Michelsen et al.[86] is implemented in `fugrho_saft.m`.
- d) **\Tests_docs**: contains a set of predetermined tests to assure the integrity of the code after new releases. Furthermore, it contains clear documentation generated using the ‘m2html’ documentation system by artefact™.
- e) **\Algorithms**: contains the different calculation methods such as phase equilibrium algorithms or methods for the calculation of transport properties.
- f) **\Fitting**: contains the routines required to fit the model parameters to the experimental data provided by the user in one or more `.txt` files.

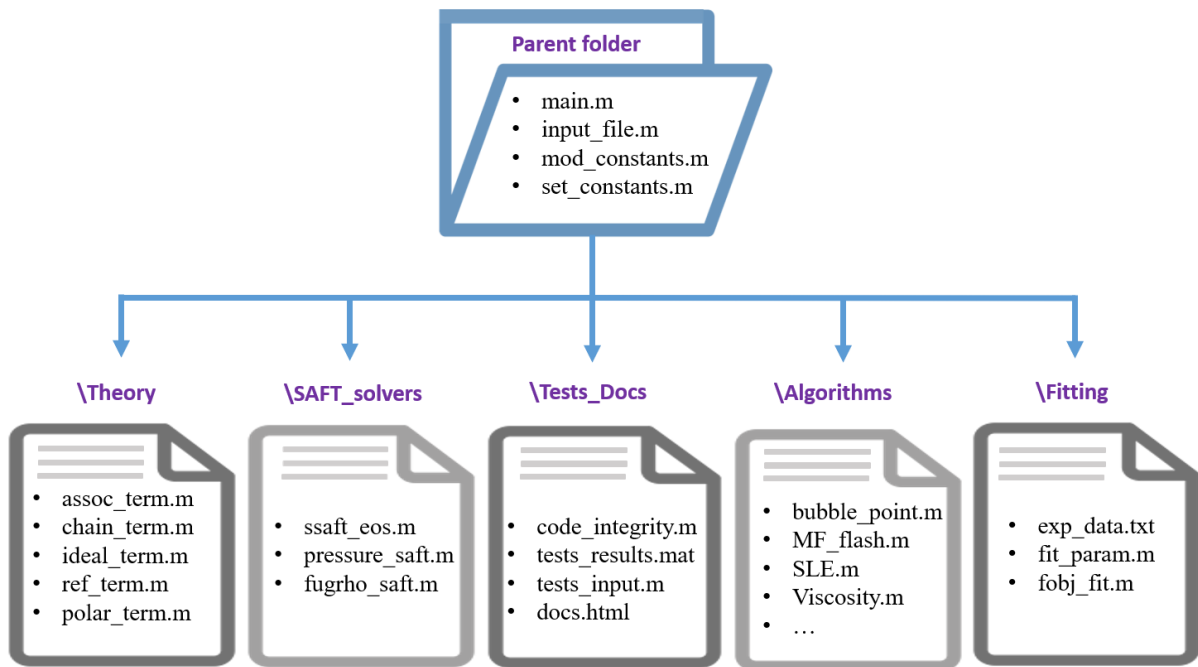


Figure 2.4. Organization of the source code developed in this work.

For a better understanding of the code structure and how it can be used to perform the calculations, a simplified dependency diagram is provided in **Figure 2.5**.

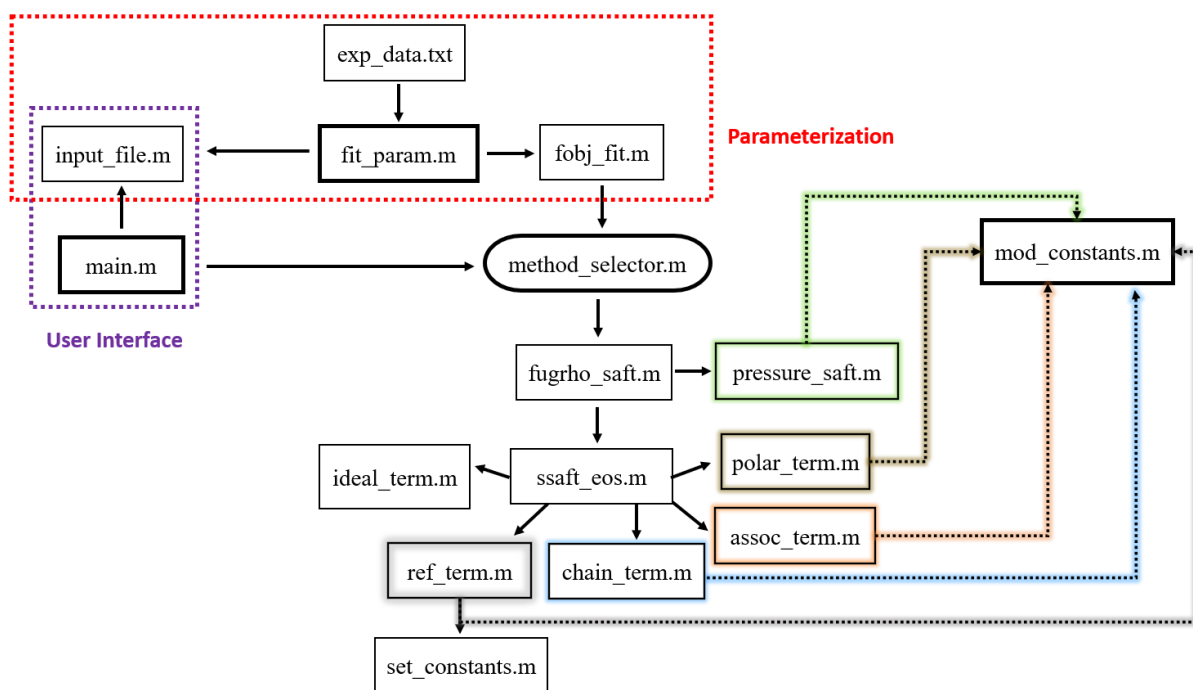


Figure 2.5. Dependency graph of the source code developed in this work.

To perform any type of calculations the user must provide the necessary input in the ‘input_file.m’ file (model parameters, critical and melting properties, molecular weight, among others for every component of the system). Additionally, in the ‘main.m’ file the type of calculation to carry out and the input conditions for the calculation must be provided (e.g., calculate a bubble point for an equimolar mixture at given (T, p) conditions). These two files belong to the purple region of the diagram in **Figure 2.5** and essentially constitute the part of the code that could be replaced by a Graphical User Interface (GUI) in a more advanced software.

The region in red represents the starting files to carry the model’s parameterization. The ‘input_file.m’ file should be provided using any reasonable estimates for the unknown parameters, the experimental data to use in the fitting is provided in one or more .txt files and the optimization functions must be tailored depending on the type of experimental data available, although default cases such as fitting the model to vapor pressures and saturated liquid densities (the most common approach) exist.

Both a calculation with the model or its parameterization calls the necessary calculation methods to describe the desired property (e.g., phase equilibrium algorithms). This occupies the central position of the diagram in **Figure 2.5** and connects the user’s task with the theory. Every method does some sort of a call to the theory to obtain at least the fugacity coefficients of the different components or the density of the system. These two properties (among many others like A, G, H, S, U, u_i , and all sorts of derivative

properties like C_p , C_v , α_p , and k_T) are obtained in the routine ‘fugrho_saft.m’ that, as previously mentioned, solves the density implicit EoS. Essentially, for a given specified pressure, p^{spec} , the density is solved iteratively until the value of pressure obtained by the EoS match that of p^{spec} . Obviously, this requires multiple calls to the SAFT theory through the ‘ssaft_eos.m’ routine. This routine converts the input from real units provided by the user to the reduced units used in the theory (c.f. **Section 2.1**), solves all the necessary mathematical expressions to obtain the contributions of the different terms to the properties mentioned before. To speed up the process, and as in intermediate steps only the calculation of pressure is required, a routine that only calculates the pressure (avoiding the calculation of compositional derivatives for the chemical potentials and others) is also provided (i.e., ‘pressure_saft.m’). After all this, the results are returned to the ‘main.m’ or ‘fit_param.m’ files (depending on whether it is a calculation or model’s parameterization) for the visualization of results.

Currently, the software is endowed with the following calculation methods/routines, that are available at my Github repository (<https://github.com/eacrespo15/PhaseEquilAlgor>):

- **VLE_PTFLASH.m**: This file contains a two-phase PT-FLASH that can be used with or without acceleration methods either through the Dominant Eigen Value Method (DEVM) or through extrapolation steps. This function calls both a Rachford-Rice equation solver (RR_solver.m) and a stability analysis for the system (stability_analysis.m).
- **Bubble_point.m**: this file contains algorithms for bubble/dew temperature/pressure calculations of multi component systems. Derivatives of the natural logarithm of the fugacity coefficients are avoided for increased speed.
- **MFFLASH_GUPTA.m**, **MFFLASH_HEIDEMANN.m**, **MFFLASH_MICHELSEN.m**: Clearly, multiphase flash calculations are among the trickiest calculations to perform. Therefore, three different algorithms, whose convergence speed and robustness may vary depending on the type of system under study, were implemented.
- **LLE_BINARY.m** and **LLE_TERNARY.m**: alternative simpler methods to solve liquid-liquid equilibrium (LLE) problems of binary or ternary systems using the iso-fugacity criterion.
- **SLE_BINARY.m**: to describe the SLE of DESs, solubility calculations in binary mixtures were implemented. The implemented routines allow for the inclusion of solid-solid transitions and heat capacity differences upon fusion if such data is available.
- **SSViscosity.m**: Implements the Free Volume Theory for viscosity calculations.[71] The current implementation allows for the use of three different mixing rules for the dense term.

2.2- Molecular Dynamics Simulations

A MD simulation is a technique to produce a phase space dynamical trajectory for a system composed of N particles, by integrating the Newton's equations of motion:

$$\frac{\partial^2 r_i}{\partial t^2} = f_i = -\frac{\partial}{\partial r_i} U(r_1, r_2, \dots, r_N) \quad (2.58)$$

where $U(r_1, r_2, \dots, r_N)$ is the potential energy of the system as a function of the coordinates of the N particles and f_i is the force acting on particle i . From the trajectory, both equilibrium and transport properties of a given system can be obtained, resembling a system obeying the laws of classical mechanics.[95]

In many aspects, MD simulations somehow reproduce the way experiments are carried out. In a real experiment, a sample of a given material is subject to an experimental apparatus to obtain certain properties and, if they are subject to statistical noise, the more measurements are taken of the same property, the more accurate our 'averaged' result becomes. In MD simulations, a similar idea is followed. First, a reasonable configuration of the system is created by defining the initial positions and velocities for every particle in the system. Then, an equilibrium step is followed until the system no longer change with time and the system have reached the desired (p, ρ, T) conditions. Once the system is equilibrated, the production run can be performed, in the desired ensemble. Here, the simulation time should be much longer than the relaxation time of the property of interest and sufficiently long to ensure the validity of the ergodic hypothesis, i.e., the time-average of a given property coincides with the ensemble average. Finally, the simulated trajectory file provides the particle positions, velocities and forces as a function of time, thus relevant system's properties can be obtained, by expressing them in terms of the positions and momentum of the particles can be obtained.[95]

To solve the Newton's equations of motion, the forces acting on every particle must be determined in every time step, usually using pairwise additive interactions. Therefore, a mathematical expression describing the dependence of the system's energy with the coordinates and interactions between the particles, i.e., a forcefield (FF) is required.[96] There are many FFs available in the literature, with distinct degrees of complexity, and applicable to the study of different types of systems. Ideally, it must be simple enough to be quickly evaluated at each iteration, but sufficiently detailed to properly reproduce the system's thermodynamic behaviour.

Despite the pretentious analogy of MD modelling as a 'virtual experiment', the aim of a MD simulation is not to reproduce experiments but rather to provide a better understanding of the microscopic behaviour of the system leading to the phenomena being observed at the macroscopic scale, or to obtain

qualitative predictions of the behaviour expected at conditions that cannot be easily reproduced in experiments. Nonetheless, MD simulations represent an efficient method to explore the structure and dynamics of complex systems with their accuracy and reliability depending on the quality of the FF chosen to describe the intra- and intermolecular interactions.

The use of MD simulations is clearly a good complement to SAFT-type EoSs, as both tools combined can provide an overall description of the system. While EoSs can be used to quickly obtain macroscopic phase equilibrium and different thermophysical properties, MD simulations allow for a better understanding of the system's behaviour at the molecular level. As an example, they can be used to provide useful insights on micelle formation or to investigate the self-assembly phenomena and the formation of different LC phases of surfactants in water or multi-component systems, compute structural properties such as the rdf, or structure factors comparable to X-ray diffraction experimental data, dynamical properties such as diffusion coefficients, among others.

It must be noticed that MD remains a compromise between computational efficiency and scale resolution (c.f. **Figure 2.6**). Atomistic or AA models (i.e., the contribution of each atom is taken into account in the calculation) can indeed provide detailed and precise information about the initial stages of micelle formation in diluted systems but are unable to address the time and size scales relevant for the self-assembling and mesophase transition processes. In this regard, the required relaxation times, typically in the order of microseconds and at a nanometer scale, are unattainable by AA models unless preformed structures are used. Alternatively, by reducing the number of interaction centres, CG models have been demonstrated as a good alternative to the more computational demanding AA models. Thus, by grouping a certain number of atoms into a single interaction site, the number of particles and pairwise interactions in the system are severely decreased, significantly reducing the computational cost of the simulations. Hence, these models can tackle larger systems for longer simulation times and, even though some atomistic structural details may be lost in this simplification, the results obtained so far have been really promising.

Naturally, the performance of a CG model heavily relies on the FF accuracy and on an appropriate CG mapping of the different atoms of the real system. Despite the significant decrease of interaction sites, the model must still capture the essential physico-chemical features of the molecules. Given the empirical nature of most CG FFs, their predictive power and transferability is often limited, and simulations carried out at conditions that differ significantly from those used in the FF parameterization should be carefully analysed.

In this work, CG-MD simulations are used to investigate the surfactant-like behaviour of C_iE_j aqueous solutions and multicomponent systems and, considering its highly transferable character, the MARTINI FF, proposed by Marrink et al.,[52] is used, being properly described in the next section.

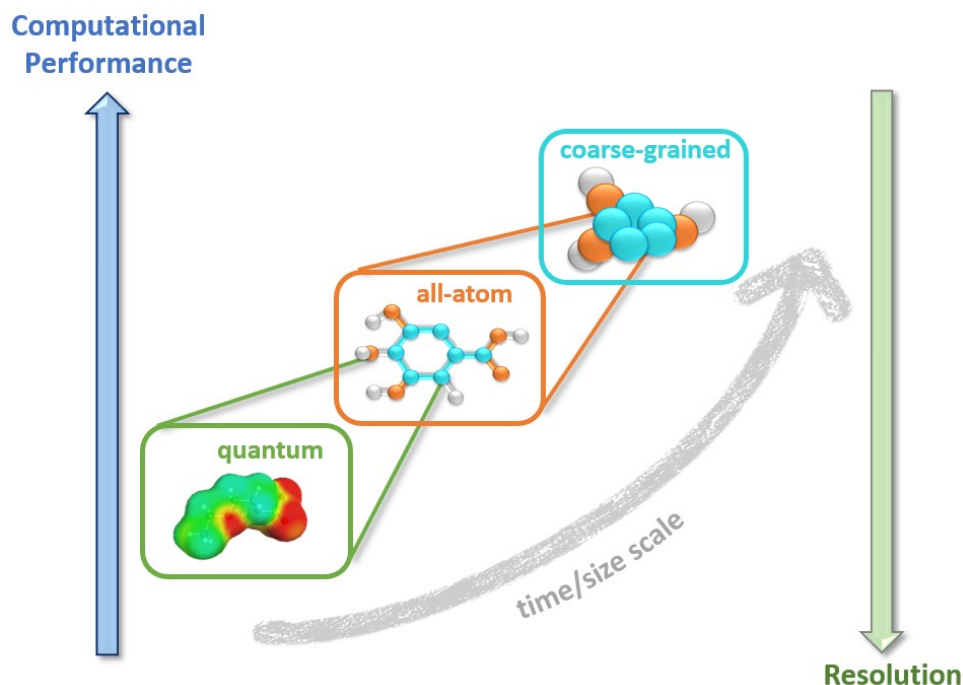


Figure 2.6. Molecular modelling at different resolutions.

2.2.1- MARTINI Forcefield

The MARTINI FF was first developed in 2003 for the study of bio(molecular) systems whose relevant timescales are typically unattainable using atomistic MD simulations, such as the study of lipid membranes.[97,98] A few years later, in 2007, an improved version of the CG FF, referred to as MARTINI 2 and used throughout this work, was proposed to overcome some of the limitations observed in the first studies such as the excessively coarsened definition of the interactions or the unrealistic tendency of water to freeze at room temperature.[52]

Although initially developed for biomolecular simulations of phospholipids, it has been increasingly successfully applied for a variety of chemical, non-biological, systems due to its distinct development philosophy.[99,100] Instead of focusing on an accurate reproduction of structural details, under certain conditions, the MARTINI FF aims at providing a general CG modelling framework useful for a broader range of applications, without the need to reparametrize the model. This remarkable transferability is achieved by a modular mapping and parameterization scheme based on a limited

number of building blocks (beads), whose calibration was carried against experimental thermodynamic properties, in particular oil/water partitioning coefficients.[52,100]

In the MARTINI FF, four non-hydrogen atoms are mapped into a single CG bead (interaction centre) which resembles their physico-chemical properties. This kind of approach makes it easy to build the CG models of different molecules based on a common set of beads, in a systematic manner. The MARTINI 2 FF encompasses four main bead types: polar (P), nonpolar (N), apolar(C), and charged (Q) with different sub-types depending on the degree of polarity or the hydrogen bonding capabilities implicitly included in Q or N beads. This allows for a more realistic representation of the chemical nature of the subjacent building block. Thus, the Q and N bead types have four subtypes each that are distinguished by their hydrogen bonding ability in between donor (d), acceptor (a), donor + acceptor (da), or none (0), the main difference being related to their self-interaction strength. The P and C bead types have five subtypes each to represent different polarity degrees in a 1-5 scale where 1 describes a low polarity bead and 5 denotes the more highly polar bead type. This yields a total of 18 different bead types that can be used to map any given molecule. For computational efficiency, all the beads have the same mass, equivalent to that of four water molecules (four water molecules are represented by a P4 bead type in the MARTINI FF).[100]

The MD simulations using the MARTINI FF were carried out using the GROMACS package,[101] and the potential energy of the system comprises both bonded and nonbonded interactions, as given in **eq. 2.59**.

$$U = \sum_{bonds} \frac{1}{2} k_b (r - r_0)^2 + \sum_{angles} \frac{1}{2} k_a (\theta - \theta_0)^2 + \sum_{torsions} \frac{V_n}{2} [1 + \cos(n\phi - \delta)] + \sum_{improper} V_{imp} + \sum_{LJ} 4\epsilon_{ij} \left[\left(\frac{\sigma_{ij}}{r} \right)^{12} - \left(\frac{\sigma_{ij}}{r} \right)^6 \right] + \sum_{elec} \frac{q_i q_j}{4\pi\epsilon_r r_{ij}} \quad (2.59)$$

The first four terms are the bonded interactions with harmonic functions for the bond stretching, angle bending and dihedral torsion, respectively. The last two terms are the nonbonded interactions. The first of those terms is a shifted LJ 12-6 potential energy function, expressed by **eq. 2.60**:

$$U_{LJ}(r) = 4\epsilon_{ij} \left[\left(\frac{\sigma_{ij}}{r} \right)^{12} - \left(\frac{\sigma_{ij}}{r} \right)^6 \right] \quad (2.60)$$

where σ_{ij} is the closest approach distance between two interacting beads and assumed to have an effective size of 0.47 nm, except for the interactions between charged ‘Q’ beads and the most apolar types ‘C1’ and ‘C2’ where this parameter is set to 0.62 nm. Concerning the ϵ_{ij} interaction energies, a total of 10 interaction levels, with energies between 2.0 and 5.6 kJ/mol were proposed and assigned to the different bead-bead interaction pairs, according to the interaction matrix developed by Marrink et

al.[52] The assignment of a given level to a particular bead-bead pair was carried out based on the experimental water-oil partitioning of small molecules that are represented by each of the beads.

The last term in the total potential energy calculates interactions between charged Q-beads, as they bear an explicit full charge q_i , a shifted Coulombic potential energy function (eq. 2.61) is used to describe the interaction between charged beads, using an empirical relative dielectric constant $\epsilon_r = 15$ for explicit screening.

$$U_{coul}(r) = \frac{q_i q_j}{4\pi\epsilon_r r_{ij}} \quad (2.61)$$

For cases where a 4:1 mapping is not appropriate, such as to preserve the geometry of ring structures where a 2:1 or 3:1 mapping is more appropriate, a special particle set, denoted by the letter ‘S’ is introduced. For self-interactions between ‘S’ type beads, the value of σ_{ij} is reduced to 0.43 nm and the value of ϵ_{ij} is scaled to 75% of its original value. This modification allows S-type beads to pack more closely together allowing a more accurate representation of this type of components.

While the non-bonded interactions are described following a “top-down” approach by using experimental data, the information required to describe the bonded interactions is typically extracted via a “bottom-up” approach using data obtained from atomistic models and quantum calculations. Typically, the bonded parameters are optimized to improve the agreement between the distribution profiles obtained in AA and CG simulations in an iterative procedure.[100]

To illustrate the CG mapping of a molecule using the MARTINI FF, a sketch of the CG mapping for the 1-tetradecyl-3-methylimidazolium cation [$C_{14}mim^+$] proposed in a work co-authored by the candidate[102] is presented in **Figure 2.7**. As can be seen, the cation was divided into seven different beads following a 3:1/4:1 mapping. The special bead type ‘S’, often used to map aromatic rings, was selected to reproduce the imidazolium ring. In this work, the [$C_n m m$][Cl] geometries were first taken from ad-hoc AA-MD simulations, using the well-known and widely used Canongia-Lopes FF.[103,104] Then, MD simulations of individual IL moieties were run under very diluted conditions at both, the AA and CG levels, where the AA structure is taken as a reference to find the proper set of CG beads and bonded parameters. Thus, the best agreement was found for the following mapping: one SQd bead type (charged and hydrogen bond donor) comprising the hydrogen atom bonded to the carbon atom between the two nitrogen atoms of the ring; one bead type SP5 for the stronger polar region of the aromatic ring, and a SP1 bead to represent the less polar part of the ring. For the alkyl chain, one bead type SC1 (aromatic strongly apolar bead) was used to connect the head-group with alkyl-chain tail that is mapped using C1 beads (the most apolar beads in the MARTINI model). The purpose of using a SC1 bead near the head instead of C1 beads was twofold: Firstly, it allows to better represent the total number of carbon

atoms, decreasing the degree of bead overlapping. Secondly, it allows a smoother transition between a very polar region of the imidazolium cation (the head group) and the strongly apolar alkyl-chain tail.

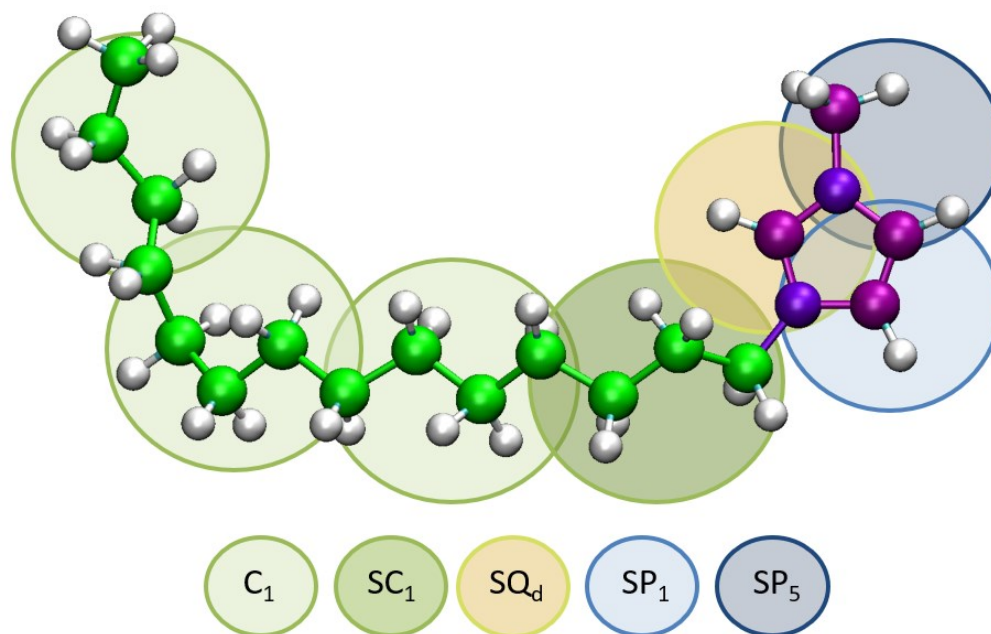


Figure 2.7. Sketch of the CG mapping for the 1-tetradecyl-3-methylimidazolium cation and corresponding bead types under the MARTINI forcefield.[52]

This example illustrates the versatility of the MARTINI FF that, along with its inherent transferability and the good results previously obtained when investigating the self-assembly of a large number of amphiphilic compounds,[102,105–110] suggests that it is a valuable tool to study the surfactant-like behaviour of the C_iE_j molecules mentioned in **Chapter 1**. As such, a CG-MD framework was selected under the MARTINI FF to analyse the phase behaviour of these non-ionic surfactants in water as well as in multi-component systems, as reported in **Chapter 5**.

3- Thermodynamic Modelling of Glycols and Glymes

"All models are wrong, but some are useful."

George E.P. Box

3.1- A simple, yet robust, soft-SAFT model for glycols

The content of this section is based on the following published works, developed in the framework of this PhD thesis, where E.A. Crespo was responsible for the modelling tasks and for writing the manuscripts, with substantial contributions from the remaining authors.

- Emanuel A. Crespo, João M.L. Costa, Zulkhimali B.M.A. Hanafiah, Kiki A. Kurnia, Mariana B. Oliveira, Fèlix Llovell, Lourdes F. Vega, Pedro J. Carvalho, and João A.P. Coutinho, “*New measurements and modelling of high-pressure thermodynamic properties of glycols*”, *Fluid Phase Equilibria*, 436 (2017) 113-123, DOI: 10.1016/j.fluid.2017.01.003.
- Emanuel A. Crespo and João A.P. Coutinho, “*A Statistical Associating Fluid Theory Perspective of the Modeling of Compounds Containing Ethylene Oxide Groups*”, *Ind. Eng. Chem. Res.* 2019, 58, 3562-3582, DOI: 10.1021/acs.iecr.9b00273

Introduction

In soft-SAFT, as in any molecular-based EoS, the adequate selection of a CG model, capable of representing the basic physical features of the compounds, is key for a good performance of the model. As detailed in **Chapter 2.1**, soft-SAFT relies on the pre-selection of a molecular model for each pure compound. This model requires five parameters to fully characterize an associating component i , as it is the case for glycols. For the physical part three parameters are necessary, the number of segments in the chain, m_i , the monomers diameter, σ_{ii} , and the dispersive energy between monomers, ε_{ii} . For the association term, a proper association scheme specifying the number/type of association sites and the interactions allowed to occur, must be assigned to each associating species present in the system. Then, the energy ($\varepsilon^{A_i B_i}$ or ε^{HB}) and volume ($\kappa^{A_i B_i}$ or κ^{HB}) of association must be defined for each pairwise site-site interaction, although typically they are all considered equivalent within a same species so that a total of five parameters become necessary.

The first relevant work on the SAFT modelling of glycols appeared 10 years after the advent of SAFT when, in 2000, Wiesmet et al.,[111] applied the CK-SAFT EoS to describe the phase equilibria of binary systems composed of polyethylene glycols (PEG) with a molecular weight $M_w = 200 - 8000 \text{ g/mol}$ with either CO_2 , n -propane, or N_2 . Even though PEG molecules can self-associate via one of the hydroxyl end-groups with either the oxygen atoms in the polymer backbone, or with a hydroxyl end-group in a neighbour molecule, only the hydrogen bonding character of the hydroxyl groups was considered, when assigning an association scheme. Furthermore, even though each PEG molecule contains two hydroxyl end-groups, only two association sites were ascribed to each PEG molecule,

following the simple ‘2B’ association scheme, typically suggested for alkan-1-ols that contain a single hydroxyl group. This association scheme contains only one positive/donor ‘A’ site accounting for the H-atom of the hydroxyl group, and a negative/acceptor ‘B’ site accounting for the lone electron pairs of the oxygen atom, allowing for ‘A-B’ interactions. Given the negligible vapor pressures for PEGs, the PEG non-associating parameters were regressed from a set of 61 pressure-density-temperature ($p\rho T$) experimental data points in wide temperature and pressure ranges obtained for only one M_w , PEG 7500, while the associating parameters were directly transferred from those of ethanol. Due to the simplicity of the approach (both the association scheme employed, and the experimental data used for parameterization), the successful description of the mixtures was found to require the use of complex binary interaction parameters (linear and quadratic temperature-dependencies). Afterwards, several modelling works using SAFT-based models to describe the phase equilibria of systems containing glycols have been reported in the literature, and are summarized in **Table B.1**, in **Appendix B**.

From this literature survey, discussed in more detail in the published review[112], a few important observations arise. First, it shows that different SAFT variants have been applied to the thermodynamic modelling of glycols, although more than half of the works published in this topic were carried out using the Cubic-Plus-Association (CPA) EoS, where a cubic EoS, namely PR or SRK is coupled with the association term derived from the SAFT theory. This is in part, due to the long-term interest of Kontogeorgis and co-workers in gas-hydrate related systems, but also because CPA has the advantage, compared with other variants that, in the absence of associating components, it is reduced to a classical cubic EoS, with which the Oil & Gas industry is much more familiar, facilitating its wide adoption.

Secondly, as depicted in **Figure 3.1**, a variety of association schemes (detailed in **Table 3.1**) have been employed to describe the associating behaviour of glycols. From **Figure 3.1**, it is clear that the ‘4C’ scheme has been by far the most adopted scheme to describe glycols and, from an analysis of the literature, even though it does not explicitly account for the hydrogen bonding acceptor character of the inner EO groups of the glycol molecule, no significant improvements in terms of accuracy were observed when more complex association schemes were applied, especially if considering the increased computational cost of using a more complex association term.

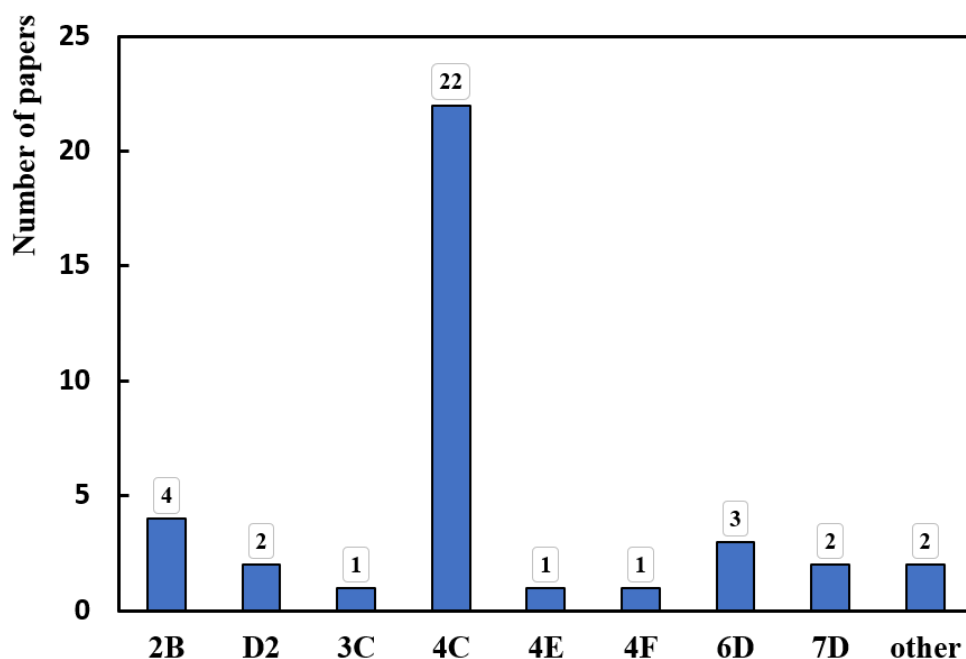


Figure 3.1. Association schemes (c.f. Table 3.1) used to describe the hydrogen-bonding character of glycols in the framework of association models.

Table 3.1. Association schemes employed in the modelling of glycols using either SAFT or CPA. Blue and red colours are used to define positive and negative sites that can only interact with the opposite sign, while green represents binary sites that can interact with both positive and negative sites.

Designation	N° of Association Sites			Schematic Representation
	+	-	+/-	
2B	1	1	-	
4C	2	2	-	
6D	2	4	-	
7D	2	5	-	
D2	-	-	2	
3C	1	1	1	
4E	1	1	2	
4F	-	2	2	

Finally, as illustrated in **Figure 3.2**, the majority of publications dealing with the thermodynamic modelling of glycols using association models is focused only in the first four members of the series, especially EG and TriEG due to their widespread use as gas hydrate inhibitors and dehydration agents. This is despite the importance that achieving an accurate modelling of higher chain length members has in ensuring the robustness of the molecular models and parameters proposed, and in certifying that the influence of the inner oxyethylene repeating units is being well captured by the model.

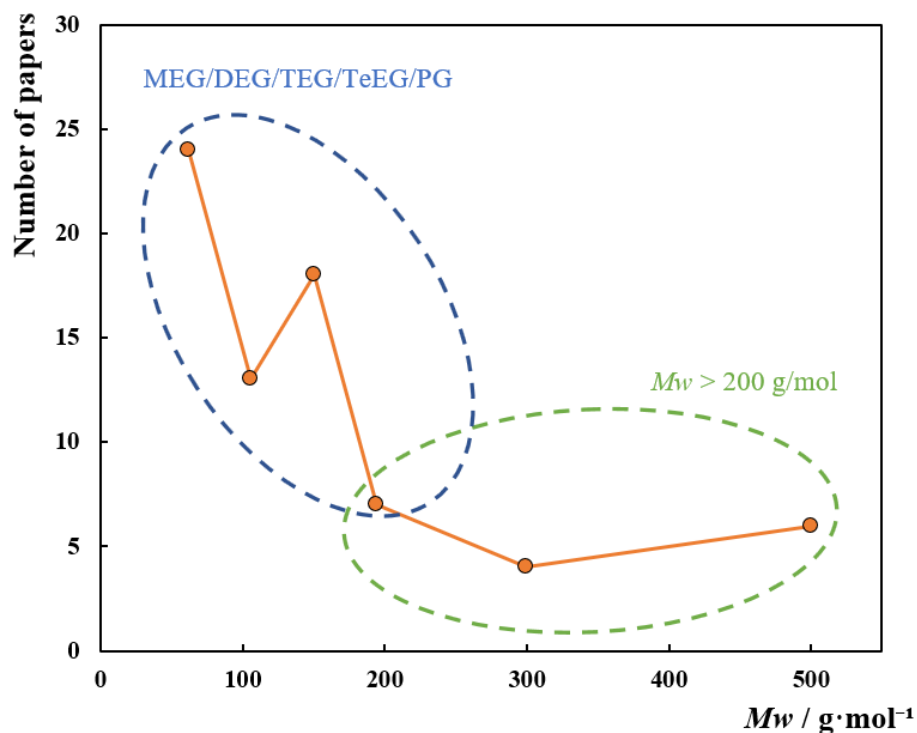


Figure 3.2. Number of modelling works (c.f. **Table B.1.**) using SAFT or CPA as a function of the glycols M_w . The points 300 and 500 represent the works with a M_w in the range of 200-400 g/mol and higher than 400 g/mol, respectively.

According to the literature survey in **Table B.1.**, the only attempt to model both low and high M_w glycols using the same model was carried out in the works of Pedrosa et al.,[75,113] using the soft-SAFT EoS. Initially, the modelling of low molecular weight glycol oligomers (from EG to TeEG) was addressed.[75] Then, as the associating parameters of any glycol had been fixed to those of EG and the non-associating parameters were found to correlate with the glycols' M_w , the same model was later applied for the modelling of PEGs with different M_w in the range of 200-8000 g/mol, and used to describe binary mixtures of PEGs with light gases, water, alcohols, or aromatic compounds.[113]

Concerning pure glycol oligomers, even though an excellent agreement was obtained for the temperature-density diagrams and vapor pressures,[75] the model fails to accurately describe the pressure effect on the glycols' behaviour, leading to large deviations from the experimental data when it is applied to describe the more sensitive second-order derivative properties such as k_T . This is shown more clearly in **Figure B.1** in **Appendix B**. Obviously, when the model is later applied to describe binary mixtures, the use of a binary interaction parameter helps masking this kind of subtle model deficiencies, and a good description of the experimental data can still be achieved. Nonetheless, an improvement of the molecular model of the pure components in what concerns a better description of the pressure effect can result in an enhanced predictive ability when the model is used to describe higher chain length homologues or blends, in the reduction of the binary interaction parameter's magnitude, or in better predictions for ternary/multicomponent systems when the model is used to simulate an entire process.

Therefore, in this work, an improved CG model for glycols is proposed, aiming at an enhanced accuracy in terms of the second-order derivative properties compared with the model of Pedrosa et al. [75]. The new model should be applicable to glycols of different M_w and make use of a computational efficient association scheme.

Modelling Approach

In the work of Pedrosa et al.[75], the glycol oligomers were considered as LJ chains with two square-well sites embedded off-centre in two of the LJ segments, following a 2B association scheme, and the pure-component parameters were obtained by fitting to available VLE data (saturation liquid densities and vapor pressures) for the first four members of the series (EG to TeEG) that was accurately described through fitting. The '2B' association scheme is typically used to describe alkan-1-ols that contain only one hydroxyl group. In theory, this makes it oversimplified to describe glycols that contain two hydroxyl groups, especially considering that the hydrogen bonding character of the inner EO groups is already being neglected. Under a '2B' scheme, either one negative site describes the effect of the lone electron pairs in both oxygen atoms and one positive site describes the effect of both hydrogen atoms or as illustrated in **Table 3.1**, one hydroxyl group is considered as an acceptor and the other as donor of hydrogen bonds.

Clearly, a more accurate representation of the glycols behaviour can be achieved using the '4C' association scheme that, as depicted in **Figure 3.1**, is the most widely applied scheme to glycols but results in an increased number of association sites. In this work, an alternative approach is considered

through the introduction of the so-called binary association sites, i.e., association sites that can interact with both negative and positive sites. Therefore, as represented in **Figure 3.3**, two equivalent association sites are assigned to the molecule, one site type ‘A’ and one site type ‘B’, each representing one of the hydroxyl end-groups, and, contrarily to what occurs in a ‘2B’, all kind of interactions are allowed (‘A–A’, ‘B–B’, and ‘A–B’). This allows to account for the dual positive-negative nature of the hydroxyl groups, without an increase on the total number of association sites.

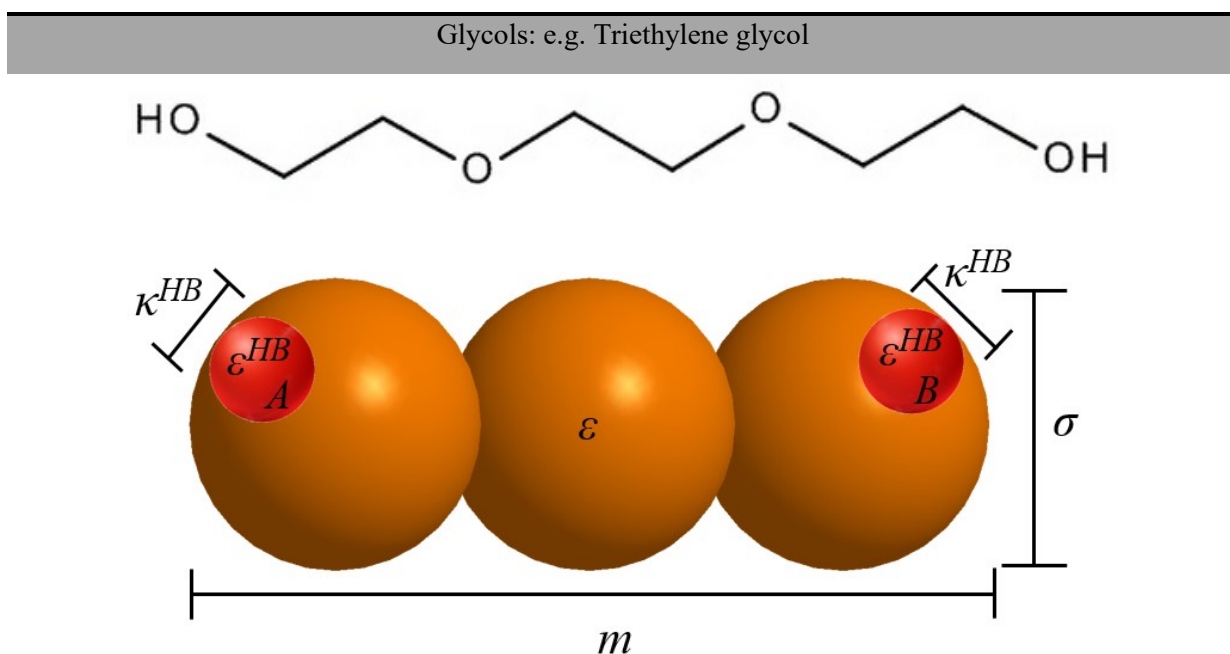


Figure 3.3. Sketch of the molecular model proposed for glycols, illustrated for TriEG.

Furthermore, even though fitting the pure-component parameters to experimental VLE data of the pure fluid is the traditional parameterization approach for SAFT-type EoSs, recent developments on SAFT-type EoSs have emphasized the importance of adjusting the EoS molecular parameters against properties affected by association, aiming to obtain a realistic balance between dispersive and associative interactions,[114] and several researchers highlighted the importance of using additional data (e.g. enthalpies of vaporization, monomer fractions, or derivative properties) in the parameterization procedure.[115,116] Although the selection of the most reliable properties for the fitting is still under discussion, the simultaneous description of vapor pressures and density along with its pressure and temperature derivatives appears as the most relevant.[117] Accordingly, in order to improve the description of the pressure effect with the new model, and to provide a better description of second-order derivative properties, an isotherm at 323 K of high-pressure liquid densities and of k_T data (up to 95

MPa) were included in the experimental dataset that also contained the usual vapour pressures and saturated liquid densities.

Results

The work of Oliveira et al.[117] focused on the role of derivative properties in the development of new procedures for enhancing the transferability of SAFT molecular parameters proposed the use of a coupling factor, δ , in the soft-SAFT fitting procedure, to change the weight of one set of properties comprising VLE data over another containing high-pressure density data or derivative properties. Here, following those suggestions, the following objective function (OF) was used in the parameters' optimization:

$$OF = \frac{\delta}{N} \left[0.80 \sum_{i=1}^N \frac{\rho^{calc} - \rho^{exp}}{\rho^{exp}} + 0.20 \sum_{i=1}^N \frac{p^{*,calc} - p^{*,exp}}{p^{*,exp}} \right] + \frac{1 - \delta}{M} \left[0.90 \sum_{i=1}^M \frac{p\rho T_{323K}^{calc} - p\rho T_{323K}^{exp}}{p\rho T_{323K}^{exp}} + 0.10 \sum_{i=1}^M \frac{k_{T_{323K}}^{calc} - k_{T_{323K}}^{exp}}{k_{T_{323K}}^{exp}} \right] \quad (3.1)$$

where, δ is the coupling factor, N and M are the number of experimental phase equilibrium and high-pressure points, respectively. A δ of 0.5 was found to provide the best results as previously suggested by Oliveira et al.[117]. The weights 0.80 and 0.20 were directly taken from previous contributions,[72,117] while those from the high-pressure term have been here found to provide the most accurate results. In addition, having now data available for more members of the series, it allows assessing the model and parameters in a more robust manner, hence, the model parameterization was carried for the first six glycol oligomers, up to hexaethylene glycol (HeEG). However, for the pentaethylene glycol (PeEG) and HeEG, no VLE data is currently available, making the parameters determination for these two compounds only feasible by using the second term of **eq. 3.1**.

As depicted in **Figures 3.4** and **3.5**, the selected molecular model, using the optimized molecular parameters reported in **Table 3.2**, provides an excellent description of the VLE of pure glycol oligomers, with overall percentage average relative deviations (%ARD) – **eq. 3.2** – for the compounds' vapor pressure, saturated liquid and vapor densities of 9.61, 0.28 and 9.05, respectively. As commonly done for homologous series of compounds, and as will be further discussed in the next section, the association parameters were kept fixed for the different glycols to the values obtained for TriEG, except for EG that presents a slightly higher association energy.

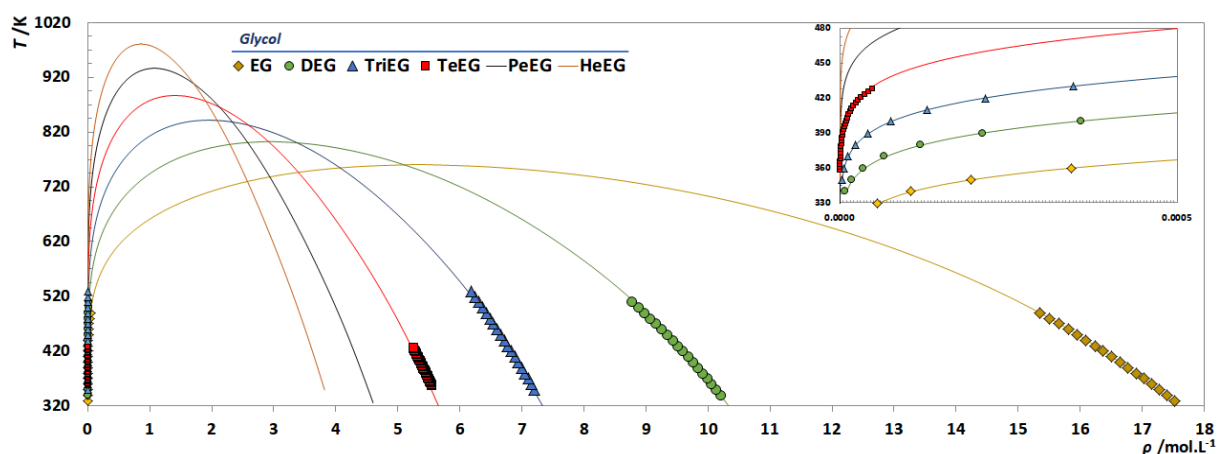


Figure 3.4. Saturated liquid and vapor densities as a function of temperature for the EG, DEG, TEG, and TeEG. The solid lines represent the soft-SAFT EoS fit to the experimental data,[118] for EG, DEG, TEG, and TeEG, while for PeEG and HeEG, predictions are provided.

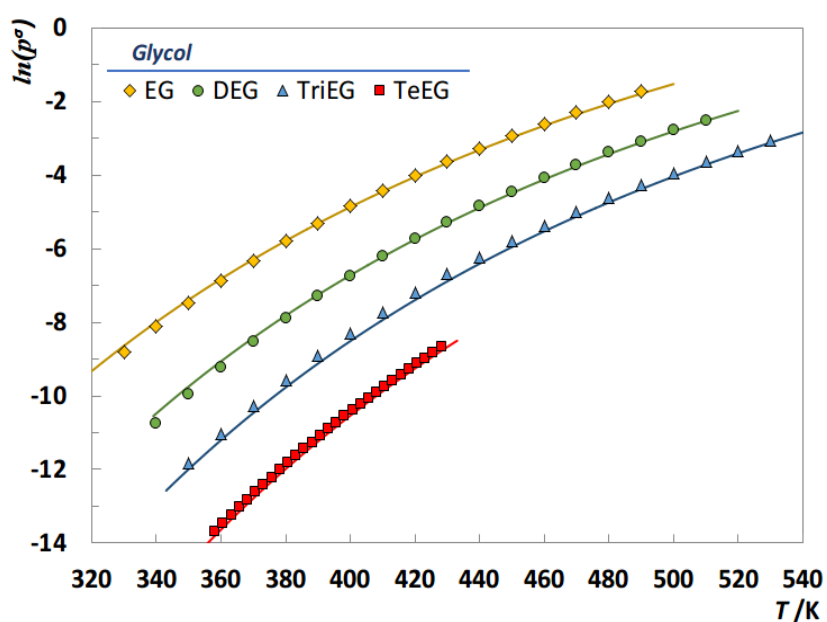


Figure 3.5. Logarithm of the vapor pressure, as a function of temperature for glycol oligomers. The solid lines represent the soft-SAFT EoS fit to the experimental data.[118]

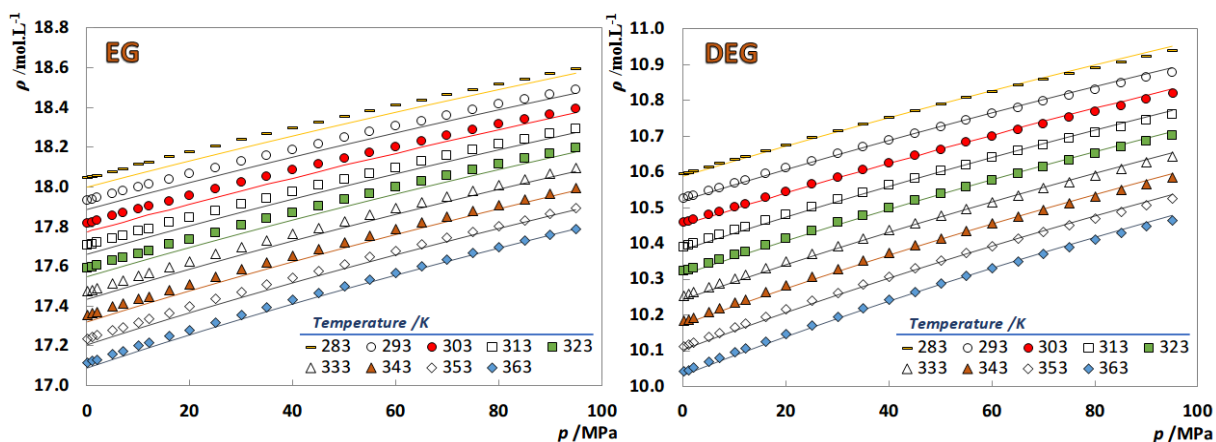
$$\%ARD = \frac{100}{N} \sum_{i=1}^N \left| \frac{x_i^{calc} - x_i^{exp}}{x_i^{exp}} \right| \quad (3.2)$$

Table 3.2. soft-SAFT pure-component parameters for glycols.

	m_i	$\sigma_{ii}(\text{\AA})$	$\varepsilon_{ii}/k_B(K)$	$\varepsilon^{HB}/k_B(K)$	$\kappa^{HB}(\text{\AA}^3)$
EG	1.951	3.533	325.10	4140	2600
DEG	2.825	3.733	342.77	3891	2600
TriEG	3.525	3.887	346.18	3891	2600
TeEG	4.311	3.964	349.14	3891	2600
PeEG	5.256	3.970	351.65	3891	2600
HeEG	6.175	3.983	354.44	3891	2600
PEG400	8.321*	4.049*	357.47*	3891	2600

*Extrapolated from eqs. 3.3-3.5.

The optimized parameters were also used to predict the high-pressure liquid densities of the different glycol oligomers for isotherms other than 323K (which was included in the experimental data set considered for the optimization procedure), and as depicted in **Figure. 3.6**, soft-SAFT provides a very good description of the $p\rho T$ diagrams of the studied compounds in a wide temperature and pressure range, with %ARDs lower than 0.20 for all the compounds. No systematic degradation of the quality of the results with pressure, temperature or M_w was observed, highlighting the robustness of the new parameters.



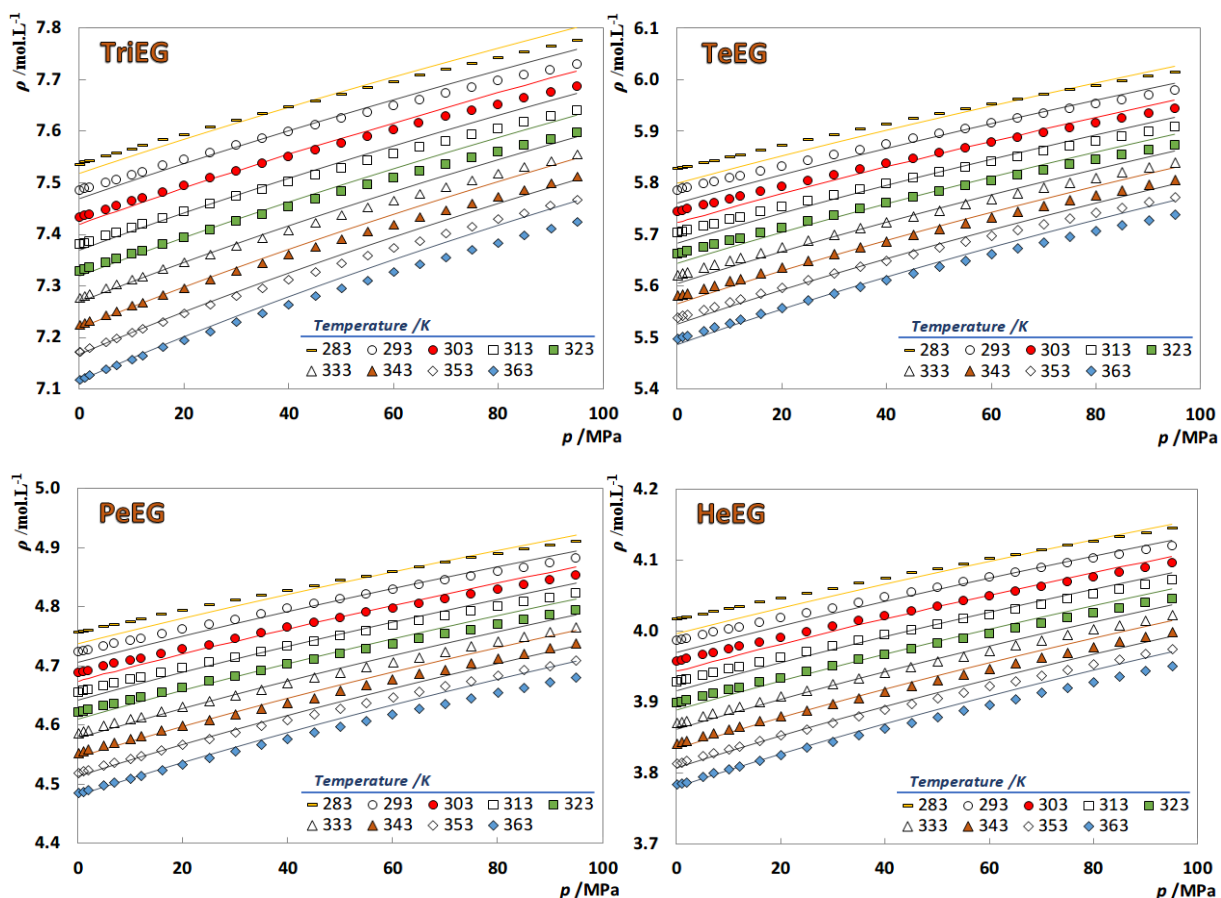


Figure 3.6. Density as a function of pressure and temperature for different glycols. The symbols represent experimental data,[119] while the solid lines represent the soft-SAFT results.

Furthermore, as commonly done for homologous series of compounds,[72–77,79,119–121] the optimized molecular parameters were successfully correlated with the glycols' M_w , in order to identify linear trends that may allow the prediction of the behaviour and properties of other glycols not used in the model's development. As depicted in **Figure 3.7**, the soft-SAFT molecular parameters for the non-associating part ($m, m\sigma^3, m\epsilon/k_B$) present a linear dependency with the glycols' M_w , which can be described by the following equations:

$$m = 0.01894 M_w (g \cdot \text{mol}^{-1}) + 0.7461; R^2 = 0.9976 \quad (3.3)$$

$$m\sigma^3 = 1.38015 M_w (g \cdot \text{mol}^{-1}) + 0.26992; R^2 = 1.000 \quad (3.4)$$

$$m\epsilon/k_B = 6.93761 M_w (g \cdot \text{mol}^{-1}) + 199.509; R^2 = 0.9974 \quad (3.5)$$

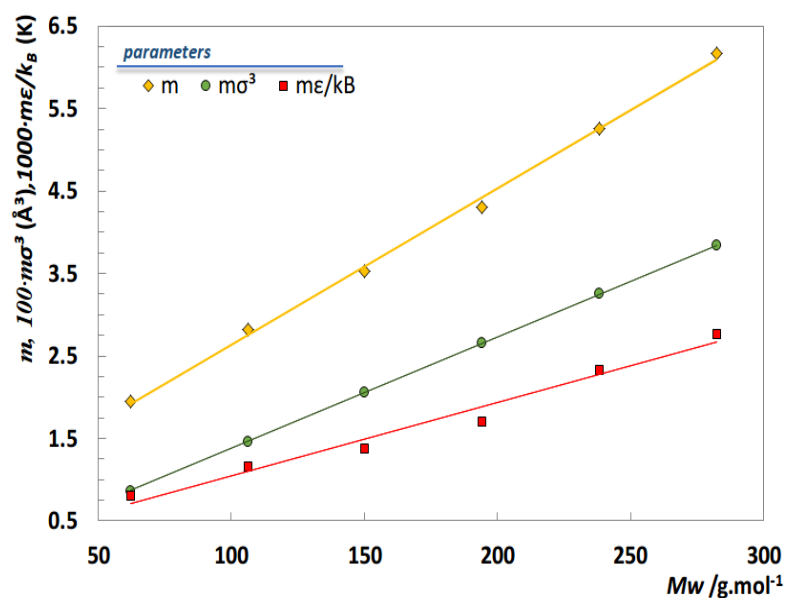


Figure 3.7. soft-SAFT molecular parameters as a function of the glycols molecular weight.

These relationships are possible due to the enhanced physical meaning of the soft-SAFT molecular parameters that allow the prediction of thermodynamic properties for other members of the homologous series. $m\sigma^3$ is directly related to the volume occupied by the molecule, while $m\epsilon/k_B$ refers to the energy of interaction per molecule, and both are expected to increase linearly due to the addition of EO groups. To evaluate the predictive ability of these correlations, the prediction of the $p\rho T$ data for PEG400 was attempted. PEG400 is usually a mixture of polyols with the generic formula $C_{2n}H_{4n+2}O_{n+1}$, with n between 8.2 and 9.1, and a M_w ranging from 380 to 420 $\text{g}\cdot\text{mol}^{-1}$. This mixture of polyols was treated following a pseudo-pure component approach with an average M_w of 400 $\text{g}\cdot\text{mol}^{-1}$, and the correspondent physical molecular parameters extrapolated from eqs. 3.3-3.5. The association parameters were kept constant for the whole series, except for EG. The representation of PEG 400 high-pressure density is shown in **Figure 3.8** and show a very good agreement with the experimental data, with a %ARD of only 0.22%.

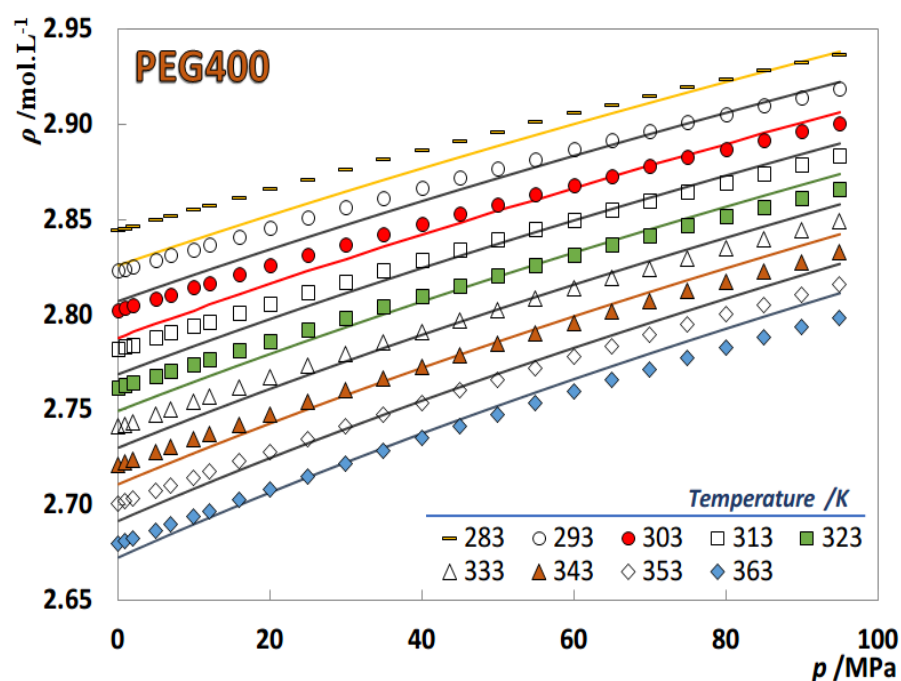
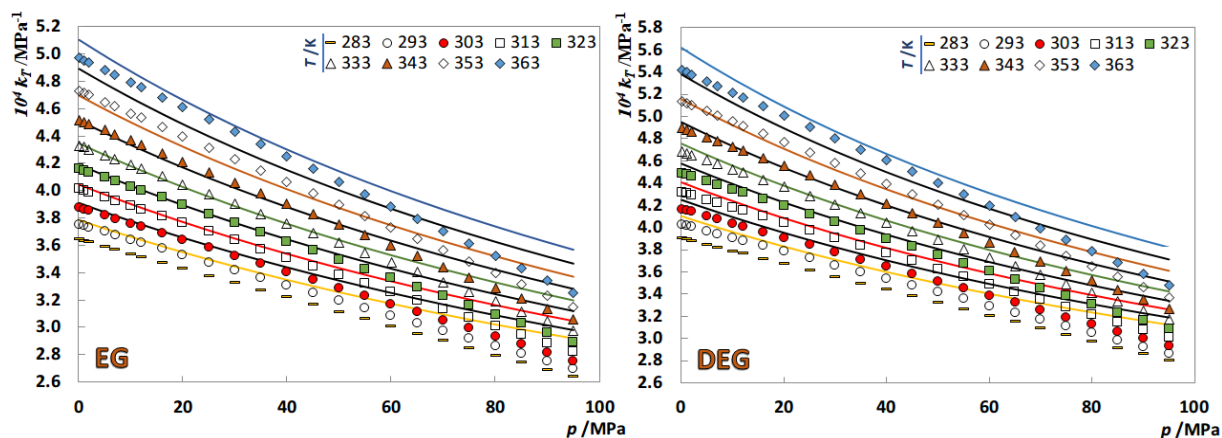


Figure 3.8. Density as a function of pressure and temperature for the PEG400. Symbols represent experimental data,[119] while the solid lines depict the soft-SAFT EoS predictions.

The values of k_T of the different glycols, estimated from the experimental $p\rho T$ data, were also calculated using the soft-SAFT EoS applying eq. 3.6 to the SAFT theory. This property reflects the volumetric changes of the pure glycol with pressure at a fixed temperature and, as can be seen in **Figure 3.9**, a clear dependency with pressure and temperature is observed, decreasing significantly as the pressure increases and temperature decreases. This behaviour is, as depicted in the same figure, well captured by the model even though a degradation of the predictions is observed as the glycols' chain length is increased.

$$k_T = \left(\frac{\partial \ln(\rho)}{\partial p} \right)_T \quad (3.6)$$



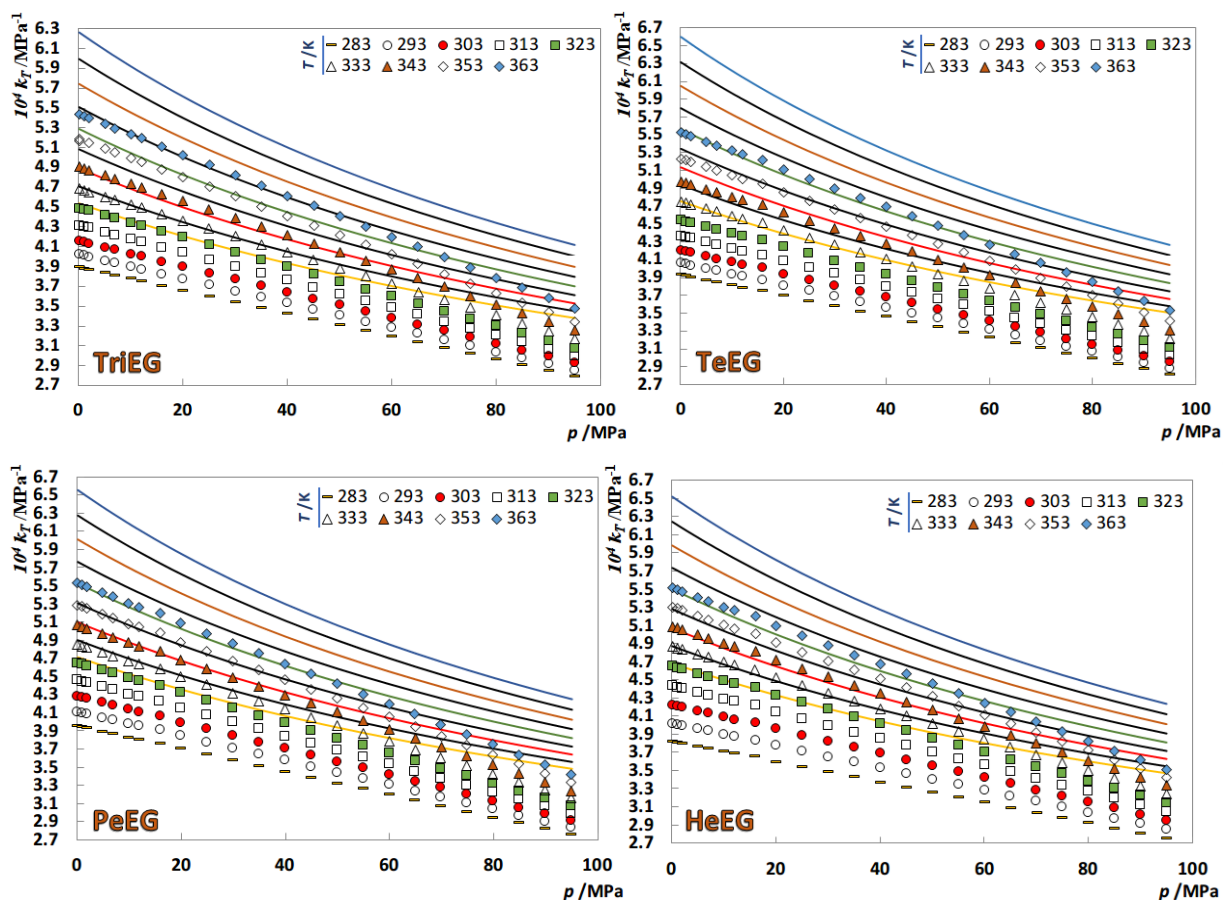


Figure 3.9. Isothermal compressibility of pure glycols as a function of pressure and temperature. Symbols represent estimates from the experimental ppT data,[119] while the solid lines represent the soft-SAFT predictions.

The α_p of the studied glycols were also predicted from the EoS modelling using the definition in eq. 3.7. The soft-SAFT predictions are plotted in **Figure 3.10**, along with the estimates from experimental data.[119] This property reflects the volumetric changes with temperature at a fixed pressure and present similar pressure and temperature dependencies to those of k_T , although becoming less pronounced as the chain length increases, an effect that is well predicted by the soft-SAFT model. Moreover, and as the pressure increases, the isobaric thermal expansivity presents a cross-over point, which can be understood as a macroscopic manifestation of the association phenomenon occurring at the molecular level, with the temperature increase leading to the breaking of hydrogen bonds, decreasing the magnitude of the intermolecular interactions that become dominated by dispersive forces. As depicted in **Figure 3.10**, soft-SAFT is capable of correctly describing this property and of predicting, although at higher pressures than observed in the experiments (for EG and DEG the crossover point exists beyond the pressure range shown in **Figure 3.10**), the occurrence of the above-mentioned phenomena.

$$\alpha_p = \left(\frac{\partial \ln(\rho)}{\partial T} \right)_p \quad (3.7)$$

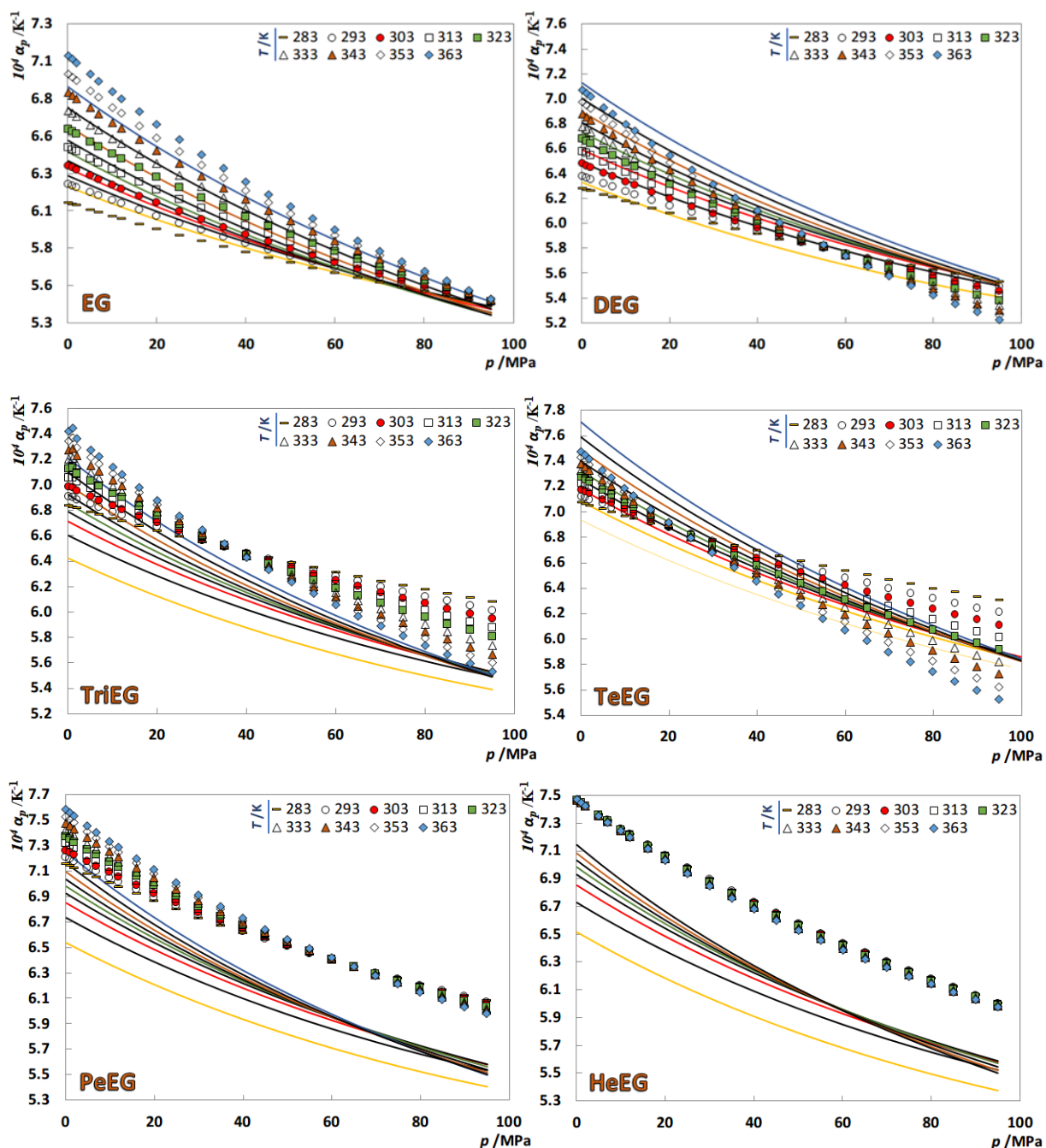


Figure 3.10. Isothermal expansivity of pure glycols as a function of pressure and temperature. Symbols represent estimates from the experimental data,[119] while the solid lines represent the soft-SAFT predictions.

Conclusions

In this work, a new CG model for glycols was developed in the framework of the soft-SAFT EoS. Aware of the limitation of the previous model by Pedrosa et al.[75] concerning the description of the pressure effect and second-order derivative properties, a new set of optimized molecular parameters was determined using the pure fluids VLE data (vapor pressures and saturated liquid densities), available for the glycol oligomers up to TeEG, and one isotherm of new experimental $p\rho T$ and k_T data, measured for glycol oligomers up to HeEG. Simultaneously, a more realistic association scheme, where the dual positive-negative nature of the terminal OH groups is considered, was assigned to the glycol molecules.

The optimized parameters and refined CG model were shown to provide an excellent description of the glycols VLE and $p\rho T$ data, while allowing for an improved description of the derivative properties, including the prediction of a crossover point in the isobaric expansivities, which demonstrates the ability of the model to capture the existent balance between hydrogen bonding and dispersive interactions. Furthermore, as previously done for other families of compounds, the molecular parameters were correlated with the glycols' M_w , while the association parameters were kept constant for all the members of the series (except for EG). The soft-SAFT EoS predictive ability was further evaluated by predicting the glycols and a light PEG (PEG400) high pressure density data in the entire pressure and temperature range. As shown, the new modelling scheme yielded a very good description of the $p\rho T$ data, with an %ARD of 0.17% for the studied glycol oligomers and of only 0.22% for the PEG 400 (note that no experimental data for the latter was used in the model's parameterization).

3.2- Extending the model to glymes

The content of this section is based on the following published works, developed in the framework of this PhD thesis, where E.A. Crespo was responsible for the modelling tasks and for writing the manuscripts, with substantial contributions from the remaining authors.

- Pablo Navarro, Emanuel A. Crespo, João M.L. Costa, Fèlix Llovell, Julián García, Francisco Rodríguez, Pedro J. Carvalho, Lourdes F. Vega, and João A.P. Coutinho, “*New Experimental Data and Modeling of Glymes: Toward the Development of a Predictive Model for Polyethers*”, Ind. Eng. Chem. Res, 56 (2017) 7830-7844, DOI: 10.1021/acs.iecr.7b01532.
- Emanuel A. Crespo and João A.P. Coutinho, “*A Statistical Associating Fluid Theory Perspective of the Modeling of Compounds Containing Ethylene Oxide Groups*”, Ind. Eng. Chem. Res. 2019, 58, 3562-3582, DOI: 10.1021/acs.iecr.9b00273

Introduction

When compared with glycols, studies involving the application of SAFT-type EoSs to the thermodynamic modelling of glymes are much scarcer. From a literature survey,[112] only three works were found, all concerning the modelling of di-alkyl ethers.

Kiesow et al.,[122] applied the PC-SAFT EoS to study the oiling-out effect of blends of polyethylene glycol dimethyl ethers (PEGDME). The phase equilibria of two different blends, PEGDME 2000 and PEGDME 1000 in different solvents, namely diethylketone, ethylacetate, and 2-propanol were investigated. As the modelling of smaller glymes was not addressed in this work, the PEGDME blends were modelled under a pseudo-pure component approach in which their molecular parameters (m_i as a function of M_w) had to be regressed along with a BIP to the solubility data of PEGDME 2000 + diethylketone. The BIP of PEGDME/ethyl acetate and PEGDME/2-propanol were then fitted to the correspondent solubility data. Afterwards, the parameters were transferred to PEGDME 1000 and used to satisfactorily predict the solubility data in the different solvents.

Nannan et al.,[123] applied the same EoS to the modelling of PEGDME solvents, but in this case, the pure-component parameters for the first four members of the di-alkyl glymes, namely ethylene glycol dimethyl ether (EGDME), diethylene glycol dimethyl ether (DEGDME), triethylene glycol dimethyl ether (TriEGDME), and tetraethylene glycol dimethyl ether (TeEGDME) were first obtained by fitting to the experimental VLE data of the pure fluids. Then, the optimized parameters were used to develop correlations as a function of the glymes' M_w . These correlations were then used to obtain the pure-component parameters for glymes containing 5 to 9 EO groups and used to predict the Selexol's liquid

density, and heat capacity, considering an approximate mixture composition, achieving a reasonable agreement with the experimental data. Polishuk and Yitzhak,[124] applied the SAFT + Cubic EoS[125] to describe the properties of TriEGDME. Even though the proposed parameters were shown to be able to accurately describe the liquid densities, speed of sound, and isothermal compressibility, results for the vapor pressure were not provided. Furthermore, the simultaneous accurate description of both densities and derivative properties may be attributed to the higher number of parameters required by this particular EoS, where five parameters are necessary to describe a non-associating molecule.

All these three works describe the di-alkyl glymes as non-associating species, which although true in the works of Nannan et al.,[123] and Polishuk and Yitzhak,[124] where only pure components were addressed, constitutes an approximation to be aware of in the work of Kiesow et al.,[122] where binary mixtures with self-associating components, such as 2-propanol, were also described. From these works, only the work of Nannan et al.,[123] addressed the modelling of both low and high M_w di-alkyl glymes, but none of them addressed both mono- and di- alkyl glymes in the same study, nor the importance of including derivative properties in the model's parameterization.

Therefore, given the encouraging results obtained for glycols in the previous section, the same modelling approach is here extended for the thermodynamic modelling of glymes (glycol ethers). Within the same laboratory where this PhD project was carried out, new ppT data was measured for eight different glymes in wide ranges of temperature (283 – 363 K) and pressures (0.1 – 95 MPa) and used in this work to guide the selection and optimization of the soft-SAFT model parameters for glymes. The investigated compounds and the range of experimental conditions allow to analyse the performance of the model to describe the combined effects of pressure, temperature, number of EO groups, and the loss of the capability to establish hydrogen bonds, through the replacement of the hydroxyl groups by a methyl or ethyl group, on densities and second-order derivative properties. Ultimately, the robustness of the proposed molecular model is tested against density data available in literature for polyethylene glycol dimethyl ether 250 (PEGDME250), a blend of di-alkyl ethers similar to the Selexol solvent used in natural gas processing.

The proposed molecular parameters were further correlated with the glymes' M_w , as commonly performed for homologous series, and were compared to the parameters obtained for other well-established families, allowing a thorough discussion on their physical meaning and on the reliability of the applied model. It is shown how paying attention to one of the strongest features of SAFT-type equations, as the physical meaning of its parameters, is crucial to allow the development of reliable models for different families of compounds.

Modelling Approach

A careful selection of a number of different glymes that would allow the evaluation of different structural effects such as the compounds' chain length and the replacement of the hydrogen (s) of the glycols hydroxyl group(s) with a methyl or ethyl group on their thermophysical properties was carried out. Hence, eight different glymes were studied here, four mono-alkyl ethers: ethylene glycol ethyl ether (EGEE), diethylene glycol ethyl ether (DEGEE), diethylene glycol methyl ether (DEGME), and tetraethylene glycol methyl ether (TeEGME), and four di-alkyl ethers: diethylene glycol diethyl ether (DEGDDE), diethylene glycol dimethyl ether (DEGDME), triethylene glycol dimethyl ether (TriEGDME), and tetraethylene glycol dimethyl ether (TeEGDME). The chemical structures of these glymes are shown in **Table 3.3**.

Table 3.3. Name, chemical structure, and molecular weight of the studied glymes.

Compound	Chemical structure
Ethylene glycol ethyl ether (EGEE) $M_w = 90.12 \text{ g}\cdot\text{mol}^{-1}$;	
Diethylene glycol ethyl ether (DEGEE) $M_w = 134.17 \text{ g}\cdot\text{mol}^{-1}$;	
Diethylene glycol diethyl ether (DEGDDE) $M_w = 162.23 \text{ g}\cdot\text{mol}^{-1}$;	
Diethylene glycol dimethyl ether (DEGDME) $M_w = 134.17 \text{ g}\cdot\text{mol}^{-1}$;	
Triethylene glycol dimethyl ether (TriEGDME) $M_w = 178.23 \text{ g}\cdot\text{mol}^{-1}$;	
Tetraethylene glycol dimethyl ether (TeEGDME) $M_w = 222.28 \text{ g}\cdot\text{mol}^{-1}$;	
Diethylene glycol methyl ether (DEGME) $M_w = 120.15 \text{ g}\cdot\text{mol}^{-1}$;	
Tetraethylene glycol methyl ether (TeEGME) $M_w = 208.25 \text{ g}\cdot\text{mol}^{-1}$;	

These glymes are here modelled following the same philosophy as previously proposed for glycols. Hence, for each mono-alkyl ether, one associating site 'A' (binary) is assigned, mimicking the dual donor/acceptor nature of the hydroxyl group, and allowing for 'A-A' interactions. Conversely, the di-alkyl ethers studied in this work are considered as non-associating compounds given the absence of hydroxyl end groups. The hydrogen bonding character of the inner EO groups is, in this case, implicitly accounted for by the specific values of the non-associative molecular parameters, without the inclusion of the association term. This strengthens the importance of obtaining optimal molecular parameters for the different species, not only in terms of fitting accuracy, but also in terms of physical meaning and

consistency as, for instance, the values of the molecular parameters are the only thing distinguishing the CG model of di-alkyl glymes and n -alkanes. A sketch of the proposed molecular models for glymes is depicted in **Figure 3.11**.

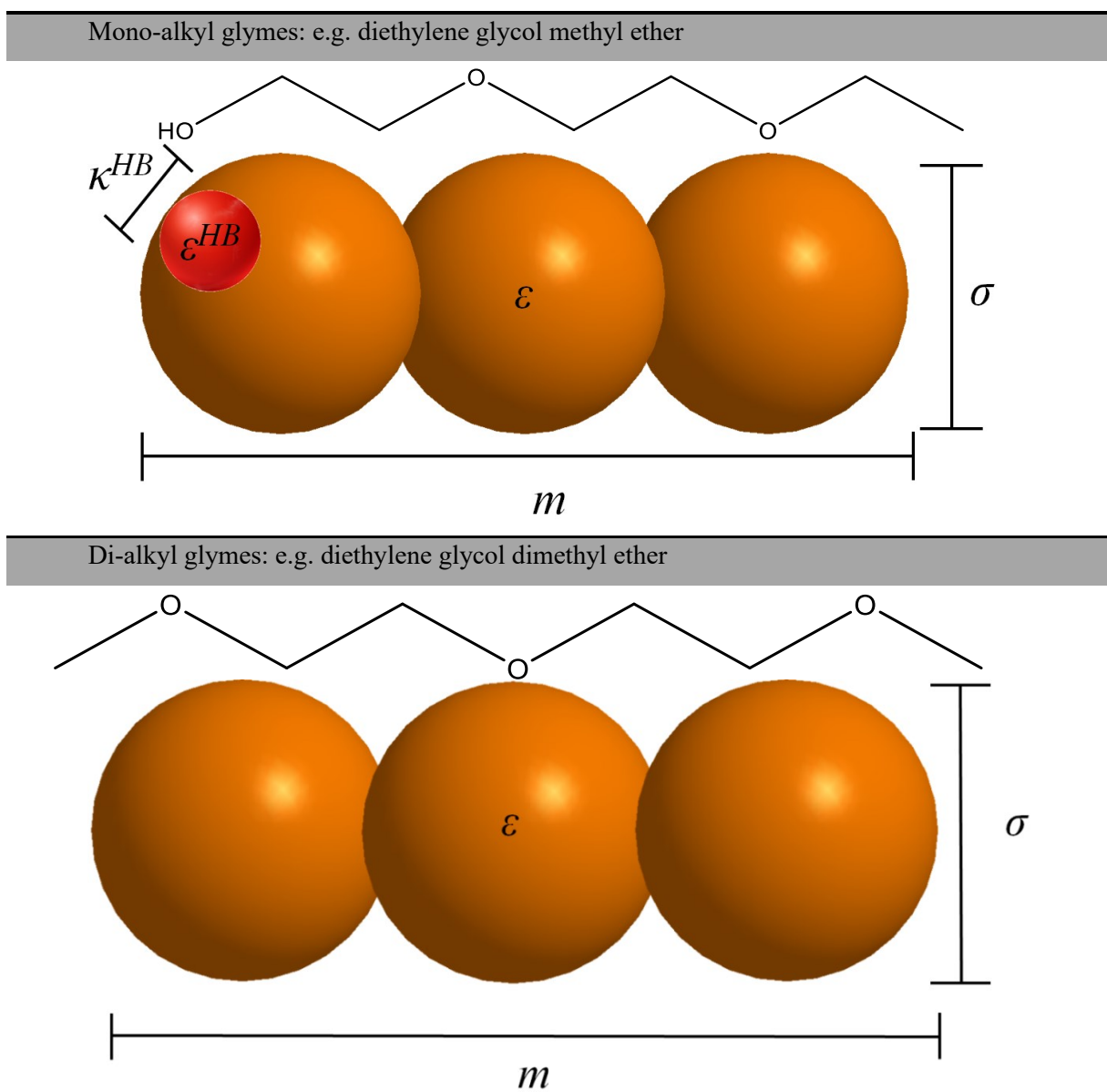


Figure 3.11. Sketch of the proposed molecular models for mono- and di-alkyl glycol ethers.

Results

The parameterization of the different glymes was carried out using the same OF used for glycols (eq. 3.1) and the optimal soft-SAFT pure-component parameters are reported in **Table 3.4**, along with the %ARD relatively to the experimental $p\rho T$ data, and to the estimated k_T , and α_P data.

Table 3.4. soft-SAFT pure-component parameters for the studied glymes and deviations from the experimental data.

Glyme	m_i	σ_{ii} (Å)	ε_{ii}/k_B (K)	ε^{HB}/k_B (K)	κ^{HB} (Å ³)	%ARD _{$p\rho T$}	%ARD _{k_T}	%ARD _{α_P}
EGEE	2.705	3.721	294.87	3450	2600	0.086	5.62	3.90
DEGME	2.995	3.889	330.50	3450	2600	0.13	9.63	2.80
DEGEE	3.165	4.009	331.00	3450	2600	0.16	9.13	5.14
TeEGME	4.481	4.061	353.23	3450	2600	0.17	12.9	5.75
DEGDME	3.300	3.955	308.15	-	-	0.28	17.2	2.60
DEGDDE	3.586	4.165	309.43	-	-	0.35	20.2	6.10
TriEGDME	4.021	4.039	318.12	-	-	0.34	22.3	3.09
TeEGDME	4.696	4.107	322.68	-	-	0.41	28.4	2.95
PEGDME298	5.913*	4.166*	330.85*	-	-	-	-	-

*- Extrapolated from eqs. 3.10-3.12.

The results obtained for the saturated liquid densities and vapor pressures of pure glymes using these parameters are presented in **Figure 3.12** and **Figure 3.13**. A good description of the glymes' VLE is obtained with overall %ARDs for the glymes' saturated liquid and vapor densities and vapor pressures of 0.33%, 7.66%, and 7.80%, respectively. These values are similar to those obtained for glycols, although with a slight improve of the vapor pressures' description.

The soft-SAFT description of the high-pressure liquid densities of the different glymes is shown in **Figure 3.14**, and as can be observed the molecular model and assumptions proposed here allow for a very good description of the experimental data with a maximum %ARD of 0.41%, as reported in **Table 3.4**.

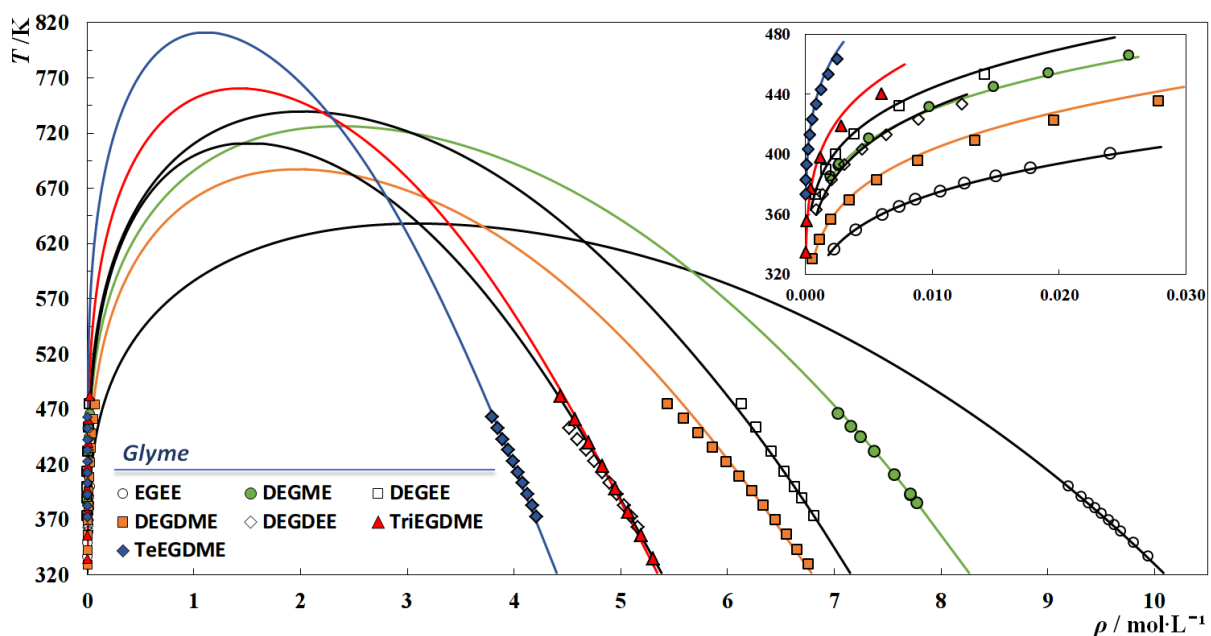


Figure 3.12. Saturated liquid and vapor densities as a function of temperature for different glymes. Symbols represent experimental data,[118] while the solid lines depict the soft-SAFT EoS fitting to the data.

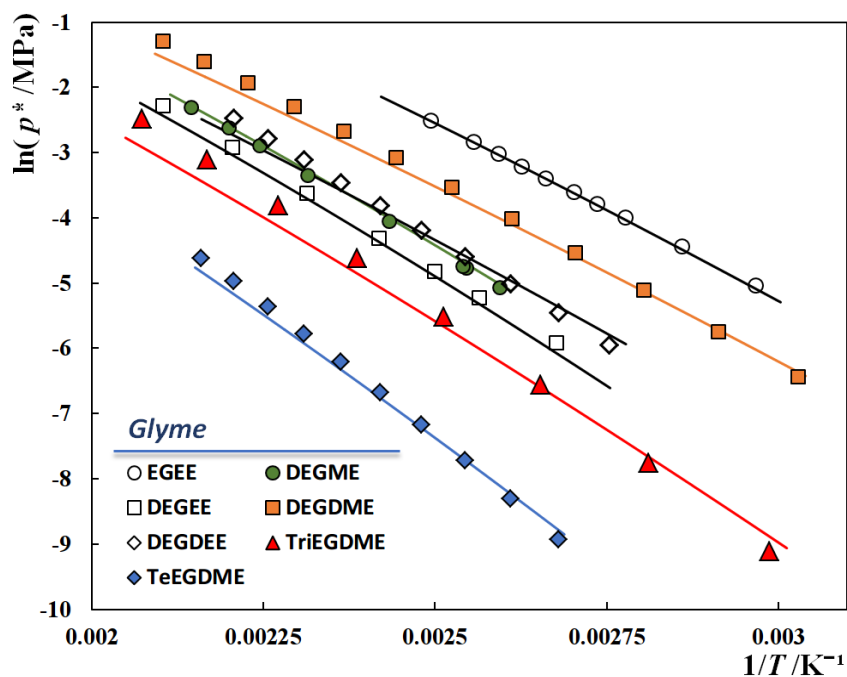
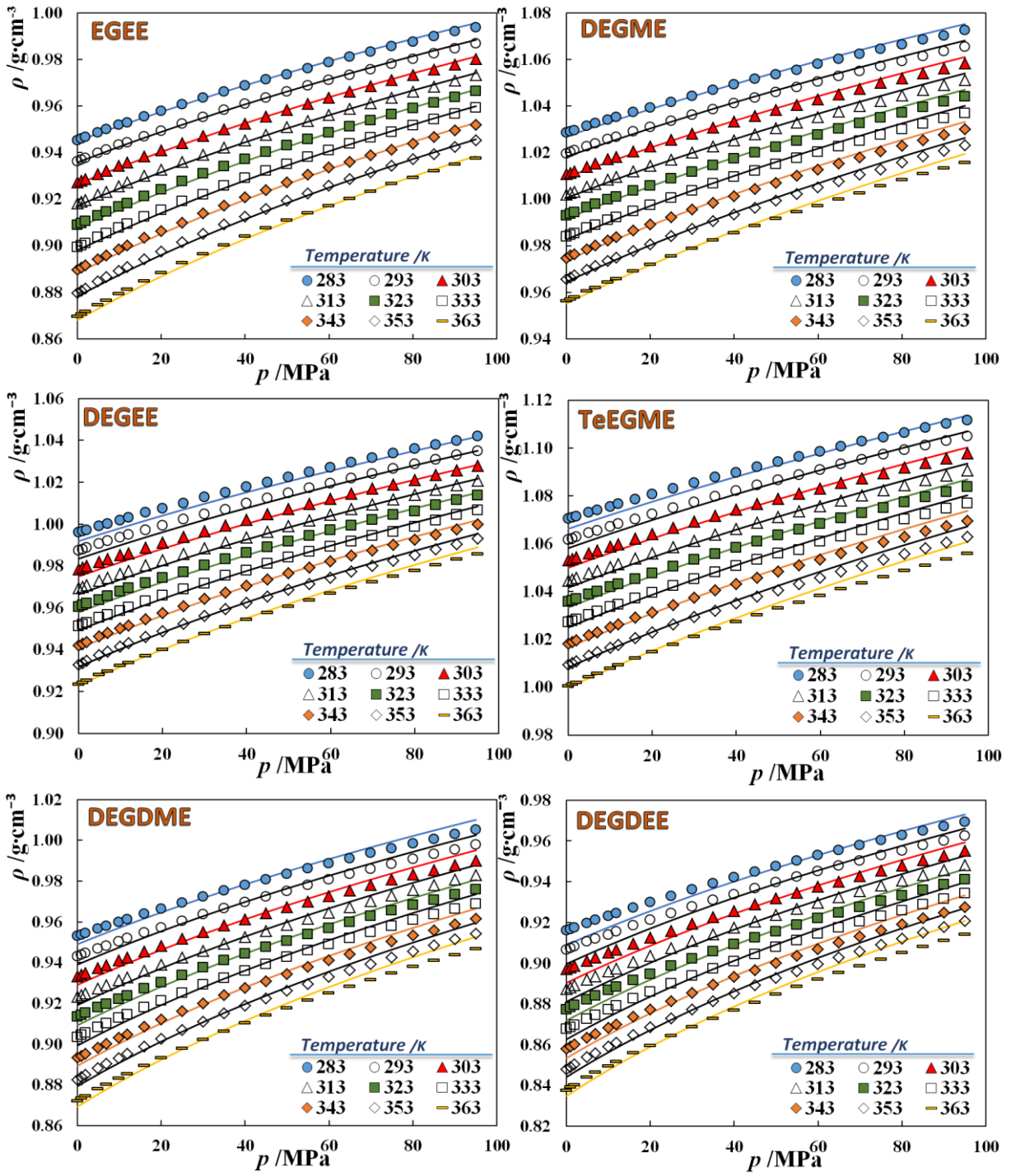


Figure 3.13. Logarithm of the vapor pressure, p^* , as function of the inverse of temperature for the studied glymes. Symbols represent experimental data,[118] while the solid lines represent the soft-SAFT EoS fitting to the data.



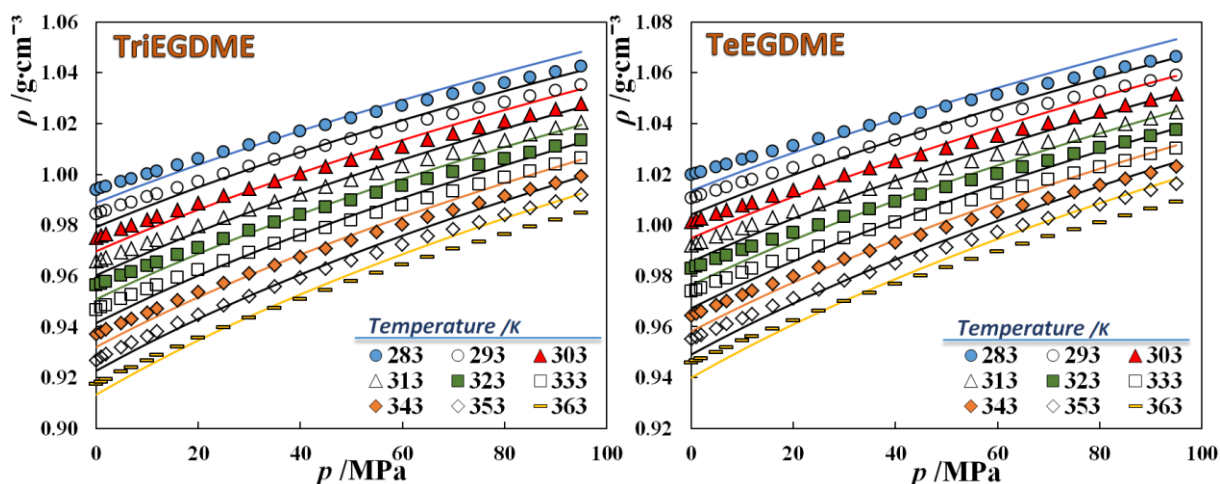


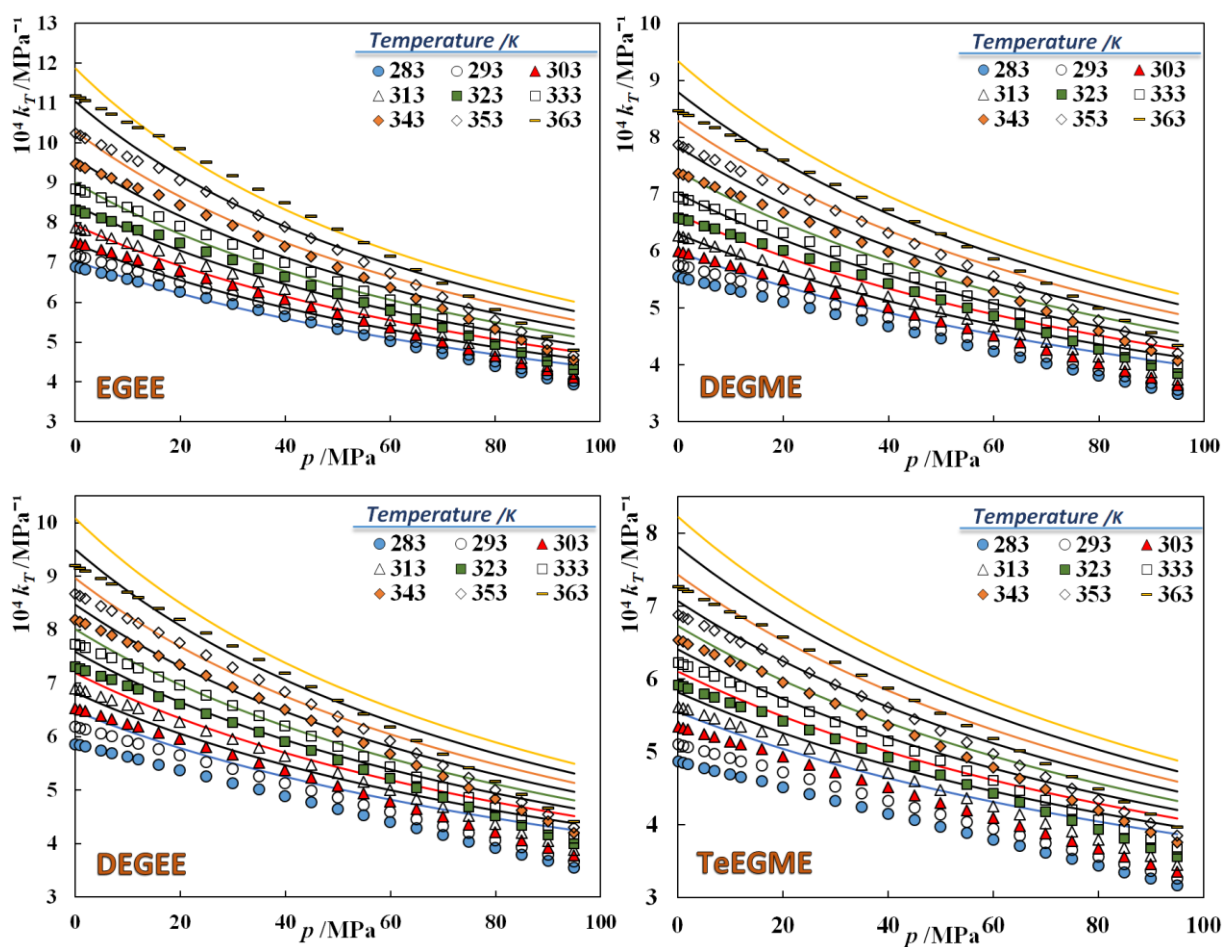
Figure 3.14. Density as a function of p and T of the studied glymes. Symbols represent the experimental data,[120] while the solid lines represent the soft-SAFT results.

As can be inferred from **Table 3.4**, low deviations of the experimental $p\rho T$ data were obtained with an overall %ARD of 0.240%. The very good description of the experimental data shows that the addition of one single isotherm (@323K) of high-pressure data to the experimental data set used for the model's parameterization, enables the model to correctly describe the effect of both temperature and pressure in the entire temperature and pressure ranges where experimental data has been measured.

Nevertheless, it can be observed that these deviations tend to increase both with the chain length of the glyme and with the removal of the hydroxyl end groups (i.e., from mono-alkyl ethers to di-alkyl ethers). This increase with the removal of the hydroxyl end groups shows the relative importance of the EO groups being neglected (in terms of association sites), since when a hydroxyl end group is present and self-association of the molecule considered (as it is the case for mono-alkyl ethers), the associating interactions involving the EO groups can still be masked by the association term. Conversely, for the di-alkyl ethers, modelled here as non-associating species, the model does not consider the EO groups any different than the alkyl groups in an n -alkane molecule. Instead, the influence of the EO groups in the overall energy of the molecule is implicitly considered by the specific values of the physical parameters. Moreover, the increase of the glymes' chain length also deteriorates the description of the high-pressure thermodynamic properties, as previously observed for glycols in **Chapter 3. 1**.

A challenging test to any molecular approach would be to check its ability to provide other thermodynamic properties of the studied glymes not used for the model parameterization. Therefore, as derivative properties usually present some singularities observed experimentally,[126] an accurate description of the physical features behind second-order derivative properties remains highly relevant to

validate the model proposed here as well as the robustness of the fitted parameters. For this reason, the molecular parameters from **Table 3.4**, were further applied to predict the k_T and α_p of the studied glymes, whose results are shown in **Figure 3.15** and **Figure 3.16**, while the deviations to the experimental data are also reported in **Table 3.4**. As can be seen in both figures, a good qualitative (and in some cases, quantitative) agreement was found with overall %ARDs of 15.7% and 4.04% for k_T and α_p , respectively. The low deviations obtained for α_p show that, as expected, the temperature effect is very well captured by soft-SAFT. However, despite the very good qualitative description, higher deviations were observed for k_T . Again, the deviations from the experimental data were found to increase with the glymes' M_w i.e., with the increase of the number of EO groups being “neglected”.



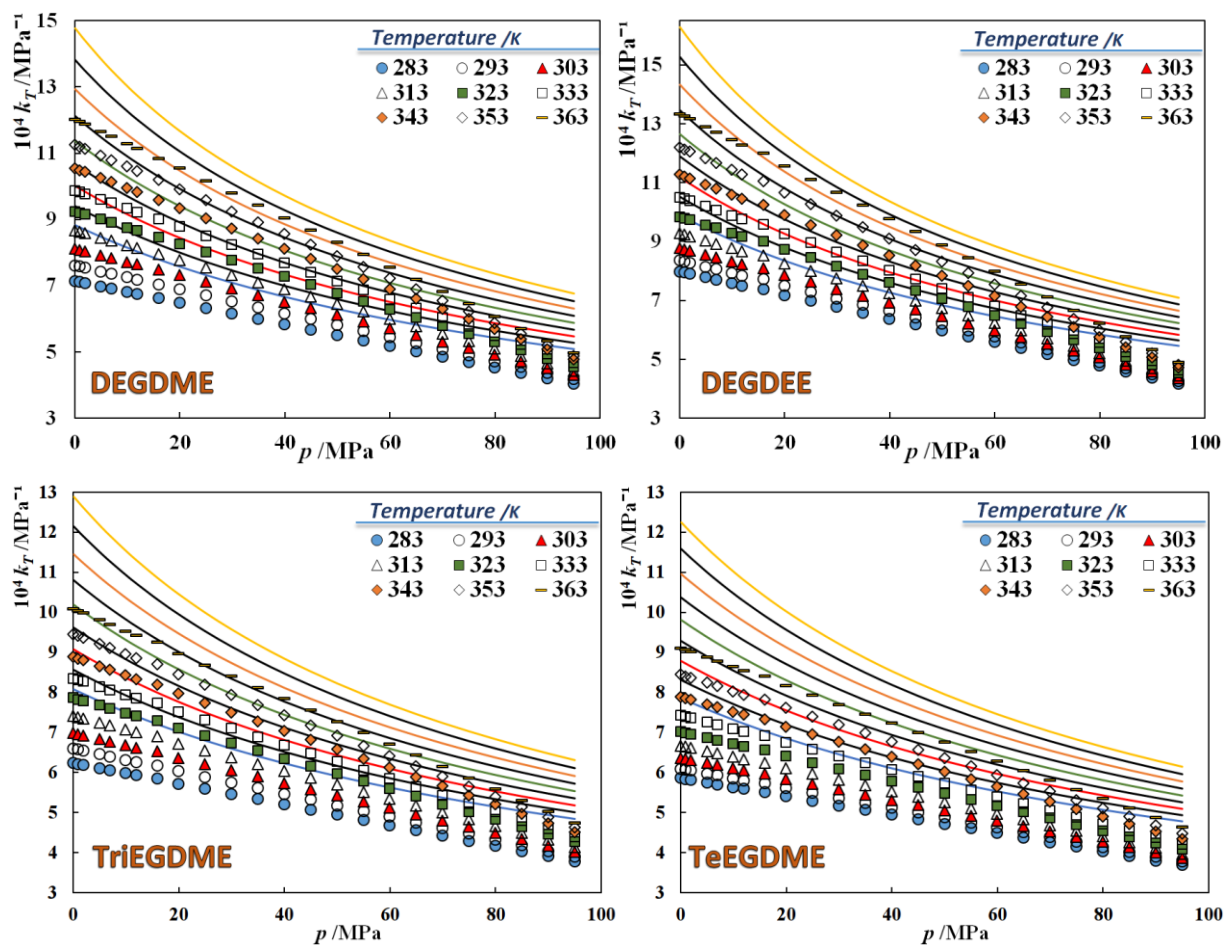
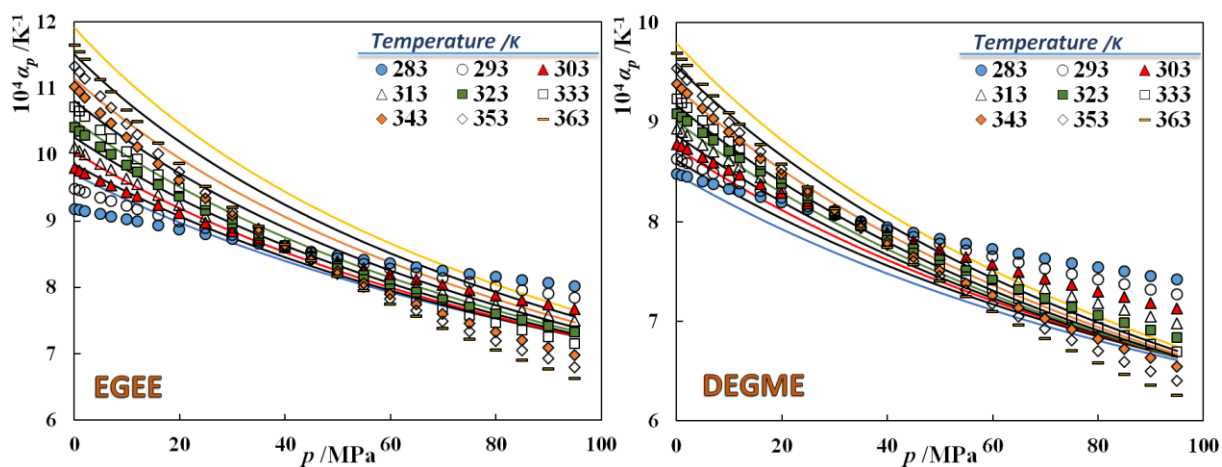


Figure 3.15. Isothermal compressibility, k_T , as function of pressure and temperature for the studied glymes. Symbols represent experimental data,[120] while the solid lines represent the soft-SAFT predictions.



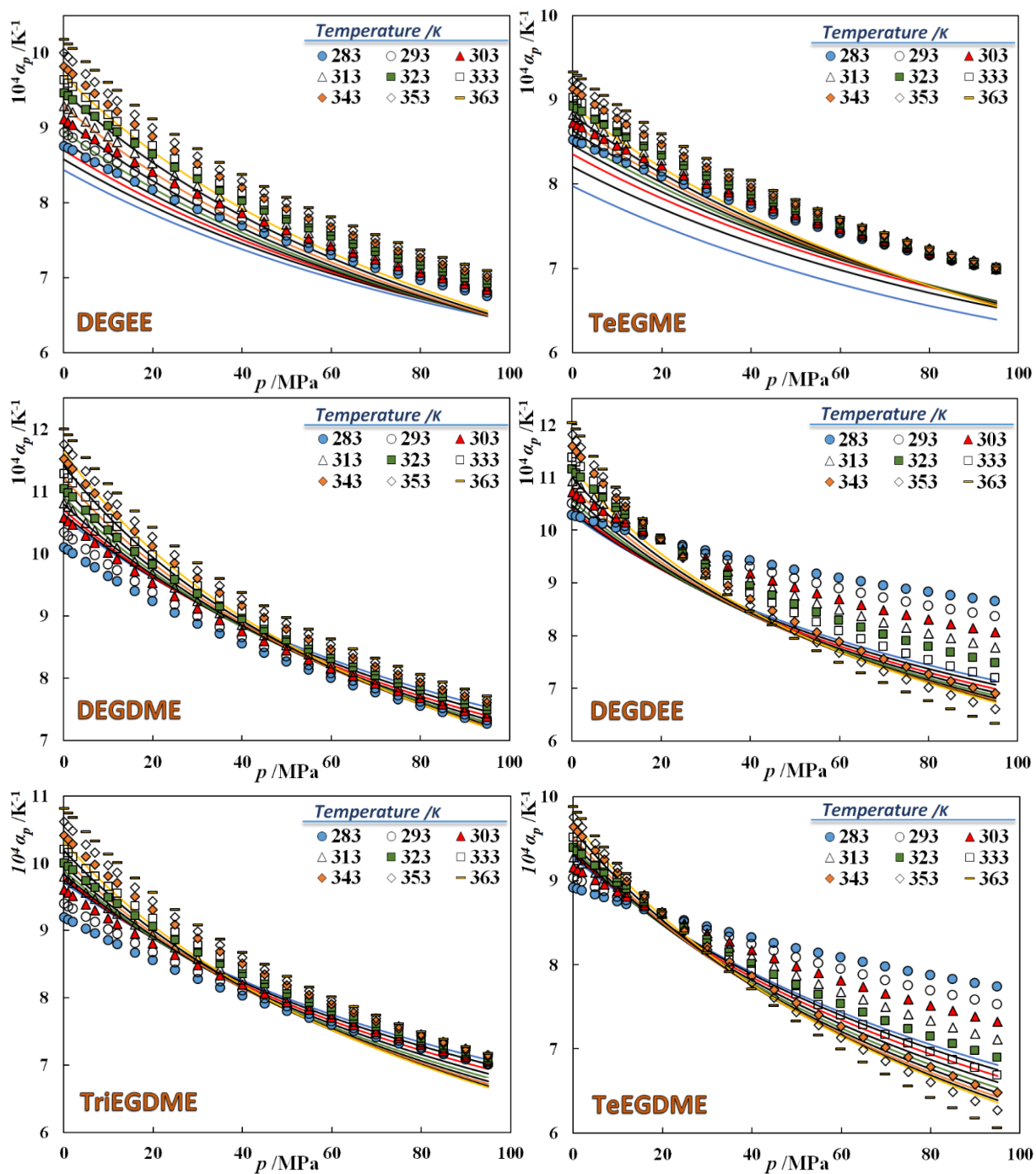


Figure 3.16. Isobaric thermal expansivity, α_p , as function of pressure and temperature for the studied glymes. Symbols represent experimental data, while the solid lines depict the soft-SAFT predictions.

As depicted in **Figure 3.15**, an increase in the number of EO groups leads to smaller temperature and pressure dependencies of k_T , which are nevertheless, well captured by the model. Additionally, and

similar to what was observed for glycols, α_p presents a crossover point related to a decrease of the intermolecular interactions, with hydrogen bonds breaking due to the temperature increase. The soft-SAFT EoS was able to correctly describe this property, and to predict the occurrence of this crossover point. However, within the experimental pressure range, the EoS predicts the crossover point only for the di-alkyl glymes. The crossover point is also predicted for the mono-alkyl glymes but at pressures ranging from 150 MPa, for TeEGME, to 650MPa, for the EGEE. The model denotes a decrease of the pressure at which the crossover point appears as the glymes' chain length increases and with the replacement of a hydroxyl end group by an alkyl group. Nonetheless, given the sensitivity of derivative properties to inaccuracies in the models or equations, the good results provide evidence of the robustness of the proposed model and molecular parameters.

As mentioned in **Chapter 2**, one of the main advantages of SAFT-type EoSs is that their parameters have a solid physical meaning. However, in several cases, SAFT models are used almost in an empirical manner, with little attention paid to the meaning of these parameters and their possible transferability. A clear example of this limitation is the case of water, for which several molecular models and sets of parameters have been proposed, even within the same SAFT variant and same type of experimental data used for the fitting procedure.[127] Therefore, when a new molecular model and parameters are proposed, a discussion on their physical meaning and transferability becomes relevant.

Since in soft-SAFT compounds are modelled as homonuclear chains, different values of m_i , σ_{ii} , and ε_{ii} are expected for each member of a homologous series. However, σ_{ii} and ε_{ii} should tend to an asymptotic value with an increase of the chain length, since the addition of more repeating units to already long chains does not significantly modify the molecules' structure, and the influence of the hydroxyl end-groups also decreases. This behaviour is depicted in **Figure. 3.17** for the different polyethers studied here (glycols and glymes), along with the parameters previously proposed for *n*-alkanes[72] and alkan-1-ols.[74] Another interesting result is that these parameters increase linearly with the M_w , within an homologous series, as showed by Kraska and Gubbins[128] and Vega and collaborators[72–77,79,90,121] for different chemical families. These physical trends observed for the pure component parameters of SAFT-type EoSs allow the transferability of the parameters to different members within a homologous series, allowing for the prediction of the thermodynamic behaviour of higher chain length members for which no VLE data are available, and no parameters were fitted. These linear trends are also observed in the molecular parameters proposed here for glymes and those previously obtained for glycols. However, since the mono-alkyl ethers (glymes m-ether in **Figure. 3.17**) are considered as associating species and the di-alkyl ethers (glymes d-ether in **Fig. 3.17**) are considered as non-associating species, significant differences between them are to be expected, especially in the

dispersive energy parameter, as can be observed in **Figure 3.17c**). Thus, both types of glymes were considered as different families and the correspondent linear trends were obtained separately for each type of glymes and are reported in **Table 3.5**.

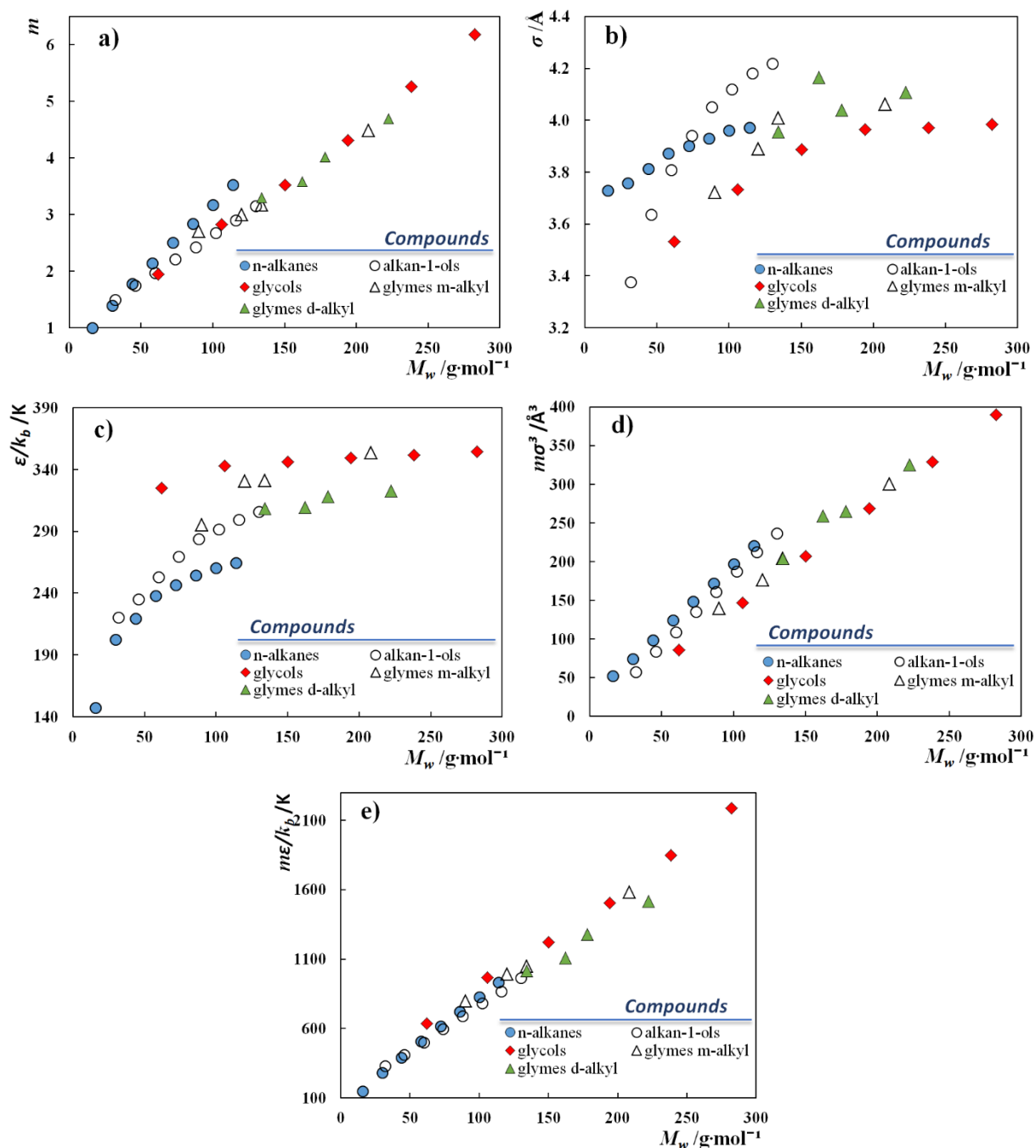


Figure 3.17. Trends of the soft-SAFT pure-component parameters for different families of compounds, as a function of their molecular weight.[120]

Table 3.5. soft-SAFT molecular parameters for glymes as a function of the molecular weight.

Mono-alkyl ethers	
$m = 0.01553 M_w(g \cdot mol^{-1}) + 1.191$	$R^2 = 0.9827$ (3.8)
$m\sigma^3 = 1.368 M_w(g \cdot mol^{-1}) + 15.90$	$R^2 = 0.9974$ (3.9)
$m \varepsilon/k_B = 6.687 M_w(g \cdot mol^{-1}) + 180.61$	$R^2 = 0.9963$ (3.10)
Di-alkyl ethers	
$m = 0.01633 M_w(g \cdot mol^{-1}) + 1.055$	$R^2 = 0.9818$ (3.11)
$m\sigma^3 = 1.327 M_w(g \cdot mol^{-1}) + 32.15$	$R^2 = 0.9743$ (3.12)
$m \varepsilon/k_B = 5.864 M_w(g \cdot mol^{-1}) + 208.59$	$R^2 = 0.9746$ (3.13)

Furthermore, the correlations with the M_w obtained for the di-alkyl ethers (eqs. 3.11-3.13) were used to predict the liquid densities at atmospheric pressure of the polyethylene glycol dimethyl ether 250 (here denoted PEGDME 298) reported by Conesa et al.[129] The mixture of ethylene glycol dimethyl ethers with different n values ($n=3$ to 9), where n is the number of EO groups, is here modelled under a pseudo-pure component approach ($n=5.723$ and $M_w=298.21$ g/mol) and, as depicted in **Figure. 3.18**, the model was able to accurately predict the experimental density data with a %ARD of only 0.35%. Note that the data was predicted from the correlations of the molecular parameters. Thus, these results support the model's transferability and validate the assumptions therein, showing that, even for a blend of di-alkyl ethers, similar to the solvent typically used in natural gas processing, the influence of the EO groups can be implicitly accounted for by the effective values of the non-associating molecular parameters.

As mentioned, the differences between the two types of glymes are expected to be more relevant on the energy parameter. Therefore, the values of m_i and σ_{ii} of both series seem to be consistent, showing a very similar linear dependency with M_w both on m_i and $m_i\sigma_{ii}^3$. However, an outlier is observed on the segment diameter of DEGDEE. This deviation of the DEGDEE pure-component parameters from the behaviour of the remaining glymes can be understood by the larger size of both diethyl end-groups, since DEGDEE was the only diethyl ether amongst the di-alkyl ethers evaluated. Moreover, and according to **Figure. 3.17a**, the linear dependency of m_i with the M_w seems to be common to the different families, except for the n -alkanes. This general behaviour of the chain length parameter shows that the introduction of inner-chain groups, like EO groups, and the removal or addition of similar functional end-groups (e.g. hydroxyl groups) have only a slight effect on m_i per unit of molar mass, but have a higher impact on the monomer's size, σ_{ii} . Note that the molecular volume is directly related to both by $m_i\sigma_{ii}^3$. As depicted in **Figure. 3.17b**, the introduction of EO groups in the glyme molecule results in lower segment diameter

increments than those observed for the methylene group addition in the *n*-alkanes and alkan-1-ols, due to the lower volume of the oxygen atoms. Moreover, the alkylation of the end groups also increases the segment diameter (CH_3O is bulkier than OH) and thus, the segment diameters proposed here for glymes are higher than the ones previously obtained for glycols.

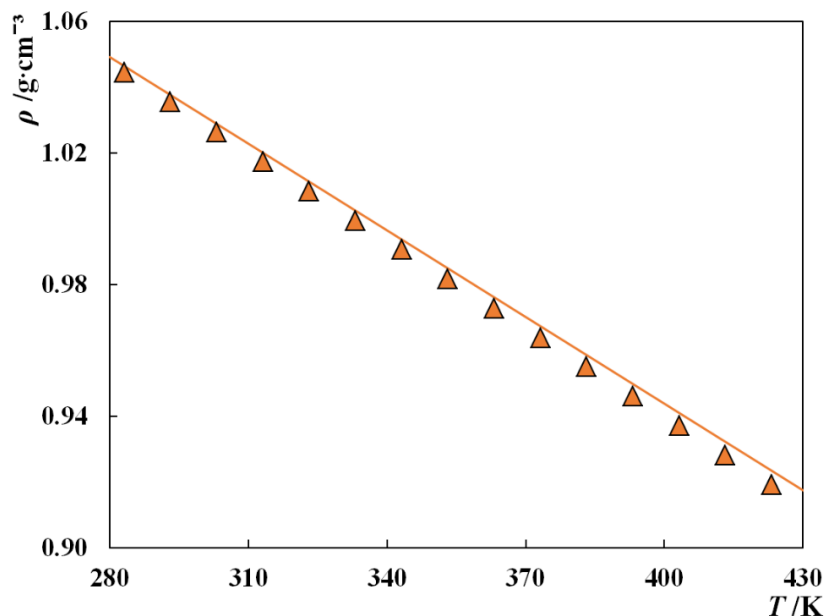


Figure 3.18. Liquid density data for PEGDME250. Symbols represent the experimental data,[129] while the solid line depicts the soft-SAFT predictions.

Concerning the dispersive energy parameter, ϵ_{ii} , significant differences are observed between the different families. As can be seen in **Figure 3.17c**, the dispersive energies proposed here for glymes and glycols show the following trend:

$$n - \text{alkanes} < di - \text{alkyl ethers} \sim \text{alkan} - 1 - \text{ols} < mono - \text{alkyl ethers} < \text{glycols}$$

The observed trend denotes that an increase in the associative character of the compound is reflected in an increase in its dispersive energy parameter, since some of the associative behaviour of the hydroxyl groups is being incorporated into the dispersive term of soft-SAFT. Moreover, the EO groups are considered in an effective manner, without the inclusion of additional sites, resulting in higher dispersive energies and explains the similarity of the values obtained for the di-alkyl glymes and the alkan-1-ols family.

Given the short range and highly directional character of association forces, the association parameters are often kept constant within each family, except for the first or first two members, as these interactions are generally not strongly influenced by the compounds' chain length except for the shortest

members of the series. The association parameters for alkan-1-ols, glycols and mono-alkyl ethers are depicted in **Figure 3.19**. Both, for glycols and alkan-1-ols, the first member (or first two members) has different association parameters compared to the heavier members, showing a much higher energy or volume of association. Note that, in this case, the association is not hindered by steric effects present within the longer molecules. For the mono-alkyl ethers studied in this work the association energy was transferred from the alkan-1-ols, while the association volume was transferred from glycols. This transferability and similarity between the association parameters of these compounds was already expected since the same associative functional groups are being considered (hydroxyl groups) with the differences between the three families being related to the number of hydroxyl end groups (justifying the different association energy values between glycols and glymes), but also due to the influence of the EO groups that can be masked by the association term (this explaining the difference in association volume of alkan-1-ols and glymes).

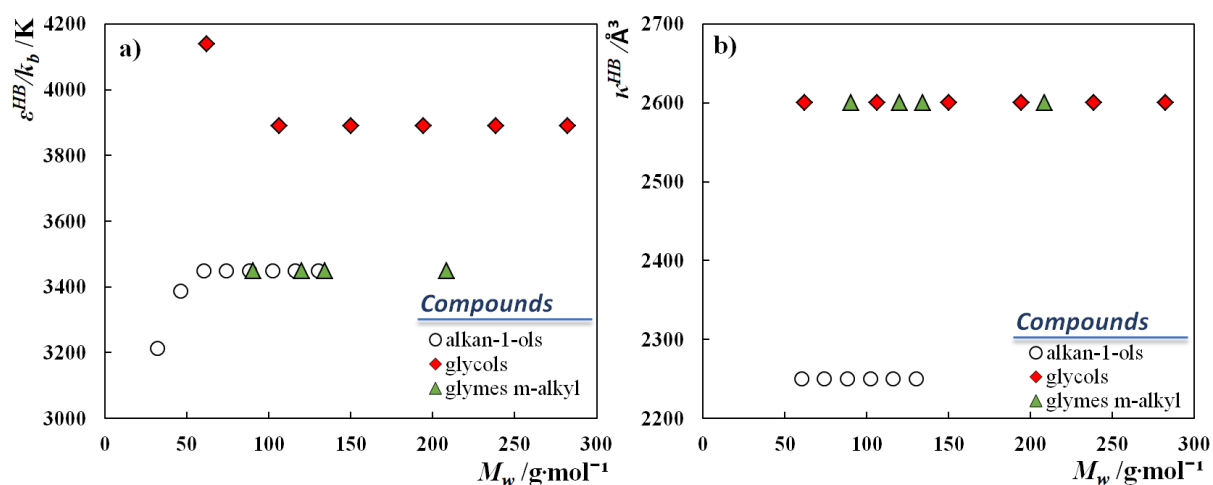


Figure 3.19. soft-SAFT association parameters for three families of compounds.

In summary, the robustness of the molecular parameters, exhibiting the expected trends and values, along with the very good descriptions obtained for VLE, $p\rho T$, and second-order derivative properties, both for glymes and glycols, emphasize the reliability of the simple model proposed here.

Conclusions

With the aim of developing a robust molecular approach and proposing reliable and transferable molecular parameters, the soft-SAFT EoS was evaluated based on newly measured $p\rho T$ data for eight different glymes, from which k_T and α_P were also determined.

Following the modelling philosophy presented in the previous section for glycols, glymes were described as homonuclear LJ chains containing one square-well site embedded off-center in one of the LJ segments, mimicking the hydroxyl end group in the case of mono-alkyl glymes, or as non-associating species in the case of di-alkyl glymes. In addition to the usual VLE data, one single density-pressure and k_T isotherms at 323 K were considered in the experimental data set used for the model's parameterization. The optimized parameters were then used to successfully describe the VLE, $p\rho T$ and second-order derivative properties in wide temperature and pressure ranges. Particularly relevant, the model was able to provide not only a good qualitative, and in some cases quantitative, description of the sensitive second-order derivative properties, but also to capture the characteristic crossover points of α_P .

The molecular parameters obtained for glymes and those previously reported for glycols were further analysed through comparison with different families of compounds, such as *n*-alkanes and alkan-1-ols to assure that the more physically meaningful set of parameters was chosen. It is important to recall that, in multi-parameter EoS models like most SAFT variants, several different sets of pure-component parameters can yield similar accuracy when used to describe the properties of the pure fluid but lead to different behaviours when applied to describe binary and multicomponent systems. For this reason, ensuring the physical meaning and consistency of the optimized parameters contributes to a more appropriate choice. The trends exhibited by the different sets of parameters obtained in this work are shown to be in good agreement with those expected, highlighting the robustness and transferability of the proposed molecular approach. Furthermore, these trends were further used to successfully predict the atmospheric pressure densities of a blend of di-alkyl glymes by modelling it as a pseudo-pure component approach.

3.3- Glycols and Glymes as physical solvents for CO₂ separation

The content of this section is based on the following published works, developed during the execution of this PhD thesis, where E.A. Crespo was responsible for all the modelling tasks and most of the writing of the manuscripts, with contributions from the other authors.

- Emanuel A. Crespo, Mónica Amaral, Cláudio Dariva, Pedro J. Carvalho, João A. P. Coutinho, Fèlix Llovell, Luís M. C. Pereira, and Lourdes F. Vega, “*Soft-SAFT EoS as a Valuable Tool for the Design of New CO₂ capture Technologies*”, Abu Dhabi International Petroleum Exhibition & Conference (2017), Society of Petroleum Engineers, DOI:10.2118/188464-MS.
- Mónica Amaral, Emanuel A. Crespo, Cláudio Dariva, Lourdes F. Vega, Pedro J. Carvalho, and João A.P. Coutinho, “*High-Pressure solubility of CO₂ in glymes*”, Fuel, 219 (2018) 120, DOI: 10.1016/j.fuel.2018.01.084.
- Emanuel A. Crespo, Pedro J. Carvalho, João A.P. Coutinho, and Lourdes F. Vega, “*Exploring Alternative Solvents for Gas Processing using the soft-SAFT EoS*”, Research and Development Petroleum Conference and Exhibition (RDPETRO 2018), 156,, DOI: 10.1190/RDP2018-41512825.1

Introduction

Among the different processes for CO₂ capture, the oxygenation of alkyl chains is a well-known approach for enhancing the CO₂ solubilities,[130] being the basis of the two most successful industrial processes for natural gas sweetening (removal of H₂S, CO₂ and mercaptans from the natural gas to make it suitable for transportation), namely Rectisol[131] and Selexol.[20] For the same reason, several polyethers including glycols, glymes and polymers have been attracting considerable attention as feasible candidates to CO₂ capture but, despite the industrial interest for these systems, the CO₂ sorption mechanism in these solvents is still unclear. Therefore, the development and optimization of more efficient separation processes for CO₂ separation remains a challenging task to the Oil & Gas industry, closely tight to the fundamental understanding of the interactions between the gas and the solvent and, consequently, to an accurate description of the thermodynamic behaviour of the relevant mixtures.

In the previous sections, the development of a reliable CG model for both glycols and glymes, in the framework of the soft-SAFT EoS, was presented, and correlations that allow to obtain the molecular model parameters for any glycol or glycol ether, using solely the M_w as an input, were proposed. In this model, one single association site (binary type) is assigned per each hydroxyl end-group in the molecule,

while implicitly accounting for the presence of the inner EO groups, and thus of the lone electron pairs of the oxygen atom, through the effective values of the parameters, without the inclusion of additional association sites. Despite its simplicity, the model was shown to accurately describe the properties of the pure fluid and to be easily transferable to compounds not included in the parameterization procedure. Here, these models are applied to the modelling of the phase equilibria of their binary mixtures with CO₂ and CH₄ (the main component in natural gas), assessing its performance when used to describe these highly relevant systems.

Modelling Approach

While the model for the glycols and glymes have been discussed in the previous sections, molecular models for CO₂ and CH₄ are also required. In this work both models were inherited from previous publications. CH₄ is modelled as a non-associating species with a spherical shape ($m_i = 1$), whose diameter and dispersive energy parameters have been proposed by Pàmies and Vega.[72] For CO₂, a molecular model previously proposed by Pedrosa et al.[75] was adopted. It describes CO₂ as a non-associating LJ chain, in which the quadrupolar interactions are explicitly considered, by enabling the polar term of the soft-SAFT theory (see **Chapter 2.1**). The pure-component parameters for the two gases are provided in **Table 3.6**. Once the molecular models and parameters for both the gas and the solvents are established, soft-SAFT can be used to model the phase equilibrium of the correspondent binary mixtures.

Table 3.6. soft-SAFT pure-component parameters used in this work.

Compound	Mw (g/mol)	m_i	σ_{ii} (Å)	ϵ_{ii}/k_B (K)	ϵ^{HB}/k_B (K)	κ^{HB} (Å ³)	$10^{40}Q_{exp}$ (C · m ²)	x_p	Reference
CO ₂	44.01	1.571	3.184	160.20	-	-	4.40	1/3	[75]
CH ₄	16.04	1.000	3.728	147.20	-	-	-	-	[72]
TriEGMME	164.20	3.736 ^a	4.008 ^a	342.23 ^a	3450 ^b	2600 ^b	-	-	-
PEGDME250	250	5.130 ^c	4.140 ^c	326.43 ^c	-	-	-	-	-

^aextrapolated from eqs. 3.8-3.10; ^btransferred from other mono-alkyl glymes; ^cextrapolated from eqs. 3.11-3.13.

Results

Even though glymes have a much higher affinity towards CO₂ than glycols, this section is started by assessing the performance of the EoS to describe an example of a binary mixture glycol + CO₂. Jou et al.[132] measured the solubility of CO₂ in DEG in a wide temperature range, namely 298.15–398.15 K. The soft-SAFT modelling results for this mixture are shown in **Figure 3.20**, and as can be observed, by using one temperature-dependent binary interaction parameter, ξ , correcting the magnitude of the unlike dispersive energies, an accurate description of the experimental data, with a %ARD of only 5.61 %, is obtained. Surprisingly, even though association sites were not included to explicitly model the hydrogen bonding acceptor behaviour of the EO groups, that probably being one of the reasons why a temperature-dependency was necessary in the first place, values of ξ lower than one were required, indicating that the unlike dispersive energy between the molecules was overestimated by the combining rules. Nevertheless, the temperature-dependence of the binary parameters is very weak, with the values ranging from 0.975 to 0.933 in a 100 K interval, seeming to reach an asymptotic value at higher temperatures where hydrogen bonding becomes less relevant. In the 293–393 K range, the binary interaction parameter can be easily described by a second-order polynomial expression (c.f. **Figure 3.20b**) that can be expressed by **eq. 3.14**.

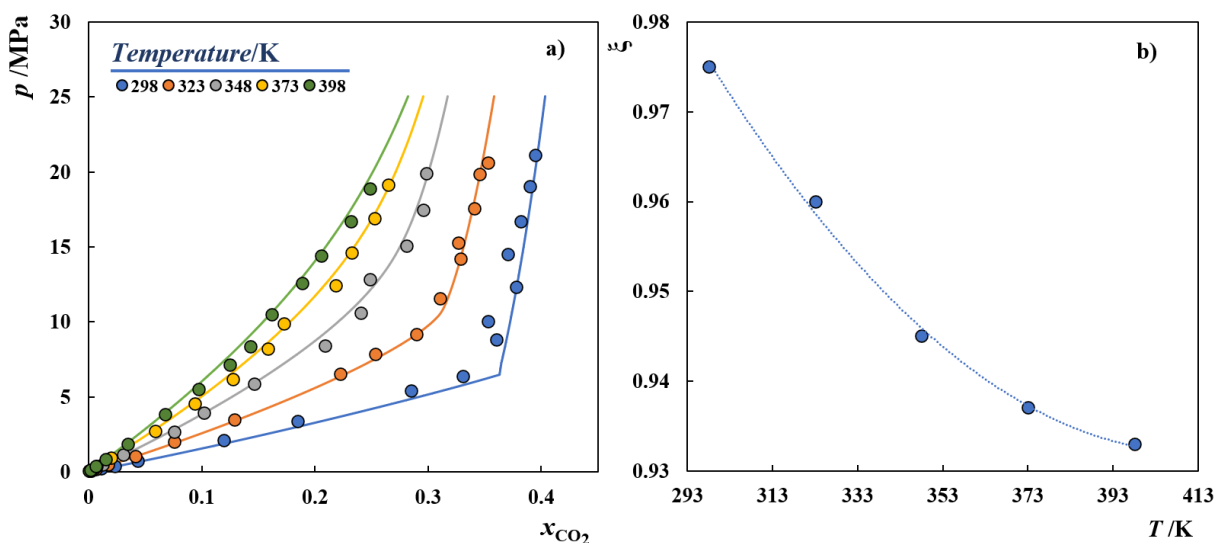


Figure 3.20. a) VLE for the system DEG + CO₂. Symbols represent experimental data, while the solid lines depict the soft-SAFT results.[132] b) Temperature-dependent binary interaction parameter used in the calculations.

$$\xi_{DEG-CO_2} = 3.314 \times 10^{-6}(T/K)^2 - 2.736 \times 10^{-3} T/K + 1.497; R^2 = 0.998 \quad (3.14)$$

Carvalho and Coutinho[133] have previously reported that the deviations from the ideal behaviour observed in CO₂ solutions in low-volatility physical solvents are typically small and largely dominated by entropic effects, mostly derived from the solute-solvent size and shape asymmetries that are responsible for important free-volume contributions. The authors also observed that, when expressed in molality, the pressure vs concentration phase diagrams are, within the experimental uncertainty, solvent independent and can thus be correlated as a single function of temperature. For this reason, even though molar units are used within an EoS, an appropriate analysis of solubility data should be first made with the solubility data expressed in molality to remove the M_w effect and provide a truthful comparison of the solubility in the different solvents. Such a comparison is provided in **Figure 3.21** and, as can be observed, while DEG presents an ideal behaviour, in agreement with the correlation proposed by Carvalho and Coutinho[133], glymes present much higher solubilities, with their behaviour starting to deviate from the correlation at pressures lower than 5 MPa (the validity range of the correlation).

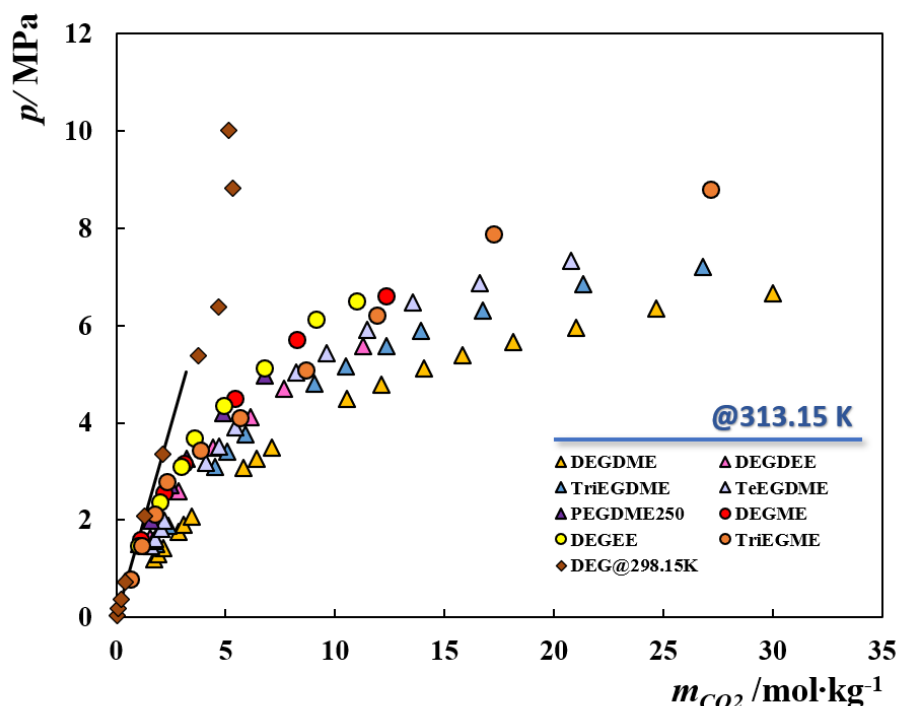
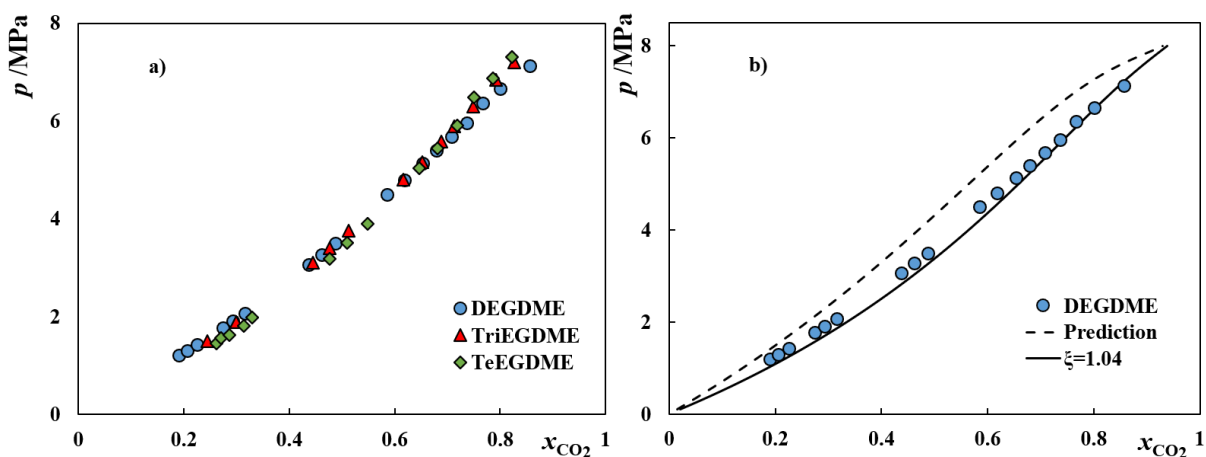


Figure 3.21. Solubility of CO₂ in different glymes and DEG at 313.15 K.[11,16,17,19,132] The solid line depicts the correlation proposed by Carvalho and Coutinho[133] for the CO₂ solubility in ideal low-volatility physical solvents.

It is also clear that di-alkyl glymes have much higher affinity towards CO₂, exhibiting much higher solubilities under the same conditions than those exhibited by mono-alkyl glymes and glycols. For this reason, they are used in a blend as solvent in the Selexol process and have been the motivation of some

experimental works. Kodama et al.[17] measured the solubility of CO₂ in different di-alkyl ethers, namely DEGDME, TriEGDME, and TeEGDME at 313.15 K, analysing the effect of the compounds' chain length on the phase equilibria. As depicted in **Figure 3.22a**), the solubility was observed to rapidly increase with pressure, but to be rather insensitive to changes in the glymes M_w (and consequently on the number of EO groups). This being observed with the solubilities expressed in terms of molar fraction of gas, leads to the distinct behaviour observed in **Figure 3.21**, where the solubility, when expressed in terms of molality, varies across the different di-alkyl glymes. This suggests that the CO₂ sorption behaviour in glymes, although mainly affected by entropic effects, is also influenced by enthalpic contributions. Nevertheless, as depicted in **Figure 3.22**, soft-SAFT can provide very good predictions of the solubility data, even without the use of an adjustable binary interaction parameter (i.e., $\xi = 1$), predicting a very subtle change in the shape of the solubility curve as the glymes chain length is increased, something that the experimental data seems to suggest as denoted by the crossover point observed in **Figure 3.22a**), where the solubilities increase as the chain length is increased at lower pressures, but showing the opposite behaviour at higher pressures.

If a higher degree of accuracy is desired, it can be obtained by applying very small corrections to the unlike dispersive energy, using ξ in the interval 1.00–1.04. The use of these corrections yields an accurate description of the experimental data with %ARD of only 5.30, 4.42, and 2.80, for DEGDME, TriEGDME, and TeEGDME, respectively. As expected, both the deviations from the experimental data and the magnitude of the correction applied increase with the deviation from the ideal behaviour of a low-volatility physical solvent that, as depicted in **Figure 3.21**, increases in the following order: DEGDME>TriEGDME>TeEGDME.



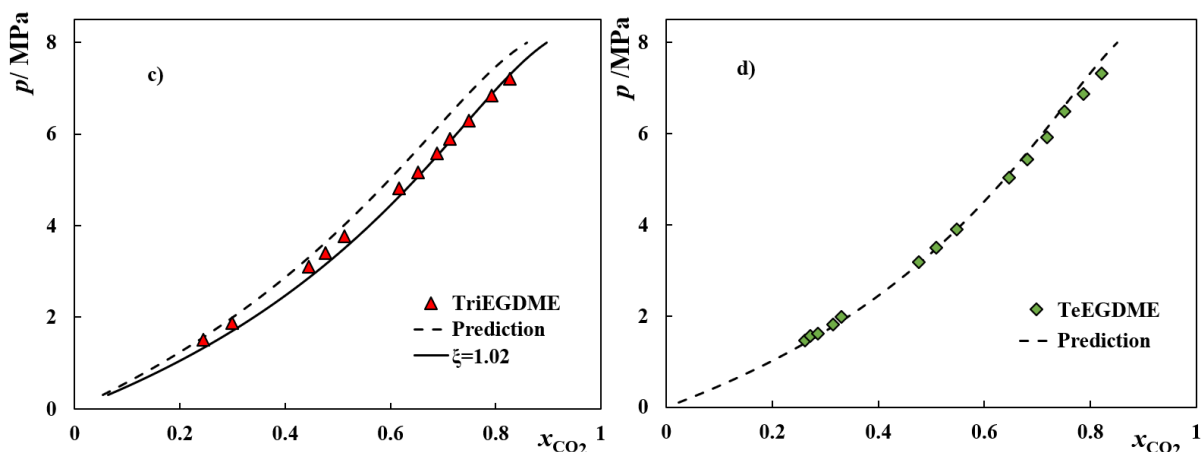


Figure 3.22. CO_2 solubilities in di-alkyl ethers at 313.15 K. Symbols represent the experimental data,[17] while the dashed and solid lines depict the soft-SAFT predictions and fitting to the experimental data, respectively.

In the same publication, experimental values for the saturated densities of both the liquid and vapour phases were reported, and are depicted in **Figure 3.23**, for the system DEGDM + CO_2 , along with the soft-SAFT calculations, with and without using the binary interaction parameter adjusted to the solubility data. While both calculations yield similarly accurate results for the vapour densities, the use of the binary parameter marginally improves the description of the liquid phase density.

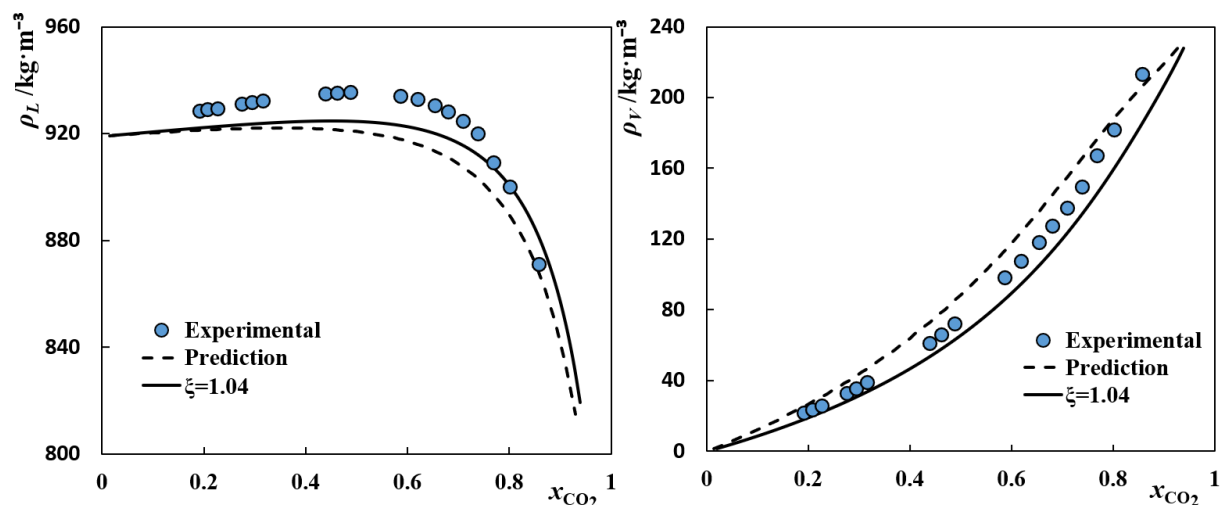


Figure 3.23. Saturated liquid and vapor densities at equilibrium for the DEGDM + CO_2 system. Symbols represent experimental data,[17] while the lines depict the soft-SAFT results.

Considering the transferability of the soft-SAFT molecular parameters already discussed, the binary mixtures of CO_2 with a wider range of glymes is next described. For instance, the correlations previously proposed for mono-alkyl glymes, and di-alkyl glymes were used to obtain the pure-

component parameters for triethylene glycol methyl ether (TriEGME) and PEGDME 250, whose values are provided in **Table 3.6**, for which experimental CO₂ solubility data are available.[11,16] As depicted in **Figure 3.24**, soft-SAFT is able to accurately describe these systems using the extrapolated parameters and using a binary interaction parameter of the same magnitude to those applied before (1.025 for TEGME and 0.98 for PEGDME250). Particularly remarkable is the fact that, even though a state-independent binary interaction parameter was applied, the experimental data could be successfully described over a wide temperature range (from 293 to 373 K) with overall %ARD of only 8.78 and 10.50 for TEGME and PEGDME250, respectively. The need for a temperature-dependent binary parameter in DEG (c.f., **Figure 3.20**), contrarily to what is observed here with glymes, is probably related to the higher influence of temperature upon the hydrogen bonding contribution that, as previously discussed, is much more significant in glycols than in glycol ethers.

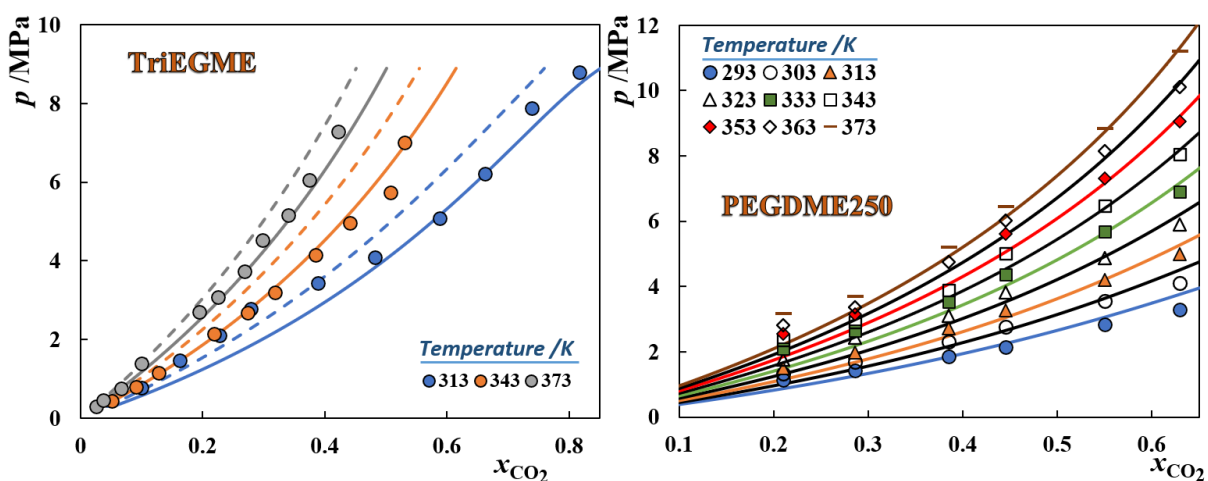


Figure 3.24. CO₂ solubilities as a function of temperature for TriEGME and PEGDME250. Symbols represent experimental data,[11,16] while the solid lines depict the soft-SAFT results.

Furthermore, the binary interaction parameter applied to describe the phase equilibria of CO₂ with the different glymes was found to correlate linearly with the glyme's M_w , according to the following expression:

$$\xi_{glyme-CO_2} = -5.021 \times 10^{-4} M_w (g \cdot mol^{-1}) + 1.108; R^2 = 0.990 \quad (3.15)$$

Also interesting is the fact that although mono-alkyl glymes and di-alkyl glymes are modelled as two different families (with the latter being considered as a non-associating species), the binary interaction parameter considered for the system with TriEGME fits well into the same relationship as those applied for the mixtures with di-alkyl glymes and the PEGDME 250 blend. As a remainder, this parameter is related to the asymmetry in the van der Waals interactions, not on the association, hence,

the results obtained here reinforce the consistency and reliability of the molecular model developed in the previous chapter.

When assessing and comparing the performance of new solvents for CO₂ capture, an important metric to calculate is the thermal cycle capacity (TCC), which is here defined as the difference between the CO₂ solubilities, expressed in molality, in each solvent at two different temperatures at a given process pressure, to evaluate their absorption/desorption capacity per cycle of regeneration. Therefore, the solubilities at two different temperatures (298 and 373 K) were predicted using the binary interaction parameters given by eqs. 3.14 and 3.15, at a system's pressure of 5 MPa and the results are reported in Table 3.7. As can be observed, the TCC values of a polyether as a solvent for CO₂ decrease with the introduction of hydroxyl end-groups in the solvents structure and with the increase of the M_w . While the former might be explained by the fact that a higher self-association of the solvent results in decreased interactions with the gas, the latter can be due to the increase of steric hindrance as the solvent molecules become bulkier and the inner oxygenated groups become less accessible to the gas molecules.

Table 3.7. Thermal cycle capacities predicted by soft-SAFT for the different solvents at 5 MPa.

Compound	$m_{CO_2}(\text{mol}\cdot\text{kg}^{-1})$ @298 K	$m_{CO_2}(\text{mol}\cdot\text{kg}^{-1})$ @373 K	TCC(mol·kg ⁻¹)
DEG	3.887	1.043	2.844
TriEGME	14.038	3.120	10.918
DEGDME	30.506	4.785	25.720
TriEGDME	19.583	3.693	15.890
TeEGDME	13.789	3.040	10.748
PEGDME250	9.935	2.554	7.380

While carrying the work presented in this doctoral thesis, the CO₂ solubilities in four different glymes, namely DEGME, DEGEE, DEGDME, and DEGDEE, in wide temperature (293–353 K) and pressure (up to 13 MPa) ranges were measured, in the same research lab, by Amaral et al.[19] This data is shown in Figure 3.25, and as previously suggested when analysing Figure 3.21, the substitution of one hydrogen atom in the hydroxyl end-group by an ethyl or methyl group leads to increased solubilities, as can be observed when comparing the data obtained for DEGME/DEGDME and DEGEE/DEGDEE, an effect that gets weaker, as the temperature is increased.

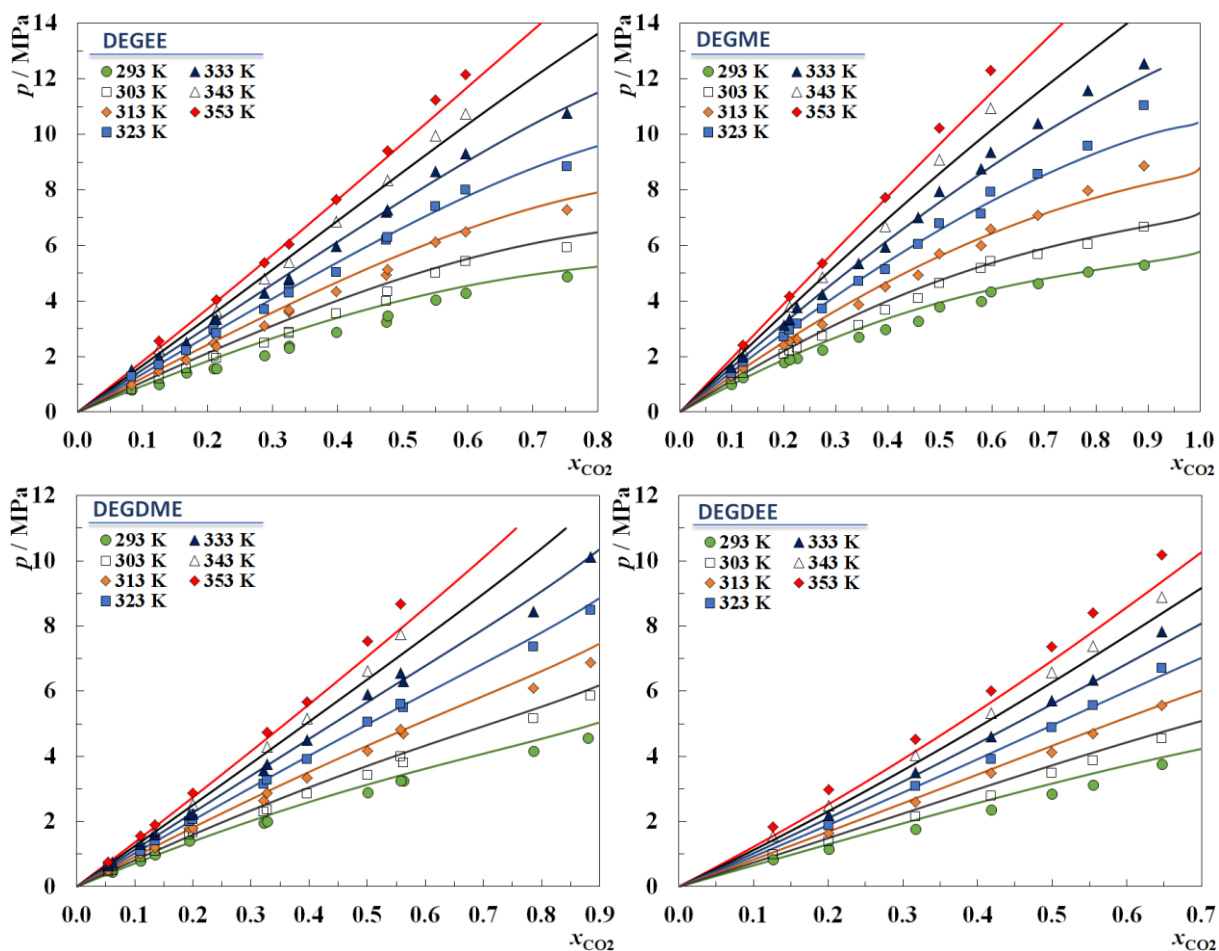


Figure 3.25. Pressure-composition diagrams at different temperatures for the binary systems: CO_2 + DEGEE, DEGME, DEGDME, and DEGDEE. Symbols represent experimental data,[19] while the solid lines represent the soft-SAFT results, using the temperature-dependent binary interaction parameters from **Table 3.8**.

The soft-SAFT EoS was also applied to describe this set of experimental data, but as reported in **Table 3.8**, in this case, two binary interaction parameters (η correcting the unlike segment size diameter and ξ correcting the magnitude of the unlike dispersive interactions), all very close to unity, were necessary to achieve a good quantitative description of the data plotted in **Figure 3.25**. Although size-related binary parameters are generally avoided when dealing with mixtures with similar chemical groups, huge size/shape differences between the two compounds, or their sparse sphericity may require the use of said parameter to allow the model to accurately describe the data, while consequently decreasing the correction triggered by the energy binary parameter, which would otherwise account for both size/shape and energetic effects.

Nevertheless, one of the main advantages of using molecular-based EoSs is that, even in challenging systems, their parameters are usually independent of state conditions such as temperature

and pressure. Here, the high-pressure phase diagrams calculated with soft-SAFT were obtained using a state-independent size binary parameter, $\eta = 1.028$, across the four systems. The value of the parameter, greater than one, indicates that the volume occupied by the molecules in the mixture is higher than the ideal case (Lorentz-Berthelot's rule with $\eta = 1$). The energy binary parameter, ξ , was fitted individually to the experimental solubility data at 323 K for each mixture and used to successfully predict the remaining isotherms. Contrarily to what was observed when analysing literature data, values lower than unity were observed in all cases that as explained above are due to the use of a $\eta > 1$ that decreases the magnitude of the correction to be applied in the energy parameter. Furthermore, the values of ξ were found to decrease with the increase of the glyme's chain length and/or with the removal of the hydroxyl end-group, the latter being expected because of the simplifications within the glyme's molecular model that, by considering DEGDME and DEGDEE as non-associating species result in increased values of the dispersive energy of the pure-component.

Table 3.8. Binary interaction parameters used in the soft-SAFT calculations and deviations from the experimental data reported by Amaral et al.[19]

$CO_2 +$	η_{ij}	ξ_{ij}	%ARD
DEGME	1.028	0.995	3.86
DEGEE	1.028	0.974	6.62
DEGDME	1.028	0.991	3.70
DEGDEE	1.028	0.960	5.93

From the four systems presented in **Figure 3.25**, only the binary mixture $CO_2 +$ DEGDME was presented before in **Figure 3.22**, where it was modelled using a different binary interaction parameter, given the disagreement between the two datasets. Moreover, Kodama et al.[17] reported solubility data only at 313 K which may hinder the correct assessment of the system's physics, and its dependency with temperature, which consequently may prevent the selection of the most adequate modelling approach for these kind of systems. More importantly, such distinct results reinforce the need for more reliable solubility data in wide temperature and pressure ranges to guide the development of semi-predictive models that can then be used in the design of new CO_2 separation systems. Therefore, new experimental data, expanding the number of systems investigated in **Figure 3.25**, is welcome for a careful selection of glymes that would allow the study of different aspects of the glymes structure on their interactions with CO_2 , similar the selection done in **Chapter 3.2** for the development of the molecular model for glymes.

At the moment of writing, experimental measurements of the CH₄ solubility in wide temperature (293-353K) and pressure (up to 20MPa) ranges for a selection of different glymes are being undertaken in the same research lab. Therefore, the model developed for glymes in **Chapter 3.2**, is here applied, along with the CH₄ model by Pàmies and Vega,[72] for the description of the raw data obtained so far.

Figure 3.26 illustrates the methane experimental solubility measured in TriEGDME and DEGEE along with the soft-SAFT modelling using the molecular parameters for glymes presented in **Section 3.2**. As depicted, and in accordance to what was previously observed in other physical solvents such as ionic liquids (ILs),[134] the temperature effect in the methane solubility is negligible, with soft-SAFT being able to capture such behaviour using one state-independent binary interaction parameter, whose value, although increasing with the solvent's M_w , is only marginally influenced by the glyme considered (e.g. $\xi = 0.915$ for TriEGDME and $\xi = 0.90$ for DEGEE). The value of the energy parameters applied, which are lower than unity, highlight the weak interactions between CH₄ and glymes, reinforcing the positive deviations from the ideal behaviour that characterize these mixtures. Particularly interesting, soft-SAFT was able to predict, in the correct range of pressures, the inversion point on the methane solubility with temperature, due to its supercritical state.

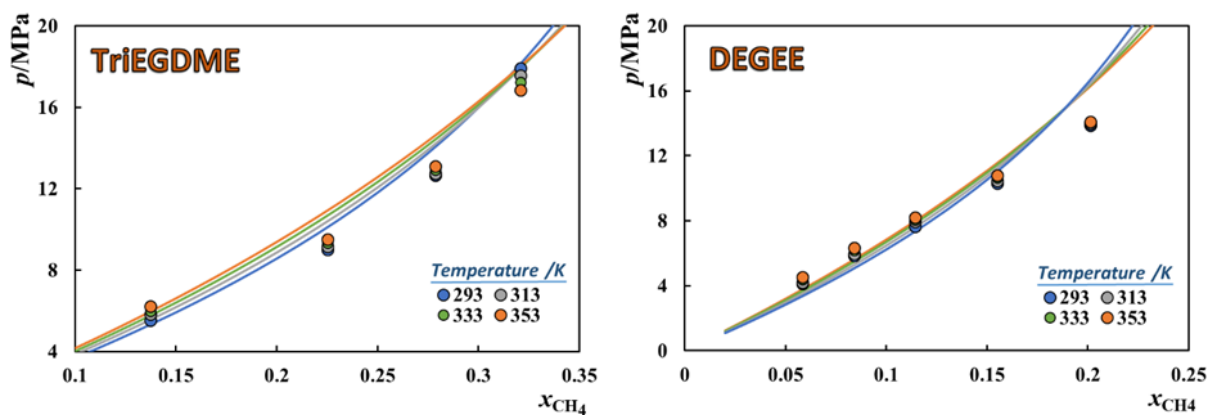


Figure 3.26. CH₄ solubilities in TriEGDME and DEGEE. Symbols represent experimental measurements, while the solid lines depict the soft-SAFT fitting to the experimental data.

Given the good performance of soft-SAFT when used to describe the solubilities of both CH₄ and CH₂ in glymes, it can be used to predict the ideal gas selectivities (S_{CO_2/CH_4}) through **eq. 3.16**, using the Henry's constants calculated from the soft-SAFT EoS results as the limiting slope of the solubility curve as the gas composition in the liquid phase approaches zero.

$$S_{CO_2/CH_4} = \frac{H_{CH_4 glyme}}{H_{CO_2 glyme}} \quad (3.16)$$

This is illustrated in **Figure 3.27** for DEGDEE and as it can be observed, glymes are very selective towards CO₂ although the selectivity decreases linearly with temperature, since even though the solubility of CH₄ is temperature independent, the CO₂ solubility greatly decreases as the temperature increases.

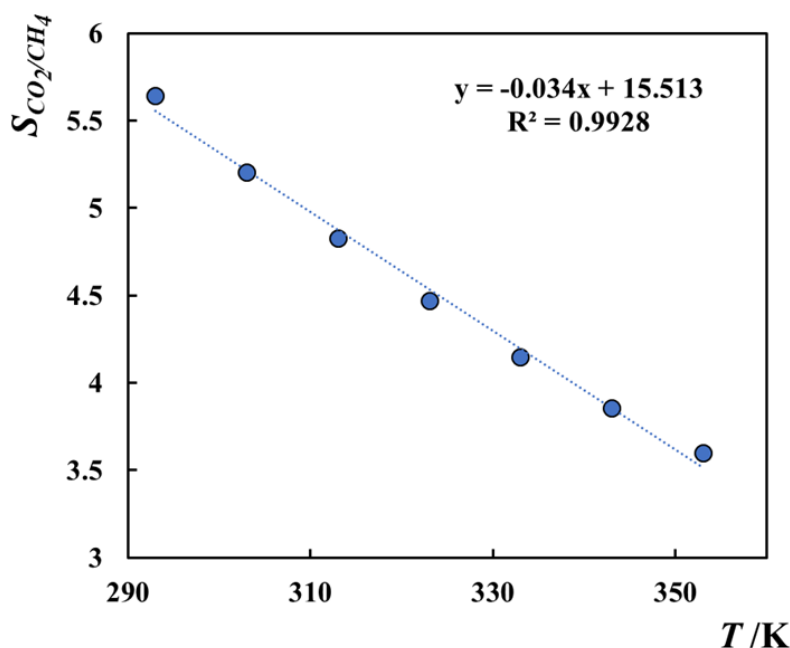


Figure 3.27. Selectivity CO₂/CH₄ in DEGEE, as predicted by the soft-SAFT EoS.

Conclusions

In this section, the soft-SAFT molecular models previously developed for glycols and glymes were used to successfully describe the CO₂ and CH₄ solubilities in those systems, and to rationalize about the magnitude of the interactions between the gas and the solvent as a function of the solvent's structure. Although good results could always be obtained, different experimental data sources were found to disagree with each other for a few systems, requiring a different modelling approach and highlighting the need for additional reliable data. Nevertheless, using literature solubility data available for a number of different glymes, the binary interaction parameter between the gas and the solvent was found to correlate with the solvent's M_w , allowing the proposal of a fully predictive model for the prediction of CO₂ solubilities in any glyme, in the absence of experimental data for the pure solvent and the mixture. Such a tool based on an EoS can be useful for solvent screening purposes as it can quickly provide useful information such as solubility, densities, thermal cycle capacities and selectivity.

3.4- Aqueous solutions of glycols and glymes

The content of this section is based on the following published manuscripts, where E.A. Crespo was responsible for the modelling tasks and for writing the manuscripts, with substantial contributions from the remaining authors.

- Naima Chouireb, Emanuel A. Crespo, Luís M.C. Pereira, O. Tafat-Igoudjilene, Lourdes F. Vega, João A.P. Coutinho, and Pedro J. Carvalho, “*Measurement and Modeling of Isobaric Vapor-Liquid Equilibrium of Water + Glycols*”, Journal of Chemical and Engineering Data, 63 (2018) 2394-2401, DOI: 10.1021/acs.jced.7b00945.
- Emanuel A. Crespo, Naima Chouireb, O. Tafat-Igoudjilene, Lourdes F. Vega, Pedro J. Carvalho, and João A.P. Coutinho, “*Isobaric Vapor-Liquid Equilibrium of Water + Glymes Binary Mixtures: Experimental Measurements and Molecular Thermodynamic Modelling*”, Fluid Phase Equilibria, 513 (2020), 112547, DOI: 10.1016/j.fluid.2020.112547

Introduction

Regardless of its source, raw natural gas is significantly different from end-use natural gas, which is almost pure CH₄. Instead, natural gas is a mixture of methane with different hydrocarbons such as ethane, propane, butane, i-butane, and a fraction of C₅+, along with several impurities such as H₂O, H₂S, CO₂, N₂, mercaptans, among others. Consequently, the natural gas stream must be processed to remove the undesired hydrocarbons and impurities to meet the required specifications for pipeline transportation and final use. This purification processes involves different sequential stages, starting with the removal of oil and condensates, dehydration/water removal, the separation of natural gas liquids, and finally the sweetening of the gas through the removal of sulphur-containing compounds, and acid gases such as H₂S and CO₂, whose presence in the final product is highly undesirable, to avoid the formation of sulfuric and carbonic acid that are highly corrosive for equipment and pipelines.[135]

Glycols are the main dehydration agents and thus knowledge on the glycols + water phase equilibrium is of ubiquitous importance. Then, given the possible occurrence of residual water in the natural gas stream entering the gas sweetening process, a reliable knowledge of the phase behaviour and interactions exhibited by aqueous glycol ether systems is also required, not to mention that such knowledge is also useful for applications in other industries as glymes are often found in several personal, household, and industrial products containing water such as water-based paints, dyes, sunscreens, cosmetics, etc.[136] For these reasons, accurately modelling the phase equilibria of aqueous solutions of both glycols and glymes is highly relevant for the Oil & Gas industry, as a further validation of the CG models developed in **Chapter 3.1** and **Chapter 3.2**, before their adoption to more complex systems.

Modelling Approach

The soft-SAFT models for glycols and glymes have been already described in the previous sections and are here applied in a transferable manner. The investigation of glycols + water binary mixtures is extended to some polyethylene glycols (PEGs) with M_w in the 400–6000 g·mol⁻¹ range, whose pure-component parameters were obtained by extrapolation from the correlations obtained for the glycol oligomers, using **eqs. 3.3-3.5** with the values being provided in **Table 3.9**.

Water is modelled following the work of Vega et al.,[137] where it is described as a LJ sphere with a 4-site associating model, the ‘4C’ association scheme, that assigns to the water molecule, two sites type ‘B’ representing the hydrogen atoms and two sites type ‘C’ representing the lone electron pairs on the oxygen atom, with ‘B–C’ interactions being allowed in pure-water and both sites allowed to interact with the binary sites present in the glycol molecules. The water pure-component parameters are also provided in **Table 3.9**.

Table 3.9. soft-SAFT pure-component parameters for water and different PEGs.

Compound	M_w (g/mol)	m_i	σ_{ii} (Å)	ε_{ii}/k_B (K)	ε^{HB}/k_B (K)	κ^{HB} (Å ³)
PEG 400*	400	8.321	4.049	357.47	3891	2600
PEG 600*	600	12.110	4.090	360.20	3891	2600
PEG 1500*	1500	29.156	4.141	363.76	3891	2600
PEG 6000*	6000	114.386	4.168	365.65	3891	2600
Water[137]	18.02	1.000	3.154	365.00	2388	2932

*-Non-associating parameters extrapolated from **eqs. 3.3-3.5** and associating parameters transferred from glycol oligomers.

Results – Glycols + Water

Experimental isobaric VLE data (i.e., boiling temperatures) are available for binary mixtures of water with EG, DEG, TriEG, and TeEG at three different pressures, and are presented in **Figure 3.28**, along with the soft-SAFT results. In the same figure, a comparison between soft-SAFT calculations as predicted from the pure-component parameters, i.e., with $\xi = 1$ (dashed lines in the figure) and the soft-SAFT fitting to the experimental data (solid lines in the figure), using one state-independent binary interaction parameter, correcting the mixtures dispersive energy, is presented. The soft-SAFT predictions exhibit a systematic underprediction of the mixtures boiling temperatures. Conversely, the use of the binary parameter, whose values are provided in **Table 3.10**, allows for an excellent agreement with the experimental data with an overall %ARD of only 3.82 %. All the binary parameters have values greater than one, suggesting the existence of strong interactions between glycols and water, whose magnitude

are underestimated by the model. This binary parameter is found to increase with the glycol's chain length, in agreement with the increase in the mixtures' boiling temperatures, due to the increase of the van der Waals dispersion forces. Furthermore, looking at **Figure 3.28**, small deviations in the water-rich phase can be observed, with the model underestimating the boiling temperature of the mixture. This is due to the slight overestimation of pure water's vapor pressure by the soft-SAFT model. Although this could be improved by refitting the water model without forcing it to have a spherical shape (m_i not necessarily equal to 1) the differences are still negligible.

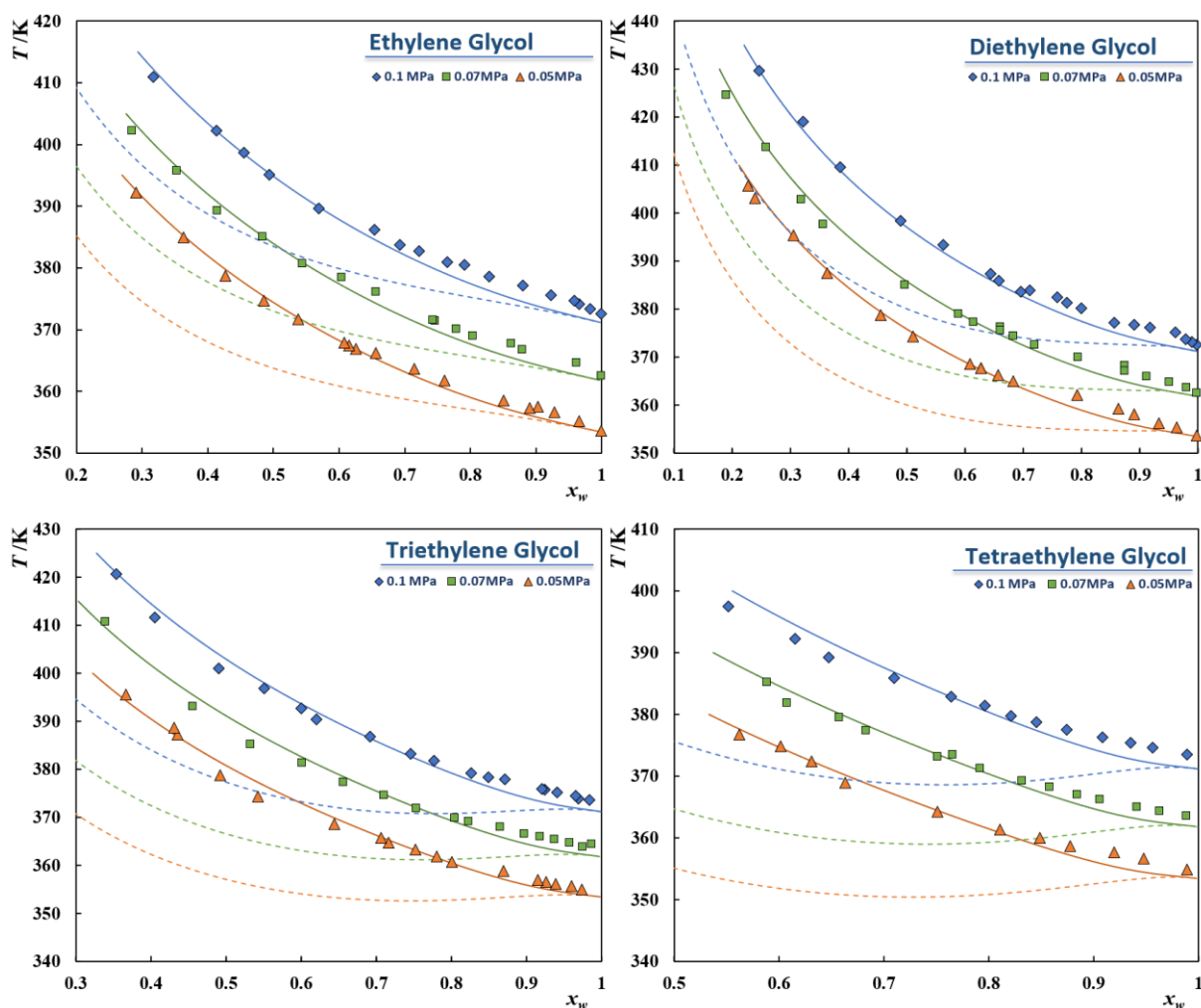


Figure 3.28. Isobaric temperature-composition diagrams of the glycols + water binary systems. The symbols represent experimental data,[138] while the dashed and solid lines represent the soft-SAFT EoS predictions and fitting to the data.

Table 3.10. Binary interaction parameters and deviations from the experimental data for glycols + water systems.

	ξ_{ij}	%ARD (x)	%ARD (y)
EG + H ₂ O	1.130	3.87	5.49
DEG + H ₂ O	1.135	4.33	5.63
TriEG + H ₂ O	1.175	3.93	5.74
TeEG + H ₂ O	1.185	3.14	5.09

The water activity coefficients (γ_w) estimated from the mixtures boiling temperatures can be used to evaluate the non-ideality of aqueous systems, using the generalized modified Raoult's law, expressed by eq. 3.17:

$$\gamma_w = \frac{y_w \varphi_w^V p}{x_w \varphi_w^L p_w^*} \quad (3.17)$$

where, p is the system's pressure, p_w^* is the water vapor pressure at the system's temperature, φ_w^V and φ_w^L are the fugacity coefficients of water in the vapor and liquid phase, respectively. x_w and y_w are the water mole fractions in the liquid and vapor phase, respectively. As the pressures investigated in this work are low, the fugacity coefficients are close to unity. Furthermore, due to the glycols low volatility (soft-SAFT results show glycol mole fractions, in the vapor phase, always lower than 10%), the system vapor phase can be approximately considered as pure water, allowing eq. 3.17 to be simplified as eq. 3.18 that can be used to estimate γ_w and grasp about the magnitude of the interactions between the two species.

$$\gamma_w = \frac{p}{x_w p_w^*} \quad (3.18)$$

The γ_w estimated from the mixtures boiling temperatures and predicted with soft-SAFT EoS are depicted in **Figure 3.29**. As can be observed, a good agreement between experimental data and model results is found considering the simplifications made in the estimation of the activity coefficients. The high deviations observed for EG are most probably due to the oversimplifications of the model used for the estimation of the activity coefficients from the experimental data, as EG presents a considerably higher volatility than their homologous and consequently, the vapor phase is richer in this compound than for the rest of the series. An additional explanation is that the water-EG hydrogen bonding interactions, which are dominant, given the short length of the EG are not well described by the simplified model, as the OH group is represented only by one associating site. The assumptions in the estimates and the molecular model seem to be good for the rest of the mixtures, as the glycols increase their molecular weight. Also, as shown in **Figure 3.29**, the systems studied present γ_w very close to 1 for low glycol concentrations, where water-water interactions dominate.

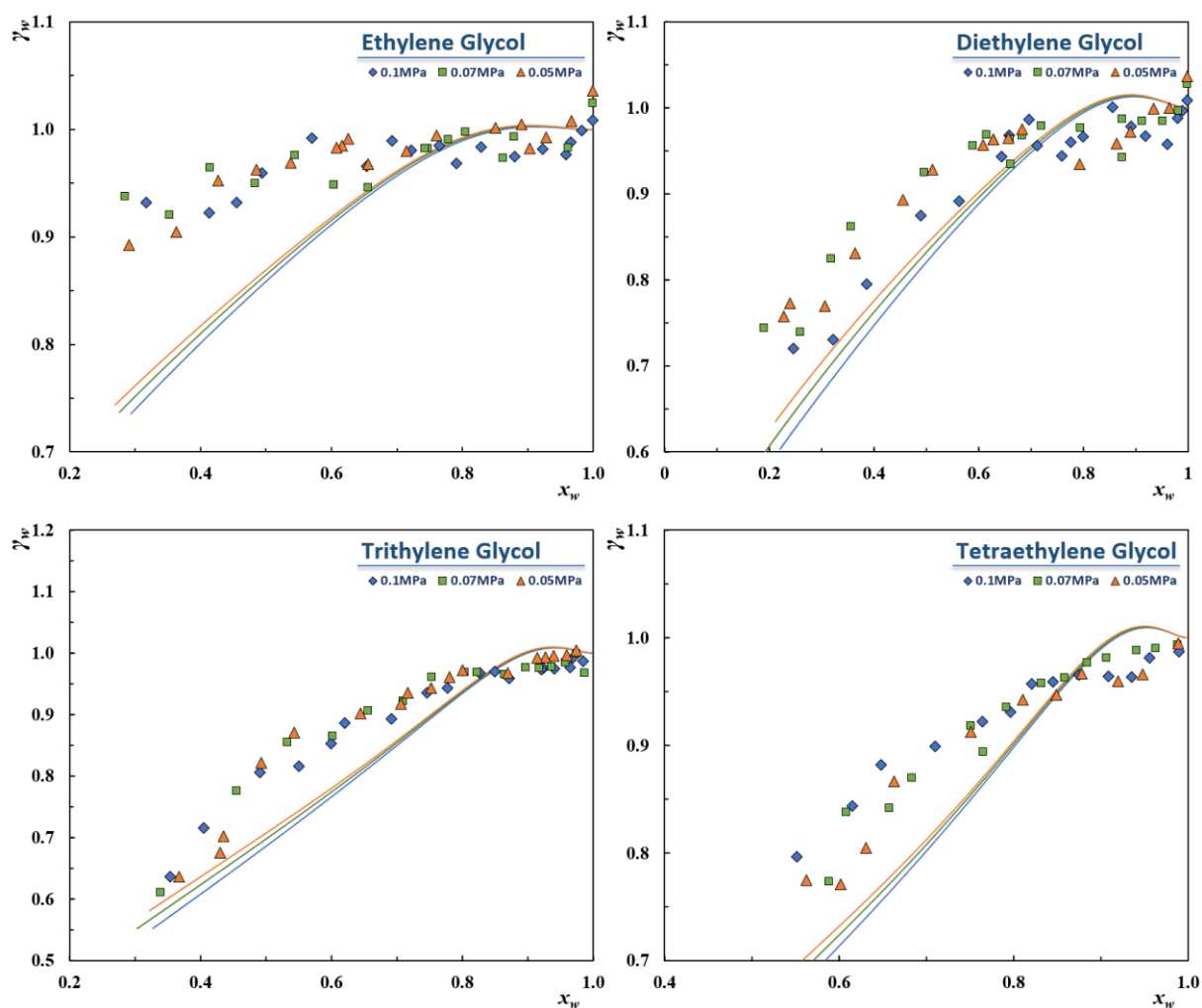


Figure 3.29. Water activity coefficients for the binary systems water + glycols at three different pressures. Symbols represent estimates from the experimental boiling temperatures,[138] while the solid lines represent the soft-SAFT calculations.

Furthermore, as the glycols chain length increases, soft-SAFT predicts the existence of a maximum on γ_w (values very close to one) at high water concentrations, denoting a region in which unfavorable interactions dominate the system. This suggests that as the size of the glycol molecules increase, their interactions with water decrease in the full solvation regime. It is also observed that for higher mole fractions of glycol there is a regular decrease of the water activity coefficients, denoting the existence of favourable intermolecular interactions between the two species; contrarily to what it is observed in the solvation regime, it increases with increasing glycols chain length. Nevertheless, this is translated into values of the binary interaction parameters applied within soft-SAFT that also increase following the same trend. It is important to remark that the mixtures behaviour has been corrected just

with one binary parameter for the van der Waals interactions, while the cross-association, hydrogen bonding interactions, were always calculated from the combining rules discussed in **Chapter 2.1**, in a predictive manner.

As in the previous section, molecular parameters for compounds not included in the fitting procedure, and for which little or no pure-component data is available for parameterization, as it is the case for longer PEGs, can be obtained from the correlations developed in **Chapter 3.1**. Therefore, the correlations proposed before were here applied to obtain the soft-SAFT parameters for PEGs of different M_w as listed in **Table 3.9**, to further demonstrate the robustness of soft-SAFT EoS to investigate the VLE of PEGs + water binary systems.

Ninni et al.[139] reported water activities (a_w) in PEG aqueous solutions at 298 K for PEG molecular weights ranging between 200 and 200000 g·mol⁻¹, while Herskowitz and Gottlieb[140] reported experimental water activities in PEG (200-6000 g/mol) solutions in the 293.1-333.1 K temperature range. However, most of this data is limited to very high mole fractions of water providing little insights into the overall systems behaviour. Thus, only selected data for PEG 400, PEG 600, PEG 1500 and PEG 6000 over a broader concentration range were modelled here using soft-SAFT EoS, with the water activities being obtained from applying the relationship between a_w and γ_w (**eq. 3.19**).

$$a_w = \gamma_w x_w \quad (3.19)$$

As depicted in **Figure. 3.30**, a binary interaction parameter $\xi = 1.220$ was found to provide a good description of the water activities in a PEG 400 aqueous solution. As this parameter corrects the van der Waals energy parameter, it is expected that by increasing the glycols chain length, its value should tend to an asymptotic behaviour as the magnitude of the interactions between the two components becomes independent of the glycols chain length. Therefore, the BIP fitted to the binary system PEG 400 + water was used to predict the water activities in aqueous solutions of PEG 600/1500/6000 at different temperatures and as depicted in **Figure. 3.30**, a very good description of the experimental data was achieved.

The good results obtained for PEG 600, 1500 and 6000 are particularly remarkable as they represent full predictions of the model with the PEG pure-component parameters being obtained from the correlations proposed in **Chapter 3.1** and the binary parameter being transferred from PEG 400. Moreover, as explained in the before, a simplified molecular model is being used to describe the PEG molecules, where the hydrogen-bonding character of each of the hydroxyl end-groups is mimicked through one association site only and the influence of the high number of EO groups is being accounted implicitly by the specific values of the parameters. An additional simplification is related to the polymer's molecular mass distribution as these polymers are in fact mixtures of PEGs with different

molecular weights, which are in soft-SAFT described under a pseudo-pure component approach. This seems to be particularly important in PEG 400, where the water activities calculated with soft-SAFT are for water-rich solutions higher than those observed experimentally, suggesting that the distribution of the PEG 400 may be displaced towards higher values. Additionally, as observed both experimentally and with the modelling results for PEG 600 and PEG 1500, temperature plays a minor role on the magnitude of the interactions between the two components, with soft-SAFT predicting a minor decrease on the water activities as the temperature increases.

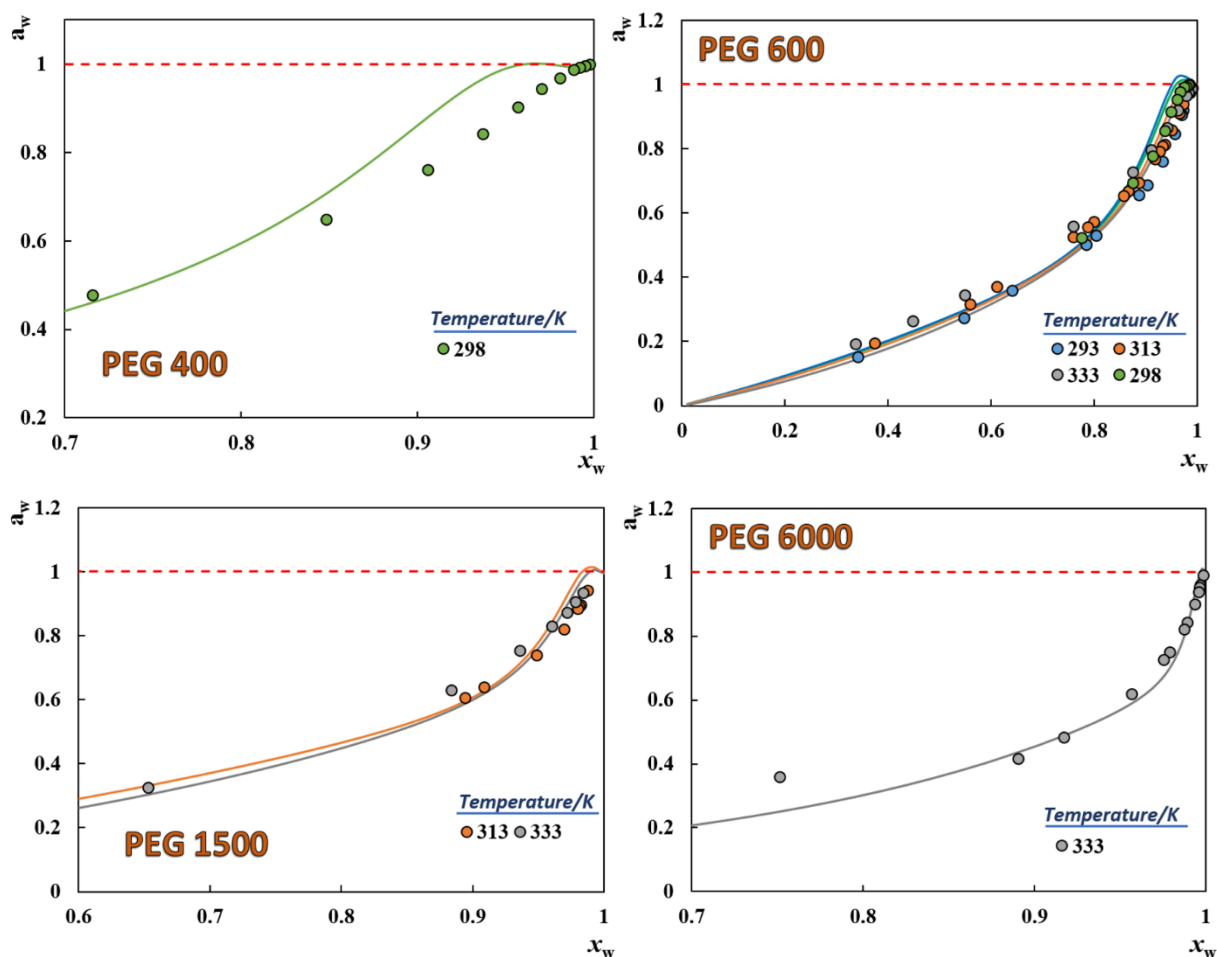


Figure 3.30. Water activity for the binary system water + PEGs. Symbols represent experimental data,[139–141] while the solid lines represent the soft-SAFT results, using $\xi = 1.22$.

Results – Glymes + Water

Experimental isobaric VLE data (i.e., boiling temperatures) is available for binary mixtures composed of water and six different glymes, namely EGEE, DEGME, DEGEE, DEGDME, TriEGDME, and TeEGDME. The data was measured at three different pressures, namely 0.10, 0.07 and 0.05 MPa and glyme mole fractions up to 0.7, corresponding to equilibrium temperatures up to 395 K.[142] This data is presented in **Figure 3.31**, along with the soft-SAFT calculations carried out in this work. As expected, given the lower volatility of the glyme compared with water, the mixture's boiling temperature increases with the glymes mole fraction for all cases. In the water-rich region ($0.8 \leq x_w \leq 1$), there is only a slight increase of the equilibrium temperature as glyme is added to the system. Conversely, in the glycol ether-rich region, a steep increase of the systems temperature towards the boiling temperature of the pure glyme can be observed.

Given the complexity of most aqueous systems, thermodynamic models are frequently unable to correctly predict their phase behaviour. In this work, as demonstrated in **Figure B.2.**, when the soft-SAFT EoS was used in its purely predictive form, i.e., $\xi = 1$, the model predicts the immiscibility of the two compounds in the liquid phase, a behaviour that is contrary to the one observed experimentally. Furthermore, the model predicts that the degree of immiscibility between the studied glymes and water increases dramatically for the di-alkyl glymes, most probably due to the absence of explicit association sites to mimic the existence of hydrogen bonding between the water molecules and the inner EO groups that enhances the miscibility. This result suggests that, somehow, being able to represent the hydrogen bonding acceptor character of EO groups (e.g., by adding one acceptor association site or one per each EO group) might be relevant especially when modelling aqueous systems, with the water molecules small size and high mobility contributing to an easier access to the EO groups for hydrogen bonding. This is something to be addressed in the next chapter of this project, when applying a heteronuclear SAFT variant to the modelling of EO-containing systems.

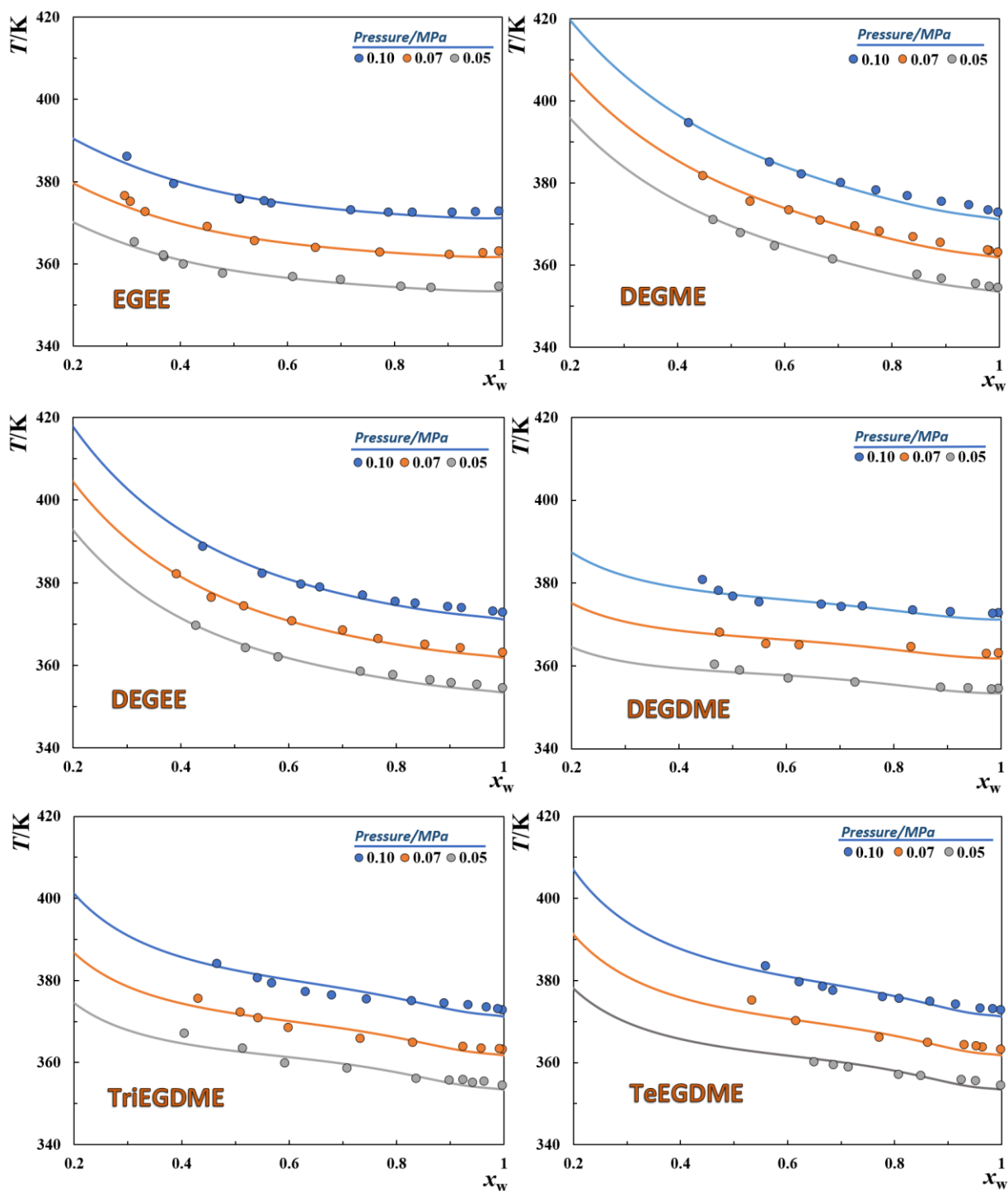


Figure 3.31. Isobaric temperature-composition phase diagrams of the binary glyme+ water mixtures. Symbols represent experimental data,[142] while the solid lines represent the soft-SAFT results, using the binary interaction parameters from Table 3.11.

Consequently, to accurately describe the experimental data, a binary interaction parameter correcting the non-ideality of the mixtures on a coarse-grained manner is necessarily fitted to the experimental data at 0.07 MPa and used to predict the remaining isobars. In this case, a state-independent parameter used to correct the unlike dispersive energy, ξ , is used, while no corrections were applied to the size parameter. As depicted in **Figure 3.31**, an excellent description is obtained for all the studied systems with average absolute deviations in temperature (%ARD) lower than 1.30 K. The deviations from the experimental data of each system and the values of the binary interaction parameter used in the calculations are provided in **Table 3.11**. All the binary parameters were found to be higher than one, suggesting that the model underestimates the interactions between the two species.

Table 3.11. Binary interaction parameters for the system glymes + water, and the deviations between the model calculations and the experimental data.

Water +	ξ	$AAD(T)/K$	%ARD(γ_w)
EGEE	1.105	0.814	18.7
DEGME	1.145	1.10	4.53
DEGEE	1.170	0.873	4.24
DEGDME	1.210	0.975	9.31
TriEGDME	1.220	1.27	5.04
TeEGDME	1.220	1.13	4.34

$$\frac{AAD(T)}{K} = \frac{1}{N} \sum_{i=1}^N |T_i^{calc} - T_i^{exp}| \quad (3.20)$$

$$\%ARD(\gamma_w) = \frac{100}{N} \sum_{i=1}^N \frac{|\gamma_{w,i}^{calc} - \gamma_{w,i}^{exp}|}{\gamma_{w,i}^{exp}} \quad (3.21)$$

In the previous section, the binary interaction parameter between glycols and water was found to increase with the glycols chain length until reaching an asymptotic behaviour for PEG 400 resulting in a value that could then be used for reasonable predictions of the behaviour for higher chain length polymers. Here, a similar trend is observed, with the values of the binary parameter increasing with the glyme's M_w until reaching what seems to be an asymptotic value of 1.22 for TriEGDME onwards, this being curiously the same asymptotic value found before for glycols + water mixtures. Although, there is no experimental data available to evaluate the predictive ability of the model for higher chain length homologues as previously done for glycols, the common roots of both models, and the similar asymptotic

behaviour of the binary parameter, suggest that this model can be used to obtain reliable predictions of the VLE of heavier glymes in water than those studied in this work.

The boiling temperatures of the pure glymes and that of their aqueous mixtures at three different compositions (glyme mole fraction of 0.25, 0.50, and 0.75) as calculated by the soft-SAFT EoS are plotted in **Figure 3.32**. This figure suggests that the mixtures boiling temperatures increase with the glymes chain length, as expected due to an increase of both the van der Waals dispersion forces and the polar interactions involving the EO groups, with the temperature increasing in the following order: *DEGDME* < *TriEGDME* < *TeEGDME*. However, the replacement of a methyl group by an ethyl group and the removal of the terminal hydroxyl group of mono-alkyl glymes have the opposite effect, lowering the equilibrium temperature. If the latter effect is relatively easy to understand due to the lower number of hydrogen bonds that can be established once a highly associative functional group is removed, the former is more convoluted with a possible explanation being that the existence of a bulkier terminal group hinders the otherwise easy access of water molecules to the inner EO groups, diminishing the magnitude of the cross-interactions.

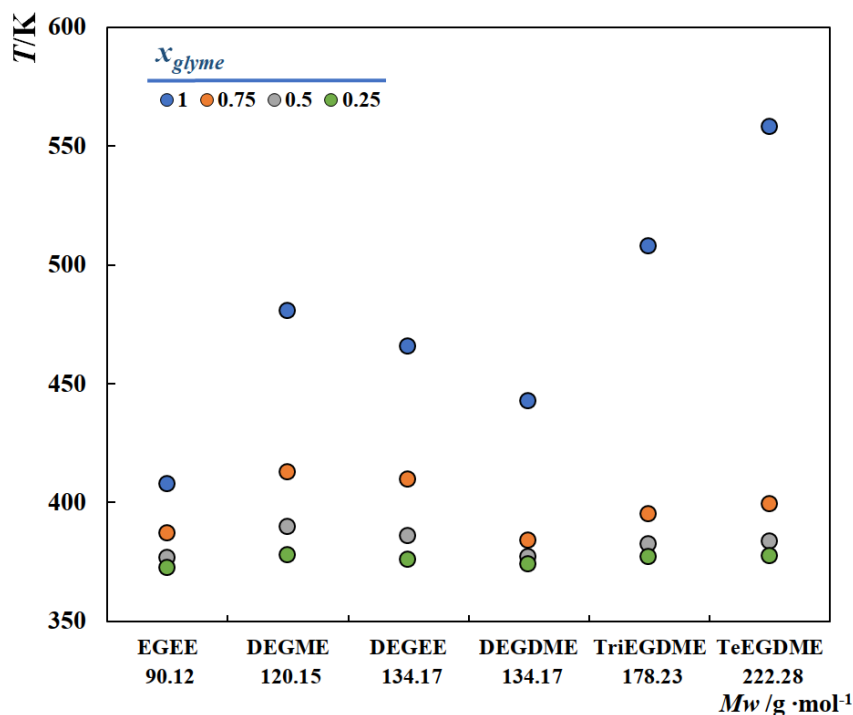


Figure 3.32. Boiling temperatures (@1atm) of the pure glymes and their aqueous solutions at different concentrations as calculated with soft-SAFT EoS.

As previously done for glycols + water systems, the water activity coefficients in the glymes + water systems were also estimated from the experimental VLE data, using **eq. 3.18**, and the results are plotted in **Figure 3.33**, along with the soft-SAFT predictions that are always obtained using the more rigorous expression in **eq. 3.17**. As can be observed, a reasonable agreement between the experimental estimates and the modelling results is found for most systems, despite the simplifications considered when treating the experimental data. The %ARD between the two sets of data are reported in **Table 3.11**, and highlight the high deviations observed for the lighter glyme investigated. This is expected, considering the high volatility of EGEE and the consequent increase of its concentration in the vapor phase that can no longer be neglected as done when using **eq. 3.18** with the experimental data.

Contrarily to what was observed with glycols, γ_w were found to be higher than 1 in the concentration range where experimental measurements were carried, denoting the existence of weaker interactions in the mixture than those observed in the pure compounds. For the mono-alkyl glymes, γ_w decrease with the increase of the glymes chain length (e.g., $\gamma_w(DEGME) < \gamma_w(EGEE)$) probably due to the increase of the number of EO groups that can interact favourably with the water molecules. Conversely, following the same reasoning as for the decrease of the boiling temperatures, the replacement of a terminal methyl group by an ethyl group increases the water activity coefficients. Furthermore, γ_w in the systems with di-alkyl glymes suggest that the removal of the terminal hydroxyl group reduces, as expected, the interactions with water, translated into an increase of the water activity coefficients (e.g., $\gamma_w(DEGDME) > \gamma_w(DEGME)$)

Although there is no experimental data in the glycol rich region of the vapor-liquid phase diagram, the soft-SAFT EoS was used to predict γ_w in the whole concentration range (water mole fractions ranging from 0.01 to 1) and show the existence of a maximum on the γ_w in all systems, whose value decreases when increasing the glymes' chain length, adding a terminal hydroxyl group, or through the replacement of a terminal ethyl group by a methyl counterpart. This agrees with the effect of these same structural changes on the boiling temperatures, as previously discussed and shown in **Figure 3.32**.

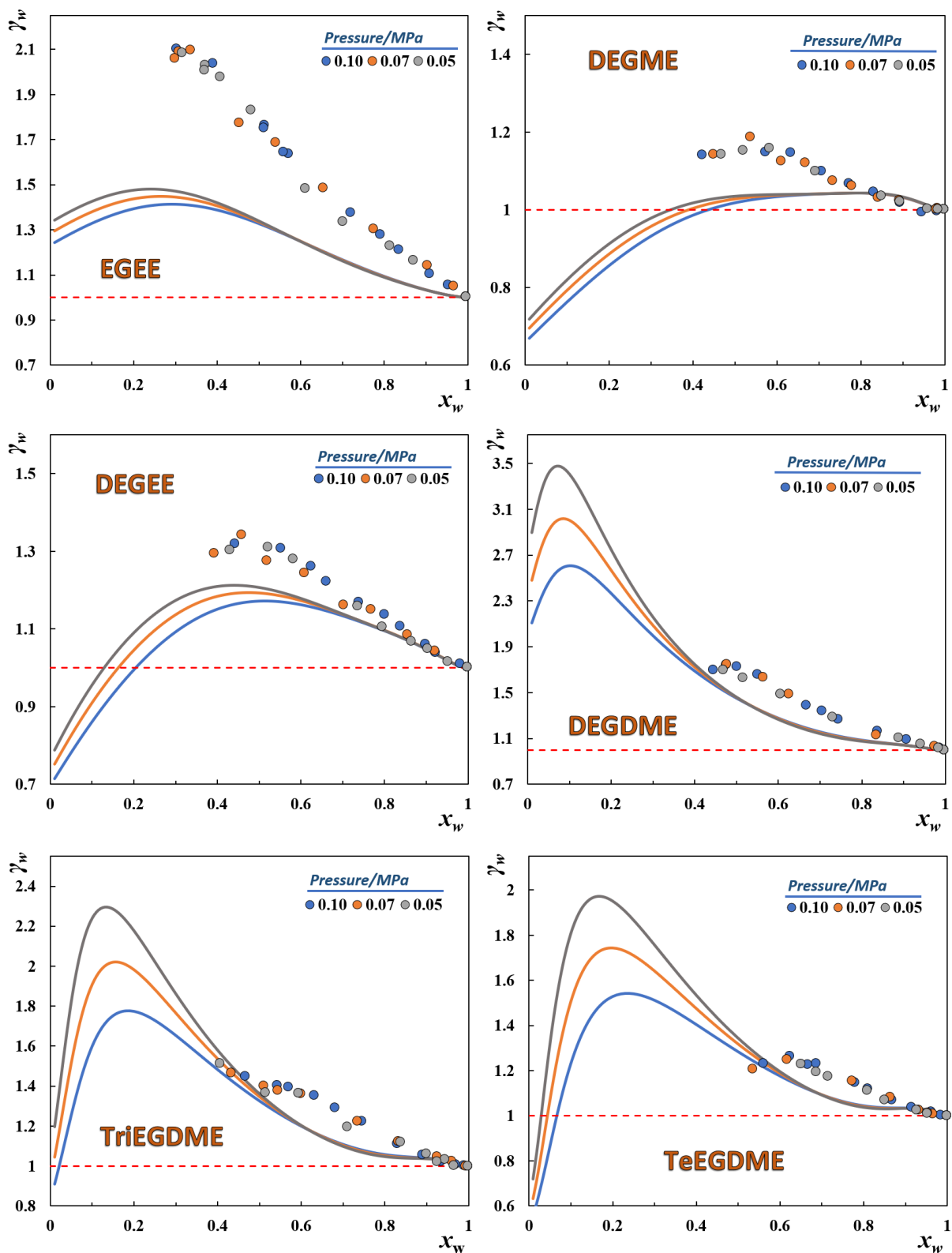


Figure 3.33. Water activity coefficients for glyme + water binary mixtures. Symbols represent estimates obtained from the experimental boiling temperatures,[142] while the solid lines depict the soft-SAFT predictions.

Conclusions

In this section, the soft-SAFT molecular models previously developed for glycols and glymes were used to successfully describe the isobaric VLE data of several binary mixtures glycols + water and glymes + water, and to provide useful insights into the magnitude and type of interactions established in those systems, and how they are affected by structural changes on the glycol/glyme molecule. To obtain an accurate description of the experimental data, a state-independent binary interaction parameter, correcting the mixtures dispersive energy, was used in all systems. This binary parameter was always higher than one, highlighting the model's underestimation of the glycol/glyme – water interactions that, in the absence of the binary parameter, may lead to immiscibility in some of the investigated systems.

The investigation of a reasonable number of systems allowed to observe that the binary interaction parameter necessary for capturing the behaviour of these mixtures tends to increase with the glycols/glymes' chain length towards an asymptotic value around 1.22 for both types of polyethers. This value was shown to be able to provide reasonable predictions of the behaviour for mixtures containing their heavier homologues.

From the experimental boiling temperatures, the water activity coefficients were estimated and compared with the values predicted by the soft-SAFT EoS. Except for the systems where the polyether has a considerable volatility, a good agreement between the experimental estimates and the model predictions was obtained, suggesting that the values predicted by the model can indeed be used to rationalized about the interactions present in the system. For glycols + water systems, γ_w were very close to 1 in the solvation regime, but when the glycols mole fraction is increased a regular decrease of γ_w to values considerably lower than 1, suggesting the existence of strong interactions between water and the glycols. Conversely, in the glymes + water systems, due to the decreased number of OH groups and consequent decrease in hydrogen bonding, γ_w were always higher than one in the concentration region where the experimental measurements took place. Both, the replacement of a terminal ethyl group by a shorter methyl group or the removal the terminal hydroxyl group results in a decrease of the equilibrium temperature, translated into an increase of γ_w .

Overall, the CG models proposed before represent a useful tool to provide not only a good description of the experimental data, but also reliable predictions and useful insights into the thermodynamic behaviour of water + glycol/glyme systems.

4- EoS modelling of C_iE_j surfactants: The Fallacy of Heteronuclear SAFT Variants

“What is simple is always wrong. What is not is unusable.”

Paul Valéry

4.1- Introduction

Even though SAFT-type models have been around for over 30 years, research on applied thermodynamics, focused on the development/improvement of these models, continues to be a very active research topic, with part of the efforts being devoted to improving the predictive ability and parameters transferability of the EoS. As such, different attempts aiming at transferring the model parameters between different compounds of a given homologous series or different families have been reported. Several authors have shown that simple empirical relationships between the molecular parameters and the molecular weight/carbon number of the molecules can be drawn for a given homologous series, allowing the inter/extrapolation of the model parameters to compounds of different chain length, this being successfully applied in **Chapter 3**. However, as the fluids become more complex, the performance of the extrapolated parameters deteriorates for increased chain lengths, especially if the underlying CG model of the smaller oligomers is too simplistic.

To avoid extensive parameterizations, and because SAFT models are often used for the prediction of binary or multicomponent systems, for which experimental data is not readily available for one or more of the compounds, pseudo-GC methods, in which the pure-component parameters are obtained from mixing rules that combine group-specific parameters, have also been proposed and applied to some of the most successful SAFT variants, such as SAFT-0,[143] SAFT-VR,[143] PC-SAFT,[144–146] and sPC-SAFT[147,148], being used for the successful description of a wide variety of fluids.[143–151].

Alternatively, instead of applying a GC treatment directly to the pure-component parameters, a more physically meaningful approach would be to develop the underlying theory explicitly in terms of the different functional groups making up the molecule. In this way, the monomeric segments on the chainlike fluid are no longer identical, as occurred with the more common homonuclear SAFT variants. This means that the energy and size characterizing the different monomers are no longer equal to an averaged compound-specific value but can now account for the molecules' heterogeneity and the differences between the functional groups making up the molecule. This has led to the development of heteronuclear SAFT models, the most successful being SAFT- γ ,[67,152] GC-SAFT-VR,[66] and SAFT- γ -Mie[68] that have been applied for the successful description of systems containing different types of compounds including alkanes,[66–68,153] perfluoroalkanes,[154] alkenes,[67,153] alcohols,[67,155] aromatics,[66,67,153,156] ketones,[66,152] acids,[152,153] amines,[152] esters,[66,68,157] and polymers[158], with accuracies similar (and in some cases better) than those obtained using the more traditional homonuclear variants.

Therefore, the use of heteronuclear SAFT variants is often viewed as a way to improve the predictive ability and parameter transferability of advanced association models, being particularly appealing to deal with molecules for which pure-component experimental data, necessary to parameterize the homonuclear models, is unavailable, as it is the case for most C_iE_j surfactants mentioned in **Chapter 1**, that typically exist in the form of their aqueous solutions. However, in most of these works using either ‘pseudo-group’ GC methods or heteronuclear SAFT models, the study of a different family/type of compounds often results in the introduction of a new functional group, a new version of an existing group (e.g., due to changes in its position within the molecule), or a simple refitting of a given functional group. This not only leads to extensive parameter tables that may contain multiple versions of a same group, but also hinders the assessment of the ‘true’ transferability of group-specific parameters across different types of compounds, something that is widely recognized as the brand of heteronuclear models.

Hence, the question persists, does the good agreement with experimental data for a multifunctional compound using these models results from a better representation of the effect of the individual groups on the thermodynamic behaviour of the fluid? Or the fitting of a new group at each stage of development of a molecular model, even if a small number of adjustable parameters is present, masks any deficiencies on the functional groups that are common to other families? As an example, when a carboxylic acid is modelled using a heteronuclear SAFT model, CH_3 , CH_2 , and $COOH$ groups are involved. The CH_3 and CH_2 groups are transferred from those previously fitted to the thermodynamic behaviour of *n*-alkanes but are they accurately describing the effect of these groups on the carboxylic acid’s behaviour, or are the deficiencies being masked by the parameterization of the $COOH$ group? If the latter is true, then the $COOH$ parameters will be affected and will probably fail when used to describe multifunctional molecules that contain $COOH$ groups along with functional groups other than CH_3 and CH_2 .

This work aims at investigating whether the additional complexity (and thus decreased computational efficiency) of a heteronuclear treatment of the SAFT theory results in an enhanced transferability of the model parameters across different families of compounds, effectively avoiding the need of extensive parameterizations and improving the overall predictive ability of SAFT-type models. For this analysis, one of the most prominent heteronuclear SAFT-type EoSs, SAFT- γ -Mie[68] described in **Chapter 2.1.3**, is used to carry a case study involving some different (yet related) families of compounds, containing a small number of common functional groups, for which the EO-based compounds mentioned in **Chapter 1** stand as a suitable option.

Glycols, glymes, and C_iE_j surfactants can all be decomposed into four main functional groups (CH_3 , CH_2 , OH , and the EO group - CH_2OCH_2), only one of which is not found in the well-known *n*-

alkanes and alkan-1-ols series. In these compounds, as they are made up of the same functional groups, no additional parameterizations should be carried between them to obtain a reasonable description of the system, allowing the evaluation of the ‘true’ capability of heteronuclear SAFT variants. In this way, even though experimental data is not available for most pure C_iE_j surfactants, all its functional groups can be adequately parameterized using abundant data from the other compounds (e.g., EO group is present in both glycols and glymes, for which experimental data is widely available), and a highly predictive tool to describe these surfactants and to screen their phase behaviour in water could, in theory, be obtained.

4.2- SAFT modelling of C_iE_j surfactants and the case for a predictive tool

SAFT-based approaches have long been used to provide useful information regarding different aspects of surfactant-like behaviour, including correlating the critical micellar concentration (*cmc*), [159] investigate the aggregate formation and fraction of unbounded molecules, [83] or through coupling with the density functional theory (DFT) study the influence of surfactant structure on micelle formation, surface and interfacial tensions, and obtain density profiles at oil-water interfaces. [160–162] However, the complex phase behaviour observed in aqueous solutions of C_iE_j surfactants, characterized by displaying closed-loop immiscibility, is clearly overlooked, despite the importance that being able to accurately describe the phase behaviour of this binary system has on later predicting the behaviour of complex aqueous formulations containing these surfactants, such as those used in EOR or in the detergents and cosmetics industry.

For very light surfactants, vapor pressures and liquid densities are available and the common parameterization methodologies have been applied with PC-SAFT and CPA EoSs to describe the phase behaviour of C_1E_1 , C_2E_1 , C_4E_1 , and C_4E_3 in water. [163,164] Conversely, to the best of my knowledge, only García-Lisbona et al. [165,166] have systematically addressed the modelling of higher surfactants using a SAFT-type EoS, namely SAFT-HS [167]. In a first work, [165] they applied the model to describe the phase equilibria of binary aqueous solutions of C_4E_1 and $C_{10}E_5$. The surfactant molecules were described as associating chains containing three associating sites to represent the hydroxyl end group: one negative site ‘e’, one positive site ‘H’, and an additional negative site ‘e*’ that was only able to establish cross-interactions with water, i.e., ‘e*–H’ interactions between surfactant molecules were not allowed. Additionally, three negative association sites ‘O’ per EO group are used to mimic the cross-interactions between water and the ether oxygen atoms, while ‘O–H’ self-interactions were also forbidden; the steric hindrance is allegedly too large for those interactions to occur favourably. The number of segments was obtained from an empirical expression and the non-associating parameters, σ

and ε were transferred from *n*-alkanes, while the self-association parameters ('e-H') were fitted to the vapor pressures of C₄E₁. Concerning the unlike interactions between the hydroxyl group and water ('e*-W'), the parameters were transferred from the system 1-butanol + water, and the cross-association energy for interactions through the EO groups with water ('O-W') was fitted to the LLE data of C₄E₁ + water and transferred for the modelling of C₁₀E₅. Following this approach, the cross-dispersive energy parameter between the surfactant and water, ε_{12} , was necessarily fitted to each individual system to reproduce the formation of a closed loop immiscibility region. In a subsequent publication,[166] the study was extended to the aqueous solutions of a wide range of surfactants, assessing the model parameters transferability to different C_iE_j surfactants through an examination of their cloud curves. The general trends could be reproduced using transferred parameters, except for the ε_{12} that was confirmed to be necessarily fitted individually to the LCST of the LLE of each C_iE_j + water system for the model to be able to describe the closed-loop immiscibility regions, with both the critical temperatures and the extent of immiscibility being in good agreement with the experimental data. Nevertheless, the authors were able to find a quadratic dependence of ε_{12} on *j* and, assuming a linear dependence on *i*, a general relationship for $\varepsilon_{12} = f(i, j)$ was proposed, conferring a certain predictive ability to the developed model.

Despite the good results obtained by Nieves García-Lisbona and co-workers,[165,166] the use of this model for the design and simulation of new processes using these surfactants is made difficult for several reasons:

- SAFT-HS EoS is not implemented in common commercial process simulators, and the wider adoption of other homonuclear SAFT variants like PC-SAFT and CPA over the last decades make it highly unlikely that it will ever be.
- The number of association sites chosen to represent the EO group (3) was chosen arbitrarily to obtain the best agreement with the experimental data rather than following theoretical basis. Two sites would have seemed more obvious (i.e., one per each lone electron pair)
- It makes use of a very complex and somewhat empirical association scheme. Some of the specific issues are a) 'H-e*' and 'O-H' interactions are forbidden, despite involving sites of opposite hydrogen bonding ability. This would require the software to allow the user the possibility to specify all the pairwise cross-interaction parameters on the interaction matrix, which although extremely useful in some cases, is, to the best of my knowledge, yet to be implemented in commercial software. b) For larger surfactants, the use of three association sites per each EO group would result in a high number of association sites and thus on an

increased computational cost of the calculations. Probably a similar accuracy could be obtained using one single negative association site per EO group to account for the hydrogen bonding acceptor character of this group, but results were not provided to corroborate or discredit such claim.

- The parameterization of the interactions involving the EO group is solely based on C_4E_1 , which, due to its very low M_w (only contains one EO group) and different nature, may not be appropriate for the modelling of its heavier homologues.

For these reasons, the development of a thermodynamic modelling framework for C_iE_j surfactants with enhanced predictive ability, based on the SAFT- γ -Mie EoS, would allow to overcome some of these limitations, fostering its use for large-scale applications. First, this EoS has been increasingly applied in the literature since its inception, being by far the most widely acknowledged heteronuclear SAFT model, and it is already implemented in gPROMS® process simulator by Process Systems Enterprise. Secondly, the model parameterization is made completely independent of data on C_iE_j -based systems. Finally, a simple but physically meaningful association scheme can be applied to each functional group, decreasing the total number of association sites assigned to a surfactant molecule, without sacrificing accuracy. So, the question is: are heteronuclear SAFT EoSs the answer?

4.3- Results

n-alkanes

Due to the importance of CH_3 and CH_2 groups for the modelling of a wide variety of compounds, including those of interest to this work, the parameterization proposed by Papaioannou et al.[68] in the original SAFT- γ -Mie paper is here revisited. Both the group-specific parameters and the unlike interactions between the methyl and methylene functional groups, reported in **Table 4.1** and **Table 4.2**, were obtained by fitting to experimental data for vapor pressure, saturated liquid density, and single-phase density of *n*-alkanes from ethane to *n*-decane, and exhibit %ARD of 1.55 and 0.59 for vapor pressure and saturated liquid density data, respectively.

As shown in **Figure C.1** and **Figure C.2**, in **Appendix C**, the performance of the model in describing the vapor pressure and the saturated liquid density is indeed remarkable except for ethane and *n*-propane. This is however expected since they are the shortest oligomers of the *n*-alkanes series and the thermodynamic behaviour of the first members of a homologous series of compounds can deviate from their heavier homologous. In the same work, Papaioannou et al.[68] showed that, using these parameters,

good predictions for the thermodynamic behaviour of n -alkanes of longer chain lengths (up to C30) could be obtained, including a good description of second-order derivative properties such as the isobaric and isochoric heat capacities (c_p and c_v), speed of sound (u), isothermal compressibility (k_T) and isobaric expansivity (α_p). Additionally, as it is shown in **Figure C.3**, a good prediction of vaporization enthalpies can also be obtained for n -alkanes up to at least 20 carbon atoms.

Another important test for the validity of the CH₃ and CH₂ parameters is the modelling of binary mixtures of n -alkanes. Papaioannou et al.[68] showed that, using these parameters, excellent descriptions of both the VLE and excess properties, namely the excess speed of sound and excess molar volumes, could be obtained. Particularly remarkable, is the good agreement with the experimental data obtained for highly asymmetrical systems (e.g., n -propane + n -hexacontane). In addition, it is shown in **Figure C.4**, in **Appendix C**, that the model is able not only to successfully describe both isothermal and isobaric vapor-liquid equilibrium (VLE) of binary n -alkane mixtures, but also their densities, even at high pressures. For all these reasons, the parameters previously estimated for the methyl and methylene groups (and their unlike interaction) by Papaioannou et al. [68] will be used throughout this work.

Table 4.1. Group specific parameters used in the SAFT- γ -Mie EoS calculations.

Group	ν_k	S_k	λ_{kk}^r	λ_{kk}^a	$\sigma_{kk}(\text{\AA})$	$\epsilon_{kk}/k_B[\text{K}]$	$NS_{k,H}$	$NS_{k,e1}$	$NS_{k,e2}$	Ref.
CH ₃	1	0.57255	15.050	6	4.0772	256.77	-	-	-	[68]
CH ₂	1	0.22932	19.871	6	4.8801	473.39	-	-	-	[68]
CH ₂ OH	2	0.58538	22.699	6	3.4054	407.22	1	2	-	[168]
H ₂ O	1	1.00000	17.020	6	3.0063	266.68	2	2	-	[153]
OH	1	0.82154	10.316	6	2.8965	350.00	1	2	-	This work
EOa	2	0.55560	11.860	6	3.8050	277.39	0	0	1	This work
EOb	1	0.55386	10.000	6	4.8330	367.68	0	0	1	This work
EOg	2	0.55560	20.011	6	3.805	394.26	0	0	1	This work
CH ₃ Oa	1	0.6860	10.05	6	3.9910	473.50	0	0	1	This work
CH ₃ Og	1	0.9650	10.26	6	3.5690	493.48	0	0	1	This work

Table 4.2. Unlike physical interaction parameters used in the SAFT- γ -Mie EoS calculations.

Group k	Group l	$\epsilon_{kl}/k_B(K)$	λ_{kl}^r	Ref.
CH ₃	CH ₂	350.77	CR	[68]
CH ₃	CH ₂ OH	333.20	CR	[168]
CH ₃	H ₂ O	358.18	100.00	[168]
CH ₃	OH	249.96	CR	This work
CH ₂	H ₂ O	423.63	100.00	[168]
CH ₂	CH ₂ OH	423.17	CR	[168]
CH ₂	OH	352.53	CR	This work
CH ₂ OH	H ₂ O	353.37	CR	[168]
OH	H ₂ O	323.55	CR	This work
EOa	CH ₃	383.60	CR	This work
EOa	CH ₂	296.00	CR	This work
EOa	OH	472.44	CR	This work
EOa	H ₂ O	289.44	CR	This work
EOb	CH ₃	443.01	CR	This work
EOb	CH ₂	262.27	CR	This work
EOb	OH	351.21	CR	This work
EOb	H ₂ O	261.54	CR	This work
EOg	CH ₃	269.10	CR	This work
EOg	CH ₂	325.24	CR	This work
EOg	OH	451.94	CR	This work
EOg	H ₂ O	340.65	CR	This work
CH ₃ Oa	CH ₃	458.70	CR	This work
CH ₃ Oa	EO	232.41	CR	This work
CH ₃ Oa	H ₂ O	279.30	CR	This work

CH₃Og	CH₃	478.68	CR	This work
CH₃Og	EO	293.53	CR	This work
CH₃Og	H₂O	335.74	CR	This work

CR- Combining rule (eq. 2.55)

n-alkanes + water mixtures

As mentioned in the introduction, the EO-containing compounds that are the cornerstone of this work present a rich and varied phase behaviour when in aqueous solutions. Therefore, the modelling of their mixtures with water will also be considered throughout this work to evaluate the performance of the SAFT- γ -Mie EoS and the transferability of parameters, across the different families of compounds. Consequently, it is important to have an accurate and robust parameterization of water and of their unlike interactions with the groups of interest.

Dufal et al.[153] were the first to propose a parameterization of the water molecule, in the framework of SAFT- γ -Mie, along with parameters for the unlike interactions between water and a considerable number of functional groups. Of special relevance to this work are the water group specific parameters (reported in **Table 4.1** and **Table 4.3**), and the parameters characterizing their unlike interaction with the methyl and methylene groups, reported in **Table 4.2**. Although details concerning the experimental data used in the fitting of such parameters were not provided, the model was shown to provide a good description of the very low mutual solubilities exhibited in water + benzene and water + *n*-hexane systems, and a good prediction of the excess isobaric heat capacity (C_p^E) of acetone + water mixtures. In a subsequent study by the same group,[168] the authors found that, using this parameterization, a good description of the *n*-alkane solubility in the water-rich phase could only be obtained for medium chain length hydrocarbons. Therefore, the parameters characterizing the unlike interaction between the alkyl groups and water were refined, considering both the ϵ_{kl} and λ_{kl}^r as adjustable parameters. While keeping the water molecule parameters equal to those previously reported,[153] three-phase vapor-liquid-liquid equilibrium (VLLE) solubility data for aqueous mixtures of *n*-pentane and *n*-octane, over an extended temperature range, and the coexisting liquid compositions at 298 K, along the three-phase region, for mixtures of *n*-hexane and *n*-decane mixtures were used to obtain the unlike parameters mediating the H₂O-CH₃ and H₂O-CH₂ interactions, reported in **Table 4.2**.

Table 4.3. Site-site hydrogen-bonding parameters used in the association term.

Group k	Group l	Site a of group k	Site b of group l	$\varepsilon_{kl,ab}^{HB} [K]$	$\kappa_{kl,ab}^{HB} / [\text{\AA}^3]$	Reference
H ₂ O	H ₂ O	H	e ₁	1985.4	101.69	[153]
CH ₂ OH	CH ₂ OH	H	e ₁	2097.9	62.309	[168]
CH ₂ OH	H ₂ O	H	e ₁	621.68	425.00	[168]
CH ₂ OH	H ₂ O	e ₁	H	2153.2	147.40	[168]
OH	OH	H	e ₁	2491.9	21.340	This work
OH	H ₂ O	H	e ₁	1690.5	37.640	This work
OH	H ₂ O	e ₁	H	2064.83	179.98	This work
EOa	OH	e ₂	H	2523.3	21.340	This work
EOa	H ₂ O	e ₂	H	1381.95	315.32	This work
EOb	OH	e ₂	H	745.29	678.20	This work
EOb	H ₂ O	e ₂	H	2461.63	15.01	This work
EOg	OH	e ₂	H	1196.0	21.340	This work
EOg	H ₂ O	e ₂	H	1319.83	61.18	This work
CH ₃ Oa	H ₂ O	e ₂	H	2793.22	14.96	This work
CH ₃ Og	H ₂ O	e ₂	H	3161.61	15.00	This work

As shown in **Figure 4.1**, these new parameters allowed for a considerable improvement on the description of the n -alkanes solubility in water, while preserving a similar accuracy when describing the water solubility in n -alkanes (cf. Hutacharoen et al.[168]).

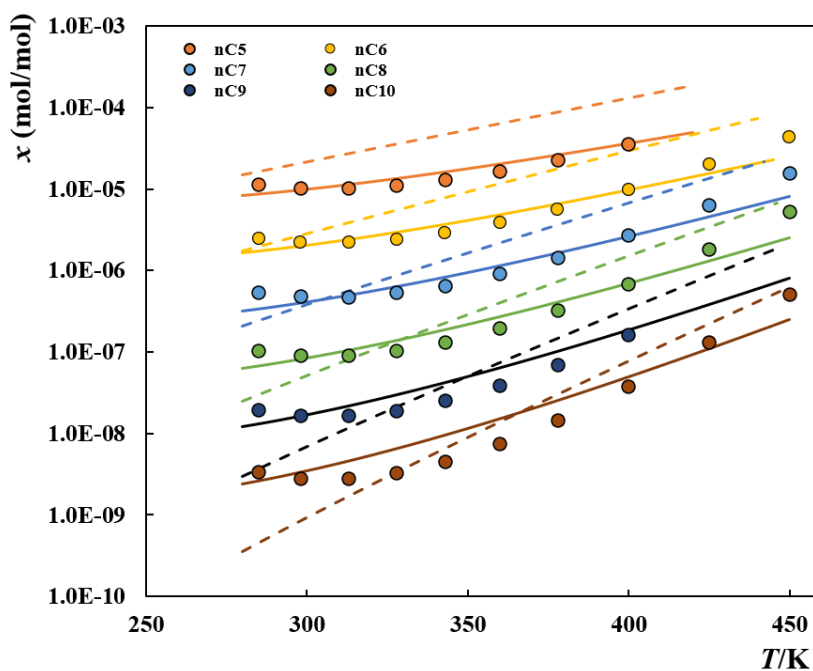


Figure 4.1. Solubility of *n*-alkanes in water. Symbols represent experimental data,[169–174] while the solid lines and dashed lines represent the SAFT- γ -Mie results using the unlike interaction parameters with alkyl groups proposed by Hutacharoen et al.[168] and Dufal et al.[153], respectively.

alkan-1-ols

Once the alkyl groups are established within the GC framework, they can be transferred to the modelling of more complex compounds, through the successive introduction of additional groups. The compounds of interest to this work contain one or two terminal alcohol groups, also present in the much simpler alkan-1-ols. Evidently, alcohol groups can be modelled either as the hydroxyl group itself (i.e., OH), or along with the methylene group to which it is bonded, considering it as a CH₂OH group.

Hutacharoen et al.[168] have proposed a parameterization for the study of 1-alcohols in the framework of SAFT- γ -Mie. In their work, a new CH₂OH group, whose parameters are reported in **Table 4.1** and **Table 4.3**, was introduced. As reported in **Table 4.1**, the CH₂OH group proposed contains two identical segments and, being an associating group, a 3B association scheme, according to the nomenclature proposed by Huang and Radosz[58] was assigned. The new group contains two association site types: two sites type ' e_l ' representing the two lone electron pairs on the oxygen atom, and one site type ' H ', representing the hydrogen atom of the hydroxyl group, with only unlike site-site interactions being allowed. The parameters obtained for the CH₂OH and its unlike interactions with CH₃ and CH₂ groups were obtained by fitting to the vapor pressure and saturated-liquid density of pure *n*-alkan-1-ols from ethanol to *n*-decan-1-ol, along with the LLE data for *n*-tetradecane + ethanol.

Although this model is able to successfully describe both the pure-component properties of alkan-1-ols and the phase equilibria of binary mixtures n -alkanes + alkan-1-ols and water + alkan-1-ols, a new parameterization of the hydroxyl group, considering it as an OH group, instead of a CH₂OH, is proposed in this work. The idea is not to replace the parameterization proposed by Hutacharoen and co-workers,[168] but rather to be able to test the two alternatives in the modelling of other families of compounds, and evaluate the transferability of the hydroxyl group across the different compounds of interest. To parameterize the new OH group, only one segment was considered (i.e. $v_k^* = 1$) and, similarly to the CH₂OH group available in the literature, the 3B association scheme was assigned to represent its hydrogen bonding character. The attractive exponent, λ_{kk}^a , was fixed to the default value of 6 as commonly done for most groups,[153] while the remaining unknown parameters, S_k , λ_{kk}^r , σ_{kk} , ϵ_{kk}/k_B , $\epsilon_{kl,ab}^{HB}$, $\kappa_{kl,ab}^{HB}$, and the parameters characterizing the unlike dispersive energy with the CH₃ and CH₂ groups were regressed from the vapor pressures and saturation liquid densities of pentan-1-ol, hexan-1-ol, octan-1-ol, and decan-1-ol, along with the VLE of butan-1-ol + n -decane mixture. The OH-group specific parameters obtained are reported in **Table 4.1** and **Table 4.3**, while those mediating the unlike interactions with the alkyl groups are provided in **Table 4.2**. Comparing to the CH₂OH parameters reported in the literature, the new OH parameters show a much lower repulsive exponent of the Mie potential, which is coherent with the lower ‘OH–OH’, ‘OH–CH₂’ and ‘OH–CH₃’ dispersive energies obtained.

This difference may be due to the fact that, contrarily to the parameterization carried out by Hutacharoen and co-workers,[168] pure fluid data for ethanol and propan-1-ol were not included in the experimental dataset used for the fitting, which could force the repulsive exponent of the Mie potential towards higher values. Instead, it was opted to exclude them from the dataset as the shortest oligomers of a given homologous series can have a slightly different behaviour than their higher chain length homologues, since the global effect of the presence of a terminal alcohol group can be affected by the very small alkyl chain attached to it. Consequently, as reported in **Table 4.4**, the deviations between the model calculations and the VLE experimental data for pure ethanol are higher than those obtained using the CH₂OH group available in literature[168]. On the other hand, for most of the remaining oligomers, including propan-1-ol, the new parameterization yields a better description of the data.

To enhance the robustness of the OH group parameterization, the VLE of butan-1-ol and + n -decane mixture was also considered in the fitting procedure. Then, as all the necessary parameters were available, the model was used to predict the VLE of 25 different binary alkan-1-ols + n -alkanes mixtures. The deviations from the experimental data are reported in **Table 4.5**, along with those obtained if a

CH₂OH group is considered and as can be gauged from the table, both models have a similar accuracy, although the new OH group shows lower deviations for 17 out of the 25 mixtures investigated. Nevertheless, in most cases the differences between the two models are negligible, and the highest deviations are usually observed on the dew pressures of systems where experimental data is only available on a very narrow region of the phase diagram (e.g., butan-1-ol + *n*-dodecane and tetradecan-1-ol + *n*-undecane).

Table 4.4. Deviations between the SAFT- γ -Mie EoS results and the experimental data[118] for the vapor pressure, saturation liquid density and vaporization enthalpy of pure alkan-1-ols, using the alcohol group parameterized as an OH (this work) or as a CH₂OH[168].

Compound	<i>T</i> -range (K)	%ARD _{OH} $p^*/\rho_L/H_{\text{vap}}$	%ARD _{CH₂OH} $p^*/\rho_L/H_{\text{vap}}$
ethanol	200-510	5.06/2.60/2.25	2.27/2.64/1.59
propan-1-ol	200-530	5.85/1.48/2.01	6.91/1.35/1.58
butan-1-ol	220-550	3.39/1.26/5.07	7.51/1.44/5.14
pentan-1-ol	240-580	4.95/1.61/6.67	3.37/2.03/6.01
hexan-1-ol	250-600	2.90/2.38/5.79	3.20/2.93/5.31
octan-1-ol	280-640	2.12/2.12/10.92	6.00/2.90/10.24
decan-1-ol	290-660	2.56/2.24/8.61	3.62/2.93/8.55

Table 4.5. Binary alkan-1-ols + *n*-alkanes systems studied in this work, using the SAFT- γ -Mie EoS and the correspondent deviations from the experimental data modelling the hydroxyl groups as an OH (this work) or as a CH₂OH group[168].

System	<i>T</i> (K)	<i>P</i> (kPa)	%ARD _{OH}	%ARD _{CH₂OH}	Exp. Ref.
ethanol + propan-1-ol	303.15	12-16.02	7.58	3.86	[175]
ethanol + <i>n</i> C ₄	323-423	28-3800	2.69/4.30	4.00/7.23	[176]
ethanol + <i>n</i> C ₆	328-473	46-3484	2.23/2.75	5.72/5.54	[177]
ethanol + <i>n</i> C ₇	303.15	4-11	1.48	3.32	[175]
ethanol + <i>n</i> C ₁₁	333-353	0.5-106	7.15	8.68	[178]
propan-1-ol + <i>n</i> C ₆	338-348	21-138	2.53/4.64	6.08/6.37	[179]
propan-1-ol + <i>n</i> C ₇	303.15	5-11	1.05	4.09	[175]
propan-1-ol + <i>n</i> C ₁₁	333-353	0.5-51	7.95	10.5	[178]
butan-1-ol + <i>n</i> C ₅	333-393	8-918	3.37/6.21	2.27/7.65	[180]
butan-1-ol + <i>n</i> C ₆	323	21-55	5.56/1.85	1.03/0.48	[181]
butan-1-ol + <i>n</i> C ₇	313.15	2.5-13.2	2.43/2.13	1.96/1.71	[182]

butan-1-ol + nC_8^*	382-399	101.3	0.838*	1.79*	[183]
butan-1-ol + nC_8	313-373	2.4-76	4.48/2.49	6.06/4.42	[184,185]
butan-1-ol + nC_9	323	4.7-5.7	3.15/2.96	4.48/3.25	[181]
butan-1-ol + nC_{10}	358-388	5-92.5	3.56/2.95	5.45/4.37	[186]
butan-1-ol + nC_{11}	353-373	1.7-52.6	5.51	5.96	[178]
butan-1-ol + nC_{12}	313.15	0.05-2.5	5.67/19.1	3.93/16.8	[182]
pentan-1-ol + nC_5	303	0.4-82	5.28	3.55	[187]
pentan-1-ol + nC_7	348-368	7-92	0.86/0.77	3.14/1.08	[188]
pentan-1-ol + nC_9^*	406-424	101.3	0.381*	1.23*	[189]
hexan-1-ol + nC_6^*	342-422	101.3	1.233*	1.152*	[190]
hexan-1-ol + nC_7^*	371-428	101.3	1.873*	2.981*	[190]
octan-1-ol + nC_6	313.15	8.8-35.9	3.55	2.53	[181]
dodecan-1-ol + nC_6	298.15	7-19.7	1.96	1.57	[181]
dodecan-1-ol + nC_{11}	393-413	0.5-20.5	3.61	3.65	[178]
tetradecan-1-ol + nC_{11}	393-413	0.1-20.5	2.64/14.4	3.60/14.1	[178]

*Isothermal VLE – the deviations provided are an average absolute deviation in T (K).
When deviations are reported as a pair of values they are related to bubble/dew pressures.

alkan-1-ols + water mixtures

With the OH parameters and their unlike interactions with the alkyl groups defined, the model can be used to investigate the phase equilibria of alkan-1-ols + water mixtures. Contrarily to the n -alkanes + water mixtures where the presence of weak attractive interactions dominates the systems behaviour, in the case of alkan-1-ols + water mixtures, hydrogen bonding also plays an important role, with the fluid phase behaviour of these mixtures resulting from a delicate balance between the two types of interactions.

Consequently, while all n -alkanes are fully immiscible in water (mutual solubilities are very low), methanol, ethanol and propan-1-ol are fully miscible in water, and thus the phase diagram of their aqueous mixtures, consists of a simple VLE. Conversely, from butan-1-ol onwards, alkan-1-ols are only partly miscible in water (the water solubility in the alcohol-rich phase being much higher than the solubility of the alcohol in water-rich phase), and thus the isobaric temperature-composition (T - x) phase diagrams usually consist of a vapor-liquid-liquid equilibrium (VLLE).

To be able to model these mixtures, the unlike interaction parameters (dispersive energy and hydrogen bonding parameters) between the alcohol groups and water must be first estimated from experimental data. As previously done by Hutacharoen et al.[168] for the CH_2OH group, the unknown

parameters between the new OH group and water were regressed from the LLE data of the octan-1-ol + water mixture and the final values are reported in **Table 4.2** and **Table 4.3**. Afterwards, the parameters were used to predict the VLE and/or LLE data for alkan-1-ols + water mixtures from ethanol to dodecan-1-ol, an example being the satisfactory prediction of the VLLE phase diagram of the pentan-1-ol + water mixture shown in **Figure 4.2**.

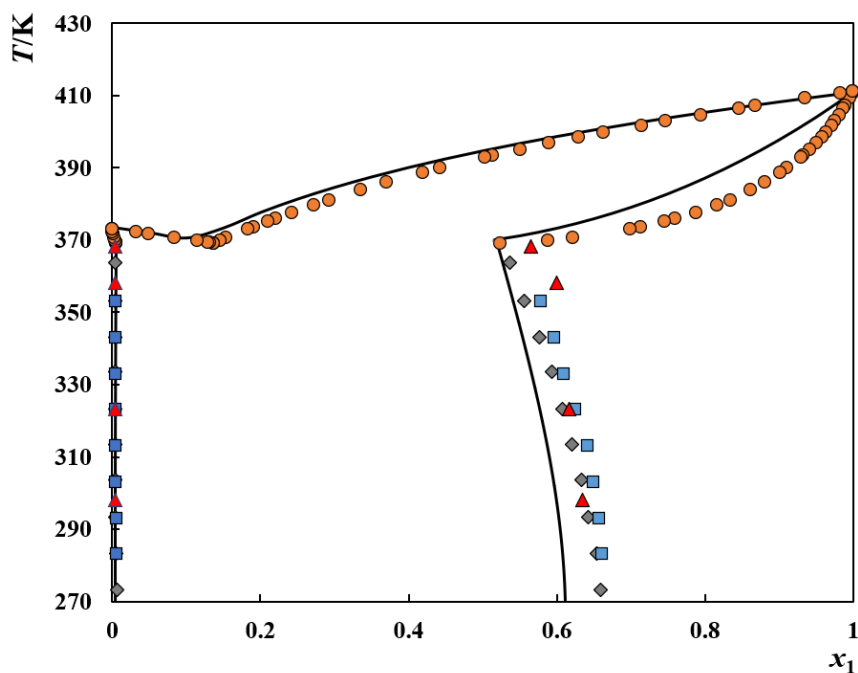


Figure 4.2. VLLE of pentan-1-ol (1) + water (2) at atmospheric pressure. Symbols represent experimental data, [191–194] while the solid lines depict the SAFT- γ -Mie EoS predictions using the new OH group parameters.

The performance of the new parameterization for the alcohol group, when used to describe alkan-1-ol + water mixtures, was further compared with the CG model that considers a CH_2OH group, and the deviations from the experimental data are reported in **Table 4.6**. As can be seen in **Figure 4.3**, both approaches have a similar performance when used to describe the mutual solubilities in such mixtures. The deviations from the LLE experimental data show that the new approach performs better in the alcohol phase and in the water-rich phase for the shorter alcohols, while the CH_2OH approach performs better in the water-rich phase of longer alcohols. In terms of VLE, both models have a similar accuracy, and reasonable results can be obtained, especially if considering that VLE data was not used in the parameterization of the unlike parameters between the alcohol and water groups.

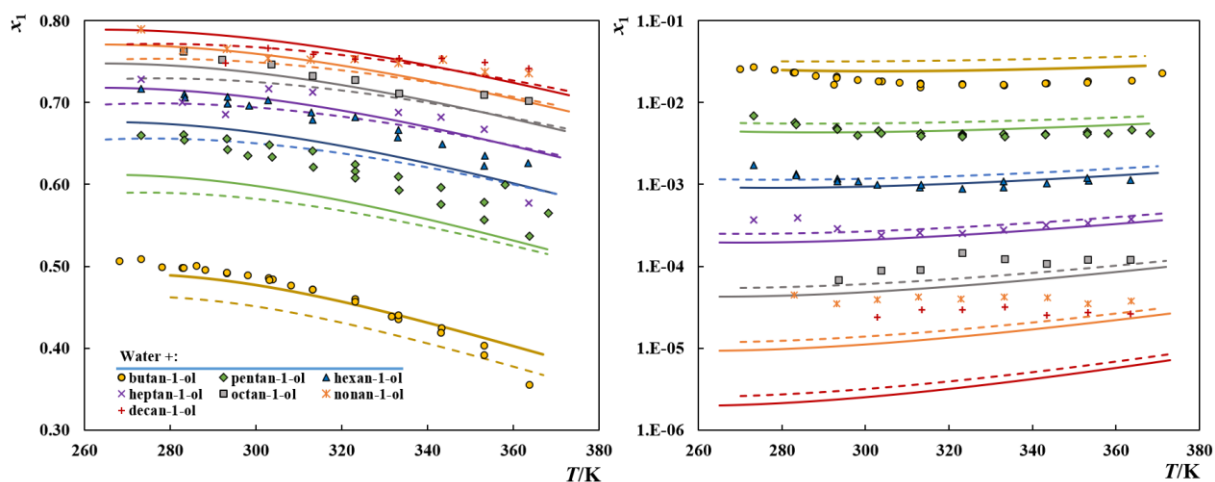


Figure 4.3. LLE of alkan-1-ol (1) + water mixtures. (left) alcohol rich phase (right) aqueous phase. Symbols represent experimental data (c.f. **Table 4.6**) while the solid and dashed lines represent the SAFT- γ -Mie results using an OH or a CH₂OH group, respectively.

Table 4.6. Binary alkan-1-ols + water systems studied in this work, using the SAFT- γ -Mie EoS and the correspondent deviations from the experimental data modelling the hydroxyl groups as an OH (this work) or a CH₂OH group.[168]

<i>Vapor-Liquid Equilibrium</i>				
System	<i>P</i> (kPa)	<i>AAD</i> (<i>T</i>)/ <i>K</i> _{OH}	<i>AAD</i> (<i>T</i>)/ <i>K</i> _{CH₂OH}	<i>Exp. Ref.</i>
ethanol + water	13-33	3.01/2.89	3.12/3.15	[195]
propan-1-ol + water	30-100	5.21/4.80	5.43/5.00	[196]
butan-1-ol + water	101.3	3.67/3.16	3.94/3.36	[197]
pentan-1-ol + water	101.3	4.99/1.87	5.06/1.96	[191]
hexan-1-ol + water	101.3	7.44/1.87	7.14/1.86	[198]
<i>Liquid-Liquid Equilibrium</i>				
	<i>T-range</i> (K)	% <i>ARD</i> (<i>x</i>) _{OH}	% <i>ARD</i> (<i>x</i>) _{CH₂OH}	<i>Exp. Ref.</i>
butan-1-ol + water	273-363	3.09/34.5	6.16/77.0	[199–201]
pentan-1-ol + water	273-363	5.03/19.5	7.20/38.2	[191–194]
hexan-1-ol + water	273-363	5.76/21.0	6.46/31.3	[192,202]
heptan-1-ol + water	273-363	3.13/18.0	3.43/16.7	[192]
octan-1-ol + water	283-363	1.27/42.1	2.52/25.5	[192,203,204]
nonan-1-ol + water	273-363	1.58/63.9	2.40/53.0	[201]
decan-1-ol + water	293-363	1.42/86.4	1.08/82.1	[201]

In VLE calculations the pair of deviations presented are related to the Bubble/Dew temperatures and are reported as an average absolute deviation in terms of temperature. In the LLE calculations, the values reported are for the alcohol/aqueous phase and are reported as %ARD.

α, ω – alkanediols

As mentioned above the main goal of this work is to evaluate the transferability of parameters and the predictive ability of heteronuclear SAFT-type EoSs. This means to evaluate the performance of group-specific and unlike interaction parameters across different families, whose study does not require the simultaneous introduction and fitting of additional groups. Having parameterized the alkyl groups and the alcohol group that, as seen in the previous sections, can be modelled either using an OH or a CH_2OH bead, one class of compounds that can be studied without further parameterizations is the α, ω – alkanediols. Experimental data is available for the pure fluid densities and vapor pressures from 1,2-ethanediol, to 1,5-pentanediol.[118] Hence, the parameters previously reported in **Tables 4.1-4.3**, were used in a predictive manner to calculate these properties. Such calculations are illustrated in **Figure 4.4** for 1,3-propanediol and 1,5-pentanediol, while the deviations from the experimental data for all the four compounds are reported in **Table 4.7**. As shown in **Figure 4.4**, both approaches fail to accurately describe these fundamental properties of pure α, ω – alkanediols. Although a reasonable description of density data could be obtained using the new OH group, especially at low temperatures, the description of the vapor pressures is very poor for all the compounds, using both approaches, with deviations ranging between 17.5 and 48.3%. These results are a first indication of the limited transferability of group and unlike parameters across different families, suggesting that the effect of the hydroxyl groups in a fluid's behaviour, or at least, the additive effect of having multiple units of it in a given compound may not be correctly accounted for by using multiple alcohol groups in a heteronuclear EoS.

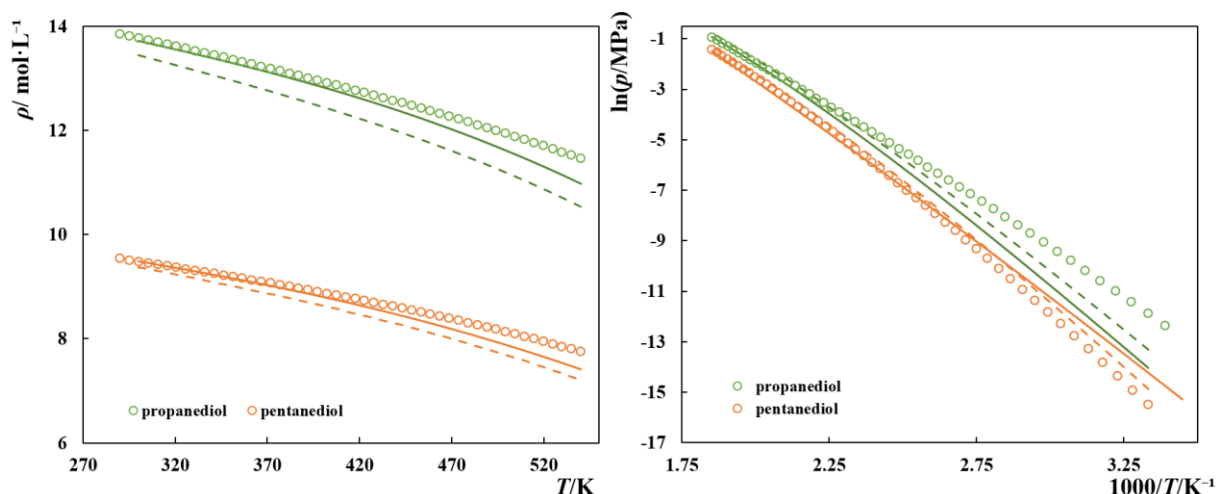


Figure 4.4. Densities and vapor pressures for α, ω -alkanediols. Symbols represent experimental data[118] while the solid and dashed lines represent the SAFT- γ -Mie EoS results using an OH or a CH_2OH to describe the alcohol groups, respectively.

Table 4.7. Deviations between SAFT- γ -Mie results and the experimental data for pure α , ω – alkanediols with heteronuclear SAFT- γ -Mie.

Compound	<i>T</i> -range (K)	%ARD _{OH} p^*/ρ_L	%ARD _{CH₂OH} p^*/ρ_L
1,2 – ethanediol	280-640	48.3/0.80	33.9/5.45
1,3 – propanediol	300-540	43.1/1.46	31.8/4.46
1,4 – butanediol	300-540	17.5/0.93	20.2/3.37
1,5 – pentanediol	300-540	26.8/1.55	31.5/3.49

Additional calculations (not shown here) were carried out to understand what would be needed to accurately describe α , ω – alkanediols. Using the new OH group to represent the alcohol groups, a refitting of S_k , ϵ_{kk}/k_B , $\epsilon_{kl,ab}^{HB}$, $\kappa_{kl,ab}^{HB}$ parameters was found necessary, and the refined parameters are provided in **Table 4.8**. As can be observed, ϵ_{kk}/k_B and $\kappa_{kl,ab}^{HB}$ are constant for all the compounds, while the S_k and $\epsilon_{kl,ab}^{HB}$ were found to correlate linearly with the carbon number for the lighter alkanediols (ethanediol up to hexanediol), with the values of hexanediol being transferable for the heavier members. Using these parameters, a good description of the liquid densities and vapor pressures for α , ω – alkanediols up to 1,10-decanediol can be obtained. Experimental data is also available for the LLE of binary mixtures composed of EG (1,2 – ethanediol) with either *n*-propane, *n*-hexane, and *n*-heptane that could be accurately described using these refined parameters.

Table 4.8. Refined parameters for the OH group to accurately describe the properties of α,ω - alkanediols.

α , ω - alkanediols	S_k	ϵ_{kk}/k_B (K)	$\epsilon_{kl,ab}^{HB}$ (K)	$\kappa_{kl,ab}^{HB}/\text{\AA}^3$
1, 2 – ethanediol	0.7785	307.8	2041.8	50.79
1, 3 – propanediol	0.7911	307.8	2081.0	50.79
1, 4 – butanediol	0.8028	307.8	2192.2	50.79
1, 5 – pentanediol	0.8086	307.8	2204.1	50.79
1,6 – hexanediol	0.8215	307.8	2249.0	50.79

Pure glycols and their mixtures with *n*-heptane

The alkyl and alcohol groups having been defined, the performance of SAFT- γ -Mie EoS, when used to describe the thermodynamic behaviour of compounds containing EO groups, can be investigated. Although their chemical structure is typically expressed as $\text{H}-(\text{OCH}_2\text{CH}_2)_n\text{OH}$, three different approaches were considered in this work to sub-divide the glycol molecules into groups. These approaches are schematically represented in **Figure 4.5** for TriEG: approach A is based on the chemical formula presented above so that each glycol consists of a terminal hydroxyl group, and n EO groups, each described as an $-\text{OCH}_2\text{CH}_2$ unit. Alternatively, approach B and C attempt to retain the identity of both end groups by considering that a glycol has two terminal alcohol groups and, consequently two CH_2 groups and $n - 1$ EO groups represented as either a CH_2OCH_2 (approach B) or $-\text{CH}_2\text{CH}_2\text{O}$ (approach C). Given the nature of the SAFT- γ -Mie EoS, approach B and C are indistinguishable, since the connectivity between the different groups is not explicitly considered in the theory, as conveniently explained in the work of Papaioannou et al.[68]

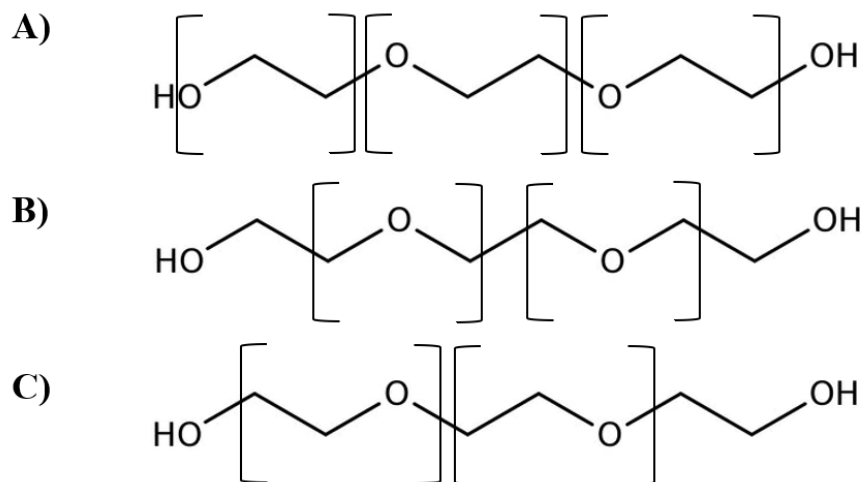


Figure 4.5. Approaches considered to subdivide the glycol molecules in the framework of a heteronuclear model.

Considering the slightly better performance of the OH group proposed in this work compared with the literature CH_2OH group to describe alcohol groups, observed before, and because only the OH group is coherent with the approach A in **Figure 4.5**, the OH group will be adopted as the primary option throughout the rest of this work to represent alcohol groups. Nonetheless, assessments of the performance of the model using a CH_2OH group were carried out, but no significant advantages were found for the systems investigated.

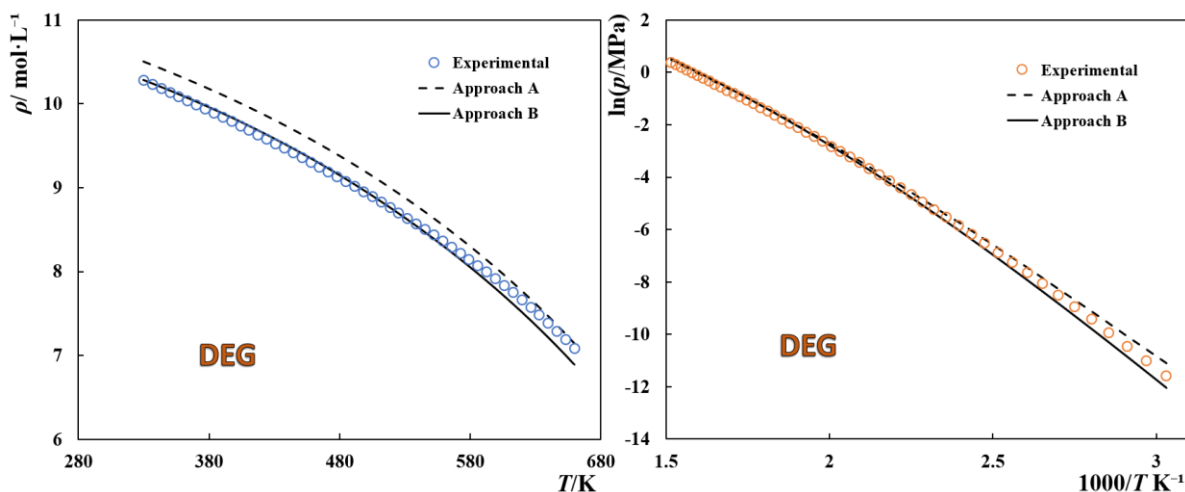
To the best of my knowledge, this is the first time that the EO group parameterization is carried out using the SAFT- γ -Mie EoS to describe glycols or glymes. Therefore, considering $\lambda_{EO-EO}^a = 6$, as

previously suggested for most groups, the remain unknown parameters necessary to define an EO group are v_{EO}^* , S_{EO} , λ_{EO-EO}^r , σ_{EO-EO} , ε_{EO-EO} . Furthermore, to model a pure glycol oligomer, the unlike interaction parameters with the remaining groups are also required, namely the unlike dispersive energies between the EO groups and the alkyl or alcohol groups, i.e., ε_{EO-CH_3} , ε_{EO-CH_2} , and ε_{EO-OH} . Moreover, the EO group, due to the lone electron pairs on the oxygen atom can establish hydrogen bonds, so their associative behaviour can be modelled by considering the existence of acceptor association sites type ‘ e_2 ’ that can interact for example with the ‘H’ donor site on the alcohol groups. Hence, two additional parameters are required, namely the energy and volume of association between said sites, $\varepsilon_{EO-OH,e_2-H}^{HB}$, $\kappa_{EO-OH,e_2-H}^{HB}$.

All the unknown parameters were obtained by fitting to experimental data available in literature for pure glycol oligomers and their mixtures with n -alkanes, namely the vapor pressures and saturated liquid densities of pure diethylene glycol (DEG), triethylene glycol (TriEG), the saturated liquid densities of tetraethylene glycol (TeEG), and the LLE data for the systems DEG + n -heptane and TriEG + n -heptane. The vapor pressures of the TeEG were not considered in the parameterization dataset due to the very high uncertainty of the data available in literature, partially related with the very low volatility of TeEG at low to medium temperatures, as previously discussed by other authors.[7] Due to the very high number of unknown parameters involved, a sequential parameterization procedure was considered. In an initial step the association parameters between EO and OH groups were set equal to those mediating the hydrogen bonding between OH groups. Simultaneously, only the pure-component data was considered so that the unlike interaction parameter with the CH_3 group was not necessary in this first step. The initial results suggested that for approach A, EO groups should be modelled using two segments ($v_k^* = 2$), since all the tests carried using only one segment resulted in shape factors always tending to the upper limit of 1. On the contrary, for approach B, the results suggested the use of a single but larger bead to model the EO group, i.e., with a higher value of σ_{EO-EO} . Once the number of segments was defined, further optimization iterations were carried out to significantly narrow the range of optimal values for S_{EO} , λ_{EO-EO}^r , σ_{EO-EO} in each approach. In a subsequent stage, the selected mixture data was included in the parameterization dataset and all the unknown parameters were fitted using the optimal parameter ranges obtained in the previous step, considering zero, one or two association sites of type ‘ e_2 ’ per EO group. Concerning the number of association sites, the results obtained suggest that the associating behaviour of EO should not be neglected but using one or two association sites result in a very similar performance of the model. Therefore, considering that such a GC-based transferable model should be suitable for a wide range of chain length, only one association site, type ‘ e_2 ’ per EO group was considered

to decrease the computational burden of evaluating the association term. The final values of the parameters obtained for the EO group following the two approaches, ‘EOa’ and ‘EOb’ are reported in **Tables 4.1-4.3**, while the results of the fitting are shown in **Figure 4.6** for the pure fluid data (including the prediction of TeEG vapor pressures), and in **Figure 4.7** for the LLE of glycols + *n*-heptane systems. The prediction of EG saturated liquid densities and vapor pressures are also provided in **Figure C.5.**, in **Appendix C**.

As can be seen in **Figure 4.6**, and by the deviations from the experimental data reported in **Table 4.9**, both approaches show significant deviations from the experimental vapor pressures, especially at lower temperatures where the pressure values become very small. For the saturation liquid densities, the deviations are much smaller but only approach B is able to describe density data with an accuracy similar to that obtained using homonuclear SAFT models.[119] The two modelling approaches were further used to predict the $p\rho T$ data previously reported for glycols in the 283-363 K and 0.1-95 MPa temperature and pressure ranges,[119] and the deviations from the experimental data are also presented in **Table 4.9**. The results show that approach B is, as previously seen, much better than approach A to describe glycols densities, even at high pressures, as shown in **Figure 4.8**, but the deviations exhibited by approach A (see data description in **Figure C.6** in **Appendix C**) have decreased considerably when compared to the saturated liquid densities, suggesting that the pressure effect on density is well captured by this approach, but there are increasing deviations with temperature that are more relevant on the saturated liquid densities due to the broader temperature range considered.



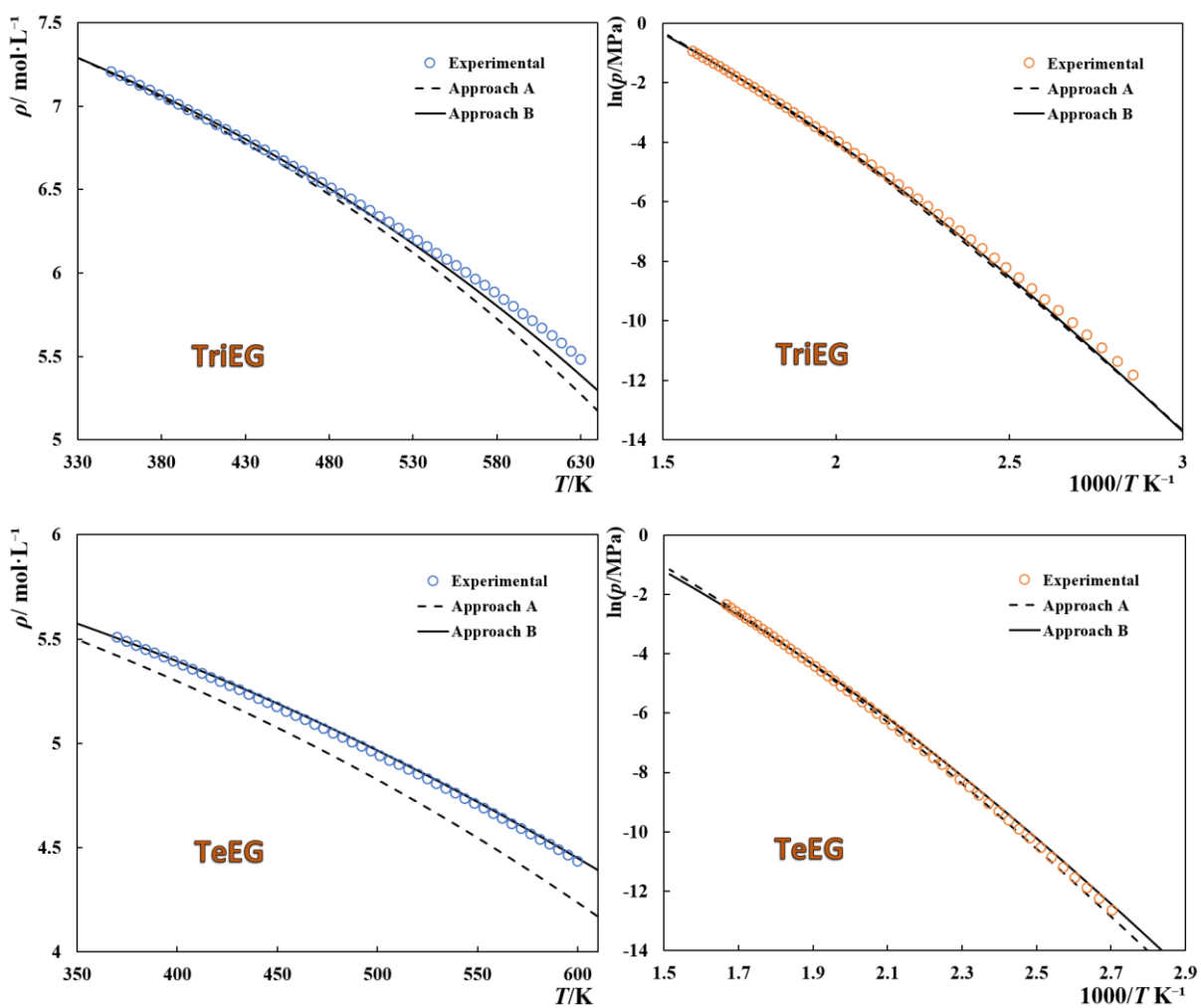
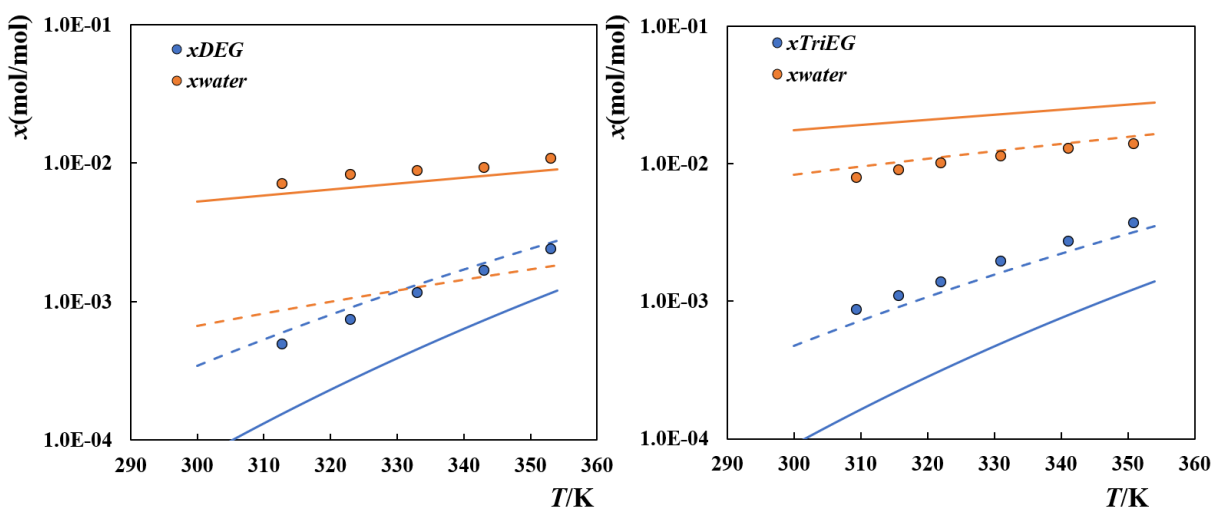


Figure 4.6. Saturation liquid densities and vapor pressures of pure glycol oligomers. Symbols represent experimental data,[118] while the lines depict the SAFT- γ -Mie results, using two different approaches.



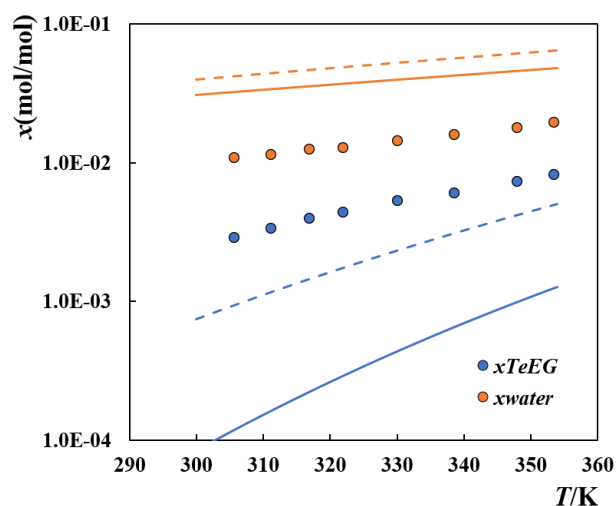


Figure 4.7. LLE of glycol + *n*-heptane systems. Symbols represent experimental data[205] while the dashed and solid lines represent the SAFT- γ -Mie results using approach A and approach B, respectively.

Table 4.9. Deviations between the experimental data for pure glycols[49] and the SAFT- γ -Mie results, expressed in %ARD.

	Approach A			Approach B		
	ρ_L	p^*	$p\rho T$	ρ_L	p^*	$p\rho T$
MEG	7.66	58.09	-	1.02	42.09	-
DEG	2.36	14.52	2.105	0.77	13.44	0.188
TriEG	1.25	14.11	0.242	0.52	9.24	0.342
TeEG	2.54	5.91	0.850	0.28	11.16	0.520
PeEG	-	-	1.620	-	-	0.574
HeEG	-	-	2.097	-	-	0.634

Concerning the LLE of mixtures with *n*-heptane shown in **Figure 4.7**, approach A shows a remarkable accuracy in describing the TriEG + *n*-heptane system (deviations reported in **Table C.1.**, in **Appendix C**), while the deviations increase considerably for the mixtures containing DEG or TeEG, especially in the glycol-rich phase. For approach B the deviations are very high in all cases, although a better performance than with approach A was obtained in the glycol-rich phase of the mixtures with DEG and TeEG. At this stage it is not possible to confidently determine which of the two approaches is better, although the results suggest that approach A might be better only for specific glycol chain lengths, namely for the case of TriEG, approach B might be better overall, especially in the description of pure component properties. Therefore, both modelling approaches will be considered in the next section for the study of glycol + water mixtures.

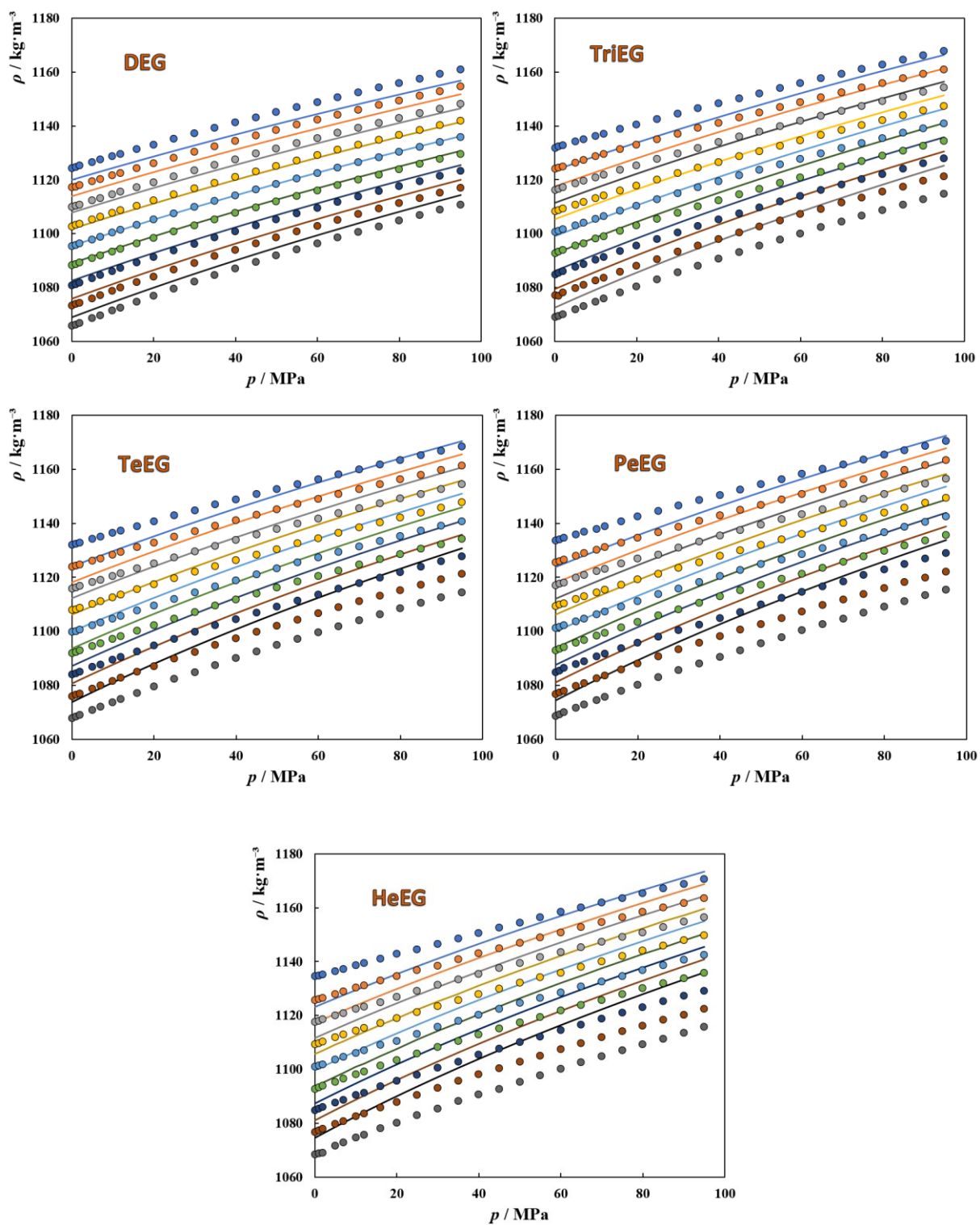
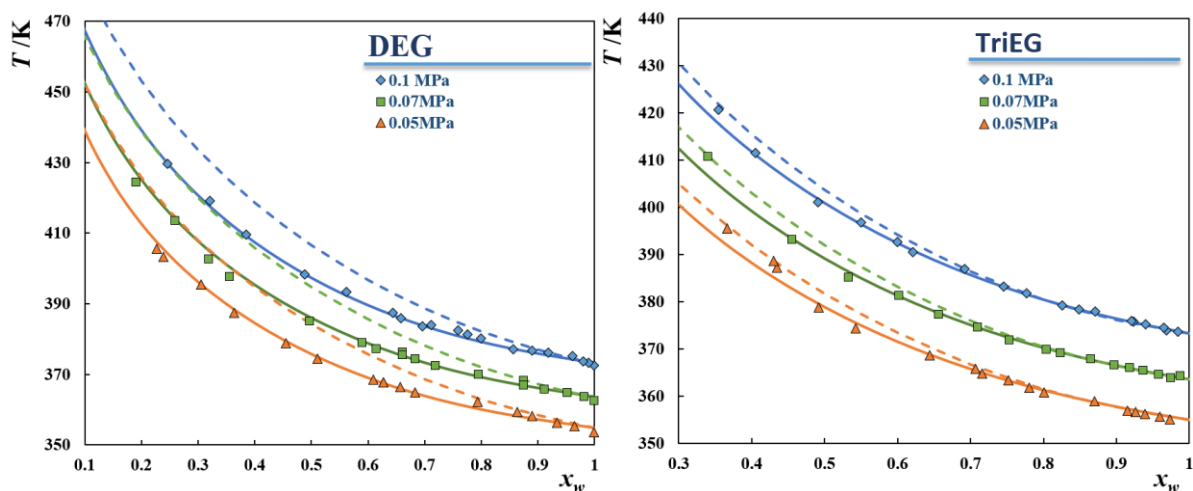


Figure 4.8. $p\rho T$ of pure glycols. Symbols represent experimental data,[119] while the solid lines depict the SAFT- γ -Mie results following approach B.

Glycols + water mixtures

Having estimated the parameters for the new EO group and their unlike interactions with the alkyl and hydroxyl groups, it is now possible to investigate the performance of the model when used to describe glycol aqueous solutions, to further compare the performance of the two modelling approaches considered in the previous section. For such calculations, the parameters characterizing the unlike interactions between the EO groups and water must be defined, namely ε_{EO-H_2O} , $\varepsilon_{EO-H_2O,e_2-H}^{HB}$, and $\kappa_{EO-H_2O,e_2-H}^{HB}$. These parameters were here regressed from available experimental data for the VLE of DEG, TriEG, and TeEG aqueous solutions at 0.1 MPa, and used to predict the behaviour at two other pressures, 0.05 and 0.07 MPa.

The results of the fitting procedure are shown in **Figure 4.9**, and the deviations from the experimental data, reported as average absolute deviation (K), are provided in **Table 4.10**. As can be observed in the figure, approach A shows a better agreement with the experimental boiling temperatures for the three systems, especially for DEG + water for which, a quantitative agreement using approach B would require a further tuning of the $\varepsilon_{EO-H_2O,e_2-H}^{HB}$ parameter to a value different than those used for their higher chain length homologues. Moreover, using approach B, one can observe that while increasing the glycols chain length, the model goes from overestimating to underestimating the boiling temperatures, i.e., from overestimating to underestimating the water-glycol interactions.



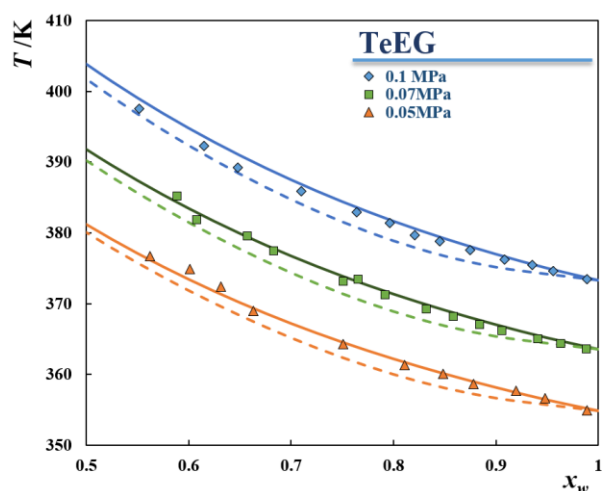


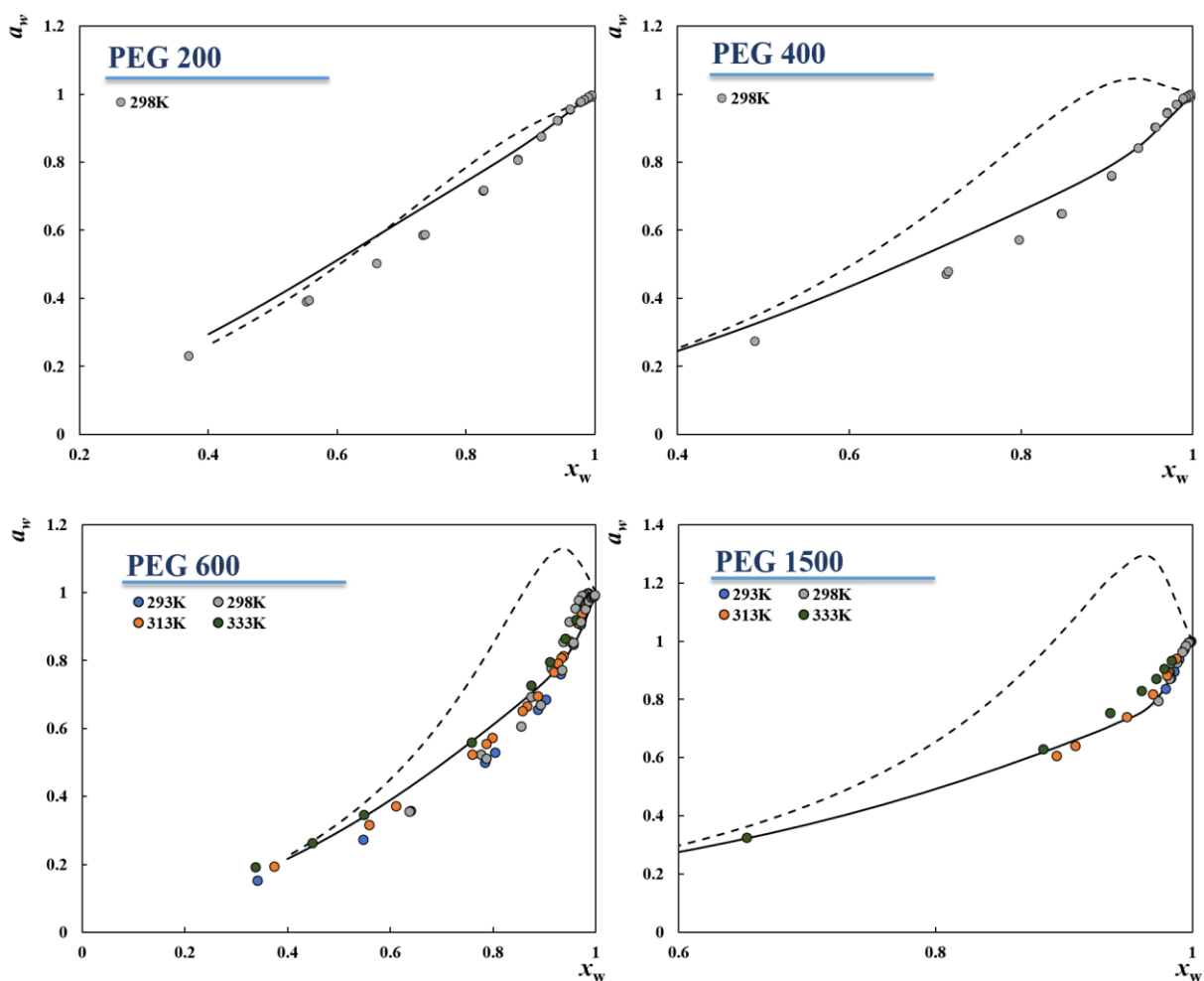
Figure 4.9. VLE of glycol + water systems. Symbols represent experimental data,[138] while the solid and dashed lines represent the SAFT- γ -Mie results using approach A and approach B, respectively.

Table 4.10. Deviations between the modelling results and the VLE experimental data for glycol + water systems.[138–140]

System	Approach A	Approach B
	<i>AAD (T) / K</i>	
DEG + water	0.76	5.55
TriEG + water	0.60	0.92
TeEG + water	0.57	1.53
System	<i>%ARD (a_w)</i>	
PEG 200 + water	4.28	5.96
PEG 400 + water	3.72	16.78
PEG 600 + water	7.29	22.93
PEG 1500 + water	4.07	50.39
PEG 6000 + water	5.07	33.45

PEGs are not as useful for the Oil & Gas industry as glycol oligomers but, as previously seen in **Chapter 3.4**, different authors[139–141] have reported the water activities in PEG aqueous solutions for polymers of different M_w and at different temperatures. As the parameters governing the interactions between EO groups and water are already defined, the model can be used to predict the behaviour of such systems. Therefore, and as for higher M_w polymers the temperature effect on the water activities is negligible, the results of these predictions at 298.15 K are shown in **Figure 4.10** for PEGs with M_w in the range 200–6000 g/mol, while the deviations from the experimental data are reported in **Table 4.10**. As depicted in the figure, approach A performs much better than approach B, providing an excellent agreement with the experimental data, while approach B not only shows considerable deviations from the experimental data, but also shows a different qualitative behaviour with the model predictions showing the existence of a maximum on the water activities that is not observed experimentally.

The results obtained for the glycols + water and PEG + water systems show that despite the slightly better performance of approach B to describe the properties of pure small glycol oligomers, approach A performs much better when the parameters are used to predict the behaviour of mixtures, namely glycols with either *n*-heptane or water. This reinforces the already known importance of including mixture data in the parameterization of SAFT model parameters, or at least their use to guide the selection of the most appropriate parameter set.[7,206]



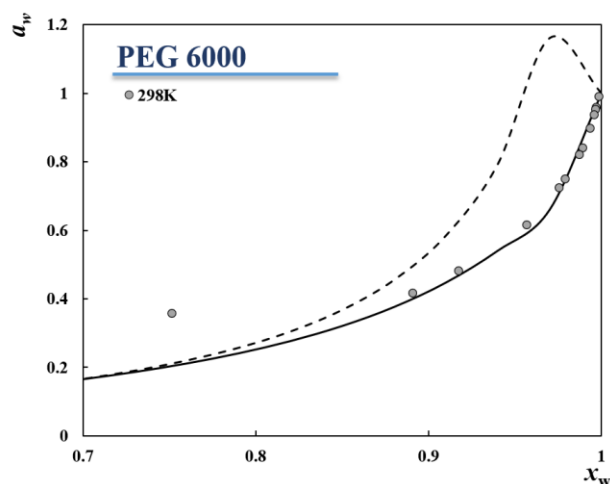


Figure 4.10. Water activity for binary systems PEG + water. Symbols represent experimental data,[139–141] while the solid and dashed lines represent the SAFT- γ -Mie predictions using approach A and B, respectively.

At higher pressures, PEG + water systems exhibit a closed-loop immiscibility region, presenting both a LCST and UCST that results from a delicate balance between the hydrogen bonding and the weaker van der Waals interactions.[207,208] Unfortunately, none of the two approaches was able to predict this phase behaviour under a broad range of (T, p, x) conditions tested around the experimental values. As an example, PEG 3350 + water exhibit a closed loop immiscibility between 420-520 K for polymer weight fractions between ~ 0 and 0.5 which corresponds to a polymer mole fraction of less than 0.005. If isothermal flash calculations are carried out in this temperature interval and for a feed containing a polymer mole fraction ranging between 0 and 0.005, the model always predicts a single phase or a single liquid phase with a pure water vapor phase if the pressure is lower than the water's vapor pressure at the given temperature.

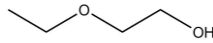
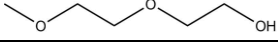
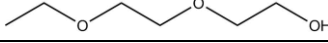
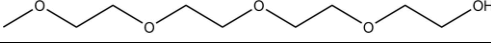
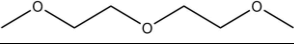
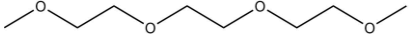
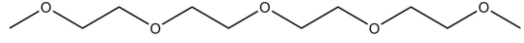
A possible reason for the inability to reproduce such phase diagrams is that the delicate balance between hydrogen bonding and van der Waals interactions is strongly affected by temperature. Therefore, the use of temperature-dependent parameters to describe the cross-interactions between the polymer and water may be needed to capture the closed-loop immiscibility exhibited by these polymer/water systems. Unfortunately, the g-SAFT® software by PSE used in this work for the calculations with SAFT- γ -Mie does not allow for the use temperature-dependent parameters to further analyse this issue.

Pure glymes

The glymes investigated in this work are presented in **Table 4.11** along with their decomposition into different functional groups. Considering the group decomposition for the mono-alkyl ethers, EGEE, DEGME, DEGEE, and TeEGME can be modelled using the same functional groups previously considered for glycols, without any further fitting. Therefore, the group and unlike interaction parameters already defined in the previous sections, using the ‘EOa’ for the EO group, were used to predict the vapor pressures and saturation liquid densities of the different mono-alkyl glymes, and these are depicted in **Figure 4.11a** and **Figure 4.12a**, respectively. As can be observed, the transferred parameters are unable to properly describe the thermodynamic behaviour of pure glycol ethers showing very high deviations from the experimental data (reported in **Table C.2**, in **Appendix C**). Additional attempts using the modelling approach B presented in the previous section also resulted in a similar or even lower performance.

To improve such results, and to have a set of parameters that adequately describes glymes (and that, consequently may, or may not, be more appropriate for the modelling of C_iE_j surfactants at a later stage), a reparameterization of the energy-related parameters involving the EO group was carried out originating a new version of the EO group: ‘EOg’ – approach G. The refined parameters, namely the self-interaction parameters $\varepsilon_{EOg-EOg}$ and $\lambda_{EOg-EOg}^r$, and the unlike dispersive energy parameters with the CH₃, CH₂ and OH groups were regressed using the VLE experimental data of mono-alkyl glymes, and the new parameters are reported in **Table 4.1** and **Table 4.2**. The results of this fitting are shown in **Figure 4.11b** and **Figure 4.12b** and, as can be observed, although there is a considerable improvement of the results, the deviations from the experimental data are still considerable (cf. **Table C.2**).

Table 4.11. Glymes investigated in this work and its decomposition into functional groups for their modelling with heteronuclear SAFT- γ -Mie.

Glyme	Group decomposition	Chemical structure
EGEE	1xCH ₃ ; 1xCH ₂ ; 1xOH; and 1xEO	
DEGME	1xCH ₃ ; 1xOH; and 2xEO	
DEGEE	1xCH ₃ ; 1xCH ₂ ; 1xOH; and 2xEO	
TeEGME	1xCH ₃ ; 1xOH; and 4xEO	
DEGDME	1xCH ₃ ; 2xEO; and 1xCH ₃ O	
TriEGDME	1xCH ₃ ; 3xEO; and 1xCH ₃ O	
TeEGDME	1xCH ₃ ; 4xEO; and 1xCH ₃ O	

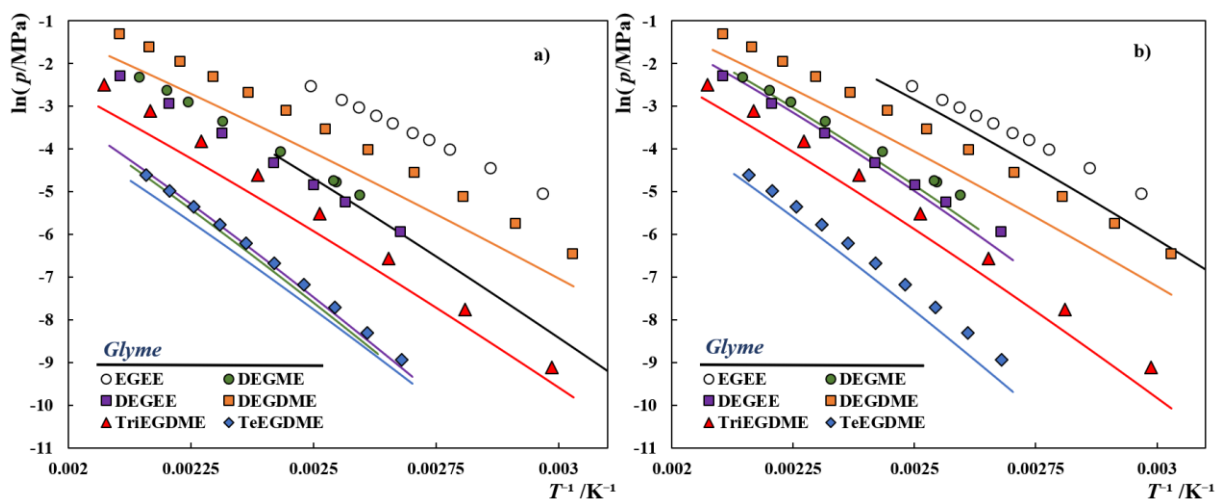


Figure 4.11. Vapor pressures of pure glymes. Symbols represent experimental data[118], while the solid lines depict the SAFT- γ -Mie results using a) approach A; b) approach G.

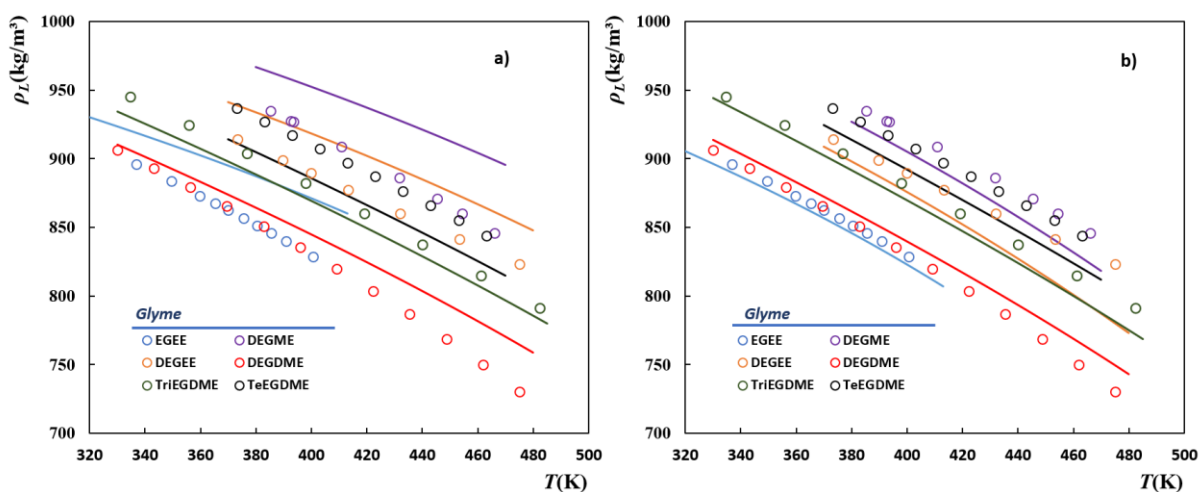


Figure 4.12. Saturation liquid densities of pure glymes. Symbols represent experimental data, while the solid lines depict the SAFT- γ -Mie results using a) approach A; b) approach G.

The very low accuracy of the model, when used to describe pure glymes, suggests that the effect of some of the functional groups composing the mono-alkyl glymes are not well captured by the model, even though the ‘EOg’ group has been parameterized to pure glymes VLE data. This is in good agreement with the lack of transferability previously observed for the hydroxyl group, whose transferability from alkan-1-ols to α, ω – alkanediols and glycols seems to be very limited. In the previous sections, this could be partially explained by the additive effect of having multiple OH groups in the same molecule as both α, ω – alkanediols and glycols have two terminal hydroxyl groups, but this is not the case for the mono-alkyl glymes studied here, where only one terminal hydroxyl group (as in alkan-

1-ols) is present and still, huge deviations from the experimental data are observed, despite the refinement of the parameters, especially in the vapor pressures.

Conversely, according to the group decomposition proposed in **Table 4.11**, the study of di-alkyl glymes requires the introduction of a new CH₃O group. The parameters characterizing this new group and their unlike interactions with CH₃ and EO groups also present in di-alkyl glymes were obtained by fitting to the experimental vapor pressures and saturated liquid densities of DEGDME, TriEGDME, and TeEGDME available in the DIPPR database,[118] and the final values of the parameters are reported in **Table 4.1** and **Table 4.2** as ‘CH₃Oa’ and ‘CH₃Og’ groups, whether the EO group was modelled following approach A or the new approach G. The results of the fitting are also shown in **Figure 4.11** and **Figure 4.12** and the deviations from the experimental data are also reported in **Table C.2**. Following approach A, as a parameterization of the new group is involved, the accuracy on the description of di-alkyl glymes is better than that previously observed for mono-alkyl glymes, especially in the vapor pressures, although high deviations are still observed, reinforcing the poor transferability of the remaining functional groups. Concerning approach G, a similar accuracy was obtained for both types of glycol ethers (note that in both cases, a parameterization step was taken for both types of glymes), with densities being better described for di-alkyl glymes and vapor pressures for the mono-alkyl glymes.

Having available experimental data for the high-pressure liquid densities of different glycol ethers,[120] both modelling approaches (A and G) were used to predict the density in a wide temperature (283-363 K) and pressure (0.1-95 MPa) ranges and the results are shown in **Figure C.7** and **Figure C.8**, in **Appendix C**. The deviations from the experimental data provided in **Table C.2** show that despite the extra parameterization step in approach G, the accuracy of both approaches in predicting the $p\rho T$ data is similar, reinforcing the idea that the extra parameterization did not solve the issues associated with the transferred groups (OH, CH₃, and CH₂). Nonetheless, the deviations are lower than those observed for the saturation liquid densities, suggesting that the models perform much better at lower temperatures, far from the saturation conditions.

Glymes + water mixtures

As discussed in **Chapter 3.4**, the experimental boiling temperatures of aqueous solutions of six different glymes were reported at three different pressures (0.10, 0.07, and 0.05 MPa).[138] Hence, in this section, the existent CG water model is used along with the two glymes modelling approaches (A and G), discussed previously, to describe the available experimental data. For mono-alkyl glymes, using approach A, all the necessary parameters are already available, since the unlike interactions between EO and H₂O groups were already characterized while studying glycols + water mixtures. On the other hand, for approach G, the required ε_{EO-H_2O} , $\varepsilon_{EO-H_2O,e_2-H}^{HB}$, and $\kappa_{EO-H_2O,e_2-H}^{HB}$ parameters have to be fitted to the experimental data at 0.1 MPa for EGEE, DEGME, and DEGEE aqueous solutions and used to predict the behaviour at the two other pressures investigated. For di-alkyl glymes, as a new CH₃O group was introduced, the parameters characterizing the unlike interactions between this group and water are necessary in both approaches and were fitted to the experimental VLE data of aqueous solutions of DEGDME, TriEGDME, and TeEGDME at 0.1 MPa.

The modelling results are shown in **Figure 4.13**, and the deviations from the experimental data, reported as AAD(*T*) in K, are provided in **Table C.3**, in **Appendix C**.

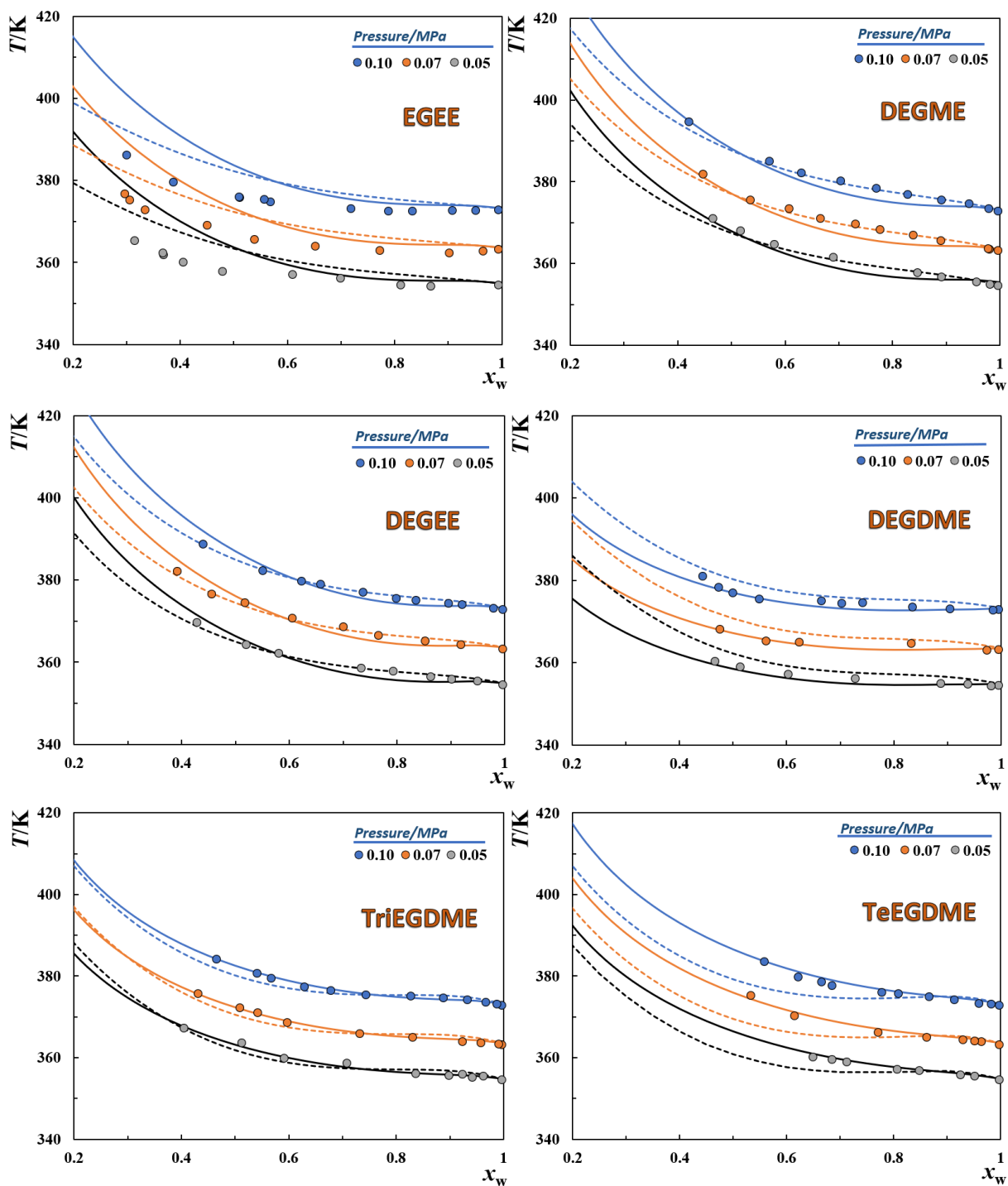


Figure 4.13. Boiling temperatures of glymes + water mixtures at different pressures. Symbols represent experimental data[142] while the solid and dashed lines represent the SAFT- γ -Mie results using approach A and approach G, respectively.

As expected, for the mono-alkyl glymes, approach G performs slightly better than approach A, since the unlike interactions between ‘EOg’ and water were specifically parameterized for these systems. Nevertheless, the results obtained using approach A suggest the robustness of this modelling approach when used to describe the VLE of aqueous solutions of EO-containing compounds, as previously seen for glycol + water mixtures. For the di-alkyl glymes, where the CH₃O-water interaction parameters were fitted in both cases, approach A provides the most accurate results, reinforcing the overall robustness of approach A.

The good performance of approach A when used to describe the VLE of aqueous solutions of both glycols and glymes is observed despite this model presents considerable deviations from the experimental vapor pressures of the pure glycols/glymes, for which approach B and approach G yielded the best results, respectively. Considering that approach A was also slightly better in describing the glycols + *n*-heptane mixtures presented in **Figure 4.7**, this is another indication that mixture data should indeed be included in the parameterization datasets, at least to select the most appropriate set of parameters as clearly, a better representation of pure-component properties does not necessarily result in a better description of the mixtures behaviour, and there may even exist different sets of parameters yielding results with a similar accuracy in what concerns pure-component properties, but completely different performances in binary and multi-component systems. This is yet another advantage of heteronuclear models, whose parameterization is much more flexible in terms of including mixture data that can, in these models, represent up to 100% of the experimental dataset considered.

C_iE_j + water mixtures

The final goal of this chapter was to evaluate the performance of a heteronuclear SAFT variant in describing the phase behaviour of aqueous solutions of C_iE_j non-ionic surfactants. Therefore, the performance of the three modelling approaches previously discussed for glycols and glymes (A, B, and G) in describing these systems is evaluated, since these surfactants are only composed of CH₃, CH₂, EO, and OH groups, all of them extensively analysed in the previous sections.

C₄E₁ is the shortest of this type of compounds and due to its low melting point, one of the few for which pure fluid experimental data is available. Therefore, the three modelling approaches were first used to predict the liquid densities and vapor pressures of C₄E₁, and the results are shown in **Figure 4.14** below.

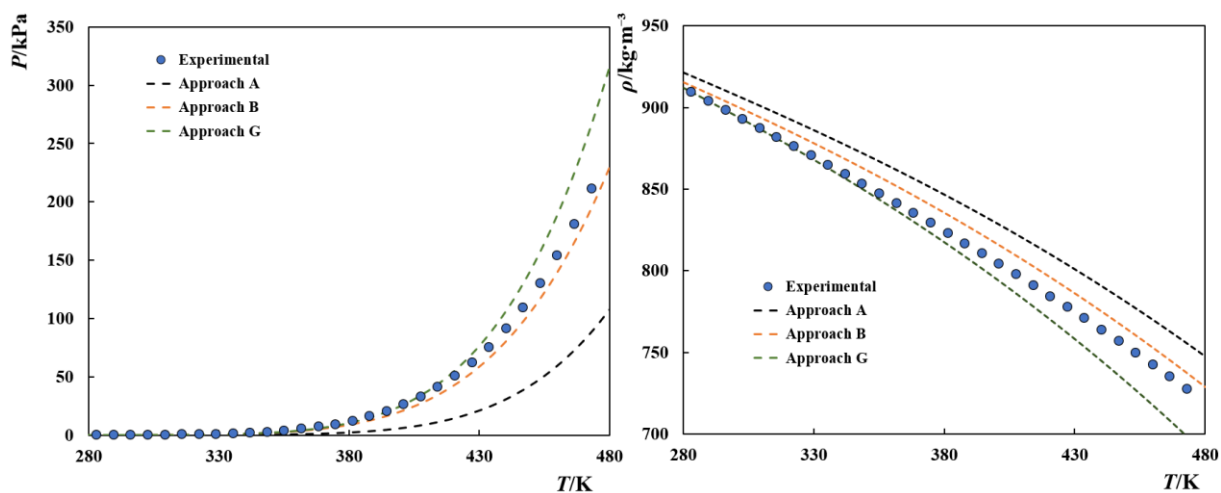


Figure 4.14. Vapor pressures and liquid densities of pure C_4E_1 . Symbols represent experimental data[118] while the dashed lines represent the modelling predictions using different approaches in SAFT- γ -Mie.

From the figure, one can observe that while the modelling approach A clearly fails to describe both properties, the modelling approach B provides a reasonable prediction of both properties, slightly overpredicting the liquid density and underpredicting the vapor pressures. On the other hand, approach G seems to provide a good description of the experimental data at low temperatures, while presenting similar deviations to those exhibited by approach A at higher temperatures.

Concerning the aqueous solutions of C_iE_j surfactants, one of the main features is the presence of an immiscibility region in their phase diagram. Usually, at very low temperatures, the system consists of a homogeneous solution but, with increasing temperature, a phase separation occurs above a lower critical solution temperature (LCST), into a water-rich phase and a surfactant-rich phase. This immiscibility can persist at higher temperatures, although in many cases it disappears above an upper critical solution temperature (UCST), resulting in a closed-loop LLE, which is commonly observed in $C_iE_j + \text{water}$ mixtures. This phenomenon results from a delicate balance between energetic and entropic contributions to the systems energy, where the magnitude of both the van der Waals and hydrogen bond interactions play a crucial role. If at very high temperatures, the system maximizes its entropy by being homogeneous, the presence of unfavourable van der Waals forces between water and the surfactant induce phase separation as the temperature is decreased below the UCST. However, if the temperature is further decreased (to temperatures lower than the LCST) the enthalpic contribution due to the very strong attractive hydrogen bonding interactions between the two species overcomes the other effects, resulting in the formation of a single phase. Obviously, capturing such delicate balances between entropic/energetic contributions and the magnitude of van der Waals/hydrogen bonding forces is a

challenging task to any thermodynamic model, and represent a stringent test to the transferability of the SAFT- γ -Mie EoS parameters obtained in the previous sections. Therefore, the three modelling approaches were used to predict the phase behaviour of four surfactants, namely C_4E_1 , C_6E_2 , C_8E_4 , and $C_{10}E_4$, in water, and the results are depicted in **Figure 4.15**. From these systems, the experimental data reported for aqueous solutions of C_6E_2 and C_8E_4 do not exhibit the presence of a UCST. Often this is because the systems were not investigated at sufficiently high temperatures due to the temperature instability of the molecules, but an UCST is also expected to exist for these systems.

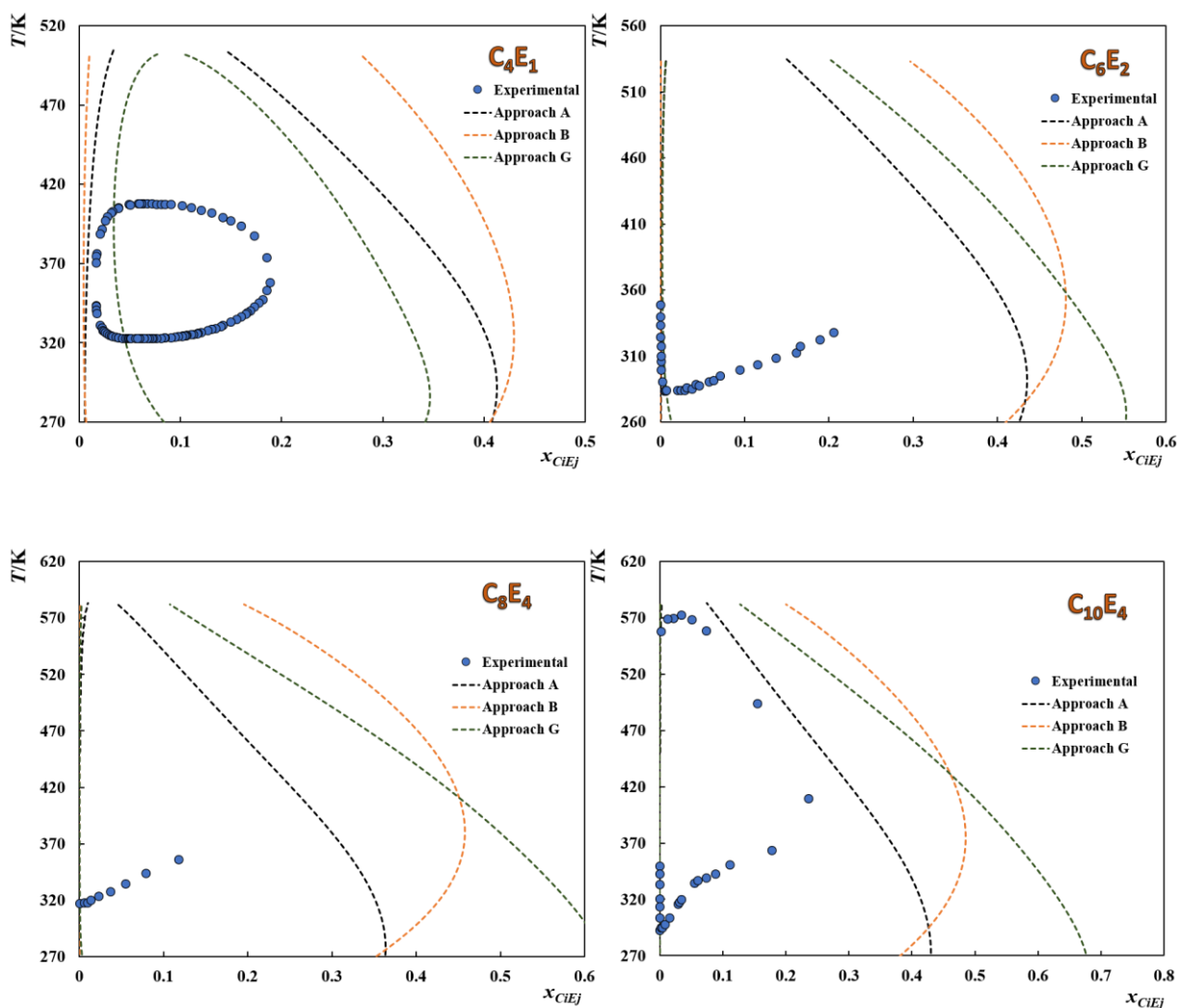


Figure 4.15. LLE of C_iE_j + water systems. Symbols represent experimental data,[209–213] while the dashed lines represent the modelling predictions using the different modelling approaches.

The modelling results in **Figure 4.15** show that none of the three approaches can adequately describe any of the selected systems. As an example, none of the modelling approaches predicted the occurrence of a LCST above the freezing temperature of water (273 K). Moreover, except for the modelling approach G on the C_4E_1 system, the models do not predict the occurrence of a UCST in a reasonable temperature range, but rather a transition from a LLE to a VLE at higher temperatures. Also clear from **Figure 4.15** is that, except for the C_4E_1 system for which approach G seems to provide the most reasonable description of the system, approach A presents the best results for the remaining systems by predicting a narrower immiscibility gap than those predicted by the remaining approaches. This agrees with the results previously obtained for glycols and glymes, where approach A, despite having the worst performance when used to describe the pure EO-containing compounds, seems to have the best performance when used to model mixtures.

As the model parameters transferred from the compounds studied in the previous sections did not yield a closed-loop type LLE for the selected systems, further calculations were carried out by refitting the unlike interaction parameters between the EO group and the water molecules, namely ϵ_{EO-H_2O} , and $\epsilon_{EO-H_2O,e2-H}^{HB}$, specifically to match the closed-loop LLE data of $C_iE_j + \text{water}$ systems. The results of such calculations are shown below in **Figure 4.16** for two different scenarios: represented with a red line are the results of the model when the above-mentioned parameters are fitted to the LLE data of $C_4E_1 + \text{water}$ system, while a blue line represents the results of the model when those same parameters are fitted to the LLE data of $C_{10}E_4 + \text{water}$ system. The results obtained show that, as previously discussed, whenever a parameterization is carried while studying a new family of compounds, good results, at least qualitatively, can be obtained for most systems. In this case, when the unlike interaction parameters between EO groups and water are fitted to LLE experimental data of a representative $C_iE_j + \text{water}$ system, their characteristic closed-loop immiscibility gap is always captured by the model, contrarily to the pure predictions shown in **Figure 4.15**.

However, even by refitting these parameters using data for a representative system, the agreement with the experimental data is still far from perfect (this is partially due to the limitations of the remaining transferred parameters, as discussed previously). Moreover, the new parameters are not necessarily transferable to other chain lengths of the hydrophobic or hydrophilic moieties of the surfactant, with the performance of the model deteriorating considerably between the different systems. This is shown by the example presented in **Figure 4.16**. Here, when using parameters fitted to the LLE data of $C_4E_1 + \text{water}$ system, very high deviations between the model predictions and the experimental data for the $C_8E_4 + \text{water}$ system are obtained while, when using parameters that were regressed from LLE experimental

data for $C_{10}E_4$ + water system, the critical temperatures of the C_4E_1 + water system are much higher/lower than the experimental UCST/LCST. The results obtained also suggest that a simultaneously good agreement with both the critical temperatures and the two-phase compositions may be quite difficult to obtain, at least using temperature-independent parameters, as a best description of the phase compositions (blue line) is usually obtained at the expense of higher deviations in the critical temperatures.

As clearly suggested by the good results obtained for $C_{10}E_4$, a better agreement can be obtained if a similar approach to that presented in the literature[166] is followed, and the values of the parameters are fitted individually to each system. In that case, even though most of the parameters transferability will be lost, the model would still retain the other advantages discussed in **Chapter 4.2** compared with the model proposed by Garcia-Lisbona et al.[166], namely the fact that SAFT- γ -Mie EoS is already implemented in commercial process simulators, and it allows for a decrease in the total number of association sites assigned to each surfactant molecule, as the EO group contains only one negative association site instead of three as proposed in the literature, which may contribute to a higher computational efficiency of the method.

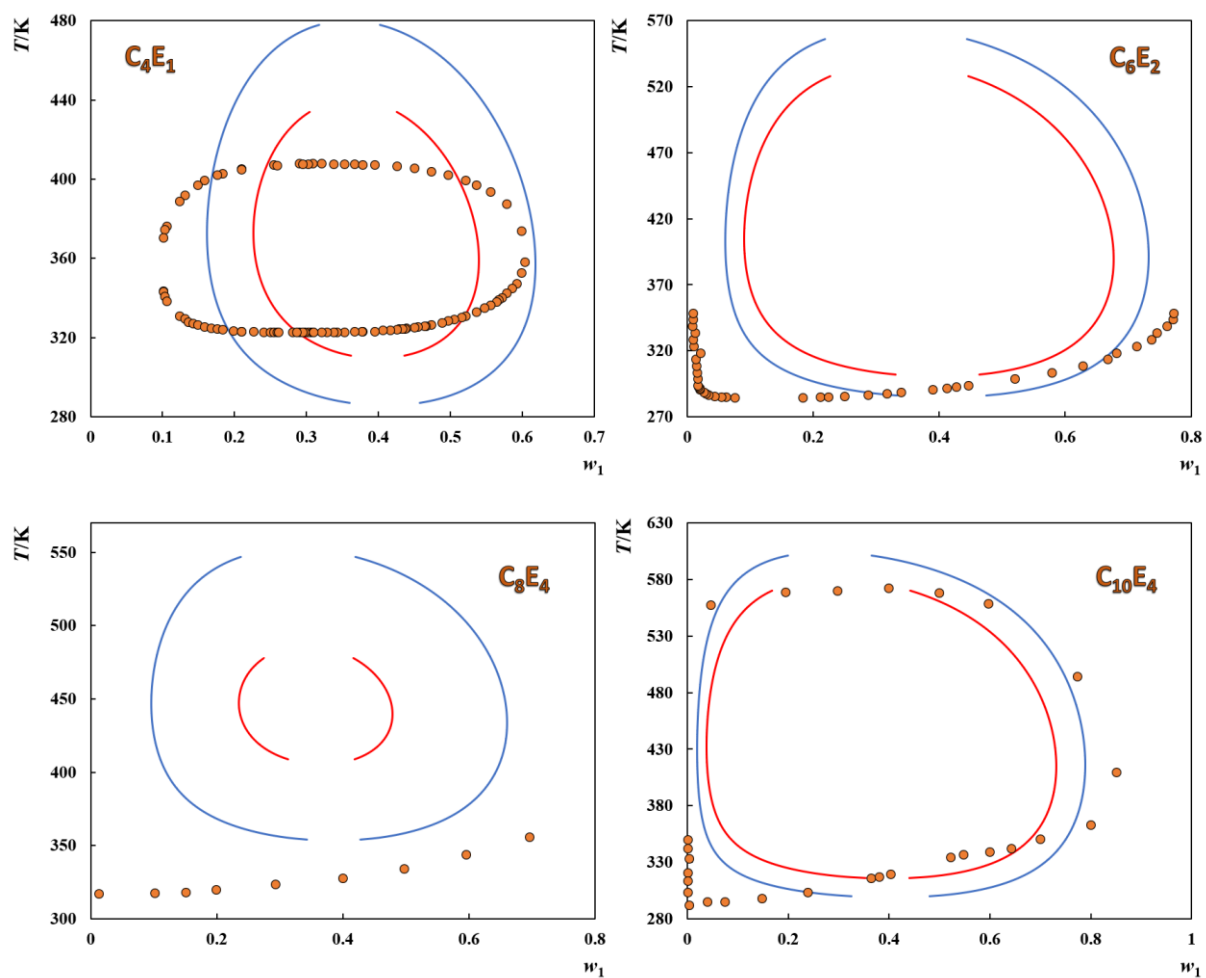


Figure 4.16. LLE of C_iE_j (1) + water (2) systems. Symbols represent experimental data[209–213] while the red and blue lines represent the SAFT- γ -Mie results when the EO- H_2O unlike interaction parameters were fitted to the experimental data for the C_4E_1 and $C_{10}E_4$ systems, respectively.

4.4- Conclusions

In this chapter, a heteronuclear SAFT-type EoS, namely the SAFT- γ -Mie EoS, was applied to the thermodynamic modelling of EO-containing compounds, aiming to evaluate the transferability of the model parameters and if the additional complexity of the heteronuclear treatment of the SAFT theory, leads to an enhancement of the predictive ability and transferability of SAFT models. To accomplish this objective, three families of EO-containing compounds were selected: glycols, glymes (or glycol ethers), and CiEj surfactants, all composed of only CH₃, CH₂, OH, and EO groups, and thus a suitable choice for tackling the objectives of this study.

Although CH₃, CH₂, and OH groups are usually transferred from the well-known families of *n*-alkanes and alkan-1-ols and their parameters are usually considered to be good for further applications, this work started by analysing the performance of such parameters. The results obtained showed that the OH group, typically parameterized using experimental data of alkan-1-ol containing systems, fails to describe other type of components, namely α , ω – alkanediols, for which very high deviations from the experimental data were observed, suggesting that the OH group is not readily transferable to other families. Therefore, when the OH group is used to model glycols, not only the influence of the OH groups in the glycols' behaviour is not well captured by the model, but the parameterization of the newly introduced EO group is affected, with some of the deviations induced by the problems of the OH group being masked by the proposed EO parameters, perpetuating the problem, with every new addition to the molecular structure.

The results obtained for glycols showed that the model is able to provide reasonably accurate results only when a parameterization is involved, as it is the case of the pure glycol properties or even of the VLE of their aqueous solutions, where the EO-water unlike interaction parameters were parameterized, but fails when used in a purely predictive manner such as in the prediction of the LLE of PEG/water systems, demonstrating the inability of the model parameters to be transferred across different types of phase equilibria. Afterwards, when the new EO parameters were used to study glymes, the results showed that not only the parameters are not transferable across different types of phase equilibria but they also fail when used across different families of compounds since the model was unable to provide reasonable predictions for pure glymes or their mixtures with water, allowing for a similar conclusion to that reached based on the results obtained for the OH group in the study of α , ω – alkanediols. On the other hand, by reparametrizing the EO group using the glymes experimental data, a much better agreement with the experimental data could be obtained, reinforcing the idea that a (small

or large) reparameterization is always present behind the good results commonly reported with heteronuclear SAFT models.

In the final section, the different modelling approaches (those built using glycols experimental data and those based on glymes) were extended for the modelling of C_iE_j surfactants in water and again, the results showed that, without a tweaking of the EO-water and/or OH/water unlike interaction parameters for this type of systems, not even a qualitative agreement with the experimental data could be obtained, with all the modelling approaches failing to predict the existence of a well reported LCST. Nevertheless, given the lack of works in the literature addressing the modelling of phase equilibria of C_iE_j surfactants in water, a useful model can still be obtained if the unlike interaction parameters governing the magnitude of the dispersive and hydrogen bonding interactions between the EO groups and water are fine-tuned to each system.

The global conclusion of this comprehensive work is that the parameters for the heteronuclear SAFT models are not readily transferable across different types of compounds, thus limiting much of the predictive capability of this type of models that is usually suggested as their greatest advantage over homonuclear SAFT variants.

5- Molecular Dynamics Simulations of Surfactant Systems

“Almost all aspects of life are engineered at the molecular level, and without understanding molecules we can only have a very sketchy understanding of life itself”

Francis Crick

5.1- Unveiling the phase behaviour of C_iE_j surfactants in water through CG-MD simulations

The content of this section is based on the following published manuscript, where E.A. Crespo was responsible for the modelling tasks and for writing the manuscripts, with substantial contributions from the remaining authors.

- Emanuel A. Crespo, Lourdes F. Vega, Germán Pérez-Sánchez, and João A.P. Coutinho, “*Unveiling the phase behavior of C_iE_j non-ionic surfactants in water through coarse-grained molecular dynamics simulations*”, *Soft Matter*, 2021, Advance Article, DOI: 10.1039/D1SM00362C

Introduction

C_iE_j surfactants have a wide number of applications, across different industrial segments that goes well beyond their use in the Oil & Gas industry for EOR. From detergents and cosmetics to enhanced oil recovery, many other applications such as drug delivery, emulsification, proteins purification and crystallization, and others in the agriculture, textile, and paper industries have been reported.[214–216] Most of their success in all these applications is due to their ability to, once in aqueous solution, self-assemble to form a variety of 3-D structures with a controllable morphology, ranging from simple spherical, rod, disk or worm-like micelles at low surfactant concentrations, to the formation of more complex LC phases (e.g. hexagonal (H_1) or lamellar (L_α) phases) at higher concentrations.[217] Furthermore, C_iE_j surfactants are often known as reference detergents, and as archetypal systems to study fundamental aspects of non-ionic surfactant solutions in order to better understand their behaviour. Owing to their simple molecular architecture, they are easy to synthesize (several C_iE_j grades are commercially available), and their properties can be tuned, aiming at a specific application (e.g. for use in a particular reservoir), by manipulating their structural and physico-chemical properties such as the length of the hydrophobic tail and hydrophilic moiety of the molecule.[218] As an example, the shapes and sizes of the self-assembled structures of systems containing C_iE_j surfactants are useful as templates in the development of new tailor-made materials, such as nano-porous structures with dimension-controlled pores.[219]

Therefore, understanding and ultimately predict the role of the surfactants molecular structure on the properties of their aqueous micellar solutions, and on the morphology of the self-assembled structures, is highly relevant for the design and synthesis of new compounds and materials of interest for many applications.[220] On the other side, for some aspects of industrial handling, processing and

transportation, it is important to avoid the formation of LC phases that often exhibit marked gel-like properties, with considerable high viscosities hampering the preparation of useful formulations.[221]

Given the importance of these surfactants, both from a fundamental and a practical point of view, several experimental techniques were employed to characterize their rich phase behaviour in water, providing useful information both in the micellar regime,[222,223] and at higher amphiphile concentrations, where techniques like small-angle X-ray scattering (SAXS), small-angle neutron scattering (SANS), and polarizing optical microscopy (POM), among others, allow to investigate the formation of different LC phases and display their phase diagrams.[210,224] Unfortunately, an unequivocal identification of the mesophase formed under certain thermodynamic conditions and its microscopic structure is not an easy task, being the origin of conflicting results, especially when different experimental techniques are used. As an example, the phase diagram of $C_{10}E_5/H_2O$ reported by Nibu and Inoue[225] describes the existence of a bi-continuous cubic phase (V_1) in the composition range between the L_α and H_1 phases, while in the study of Lang and Morgan,[209] only the L_α and H_1 phases were reported; similar issues were also reported for other surfactants such as $C_{10}E_6$,[225–227] $C_{12}E_2$,[228,229] $C_{12}E_6$,[210,230] $C_{12}E_8$,[210,231–233]

By establishing a link between molecular structure and the fluids microscopic behaviour, MD simulations can be used to enhance the ability to identify the various phases observed experimentally and discern the most plausible and stable ones. Furthermore, MD simulations provide useful insights into the mechanisms driving micellization, clouding or self-assembly phenomena. Atomistic models, although being able to provide detailed and precise information about the initial stages of micelle formation in diluted systems,[216,220,234–237] are unable to address the time and size scales relevant for the self-assembling and mesophase transition processes. In this regard, the required relaxation times, typically in the order of microseconds at the nanometer scale, leave the AA models out of the way unless preformed structures are used as initial state for the simulations. Conversely, CG models, constructed by grouping a certain number of atoms into a single interaction site, significantly reduce the computational demand, being a powerful tool to investigate the surfactant self-assembly and, consequently, to investigate the mesophase behaviour of C_iE_j surfactants in water.

Shinoda and co-workers[238] were the first to propose a CG model for the C_iE_j surfactants. In their work, the intramolecular potentials were fitted to reproduce the bond and angle distributions obtained from more detailed AA-MD simulations, while the intermolecular interactions were fitted using density, surface tension and hydration free energy experimental data. However, for the interaction between the EO groups and water, since hydration free energy data was not available, they used structural data of the L_α phase in the $C_{12}E_2$ /water system (e.g., lamellar spacing and molecular area) to parameterize

this interaction and showed that the model was able to correctly describe such phase. Only on a later study carried out by the same authors,[239] the transferability and versatility of the model was assessed by extending the model to the $C_{12}E_6$ surfactant. The model predicted the existence of the micellar, H_1 (although thin water channels were found to persist between the cylinders), and L_α phases at 20, 50 and 80 %wt of surfactant concentration, respectively, in agreement with experimental reports.[210,230]

The majority of the CG modelling of C_iE_j surfactants in water[107,214,240–242] relied on the MARTINI FF, which although initially proposed for biomolecular simulations of phospholipids, has been increasingly applied for a variety of chemical systems.[243] The adoption of the MARTINI FF is mainly due to its remarkable transferability, since it proposes a general coarse-graining framework, where molecules are mapped from a few pre-defined bead types (with different polarities and hydrogen bonding capabilities), whose interaction LJ potentials are systematically parameterized to match densities, self-diffusion constants, and partitioning free-energies of representative building blocks.[52] This FF have thus been successfully applied to investigate the *cmc* and aggregation number (N_{agg}) of C_iE_j surfactants in water.[214] The micellar assemblies of $C_{12}E_5$ and the existence of a sphere-to-rod transition with increasing surfactant concentrations,[107,244] or the self-assembly of micellar, hexagonal and lamellar phases of $C_{12}E_j$ ($j = 2, 4, 6$) surfactants were also tackled.[241] Despite some promising results, the models available exhibited a limited transferability to compounds with a larger number of EO groups and the existent MARTINI beads were shown to be too hydrophilic to accurately represent an EO group,[241,243] being inappropriate for simulations in non-polar media.

To overcome such limitations, and to increase the numerical stability of these models, Grunewald et al,[245] recently proposed a new MARTINI bead to represent EO groups, carrying a systematic parameterization to ensure its full compatibility with the whole MARTINI energy matrix of interactions. The new model was successfully applied to describe the densities of bulk PEO oligomers, long-range structural properties of different PEO chains, structural properties of lipid bilayers containing pegylated lipids, and the phase behaviour of some C_iE_j surfactants, paving the way to the simulation of more complex systems containing EO groups. However, as previously done in the work of Rossi et al.[241], the simulations of C_iE_j surfactants in water were carried only for three specific concentration/chain length pairs, namely $C_{12}E_2$, $C_{12}E_4$, and $C_{12}E_6$, with a surfactant composition of 71.1, 53, and 50 % (w/w), respectively. Consequently, before using this surfactant model for more complex studies, such as in multi-component systems (e.g., by adding an oil, a salt, or a co-solvent to the aqueous solution), it is vital to assess the performance of the above-mentioned model under a wide variety of conditions and C_iE_j surfactants. Therefore, the main aim of this work is to extend the MARTINI model for a wide range of C_iE_j surfactants by carrying a systematic assessment of its performance to evaluate its reliability. The

effect of chain length (of both the hydrophobic and hydrophilic moieties) and the surfactant concentration on the phase behaviour of C_iE_j /water is presented, while spanning a wide range of hydrophilic-lipophilic balance (HLB) values.

Methodology

The MD simulations performed in this work were carried out using the GROMACS 2019 package,[101] integrating the equations of motion using the leap-frog algorithm with a time step of 20 fs. The potential energy in the C_iE_j surfactant CG model proposed by Grunewald et al.[245] is obtained as a sum of the contributions due to bond stretching, angle bending (including the use of a “restricted bending” potential developed by Bulacu and co-workers[246] for improved stability when one of the angles approaches 180°), and dihedrals for bonded interactions and a Lennard-Jones (LJ) potential to describe the non-bonded interactions. Examples of topology (.itp) files for a surfactant molecule were provided together with the original publication of the EO bead in the work of Grunewald et al,[245] while a schematic representation of the CG mapping considered for the $C_{12}E_6$ surfactant is provided in **Figure 5.1** as an example of the surfactants studied in this work. The alkyl groups are described using a 4:1 mapping by the apolar C_1 bead proposed in the original MARTINI FF;[52] the EO groups are represented by the EO bead (OCH_2CH_2) proposed by Grunewald et al,[245] and the terminal hydroxyl group is modelled using a small-type polar bead, SP_2 , from the original MARTINI FF.[52]

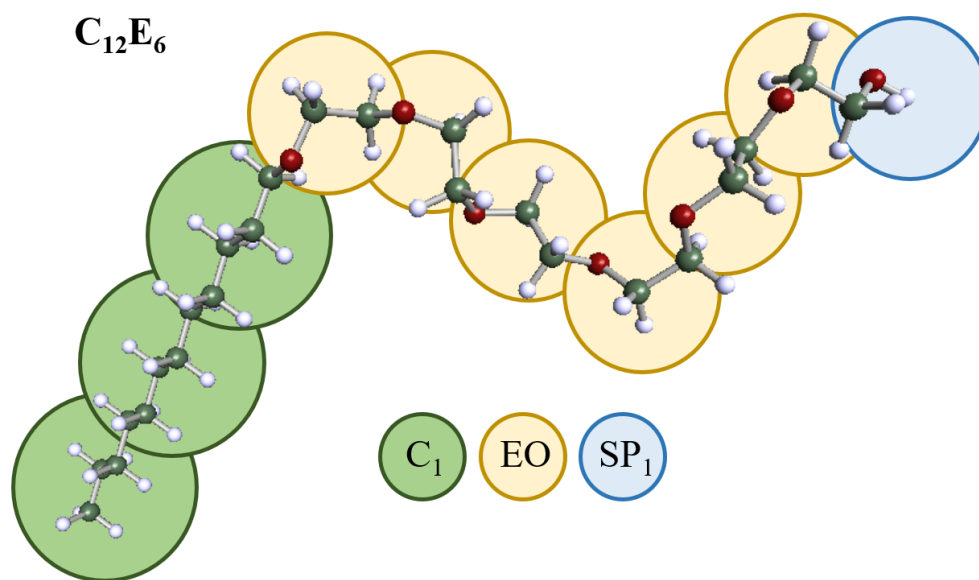


Figure 5.1. Schematic representation of the CG mapping considered for the $C_{12}E_6$ surfactant.

Non-bonded interactions were computed using a Verlet cut-off scheme (Potential-shift-verlet modifier) with a cut-off length of 1.1 nm, changing the verlet-buffer-tolerance from its default value ($5 \cdot 10^{-3}$) to 10^{-5} kJ/mol/ps. The temperature of the simulation boxes was fixed using the velocity-rescaling thermostat,[247] with a coupling time constant, $\tau_T = 1.0$ ps, while the pressure coupling was assured by the Parrinello-Rahman barostat[248] with a coupling time constant, $\tau_P = 24.0$ ps. Before the production runs in the NpT ensemble, an equilibration procedure was followed for every simulation: an energy minimization step using the steepest descent method to prevent short-range contacts between atoms, followed by a short NVT run to ensure the right temperature of the simulation (5-10 ns) and a short simulation in the NpT ensemble to equilibrate the system's density (20 ns). During the NVT equilibration step, the LINCS algorithm[249] was used to constrain the bond lengths to facilitate the equilibration of temperature in some of the more concentrated systems. For the production runs, the total energy profile of the systems was monitored, and the equilibrium assumed when the energy remained constant for at least 1 μ s, with an energy drift lower than 10 kJ/mol. A total simulation time of 6 μ s was observed to be sufficient to ensure that all the investigated systems have reached their final equilibrium state. The equilibrium was also confirmed by monitoring temperature, pressure, and density of the system as well as by visual inspection of the simulation boxes. To confirm that the simulations did not become trapped in a local minimum, as it may occur in CG simulations due to high energy barriers, the first 4 μ s were carried out at the simulation temperature (333 K was used for all systems), followed by 1 μ s at a higher temperature (363 K), and an additional 1 μ s at the simulation temperature. This procedure was shown in a recent work with imidazolium-based ionic liquids (ILs) to help simulations reach their final equilibrium structure and overcome local minima.[102]

Every simulation was carried out using a cubic box with periodic boundary conditions (PBC) and an initial random configuration, generated using the PACKMOL code.[250] Simulations were visualized using the Visual Molecular Dynamics (VMD) software package,[251] and the micellar aggregates were analysed using an in-house code[108] inspired by the Hoshen-Kopelman cluster-counting algorithm.[252] This algorithm considers that two surfactant molecules belong to the same aggregate when their tail sites are separated by less than a certain threshold, which is usually defined by the first minimum of the respective radial distribution functions. The aggregate sizes can then be monitored along the simulation trajectory, until reaching their final equilibrium value.

Simulated Systems

As mentioned in the introduction, the aim of this study is to extend the Grunewald et al.[245] model for a wide range of C_iE_j surfactant aqueous solutions. Bearing in mind the transferability offered by the MARTINI model, this should allow to validate this framework for further studies of multicomponent systems containing such compounds. Therefore, twelve different surfactants, with diverse chain lengths of both the alkyl tail and hydrophilic moiety were selected to investigate the relationship between molecular structure and phase behaviour. The simulated systems are reported in **Table 5.1** displaying a range of alkyl-chain lengths $i = 8, 12,$ and 16 , while the number of EO units, j , varies between 2 and 23 . The expression proposed by Griffin[253] to determine the hydrophilic-lipophilic balance (HLB) values was applied to the selected surfactants, as follows:

$$HLB = 20 * \frac{M_h}{M} \quad (5.1)$$

where M_h is the molar mass of the hydrophilic segment and M is the molar mass of the surfactant molecule. The values obtained from **eq. 5.1** are also provided in **Table 5.1**. As can be gauged from **Table 5.1**, the selected surfactants span a wide range of HLB values (8.17-17.4), especially in the water-soluble region of the scale (values between 10-20 characterize water-soluble surfactants).

The overall C_iE_j /water systems were simulated at least at four different surfactant concentrations, namely 15, 30, 50, and 70 wt%. A few additional simulations at different concentrations were carried out for specific systems, whenever appropriate for further comparisons with experimental reports. Although there is a marked temperature effect on the phase diagram of C_iE_j /water systems (e.g., sphere to rod transitions, clouding phenomena, etc.), the MARTINI FF suffers from a poor temperature transferability, mainly due to the lack of an accurate representation of certain nonbonded interactions, such as the hydrogen bond orientation. Consequently, changes in temperature are mainly advantageous to reduce the mixing entropy and to increase the kinetic energy, helping to avoid local minima during the calculations. Therefore, all the simulations were carried out at 333 K, a temperature slightly higher than most experimental observations.

Table 5.1. Non-ionic surfactants studied in this work.

Surfactant	HLB	Experimental observations reported in Literature	Ref.	wt% of C_iE_j in CG-MD simulations (%wt)	Phases observed in the simulations
C_8E_6	14.9	H_1	[210,227]	15/30/50/60/70	L_1, H_1
C_8E_{12}	17.0	No mesophases were observed	[210]	15/30/50/70	L_1
$C_{12}E_2$	8.17	$W, L_3, L_2, V_2^{(1)}, V_2^{(2)}, L_\alpha$	[228,229]	15/30/45/50/70	W, L_3^*, L_α
$C_{12}E_4$	11.2	$W, L_3, L_2, L_1, L_\alpha$	[210]	15/30/53/70/80	$L_1, L_\alpha^H, L_\alpha$
$C_{12}E_6$	13.0	H_1, L_α, V_1	[210,230]	15/30/50/70/80	$L_1, H_1, V_1, L_\alpha^H, L_\alpha$
$C_{12}E_{10}$	15.0	H_1, L_2, L_1	[254]	15/30/50/70/85	L_1, H_1
$C_{12}E_{12}$	15.6	$Fm3m, Im3m, Pm3n, H_1$	[255]	15/30/50/70/82	L_1, H_1
$C_{12}E_{23}$	17.4	L_1, I_1, L_2	[254]	15/30/50/70	L_1
$C_{16}E_4$	9.62	$W, L_2, L_3, V_2, L_\alpha$	[210]	15/30/50/70	L_1, V_1, L_α
$C_{16}E_6$	11.5	$N_c, L_1, L_\alpha^H, H_1, V_1, Int, L_\alpha, L_\beta$	[256,257]	15/30/40/50/70	$L_1, H_1, Int, L_\alpha^H, L_\alpha$
$C_{16}E_8$	12.8	$W, L_1, I_1, H_1, V_1, L_\alpha, L_2$	[210]	15/30/50/70/80	$L_1, I_1^*, V_1, L_\alpha$
$C_{16}E_{12}$	14.5	$W, L_1, I_1, H_1, V_1, L_\alpha$	[210]	15/30/50/70/90	L_1, V_1, L_α

Nomenclature: L_1 – Micellar Solution; L_2 – Surfactant liquid; L_3 – ‘critical’ aqueous surfactant solution; I_1 - cubic phase of close-packed micelles; H_1 - normal Hexagonal phase; V_1 – normal bi-continuous cubic phase; L_α – Lamellar phase; V_2 – Reversed bi-continuous cubic phase; $V_2^{(1)}$ – bi-continuous cubic phase with $Pn3m$ symmetry; $V_2^{(2)}$ – bi-continuous cubic phase with $Ia3d$ symmetry; W – water containing surfactant unimer, usually continuous with L_1 ; $Fm3m/Im3m/Pm3n$ – different arrangements of a micellar cubic phase; N_c - lyotropic nematic phase composed of rod-shaped micelles; L_α^H – lamellar phase with water-filled defects; L_β – Gel phase; Int – non-cubic phases between H_1 and L_α occurring in C_iE_j /water systems when long alkyl chains prevent the formation of V_1 .
* - the system is in a transition towards the indicated mesophase.

Results and Discussion

Aqueous solutions of C_iE_j surfactants with short alkyl tails ($i < 8$) usually do not exhibit the formation of LC phases with a consequent mesophase instability for lower i surfactants caused by the entropy increase associated with the formation of small micelles from rods or bilayers. Therefore, their phase diagrams usually feature only a two-phase liquid-liquid equilibrium (LLE) characterized by a lower critical solution temperature (LCST) and, in some cases, exhibiting a closed-loop type behaviour with an upper critical solution temperature (UCST) emerging at higher temperatures. Examples of such phase diagrams were reported by Christensen and co-workers for both types of diagrams,[258] and are widely available in literature for a considerable number of surfactants.

The clouding phenomena leading to the phase separation is mainly driven by a temperature effect leading on long-range concentration fluctuations and a hypothetical micellar growth that are thought to be in the origin of the phase transition.[259,260] Unfortunately, as mentioned in the previous section, the CG models have a limited ability on capturing the effect of temperature. For this reason, the study of the macroscopic LLE of these surfactant solutions is better tackled using other types of modelling techniques such as umbrella-sampling MD simulations, thermodynamic integration or the use of advanced molecular-based EoSs as discussed in the previous chapter.[50,51] Instead, the MD simulations carried here are focused on investigating the formation of the lyotropic LC phases observed for surfactants possessing higher alkyl chain lengths (typically $i \geq 8$) as well as the impact of the surfactant molecular structure and concentration. The different phases observed in the CG-MD simulations are summarized in **Table 5.1** and will be discussed in the following sections, before concluding with some remarks on the more diluted micellar phase.

C₈ surfactants

The C₈ surfactant in water with two different EO groups, namely the C₈E₆ and C₈E₁₂, were simulated. For the former, Clunie et al.[227] and Marland et al.[261] reported the existence of a H₁ phase in a narrow temperature range for surfactant concentrations between 50 and 70 wt%. The MD results for C₈E₆ at this concentration range are shown in **Figure 5.2**. At 50 wt%, the C₈E₆ system revealed the formation of cylindrical micelles resembling the hexagonal arrangement. Conversely, at 70 wt% concentration the C₈E₆ system displayed a transition state towards the formation of layers, in what should be the initial stage of the L_α phase that although not observed here, has been reported experimentally for C₁₀E₆. [209] Both concentrations were in reasonable agreement with the experimental reports since the 50 and 70 wt% concentrations are the lower and upper limits for the H₁ mesophase observed. An

additional simulation at 60 wt% (the concentration at which such phase is, according to the literature, present in a wider temperature range) was carried out and the final equilibrium state is also shown in **Figure 5.2**. It clearly shows the hexagonal arrangement of the cylindrical micelles. The individual cylindrical micelles and their long-range organization can be clearly seen in **Figure D.1**, in Appendix D.

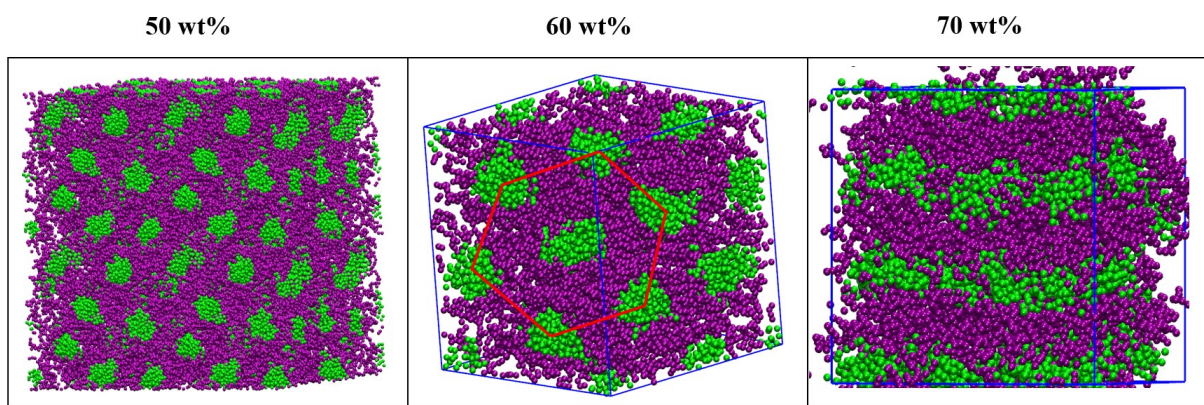


Figure 5.2. CG-MD simulations of C_8E_6 in water at different surfactant concentrations. Green represents the alkyl tail beads, while purple is used to represent the beads of the hydrophilic moiety. Water molecules are omitted for a clearer visualization.

At lower concentrations, 15 wt% and 30 wt%, the MD C_8E_6 simulations were in good agreement with the literature reports.[227,261] As shown in **Figure D.2** in Appendix D, both concentrations consisted in a simple micellar solution with individual spherical or near-spherical micelles. Nonetheless, an increase in the size and elongation of the micelles was observed as the surfactant concentration increased, leading to a sphere-to-rod transition of the micelles being observed from 15 to 30 wt% of surfactant.

For the C_8E_{12} system, the increased number of EO units (higher HLB), exhibited a much higher affinity with water molecules that makes it much less prone to the formation of mesophases. Mitchell et al.[210] reported the absence of mesophases in aqueous solutions for C_8E_4 , C_8E_8 , and C_8E_{12} . The CG-MD simulations, whose final snapshots are depicted in **Figure D.3** in Appendix D, were able to accurately capture the higher water affinity induced by the extra EO units. **Figure D.3** shows the existence of dispersed micelles of different sizes and shapes in the 15-50 wt% concentration range. Nonetheless, at 70 wt%, the simulation reveals the initial stages of formation of a H_1 – like phase that was not previously reported in the literature. This is the first time that the MARTINI FF is applied to C_iE_j surfactants with $i \neq 12$ and it is in good agreement with the experiments, especially when predicting the mesophase instability of C_8 surfactants with a higher number of EO groups, which can be interpreted as an indicator of the good transferability of the C_iE_j CG model.

C₁₂ surfactants

It is widely accepted that, by increasing the alkyl chain length, the mesophase instability previously observed for C₈ surfactants is decreased. The interactions between alkyl tails favour the formation of LC phases even for those surfactants containing relatively short hydrophilic segments. To assess whether the MARTINI FF can capture such behaviour, CG-MD simulations of six different C₁₂ surfactants with a different number of EO groups in water were carried out, allowing to systematically study the effect of the number of EO units in the mesophase formation, spanning a wide range of HLB values (8.17-17.4).

At low HLB (lower number of EO units), Funari et al.[228] reported the phase diagram for the C₁₂E₂/water system. A striking feature of such phase diagram is the absence of an isotropic micellar phase in the low surfactant concentration regime, conversely to most surfactant solutions. Instead, at 298 K, the micellar solution is replaced by a L_α phase – that is thought to coexist in equilibrium with water containing surfactant unimers. This L_α phase, present even at very low concentrations, is further found to persist up to approximately 80 wt% of surfactant concentration. The diagram proposed also suggests the formation of two reversed bi-continuous cubic phases with different morphologies (V₂⁽¹⁾ and V₂⁽²⁾) and a sponge-like phase L₃ between 40-60 wt% in a narrow temperature range above the 303 K. A few years later, the same system was revisited by Lynch et al.[229] that proposed a new phase diagram for the same system. This new diagram essentially shares the same features described by Funari except for the presence of miscibility gaps between L₃/ V₂⁽¹⁾ and in between the two bi-continuous phases.

The CG-MD simulation results for the C₁₂E₂ system are shown in **Figure 5.3** where the L_α phase is indeed observed at low surfactant concentrations (15 wt%) persisting up to 70 wt%, in excellent agreement with the experiments.[228,229] Literature CG-MD simulations have previously been carried out for this system but only at very high surfactant concentrations (around 70 wt%) for which the lamellar phase was also reported.[241,245] This is the first time that the formation of such phase in the low concentration regime, starting from a random configuration of the system, is reported using CG-MD simulations. Unfortunately, no evidence for the formation of L₃ and V₂ phases was found in the simulations, what must be related to the narrow (*T, x*) experimental range in which they were observed experimentally. Accordingly to Funari et al.,[228] the interconversion between the V₂ phases is mainly driven by temperature rather than by surfactant concentration, thus being difficult to capture this phase in CG-MD simulations. Nonetheless, an additional simulation at 45 wt% was carried out at 303 K where Lynch and co-workers[229] reported the existence of an L₃ phase. The CG-MD result shown in **Figure 5.3**, points towards the formation of bended bilayers that can represent an intermediate stage towards the formation of a sponge-like phase, commonly suggested as a possible structure of the L₃ phase.

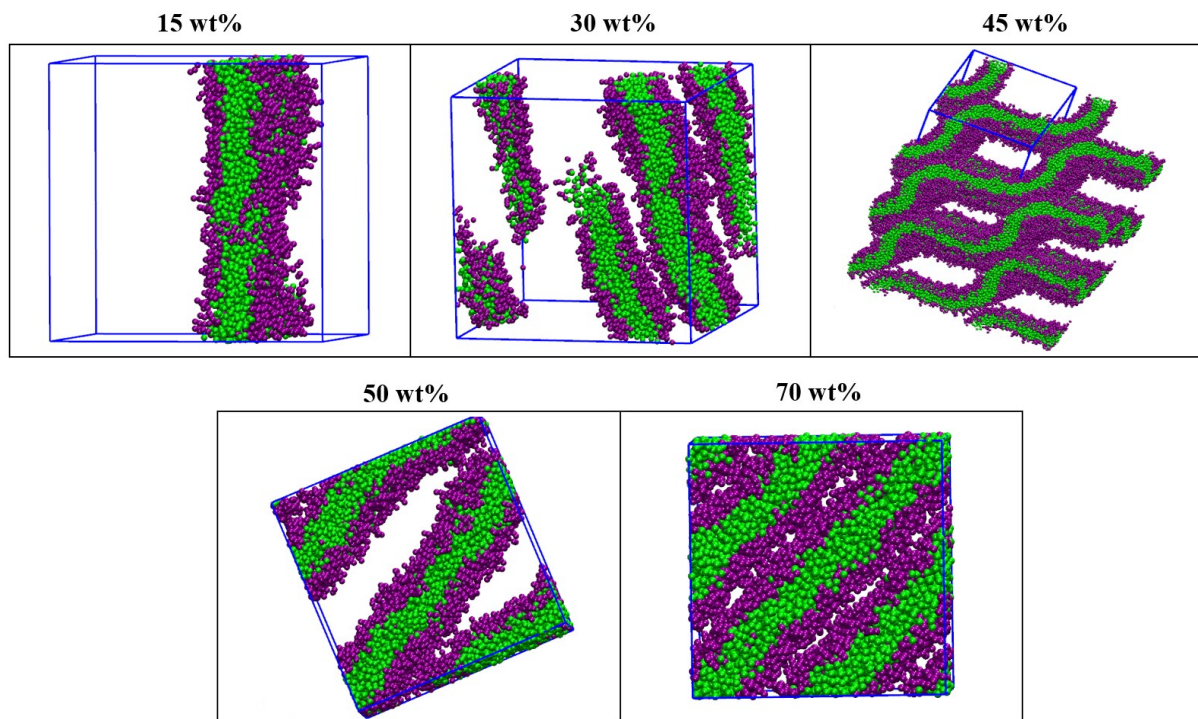


Figure 5.3. CG-MD simulations for $C_{12}E_2$ in water at different surfactant concentrations. Colours as in **Figure 5.2**.

For $C_{12}E_4$, Mitchell et al.[210] proposed a similar behaviour, with the system exhibiting a $W + L_\alpha$ dispersion at lower surfactant concentrations and a single L_α in the range of 25-75 wt%. The increased EO units in $C_{12}E_4$ promoted that V_2 phases are no longer observed. This system was previously modelled through CG-MD simulations by Rossi et al.[241] and Grunewald et al.,[245] but only at 53 wt% of surfactant for which, a defected lamellar phase (L_α^H) was observed, i.e., the bilayers contained water-filled defects in the form of pores or necks.[262] In the simulations, displayed in **Figure D.4**. in Appendix D, this phase was found at 53 wt% persisting up to at least 70 wt% of surfactant concentration. Only above 80 wt%, near the upper concentration limit reported in literature, a perfect lamellar phase was observed. Curiously, as can be observed in the same figure, at lower surfactant concentrations, disperse rod-like micelles are found in solution, instead of the $W + L_\alpha$ dispersion suggested by Mitchell et al.[210] Nevertheless, although the model was not able to reproduce the L_α phase at low surfactant concentrations, as happens for the $C_{12}E_2$, it still predicts a lower surface curvature and the consequent inability of the system to produce spherical micelles for a surfactant with such a low HLB.

Clunie et al.[230] reported that the phase diagram for the aqueous solution of $C_{12}E_6$ exhibits a $L_1/H_1/L_\alpha$ sequence. The proposed phase diagram shows an unusual region of micellar phase L_1 between H_1 and the L_α . However, this was not supported by Mitchell et al.[210] in a later study that reported the archetypical sequence of $L_1/H_1/V_1/L_\alpha$ phases. In previous studies using CG-MD simulations, only the L_1

and H_1 phases were observed. Thus, in this work, the concentration screening allowed to investigate the formation of all the reported phases, as depicted in **Figure 5.4**. The increased hydrophilicity of the $C_{12}E_6$ yielded a micellar solution at 15 wt%, with the micelles adopting a near spherical shape, contrarily to what it was observed for the lower HLB surfactant $C_{12}E_4$. At 30 wt%, the micelles are larger and adopted a rod-like shape that are at the origin of the cylindrical rods that later form the H_1 -like phase observed at 50 wt%, in excellent agreement with the experiments.[230]

In contrast, the simulation at 70 wt% (333 K) revealed the formation of a lamellar phase containing water-filled pore defects, as previously observed for the $C_{12}E_4$ system. According to Mitchell and co-workers,[210] at this concentration range, the expected phase can be either L_α or V_1 depending on temperature. Therefore, and since the L_α^H is a transition towards L_α , an additional simulation at a lower temperature (303 K) was carried out. In **Figure 5.4**, it can be noticed an intermediate V_1 -like phase with different layers interconnected. Despite the limitation of capturing the effect of temperature in CG-MD simulations, the $V_1 \rightarrow L_\alpha$ transition was indeed promoted by a temperature increase, in agreement with experiments. This is not the usual case, especially when dealing with the I_1 and the H_1 -like phases. The energy barriers during the mesophase formation in CG-MD simulations, usually prevent the system to reach the proper equilibrium state unless higher simulation temperatures are considered. This was previously discussed for the phase behaviour of imidazolium based ILs.[102]

The presence of a defected lamellar phase in C_iE_j /water systems, as found in the simulations, seems to be the most stable phase for the $C_{12}E_6$ /water system at around 70 wt% concentration. The defected lamellar phase was first reported for $C_{22}E_6$,[263] $C_{16}E_6$,[256] and $C_{30}E_9$ [264] systems and thought to be induced by the increased alkyl chain lengths with limited flexibility, as a way to increase the EO hydration, without changing the surface area per molecule. However, a few years later, Constantin et al.[262] demonstrated that such phase also occurs for surfactants with lower alkyl chains, namely $C_{12}E_6$, at around 65 %wt, in a remarkable agreement with the CG-MD simulations carried out in this work.

Since the L_α phase appeared at even higher surfactant concentrations (up to 85 wt%), an additional simulation at 80 wt % was carried out for this system. The final simulation snapshot is displayed in **Figure 5.4**, revealing the formation of a defect-free L_α phase. This is in excellent agreement with the work of Mitchell et al.,[210] with all the four different phases being observed in the CG-MD simulations. It must be noticed that the model correctly captured the structure and formation of the L_α phase for this $C_{12}E_6$ system, a phase that was not clearly observed for C_8E_6 . This can be ascribed to the increased interactions between alkyl chains and demonstrates the ability of the model to capture the delicate balance of forces behind the formation of the L_α phase.

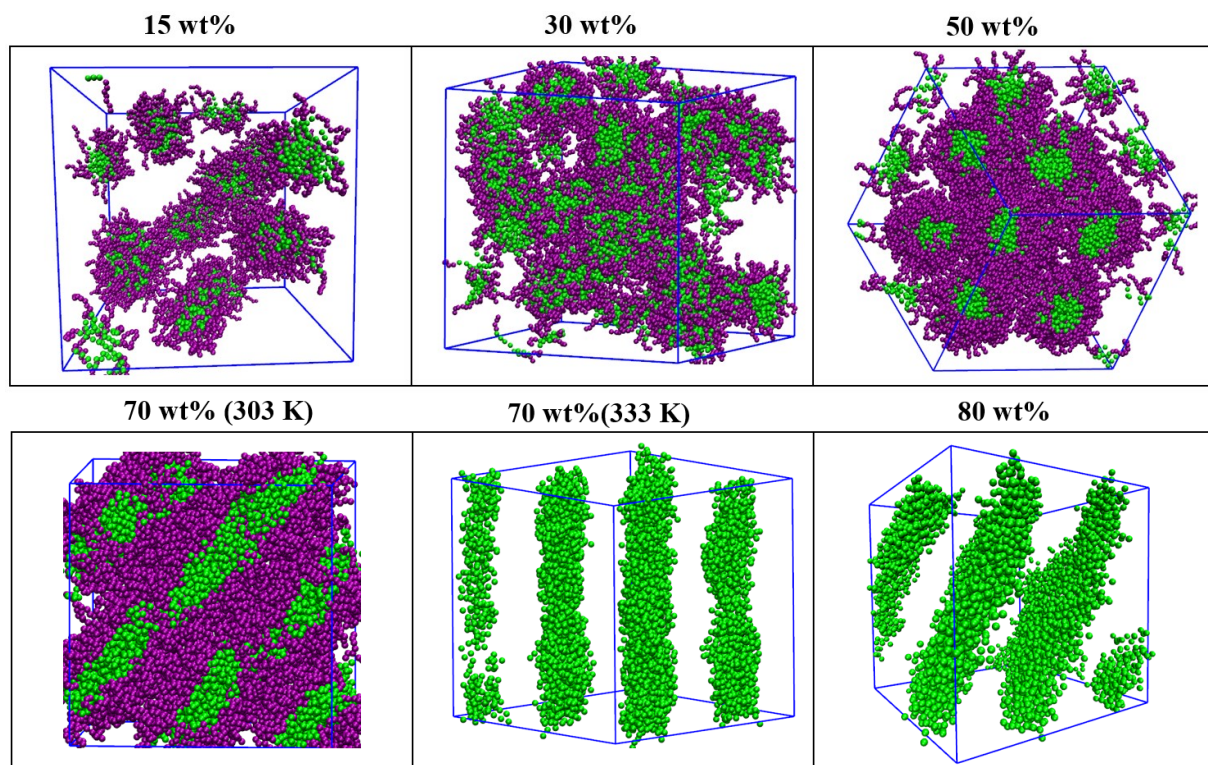


Figure 5.4. CG-MD simulations for $C_{12}E_6$ in water at different surfactant concentrations. Colours as in **Figure 5.2**.

A further increase in the number of EO units to 10, reveals a decrease in the stability of the lamellar L_α phase. As a consequence, Patrick et al.[254] suggested that, depending on the surfactant concentration, the $C_{12}E_{10}$ /water system is either in a micellar solution or in a H_1 phase. Our CG-MD simulations, shown in **Figure D.5** in Appendix D, suggest that the model can capture such effect for concentrations below 50 wt%, revealing the presence of micelles whose shape and size vary when the surfactant concentration is increased (spherical micelles \rightarrow micelle rods \rightarrow long cylindrical rods). The elongated cylindrical micelles observed at 50 wt% revealed the initial stages of the H_1 phase formation, later observed at 70 wt%, in excellent agreement with literature as shown in **Figure 5.5**. When the surfactant concentration is further increased to 85 wt%, the CG-MD simulations predict the formation of a V_1 phase. Although this V_1 phase was not reported experimentally, it is a well-known feature of this type of systems, being, according to experimental results, also present in $C_{12}E_8$ and, in a very narrow range of conditions, in the $C_{12}E_9$ system.[233,265] It must be pointed out that the L_α phase was not observed in the CG-MD simulations carried in this work for the $C_{12}E_{10}$ /water system, confirming the absence of such phase, as previously reported experimentally for the $C_{12}E_9$ system.[265]

70 wt% – Frontal View

70 wt% – Side View

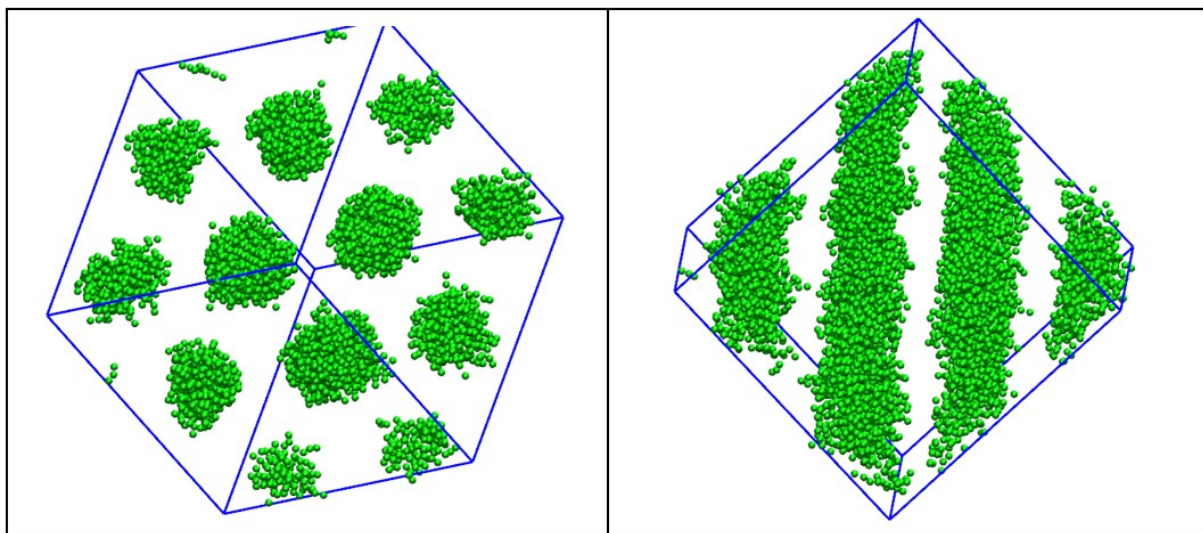


Figure 5.5. Spatial organization of the alkyl tails in the H_1 phase observed in the $C_{12}E_{10}/H_2O$ system at 70 wt% concentration.

Continuing the trend of decreasing the stability of the lamellar phase, the $C_{12}E_{12}/water$ system showed a similar behaviour with the exception that, contrarily to $C_{12}E_{10}$, POM observations and low angle X-ray studies carried out by Mitchell et al.[210] revealed the formation of a cubic phase with two different morphologies in the 30-55 wt% concentration range, prior to the formation of the H_1 phase. A subsequent study developed by Sakya et al.[255] reinforced the results of Mitchell et al.[210] but stressed the existence of a third morphology of the cubic phase in a very narrow range of (T, x) conditions. The results of the CG-MD simulations for the $C_{12}E_{12}$ system are presented in **Figure 5.6**, confirming the decrease in the stability of the lamellar phase. At 15 wt%, the model predicted the formation of a micellar phase with near-spherical micelles in good agreement with the phase diagram reported by Sakya et al.[255] According to this study, at higher concentrations, a cubic phase with different structures is expected but such well-defined cubic phases could not be well reproduced by the model. At 50 wt%, cylindrical rod micelles were found instead, that represent the precursor of the H_1 phase at this concentration and found to persist up to higher surfactant concentrations. Accordingly, in the CG-MD simulation at 70 wt%, a H_1 phase is predicted by the model. A further increase of the surfactant concentration (82 wt%) does not lead to a clear L_α phase. Instead, at this concentration, the system seems to be in an intermediate phase between H_1 and a L_α^H -like phase, similarly to what was observed for $C_{12}E_{10}$.

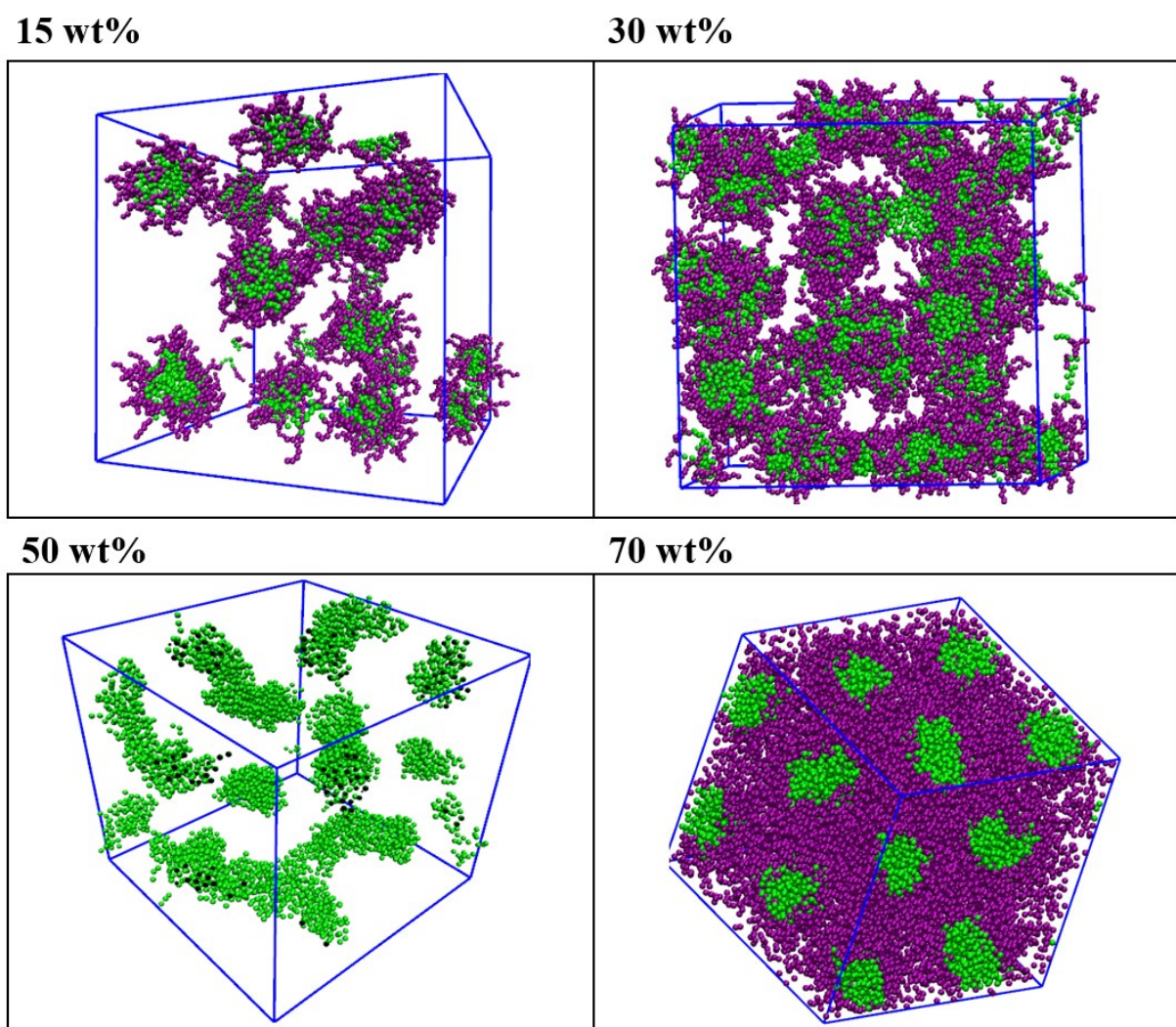


Figure 5.6. CG-MD simulations for $C_{12}E_{12}/H_2O$ at different surfactant concentrations. Colours as in **Figure 5.2**. Black represents the direction of plane in which the content of the box was cut to allow for a clearer visualization.

Among the twelve different surfactants analysed in this work, the $C_{12}E_{23}$ represents the molecule with the highest number of EO units (highest HLB). Due to the increased hydrophilicity, Patrick et al.[254] reported the absence of mesophases in $C_{12}E_{23}$ except for the formation of the I_1 phase, although no temperature and concentration conditions were provided. The CG-MD simulations for this surfactant confirmed the absence of ordered phases. Instead, a random dispersion of spherical or rod-like micelles (depending on the concentration) was observed in all simulations as illustrated in **Figure D.6.** in Appendix D. In fact, even for very high concentrations (e.g., 50 or 70 wt%), most of the micelles retain its sphericity, contrarily to what is observed for surfactants with a lower HLB.

Overall, the results predicted for C_{12} surfactants showed a good agreement with literature reports, especially considering the CG nature of the model and its inherent transferability. Previous models could not reproduce the phase behaviour of surfactants with a considerable number of EO units. Nevertheless, the MARTINI FF successfully provided a reasonable description of C_iE_j surfactants with EO groups up to 23 units. Moreover, the model was able to predict the inability to form spherical micelles when the number of EO groups is low ($j = 2, 4$) as well as how the lamellar phase is the most stable phase for such surfactants. Simultaneously, the model was able to predict how the increased hydrophilicity first induces the instability of the lamellar phase and, then the hexagonal phase emerges for even larger hydrophilic heads. In summary for $C_{12}E_j$ surfactants, increasing j , and consequently the HLB, changes the first mesophase from lamellar to hexagonal, and possibly to a cubic-like phase or a micellar solution. This is in good agreement with experiments and the model seems to predict that, as the size and consequently the area occupied by the hydrophilic group is increased, the surfactant packing favors the formation of curved interfaces (spheres and cylinders) over planar ones (bilayers) as observed in both the simulations carried here and in the experimental data reported in the literature.

C_{16} surfactants

Previous CG-MD studies of aqueous solutions covering C_iE_j surfactants were restricted to $i = 12$ and three different EO groups, $j = 2, 4, 6$. Bearing in mind the effect that longer alkyl chains could have in the mesophase behaviour, a set of CG-MD simulations were carried out for C_{16} surfactants with different number of EO units.

Mitchell et al.[210] reported the phase diagram for $C_{16}E_4$. At low surfactant concentrations and temperatures lower than 333 K, the system exhibits a $W + L_\alpha$ dispersion with the L_α phase being replaced by an L_3 , V_2 or L_2 phase when the temperature is increased. Such phases are stable up to circa 60 wt% of surfactant concentration beyond which the lamellar phase is always the most stable phase. The CG-MD simulation results for $C_{16}E_4$ are presented in **Figure 5.7**, exhibiting elongated or rod-like micelles at 15 wt%. At 30 wt%, the system seems to be in a transition state resembling the V_1 phase that often acts as a precursor for layer-like structures such as those later observed at 50 wt%. Despite this intermediate phase was not reported by Mitchell et al.[210], it is compatible with a phase transition from the micellar rods-to- L_α phase observed at low concentrations. This is unequivocally the most stable phase at higher concentrations and is also observed in the CG-MD simulation at 70 wt%.

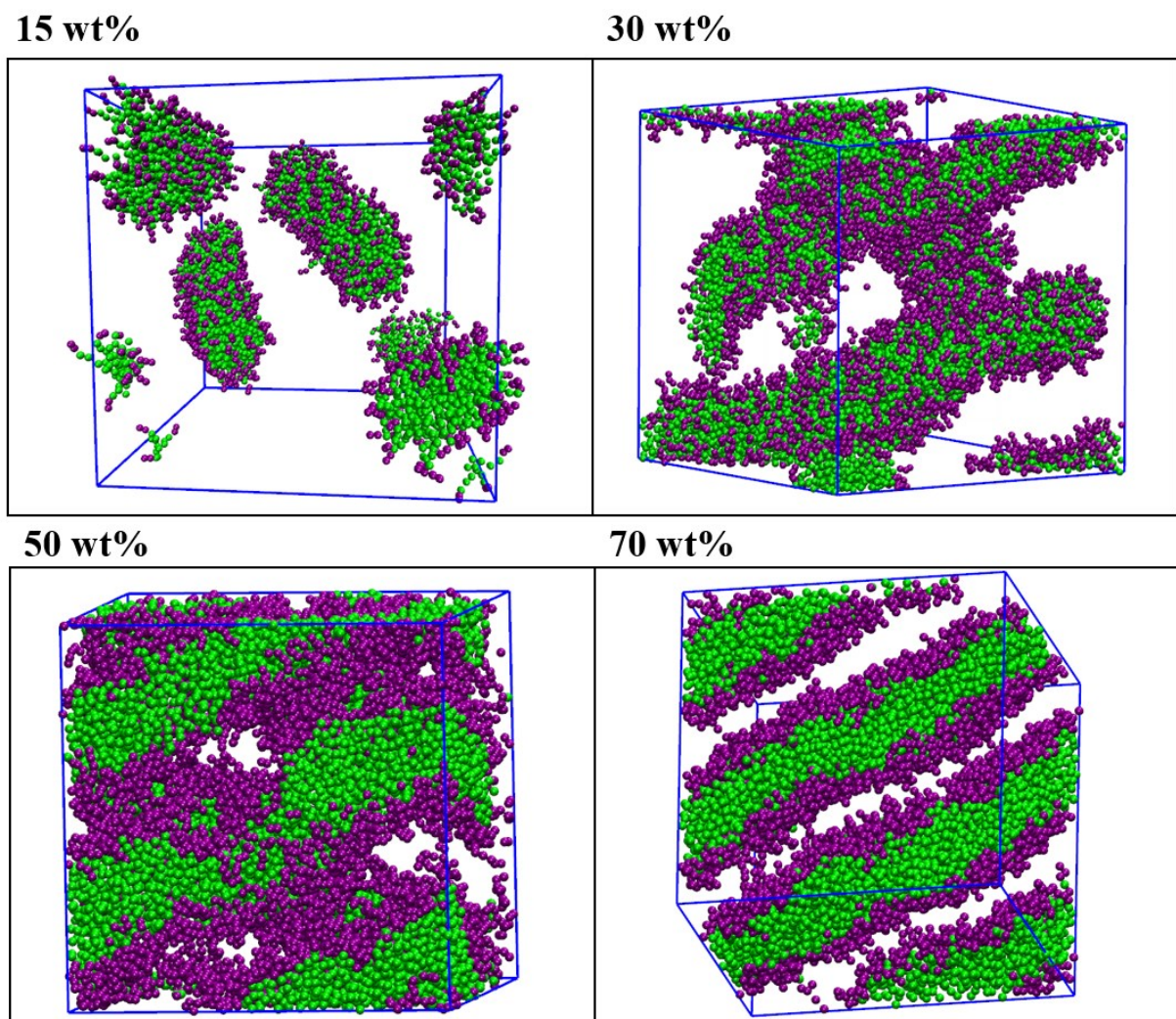


Figure 5.7. CG-MD simulations for $C_{16}E_4/H_2O$ at different surfactant concentrations. Colours as in **Figure 5.2**.

Funari et al.[256] and Fairhurst et al.[257] reported the phase diagram for the $C_{16}E_6$ /water system. Even though there are a few differences concerning the location of the phase boundaries, both studies denoted the presence of an intermediate phase, a term used here for the first time to characterize non-cubic phases between H_1 and L_α occurring in C_iE_j /water systems. Prior to the formation of the L_α phase, and because long alkyl tails cannot pack into V_1 structures,[256] the presence of both, the intermediate phase and a defected lamellar phase L_α^H , are expected to arise instead, stressing the role played by the alkyl chain conformations in controlling the transition between H_1 and L_α . The CG-MD simulations for the $C_{16}E_6$ /water system showed the change in the organization of the alkyl chains due to the increase on the surfactant concentration as presented in **Figure 5.8**. At 40 wt%, the system formed cylindrical rods resembling the H_1 phase that was reported between 35-45 wt% of surfactant concentration.[256,257] At

50 wt%, the system assembled in a mesh-like structure which is one of the possible structures suggested by Holmes and co-workers[257,266] for the intermediate phase, thought to replace V_1 for surfactants with considerably long alkyl chains. At higher surfactant concentration, the alkyl chains are already forming a L_α phase with an almost negligible presence of water-filled defects. Although the formation of a defected lamellar phase is expected between the intermediate phase and the L_α , the considerably high temperature and the high concentration contributed to the decreased number of defects found in the L_α^H phase. In **Figure D.7.** in Appendix D, another perspective of the simulation box for the 70 wt% system is shown, where one of the pore defects still present can be more easily observed.

It must be highlighted that the model was able to predict the existence of a mesh-like intermediate phase, instead of the typical V_1 phase due to the increase of the alkyl chain length, and a relatively low HLB is yet another beacon of the model prediction ability and transferability.

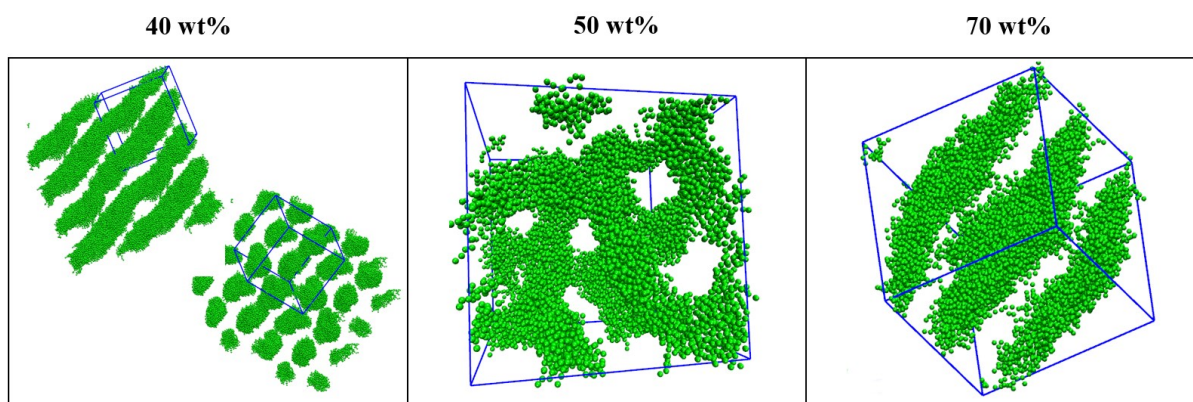


Figure 5.8. Arrangement of the alkyl tails in the $C_{16}E_6/H_2O$ system at different surfactant concentrations.

Mitchell et al.[210] reported a few years earlier that neither the intermediate or L_α^H phases were present in $C_{16}E_8$. Instead, the phase diagram displayed the archetypical progression of phases from low to high amphiphile concentrations, *i.e.*, micellar solution \rightarrow micellar cubic phase \rightarrow hexagonal columnar phase \rightarrow bi-continuous cubic phase \rightarrow lamellar phase. The CG-MD simulations results for this $C_{16}E_8$ system are shown in **Figure 5.9.** The results display a fair agreement with experiments: at 15 wt%, the system exhibited a micellar solution with the micelles retaining their sphericity up to 30 wt%. At this concentration, the presence of a cubic phase could not be clearly identified, although some sort of long-range ordering of the micelles, resembling a micellar cubic phase, is visible when compared with the results for other systems at different conditions. At 50 wt%, the hexagonal phase is expected according to the literature but only dispersed cylindrical micelles were found. Conversely, at 70 and 80 wt% the model can predict the occurrence of the V_1 and L_α phases, respectively. Perhaps, the most interesting result is that the defected lamellar phase – previously observed for $C_{16}E_6$ – was no longer observed in

this system. The model was able to capture the ability of the system to form instead a V_1 -like phase given a sufficiently large j/i ratio. It is important to stress that V_1 structures are difficult to characterize, with the best candidates being extended networks where the chain/water interface has both positive and negative curvatures, as observed in some of our simulations.[267]

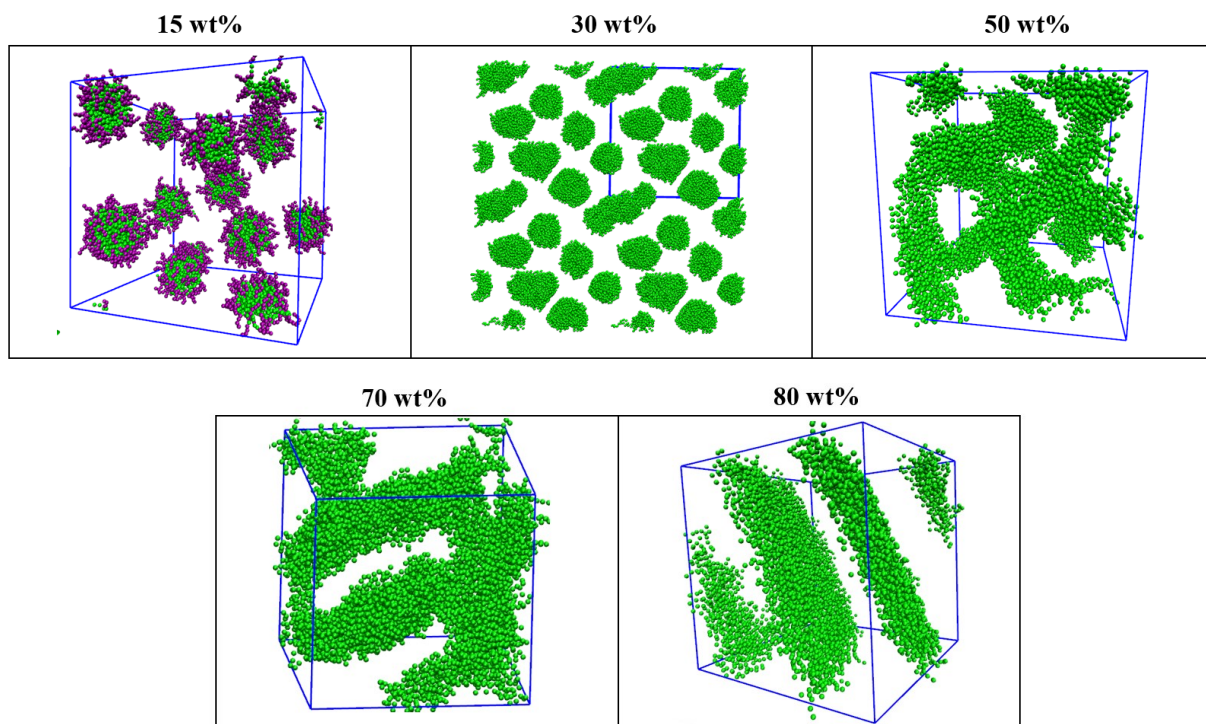


Figure 5.9. CG-MD simulations for $C_{16}E_8/H_2O$ at different surfactant concentrations. Colours as in **Figure 5.2**.

When the number of EO groups are increased, such as in $C_{16}E_{12}$, the agreement with experiments was less satisfactory. According to the work of Mitchell et al.[210] at 30, 50 and 70 wt% the I_1 , H_1 , and V_1/L_a phases are expected. The stability of the bi-continuous and lamellar phases decreases considerably and are only present in a very narrow range of concentrations. In the CG-MD simulations carried out in this work, depicted in **Figure D.8** in **Appendix D**, at 30 wt%, the cubic phase was not found and at 50 wt% the cylindrical micelles were somehow organized, but not in the expected hexagonal array. At 70 wt%, the bi-continuous cubic phase was indeed observed, as reported in the literature. However, the lamellar phase persisted to even higher concentrations (up to 90%wt) contrary what it was observed experimentally. This is, however, a common issue of MD simulations when tackling phase transitions between ordered phases such as the lamellar phase at very high concentrations. Nonetheless, the ability of the model to predict the existence of a V_1 -like phase instead of a defected lamellar phase is still a remarkable achievement of the model.

The low concentration regime

Under diluted conditions, a surfactant molecule is usually present in water as a solution of surfactant unimers or small oligomers aggregates. However, at a given temperature, once the surfactant concentration is increased beyond a certain threshold – denoted as the *cmc* –, small spherical-shaped aggregates are formed to decrease the alkyl chain area exposed to water. By increasing the surfactant concentration, the size of the micelles tends to rise, while its sphericity is severely decreased, leading to the formation of rod-like and disk-like aggregates that can be seen as precursors of long-range ordering phases such as H_1 and L_α .

Therefore, having a reasonable description of the micellar aggregates, precursors of certain mesophases, and the knowledge on how the *cmc* or N_{agg} vary with the surfactant nature, is highly relevant for the design and understanding of C_iE_j solutions. While *cmc* values are relatively easy to determine experimentally, usually capturing changes in the behaviour of relevant physical properties (e.g., conductivity, surface tension, etc.), it is a tough question for MD simulations. This is mainly due to the very low *cmc* values of non-ionic surfactants when compared to their ionic counterparts that makes it very computational demanding to systematically simulate systems at such low concentrations, even using CG models. The experimental *cmc* and N_{agg} values found in literature for the studied surfactants are provided in **Table 5.2**. In the case of the $C_{12}E_6$ aqueous solution – surfactant with an intermediate HLB value in between those studied in this work – the *cmc* reported experimentally ranges between 6.8 and $8.8 \cdot 10^{-5}$ M, while their N_{agg} are between 110-180.[222,268,269] Considering the highest concentration and the lowest N_{agg} , a simulation of only 110 molecules of surfactant requires more than 17 millions of CG water beads (68 millions of water molecules). An alternative is to perform simulations at higher concentrations but still within the micellar phase and take the average free surfactant unimer concentration as a rough estimation of the actual *cmc*. This approach has been previously used with the MARTINI FF, using a different CG mapping for the C_iE_j molecules, and found to provide a reasonable estimation of the *cmc* values, although an incorrect temperature dependency was observed.[214]

With the aim to explore the ability of the C_iE_j CG model at concentrations near the *cmc*, an additional simulation of 51 C_8E_6 molecules (the surfactant with the lowest *cmc* from those investigated in this work) was carried out at $9.8 \cdot 10^{-3}$ M. After 5 μ s of simulation, using an in-house cluster counting code, the N_{agg} was found to be 39 surfactant molecules, with 12 molecules remaining freely in the solution. The free surfactant unimers correspond to a concentration of $2.3 \cdot 10^{-3}$ M that compares reasonably well with the *cmc* values reported in literature. This fact suggests that the CG mapping proposed by Grunewald et al.,[245] and used in our study, retains the ability to provide a reasonable estimate of the *cmc* for C_iE_j surfactants in water.

Table 5.2. Micelle aggregation numbers determined from the CG-MD simulations at 15 wt% of surfactant concentration and literature values for N_{agg} and cmc .

Surfactant	N_{min}	N_{max}	N_{agg}	N_{agg}^{Lit}	Ref.	cmc^{Lit} (M)	Ref.
C ₈ E ₆	43	104	61.9	32	[270]	$\sim 9.8 \cdot 10^{-3}$	[211,270,271]
				51	[272]	$7.6 \cdot 10^{-3}$	[270]
						$1.68 \cdot 10^{-2}$	[270]
				>300	[269]	$2.3 \cdot 10^{-4}$	[269]
C ₈ E ₁₂	34	59	46.6	-		-	
C ₁₂ E ₂	-	-	-	-		$3.3 \cdot 10^{-5}$	[224]
C ₁₂ E ₄	140	329	250.0	160*	[268]	$6.0 \cdot 10^{-5*}$	[268]
							$4.33 \cdot 10^{-5}$
C ₁₂ E ₆	53	158	90.9	110	[268]	$6.8 \cdot 10^{-5}$	[268]
				144-180	[269]	$8.8 \cdot 10^{-5}$	[222]
C ₁₂ E ₁₀	38	72	58.8	-		-	
C ₁₂ E ₁₂	29	70	50.0	81	[269]	$1.4 \cdot 10^{-4}$	[224,269]
C ₁₂ E ₂₃	19	61	38.5	40	[268]	$1.0 \cdot 10^{-4}$	[268]
				41	[269]	$1.75 \cdot 10^{-4}$	[269]
C ₁₆ E ₄	176	322	250				
C ₁₆ E ₆	73	168	111.1			$1.3 \cdot 10^{-6}$	[271]
C ₁₆ E ₈	56	114	83.3	160	[269]	$5.0 \cdot 10^{-7}$	[274]
C ₁₆ E ₁₂	39	105	66.7	152	[269]	$2.3 \cdot 10^{-6}$	[269]

*values for C₁₂E₅

Lit – Literature values

The MARTINI FF has been previously applied for the prediction of the N_{agg} in aqueous solutions of C_iE_j surfactants[214] and to obtain the average size distribution of ethylene oxide urethane micelles[275]. However, in those works previous parameterizations of the EO groups were based on pre-existing MARTINI beads. Therefore, to analyse the ability of the new EO parameterization to predict the aggregation behaviour of C_iE_j surfactants, N_{agg} values, were here obtained using the cluster counting code for 15 wt% systems. It is however important to point out two aspects of the values obtained using this procedure: firstly, the N_{agg} cannot be obtained for the C₁₂E₂ system, since the L_α phase was already observed at 15 wt%. Secondly, since N_{agg} tends to increase with surfactant concentration, the values reported here are expected to be slightly higher than those predicted by the model at the cmc , especially

for those surfactants with a considerably high i to j ratio, where micellar-to-rod transition was observed at this concentration, instead of spherical micelles, as observed in $C_{12}E_4$ and $C_{16}E_4$.

The aggregation numbers (minimum, maximum, and average) obtained in the CG-MD simulations are reported in **Table 5.2** and compared with some experimental values found in the literature. It must be pointed out that the literature values should be taken with caution since diverse values were reported by different authors and, in addition, the concentrations were not always provided. **Table 5.2** exhibits a considerable disparity between the minimum and maximum micelle size. Nonetheless, the N_{agg} values obtained correctly describe the effect of the chain length, increasing with i and decreasing with j . The agreement with literature can also be considered fairly satisfactory, in particular for C_8E_6 , $C_{12}E_6$, and $C_{12}E_{23}$ systems. It is worth to highlight the excellent agreement obtained for the $C_{12}E_6$ whose $N_{agg} \sim 90.9$, which is close to the value reported in literature as shown in **Table 5.2**, $N_{agg} = 110$, and different to the $N_{agg} = 45$ previously reported by Puvvada et al.[235,276] who used a molecular thermodynamic approach to predict the micellization. Clearly, the highest deviations were observed for the C_{16} systems when comparing with the data reported by Levitz et al.[269] however, such data could have been severely overestimated. For instance, in the C_8E_6 system, micelles with more than 300 surfactant molecules were reported, even though other authors have reported values between 32 and 51 for the same system[270,272] or 80 for C_8E_5 , whose N_{agg} is expected to be higher.[268]

These results reinforce the ability of the MARTINI FF to provide a reasonable description of the low concentration micellar regime in aqueous solutions of non-ionic surfactants; however, as previously mentioned, to obtain quantitative measurements of the cmc using this type of simulations can easily become computational prohibitive, especially for the longer non-ionic surfactants with very low cmc values. One viable alternative, suggested by Anogiannakis et al.[277] is to use an implicit solvent version of the MARTINI FF to calculate such diluted properties, while retaining the original variant to study the phase behaviour at higher concentrations. In their work, after a small tweak of the interaction between the hydrophobic beads and of the electric permittivity of water, a good agreement with the cmc and N_{agg} of ionic surfactants was achieved and, considering the good description obtained here, similar results can be expected for the non-ionic surfactants. Another alternative could be the methodology proposed by Santos et al.[278] that used Monte Carlo simulations of a lattice surfactant model to determine the cmc from extrapolations of the unimer surfactant concentration. However, as exemplified above for $C_{12}E_6$, diluted simulations of these surfactants at concentrations even slightly above the cmc are computational prohibitive so that an implicit solvent model would still be required.[278]

A final model benchmark on describing the diluted region of the C_iE_j /water systems is the micellar radius. Unfortunately, experimental data was only found for $C_{12}E_6$, exhibiting a micelle radius $\sim 20 \pm 5$

Å reported by Corti et al.[222] To obtain the micelle radius from the CG-MD simulation carried out for $C_{12}E_6$ /water system at 15 wt%, the micelle density profile from the micelle centre of mass was obtained and shown in **Figure 5.10**. The micelle radius is the distance from the centre of the micelle (0) to the maximum of hydrophilic head curve (purple). Thus, the micellar radius is ~ 21.7 Å which is in excellent agreement with the literature. This suggests that the model correctly describes the molecular packing of the surfactant within the micelles.

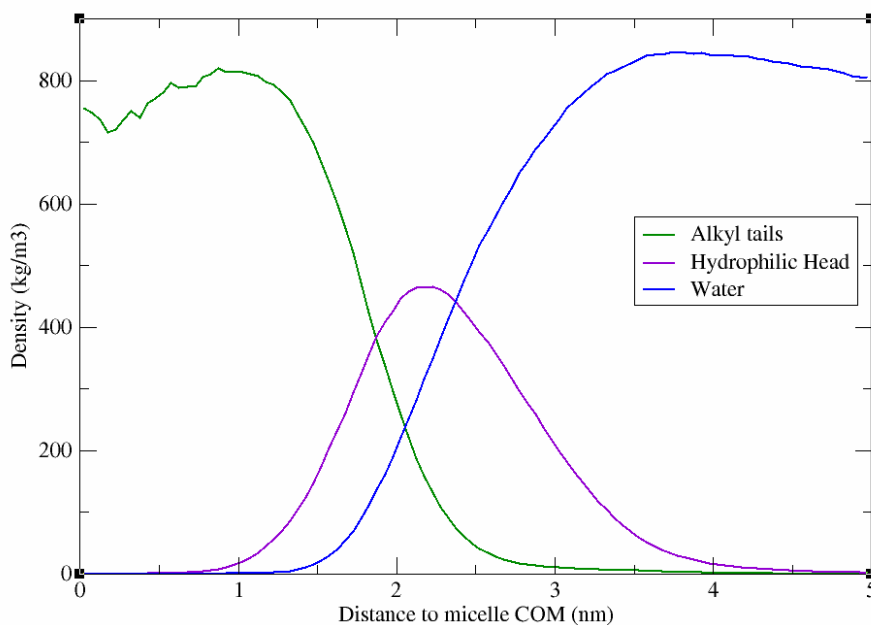


Figure 5.10. Micelle density profile for the $C_{12}E_6$ in water as obtained from the CG-MD simulation at 15 wt%.

Conclusions

In this section, an extensive analysis of the influence of molecular structure and concentration on the phase behaviour of aqueous solutions of C_iE_j surfactants was carried out using a MARTINI FF for CG-MD simulations. Twelve different surfactants with different chain lengths of both the hydrophobic and hydrophilic moieties were investigated at different concentrations, allowing to span a wide range of HLB values.

Concerning the effect of the alkyl chain length, MD simulations were able to correctly reproduce how an increase of i from 8 to 12 leads to the decrease of mesophase instability. LC phases were obtained for C_{12} surfactants, even for small hydrophilic moieties, for which a lamellar phase can be predicted even at very low surfactant loadings, in agreement with experiments. In addition, the effect of adding EO units is shown to be well captured by the model, used to simulate surfactants with up to 23 EO units, accurately describing the decreased stability of the lamellar phase when the number of EO chains are increased.

In terms of mesophase structures, the model captured the existence of intermediate phases between H_1 and L_α , other than the usual V_1 phases, typical of these types of systems. As an example, the presence of a defected lamellar phase, initially supposed to exist only for long alkyl chains ($i > 16$), was here shown also for C_{12} surfactants, in excellent agreement with some of the most recent studies.

Furthermore, the model provided a reasonable description of the micellar regime, namely the micelle radius, aggregation numbers and critical micellar concentration, in agreement with experiments, considering the uncertainty of some experimental values.

Overall, the model correctly predicted the formation of LC phases in C_iE_j systems in a wide range of concentrations in good agreement with experiments, regardless the surfactant structure, while still providing a reasonable description of diluted micellar phases. The obtained results improve the reliability of the MARTINI C_iE_j model, paving the way for the use in multi-component systems used in the industry and diverse research areas, providing some clues when experimental data is not available.

5.2- The impact of oil on the phase behaviour of C_iE_j/H_2O systems

Introduction

One of the advantages of developing a MARTINI CG-MD computer simulation framework is its transferability. Thus, the C_iE_j model discussed in the previous section can be used as a computational design tool to analyse the impact of adding other compounds, providing a tool for the computational design and analysis of new surfactant systems. This is useful not only for the Oil & Gas industry in the search for new systems relevant for EOR applications, but also in other fields where formulations typically contain this kind of surfactants, such as many detergents or cosmetics. Within EOR, before using the MARTINI FF to model the oil detachment mechanism from the rock reservoir, it is first advisable to evaluate the impact of oil, or other non-polar fluids, to the phase behaviour of the surfactant-water systems investigated in the previous chapter. This would not only allow to understand and predict how the oil affects the interfacial curvature and phase structure of the fluid, allowing the manipulation of the liquids structure, but also to enable a better understanding of the interactions established between the oil and the solution. Unfortunately, although there is a great amount of information in the literature about the macroscopic phase behaviour of these ternary systems, typically in the form of fish-shaped phase diagrams at a constant oil-to-water ratio showing the macroscopic phase separation,[279] knowledge about how an oil affects the nano-structural organization of C_iE_j -water systems are much scarcer, and are often limited to analyse the swelling or penetrating behaviour of an oil in the L_α or mesh phase.[280–282] As a consequence, phase diagrams for the ternary systems that include information about the possible LC phases are far from being common and, to the best of my knowledge, only the remarkable book written by Laughlin[283] presents a full phase diagram including the LC phases (in this case a L_α phase) for the $C_{10}E_4 + C_{16}H_{34} + H_2O$ system, at different temperatures between 19 and 60 °C.

Therefore, given the good results obtained in the previous section, CG-MD simulations are here carried out for ternary systems oil + surfactant + water to predict the impact of oil to the most common types of LC phases. The $C_{12}E_6$ surfactant is chosen as archetypal surfactant given its intermediate HLB and because in the previous chapter it was shown to form the most common phases, namely micellar, H_1 , L_α^H , and L_α . Hence, starting from the final configurations of the binary system obtained in the previous chapter at different concentrations of $C_{12}E_6$, *n*-dodecane is used as a model oil and added to the system in different amounts. Each *n*-dodecane molecule is modelled using four ‘C1’ beads, the same beads used in the surfactant tail, and commonly used to model *n*-alkanes.[52] Even though temperature has an important impact on the phase behaviour of the ternary systems,[283] especially in what concerns the

macroscopic phase split, simulations were carried out only at 313 K to investigate the effect of increasing oil amounts upon the LC phases at constant temperature. The different simulations were run for up to 8 μ s and the equilibrium was ensured, using the same settings and methodology described in the previous chapter. Simulations starting from the L_α of aqueous solutions of $C_{10}E_4$ were also carried out to enable a qualitative comparison with the results reported by Laughlin[283].

Results

The Lamellar phase (L_α)

Based on the phase diagram reported by Laughlin[283], the binary system $C_{10}E_4 + H_2O$ exhibits a L_α phase at around 60 wt% of surfactant and 313 K. This phase is shown to persist upon the addition of small amounts of oil (*n*-hexadecane) but, when the total oil concentration amounts to more than 30 wt%, a phase split is observed. To reproduce this behaviour, CG-MD simulations were carried out for $C_{10}E_4 + H_2O + n$ -dodecane mixtures. Starting from a binary mixture of $C_{10}E_4 + H_2O$ at 60 wt% of surfactant, oil molecules were added so that the total oil amount in the mixture corresponds to 10, 25 or 40 wt%. **Figure 5.11** shows the organization of the oil molecules and the alkyl tails of the surfactant. While at low oil concentrations the oil molecules move towards the inner part of the bilayers and the liquid retains the form of a L_α phase, as soon as the oil concentration is increased, the system forms an oil-rich phase. At 25 wt% of oil, except for one aggregate, all the oil is present in a continuous phase and increasing the oil concentration leads to the expected phase separation. Although simulations in rectangular boxes would make the visualization clearer, in the simulation at 40 wt% all the oil molecules are extended across the periodic boundary conditions in a continuous phase that is separated from the aqueous phase, with the surfactant molecules residing at the oil/water interface.

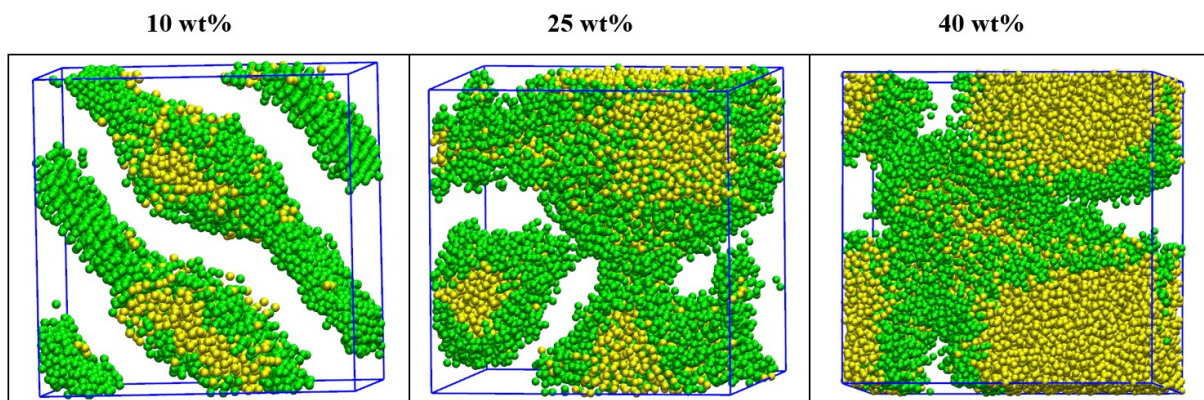


Figure 5.11. Final snapshots of the CG-MD simulations for $C_{10}E_4 + H_2O + n$ -dodecane mixtures at 313 K. Yellow represents the oil molecules, while green is used to represent the surfactant alkyl tails. Water and the polar section of the surfactants are removed for a clearer view of the system but occupy the rest of the simulation box.

This behaviour agrees with previous experimental observations and with results obtained using dissipative particle dynamics simulations, suggesting that oils with alkyl chains larger than those of the surfactant typically swells the hydrophobic region of the bilayers.[280,282] Additional simulations were carried out by replacing the *n*-dodecane by *n*-eicosane to analyse the effect of the oil's chain length but, as depicted in **Figure 5.12**, a similar qualitative behaviour was observed. Due to the increased M_w of the oil, the simulation at 25 wt% is already consistent with phase separation, with the oil molecules being in a continuous phase and, at 40 wt%, the phase separation is clearer, even using cubic simulation boxes. The earlier phase separation is, in this case, coherent with the fact that longer oils, having a larger volume contribute more to the total alkyl chain volume, encouraging the decrease of the surface curvatures and, if at sufficiently high concentrations, promoting phase separation.

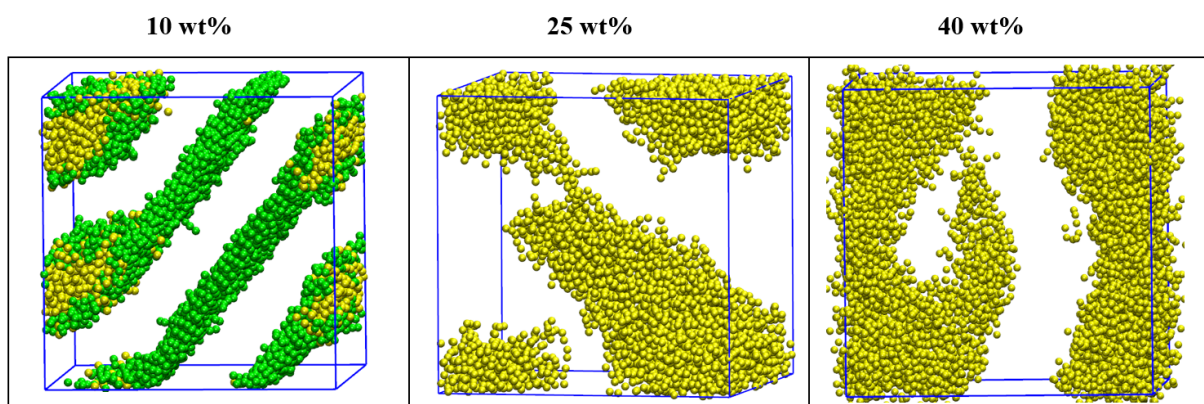


Figure 5.12. Final snapshots of the CG-MD simulations for $C_{10}E_4 + H_2O + n$ -eicosane mixtures. Colours as in **Figure 5.11**.

When replacing the $C_{10}E_4$ for the $C_{12}E_6$ surfactant, the layered-like structure of the L_α phase seems to be more stable upon the addition of oil, despite the increased HLB of this surfactant. The final snapshots of the CG-MD simulations for the $C_{12}E_6 + H_2O + n$ -dodecane mixtures are shown in **Figure 5.13** and show that only at 30 wt% the different layers start interacting with each other, leading to the formation of a bi-continuous phase that is also observed at 40 wt%. At lower oil concentrations (e.g., 10%) because the alkyl chain length of the oil is now equal to that of the surfactant tail, the oil can more easily penetrate between the alkyl chains of the surfactant, and the swelling is less intense, in agreement with what is observed experimentally.[280] Since these simulations started from the final configuration of the binary system $C_{12}E_6 + H_2O$ at 80 wt% surfactant, presented and discussed in **section 5.1**, the phase split is not observed, probably due to the very low amount of water present. It is thus reasonable to assume that the considerably high oil-to-water ratios makes the system more stable in a single bi-

continuous phase than in two phases. This agrees with the observations of Laughlin,[283] whose phase diagrams for the ternary systems usually contain a large single-phase region for water-lean mixtures.

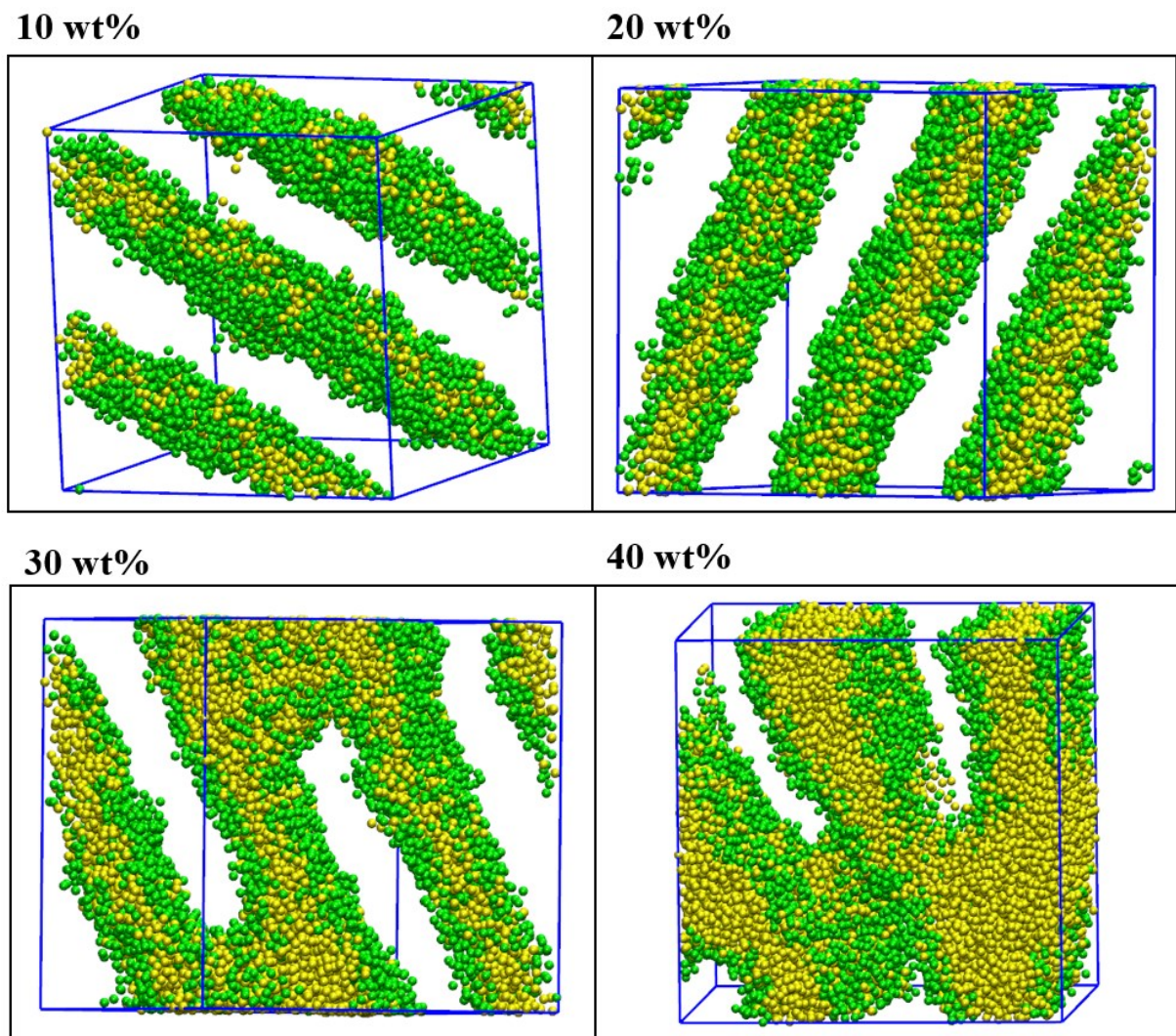


Figure 5.13. Final snapshots of the CG-MD simulations for $C_{12}E_6 + H_2O + n$ -dodecane mixtures at 313 K. The simulations start from an aqueous solution of $C_{12}E_6$ with 80 wt% of surfactant to which oil molecules were added until the total oil amounts to 10, 20, 30 and 40 wt% of the total system's weight. Colours as in **Figure 5.11**.

The Defected Lamellar Phase (L_{α}^H)

The aqueous solution of $C_{12}E_6$ at 70 wt% of surfactant consists of a L_{α}^H phase in which the hydrophobic layers contain water-filled defects. Starting from this configuration, different amounts of n -dodecane were added to the system to understand its impact on this characteristic C_iE_j phase. The results of those CG-MD simulations are shown in **Figure 5.14**. As it can be observed, when small quantities of

oil are added to the system (10 wt%), the oil molecules move towards the hydrophobic layers that self-organize and defects are no longer observed, exhibiting a L_α phase instead, the same being also observed for 20 wt% of oil. Although related to a different type of intermediate phase, Wang et al.[281] had previously reported that the addition of an oil to the mesh phase exhibited by $C_{16}E_6$ /water, in the concentration space between the H_1 and L_α phases, destabilized the intermediate phase in favour of L_α , thus a similar behaviour can be expected for a L_α^H observed in the same concentration regime.

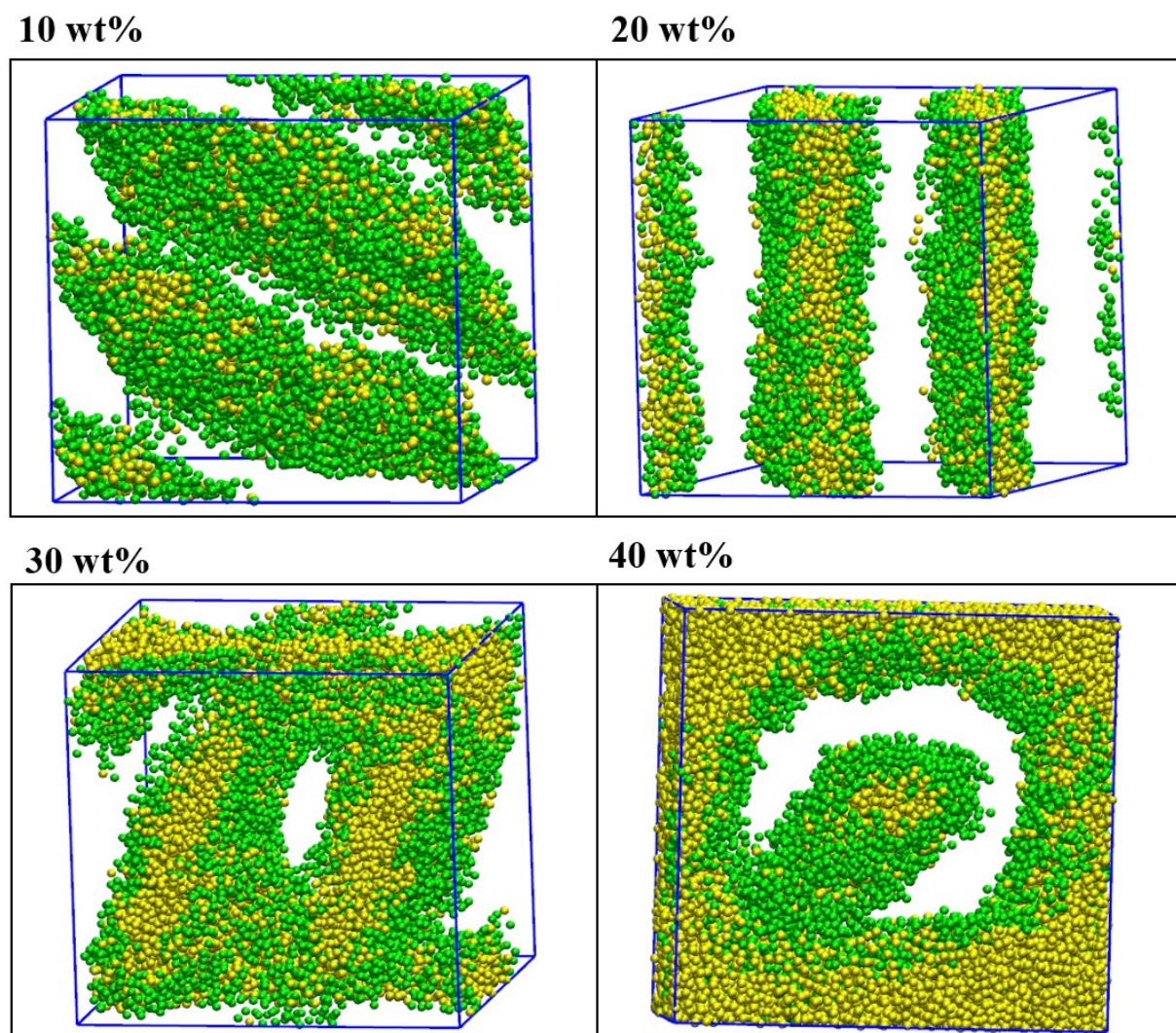


Figure 5.14. Final snapshots of the CG-MD simulations for $C_{12}E_6 + H_2O + n$ -dodecane mixtures at 313 K. The simulations start from an aqueous solution of $C_{12}E_6$ with 70 wt% of surfactant to which oil molecules were added until the oil amounts to 10, 30, and 40 wt% of the total system's weight. Colours as in **Figure 5.11**.

For higher amounts of oil (i.e., 30 wt%) a bi-continuous phase, similar to the one observed in **Figure 5.13**, is obtained. However, when the oil concentration is increased, a phase split is now expected to occur given the higher amount of water present in the system when compared with the one shown in **Figure 5.13**. Therefore, the simulation at 40 wt% shows how the oil is already in a continuous phase, except for one single aggregate that still resides within the aqueous phase. It is thus very likely that small temperature/concentration changes around this point may lead to a complete phase separation of the system.

The Hexagonal phase (H_1)

For the H_1 phase observed at 50 wt% $C_{12}E_6$ in water, an unexpected behaviour was noticed. As depicted in **Figure 5.15**, when a small amount of oil is added, the oil penetrates into the cylindrical rods, and the rods become distorted and start interacting with each other, leading to the disappearance of the H_1 phase. This is expected since experimental observations have previously suggested that the oil addition often results in a loss of phases with high mean surface curvature, favouring its conversion into phases characterized by a lower surface curvature such as bi-continuous and L_α or, in the case of large oil concentrations, a macroscopic phase split. However, at 20 wt%, upon the addition of oil, the cylinders become much thicker and distorted due to the incorporation of the oil molecules but became independent and organized in a hexagonal-like shape, although water is present in between the rods. A further increase on the amount of oil in the mixture and the systems starts a transition towards a phase split, as suggested by the snapshot of the simulation carried out at 30 wt% of oil that resembles the one observed at 40 wt% of oil shown in **Figure 5.14**. This makes it clear that as soon as the concentration of water in the mixture is increased, the amount of oil required for phase separation is decreased. This is expected since the region where the correspondent LC phase is observed in the surfactant + water binary system gets closer to interfere with the oil – water miscibility gap.

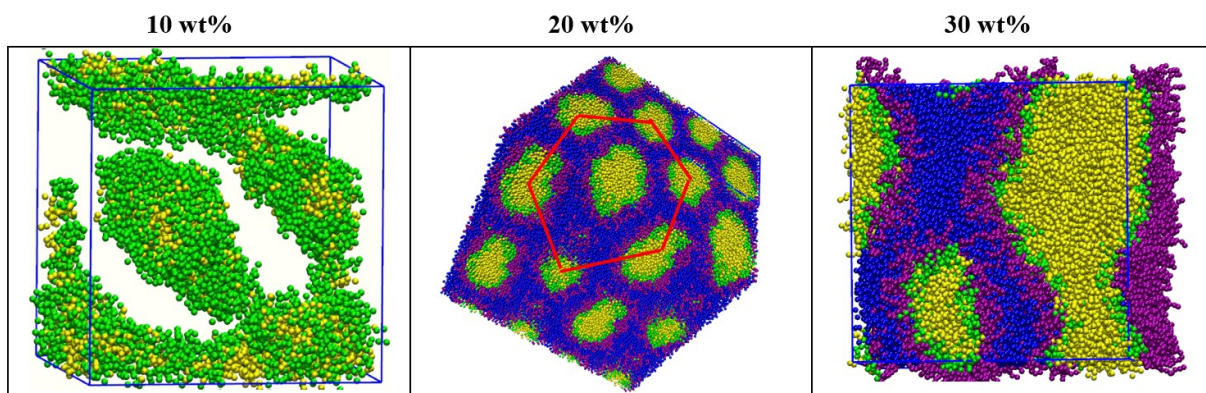


Figure 5.15. Final snapshots of the CG-MD simulations for $C_{12}E_6 + H_2O + n$ -dodecane mixtures at 313 K. The simulations start from an aqueous solution of $C_{12}E_6$ with 50 wt% of surfactant to which oil molecules were added until the oil amounts to 10, 20, and 30 wt% of the total system's weight. Yellow represents the oil molecules, green and purple are used to represent the surfactant hydrophobic and hydrophilic parts, respectively, and blue represents the water molecules.

The Micellar phase (L_1)

In EOR applications, the injection fluid usually contains a diluted aqueous solution of a given surfactant that is mixed with co-surfactants and other components before being introduced into the reservoir for the recovery of additional oil. Since the concentration of the surfactant solution is usually above the *cmc*, the system may consist of a micellar solution, typically containing individual nearly spherical micelles. Therefore, being able to capture the effect of an oil in the phase behaviour of the injection fluid, through non-invasive and cheap computational tools, is important for a better understanding of the underlying mechanism of oil recovery and, consequently, for the more efficient design of new surfactant-based injection fluids.

Starting from the binary system $C_{12}E_6 + H_2O$ at 15 wt% of surfactant concentration, discussed in the previous chapter, oil molecules were added to the system in different amounts, and CG-MD simulations were carried out to analyse the structural organization of the system. **Figure 5.16** shows the quick absorption of oil molecules into the spherical micelles, even when a small amount of oil (5 wt%) is added to the micellar solution. As can be observed, in an intermediate stage, the oil molecules start to form hydrophobic clusters before interacting with the micelles and moving towards their centre. Furthermore, as depicted in **Figure 5.17**, when more oil is added, a considerable micellar growth is observed. While the binary $C_{12}E_6 + H_2O$ mixture contained 10 micelles, the systems with 10 and 15 wt% of oil contain only 3 and 2 micelles in equilibrium, respectively. Surprisingly, despite the considerable micellar growth, the micelles retained their spherical shape, but it is likely for the micellar growth to lead

to phase separation after the merge of these two micelles upon further addition of oil or upon a temperature change.

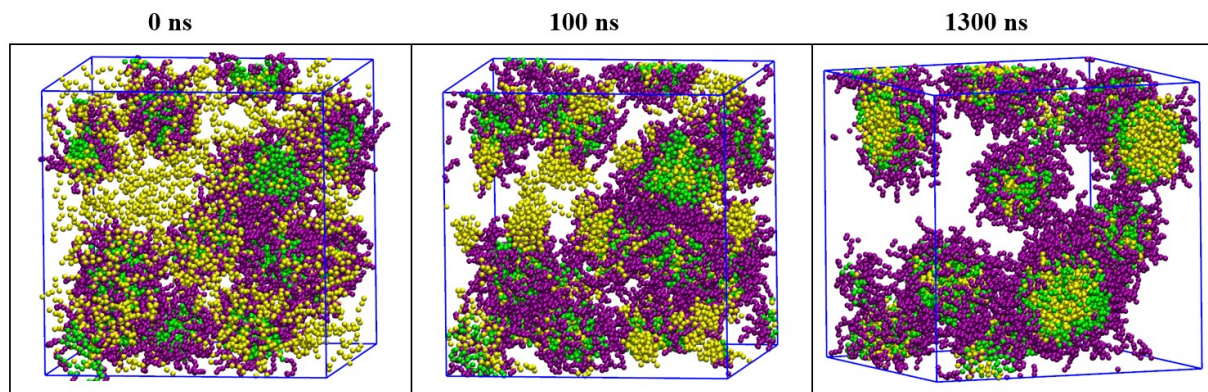


Figure 5.16. CG-MD simulations for $C_{12}E_6 + H_2O + n$ -dodecane. Oil molecules amounting to a total of 5 wt% were added to an aqueous solution of $C_{12}E_6$ at 15 wt%. Colours as in **Figure 5.15**.

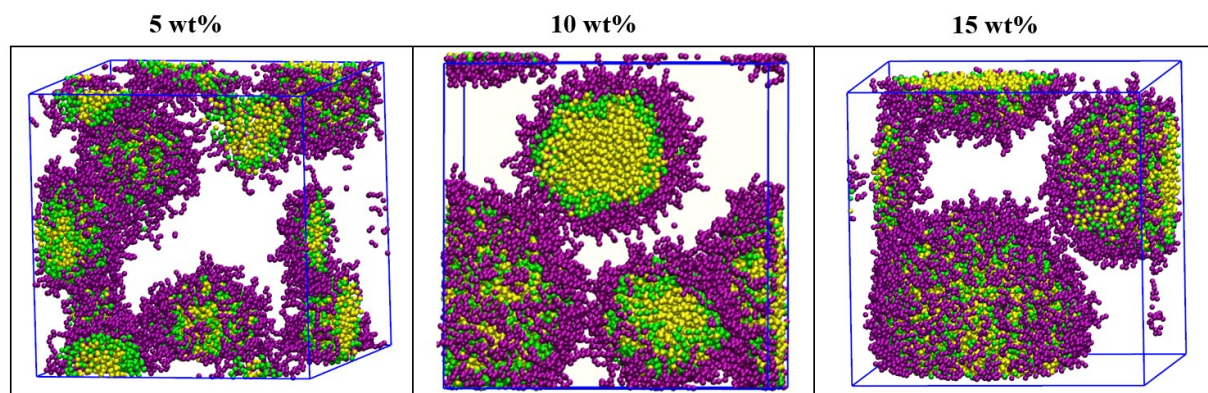


Figure 5.17. Micellar growth in $C_{12}E_6 + H_2O + n$ -dodecane mixtures as the amount of oil in the mixture increases. Colours as in **Figure 5.15**.

Conclusions

In this section, CG-MD simulations were carried out to obtain physical insights on the effect of adding oil to the mesophase behaviour of aqueous solutions of C_iE_j surfactants. Overall, in the case of LC phases like L_α , L_α^H and H_1 , when a small amount of oil is added, the oil molecules are quickly incorporated within the hydrophobic layers or the cylindrical rods making up those phases (note that in the case of a L_α^H phase, the defects in the bilayers become immediately absent upon a small addition of oil). For intermediate oil concentrations, and since the water content is usually low when these LC phases are present, the system may remain stable in a single bi-continuous phase, unless sufficiently high amounts of oil are added to induce phase separation. In summary, the addition of oil to an aqueous surfactant results in a decreased stability of phases with high mean surface curvature, favouring its conversion to phases with lower curvature such as bi-continuous and L_α that also become destabilized as soon as the amount of oil is further increased, leading to a macroscopic phase separation.

For the micellar region, when oil molecules are added, they initially form some hydrophobic clusters that then start interacting and penetrating the micelles. If the amount of oil is increased, a clear micellar growth is observed until the system separates into an oil-rich and a water-rich phases.

5.3- Perspectives on the use of CG-MD simulations for EOR applications

Introduction

Numerous experimental studies have dealt with different aspects of oil recovery upon surfactant flooding, such as phase behaviour,[284] oil/water IFT,[285] substrate wettability,[286] or foaming ability.[287] These studies demonstrate the role of surfactants in decreasing the oil – water IFT, in modifying the wetting behaviour of the rock surface, or in being able to disturb oil layers that are adsorbed at a given substrate facilitating the oil detachment from the rock.[288] Even though these studies have undoubtedly contributed to a better understanding of the macroscopic dynamics of surfactant flooding EOR processes, the wide variability in terms of reservoir rocks and crude oils poses a striking challenge for the understanding of the molecular mechanism of oil detachment under a given set of conditions. This urges the development of computational tools that can be used for screening purposes and to predict the behaviour of a given injection fluid in a specific reservoir, while probing the microscopic details of the underlying process.

Atomistic MD simulations have been successfully applied to describe the molecular scale properties of different oil/water and oil/water/surfactant interfaces, and to propose mechanisms for the oil detachment process from different surfaces.[288–292] Although these studies allowed researchers to obtain a molecular-level picture of the oil detachment process as a function of different effects such as the type and structure of the surfactant or the substrate polarity, the time and size scales attainable through AA-MD simulations prevent the study of sufficiently large systems during the whole duration of the process. Thus, AA models are computationally expensive and too slow to be efficiently used for screening purposes, or for the predictive design and evaluation of new injection fluids for a given reservoir operation. For these reasons, being able to quickly simulate the oil detachment process under different conditions without extensive parameterizations and following a straightforward procedure would be useful. The MARTINI FF offers a valuable perspective due to its transferable character, standing as an attractive alternative. Having successfully demonstrated the ability of the MARTINI FF for predicting the phase behaviour of C_iE_j + water and C_iE_j + water + oil systems in the previous sections of this chapter, a few perspectives on the use of the MARTINI FF to model the oil detachment process are here attempted. First, the MARTINI 2.0 FF,[52] used in the previous sections, was applied to model the oil detachment from a silica surface using an aqueous solution of $C_{12}E_6$. Unfortunately, the CG-MD simulations revealed an unrealistic freezing of water near the silica surface once the oil starts to form a spherical aggregate. This issue is shown to be related to deficiencies in the MARTINI water model in this version of the FF, essentially when in the presence of a surface, and not to problems in the surfactant,

oil, or surface models. Then, preliminary tests using the MARTINI 3.0 FF, recently published by Marrink and co-workers[293], showed that the improved and increased number of bead types and the availability of more CG mapping options, as well as the enhanced energy transfer between water molecules allowed to overcome this issue, enabling to explore the oil detachment process through CG-MD simulations. The preliminary results presented here suggest that once the surfactant and surface models have been adequately converted to the updated version of the FF, the MARTINI model can indeed become a very useful tool for the design and simulation of surfactant flooding processes, allowing the quick and inexpensive evaluation of different injection fluids.

Methodology

For the CG-MD simulations using the MARTINI 2.0 FF, the surfactant, water, and oil molecules were modelled using the mappings discussed in the previous sections. To model the silica substrate, a planar silica surface is considered following the guidelines presented in the work of Perrin et al.[294], where the MARTINI FF was used to investigate the structure and dynamics of polymers near a silica surface. Accordingly, each silanol group is mapped into one CG bead, namely a nonpolar bead with hydrogen-bond donor capabilities, i.e., the N_d bead type of the MARTINI framework. Perrin and co-workers[294] showed that a flat surface can be designed in order to reproduce the averaged silanol density of amorphous silica surfaces and that one single layer can be used, as additional layers do not change the surface properties. Therefore, a one-layer flat and rigid surface of silica was built using the atomistic structure encompassing three silica atoms to construct the CG model following the 3:1 mapping recommended in the MARTINI FF to model ring structures. The GROMACS tools *gmx genconf* and *gmx x2top* were used to generate the CG silica sheet from the CG unit and the topology inputs, respectively.

The CG-MD simulations are all carried out in the *NVT* ensemble to allow for the use of a rectangular box with a sufficiently large z coordinate (normal to the silica surface) to emulate a silica – water – vapor interface. Thus, a silica sheet of 168 x 225 Å was used to setup the simulation box where the water, surfactant or oil can be added accordingly. The dodecane was selected to model the oil following a 4:1 mapping and using three ‘C1’ beads from MARTINI.[52] The $C_{12}E_6$ was selected as the surfactant moiety since exhibits the archetypical surfactant phase behaviour. The standard ‘P4’ bead type water model was selected including 10% of water antifreeze ‘BP4’ beads.

Results

Tang et al.[288] have recently used AA-MD simulations to investigate the detachment process of an oil layer from an hydroxylated silica surface (with different polarities) using aqueous solutions of three different surfactants, including the non-ionic surfactant octylphenol polyoxyethylene (10) ether, being a good atomistic reference to evaluate the qualitative behaviour of the MARTINI FF in describing the same type of process. In a first step, Tang et al.[288] have randomly placed 130 *n*-dodecane molecules on the silica surface and carried out a 10 ns simulation to obtain the equilibrium adsorption configuration of the oil. Here, to validate the designed silica sheet surface, initially mapped with ‘N_d’ beads and their interactions with the oil, 1664 molecules of *n*-dodecane were randomly placed in a simulation box containing the silica surface fixed at the bottom ($z=0$) and the system was simulated for 500 ns. Starting from a random configuration, the oil molecules were found to quickly migrate towards the surface, and to organize themselves into three *n*-dodecane molecular layers parallel to the surface, in good agreement with the AA observations.[288] The density profile of the oil molecules was further determined from the CG-MD trajectory and is shown in **Figure 5.18**, along with the final snapshot of the simulation, which is presented as an inset in **Figure 5.18**. Although the location and intensity of the different peaks is different (slightly shifted towards longer distances in the CG model) than those determined by Tang et al.,[288] it could be mainly caused by the inherent oversize estimation of CG models. However, the *n*-dodecane density profile shows a reasonable qualitative agreement between them, with three clear peaks similarly distanced from each other. The first CG peak, denoting the formation of the first adsorbed layer, is very well organized across the entire surface, while the second and third peak show decreased intensities, suggesting a higher disorganization and a larger number of ‘vacancies’ in these layers.

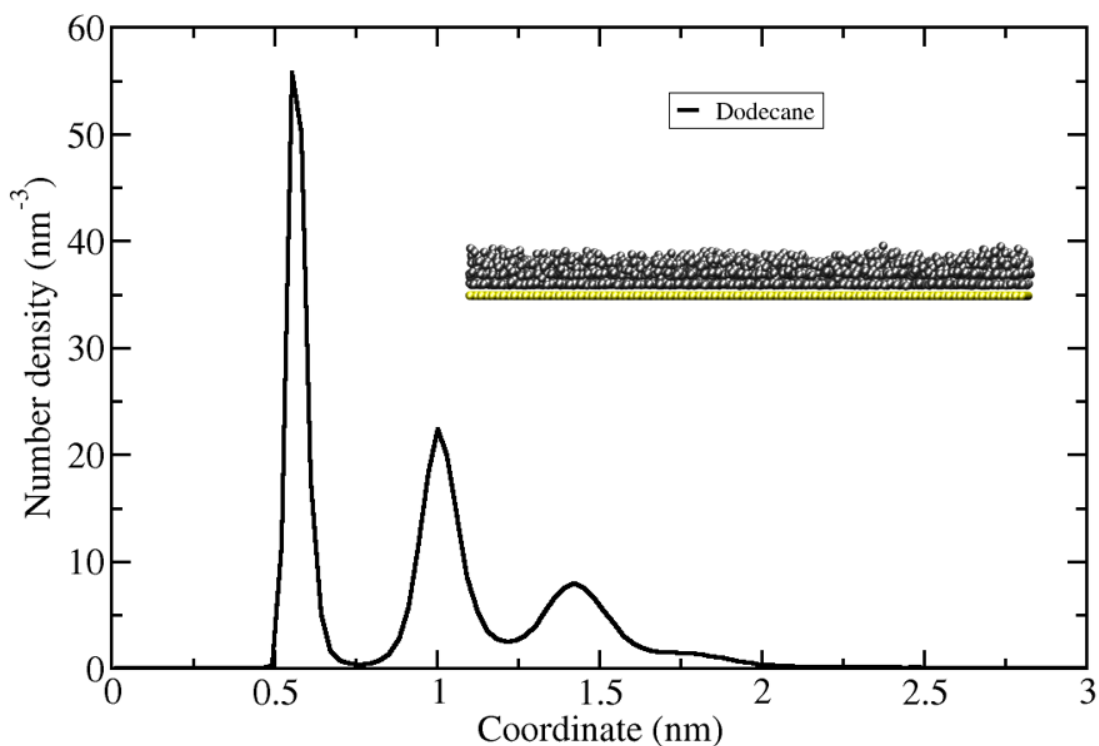


Figure 5.18. Number density of *n*-dodecane molecules as a function of the *z*-coordinate of the simulation box. The final snapshot of the CG-MD simulation of 1664 *n*-dodecane (represented in grey) near a silica surface (yellow colour) is shown as an inset.

The silica – dodecane system was used to evaluate the impact of a water column above the dodecane layer, by adding 100000 water molecules to the system. The snapshots of the simulation after 100 and 1000 ns are shown in **Figure 5.19**. Tang et al.[288] also carried AA-MD simulations in the absence of surfactant and concluded that even though the oil molecules in the top layer had been disturbed, the water molecules could not create a water channel to penetrate the oil layer, being unable to detach the oil from the silica surface. However, a distinct behaviour was observed for the CG counterpart, since although the *n*-dodecane remained attached to the silica surface for a relatively long time, after 400 ns of simulation, water molecules started to freeze despite the use of antifreeze beads and were able to penetrate the oil layer and to interact with the silica surface, as shown in **Figure 5.19**. Afterwards, due to the favourable interactions established between the surface and water, the water spreads across the surface promoting the detachment of the oil that self-assembled forming a spherical aggregate that then floated towards the top.

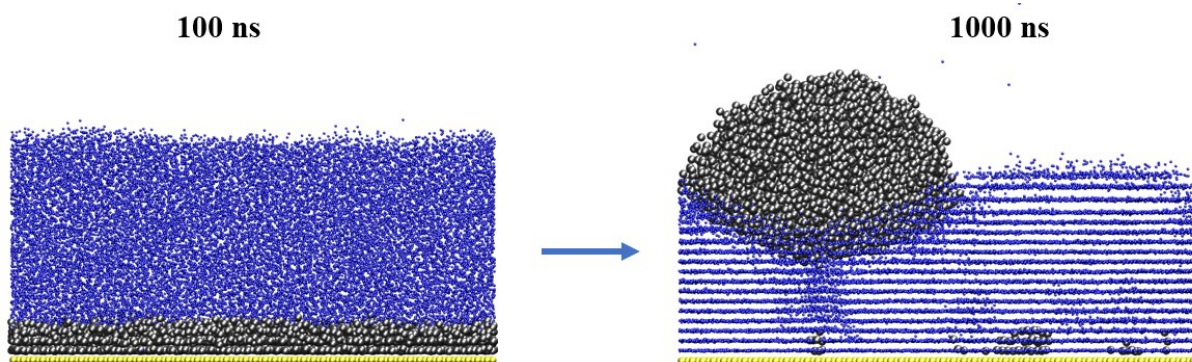


Figure 5.19. CG-MD simulation snapshots after 100 and 1000 ns of a system containing a silica surface (yellow), 1664 n-dodecane molecules (grey), and 100000 water molecules (blue).

It must be pointed out that the AA-MD simulation of Tang et al.[288] was only run for 4 ns and here the adsorbed oil was also shown to remain stable up to 400 ns, but it is arguable whether water alone can promote the oil detachment from the silica surface, even after long simulation times. An additional CG-MD simulation was carried out for a system containing four times more water to investigate whether the problem was related to the system's size. This simulation was run for 1 ns and the final snapshot is shown in **Figure E.1.**, in **Appendix E**, depicting a similar pattern, although it shows that the freezing of the water occurs only in the region closer to the silica surface and not near the liquid-vapor interface. A similar trend was also observed in the presence of surfactant, as depicted in **Figure E.2.**, although the oil was displaced much quicker. Ultimately, aiming at observing if water also freezes in the absence of both oil and surfactant, CG-MD simulations were carried out for water in contact with both the silica flat surface and a graphene sheet and the results are depicted in **Figure E.3**. As can be observed several layers of water molecules are clearly observed in both systems, although the water freezing is much more intense in the silica surface due to the much more attractive silica – water interactions, when compared with the graphene – water ones. This unrealistic behaviour of water is thought to be related to the weak energy landscape of standard water MARTINI model and other authors have also reported issues in describing the interactions between water and different surfaces, suggesting the inadequacy of the water model to describe solid-liquid properties.[294,295]

Very recently, Marrink and co-workers[293] updated the MARTINI FF to its 3.0 version, which contains an increased number of bead types, improved interaction levels and modifiers (also known as labels) to take into account some atomistic details such as the orientation of hydrogen bonds, partial charges, additional cross-interaction sigma values, self-interaction modifiers, and an improved water model, significantly expanding the capabilities of the FF. The new framework allows now much more options to address small compounds or discern monovalent ions, and the new parameterization did not

exclusively include biomolecules and other biologically relevant systems. MARTINI FF 3.0 also includes three new options to model water molecules, namely ‘W’, ‘SW’, and ‘TW’ beads which encompass 4, 3 or 2 water molecules, respectively. These new water models are expected to overcome some of the limitations of the water model used in the previous version (which usually required the addition of anti-freezing particles), being closer to the atomistic description, improving the energy transfer between water molecules, a well-known limitation of the previous version.

Therefore, to overcome the unrealistic behaviour of water near a flat surface observed in MARTINI 2, a set of CG-MD simulations were carried out using the new MARTINI 3.0 FF to reproduce the oil detachment process from a silica surface, avoiding the unrealistic water freezing issues. A special care must be taken when extending the surfactant, oil, and surface MARTINI 2 models to the new 3.0 one. The ‘TW’ water model was selected since its near atomistic resolution could better capture the energy transfer landscape of water, while for this preliminary study, the previous MARTINI 2 models are extended to the new MARTINI 3.0 by attempting similar interaction levels and a comparison with previous results, as follow:

- For the surfactant, the C₁₂E₆ 15 wt% aqueous solution was selected. This system exhibited a micellar distribution with a N_{agg} of 90, as described in **Chapter 5.1** and the new MARTINI 3.0 should capture this behaviour. Thus, after a careful bead type screening for the interaction energies, the best results were found when the alkyl tail is mapped using four ‘SC1h’ beads, ‘SN3q’ beads to represent the EO groups, and finally the SP6 bead for the surfactant head. Thereby, the C₁₂E₆ 15 wt% aqueous solution under the new mapping reproduced the micelle size and shape, exhibiting a $N_{agg} \sim 100$.
- The *n*-dodecane MARTINI 3.0 was used which is mapped with three ‘C1’ beads, as in the previous version of the FF.
- For the silica surface, the previous ‘Nd’ bead is replaced by the ‘SN1dq’ in the MARTINI 3.0 version.

The selected ‘TW’ water model should reproduce the experimental density of water. For this purpose, a simulation box containing 70862 TW particles was equilibrated and used to determine an averaged density of $0.9974 \pm 0.007 \text{ g}\cdot\text{cm}^{-3}$. Then, a CG-MD simulation containing the silica sheet and 1664 *n*-dodecane molecules was carried out and the dodecane density profile is shown in **Figure E.4.**, in **Appendix E**, and found to reproduce the results obtained with the MARTINI 2 shown in **Figure 5.18**, thus being in reasonable agreement with the AA-MD simulations of Tang and co-workers.[288] Afterwards, a water layer containing 165000 ‘TW’ beads was added to this system to evaluate whether

the dodecane layer is stable in the absence of surfactant. The system was run for 1000 ns after which the dodecane layer was completely stable as expected and, more importantly, the water molecules were not frozen conversely to what was observed using the previous version of the FF. The final snapshot of this simulation is shown in **Figure 5.20**.

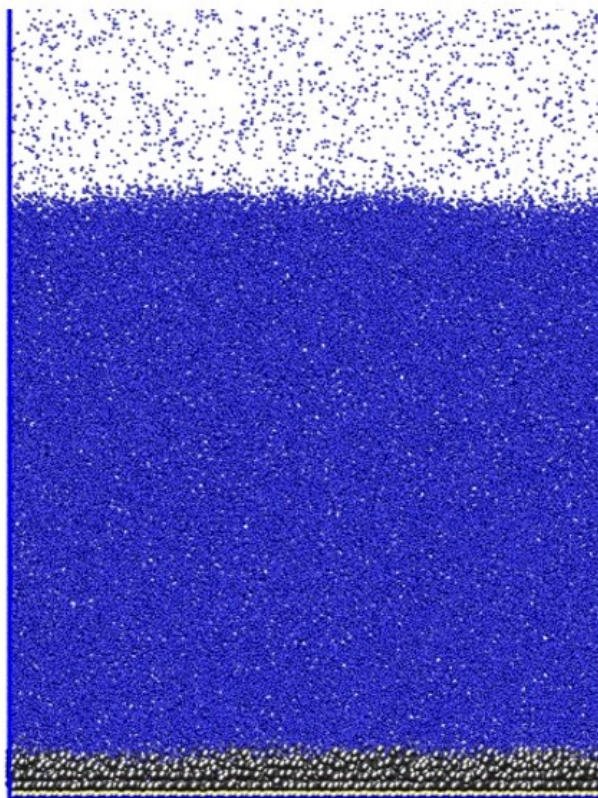


Figure 5.20. Final snapshot of the CG-MD simulation carried out for the system silica + *n*-dodecane + water using the MARTINI 3.0 FF. Yellow represents the silica surface, grey and blue represents the oil and water molecules, respectively.

Bearing in mind these encouraging results, $C_{12}E_6$ molecules were added to the silica-dodecane-water system to evaluate the effect of the surfactant in detaching the oil from the silica surface. Two different systems containing 500 and 1664 surfactant molecules were added near the oil/water interface. Remarkably, as shown in the simulation snapshots from **Figure 5.21**, the surfactant was able to induce the removal of oil from the silica surface in both systems. For the system with 500 surfactant molecules, the oil starts to aggregate after 40 ns, while in the system with 1664 surfactant molecules the oil aggregation starts right after the first 4 ns of simulation showing the dramatic role played by the surfactant in detaching the oil from the surface. Again, no unrealistic freezing of the water was observed, contrarily to the previous attempt using MARTINI 2 (**Figure E.2**.) Unfortunately, the interactions

between some of the particles still need to be optimized, as the surfactant + oil aggregate remained adsorbed at the silica surface.

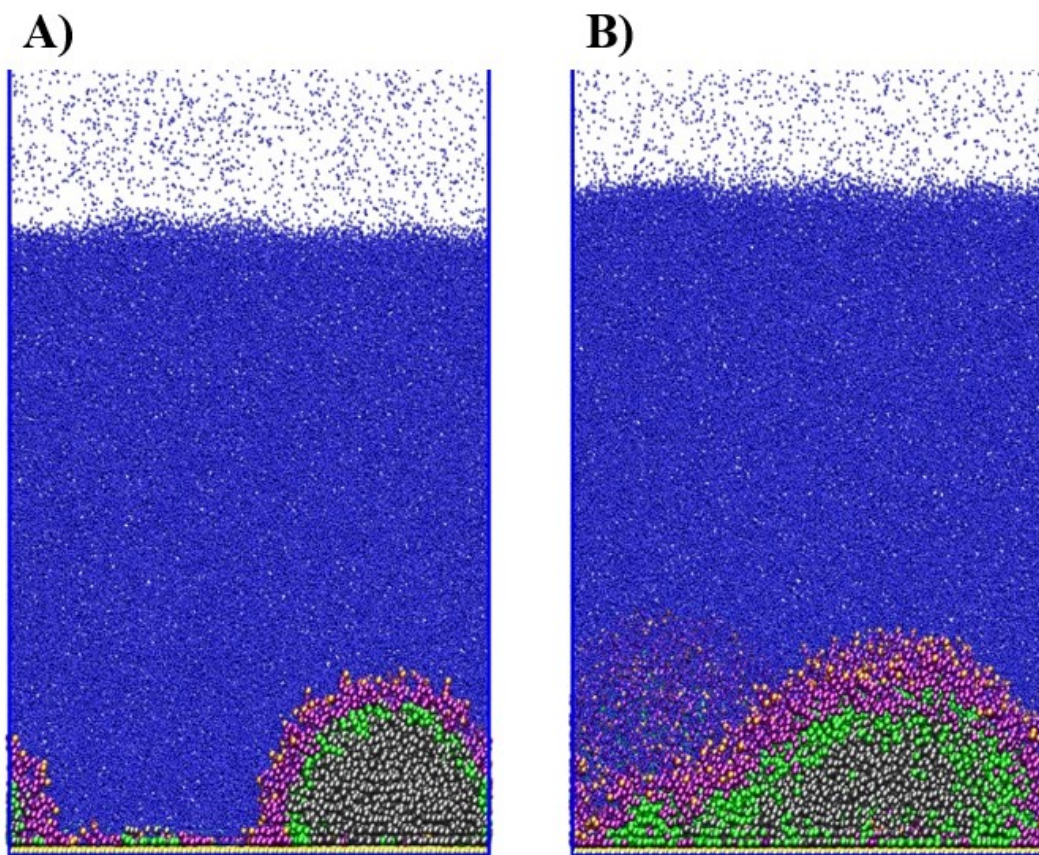


Figure 5.21. Final snapshots of the CG-MD simulations (1 ns of simulation time) of silica + *n*-dodecane + water + $C_{12}E_6$ systems using the MARTINI 3.0 FF. Yellow represents the silica surface, grey represents the *n*-dodecane, green, purple, and orange represent the alkyl tails, EO groups and alcohol group of the surfactants, and blue represents the water molecules. A) 500 molecules of $C_{12}E_6$ B) 1664 molecules of $C_{12}E_6$.

Preliminary tests showed that the main issue is related to the interactions between the ‘TW-SN1dq’ particles, whose default energy (2.0 kJ/mol) is too weak to properly describe the magnitude of the interactions between the silica surface and water. Therefore, we carried an additional simulation containing 165000 TW particles, 1664 oil molecules and 100 surfactant molecules, using an increased value of ϵ between ‘TW’ and the ‘SN1dq’ particles (3.0 kJ/mol). This simulation was run for 300 ns and the final snapshot is shown in **Figure 5.22**. As can be observed, after this correction, the surfactant + oil aggregate that is formed is easily detached from the surface in less than 20 ns of simulation and remains buoying within the aqueous phase. These encouraging results suggest that after a thorough parameterization / conversion of the surfactant model (from MARTINI 2 to MARTINI 3), and an

adequate description of the water – surface behavior, the study of the oil detachment process from a given surface, using a mesoscale CG model will indeed be possible.

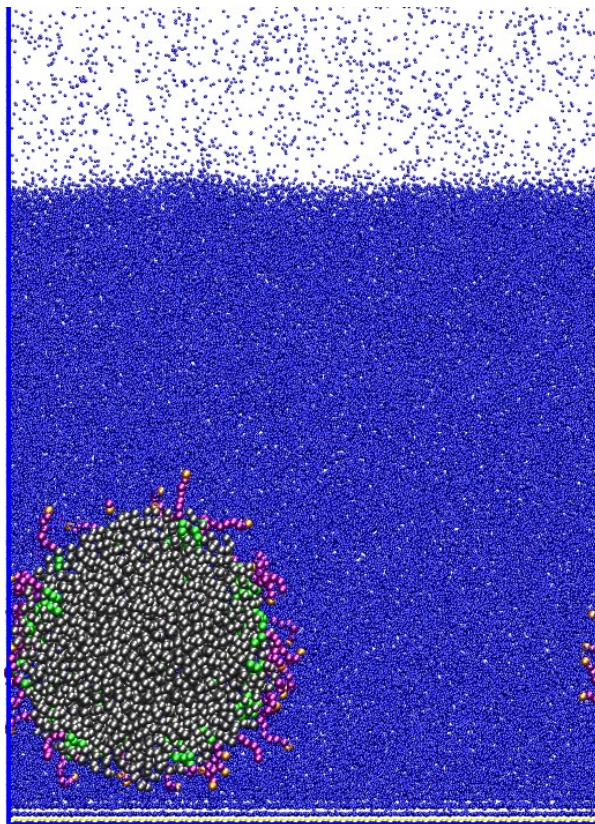


Figure 5.22. Final snapshot of the CG-MD simulations (300 ns of simulation time) of silica + n-dodecane + water + $C_{12}E_6$ systems using the MARTINI 3.0 FF, using an increased energy value for the ‘SN1dq’ – ‘TW’ interactions. Colours as in **Figure 5.21**.

Conclusions

In this section, the MARTINI FF was used as an attempt to simulate the oil detachment process from a silica surface. Using the MARTINI 2 FF used in the previous sections, the surfactant was shown to induce the removal of oil from the silica surface, but an unrealistic freezing of the water molecules was observed. This behaviour was also observed in the absence of surfactant and oil and is related to the inability of the MARTINI 2 FF to correctly describe the behaviour of water near a flat rigid surface, as had previously been reported by other authors.

Afterwards, a preliminary study on the ability of the recently published MARTINI 3.0 FF to overcome this limitation was carried out. This updated version of the FF contains an increased number of bead types and interaction levels, as well as more realistic water models. The increased complexity of the new FF requires a thorough conversion of the models that were previously developed and validated for the previous version such as the surfactant model, before it is suitable for use with the updated version of the FF. The results obtained with the new version show a good description of the silica + oil system that agrees with AA-MD simulations available in the literature. It is also shown that in the absence of surfactant, water alone cannot detach the oil from the silica surface, also in agreement with atomistic models. Furthermore, contrarily to the simulations carried out using the MARTINI 2 FF, the water molecules no longer froze near the silica surface demonstrating the reliability of the improved water models in the updated version. In a next step, surfactant molecules were added to the system and shown to induce the quick detachment of oil from the surface that forms an aggregate with the surfactant in the outer part in contact with water. However, the surfactant + oil aggregate was found to remain adsorbed at the silica surface. Additional tests suggested that the silica – water interactions could not be directly described using the default ‘SN1dq’ – ‘TW’ energy level from MARTINI 3. Therefore, by refining the magnitude of these interactions, the oil detachment process from the silica surface could be successfully captured by the model.

These preliminary results suggest that after a thorough parameterization/conversion and validation of the surfactant model developed in **Chapter 5.1** to the updated version of the MARTINI FF, and a refinement of the surface CG model to the new version of the FF, the study of the oil detachment process from a given surface using a highly transferable mesoscale CG model will be possible. This would enable the quick screening of different surfactants and different injection fluids (as co-surfactants can be easily added or mixtures of surfactants can be simulated), under different conditions or different surfaces that can represent a specific rock reservoir, expediting the initial stages of the design of new EOR operations.

6- A discussion on the thermodynamic modelling of alternative solvents

“Most innovation involves doing the things we do every day a little bit better rather than creating something completely new and different”

Darin @ The Business Warrior's Dojo

6.1- On the parameterization of SAFT models for Deep Eutectic Solvents

The content of this section is based on the following publications developed during the course of this PhD work, where E.A. Crespo was responsible for the modelling tasks and for writing the manuscripts, with substantial contributions from the remaining authors.

- Emanuel A. Crespo, João M. L. Costa, André M. Palma, Belinda Soares, M. Carmen Martín, José J. Segovia, Pedro J. Carvalho, and João A.P. Coutinho, “*Thermodynamic Characterization of Deep Eutectic Solvents at High Pressures*”, *Fluid Phase Equilibria*, 500 (2019), DOI: 10.1016/j.fluid.2019.112249
- Emanuel A. Crespo, Liliana P. Silva, Joel O. Lloret, Pedro J. Carvalho, Lourdes F. Vega, Fèlix Llovell, and João A.P. Coutinho, “*A Methodology to Parameterize SAFT-type EoSs for Solid Precursors of Deep Eutectic Solvents: The Example of Cholinium Chloride*”, *Physical Chemistry Chemical Physics*, 21 (2019), 15046-15061, DOI: 10.1039/C9CP02548K

Introduction

Over the last decades, due to issues such as global warming, the general rising of the sea level, or high indexes of atmospheric pollution, society seems to be more aware of the impact that most industrial and human activities have upon our planet’s resources and ecosystems. To stress the importance of finding novel approaches for an efficient and sustainable environmental management, the Organization of the United Nations outlined in 2015 a sustainability-oriented development plan entitled “Transforming Our World: the 2030 Agenda for Sustainable Development”. It was composed of several goals and tasks tackling a wide range of issues, in which green and sustainable chemistry is expected to play a vital role.[296] Accordingly, chemists and chemical engineers are now focusing on the development of alternative greener and more sustainable processes that can be further implemented in large-scale industries. In most chemical processes, the choice of the right solvent is crucial, as they can make up to 80% of the total volume of chemicals used and present numerous environmental, health, and waste management issues, while also being responsible for a large share of the overall energy consumption and GHG emissions of a process.[297,298] Thus, many researchers have focused on the design, characterization, and application of alternative solvents in a given process such as the use of water, supercritical fluids (e.g., CO₂), ILs, and DESs.

Firstly reported by Abbott and co-workers in 2003,[24] DES are a new class of green solvents that consist on eutectic mixtures of two or more compounds that due to strong and highly complex hydrogen-bond interactions between a hydrogen bond donor (HBD) and an hydrogen bond acceptor (HBA) exhibit

a considerable freezing temperature depression, resulting in an eutectic temperature lower than that expected for an ideal liquid phase, allowing the formation of stable liquids at relatively low temperatures with interesting solvent properties. The most common DES precursors are quaternary ammonium salts as HBAs, cholinium chloride ([Ch]Cl) being the most common due to its low cost and biodegradability, combined with different HBDs such as carboxylic acids, glycols, sugars, urea and its derivatives, aminoacids, amines, amides, alcohols and polyols, among others.

One of the most attractive properties of these systems is their ‘designer solvent’ character, as their thermophysical properties can be tailored aiming at a specific application through a proper selection of precursors and their ratio. Moreover, their ease of preparation, operation under mild conditions, inexpensive and readily available precursors, and water compatibility are often acknowledged, and contributed to the boom of DESs within industry and academia over the last decade, with a wide range of applications being reported for DESs.[299,300] Of special relevance to the Oil & Gas industry, their potential for gas separations including CO₂ capture,[26–29] enhanced oil recovery,[30,31] dearomatization, denitrogenation, and desulfurization of fuels,[27,32–35] mercury removal from petroleum,[36] and hydrate formation inhibition[37,38] has been thoroughly investigated. Surprisingly, despite the wide range of applications being reported for DESs across different industrial segments, studies on the thermodynamic modelling of DES by suitable EoSs are still scarce. This is not only due to the limited reliable experimental data available, but also due to the complexity of the hydrogen bonding network thought to be established in DESs that is still far from being fully understood,[301] and consequently are not well described by current models.

Only recently, SAFT-based models, able to explicitly account for the association phenomena have been proposed to address the modelling of DES.[302–312] However, most of those works[303–307,311] report the use of a pseudo-pure component approach to model DES, which is a crude simplification that should be avoided, as DES are mixtures of two or more individual components, significantly different from each other. This approach has several limitations, the most obvious being its inability to describe the solid-liquid phase behaviour of DES, which is of utmost importance for a better understanding of DES nature. Moreover, when using a pseudo-pure component approach, a set of molecular parameters needs to be fitted individually to each HBD to HBA ratio, i.e., the model becomes compositional dependent. Consequently, if binary interaction parameters with other species (e.g., CO₂ or H₂O) happen to be required, they also become dependent on the HBD/HBA ratio considered.

This approach has been used mainly because of the HBA’s nature that typically consist on salts with considerably high melting temperatures (e.g., [Ch]Cl has an estimated melting temperature of 597

K).[313] Thus, vapor pressures and liquid densities of the pure salts are not available and the traditional parameterization method of SAFT-type EoSs cannot be applied.

Other authors have used a more realistic individual-component approach to model DES, with the parameters describing the HBA being regressed using experimental data from diluted aqueous solutions, in which the interactions governing the system are likely to be much different than those observed in a DES. Zubeir et al.[303] applied such an approach to derive a CG model of [Ch]Cl, in the framework of PC-SAFT.[63] However, although five molecular parameters for [Ch]Cl and a temperature-dependent binary parameter with water were fitted simultaneously to the densities and osmotic coefficients at different molalities, significant deviations from the experimental data were still observed.

Llovel and co-workers[311,312] explored two different approaches to model DES within the soft-SAFT framework: treating the DES as a pseudo-pure compound, and a second approach describing the DES as a mixture of two independent constituents. In the first case, the authors fixed four molecular parameters and left only the chain length parameter, m , of the DES to become composition dependent to account for the different possible ratios, finding a linear relation with the average molecular weight of the eutectic mixture. In the second case, a molecular model for each salt 'X' and for the other precursor 'Y' is required. Taking into account that a robust molecular model and parameters are usually available for component 'Y', the molecular parameters for the salt 'X' were obtained from density data,[61] for a binary mixture 'X' + 'Y', at different X/Y ratios. Even though an accurate description of the density data and good correlations for the CO₂ solubility could be obtained, the mixtures whose data was used in the model's parameterization were often very diluted in the target component 'X', and, in some cases, an indirect regression was required (c.f. Figure 2 of Lloret et al.[311]). Moreover, using only density data to regress the parameters may prevent the model from capturing most of the system physical features as density is mainly influenced by size-related parameters, and should always be complemented with phase equilibrium data, which are greatly influenced by energy-related parameters.

A further limitation of the individual-component approaches found in literature is the use of a 2B association scheme that, although commonly used to model ionic liquids and salts, may be too simplistic to capture the highly complex hydrogen-bonding character of [Ch]Cl (and other salts) in DES. This complex behaviour was indeed evidenced through molecular dynamics (MD) simulations and ab initio calculations performed on such systems.[314–316]

This work aims at discussing and overcoming these limitations. Firstly, PC-SAFT calculations using CG models available in the literature are carried out to demonstrate why the parameterization methodology of SAFT-type EoSs is relevant, especially when addressing complex fluids like DESs. Then, by proposing an alternative methodology for the systematic parameterization of solid DES

precursors, under an individual-component approach using SAFT-type EoSs. The approach here proposed is illustrated through the development of a CG model for [Ch]Cl, the most common HBA used in DES formulations, in the framework of the soft-SAFT EoS. The model performance is then evaluated for the description of different sets of experimental data corresponding to a variety of [Ch]Cl-based eutectic mixtures in a wide range of temperature, pressure, and compositional conditions.

Why the parameterization method matters?

It was already discussed in previous chapters that the robustness and accuracy of SAFT-type EoSs rely on the careful development of the CG models representing each compound present in the system, which should be able to capture most of the compound's physical features. This includes a proper fitting of the pure-component parameters, but also the assignment of an adequate association scheme. The former includes an adequate selection of the experimental data to use for the parameters optimization, but also the care that should be taken to select the most physically meaningful set of parameters, knowing that, in SAFT models, different sets of pure-component parameters can yield similar results for the pure component or for a particular system, but different behaviour in others.

To illustrate this, the PC-SAFT EoS is first applied in this work to describe ppT data for three archetypical DESs, namely [Ch]Cl with either EG, glycerol, or urea, using CG models available in literature, that were developed in the framework of distinct applications, not necessarily related to DESs. All these four components have been previously described using PC-SAFT. Zubeir et al.[303] proposed a CG model for [Ch]Cl using the 2B association scheme (one positive and one negative association sites) to describe the CO₂ solubilities in DES, while Held and co-workers[317,318] presented a model for glycerol and urea, also using the 2B scheme. For EG, several sets of molecular parameters are available in the literature such as those reported by Atilhan and Aparicio,[319] Reschke et al.,[320] and Liang et al.[321] As density is the property going to be described here, these three CG models for EG were evaluated through the prediction of the ppT data reported by Crespo et al.[119] These predictions are shown in **Figure F.1**, in **Appendix F**, and demonstrate that only the PC-SAFT parameters proposed by Atilhan and Aparicio[319] are able to correctly describe the effect of both T and p on the densities of EG, while the other two sets yield inaccurate results, even at atmospheric pressure.

The PC-SAFT pure-component parameters used in this work are thus summarized in **Table 6.1**.

Table 6.1. PC-SAFT parameters used in this work (2B Association Scheme).

Compound	M_w (g/mol)	m_i	σ_{ii} (Å)	ε_{ii}/k_B (K)	ε^{HB}/k_B (K)	κ^{HB} (Å ³)	Ref.
[Ch]Cl	139.62	13.02	2.368	228.07	8000	0.200	[303]
EG	62.07	2.4366	3.2328	344.06	2702.6	0.02216	[319]
Glycerol	92.09	2.007	3.815	430.82	4633.5	0.0019	[318]
Urea	60.06	4.244	2.446	368.23	3068.3	0.0010	[317]

Despite the non-ideality acknowledged to DESs, their excess molar volumes (V^E) are usually small (see later in **Chapter 6.2**) and, based on the additive character of density, when V^E are small, if a thermodynamic model accurately describes the density of all pure components present in a system, which is often the case as density is normally one of the properties used in the model parameterization, the density of the mixture is at least reasonably well described by the model without any binary interaction parameters. However, from the PC-SAFT CG models presented in **Table 6.1**, only the model for EG was regressed using pure-component density data. For the remaining compounds, experimental data from very diluted aqueous solutions (typically at molar fractions of the target compound lower than 0.3) were used in the parameterization procedure.

Considering that the thermodynamic modelling of aqueous systems is a challenging task to any thermodynamic model, and that the interactions present in water are expected to be much different than those observed in other media, the models developed based on diluted aqueous solutions data are unlikely to provide a satisfactory description of the physical features of the target compound, negatively affecting the description of mixtures other than their aqueous solutions. Accordingly, and as observed in **Figure 6.1. (right)**, PC-SAFT predictions exhibit considerable deviations from the experimental density data measured in this work, especially for the mixtures with glycerol and urea. These results highlight that alternative parameterization approaches are required for a proper modelling of DESs, as CG models of compounds that are solid at room temperature, built on top of aqueous solutions data are inappropriate to describe even the simplest thermophysical properties of this class of solvents.

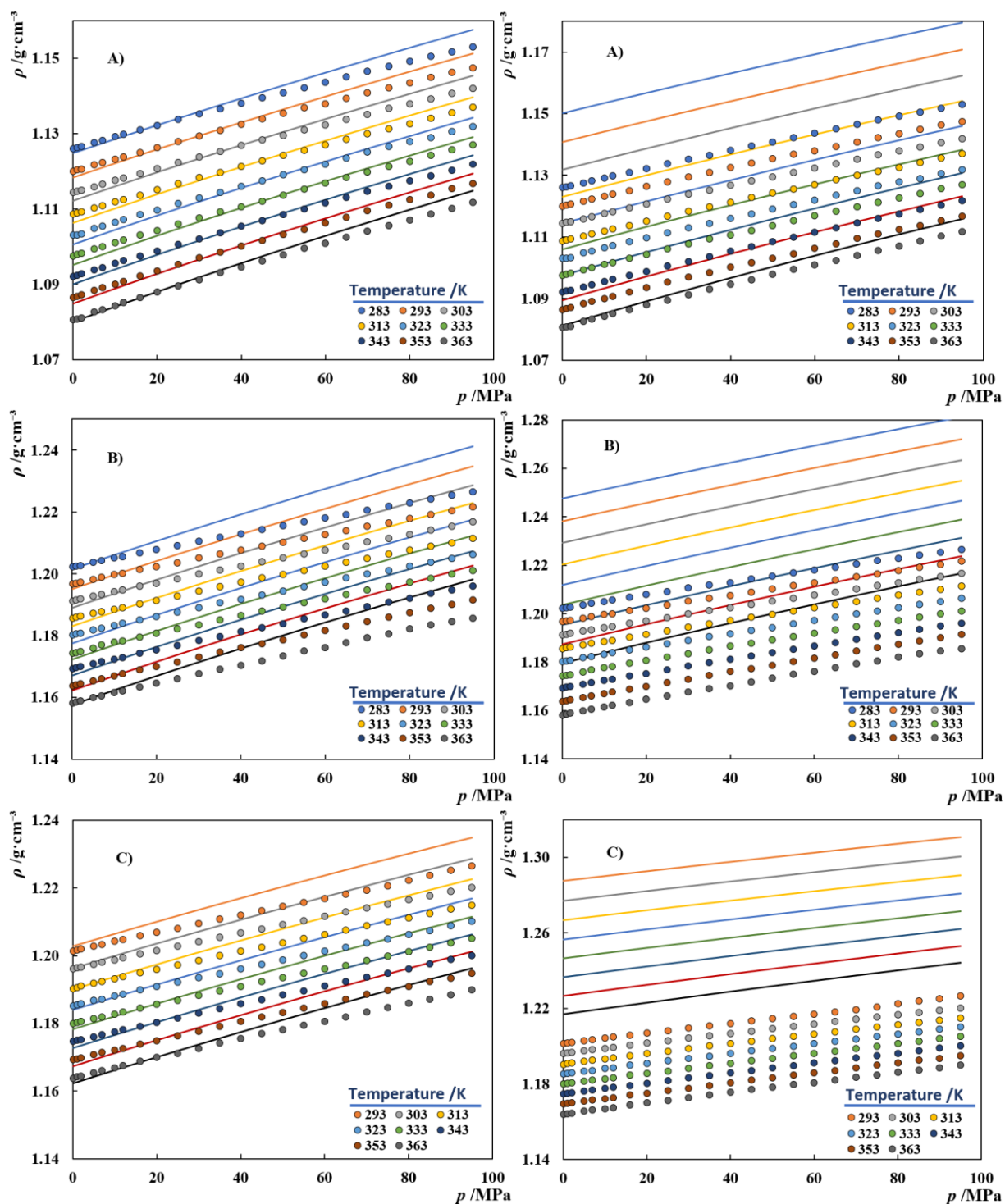


Figure 6.1. High-pressure densities of [Ch]Cl-based DESs with A) EG; B) glycerol; C) urea as HBD. Symbols represent experimental data,[322] while lines represent the PC-SAFT results with (left) and without (right) using a temperature-dependent binary interaction parameter fitted to the data.

To improve the agreement with the experimental data and try to correct the description of the temperature effect on density, a linear temperature-dependent binary interaction parameter, k_{ij} , correcting the mixtures dispersive energy was used. Although a constant binary parameter could have been preferred, it was insufficient to describe the temperature effect upon the DES densities. Hence, the final values of the binary parameters applied are summarized in **Table 6.2** while the results of such correlations are depicted in **Figure 6.1. (left)**. Using such parameters, a good description of the experimental data was obtained with an overall %ARD of only 0.270%, but there are still issues concerning the description of the pressure effect. Again, the best results were obtained for the mixture with EG since the densities of pure EG, including at high pressures, were considered in the parameterization of its model. The highest deviations were observed for the mixture with glycerol since, although both CG models of glycerol and urea were regressed from diluted aqueous solution data (including densities), higher deviations were reported for the description of the glycerol + water densities than for the aqueous solution of urea.[317,318]

Table 6.2. Binary interaction parameters used in the PC-SAFT correlations of the $p\rho T$ data of [Ch]Cl-based DES.

	$k_{ij} = a + bT/K$		
	a	b	%AARD
[Ch]Cl + EG (1:2)	0.6033	-0.001645	0.131
[Ch]Cl + Glycerol (1:2)	0.6862	-0.001599	0.415
[Ch]Cl + Urea (1:2)	0.9800	-0.002103	0.265
		Mean	0.270

Once the best possible description of the density data was achieved, it is interesting to analyse how problems in the density description propagate to the calculation of other thermophysical properties. Therefore, the Free Volume Theory (FVT), whose implementation is thoroughly described in **Appendix G**, was coupled with the PC-SAFT EoS for the correlation of the DESs viscosities. This is interesting because the FVT uses the density values retrieved from the EoS as one of their inputs.

To correlate the mixtures viscosity data, the FVT parameters (α , B , and L_v) of each pure component are required, these being typically regressed from pure fluid viscosity data. Sagdeev et al.[323] measured the viscosities of pure EG in the (0.098 – 245.2) MPa pressure and (312.5 – 464.4) K temperature ranges, while viscosity data for pure glycerol at atmospheric pressure can be retrieved from the DIPPR database.[118] Both sets of experimental data at atmospheric pressure were used to obtain the FVT parameters for EG and glycerol listed in **Table 6.3**, with the results of the fitting being depicted in **Figure F.2**, in **Appendix F**, showing AADs from the experimental data of 0.255 and 1.52 cP,

respectively. The higher deviations observed in the system with glycerol even though only data at atmospheric pressure was considered, demonstrates that although FVT contains three adjustable parameters, a good description of the pure fluid density is still highly relevant to obtain a good correlation of pure fluid viscosity data.

Table 6.3. FVT parameters used in this work.

Component	$\alpha / J \cdot m^3 \cdot mol^{-1} \cdot kg^{-1}$	B	$Lv / \text{\AA}$
Ethylene glycol	379.34	0.002434	0.03301
Glycerol	267.90	0.007701	0.00252
[Ch]Cl	190.54	0.006520	0.08776
Urea	235.94	0.009257	0.00183

Given the solid nature of [Ch]Cl, viscosity data of the pure component is not available to regress the FVT parameters and thus, viscosity data from [Ch]Cl containing mixtures were used. Hence, and with hindsight of the FVT parameters for EG and glycerol, FVT parameters for [Ch]Cl, listed in **Table 6.3**, were regressed from the viscosity data for the binary mixtures [Ch]Cl + EG (1:2) and [Ch]Cl + glycerol (1:2) at atmospheric pressure.[322] The results of the fitting are shown in **Figure F.3 A**), in **Appendix F**, and show an excellent agreement with the experimental data with AAD of only 0.923 and 0.859 cP for the mixtures with EG and glycerol, respectively. Similarly, knowing the FVT parameters for [Ch]Cl, the parameters for urea were obtained by fitting to the viscosity data for the [Ch]Cl + urea mixture. The optimized parameters are reported in **Table 6.3** and the results are also shown in **Figure F.3 B**), and as can be seen in the figure, despite three parameters are being fitted to the viscosity data, the model struggles to describe the low temperature region.

Once the FVT parameters for all the components were determined, one can predict the ηpT data available for the three systems.[322] The results of such predictions are shown in **Figure 6.2**. For the system with EG, an excellent agreement with the experimental data is observed, showing that both the effect of temperature and pressure is remarkably captured by the PC-SAFT + FVT models proposed here. On the other hand, a considerable overprediction of the pressure effect, more pronounced at lower temperatures, is observed in the system with glycerol. This is expected given the poor description of [Ch]Cl + glycerol (1:2) ρpT data by PC-SAFT previously discussed, highlighting that a good description of the mixture's density has a tremendous effect on the ability of FVT to correlate viscosity data at high pressures. For the system with urea, a reasonable agreement with the experimental data is found, although the effect of pressure is poorly described, if compared with the system with EG.

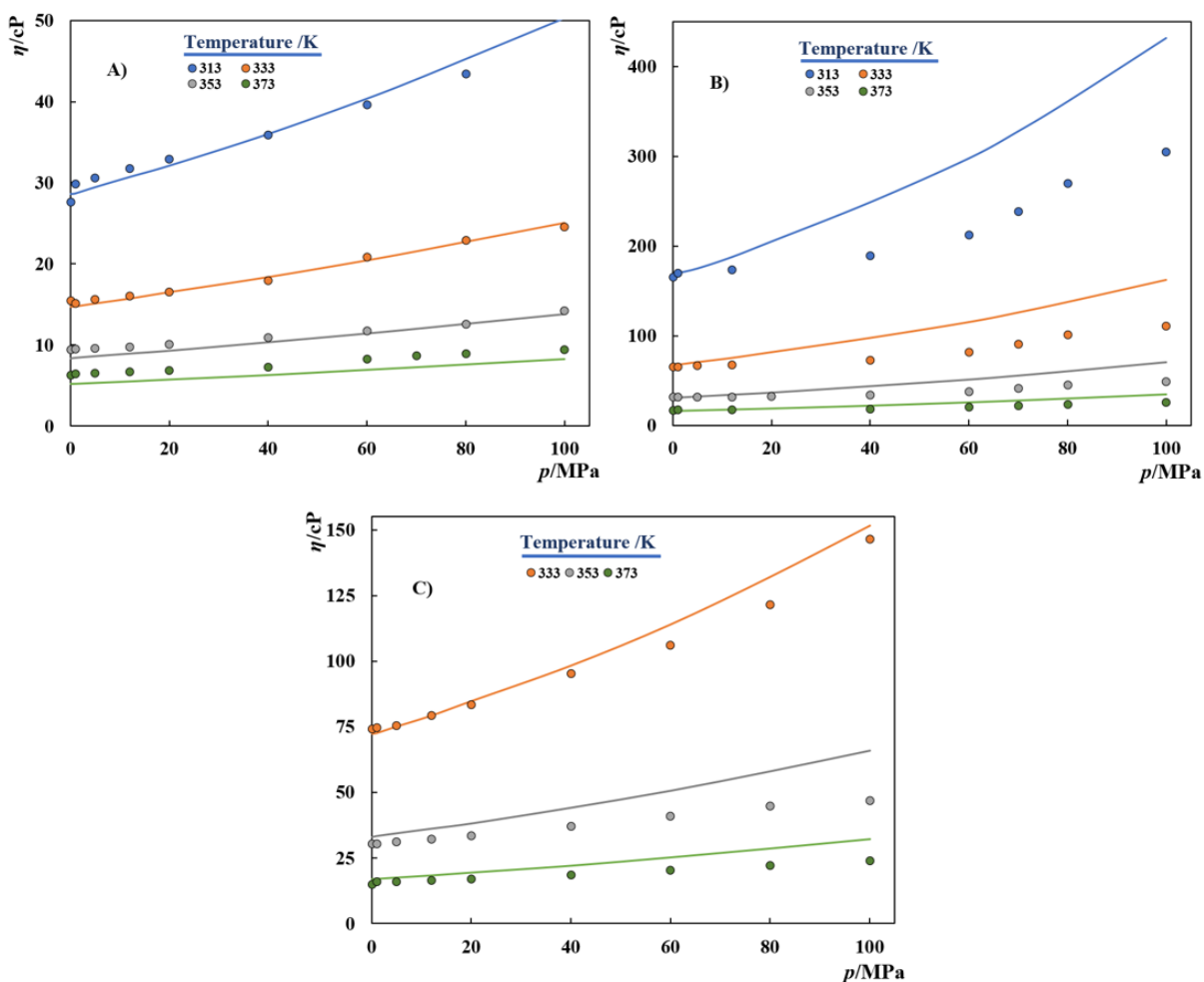


Figure 6.2. Viscosities of [Ch]Cl-based DES with different HBDs. A) EG; B) Glycerol; C) Urea. Symbols represent experimental data,[322] while the solid lines depict the results obtained with PC-SAFT + FVT.

Overall AADs against the experimental data of 0.81, 22.26, and 4.80 cP were observed for the mixtures with EG, glycerol, and urea, respectively. It is notorious that these deviations increase in the same order as those reported in **Table 6.2** for the PC-SAFT description of the $p\rho T$ data, reinforcing the importance of having an accurate description of $p\rho T$ data in wide temperature and pressure ranges with the chosen EoS prior to the correlation of viscosity data with FVT, which ultimately relies on the development of robust and accurate CG models for the DES constituents.

For most HBDs used in DES formulations the development of their CG models is a trivial task as densities and vapor pressures of the pure fluids are available and the model parameterization can be carried following the standard approach in SAFT-type EoS. However, this is not the case for most HBAs and a few HBDs (e.g., urea) which are solid at the range of working temperatures. For this type of compounds, experimental data for the pure fluids are rarely available and alternative approaches are

required. As discussed in the introduction, most literature works dealing with the thermodynamic modelling of DES, using SAFT-type EoS, follow a pseudo-pure component approach where SAFT parameters are regressed to each HBD/HBA combination. Although a pseudo-pure-component approach is an attractive approach to the modelling of some industrially important systems like polymer blends, where the different components are very similar (e.g., different chain length), this approach is inappropriate for the modelling of DES as they are mixtures of two completely different species.

Another alternative has been the use of aqueous solutions data (e.g., densities, osmotic coefficients) to regress the parameters for the target compound. Usually aqueous systems are challenging to any thermodynamic model and binary interaction parameters, sometimes temperature dependent as in the case of [Ch]Cl,[303] have to be fitted simultaneously to achieve a good agreement with the experimental data. The inclusion of such parameters may considerably affect the values of the pure-component parameters obtained, which will no longer be able to correctly capture the physical features of the target compound. Hence, and as the results obtained in this work show, the parameters obtained using such diluted data yield inaccurate results when they are applied to describe the density of DES and consequently hinder a good correlation of other thermophysical properties, e.g., viscosities. This urges the development of robust and accurate CG models that are applicable for solid DES precursors that will be discussed next.

Development of a CG model for [Ch]Cl, in the framework of the soft-SAFT EoS

In the association models currently employed in the thermodynamic modelling of DES, most DES precursors like [Ch]Cl have been modelled using the simple ‘2B’ association scheme.[302–312] This association scheme contains one proton-donor site ‘A’ and one proton-acceptor site ‘B’ with only ‘A–B’ interactions being allowed in the system. However, it seems too simplistic to capture the highly complex hydrogen-bonding character of [Ch]Cl in these solvents. In fact, ab initio calculations performed by Ashworth et al.[316] revealed that, in contrast to traditional solvents, many different types of H-bond can form in the archetypal mixture of [Ch]Cl + urea (1:2) that cannot be well captured by oversimplified models. An example is the formation of the complexed anions and cations thought to be responsible for the eutectic melting point occurring at a ratio of 1:2 ([Ch]Cl:urea) that would require more than one proton acceptor site.[316]

Therefore, considering the MD simulations and ab initio calculations available in literature for [Ch]Cl-based DES,[314,316] a 5-site association scheme is here proposed to model the salt. This scheme is sketched in **Figure 6.3**, and comprises:

-One pair of sites ‘A’ + ‘B’ mimicking the hydrogen atom and the lone electron pairs in the oxygen atom of the hydroxyl group, as commonly considered for alkan-1-ols.[74]

-One pair of sites ‘C’ + ‘D’ mimicking the cation-anion interactions as typically done for salts and ILs.[303,311,312,324,325]

-One additional ‘E’ site representing the hydrogen bond donor character of the methyl groups that, as observed by Ashworth et al.,[316] are able to establish important hydrogen bonds such as strong doubly ionic hydrogen bonds ‘CH—Cl’ in a tripod arrangement.

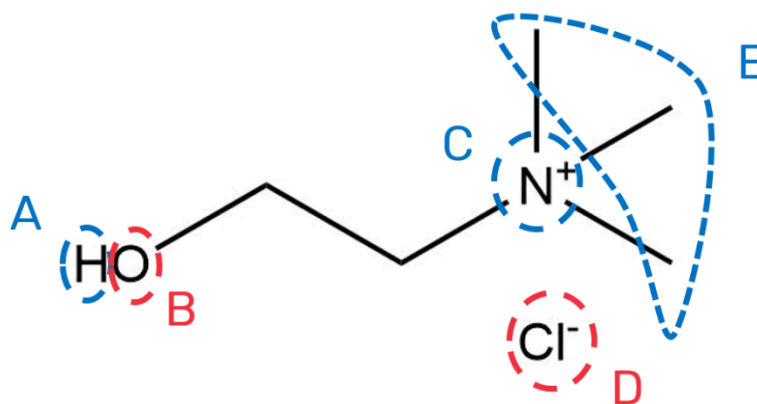


Figure 6.3. Sketch of the associating sites proposed in this work for [Ch]Cl. Blue is used for H-bond donor sites while red is used for H-bond acceptor sites.

Given this association sites distribution and the fact that association energies and volumes must be defined pairwise, a total of six association parameters (three association energies and three association volumes) are required to describe the interactions involving the hydroxyl group, cation/anion pair, and the methyl groups, within the SAFT association term. To decrease this high number of unknown parameters to be regressed from experimental data, one can take advantage of the molecular nature of soft-SAFT EoS, based on the transferability of the association parameters between chemical families as they usually describe interactions involving the same functional group. As an example, Pedrosa et al.[75] fitted the association parameters accounting for the hydrogen bond interactions through the hydroxyl end groups to the experimental data of monoethylene glycol (EG) that were later transferred to the modelling of the remaining oligomers[75] and polyethylene glycols.[113] In other works, Lloret et al.[326] and Pereira et al.[327] used soft-SAFT transferability to describe the multifunctional nature of alkanolamines with the effects of the functional groups and their interactions in water being transferred from the study of monofunctional molecules and their respective aqueous solutions. Thus, in this work, the association parameters required to describe [Ch]Cl are also transferred from previous contributions. Those necessary to describe the hydroxyl group (‘A’ and ‘B’ sites) are transferred from the alkan-1-ols family reported

by J. Pàmies,[94] while those describing the cation-anion interactions ('C' and 'D' sites) are transferred from the work of Lloret et al.[311] on the modelling of symmetrical tetraalkylammonium chlorides ([TXA]Cl). The definition of association parameters for the methyl groups is less trivial as no evident transferability is possible. Therefore, an empirical approach similar to that proposed by Folas et al.[328] to account for solvation is here applied, but in which it is the volume of interaction that is kept fixed to the association volume of the other association site involved in the H-bond, while the energy of association is taken as half of the association energy of the other site. As an example, the association parameters mediating the interactions between a site type 'E' and a H-bond acceptor site 'X' are obtained as follow:

$$\varepsilon_{E-X}^{HB} = \frac{\varepsilon_{X-X'}^{HB}}{2} \quad (6.1)$$

$$\kappa_{E-X}^{HB} = \kappa_{X-X'}^{HB} \quad (6.2)$$

Nonetheless, given the nature of the site 'E' assigned to [Ch]Cl, this site only engages in self-associating interactions with other [Ch]Cl ions (H-bonds with the chloride anion or with the lone electron pairs of the oxygen atom – 'D' and 'B' sites, respectively), while cross-association interactions with other molecules are forbidden given its unlikely occurrence.[316] The self and cross-interactions allowed to occur in a hypothetical [Ch]Cl-based DES are summarized in **Table 6.4**, along with the approach followed to obtain the corresponding association parameters.

Table 6.4. Self and cross-association interactions present in a [Ch]Cl-based DES.

	[Ch]Cl					Component 2	
	Cation (+)	Anion (-)	O (-)	H (-)	CH (+)	X (-)	Y (+)
Cation (+)	0	3384[311]	0	0	0	CR	0
Anion (-)	3384[311]	0	0	CR	EA	0	CR
O (-)	0	0	0	3450[94]	EA	0	CR
H (-)	0	CR	3450[94]	0	0	CR	0
CH (+)	0	EA	EA	0	0	0	0
X (-)	CR	0	0	CR	0	0	SA
Y (+)	0	CR	CR	0	0	SA	0

CR- Association parameters obtained through combining rules (eqs. 2.26-2.27); EA- Association parameters obtained through the empirical approach (eqs. 6.1-6.2). Red regions represent cross-association interactions while green regions represent self-association interactions.

Another issue arising when modelling [Ch]Cl and other salts used in DES formulations, is that they are solid at room temperature and thus, vapor pressures and liquid densities of the pure fluid (the properties commonly used to regress SAFT pure-component parameters) are not available, so alternative approaches must be used. In the work of Lloret et al.[311] this fact was circumvented by estimating the molecular parameters of the salt first departing from the data of the DES that this salt forms with another compound for which the pure component is well characterized (i.e. TriEG). The molecular parameters of the salt were fitted to the density of the mixture at available ratios and used to predict the behaviour of the salt with other compounds but limited experimental data was used at this time. As discussed before, CG models developed using aqueous solution data as suggested in literature[303] often yield inaccurate results when those models are later applied to the thermodynamic modelling of DES, due to the unique behaviour exhibited by most aqueous systems, and the difficulty of most models in describing them, but also due to the low concentration region of the experimental data considered in the fitting. Alternatively, in this work, it is proposed to regress the three unknown parameters of [Ch]Cl (m_i , σ_{ii} , and ε_{ii}/k_B) from experimental data obtained for a DES containing this salt, namely [Ch]Cl + EG (1:2). Hence, the experimental dataset used for the fitting consists on the $p\rho T$ data,[322] and, given the importance of including phase equilibrium data, the SLE data for this mixture.[329]

Ethylene glycol (EG) is modelled using a 2-site model as proposed by Pedrosa et al.[75] whose parameters are given in **Table 6.5**. The regression of the model parameters was carried using the 'lsqnonlin' routine of the MATLAB® software, using the Levenberg-Marquardt algorithm. The results of the fitting are depicted in **Figure 6.4**, while the [Ch]Cl pure-component parameters obtained under this approach are also reported in **Table 6.5**. The molecular parameters obtained for [Ch]Cl under this approach were found to be in good agreement with those reported by Lloret et al.[311] for [TXA]Cl salts, as the number of segments and segment's diameter are in between those obtained for tetramethylammonium chloride and tetraethylammonium chloride, as expected given the size of the different salts. Furthermore, a higher dispersive energy was obtained here for [Ch]Cl, namely $\varepsilon_{ii}/k_B = 376.64 K$, compared to the value of 360.8 K reported for [TXA]Cl salts, which is also expected given the much stronger hydrogen bonding character of [Ch]Cl. Notice that, in these CG models the associating energy and the dispersive energy are not completely isolated from each other, as both contribute to the overall energy of the molecule.

Table 6.5. soft-SAFT pure-component parameters used in this work.

Compound	M_w (g/mol)	m_i	σ_{ii} (Å)	ε_{ii}/k_B (K)	ε^{HB}/k_B (K)	κ^{HB} (Å ³)	Ref.
[Ch]Cl	139.62	4.359	3.578	376.64	3450 ^a /3384 ^b	2250 ^a /2100 ^b	This work
EG	62.07	1.751	3.668	326.05	4384	4195	[75]
TriEG	150.17	3.190	4.010	340.58	4384	4195	[75]
Glycerol	92.09	2.397	3.638	392.95	4945	2250	This work
Phenol	94.11	2.155	3.995	384.65	3099	2250	This work
Ethanol	46.07	1.740	3.635	234.80	3387	2641	[94]
Lactic acid	90.08	1.812	4.059	433.10	1510	3200	[311]
CO ₂ ^c	44.01	1.571	3.184	160.2	-	-	[75]
H ₂ O	18.02	1.000	3.154	365.00	2388	2932	[137]

^aassociation parameters for the OH group transferred from the work of Pàmies[94];

^bassociation parameters for cation-anion interactions transferred from Lloret et al.[311]

^cCO₂ parameters for the polar term: $Q = 4.40 \cdot 10^{-40} \text{ C} \cdot \text{m}^2$; $x_p = 1/3$; ref: [75]

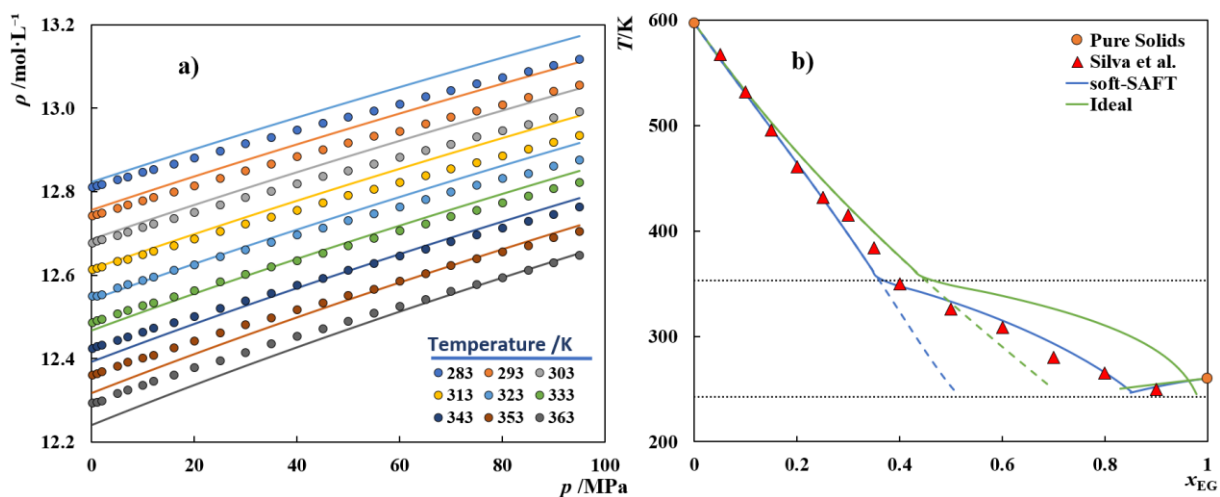


Figure 6.4. a) High-pressure liquid densities and b) SLE phase diagram for the mixture [Ch]Cl + EG (1:2). Symbols represent experimental data[322,329] while the solid lines depict the soft-SAFT results and ideal solubility curves. In b), the dashed lines represent the SLE results without accounting for the solid-solid transition of [Ch]Cl.

To achieve the good agreement with the experimental data observed in **Figure 6.4**, a binary interaction parameter, ξ_{ij} , correcting the mixtures dispersive energy, was fitted simultaneously with the three non-associating [Ch]Cl parameters. Contrarily to what was observed in the work of Zubeir et al.[303], where PC-SAFT parameters for [Ch]Cl were regressed from aqueous solutions data, the binary parameter fitted to the selected data is temperature independent and its value is reported in **Table 6.6**. Notice that a value of unity means no fitting to binary data. Additional optimizations (not shown here) revealed that the binary parameter is required not only due to the negative deviations from the ideal behaviour observed in the solid-liquid phase diagram, but mostly due to the fully predictive association matrixes considered in the association term. Similar results without a binary interaction parameter could have been obtained if one of the association parameters, e.g., the association energy for the hydroxyl group, was reoptimized for [Ch]Cl instead of directly transferred from previous works. Aiming at an increased transferability and considering the good results obtained, the first approach is selected, and as can be observed in **Figure 6.4 a**), considering the extended temperature (283-363) K and pressure (0.1—95) MPa ranges where experimental densities were available, the effect of temperature and pressure upon the DES densities are remarkably captured by the model with a %ARD of only 0.181%. The greater deviations are mostly observed at high temperatures-low pressures and low temperatures-high pressures.

Table 6.6. Binary interaction parameters used in this work. $\xi_{ij}=1.000$ means prediction from pure-component parameters.

Compound <i>i</i>	Compound <i>j</i>	ξ_{ij}
[Ch]Cl	EG	1.040
[Ch]Cl	TriEG	1.000
[Ch]Cl	Phenol	1.000
[Ch]Cl	Glycerol	1.022
[Ch]Cl	Ethanol	1.000
[Ch]Cl	Water	1.250
[Ch]Cl	Lactic acid	1.040
EG	H ₂ O	1.130[138]
Glycerol	H ₂ O	1.000
[Ch]Cl	CO ₂	1.100
EG	CO ₂	0.8321[75]
Glycerol	CO ₂	0.960
Lactic acid	CO ₂	0.760

Concerning the solubility data, the solid-liquid phase diagram reported for [Ch]Cl + EG shows that the solid-solid transition of [Ch]Cl previously reported in literature[330,331] has an impact on the mixture's phase diagram. Therefore, the modelling of the phase diagram was carried both neglecting and accounting for the existence of such phase transition, using **eq. 6.3** or **eq. 6.4**, respectively:

$$x_k \gamma_k^l = \exp \left[\frac{\Delta H_k^{sl}}{RT_{m,k}} \frac{T - T_{m,k}}{T} \right] \quad (6.3)$$

$$x_k \gamma_k^l = \exp \left[\frac{\Delta H_k^{sl}}{RT_{m,k}} \frac{T - T_{m,k}}{T} + \frac{\Delta H_k^{trs}}{RT_{trs,k}} \frac{T - T_{trs,k}}{T} \right] \quad (6.4)$$

where x_k is the solubility of a solid solute k , γ_k^l its activity coefficient in the liquid phase, T the absolute temperature, R , the ideal gas constant, $T_{m,k}$ and ΔH_k^{sl} are the melting temperature and melting enthalpy of the pure solid. $T_{trs,k}$ and H_k^{trs} required in **eq. 6.4**, represent the transition temperature and transition enthalpy for the solid-solid transition, which for [Ch]Cl have the values of 352.92 K and 17190 J/mol, respectively.[332] Both expressions neglect the effect of the heat capacity difference between the solid and liquid phases, as previously suggested by Martins et al.[301] The values of $T_{m,k}$ and ΔH_k^{sl} used in this work are given in **Table 6.7**.

Table 6.7. Melting properties used in this work.

Compound	T_m/K	$\Delta H_k^{sl}/J \cdot mol^{-1}$
[Ch]Cl	597[313]	4300[313]
EG	260.15[118]	9958[118]
Glycerol	291.33[118]	18280[118]
Lactic acid	289.82[333]	11340[333]

The results depicted in **Figure 6.4b**, show that when the solid-solid transition is explicitly considered in the modelling, an excellent description of the [Ch]Cl solubility is achieved with only small deviations in the near-transition region, probably due to the two different experimental techniques used to measure the two regions (i.e., visual vs DSC). Nonetheless in the large temperature range where the [Ch]Cl solubility was measured (280—597) K, the AAD is only 6.89 K.

Given the nature of SAFT-type equations, several pure-component parameters can yield similar results when evaluating a small experimental dataset like those usually considered during model parameterization.[7] Therefore, the CG model proposed here for [Ch]Cl was then validated through the description of the boiling temperatures of [Ch]Cl + EG mixtures.[334] As shown in **Figure 6.5**, using the pure-component parameters from **Table 6.5** and the binary interaction parameter fitted to the

densities and SLE of the eutectic solvent reported in **Table 6.6**, excellent predictions of the VLE data were obtained with an overall AAD of only 1.08 K. The small deviations observed in the glycol-rich phase are due to the overestimation of the boiling temperature of pure EG by its CG model.

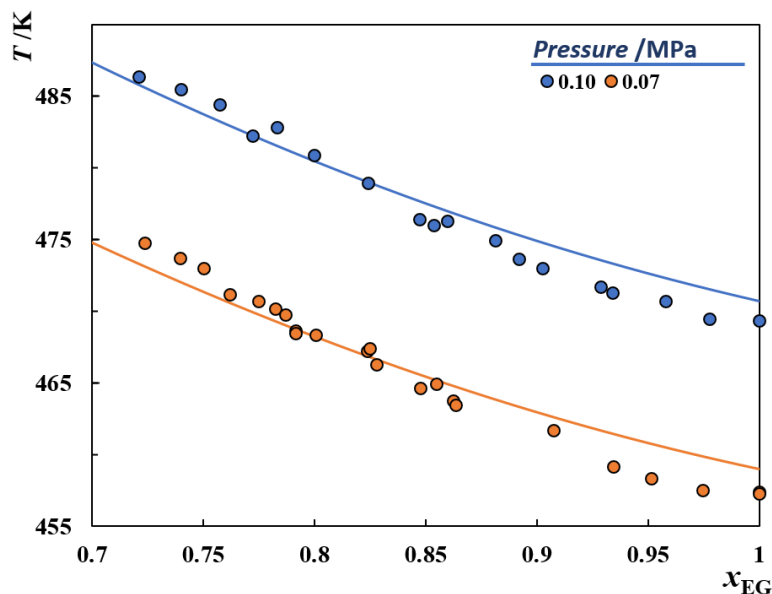


Figure 6.5. VLE for [Ch]Cl + EG mixtures. Symbols represent experimental data,[334] while the solid lines depict the soft-SAFT predictions.

Performance assessment for the [Ch]Cl CG model

Once the new CG model for [Ch]Cl was established, its performance was evaluated through the modelling of different [Ch]Cl-based DES. It was shown previously how when CG models available in literature are used to model DES, a good description of density could not be achieved even at atmospheric pressure. Therefore, the new model is first used to describe the atmospheric pressure densities of [Ch]Cl + TriEG at a 1:2 molar ratio in the (303—353) K temperature range, reported by Mjalli et al.[335]. As can be observed in **Figure 6.6a**, using the model for [Ch]Cl proposed in this work and the model for TriEG reported by Pedrosa et al.[75], whose parameters are given in **Table 6.5**, an excellent prediction of the experimental density was obtained with a %ARD of 0.106%.

Considering that DES have also been used at compositions other than the eutectic point, aiming at an increased tunability of the solvent, the effect of composition on thermophysical properties, e.g., density, must also be well described by thermodynamic models. Guo et al.[336] measured the atmospheric pressure densities of binary mixtures composed of [Ch]Cl and phenol at different HBD/HBA molar ratios in the (293—318) K temperature range. As no CG model for phenol in the framework of the soft-SAFT EoS was available in literature, new molecular parameters based on a “2B”

association scheme were regressed in this work from pure fluid VLE data. The good results of the fitting (%ARD of 0.436% and 1.58% for the liquid densities and vapor pressures, respectively) are shown in **Figure F.4** in **Appendix F**, and the parameters obtained are presented in **Table 6.5**. Using these parameters and those proposed for [Ch]Cl, an excellent agreement between the soft-SAFT predictions and the experimental data from Guo et al.[336] is achieved with a %ARD of 0.073%. These results are depicted in **Figure 6.6b**) and highlight the ability of soft-SAFT to correctly capture the effect of composition on the DES densities.

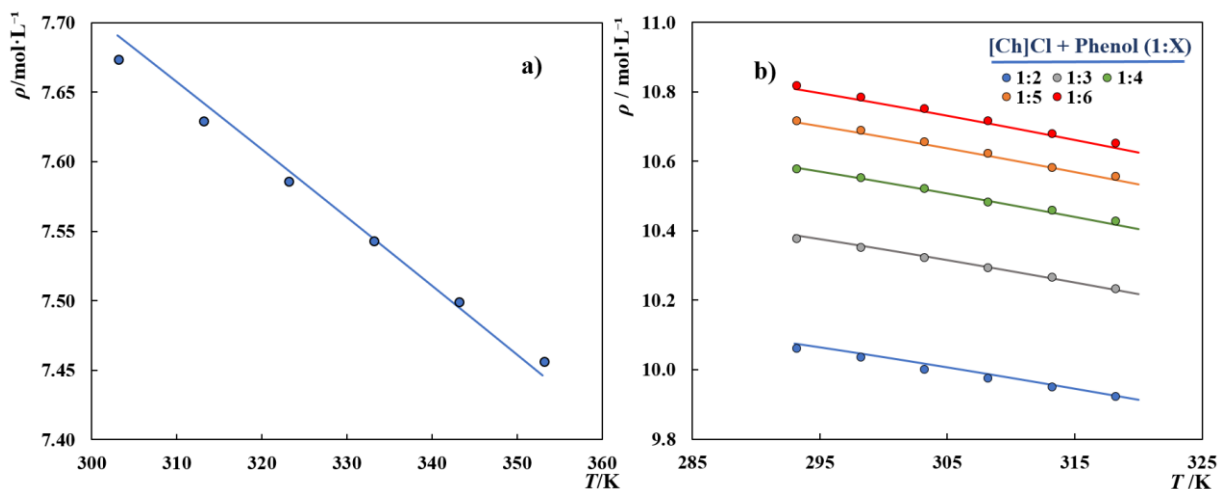


Figure 6.6. a) Densities at 0.10 MPa for [Ch]Cl + TriEG (1:2). b) Densities at 0.10 MPa for [Ch]Cl + Phenol. Symbols represent experimental data[335,336] while the solid lines depict the soft-SAFT predictions.

One of the most typical [Ch]Cl-based DES is its binary mixture with glycerol at a 1:2 molar ratio, for which densities in wide temperature and pressure ranges are available.[322] Similarly to phenol, no soft-SAFT parameters were available in literature, thus molecular parameters for glycerol were here regressed from pure fluid VLE data. The results of the fitting, using the “2B” association scheme are shown in **Figure F.5** in **Appendix F**, while the pure-component parameters obtained are given in **Table 6.5**. Despite the existence of small deviations between the soft-SAFT results and the experimental liquid densities at higher temperatures, well beyond the typical temperature range of interest for DES applications, an overall good agreement with the experimental data was found with %ARD of 1.03% and 1.75% for the liquid densities and vapor pressures, respectively. Although glycerol has a higher number of hydroxyl groups when compared to alkan-1-ols and phenol, suggesting the use of additional association sites, the “2B” association scheme yielded better results than the 4-site or 6-site association schemes tested in preliminary calculations (results not shown here). This is probably due to the relatively

small size of glycerol molecules and the consequent steric hindrance induced when bonds with other molecules are established, preventing bonding at the other free sites.

Once the CG models for the two compounds are established, soft-SAFT was applied to the prediction of the $p\rho T$ data in the entire temperature (283—363) K and pressure (0.10—95) ranges, and, as depicted in **Figure 6.7a**), a remarkable agreement with the experimental data was achieved (%ARD = 0.226%), showing that soft-SAFT is also able to capture the effect of pressure on the DES densities, even though only atmospheric pressure density data was used in the parameterization of the HBD's model, reinforcing the robustness of the model proposed here for [Ch]Cl when used to predict densities.

Abbott et al.[337] and Silva et al.[329] reported the solid-liquid phase diagram for this DES, which exhibits considerable negative deviations from the ideal behaviour were observed by the different authors, especially near the eutectic region. Consequently, when the CG models developed in this work were used to describe the [Ch]Cl solubility in glycerol (**Figure 6.8**), a binary interaction parameter (see **Table 6.6**), was required to obtain a good agreement with the experimental data. Contrarily to what was observed in the mixture with EG, the solid-solid transition of the pure salt had no visible influence on the mixtures phase diagram, hence, accurate results were only obtained when the solubility was calculated through **eq. 6.3**. The binary parameter required to accurately describe this data has a value only slightly different than the one used in the mixture with EG and was found to have a negligible impact on the DES densities, as shown in **Figure 6.7b**).

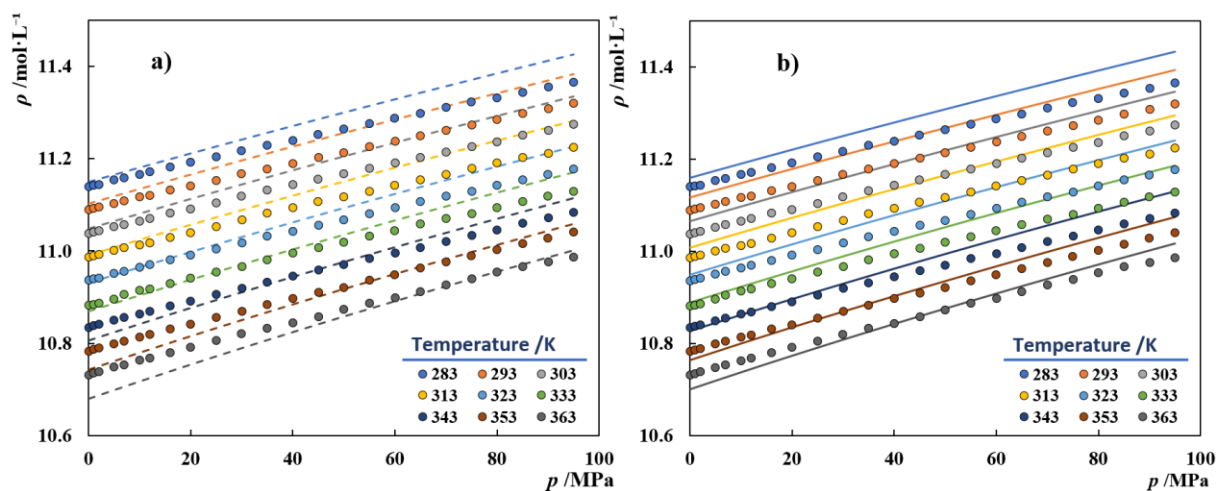


Figure 6.7. $p\rho T$ data for the [Ch]Cl + Glycerol (1:2) DES. Symbols represent the experimental data, while the lines depict the soft-SAFT results using a) $\zeta_{ij}=1$ (pure predictions); b) $\zeta_{ij}=1.022$.

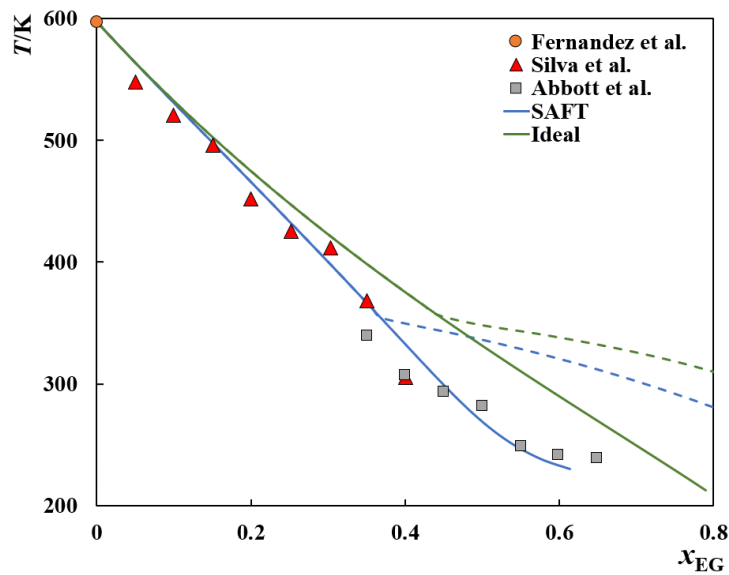


Figure 6.8. Solubility of [Ch]Cl in glycerol. Symbols represent experimental data,[313,329,337] while the dashed and solid lines represent the soft-SAFT results ($\xi_{ij}=1.022$) and ideal solubility curves, with and without accounting for the solid-solid transition of [Ch]Cl, respectively.

One of the most challenging systems involving [Ch]Cl is its aqueous solution. As previously mentioned, Zubeir et al.[303] regressed the five pure-component parameters of a PC-SAFT CG model for [Ch]Cl (“2B” association scheme) from data of its aqueous solutions, namely VLE data, in the form of osmotic coefficients, and densities at different salt concentrations ($x_{salt} < 0.33$) along with a temperature-dependent binary parameter, but significant deviations from the experimental data were still observed. In this work, using the molecular model developed for [Ch]Cl, and the 4-site CG model for water proposed by Vega et al.[137] (parameters provided in **Table 6.4**), a reasonable agreement with the experimental boiling temperatures measured by Carvalho et al.[338] (AAD = 1.22 K) and the densities at atmospheric pressure reported by Francisco et al.[339] (%ARD = 0.161%) can be obtained, as shown in **Figure 6.9**. Although an accurate prediction of the experimental densities could have been obtained solely from the pure-component parameters (see dashed lines in **Figure 6.9a**), a binary interaction parameter, $\xi_{ij}=1.25$, was necessarily fitted to the boiling temperatures at 0.10 MPa, being successfully transferred to the description of the other two isobars at lower pressures and to the description of atmospheric pressure densities (**Figure 6.9a**). In fact, similarly to what was previously observed in the system with glycerol, the binary interaction parameter had only a negligible impact upon the system’s density despite its considerable high value. This is because the ξ parameter modifies the cross-energy interaction but does not significantly affect the volume interactions, which mostly dictate the density behaviour.

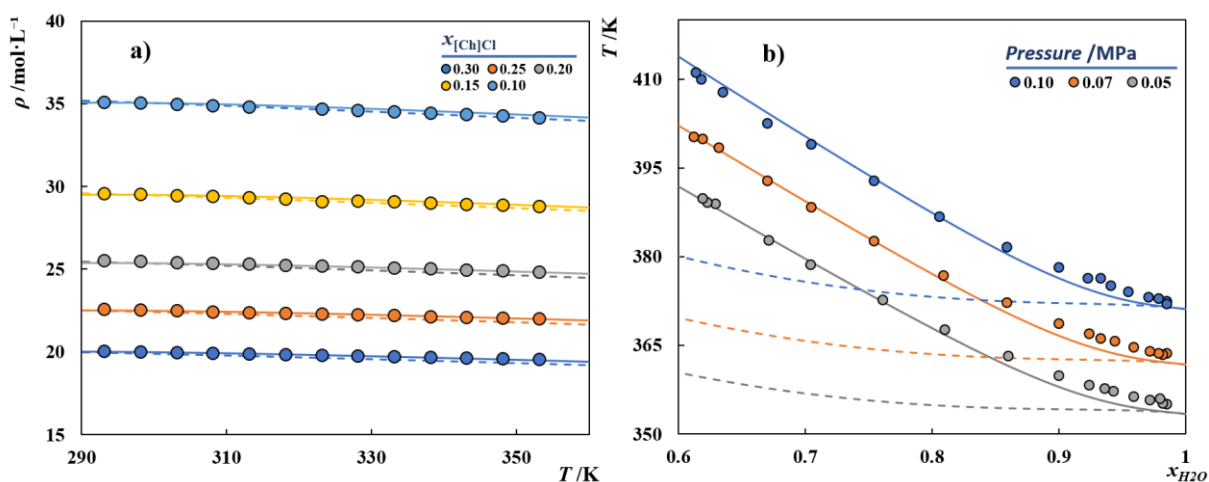


Figure 6.9. a) Densities and b) boiling temperatures of aqueous solutions of [Ch]Cl. Symbols represent experimental data,[338,339] while the solid and dashed lines represent the soft-SAFT results using $\xi=1.25$ and $\xi=1$, respectively.

In the same work, Carvalho et al.[338] also reported the boiling temperatures for the binary mixture [Ch]Cl + ethanol (EtOH) at three different pressure levels (0.10, 0.07, and 0.05 MPa). Using the CG model developed for [Ch]Cl and the soft-SAFT model for ethanol proposed by Pàmies,[94] based on a “2B” association scheme, the experimental data can be predicted. As shown in **Figure 6.10a**), an excellent agreement with the experimental data was observed, although a very narrow composition range was investigated.

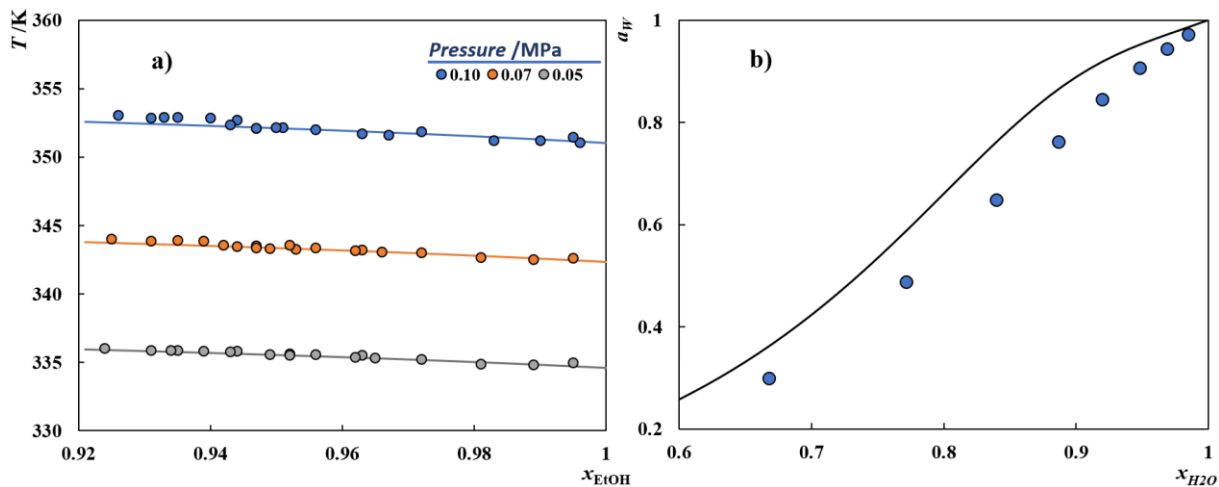


Figure 6.10. a) Boiling temperatures for [Ch]Cl + EtOH; b) Water activities at 298.2 K in aqueous solution of [Ch]Cl. Symbols represent experimental data,[338,340] while the lines depict the soft-SAFT predictions.

Khan et al.[340] reported the water activities of [Ch]Cl aqueous solution at 298.2 K. Using the binary interaction parameter between [Ch]Cl and water previously fitted to one of the isotherms on

Figure 6.9b), a reasonable prediction of the water activities at a much lower temperature was obtained. These results are depicted in **Figure 6.10b)**, where the soft-SAFT predictions show the same trend as the experimental data, highlighting the ability of the model to describe VLE data.

Having a CG model for [Ch]Cl, one could use this model to obtain the density of a hypothetical pure liquid in the temperature range of interest (**Figure 6.11a)** and compare such value with an extrapolation of the density data of its aqueous solution. Using the experimental data reported by Francisco et al.[339], and neglecting the most diluted data point, the density predicted by the CG model developed in this work captures well the trend observed experimentally, reinforcing the model's robustness. Furthermore, as shown in **Figure 6.11b)**, a linear relationship between $\ln(\rho)$ and $1/x_{H_2O}$ can be proposed, allowing a very good prediction of the density of [Ch]Cl aqueous solutions in the entire composition range.

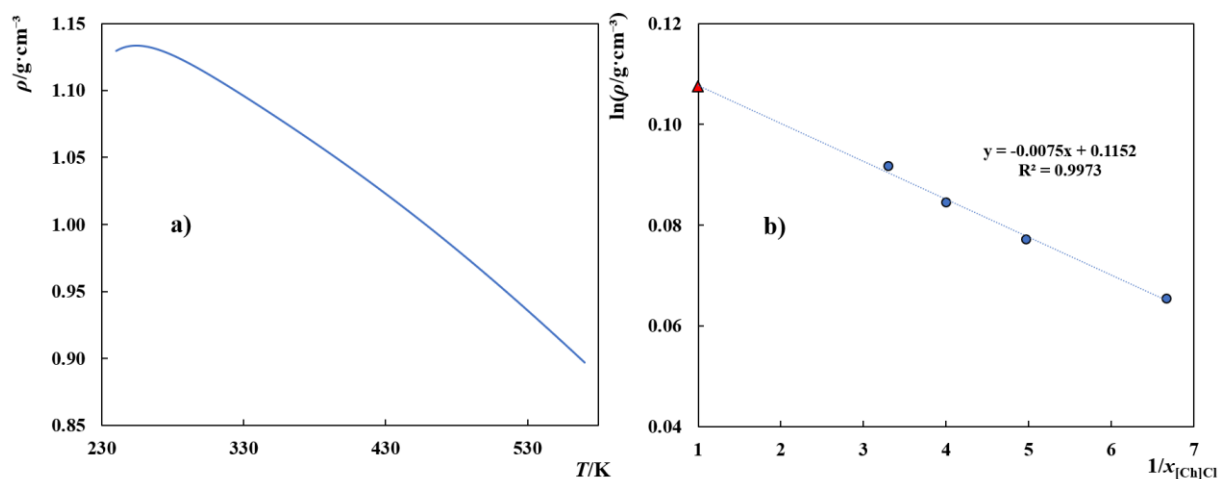


Figure 6.11. a) Density of pure [Ch]Cl as predicted by soft-SAFT. b) Density of [Ch]Cl aqueous solutions at 303.15 K. Blue circles represent experimental data from literature,[339] while the red triangle represent the hypothetical density of pure [Ch]Cl predicted by soft-SAFT at 303.15 K.

As can be observed in **Figure 6.11a)**, the density of pure [Ch]Cl, as predicted by soft-SAFT, using the CG model proposed in this work, exhibits an anomalous behaviour, displaying a maximum around 256.15 K. Some numerical pitfalls of SAFT models are known to produce unphysical behaviour and unrealistic phenomena under particular thermodynamic conditions.[341–343] Considering that [Ch]Cl melts at 597 K, these results derive from calculations performed for a hypothetical fluid well below its melting point, at a very low reduced temperature where numerical issues are also prone to appear. Therefore, although there is no experimental data corroborating or denying this behaviour, the model proposed here should not be used at temperatures lower than 256.15 K which, nonetheless, is below the temperature range for most DES applications, which are usually at room temperature.

Once the new model was successfully applied to the aqueous solutions of [Ch]Cl, it can be used to describe the effect of water upon DES thermophysical properties. This information is of key interest, not only because water absorption by DES is known to significantly influence their thermodynamic behaviour[344,345] but also because water can be deliberately added to DES in order to tune their properties, an example being the addition of water to decrease their viscosities.

Leron et al.[346] reported the densities of the [Ch]Cl + EG and [Ch]Cl + glycerol DES, both at a 1:2 molar ratio, at temperatures ranging from 298.15 to 333.15 K. Using the pure-component parameters from **Table 6.5**, and the binary parameters from **Table 6.6**, excellent predictions of the ternary mixture's densities were obtained, as shown in **Figure 6.12**. The %ARD of the soft-SAFT predictions from the experimental data are 0.449% and 0.216% for the mixture with EG and glycerol, respectively, being similar to those observed in pure DES, and lower than those observed when soft-SAFT is used to describe pure water.[127,137]

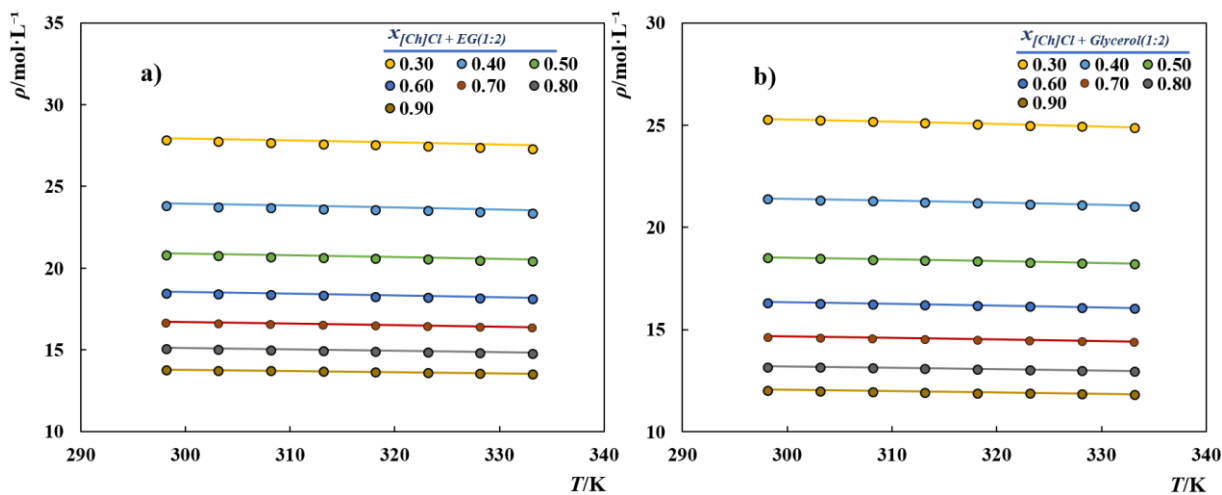


Figure 6.12. Densities of aqueous solutions of DES. a) [Ch]Cl + EG (1:2); b) [Ch]Cl + Glycerol (1:2). Symbols represent experimental data,[322] while the solid lines depict the soft-SAFT predictions.

Leron and co-workers[347,348] have measured the CO₂ solubilities in the [Ch]Cl-based DES with EG or glycerol as HBD with the latter exhibiting the highest affinity towards CO₂. The experimental solubility data in the two DES is plotted in **Figure 6.13**, along with the soft-SAFT EoS modelling. Concerning the mixture with EG, the binary interaction parameter between EG and CO₂ was retrieved from the work of Pedrosa et al.[75] where the CG models for the two compounds were first proposed, while the binary interaction parameter between [Ch]Cl and CO₂, reported in **Table 6.6**, was fitted to the isotherm at 303 K and used to predict the remaining isotherms. As can be observed in **Figure 6.13a**), a reasonable agreement with the experimental data was achieved although larger discrepancies were

observed at high temperatures. The results can however be easily improved by using a temperature-dependent binary parameter between CO₂ and either the salt or the HBD, if a higher accuracy is required. In fact, temperature-dependent binary parameters between glycols and CO₂ have already been used in soft-SAFT to better describe the interactions between glycols (e.g., diethylene glycol) and CO₂ in **Chapter 3.3**.

Once the binary parameter between [Ch]Cl and CO₂ is available, it can be used to describe the gas solubilities in the mixture with glycerol. In this system, the binary parameter between glycerol and CO₂, reported in **Table 6.6**, was fitted to the isotherm at 303 K and used to predict the data at higher temperatures. As depicted in **Figure 6.13b**), an excellent agreement with the experimental data was observed with deviations lower than those observed in the system with EG, although for the latter no binary interaction parameters between the HBD and the gas were fitted to the experimental data.

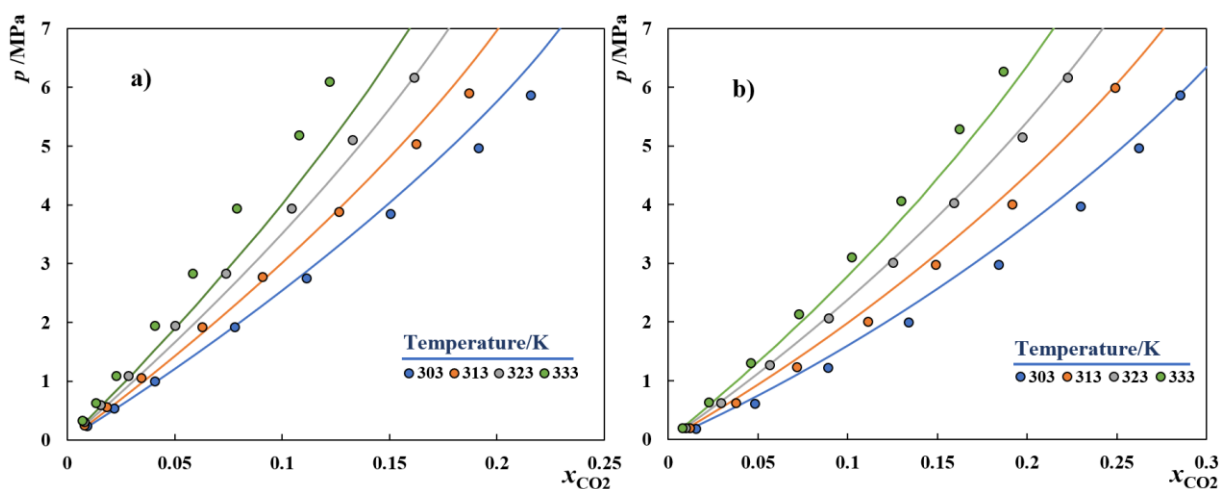


Figure 6.13. CO₂ solubilities in two different DES: a) [Ch]Cl + EG (1:2); b) [Ch]Cl + Glycerol (1:2). Symbols represent the experimental data,[347,348] while the solid lines depict the soft-SAFT results.

Considering that a molecular model within the framework of soft-SAFT was recently proposed for lactic acid by Lloret et al.[311], the CG model developed here for [Ch]Cl could be also applied to the modelling of the SLE phase diagram measured for [Ch]Cl + lactic acid mixtures reported by Crespo and co-workers[310] and the density data reported by Francisco et al.[349] measured for different HBD/HBA molar ratios. By fitting a temperature-independent binary parameter between [Ch]Cl and LA (c.f. **Table 6.6**), an excellent description of the SLE phase diagram for this mixture is achieved although no experimental data near the eutectic region is available – **Figure 6.14a**). On the contrary, a poor description of the mixture densities was obtained either with or without such binary parameter. Given the good results obtained with the model proposed here for [Ch]Cl when used to describe the densities

of different mixtures, including its challenging aqueous solution, there are reasons to believe that such discrepancies may be related to the CG model of lactic acid, whose parameters were obtained from an indirect fitting using mixtures' density data.[311] As mentioned in the introduction, this simplified approach may hinder a correct description of the compound's physical features resulting in a lower accuracy. This is corroborated by the soft-SAFT results shown in **Figure 6.14b**), as the deviations of the soft-SAFT predictions from the experimental mixture densities increase as the molar fraction of LA is increased.

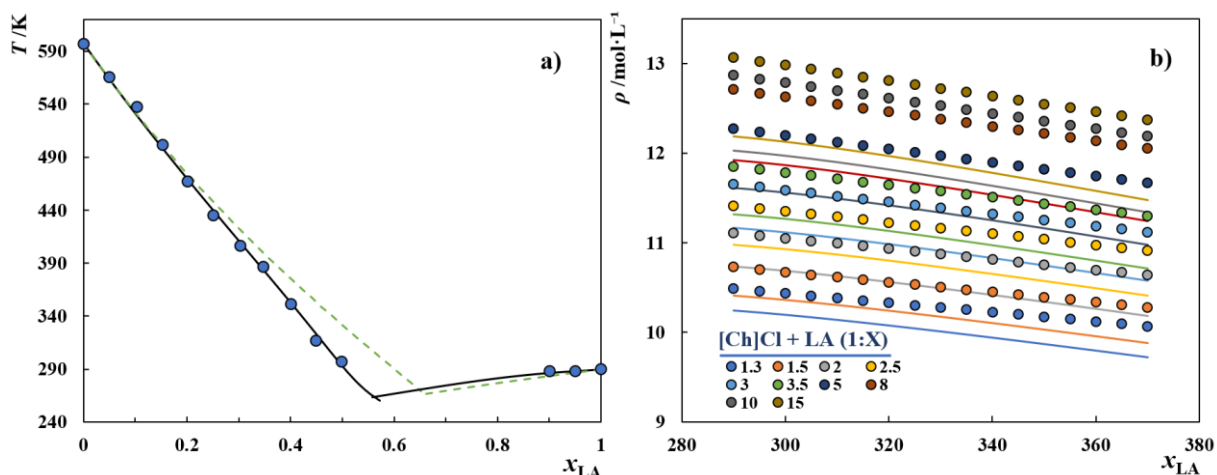


Figure 6.14. a) SLE phase diagram for [Ch]Cl + lactic acid. b) Densities of [Ch]Cl + lactic acid at different HBA to HBD molar ratios. Symbols represent experimental data,[310,349] while the solid lines depict the soft-SAFT results using $\xi=1.04$.

Francisco et al.[349] reported the CO_2 solubilities in the DES [Ch]Cl + lactic acid (1:2) in the form of isopleths with a CO_2 mole fraction ranging from 0.025 to 0.100. As the binary parameter between the salt and the HBD was defined through modelling of the SLE data of the correspondent binary mixture, only the binary parameter between lactic acid and CO_2 was directly fitted to the experimental solubility data. The results of the fitting are depicted in **Figure 6.15** and show that the model is able to provide a good description of the experimental data with a %ARD of 4.95%, although deviations increase with increasing temperatures and gas contents. However, the absorption capacity of DES seems rather limited so higher CO_2 contents than those reported by Francisco et al.[349] are unlikely to occur.

In fact, it does not make any sense that DES have been so widely investigated as alternative solvents for gas separations in literature, as a 'true' DES will never be a good solvent for gases. This is easily shown using classical thermodynamics, as the Henry constant of a gas (component 3) in a mixture of component 1 and component 2 can be obtained from the following expression:

$$\ln(H_{3,mix}) = x_1 \ln(H_{3,1}) + x_2 \ln(H_{3,2}) - a_{12}x_1x_2 \quad (6.5)$$

where $H_{3,mix}$ is the Henry constant of the gas in the mixture, $H_{3,1}$ and $H_{3,2}$ are the gas Henry's constant in component 1 and component 2, respectively, and a_{12} is a measure of the interactions between the two components. DES are assumed to arise from the existence of strong hydrogen-bonding interactions between its two precursors that often result in negative deviations from Raoult's law, i.e., $a_{12} < 0$. This implies that the Henry's constant in the mixture is larger and thus the solubility is smaller.

Conclusions

In this section, a new methodology for the parameterization of solid DES precursors in the framework of SAFT-type EoSs is shown to be necessary and proposed, overcoming the limitations of the current approaches, while achieving a better performance. The new approach was successfully illustrated for the most used DES precursor, the [Ch]Cl salt, using the soft-SAFT EoS.

Firstly, using information from MD simulations and ab initio calculations available in literature about the type and magnitude of the hydrogen-bonding interactions present in some [Ch]Cl-based DES, a more realistic association scheme with five associating sites was proposed to describe the hydrogen bonding character of [Ch]Cl. Then, the molecular parameters characterizing the associating sites were transferred from literature or obtained through an empirical approach proposed in this work without further fitting, while the non-associating pure-component parameters were obtained from fitting to experimental data that can be easily measured for any DES, namely high-pressure liquid densities and SLE data.

The accuracy and robustness of the new CG model was then demonstrated through the successful description of a wide variety of [Ch]Cl-based DES with seven different HBDs and include densities, VLE, and SLE of pure DES, and their mixtures with water and CO₂ in wide temperature, pressure and composition ranges. The new approach is easily applicable to other solid DES precursors, e.g., urea, enabling the correct thermodynamic modelling of other typical DES such as [Ch]Cl + urea which should be the aim of future works.

6.2- Remarks on the Thermodynamic Modelling of Protic ILs

The content of this section is based on the following submitted manuscript, where E.A. Crespo was responsible for the modelling tasks and for writing the manuscripts, with substantial contributions from the remaining authors.

- Emanuel A. Crespo, Liliana P. Silva, Pedro J. Carvalho, and João A.P. Coutinho, “*The Excess Molar Volumes of Protic Ionic Liquids and Its Significance to their Thermodynamic Modelling*”, submitted to Fluid Phase Equilibria.

Introduction

Over the last decade, research on PILs shows a significant increase, sustained by a large number of different applications in fields such as greenhouse gas capture, liquid-liquid extractions, polymer synthesis, as catalysts for organic synthesis, non-aqueous amphiphile self-assembly solvents, electrolytes for fuel cells, batteries, capacitors, among many others that have been summarized in comprehensive reviews.[350,351] Within the Oil & Gas industry, they have been gathering an increasing interest from both industry and academia as potential solvents for CO₂ absorption,[39–43] oil desulfurization,[44,45] methane hydration inhibition,[46] asphaltenes extraction or stabilization,[47,48] among others. However, the increasing amount of information on PILs has not been followed by the development of thermodynamic modelling approaches that can reliably provide or describe their behaviour. This is due to the lack of experimental data that can be used to provide a robust parameterization of the model, but also due to the inner complexity of PILs, resembling some of the issues faced with DESs.[334,352,353]

Although quite different in nature, PILs and DESs do share common features. Both are essentially mixtures of Lewis or Brønsted acids and bases, differing essentially in the ΔpK_a . [24,350] PILs are prepared through the stoichiometric neutralization reaction of acids and bases with the subsequent proton transfer from a Brønsted acid to a Brønsted base. This proton transfer will be complete only if the ΔpK_a is large enough (typically above 10[354]), otherwise the proton transfer will be partial with neutral molecular precursors coexisting in solution with ion pairs and ionic species. On the other hand, DESs are mixtures of weak Lewis or Brønsted acids and bases that although usually solid at room temperature, present an eutectic temperature much lower than that predicted assuming an ideal behaviour, mostly due to the presence of strong hydrogen bonding between the two molecular precursors, yielding solvents with interesting properties in a wide liquidus temperature range.[24,25] Although their differences in acidity lead to strong hydrogen bonding, no significant proton transfer takes place on these systems.

Due to the relevant role of hydrogen bonding on the behaviour of both PILs and DESs, SAFT-based models stand as one of the most appropriate and versatile tools to describe them. However, despite being already widely applied for DES,[334,352,353] the thermodynamic modelling of PILs using molecular-based EoSs is still in its infancy. Alcantara et al.[355,356] used the sPC-SAFT EoS[65] to model the high-pressure vapor-liquid equilibrium (VLE) of binary mixtures comprising CO₂ and other gases with PILs based on amines or ethanolamines and butanoic acid, by using a pseudo-pure component approach to describe the PIL, and obtaining the correspondent parameters by fitting to the experimental liquid densities and speed of sound of the PIL. Afsharpour[357] reported the use of CPA EoS to describe the CO₂ and H₂S solubility in four different PILs based on ethanolamines. The pure-component parameters for each PIL were regressed using only 12 density points at atmospheric pressure and, consequently, a complex temperature dependency of the binary interaction parameter between the gas and the IL was required to successfully describe the experimental data. Baird and co-workers[358,359] applied the ePC-SAFT[360] to describe the densities and vapor pressures of aqueous solutions of 7-methyl-1,5,7-triazabicyclo[4.4.0]dec-5-enium acetate. To better represent the complexity of PILs, both ionic and molecular species were considered; however, the proton transfer has been considered to be complete and molecular species were only considered if excess acid or base was added to the solution. Moreover, due to the number of different species, and the complex temperature-dependencies employed, a total of 17 parameters were required to fully describe the PIL aqueous solution.

Recently, the soft-SAFT EoS was used to describe carboxylate-based carboxylate-based PILs and their mixtures with CO₂[361,362], with the PIL parameters being obtained by fitting $p\rho T$ data and second-order derivative properties. In both works, even though PILs are, to a fair extent, mixtures (of neutral acid and base molecules, ion pairs and ionic species), they were modelled under a pseudo-pure component approach, as was also commonly done in the inception of DESs modelling using SAFT EoSs. Although this approach has been correctly, and with success, applied to the modelling of aprotic ILs, for PILs this approach is only adequate when the ΔpK_a is large enough[354] (typically above 10). Furthermore, even then, it is only adequate if no excess base or acid is present (note that other solvents may also displace the equilibrium).

This work aims to provide insights on why, as previously established for DESs,[334] it is important to, at least in some situations, be able to describe PILs using an individual-component approach, ideally starting from its precursors. It will be shown that, contrarily to what is observed for DES, the properties of a PIL (the density will be here used since it is the property most widely available for PILs) cannot be directly predicted from its precursors. To explain the reasons for such behaviour, a striking difference between PILs and DESs is disclosed and discussed, highlighting the distinct

challenges, compared to those found for DES, of developing SAFT models for PILs. Afterwards, it is shown how the individual-component approach can be corrected to account for the characteristic excess molar volumes (V^E) found in PILs, enhancing the predictive ability and applicability of the model, compared to the commonly used pseudo-pure component approach. All the modelling results shown in this chapter are carried out using the PC-SAFT EoS, as an example of a common SAFT-type EoS, widely implemented in thermodynamic calculation packages and most commercial process simulators.

Results and Discussion

The most common purification procedure of PILs consists of a distillation under vacuum. It is known that this process can lead to the formation of ‘mixtures’ with an acid:base proportion different than the expected 1:1 that can be related to the formation of oligomeric anions.[363–365] There are also evidences for the formation of azeotropes at molar ratios close to the 2:1 stoichiometric proportion in carboxylate-based PILs,[366] since during the distillation process, one of the precursors can be removed to a greater extent than the other, leading to a mixture enriched in the other component.[351] The strategy of using PILs with oligomeric ions or PILs with variable or poorly defined stoichiometry has been pursued with success by some authors expanding the PILs field, while making it more complex to deal with from a modelling point of view.[367–369]

Recently, the soft-SAFT EoS was used to describe carboxylate-based PILs and their mixtures with CO_2 . [361,362] Those works show that despite its good performance, the pseudo pure-component approach cannot be applied to describe mixtures containing different or variable acid:base stoichiometries, as the modelling of a different composition would require the refitting of the parameters, defining a new pseudo-pure component. Moreover, the predictive modelling of a different PIL, even if containing only common precursors with previously studied PILs, is not possible. This was the same issue previously observed in the modelling of DESs as the solvent’s properties could also be tuned by using different HBD to HBA ratios, although in the case of DESs, the use of a pseudo-pure component approach also suffers from the problem of inhibiting the study of their SLE which lays the foundation of the DES concept itself.

Therefore, a similar solution should be attempted to model PILs using a SAFT-type EoS, and the use of an individual-component approach should become standard. Hence, as most PILs investigated in literature are obtained from the mixture of an amine and a carboxylic acid, the PC-SAFT EoS parameters for monoethanolamine (MEA), diethylamine (DEA), di-n-butylamine (DBA), acetic acid, propionic acid, butanoic acid, pentanoic acid, and hexanoic acid were first retrieved from the literature,[370–375]

and verified to accurately represent their liquid densities and vapor pressures. Furthermore, new PC-SAFT parameters were obtained by fitting to experimental liquid densities and vapor pressure data for diethylethanolamine (DEEA) and methylethanolamine (MeEA). Both the literature parameters and those obtained in this work are reported in **Table 6.8**, along with all the relevant references.

Table 6.8. PC-SAFT EoS parameters used in this work and volume-shift type corrections employed.

Compound	Mw (g/mol)	m_i	σ_{ii} (Å)	ϵ_{ii}/k_B (K)	Assoc. Schem.	ϵ^{HB}/k_B (K)	κ^{HB} (Å ³)	Ref.	c_i
Diethylethanolamine	117.19	3.844	3.6406	248.55	2B	2033.2	0.02412	*	7.50
Monoethanolamine	61.08	4.521	2.6574	237.69	4C	989.9	0.18753	[370]	11.52
Diethylamine	73.14	3.424	3.3851	219.77	2B	1094.0	0.01100	[371]	20.09
Di-n-butylamine	129.24	5.095	3.5742	234.78	2B	1621.5	0.01400	[371]	10.85
Methylethanolamine	75.11	4.086	3.0108	251.41	2B	2034.4	0.02412	*	12.18
Acetic acid	60.05	2.597	3.0474	190.22	2B	2379.0	0.36832	[372]	8.94
Propionic acid	74.08	3.258	3.1047	192.67	2B	2647.5	0.19275	[373]	8.76
Butanoic acid	88.10	4.183	3.0734	198.08	2B	2409.8	0.26223	[374]	5.68
Pentanoic acid	102.13	4.300	3.3069	259.55	2B	1938.5	0.03140	[375]	5.95
Hexanoic acid	116.16	3.496	3.7510	283.68	2B	2975.7	0.00780	[375]	5.55

*- The PC-SAFT pure-component parameters for these compounds were regressed in this work by fitting to experimental liquid densities and vapor pressure data. For diethylethanolamine, the data was retrieved from references,[376–380] while for methylethanolamine data was obtained from reference [381].

These parameters were used to predict the atmospheric pressure densities of different PILs (1:1 acid:base ratio) with ammonium cations, by modelling the PILs as an equimolar mixture of the acid and the base. The results obtained for the carboxylate-based PILs are shown in **Figure 6.1** and show that the PC-SAFT EoS fails to predict the densities of these PILs, using an individual-component approach. This is different from the behaviour observed in DESs where, despite their non-ideality, the solvent densities could be easily and accurately obtained by modelling it as a mixture of the HBD and HBA, with the correspondent composition.[334]

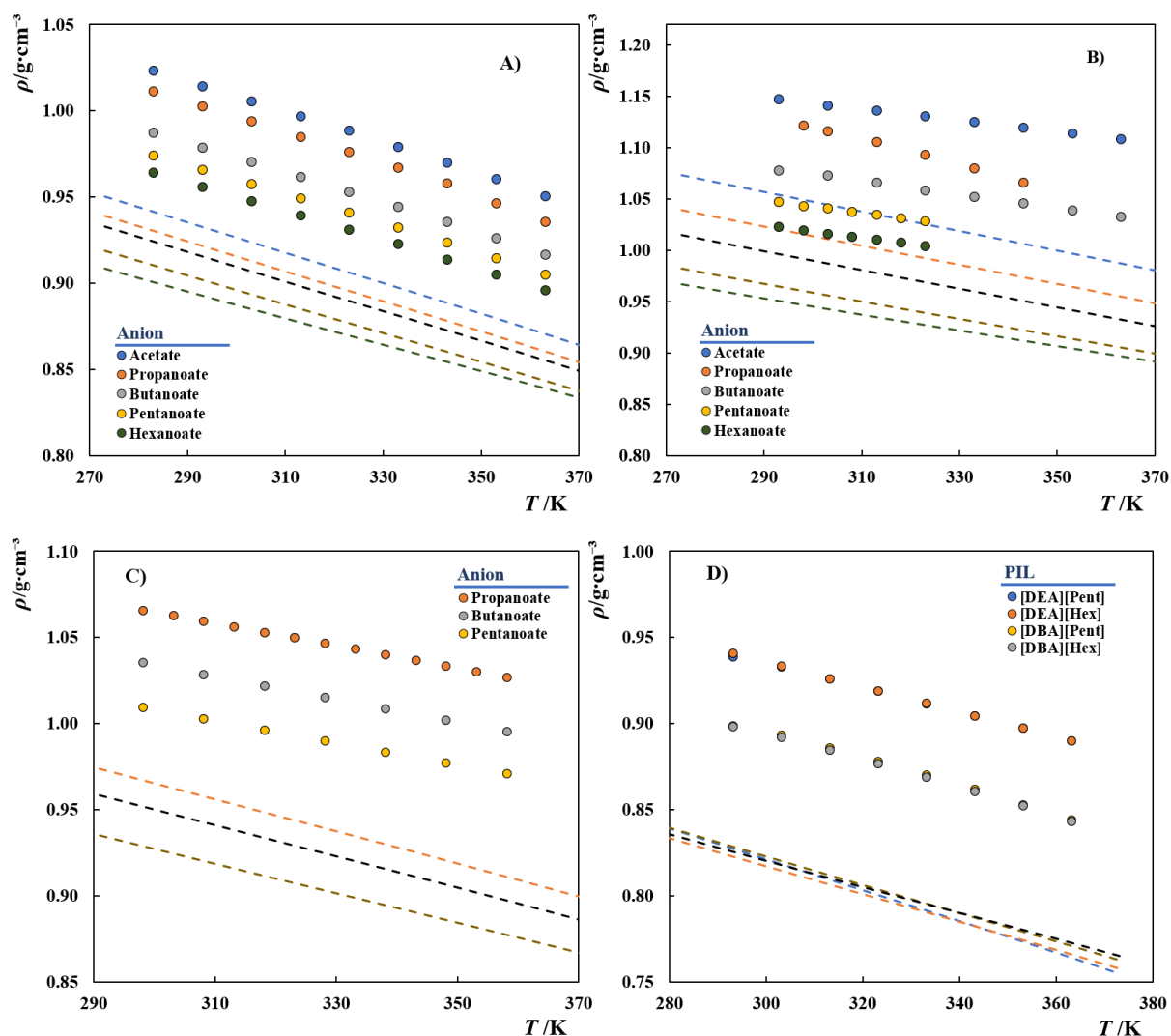


Figure 6.15. Liquid densities, at atmospheric pressure, of carboxylate-based PILs with a 1:1 acid:base ratio, with the following base precursors: A) DEEA, B) MEA, C) MeEA, and D) DEA/DBA. Symbols represent experimental data,[43,361,382–385] while the dashed lines depict the PC-SAFT predictions.

Aiming at understanding the origin of the decreased performance of the model in describing the density of PILs, the excess molar volumes (V^E) for 23 different DESs and 35 different PILs were determined from density data and are provided in **Table H.1** and **Table H.2**, in **Appendix H**. **Figure 6.16** shows the average V^E for the different systems and the same values normalized by the ideal molar volume of the mixture in order to mitigate the effect of Mw . As can be observed, despite their non-ideality, DESs exhibit very low negative V^E and, for that reason, SAFT-type EoSs could easily predict the DES densities.[334] On the other hand, PILs exhibit considerably higher V^E , whose value depends

greatly on the PIL precursors as demonstrated by the data scattering, preventing the model from accurately predict the PIL behaviour from a mixture of its precursors.

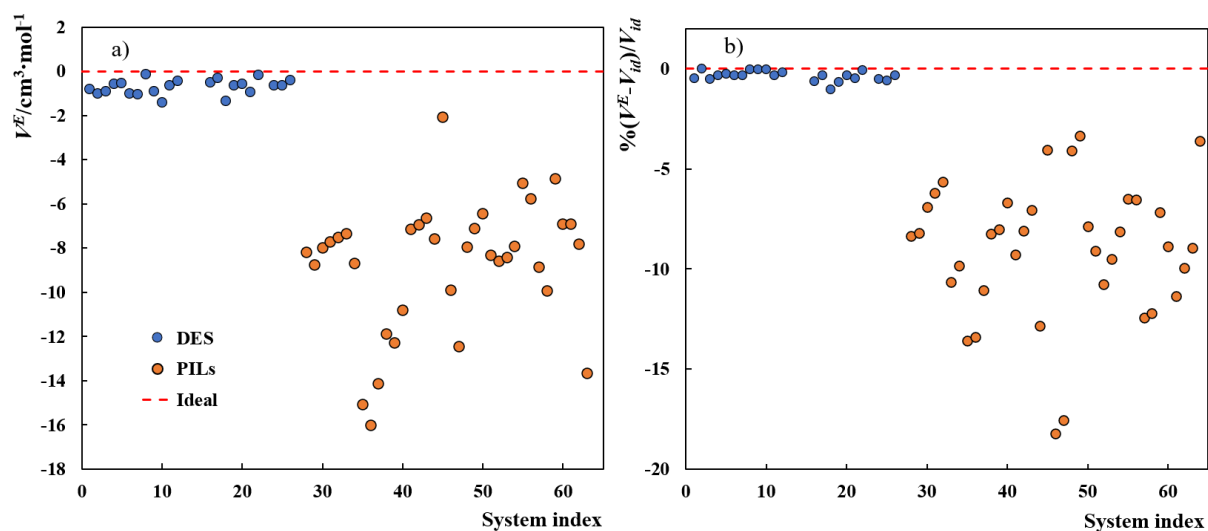


Figure 6.16. a) Excess molar volumes, V^E . b) molar volume deviation from the ideal molar volume, (V^{id}), for different PILs and DESs.

Nasrabadi and Gelb[386] used molecular dynamics simulations to investigate the effect of proton transfer on the density, viscosity and conductivity of different PILs. It was shown that PILs density increase with the degree of proton transfer that was reported to vary with the amine hybridization. This result along with the fact that the extension of proton transfer is indeed one of the main differences between DES and PILs (both are mixtures of Lewis or Brønsted acids and bases), it can be concluded that the large negative V^E observed in PILs are related to the formation of ion pairs in PILs while DES, being solely composed of neutral molecular species, present negligible V^E . Therefore, the formation of those ionic species and the effect that such formation has on the thermophysical properties must be considered when modelling PILs using molecular-based EoSs.

Clearly, one of the most appropriate methods to account for the presence of ionic species would be to use a SAFT-type EoS that contains an electrolyte term to explicitly account for Coulombic interactions, such as ePC-SAFT[360] that has already been applied to describe aprotic ILs.[387] However, in PILs, the proton transfer is incomplete and the degree of proton transfer is usually unknown. Consequently, neutral acid and base molecules coexist in solution with the ionic species, their detailed composition being unknown, hampering the application of such models. Aggregation and association of ions and neutral species, forming oligomeric ions,[365] will also take place, and applying electrolyte SAFT models would not only require a deeper knowledge of the speciation on this system than currently

exists, but also the fitting of a number of parameters to each and every species present, using a very limited amount of experimental data. In fact, for most PILs only density at atmospheric pressure is available to use in parameter regression, reinforcing the importance of measuring density in wide temperature and pressure ranges for PILs as recently discussed by us.[361] Moreover, electrolyte SAFT models are still not widely available in most commercial process simulators.

Another alternative to be further explored in this work is to account for the effect of proton transfer in the V^E of PILs in an implicit manner. Assuming that the formation of an ionic species (regardless of an ion pair or isolated ions) correspondent to the protonation/deprotonation of a given acid/base results in a given relative perturbation to the V^E , expressed in terms of percentage deviation from the ideal molar volume of the mixture of the PIL (**Figure 6.16 b**), an improved description of density, and an improved predictive ability of the model can be obtained using a volume-shift type correction expressed by **eq. 6.6**, where Vm_{mix}^C is the corrected molar volume of the PIL, Vm_{mix}^o is the molar volume of the PIL as predicted by the PC-SAFT EoS considering it as a simple mixture of its precursors, and c_i is the relative percentage correction to the molar volume of the PIL, due to the formation of the cation/anion by proton transfer from/to its correspondent precursor.

$$Vm_{mix}^C = Vm_{mix}^o \left[x_{acid} \left(1 - \frac{c_{acid}}{100} \right) + x_{base} \left(1 - \frac{c_{base}}{100} \right) \right] \quad (6.6)$$

For simplicity, **eq. 6.6** can be rewritten as **eq. 6.7**, where c_{mix} is the correction to the mixtures molar volume due to proton transfer obtained from **eq. 6.8** as a linear mixing rule of the correction parameters.

$$Vm_{mix}^C = Vm_{mix}^o \left(1 - \frac{c_{mix}}{100} \right) \quad (6.7)$$

$$c_{mix} = \sum_{i=1}^{NC} x_i c_i \quad (6.8)$$

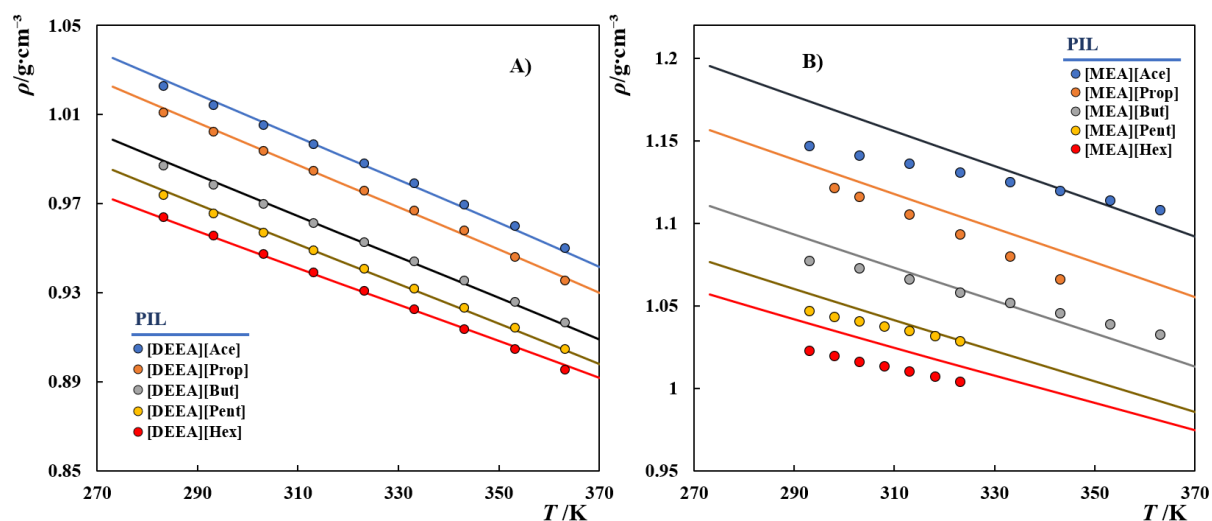
It is worth to note that the correction is here implemented in terms of relative corrections to the molar volume instead of an absolute correction, as typically done in volume-shift corrections, because the lower scattering of the data observed in **Figure 6.16 b** suggests that avoiding the effect of Mw can result in a better correlation.

This approach was thus implemented together with PC-SAFT EoS to describe the densities of PILs synthesized from the reaction of carboxylic acids (acetic up to hexanoic acid) with five different amines (DEEA, MEA, DEA, DBA, and MeEA). In a first step, the values of c_i for acetic, propanoic, butanoic, pentanoic and hexanoic acids and that of DEEA were fitted simultaneously to density data from the correspondent PILs and are reported in **Table 6.8**. As depicted in **Figure 6.17A**), this approach

allows an accurate description of the densities of PILs with DEEA as precursor. It is worth to highlight that even though the correction can only induce a y-axis translation of the PC-SAFT predicted density, an excellent description of the temperature effect is obtained through fitting. Afterwards, the c_i values for the remaining amines, namely [MEA], [MeEA], [DEA], and [DBA] were obtained by fitting to the liquid densities of a single PIL containing the correspondent amine as base precursor, namely [MEA][But], [MeEA][But], [DEA][Pent], [DBA][Pent], and used to predict the density of the PILs with the remaining carboxylic acids. As shown in **Figure 6.17 B-D**), the results display a remarkable improvement when compared to those without any correction, previously shown in **Figure 6.15**.

The good prediction of the PILs density for which no experimental data was used in the parameterization of the c_i values demonstrate the importance of accounting for the effect of proton transfer in the density modelling, and how it can be easily implemented to enhance the accuracy and the predictive ability of the model. In this way, the binary interaction parameters between the acid and the base can later be freely adjusted to describe the VLE/azeotropic behaviour of the PIL (if reliable experimental data ever becomes available), while assuring the correct description of its volumetric properties. Evidently, the densities description shown in **Figure 6.17** still have room for improvement, but the volume-shift type correction employed has several simplifications that could be overcome in a more detailed study. Firstly, the correction made to the molar volumes is temperature-independent and based on an average value of V^E in the temperature-range where experimental density data of the PIL was available (which may vary across the different PILs), while in fact the values tend to decrease with temperature, partially explaining the weak temperature dependency of the predictive results depicted in **Figure 6.17**.

Figure 6.17.



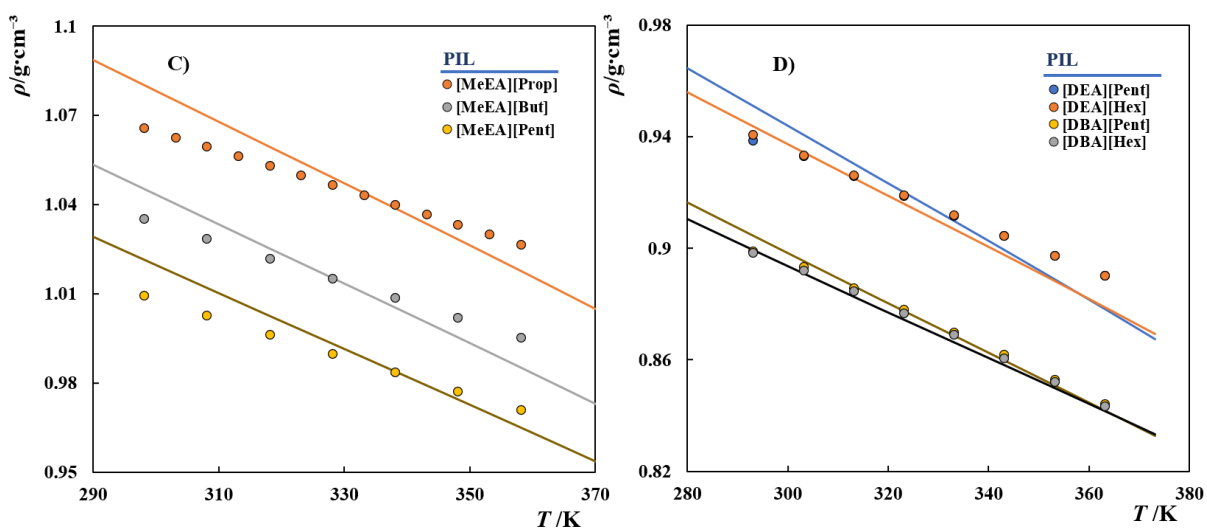


Figure 6.17. Densities at atmospheric pressure of different PILs. Symbols represent experimental data,[43,361,382–385] while the solid lines depict the PC-SAFT EoS modelling results, corrected to account for the effect of proton transfer.

Furthermore, the impact that the formation of a given cation/anion has on the PILs properties, (e.g. the presence of the acetate anion in an ion pair) is not independent of the base precursor with which it is paired, because the degree of proton transfer highly depends on the acid/base pair. This is corroborated by the work of Nasrabadi and Gelb,[386] where the degree of proton transfer was shown to decrease from primary to secondary and tertiary amines for a same carboxylate anion. The V^E values relative to the ideal volume of the mixtures determined for carboxylate-based PILs with different amines as base precursors are plotted in **Figure 6.18**, as a function of the carboxylic acid's Mw and reinforce the conclusion obtained by Nasrabadi and Gelb[386]. As the degree of proton transfer is strongly affected by the acid:base making up the PIL, being higher for primary amines, the effect on the molar volume of the PIL increases in the same direction, with the relative V^E in [MEA][X] PILs being more negative than those in the tertiary amine DEEA. **Figure 6.18** also shows that the effect on the PILs molar volume for an homologues series of carboxylic acid increases linearly with the acid's Mw . Therefore, if one wants to employ a correction as the one suggested in this work with the c_i values further depending on the base precursor, linear correlations of the c_i value as a function of the acid's Mw should be expected for a given homologous series, allowing the prediction/extrapolation of the behaviour of PILs with different chain length acids, without further measurements and parameterizations.

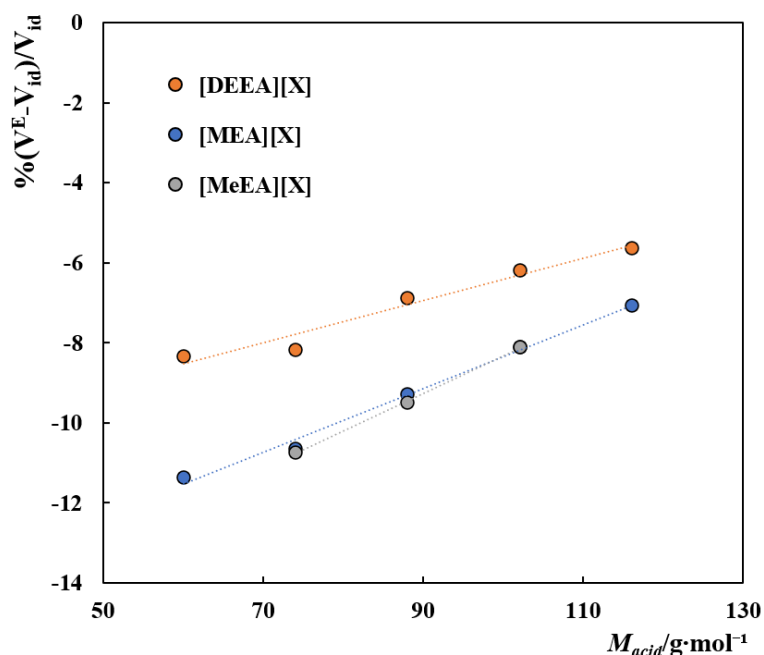


Figure 6.18. Percentage relative excess molar volumes of carboxylate based PILs with different amines as base precursors.

Finally, as initially mentioned, one of the main objectives of using an individual-component approach is to be able to predict the properties of PILs that although made up of the same precursors have distinct acid:base stoichiometric ratios. This is important because in an industrial process, the concentration of the different species will vary along the distillation columns.[366] Therefore, the modelling approach proposed in this work, with the c_i values reported in **Table 6.8**, were used to predict the densities of PILs based on the *N,N*-diethylethanolammonium cation (DEEA as base precursor) and a 2:1 acid:base ratio. The modelling results are shown in **Figure 6.19**, with and without the correction to the molar volumes and, as can be observed, using the proposed methodology, a good prediction of the composition effect on the PILs density can be obtained, without further parameterizations.

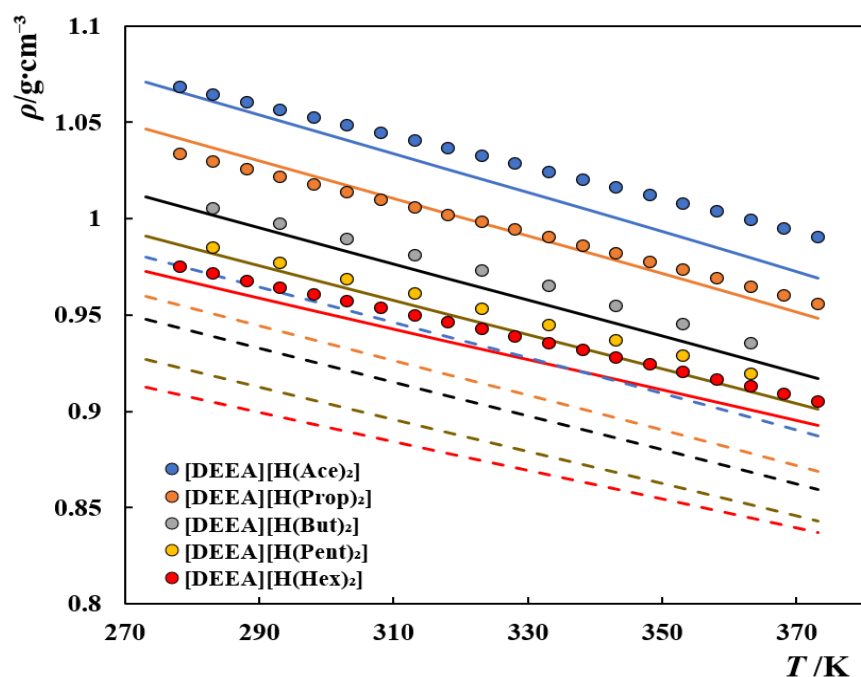


Figure 6.19. Density of PILs based on the DEEA cation. Symbols represent experimental data,[364] while the solid and dashed lines represent the PC-SAFT predictions with and without correction of the molar volumes.

Perspectives and Conclusions

In this section, a discussion on the thermodynamic modelling of PILs using SAFT-type EoSs is provided. It is discussed how, as previously proposed for DESs, being able to predict their thermodynamic behaviour from that of its precursors is useful for an enhanced predictive/extrapolative ability of the model and to enable the modelling of different acid/base compositions without additional parameterizations. Contrarily to DESs, where the behaviour of the solvent could be directly predicted from its precursors, the highly negative excess molar volumes observed in PILs, arising from the proton transfer between the acid and the base, were found to result in very poor predictions of the PILs density.

Therefore, to improve the accuracy and predictive ability of the model, a simple correction to the molar volume of the PILs is proposed, assuming that the formation of each ion in the mixture induces a certain change in the PILs molar volume. Despite the simplifications of the proposed correction, a remarkable improvement in the results is obtained with the model being able to successfully predict the densities for PILs whose data was not used in the parameterization and to predict the densities of PILs with variable stoichiometry. The results obtained highlight the importance of considering the excess volumes of PILs during the development of SAFT models and can still be further improved by avoiding some of the simplifications here adopted, such as the use of temperature-independent corrections and the assumption of a constant effect of the ionic species regardless of the PIL precursors.

7- Final Remarks

“Research is to see what everybody else has seen, and to think what nobody else has thought.”

Albert Szent-Gyorgyi

7.1- Conclusions

This thesis aimed at the development, improvement and analysis of thermodynamic modelling approaches used to describe the phase behaviour and thermophysical properties of ethylene oxide-based compounds and alternative solvents that may be relevant for the Oil & Gas industry.

After a general introduction to set the context and explain the interest from the Oil & Gas industry in these systems and in obtaining accurate thermodynamic models for them (**Chapter 1**), and a thorough description of the modelling techniques employed, namely SAFT-type EoSs and CG-MD simulations (**Chapter 2**), the work starts by showing, in **Chapter 3**, how a thermodynamic model for glycols and glymes can be simplified, improving its computational efficiency, without compromising its accuracy. In this chapter, the development of a refined CG model for glycols and glymes, with enhanced transferability, was presented, in the framework of the soft-SAFT EoS. It is the first time that, considering the chemical similarities between glycols and glymes, the same modelling approach is followed to describe both families of compounds, in a large range of molecular weights. The new model was not only shown to provide a more accurate description of the thermodynamic behaviour for low molecular weight oligomers, but also to be able to reasonable predict, without further fitting, the behaviour for compounds of increased chain length (e.g., PEGs), or blends (e.g., PEGDME 250).

Furthermore, knowing of the application of these polyethers as dehydration agents, gas hydrate inhibitors, as solvent for CO₂ separation, or acid gas removal from natural gas streams, the phase behaviour of several binary mixtures of interest (e.g., glycol/glyme + gases/water) was successfully described using the proposed model. In some cases, correlations for the necessary binary interaction parameters, as a function of the glycol/glyme molecular weight were also proposed, yielding fully predictive screening tools that can be used to investigate the effect of small structural changes on the system's behaviour, without the need for expensive measurements. As an example, the phase behaviour of a binary mixture glyme/blend of glymes + CO₂ can now be described in the absence of experimental data, i.e., the pure-component parameters for the solvent CG model are obtained from the correlations obtained for the investigated pure oligomers, and the binary parameter between the solvent and the gas is retrieved from the trends observed for the binary parameter in the studied mixtures.

C_iE_j non-ionic surfactants are made of the same functional groups present in glycols and glymes, namely CH₃, CH₂, EO, and OH but, contrarily to them, they are mostly present in the form of an aqueous solution. This poses a considerable constraint in the model parameterization, since the pure-component parameters of SAFT models are usually obtained by fitting to the experimental saturated densities and vapor pressures of the pure fluid that are in this case unavailable. For this reason, SAFT models, despite

being the most appropriate to describe associating molecules, are seldomly applied to model the phase behaviour of systems containing C_iE_j surfactants. Therefore, in **Chapter 4**, the use of a heteronuclear SAFT-type EoS, namely SAFT- γ -Mie, is proposed to describe the complex phase behaviour of C_iE_j + water mixtures. In this way, all the necessary functional groups could be parameterized by using abundant experimental data for *n*-alkanes, alkan-1-ols, glycols and glymes, where those groups are present, and used to predict the behaviour of the surfactants. Unfortunately, despite this kind of transferability being the brand of heteronuclear models, it is here shown that the transferability of a given functional group, across different families of compounds, is considerably limited, and often masked by the parameterization of an additional group. Nevertheless, even though the behaviour of C_iE_j + water mixtures could not be predicted using this approach (closed-loop immiscibility regions are not captured), it can be described by refitting the parameters governing the interactions between the EO groups and water. Thus, considering the limitations and scarcity of available SAFT models for these systems, it still represents a good starting point for future studies aiming at the extension of the model to describe surfactant-related properties like surface/interfacial tensions or CMC that, so far, have been described independently of the macroscopic phase behaviour.

These surfactants, when in aqueous solutions, self-assemble to form a variety of 3-D structures, ranging from micelles of different shapes, at low surfactant concentrations, to highly ordered liquid crystalline phases, at high surfactant loadings. In **Chapter 5**, MD simulations, using the MARTINI FF, were carried out for a large number of surfactants to unveil the mesophase behaviour of these systems, and better understand the effect of surfactant concentration and the length of the hydrophobic and hydrophilic moieties on the phase behaviour. The good agreement observed with experiments shows how a highly transferable, general-purpose FF like MARTINI, even though initially developed for MD simulations of biological systems, can be useful to provide a better understanding of chemical systems, that may be of interest for a much broader range of fields, including Oil & Gas. Once the model was shown to provide reasonable descriptions for the binary systems, remarks on its applicability to the modelling of more complex systems, such as surfactant + oil + water and surfactant + oil + water + surface were provided to guide further studies on this topic, which is particularly relevant for the development of new surfactant systems and in the design of new injection fluids to use in EOR technologies.

Finally, considering the boom of Green Chemistry, and the need for the development of more sustainable and environmentally friendly processes and technologies, **Chapter 6** discussed new modelling approaches for the description of alternative solvents being currently investigated for several applications in the Oil & Gas industry, namely DESs and PILs, using SAFT-based EoSs. In the case of

DESs, many precursors used in their preparation are solid. Consequently, vapor pressures and saturated liquid densities are unavailable to parameterize their CG models. Instead, different authors have opted to either describe the DES as a pseudo pure-component approach, or to obtain the required parameters by fitting to experimental data of their aqueous solutions. In **Chapter 6.1**, the limitations of these approaches were adequately discussed, and a new methodology for the parameterization of solid DES precursors was proposed. The methodology was illustrated for [Ch]Cl, one of the most used precursors, and shown to provide an accurate description of different [Ch]Cl-based DES. Concerning PILs, although density data is widely available, vapor pressures are negligible. Furthermore, despite being mixtures of an acid and a base, they have also often been described using a pseudo-pure component approach. This method prevents the investigation of systems with variable acid:base ratios that can be observed after the purification process, using the same model and parameters, paving the way for the development of individual-component approaches to model PILs. However, in **Chapter 6.2**, PILs are shown to exhibit considerably negative excess molar volumes, compared to those observed in DES, preventing the direct modelling of a PIL as a mixture of the acid and base used in their preparation. It is then shown how this characteristic can, and should, be incorporated in the modelling to improve the accuracy and enhance the applicability of SAFT models.

In summary, this doctoral work provides an update on the thermodynamic modelling approaches used to describe the thermodynamic behaviour of glycols, glymes, C_iE_j surfactants, DES, and PILs, as necessary for the design and simulation of new processes, and optimization of existing operations, in the Oil & Gas industry. Not only the limitations of current methods are disclosed and discussed, as alternative models or methodologies are proposed aiming at overcoming some of the existent drawbacks, or at improving their accuracy, transferability or applicability.

7.2- Future Work

Thermodynamic modelling continues to be a very active research topic; not only because new systems are being investigated for novel applications, but also because even small improvements in a certain model can justify their adoption by process and project engineers responsible for the design and simulation of industrial processes.

In **Chapter 3**, it is shown that even though computational efficiency & accuracy will always represent a compromise, many models can be considerably simplified without a noticeable influence on the accuracy. This is particularly important in SAFT-based models due to the computational burden of the association term but, unfortunately, the choice and analysis of different association schemes to apply for a given molecule are rarely discussed, even though it should be part of a systematic model development procedure. The physical meaning of the parameters, that enables the model to predict the behaviour for different compounds and mixtures than those investigated experimentally, should always be discussed appropriately when reporting new model parameters, as done in **Chapter 3.2**. This helps ensuring that a reasonable and consistent set of parameters is proposed compared with other families and decreases the probability of finding multiple set of parameters for the same compound, within the same EoS. Furthermore, as a future work, the models proposed in **Chapter 3**, should be employed to describe a wider range of binary and multi-component mixtures of interest to the Oil & Gas industry, e.g., glymes + CO₂ + H₂S + CH₄ that is relevant to reproduce a gas sweetening process, but unfortunately experimental data is not always available or is proprietary, so experimental measurements should now focus towards ternary and multi-component systems, given that binary data is becoming widely available in the literature.

The most acknowledged heteronuclear SAFT variant was shown in **Chapter 4** to exhibit a very poor transferability of the functional groups across different families for the cases considered in this PhD work. Nevertheless, given the lack of SAFT modelling approaches available to describe the behaviour of C_iE_j surfactants, and in absence of more appropriate parameterization methodologies for these molecules, these EoSs, given that they can describe the complex closed-loop immiscibility regions observed in their aqueous solutions, should still be extended in the future for the description of additional properties, relevant for surfactant-like systems, such as surface/interfacial properties, density profiles, average aggregation numbers and critical micellar concentration, whose modelling is usually addressed separately from their macroscopic phase split. Although these properties can also be obtained through

MD simulations, an integrated approach based on an EoS, able to provide both phase equilibria and this type of properties, would clearly be more computational efficient.

It was discussed in **Chapter 5**, how CG-MD simulations can be used to complement the information obtained using EoSs, by providing a link between the microscopic-level behaviour of the systems and macroscopic properties. The MARTINI FF, although initially developed for biological systems, can be extremely useful for a better understanding of chemical systems, due to its highly transferable nature. This FF was shown to be able to provide a good description of the self-assembly behaviour of $C_{12}E_8$ surfactants in water, but additional work is required prior to investigate the addition of oil, or to simulate the interactions with a surface (representing the rock reservoir) to help in the formulation of surfactant systems for EOR applications. Namely, the water model in the MARTINI 2.0 FF suffers from several limitations, and there are reasons to believe that the results obtained here, especially for the multi-component systems, can be substantially improved, by using the MARTINI 3.0 FF which was published very recently, instead of the MARTINI 2.0 version. The larger number of bead types, with smoother variations of energy, more refined mappings, and existence of more interaction levels, are expected to allow for a more appropriate modelling of the different components, and to better capture their physical features. It is expected that exploring these systems using the new version of the FF would bring exciting results and a better understanding of the phenomena going on during EOR at the microscopic level.

Concerning the modelling of alternative solvents in **Chapter 6**, the methodologies discussed here may inspire further developments in the field. For DESs, an interesting methodology is proposed but, as observed for glycols and glymes, the method can probably be simplified and become computationally more robust. The existent software must also be adapted to allow for the parameterization of pure-component parameters using different kinds of experimental data. For PILs, further experimental studies aiming at quantifying the degree of proton transfer or understanding the azeotropic behaviour of some PILs, would be useful to improve and better evaluate current thermodynamic models.

As a final thought, I feel that the applied thermodynamics community would benefit from an increased number of open-source software, by enhancing collaborative work, and by involving groups from different backgrounds, that do not have the time or resources to develop their own codes and algorithms. Or, as more simply put by Howison & Herbsleb: “It seems likely that significant software contributions to existing scientific software projects are not likely to be rewarded through the traditional reputation economy of science. Together these factors provide a reason to expect the over-production of independent scientific software packages, and the underproduction of collaborative projects, in which later academics build on the work of earlier ones.”

List of Publications

“Do not go where the path may lead, go instead where there is no path and leave a trail”

Ralph Waldo Emerson

The publications listed below refer to the scientific contributions, in the form of scientific papers published in international peer-reviewed journals, made by the candidate, during the 2017-2021 period. In the different works, **Emanuel A. Crespo** was held responsible by the modelling tasks (using SAFT models or MD simulations), and by writing/co-writing with the first author the correspondent manuscripts.

1. **Emanuel A. Crespo**, Pedro Morgado, Eduardo J. M. Filipe, and João A. P. Coutinho, “*Applying Heteronuclear SAFT models to the modelling of ethylene oxide-based compounds*”, in preparation.
2. **Emanuel A. Crespo**, Liliana P. Silva, Pedro J. Carvalho, and João A. P. Coutinho; “*The excess volumes of protic ionic liquids and its significance to their thermodynamic Modelling.*”, Fluid Phase Equilibria, submitted to Fluid Phase Equilibria (2021).
3. Liliana P. Silva, **Emanuel A. Crespo**, Mónia A. R. Martins, Ramesh L. Gardas, Lourdes F. Vega, João A. P. Coutinho, and Pedro J. Carvalho; “*Evaluating sustainable encapsulated protic ionic liquids for CO₂ capture and separation.*”, submitted to Separation and Purification Technology (2021).
4. **Emanuel A. Crespo**, Liliana P. Silva, Cristina I. P. Correia, Mónia A. R. Martins, Ramesh L. Gardas, Lourdes F. Vega, Pedro J. Carvalho, and João A. P. Coutinho; “*Development of a robust soft-SAFT model for protic ionic liquids using new high-pressure density data.*”, Fluid Phase Equilibria, 539 (2021), 113036; DOI: 10.1016/j.fluid.2021.113036
5. **Emanuel A. Crespo**, Lourdes F. Vega, Germán Pérez-Sánchez, and João A. P. Coutinho, “*Unveiling the phase behavior of C_iE_j non-ionic surfactants in water through coarse-grained molecular dynamics simulations.*”, Soft Matter (2021), Advance Article; DOI: 10.1039/D1SM00362C
6. **Emanuel A. Crespo**, Nicolas Schaeffer, João A. P. Coutinho, and Germán Pérez-Sánchez, “*Improved coarse-grain model to unravel the phase behavior of 1-alkyl-3-methylimidazolium-based ionic liquids through molecular dynamics simulations.*”, Journal of Colloid and Interface Science, 574 (2020), 324-336; DOI: 10.1016/j.jcis.2020.04.063
7. **Emanuel A. Crespo**, Naima Chouireb, O. Tafat-Igoudjilene, Lourdes F. Vega, Pedro J. Carvalho, and João A. P. Coutinho, “*Isobaric vapor-liquid equilibrium of water + glymes binary mixtures: Experimental measurements and molecular thermodynamic modelling*”, Fluid Phase Equilibria, 513 (2020), 112547, DOI: 10.1016/j.fluid.2020.112547
8. Sérgio M. Vilas-Boas, Dinis O. Abranches, **Emanuel A. Crespo**, Olga Ferreira, João A. P. Coutinho, and Simão P. Pinho, “*Experimental solubility and density studies on aqueous solutions of quaternary ammonium halides, and thermodynamic modelling for melting enthalpy estimations.*”, J. of Molecular Liquids, 300 (2020), 112281; DOI: 10.1016/j.molliq.2019.112281
9. **Emanuel A. Crespo**, Liliana P. Silva, Joel O. Lloret, Pedro J. Carvalho, Lourdes F. Vega, Fèlix Llorell, and João A. P. Coutinho, “*A methodology to parameterize SAFT-type equations of state for solid precursors of deep eutectic solvents: the example of cholinium chloride.*”, Physical Chemistry Chemical Physics, 21 (2019), 15046-15061; DOI:10.1039/C9CP02548K
10. **Emanuel A. Crespo**, João M. L. Costa, André M. Palma, Belinda Soares, M. Carmen Martín, José J. Segovia, Pedro J. Carvalho, and João A. P. Coutinho, “*Thermodynamic characterization*

- of deep eutectic solvents at high pressures*”, *Fluid Phase Equilibria*, 500 (2019), 112249; DOI: 10.1016/j.fluid.2019.112249
11. **Emanuel A. Crespo** and João A. P. Coutinho; “*A Statistical Associating Fluid Theory Perspective of the Modeling of Compounds Containing Ethylene Oxide Groups*”, *Industrial & Engineering Chemistry Research*, 58 (9), 2019, 3562-3582, DOI: 10.1021/acs.iecr.9b00273
 12. **Emanuel A. Crespo**, Liliana P. Silva, Mônia A. R. Martins, Mark Bülow, Olga Ferreira, Gabriele Sadowski, Christoph Held, Simão P. Pinho, and João A. P. Coutinho, “*The Role of Polyfunctionality in the Formation of [Ch]Cl-Carboxylic Acid-Based Deep Eutectic Solvents*”, *Industrial & Engineering Chemistry Research*, 57 (32), 2018, 11195-11209; DOI: 10.1021/acs.iecr.8b01249
 13. Mônia A. R. Martins, **Emanuel A. Crespo**, Paula V. A. Pontes, Liliana P. Silva, Mark Bülow, Guilherme J. Maximo, Eduardo A. C. Batista, Christoph Held, Simão P. Pinho, and João A. P. Coutinho, “*Tunable Hydrophobic Eutectic Solvents Based on Terpenes and Monocarboxylic Acids*”, *ACS Sustainable Chemistry & Engineering*, 6 (7), 2018, 8836-8846.
 14. **Emanuel A. Crespo**, Pedro J. Carvalho, João A. P. Coutinho, and Lourdes F. Vega, “*Exploring alternative solvents for gas processing using the soft-SAFT EoS*”, *Research and Development Petroleum Conference and Exhibition (RDPETRO 2018)*, 156, DOI: 10.1190/RDP2018-41512825.1
 15. Marcus Stuckenholtz, **Emanuel A. Crespo**, Lourdes F. Vega, Pedro J. Carvalho, João A. P. Coutinho, Wolfram Schröer, Johannes Kiefer, and Bernd Rathke, “*Vapor Liquid Equilibria of Binary Mixtures of 1-Butyl-3-methylimidazolium Triflate (C₄mimTfO) and Molecular Solvents: n-alkyl alcohols and water.*”, *Journal of Physical Chemistry B*, 122 (22), 2018, 6017-6032; DOI: 10.1021/acs.jpcc.8b03278
 16. Naima Chouireb, **Emanuel A. Crespo**, Luís M. C. Pereira, O. Tafat-Igoudjilene, Lourdes F. Vega, João A. P. Coutinho, and Pedro J. Carvalho, “*Measurement and modeling of isobaric vapor-liquid equilibrium of water + glycols.*”, *Journal of Chemical & Engineering Data*, 63 (7), 2018, 2394-2401, DOI: 10.1021/acs.jced.7b00945
 17. Monique Amaral, **Emanuel A. Crespo**, Cláudio Dariva, Lourdes F. Vega, Pedro J. Carvalho, and João A. P. Coutinho, “*High-pressure solubility of CO₂ in glymes.*”, *Fuel*, 219 (2018), 120-125; DOI: 10.1016/j.fuel.2018.01.084.
 18. **Emanuel A. Crespo**, Monique Amaral, Cláudio Dariva, Pedro J. Carvalho, João A. P. Coutinho, Fèlix Llovell, Luís M. C. Pereira, and Lourdes F. Vega, “*soft-SAFT equation of state as a valuable tool for the design of new CO₂ capture technologies*”, *Abu Dhabi International Petroleum Exhibition & Conference (2017)*, Society of Petroleum Engineers, SPE-188464-MS, DOI: 10.2118/188464-MS.
 19. **Emanuel A. Crespo**, Liliana P. Silva, Mônia A. R. Martins, Luis Fernandez, Juan Ortega, Olga Ferreira, Gabriele Sadowski, Christoph Held, Simão P. Pinho, and João A. P. Coutinho, “*Characterization and Modeling of the Liquid Phase of Deep Eutectic Solvents Based on Fatty Acids/Alcohols and Choline Chloride.*”, *Industrial & Engineering Chemistry Research*, 56 (42), 2017, 12192-12202; DOI: 10.1021/acs.iecr.7b02382
 20. Pablo Navarro, **Emanuel A. Crespo**, João M. L. Costa, Fèlix Llovell, Julián García, Francisco Rodríguez, Pedro J. Carvalho, Lourdes F. Vega, and João A. P. Coutinho, “*New Experimental*

- Data and Modeling of Glymes: Toward the Development of a Predictive Model for Polyethers*”, Industrial & Engineering Chemistry Research, 56 (27), 2017, 7830-7844; DOI: 10.1021/acs.iecr.7b01532
21. Paula V. A. Pontes, **Emanuel A. Crespo**, Mônia A. R. Martins, Liliana P. Silva, Catarina M. S. S. Neves, Guilherme J. Maximo, Miriam Dupas Hubinger, Eduardo A. C. Batista, Simão P. Pinho, João A. P. Coutinho, Gabriele Sadowski, and Christoph Held, “*Measurement and PC-SAFT modeling of solid-liquid equilibrium of deep eutectic solvents of quaternary ammonium chlorides and carboxylic acids.*”, Fluid Phase Equilibria, 448 (2017), 69-80; DOI: 10.1016/j.fluid.2017.04.007
22. **Emanuel A. Crespo**, João M. L. Costa, Zulhakimiali B. M. A. Hanafiah, Kiki A. Kurnia, Mariana B. Oliveira, Fèlix Llovel, Lourdes F. Vega, Pedro J. Carvalho, and João A. P. Coutinho, “*New Measurements and modeling of high-pressure thermodynamic properties of glycols*”, Fluid Phase Equilibria, 436 (2017), 113-123; DOI: 10.1016/j.fluid.2017.01.003
23. Naima Chouireb, Imran Khan, **Emanuel A. Crespo**, Mariana B. Oliveira, Fèlix Llovel, Lourdes F. Vega, O. Tafat-Igoudjilene, A. Ait Kaci, Luís M. N. B. F. Santos, Pedro J. Carvalho, and João A. P. Coutinho, “*Evaluation of the solvent structural effect upon the vapor-liquid equilibrium of [C₄C₁im][Cl] + alcohols*”, Fluid Phase Equilibria, 440 (2017), 36-44; DOI: 10.1016/j.fluid.2017.02.016

References

- [1] Short-term energy outlook, U.S. Energy Inf. Adm. (2021). <https://www.eia.gov/outlooks/steo/> (accessed April 23, 2021).
- [2] E.J. Gudina, L.R. Rodrigues, J.A. Teixeira, J.F.B. Pereira, J.A.P. Coutinho, L.P. Soares, Biosurfactant Producing Microorganisms and Its Application to Enhance Oil Recovery at Lab Scale, (2012). <https://doi.org/10.2118/154598-MS>.
- [3] V.A. Kuuskraa, M.L. Godec, P. Dipietro, CO₂ Utilization from “Next Generation” CO₂ Enhanced Oil Recovery Technology, *Energy Procedia*. 37 (2013) 6854–6866. <https://doi.org/10.1016/j.egypro.2013.06.618>.
- [4] A. Demirbas, H.E. Alsulami, W.S. Hassanein, Utilization of Surfactant Flooding Processes for Enhanced Oil Recovery (EOR), *Pet. Sci. Technol.* 33 (2015) 1331–1339. <https://doi.org/10.1080/10916466.2015.1060503>.
- [5] D.Y.C. Leung, G. Caramanna, M.M. Maroto-Valer, An overview of current status of carbon dioxide capture and storage technologies, *Renew. Sustain. Energy Rev.* 39 (2014) 426–443. <https://doi.org/10.1016/J.RSER.2014.07.093>.
- [6] V. Smil, *Energy transitions: global and national perspectives*, ABC-CLIO, 2016.
- [7] S.O. Derawi, M.L. Michelsen, G.M. Kontogeorgis, E.H. Stenby, Application of the CPA equation of state to glycol/hydrocarbons liquid–liquid equilibria, *Fluid Phase Equilib.* 209 (2003) 163–184. [https://doi.org/10.1016/S0378-3812\(03\)00056-6](https://doi.org/10.1016/S0378-3812(03)00056-6).
- [8] G.S. Somekh, B.O. Friedlander, Tetraethylene Glycol—A Superior Solvent for Aromatics Extraction, in: *Refin. Pet. Chem.*, American Chemical Society (ACS), 1970: pp. 14–228. <https://doi.org/10.1021/ba-1970-0097.ch014>.
- [9] X. Gui, Z. Tang, W. Fei, Solubility of CO₂ in Alcohols, Glycols, Ethers, and Ketones at High Pressures from (288.15 to 318.15) K, *J. Chem. Eng. Data*. 56 (2011) 2420–2429. <https://doi.org/10.1021/je101344v>.
- [10] S.F. Sciamanna, S. Lynn, Solubility of hydrogen sulfide, sulfur dioxide, carbon dioxide, propane, and n-butane in poly(glycol ethers), *Ind. Eng. Chem. Res.* 27 (1988) 492–499. <https://doi.org/10.1021/ie00075a020>.
- [11] A. Henni, A.E. Mather, The solubility of CO₂ in triethylene glycol monomethyl ether, *Can. J. Chem. Eng.* 73 (1995) 156–158. <https://doi.org/10.1002/cjce.5450730119>.
- [12] I. Gainar, G. Anitescu, The solubility of CO₂, N₂ and H₂ in a mixture of dimethylether polyethylene glycols at high pressures, *Fluid Phase Equilib.* 109 (1995) 281–289. [https://doi.org/10.1016/0378-3812\(95\)02729-X](https://doi.org/10.1016/0378-3812(95)02729-X).
- [13] A. Henni, P. Tontiwachwuthikul, A. Chakma, A.E. Mather, Densities and Viscosities of

- Triethylene Glycol Monomethyl Ether +Water Solutions in the Temperature Interval 25 °C–80 °C, *J. Chem. Eng. Data.* 44 (1999) 101–107. <https://doi.org/10.1021/je980127s>.
- [14] K.A.G. Schmidt, A.E. Mather, Solubility of sulphur dioxide in mixed polyethylene glycol dimethyl ethers, *Can. J. Chem. Eng.* 79 (2001) 946–960. <https://doi.org/10.1002/cjce.5450790613>.
- [15] A. Henni, P. Tontiwachwuthikul, A. Chakma, Solubilities of Carbon Dioxide in Polyethylene Glycol Ethers, *Can. J. Chem. Eng.* 83 (2005) 358–361. <https://doi.org/10.1002/cjce.5450830224>.
- [16] A.-L. Revelli, F. Mutelet, J.-N. Jaubert, High Carbon Dioxide Solubilities in Imidazolium-Based Ionic Liquids and in Poly(ethylene glycol) Dimethyl Ether, *J. Phys. Chem. B.* 114 (2010) 12908–12913. <https://doi.org/10.1021/jp1057989>.
- [17] D. Kodama, M. Kanakubo, M. Kokubo, S. Hashimoto, H. Nanjo, M. Kato, Density, viscosity, and solubility of carbon dioxide in glymes, *Fluid Phase Equilib.* 302 (2011) 103–108. <https://doi.org/10.1016/j.fluid.2010.08.014>.
- [18] A. V. Rayer, A. Henni, P. Tontiwachwuthikul, High pressure physical solubility of carbon dioxide (CO₂) in mixed polyethylene glycol dimethyl ethers (Genosorb 1753), *Can. J. Chem. Eng.* 90 (2011) 576–583. <https://doi.org/10.1002/cjce.20615>.
- [19] M. Amaral, E.A. Crespo, C. Dariva, L.F. Vega, P.J. Carvalho, J.A.P. Coutinho, High-pressure solubility of CO₂ in glymes, *Fuel.* 219 (2018) 120–125. <https://doi.org/10.1016/j.fuel.2018.01.084>.
- [20] U.O.P. LLC, Selexol Process, www.Uop.Com. (2007).
- [21] J. Ameen, S.A. Furbush, Solvent Composition Useful in Acid Gas Removal from Gas Mixtures, United States Patent Office, US3737392, 1973.
- [22] R.M. Pashley, M.E. Karaman, Surfactants and Self-Assembly, in: *Appl. Colloid Surf. Chem.*, Wiley-Blackwell, 2005: pp. 61–77. <https://doi.org/10.1002/0470014709.ch4>.
- [23] C. Negin, S. Ali, Q. Xie, Most common surfactants employed in chemical enhanced oil recovery, *Petroleum.* 3 (2017) 197–211. <https://doi.org/10.1016/J.PETLM.2016.11.007>.
- [24] A.P. Abbott, G. Capper, D.L. Davies, R.K. Rasheed, V. Tambyrajah, Novel solvent properties of choline chloride/urea mixtures., *Chem. Commun. (Camb).* (2003) 70–71. <https://doi.org/10.1039/b210714g>.
- [25] A.P. Abbott, D. Boothby, G. Capper, D.L. Davies, R.K. Rasheed, Deep Eutectic Solvents formed between choline chloride and carboxylic acids: Versatile alternatives to ionic liquids, *J. Am. Chem. Soc.* 126 (2004) 9142–9147. <https://doi.org/10.1021/ja048266j>.

- [26] G. Garcia, S. Aparicio, R. Ullah, M. Atilhan, Deep Eutectic Solvents: Physicochemical Properties and Gas Separation Applications, *Energy & Fuels*. 29 (2015) 2616–2644. <https://doi.org/10.1021/ef5028873>.
- [27] S.E.E. Warrag, C.J. Peters, M.C. Kroon, Deep eutectic solvents for highly efficient separations in oil and gas industries, *Curr. Opin. Green Sustain. Chem.* 5 (2017) 55–60. <https://doi.org/10.1016/J.COGSC.2017.03.013>.
- [28] M.H. Nematollahi, P.J. Carvalho, Green solvents for CO₂ capture, *Curr. Opin. Green Sustain. Chem.* 18 (2019) 25–30. <https://doi.org/10.1016/j.cogsc.2018.11.012>.
- [29] I.I.I. Alkhatib, M.L. Ferreira, C.G. Alba, D. Bahamon, F. Llovell, A.B. Pereiro, J.M.M. Araújo, M.R.M. Abu-Zahra, L.F. Vega, Screening of Ionic Liquids and Deep Eutectic Solvents for Physical CO₂ Absorption by Soft-SAFT Using Key Performance Indicators, *J. Chem. Eng. Data*. 65 (2020) 5844–5861. <https://doi.org/10.1021/acs.jced.0c00750>.
- [30] A. Mohsenzadeh, Y. Al-Wahaibi, A. Jibril, R. Al-Hajri, S. Shuwa, The novel use of Deep Eutectic Solvents for enhancing heavy oil recovery, *J. Pet. Sci. Eng.* 130 (2015) 6–15. <https://doi.org/10.1016/j.petrol.2015.03.018>.
- [31] M. Atilhan, S. Aparicio, Review on chemical enhanced oil recovery: Utilization of ionic liquids and deep eutectic solvents, *J. Pet. Sci. Eng.* 205 (2021) 108746. <https://doi.org/10.1016/j.petrol.2021.108746>.
- [32] H.F. Hizaddin, M.K. Hadj-Kali, A. Ramalingam, M. Ali Hashim, Extractive denitrogenation of diesel fuel using ammonium- and phosphonium-based deep eutectic solvents, *J. Chem. Thermodyn.* 95 (2016) 164–173. <https://doi.org/10.1016/j.jct.2015.12.009>.
- [33] F. Lima, M. Dave, A.J.D. Silvestre, L.C. Branco, I.M. Marrucho, Concurrent Desulfurization and Denitrogenation of Fuels Using Deep Eutectic Solvents, *ACS Sustain. Chem. Eng.* 7 (2019) 11341–11349. <https://doi.org/10.1021/acssuschemeng.9b00877>.
- [34] Z. Zhu, H. Lü, M. Zhang, H. Yang, Deep eutectic solvents as non-traditionally multifunctional media for the desulfurization process of fuel oil, *Phys. Chem. Chem. Phys.* 23 (2021) 785–805. <https://doi.org/10.1039/D0CP05153E>.
- [35] F. Lima, J. Gouvenaux, L.C. Branco, A.J.D. Silvestre, I.M. Marrucho, Towards a sulfur clean fuel: Deep extraction of thiophene and dibenzothiophene using polyethylene glycol-based deep eutectic solvents, *Fuel*. 234 (2018) 414–421. <https://doi.org/10.1016/j.fuel.2018.07.043>.
- [36] S.E.E. Warrag, E.O. Fetisov, D.J.G.P. van Osch, D.B. Harwood, M.C. Kroon, J.I. Siepmann, C.J. Peters, Mercury Capture from Petroleum Using Deep Eutectic Solvents, *Ind. Eng. Chem. Res.* 57 (2018) 9222–9230. <https://doi.org/10.1021/acs.iecr.8b00967>.

- [37] T. Aissaoui, I.M. AlNashef, Y. Benguerba, Dehydration of natural gas using choline chloride based deep eutectic solvents: COSMO-RS prediction, *J. Nat. Gas Sci. Eng.* 30 (2016) 571–577. <https://doi.org/10.1016/j.jngse.2016.02.007>.
- [38] D. Lee, W. Go, J. Oh, J. Lee, I. Jo, K.-S. Kim, Y. Seo, Thermodynamic inhibition effects of an ionic liquid (choline chloride), a naturally derived substance (urea), and their mixture (deep eutectic solvent) on CH₄ hydrates, *Chem. Eng. J.* 399 (2020) 125830. <https://doi.org/10.1016/j.cej.2020.125830>.
- [39] C. Wang, H. Luo, D. Jiang, H. Li, S. Dai, Carbon Dioxide Capture by Superbase-Derived Protic Ionic Liquids, *Angew. Chemie.* 122 (2010) 6114–6117. <https://doi.org/10.1002/ange.201002641>.
- [40] T.J. Simons, T. Verheyen, E.I. Izgorodina, R. Vijayaraghavan, S. Young, A.K. Pearson, S.J. Pas, D.R. MacFarlane, Mechanisms of low temperature capture and regeneration of CO₂ using diamino protic ionic liquids, *Phys. Chem. Chem. Phys.* 18 (2016) 1140–1149. <https://doi.org/10.1039/c5cp05200a>.
- [41] F. Li, Y. Bai, S. Zeng, X. Liang, H. Wang, F. Huo, X. Zhang, Protic ionic liquids with low viscosity for efficient and reversible capture of carbon dioxide, *Int. J. Greenh. Gas Control.* 90 (2019) 102801. <https://doi.org/10.1016/j.ijggc.2019.102801>.
- [42] X. Zhu, M. Song, Y. Xu, DBU-Based Protic Ionic Liquids for CO₂ Capture, *ACS Sustain. Chem. Eng.* 5 (2017) 8192–8198. <https://doi.org/10.1021/acssuschemeng.7b01839>.
- [43] N.M. Yunus, N.H. Halim, C.D. Wilfred, T. Murugesan, J.W. Lim, P.L. Show, Thermophysical Properties and CO₂ Absorption of Ammonium-Based Protic Ionic Liquids Containing Acetate and Butyrate Anions, *Process.* 7 (2019). <https://doi.org/10.3390/pr7110820>.
- [44] Z. Ren, L. Wei, Z. Zhou, F. Zhang, W. Liu, Extractive Desulfurization of Model Oil with Protic Ionic Liquids, *Energy & Fuels.* 32 (2018) 9172–9181. <https://doi.org/10.1021/acs.energyfuels.8b01936>.
- [45] Q. Wang, T. Zhang, S. Zhang, Y. Fan, B. Chen, Extractive desulfurization of fuels using trialkylamine-based protic ionic liquids, *Sep. Purif. Technol.* 231 (2020) 115923. <https://doi.org/10.1016/j.seppur.2019.115923>.
- [46] T. Altamash, M. Khraisheh, M.F. Qureshi, M.A. Saad, S. Aparicio, M. Atilhan, Cost-effective alkylammonium formate-based protic ionic liquids for methane hydrate inhibition, *J. Nat. Gas Sci. Eng.* 58 (2018) 59–68. <https://doi.org/10.1016/j.jngse.2018.08.002>.
- [47] L. Bai, Y. Nie, Y. Li, H. Dong, X. Zhang, Protic ionic liquids extract asphaltenes from direct coal liquefaction residue at room temperature, *Fuel Process. Technol.* 108 (2013) 94–100.

- <https://doi.org/10.1016/j.fuproc.2012.04.008>.
- [48] A.I. Ismail, A.M. Atta, M.H. El-Newehy, M.E. El-Hefnawy, Protic Asphaltene ionic liquid as asphaltene stabilizer, United States Patent-US10815433, 2020.
- [49] G.M. Kontogeorgis, G.K. Folas, Thermodynamic Models for Industrial Applications – From Classical and Advanced Mixing Rules to Association Theories, First, John Wiley & Sons, 2010.
- [50] W.G. Chapman, K.E. Gubbins, G. Jackson, M. Radosz, SAFT: Equation-of-state solution model for associating fluids, *Fluid Phase Equilib.* 52 (1989) 31–38.
[https://doi.org/10.1016/0378-3812\(89\)80308-5](https://doi.org/10.1016/0378-3812(89)80308-5).
- [51] W.G. Chapman, K.E. Gubbins, G. Jackson, M. Radosz, New reference equation of state for associating liquids, *Ind. Eng. Chem. Res.* 29 (1990) 1709–1721.
<https://doi.org/10.1021/ie00104a021>.
- [52] S.J. Marrink, H.J. Risselada, S. Yefimov, D.P. Tieleman, A.H. de Vries, The MARTINI Force Field: Coarse Grained Model for Biomolecular Simulations, *J. Phys. Chem. B.* 111 (2007) 7812–7824. <https://doi.org/10.1021/jp071097f>.
- [53] C.-C. Chen, P.M. Mathias, Applied thermodynamics for process modeling, *AIChE J.* 48 (2002) 194–200. <https://doi.org/10.1002/aic.690480202>.
- [54] M.S. Wertheim, Fluids with highly directional attractive forces. I. Statistical thermodynamics, *J. Stat. Phys.* 35 (1984) 19–34. <https://doi.org/10.1007/BF01017362>.
- [55] M.S. Wertheim, Fluids with highly directional attractive forces. II. Thermodynamic perturbation theory and integral equations, *J. Stat. Phys.* 35 (1984) 35–47.
<https://doi.org/10.1007/BF01017363>.
- [56] M.S. Wertheim, Fluids with highly directional attractive forces. III. Multiple attraction sites, *J. Stat. Phys.* 42 (1986) 459–476. <https://doi.org/10.1007/BF01127721>.
- [57] M.S. Wertheim, Fluids with highly directional attractive forces. IV. Equilibrium polymerization, *J. Stat. Phys.* 42 (1986) 477–492. <https://doi.org/10.1007/BF01127722>.
- [58] S.H. Huang, M. Radosz, Equation of state for small, large, polydisperse, and associating molecules, *Ind. Eng. Chem. Res.* 29 (1990) 2284–2294. <https://doi.org/10.1021/ie00107a014>.
- [59] Y.-H. Fu, S.I. Sandler, A Simplified SAFT Equation of State for Associating Compounds and Mixtures, *Ind. Eng. Chem. Res.* 34 (1995) 1897–1909. <https://doi.org/10.1021/ie00044a042>.
- [60] E.A. Müller, L.F. Vega, K.E. Gubbins, Molecular simulation and theory of associating chain molecules, *Int. J. Thermophys.* 16 (1995) 705–713. <https://doi.org/10.1007/BF01438855>.
- [61] F.J. Blas, L.F. Vega, Thermodynamic behaviour of homonuclear and heteronuclear Lennard-Jones chains with association sites from simulation and theory, *Mol. Phys.* 92 (1997) 135–150.

- <https://doi.org/10.1080/002689797170707>.
- [62] A. Gil-Villegas, A. Galindo, P.J. Whitehead, S.J. Mills, G. Jackson, Statistical associating fluid theory for chain molecules with attractive potentials of variable range, *J. Chem. Phys.* 106 (1997) 4168–4186. <https://doi.org/10.1063/1.473101>.
- [63] J. Gross, G. Sadowski, Perturbed-Chain SAFT: An Equation of State Based on a Perturbation Theory for Chain Molecules, *Ind. Eng. Chem. Res.* 40 (2001) 1244–1260. <https://doi.org/10.1021/ie0003887>.
- [64] J. Gross, G. Sadowski, Application of the Perturbed-Chain SAFT Equation of State to Associating Systems, *Ind. Eng. Chem. Res.* 41 (2002) 5510–5515. <https://doi.org/10.1021/ie010954d>.
- [65] N. von Solms, M.L. Michelsen, G.M. Kontogeorgis, Computational and Physical Performance of a Modified PC-SAFT Equation of State for Highly Asymmetric and Associating Mixtures, *Ind. Eng. Chem. Res.* 42 (2003) 1098–1105. <https://doi.org/10.1021/ie020753p>.
- [66] Y. Peng, K.D. Goff, M.C. dos Ramos, C. McCabe, Developing a predictive group-contribution-based SAFT-VR equation of state, *Fluid Phase Equilib.* 277 (2009) 131–144. <https://doi.org/10.1016/J.FLUID.2008.11.008>.
- [67] A. Lymeriadis, C.S. Adjiman, A. Galindo, G. Jackson, A group contribution method for associating chain molecules based on the statistical associating fluid theory (SAFT- γ), *J. Chem. Phys.* 127 (2007) 234903. <https://doi.org/10.1063/1.2813894>.
- [68] V. Papaioannou, T. Lafitte, C. Avendaño, C.S. Adjiman, G. Jackson, E.A. Müller, A. Galindo, Group contribution methodology based on the statistical associating fluid theory for heteronuclear molecules formed from Mie segments, *J. Chem. Phys.* 140 (2014) 54107. <https://doi.org/10.1063/1.4851455>.
- [69] J.S. Rowlinson, Translation of J. D. van der Waals' "The thermodynamik theory of capillarity under the hypothesis of a continuous variation of density," *J. Stat. Phys.* 20 (1979) 197–200. <https://doi.org/10.1007/BF01011513>.
- [70] J.W. Cahn, J.E. Hilliard, Free Energy of a Nonuniform System. I. Interfacial Free Energy, *J. Chem. Phys.* 28 (1958) 258–267. <https://doi.org/10.1063/1.1744102>.
- [71] F. Llovel, R.M. Marcos, L.F. Vega, Free-Volume Theory Coupled with Soft-SAFT for Viscosity Calculations: Comparison with Molecular Simulation and Experimental Data, *J. Phys. Chem. B.* 117 (2013) 8159–8171. <https://doi.org/10.1021/jp401307t>.
- [72] J.C. Pàmies, L.F. Vega, Vapor–Liquid Equilibria and Critical Behavior of Heavy n -Alkanes Using Transferable Parameters from the Soft-SAFT Equation of State, *Ind. Eng. Chem. Res.* 40

- (2001) 2532–2543. <https://doi.org/10.1021/ie000944x>.
- [73] A.M.A. Dias, J.C. Pàmies, J.A.P. Coutinho, I.M. Marrucho, L.F. Vega, SAFT Modeling of the Solubility of Gases in Perfluoroalkanes, *J. Phys. Chem. B.* 108 (2004) 1450–1457. <https://doi.org/10.1021/jp036225o>.
- [74] F. Llovell, L.F. Vega, Global Fluid Phase Equilibria and Critical Phenomena of Selected Mixtures Using the Crossover Soft-SAFT Equation, *J. Phys. Chem. B.* 110 (2006) 1350–1362. <https://doi.org/10.1021/jp0551465>.
- [75] N. Pedrosa, J.C. Pàmies, J.A.P. Coutinho, I.M. Marrucho, L.F. Vega, Phase equilibria of ethylene glycol oligomers and their mixtures, *Ind. Eng. Chem. Res.* 44 (2005) 7027–7037. <https://doi.org/10.1021/ie050361t>.
- [76] A. Belkadi, M.K. Hadj-Kali, F. Llovell, V. Gerbaud, L.F. Vega, Soft-SAFT modeling of vapor–liquid equilibria of nitriles and their mixtures, *Fluid Phase Equilib.* 289 (2010) 191–200. <https://doi.org/10.1016/j.fluid.2009.12.012>.
- [77] J.S. Andreu, L.F. Vega, Capturing the Solubility Behavior of CO₂ in Ionic Liquids by a Simple Model, *J. Phys. Chem. C.* 111 (2007) 16028–16034. <https://doi.org/10.1021/jp074353x>.
- [78] O. Vilaseca, F. Llovell, J. Yustos, R.M. Marcos, L.F. Vega, Phase equilibria, surface tensions and heat capacities of hydrofluorocarbons and their mixtures including the critical region, *J. Supercrit. Fluids.* 55 (2010) 755–768. <https://doi.org/10.1016/j.supflu.2010.10.015>.
- [79] N. Pedrosa, L.F. Vega, J. a. P. Coutinho, I.M. Marrucho, Phase Equilibria Calculations of Polyethylene Solutions from SAFT-Type Equations of State, *Macromolecules.* 39 (2006) 4240–4246. <https://doi.org/10.1021/ma060584a>.
- [80] J.K. Johnson, J.A. Zollweg, K.E. Gubbins, The Lennard-Jones equation of state revisited, *Mol. Phys.* 78 (1993) 591–618. <https://doi.org/10.1080/00268979300100411>.
- [81] J. Kolafa, I. Nezbeda, The Lennard-Jones fluid: an accurate analytic and theoretically-based equation of state, *Fluid Phase Equilib.* 100 (1994) 1–34. [https://doi.org/10.1016/0378-3812\(94\)80001-4](https://doi.org/10.1016/0378-3812(94)80001-4).
- [82] J.K. Johnson, E.A. Mueller, K.E. Gubbins, Equation of State for Lennard-Jones Chains, *J. Phys. Chem.* 98 (1994) 6413–6419. <https://doi.org/10.1021/j100076a028>.
- [83] C. Herdes, J.C. Pàmies, R.M. Marcos, L.F. Vega, Thermodynamic properties and aggregate formation of surfactant-like molecules from theory and simulation, *J. Chem. Phys.* 120 (2004) 9822–9830. <https://doi.org/10.1063/1.1714853>.
- [84] E.A. Muller, K.E. Gubbins, An Equation of State for Water from a Simplified Intermolecular Potential, *Ind. Eng. Chem. Res.* 34 (1995) 3662–3673. <https://doi.org/10.1021/ie00037a055>.

- [85] S.P. Tan, H. Adidharma, M. Radosz, Generalized Procedure for Estimating the Fractions of Nonbonded Associating Molecules and Their Derivatives in Thermodynamic Perturbation Theory, *Ind. Eng. Chem. Res.* 43 (2004) 203–208. <https://doi.org/10.1021/ie034041q>.
- [86] M.L. Michelsen, Robust and Efficient Solution Procedures for Association Models, *Ind. Eng. Chem. Res.* 45 (2006) 8449–8453. <https://doi.org/10.1021/ie060029x>.
- [87] G. Stell, J.C. Rasaiah, H. Narang, Thermodynamic perturbation theory for simple polar fluids. II, *Mol. Phys.* 27 (1974) 1393–1414. <https://doi.org/10.1080/00268977400101181>.
- [88] K.E. Gubbins, C.H. Twu, Thermodynamics of polyatomic fluid mixtures—I theory, *Chem. Eng. Sci.* 33 (1978) 863–878. [https://doi.org/10.1016/0009-2509\(78\)85176-8](https://doi.org/10.1016/0009-2509(78)85176-8).
- [89] M. Luckas, K. Lucas, U. Deiters, K.E. Gubbins, Integrals over pair- and triplet-correlation functions for the Lennard-Jones (12–6)-fluid, *Mol. Phys.* 57 (1986) 241–253. <https://doi.org/10.1080/00268978600100191>.
- [90] F.J. Blas, L.F. Vega, Prediction of Binary and Ternary Diagrams Using the Statistical Associating Fluid Theory (SAFT) Equation of State, *Ind. Eng. Chem. Res.* 37 (1998) 660–674. <https://doi.org/10.1021/ie970449+>.
- [91] N.F. Carnahan, K.E. Starling, Equation of state for nonattracting rigid spheres, *J. Chem. Phys.* 51 (1969) 635–636. <https://doi.org/10.1063/1.1672048>.
- [92] T. Boublík, Hard-Sphere Equation of State, *J. Chem. Phys.* 53 (1970) 471–472. <https://doi.org/10.1063/1.1673824>.
- [93] G.A. Mansoori, N.F. Carnahan, K.E. Starling, T.W. Leland Jr, Equilibrium thermodynamic properties of the mixture of hard spheres, *J. Chem. Phys.* 54 (1971) 1523–1525. <https://doi.org/10.1063/1.1675048>.
- [94] J. Pàmies Corominas, Bulk and interfacial properties of chain fluids: a molecular modelling approach, Ph.D. Thesis. Univ. Rovira i Virgili. (2004).
- [95] D. Frenkel, B. Smit, Chapter 4 - Molecular Dynamics Simulations, in: D. Frenkel, B.B.T.-U.M.S. (Second E. Smit (Eds.)), Academic Press, San Diego, 2002: pp. 63–107. <https://doi.org/10.1016/B978-012267351-1/50006-7>.
- [96] M.A. González, Force fields and molecular dynamics simulations, *JDN.* 12 (2011) 169–200. <https://doi.org/10.1051/sfn/201112009>.
- [97] S.J. Marrink, A.E. Mark, Molecular Dynamics Simulation of the Formation, Structure, and Dynamics of Small Phospholipid Vesicles, *J. Am. Chem. Soc.* 125 (2003) 15233–15242. <https://doi.org/10.1021/ja0352092>.
- [98] S.J. Marrink, A.H. de Vries, A.E. Mark, Coarse Grained Model for Semiquantitative Lipid

- Simulations, *J. Phys. Chem. B.* 108 (2004) 750–760. <https://doi.org/10.1021/jp036508g>.
- [99] S.J. Marrink, D.P. Tieleman, Perspective on the Martini model, *Chem. Soc. Rev.* 42 (2013) 6801–6822. <https://doi.org/10.1039/C3CS60093A>.
- [100] B.M.H. Bruininks, P.C.T. Souza, S.J. Marrink, A Practical View of the Martini Force Field, in: M. Bonomi, C. Camilloni (Eds.), *Biomol. Simulations Methods Protoc.*, Springer New York, New York, NY, 2019: pp. 105–127. https://doi.org/10.1007/978-1-4939-9608-7_5.
- [101] M.J. Abraham, T. Murtola, R. Schulz, S. Páll, J.C. Smith, B. Hess, E. Lindahl, GROMACS: High performance molecular simulations through multi-level parallelism from laptops to supercomputers, *SoftwareX.* 1–2 (2015) 19–25. <https://doi.org/10.1016/j.softx.2015.06.001>.
- [102] E.A. Crespo, N. Schaeffer, J.A.P. Coutinho, G. Perez-Sanchez, Improved coarse-grain model to unravel the phase behavior of 1-alkyl-3-methylimidazolium-based ionic liquids through molecular dynamics simulations, *J. Colloid Interface Sci.* 574 (2020) 324–336. <https://doi.org/10.1016/j.jcis.2020.04.063>.
- [103] J.N. Canongia Lopes, J. Deschamps, A.A.H. Pádua, Modeling Ionic Liquids Using a Systematic All-Atom Force Field, *J. Phys. Chem. B.* 108 (2004) 2038–2047. <https://doi.org/10.1021/jp0362133>.
- [104] J.N. Canongia Lopes, A.A.H. Pádua, Molecular Force Field for Ionic Liquids III: Imidazolium, Pyridinium, and Phosphonium Cations; Chloride, Bromide, and Dicyanamide Anions, *J. Phys. Chem. B.* 110 (2006) 19586–19592. <https://doi.org/10.1021/jp063901o>.
- [105] R. Wu, M. Deng, B. Kong, X. Yang, Coarse-Grained Molecular Dynamics Simulation of Ammonium Surfactant Self-Assemblies: Micelles and Vesicles, *J. Phys. Chem. B.* 113 (2009) 15010–15016. <https://doi.org/10.1021/jp906055d>.
- [106] A. V Sangwai, R. Sureshkumar, Coarse-Grained Molecular Dynamics Simulations of the Sphere to Rod Transition in Surfactant Micelles, *Langmuir.* 27 (2011) 6628–6638. <https://doi.org/10.1021/la2006315>.
- [107] M. Velinova, D. Sengupta, A. V Tadjer, S.-J. Marrink, Sphere-to-Rod Transitions of Nonionic Surfactant Micelles in Aqueous Solution Modeled by Molecular Dynamics Simulations, *Langmuir.* 27 (2011) 14071–14077. <https://doi.org/10.1021/la203055t>.
- [108] G. Pérez-Sánchez, J.R.B. Gomes, M. Jorge, Modeling Self-Assembly of Silica/Surfactant Mesoporous Structures in the Templated Synthesis of Nanoporous Solids, *Langmuir.* 29 (2013) 2387–2396. <https://doi.org/10.1021/la3046274>.
- [109] G. Pérez-Sánchez, S.-C. Chien, J.R.B. Gomes, M.N. D. S. Cordeiro, S.M. Auerbach, P.A. Monson, M. Jorge, Multiscale Model for the Templated Synthesis of Mesoporous Silica: The

- Essential Role of Silica Oligomers, *Chem. Mater.* 28 (2016) 2715–2727.
<https://doi.org/10.1021/acs.chemmater.6b00348>.
- [110] S.-C. Chien, G. Pérez-Sánchez, J.R.B. Gomes, M.N.D.S. Cordeiro, M. Jorge, S.M. Auerbach, P.A. Monson, Molecular Simulations of the Synthesis of Periodic Mesoporous Silica Phases at High Surfactant Concentrations, *J. Phys. Chem. C.* 121 (2017) 4564–4575.
<https://doi.org/10.1021/acs.jpcc.6b09429>.
- [111] V. Wiesmet, E. Weidner, S. Behme, G. Sadowski, W. Arlt, Measurement and modelling of high-pressure phase equilibria in the systems polyethyleneglycol (PEG)–propane, PEG–nitrogen and PEG–carbon dioxide, *J. Supercrit. Fluids.* 17 (2000) 1–12.
[https://doi.org/10.1016/S0896-8446\(99\)00043-1](https://doi.org/10.1016/S0896-8446(99)00043-1).
- [112] E.A. Crespo, J.A.P. Coutinho, A Statistical Associating Fluid Theory Perspective of the Modeling of Compounds Containing Ethylene Oxide Groups, *Ind. Eng. Chem. Res.* 58 (2019) 3562–3582. <https://doi.org/10.1021/acs.iecr.9b00273>.
- [113] N. Pedrosa, L.F. Vega, J.A.P. Coutinho, I.M. Marrucho, Modeling the Phase Equilibria of Poly(ethylene glycol) Binary Mixtures with soft-SAFT EoS, *Ind. Eng. Chem. Res.* 46 (2007) 4678–4685. <https://doi.org/10.1021/ie0701672>.
- [114] T. Lafitte, M.M. Piñeiro, J.-L. Daridon, D. Bessières, A Comprehensive Description of Chemical Association Effects on Second Derivative Properties of Alcohols through a SAFT-VR Approach, *J. Phys. Chem. B.* 111 (2007) 3447–3461. <https://doi.org/10.1021/jp0682208>.
- [115] G.N.I. Clark, A.J. Haslam, A. Galindo, G. Jackson, Developing optimal Wertheim-like models of water for use in Statistical Associating Fluid Theory (SAFT) and related approaches, *Mol. Phys.* 104 (2006) 3561–3581. <https://doi.org/10.1080/00268970601081475>.
- [116] A. Grenner, G.M. Kontogeorgis, M.L. Michelsen, G.K. Folas, On the estimation of water pure compound parameters in association theories, *Mol. Phys.* 105 (2007) 1797–1801.
<https://doi.org/10.1080/00268970701416597>.
- [117] M.B. Oliveira, F. Llovel, J.A.P. Coutinho, L.F. Vega, New Procedure for Enhancing the Transferability of Statistical Associating Fluid Theory (SAFT) Molecular Parameters: The Role of Derivative Properties, *Ind. Eng. Chem. Res.* 55 (2016) 10011–10024.
<https://doi.org/10.1021/acs.iecr.6b02205>.
- [118] T.E. Daubert, H.M. Sibul, C.C. Stebbins, R.P. Danner, R.L. Rowley, M.E. Adams, W. V Wilding, T.L. Marshall, *Physical and Thermodynamic Properties of Pure Chemicals: DIPPR: Data Compilation: Core + Supplements 1-10*, Taylor & Francis, 2000.
<https://books.google.pt/books?id=MQOjPQAACAAJ>.

- [119] E.A. Crespo, J.M.L. Costa, Z.B.M.A. Hanafiah, K.A. Kurnia, M.B. Oliveira, F. Llovell, L.F. Vega, P.J. Carvalho, J.A.P. Coutinho, New measurements and modeling of high pressure thermodynamic properties of glycols, *Fluid Phase Equilib.* 436 (2017) 113–123. <https://doi.org/10.1016/j.fluid.2017.01.003>.
- [120] P. Navarro, E.A. Crespo, J.M.L. Costa, F. Llovell, J. García, F. Rodríguez, P.J. Carvalho, L.F. Vega, J.A.P. Coutinho, New Experimental Data and Modeling of Glymes: Toward the Development of a Predictive Model for Polyethers, *Ind. Eng. Chem. Res.* 56 (2017) 7830–7844. <https://doi.org/10.1021/acs.iecr.7b01532>.
- [121] J.S. Andreu, L.F. Vega, Modeling the Solubility Behavior of CO₂, H₂, and Xe in [Cn-mim][Tf₂N] Ionic Liquids, *J. Phys. Chem. B.* 112 (2008) 15398–15406. <https://doi.org/10.1021/jp807484g>.
- [122] K. Kiesow, F. Ruether, G. Sadowski, Solubility, crystallization and oiling-out behavior of PEGDME: 1. Pure-solvent systems, *Fluid Phase Equilib.* 298 (2010) 253–261. <https://doi.org/10.1016/J.FLUID.2010.08.005>.
- [123] N.R. Nannan, C.M. De Servi, T. van der Stelt, P. Colonna, A. Bardow, An Equation of State Based on PC-SAFT for Physical Solvents Composed of Polyethylene Glycol Dimethylethers, *Ind. Eng. Chem. Res.* 52 (2013) 18401–18412. <https://doi.org/10.1021/ie401456q>.
- [124] I. Polishuk, A. Yitzhak, Modeling Viscosities of Pure Compounds and Their Binary Mixtures Using the Modified Yarranton–Satyro Correlation and Free Volume Theory Coupled with SAFT+Cubic EoS, *Ind. Eng. Chem. Res.* 53 (2014) 959–971. <https://doi.org/10.1021/ie4030352>.
- [125] I. Polishuk, Hybridizing SAFT and Cubic EOS: What Can Be Achieved?, *Ind. Eng. Chem. Res.* 50 (2011) 4183–4198. <https://doi.org/10.1021/ie102420n>.
- [126] F. Llovell, C.J. Peters, L.F. Vega, Second-order thermodynamic derivative properties of selected mixtures by the soft-SAFT equation of state, *Fluid Phase Equilib.* 248 (2006) 115–122. <https://doi.org/10.1016/j.fluid.2006.07.018>.
- [127] L.F. Vega, F. Llovell, Review and new insights into the application of molecular-based equations of state to water and aqueous solutions, *Fluid Phase Equilib.* 416 (2016) 150–173. <https://doi.org/10.1016/j.fluid.2016.01.024>.
- [128] T. Kraska, K.E. Gubbins, Phase Equilibria Calculations with a Modified SAFT Equation of State. 1. Pure Alkanes, Alkanols, and Water, *Ind. Eng. Chem. Res.* 35 (1996) 4727–4737. <https://doi.org/10.1021/ie9602320>.
- [129] A. Conesa, S. Shen, A. Coronas, Liquid Densities, Kinematic Viscosities, and Heat Capacities

- of Some Ethylene Glycol Dimethyl Ethers at Temperatures from 283.15 to 423.15 K, *Int. J. Thermophys.* 19 (1998) 1343–1358. <https://doi.org/10.1023/A:1021927417610>.
- [130] P.J. Carvalho, K.A. Kurnia, J.A.P. Coutinho, Dispelling some myths about the CO₂ solubility in ionic liquids, *Phys. Chem. Chem. Phys.* 18 (2016) 14757–14771. <https://doi.org/10.1039/C6CP01896C>.
- [131] L. Engineering, Rectisol Wash, (2007). <http://www.linde-engineering.com>.
- [132] F.-Y. Jou, F. Otto, A. Mather, Solubility of H₂S and CO₂ in diethylene glycol at elevated pressures, *Fluid Phase Equilib.* 175 (2000) 53–61. [https://doi.org/10.1016/S0378-3812\(00\)00440-4](https://doi.org/10.1016/S0378-3812(00)00440-4).
- [133] P.J. Carvalho, J.A.P. Coutinho, On the nonideality of CO₂ solutions in ionic liquids and other low volatile solvents, *J. Phys. Chem. Lett.* 1 (2010) 774–780. <https://doi.org/10.1021/jz100009c>.
- [134] P.J. Carvalho, J.A.P. Coutinho, The polarity effect upon the methane solubility in ionic liquids: a contribution for the design of ionic liquids for enhanced CO₂/CH₄ and H₂S/CH₄ selectivities, *Energy Environ. Sci.* 4 (2011) 4614–4619. <https://doi.org/10.1039/C1EE01599K>.
- [135] M.I. Stewart, Gas Sweetening, in: *Surf. Prod. Oper.*, 3rd ed., Gulf Professional Publishing, Boston, 2014: pp. 433–539. <https://doi.org/10.1016/B978-0-12-382207-9.00009-3>.
- [136] M. Pastor-Belda, N. Campillo, M. Hernández-Córdoba, P. Viñas, Gas chromatography with mass spectrometry for the quantification of ethylene glycol ethers in different household cleaning products, *J. Sep. Sci.* 39 (2016) 2292–2299. <https://doi.org/10.1002/jssc.201600180>.
- [137] L.F. Vega, F. Llovel, F.J. Blas, Capturing the Solubility Minima of n-Alkanes in Water by Soft-SAFT, *J. Phys. Chem. B.* 113 (2009) 7621–7630. <https://doi.org/10.1021/jp9018876>.
- [138] N. Chouireb, E.A. Crespo, L.M.C. Pereira, O. Tafat-Igoudjilene, L.F. Vega, J.A.P. Coutinho, P.J. Carvalho, Measurement and Modeling of Isobaric Vapor–Liquid Equilibrium of Water + Glycols, *J. Chem. Eng. Data.* 63 (2018) 2394–2401. <https://doi.org/10.1021/acs.jced.7b00945>.
- [139] L. Ninni, M.S. Camargo, A.J.A. Meirelles, Water activity in poly(ethylene glycol) aqueous solutions, *Thermochim. Acta.* 328 (1999) 169–176. [https://doi.org/10.1016/S0040-6031\(98\)00638-8](https://doi.org/10.1016/S0040-6031(98)00638-8).
- [140] M. Herskowitz, M. Gottlieb, Vapor-Liquid Equilibrium in Aqueous Solutions of Various Glycols and Poly (ethylene glycols). 3. Poly (ethylene glycols), *J. Chem. Eng. Data.* 30 (1985) 233–234. <https://doi.org/10.1021/je00040a033>.
- [141] A. Eliassi, H. Modarress, G.A. Mansoori, Measurement of Activity of Water in Aqueous Poly(ethylene glycol) Solutions (Effect of Excess Volume on the Flory–Huggins χ -Parameter),

- J. Chem. Eng. Data. 44 (1999) 52–55. <https://doi.org/10.1021/je980162z>.
- [142] E.A. Crespo, N. Chouireb, O.T. Igoudjilene, L.F. Vega, P.J. Carvalho, J.A.P. Coutinho, Isobaric vapor-liquid equilibrium of water + glymes binary mixtures: Experimental measurements and molecular thermodynamic modelling, *Fluid Phase Equilib.* 513 (2020) 112547. <https://doi.org/10.1016/j.fluid.2020.112547>.
- [143] S. Tamouza, J.-P. Passarello, P. Tobaly, J.-C. de Hemptinne, Group contribution method with SAFT EOS applied to vapor liquid equilibria of various hydrocarbon series, *Fluid Phase Equilib.* 222–223 (2004) 67–76. <https://doi.org/10.1016/J.FLUID.2004.06.038>.
- [144] J. Vijande, M.M. Piñeiro, D. Bessieres, H. Saint-Guirons, J.L. Legido, Description of PVT behaviour of hydrofluoroethers using the PC-SAFT EOS, *Phys. Chem. Chem. Phys.* 6 (2004) 766–770. <https://doi.org/10.1039/B312223A>.
- [145] J. Vijande, M.M. Piñeiro, J.L. Legido, D. Bessières, Group-Contribution Method for the Molecular Parameters of the PC-SAFT Equation of State Taking into Account the Proximity Effect. Application to Nonassociated Compounds, *Ind. Eng. Chem. Res.* 49 (2010) 9394–9406. <https://doi.org/10.1021/ie1002813>.
- [146] J. Vijande, M.M. Piñeiro, J.L. Legido, Group-Contribution Method with Proximity Effect for PC-SAFT Molecular Parameters. 2. Application to Association Parameters: Primary Alcohols and Amines, *Ind. Eng. Chem. Res.* 53 (2014) 909–919. <https://doi.org/10.1021/ie4023786>.
- [147] A. Tihic, G.M. Kontogeorgis, N. von Solms, M.L. Michelsen, L. Constantinou, A Predictive Group-Contribution Simplified PC-SAFT Equation of State: Application to Polymer Systems, *Ind. Eng. Chem. Res.* 47 (2008) 5092–5101. <https://doi.org/10.1021/ie0710768>.
- [148] A. Tihic, N. von Solms, M.L. Michelsen, G.M. Kontogeorgis, L. Constantinou, Analysis and applications of a group contribution sPC-SAFT equation of state, *Fluid Phase Equilib.* 281 (2009) 60–69. <https://doi.org/10.1016/j.fluid.2009.04.003>.
- [149] S. Tamouza, J.-P. Passarello, P. Tobaly, J.-C. de Hemptinne, Application to binary mixtures of a group contribution SAFT EOS (GC-SAFT), *Fluid Phase Equilib.* 228–229 (2005) 409–419. <https://doi.org/10.1016/j.fluid.2004.10.003>.
- [150] T.X. Nguyen Thi, S. Tamouza, P. Tobaly, J.-P. Passarello, J.-C. de Hemptinne, Application of group contribution SAFT equation of state (GC-SAFT) to model phase behaviour of light and heavy esters, *Fluid Phase Equilib.* 238 (2005) 254–261. <https://doi.org/10.1016/j.fluid.2005.10.009>.
- [151] F.T. Peters, F.S. Laube, G. Sadowski, Development of a group contribution method for polymers within the PC-SAFT model, *Fluid Phase Equilib.* 324 (2012) 70–79.

- <https://doi.org/10.1016/j.fluid.2012.03.009>.
- [152] A. Lymeriadis, C.S. Adjiman, G. Jackson, A. Galindo, A generalisation of the SAFT- γ group contribution method for groups comprising multiple spherical segments, *Fluid Phase Equilib.* 274 (2008) 85–104. <https://doi.org/10.1016/j.fluid.2008.08.005>.
- [153] S. Dufal, V. Papaioannou, M. Sadeqzadeh, T. Pogiatis, A. Chremos, C.S. Adjiman, G. Jackson, A. Galindo, Prediction of Thermodynamic Properties and Phase Behavior of Fluids and Mixtures with the SAFT- γ Mie Group-Contribution Equation of State, *J. Chem. Eng. Data.* 59 (2014) 3272–3288. <https://doi.org/10.1021/je500248h>.
- [154] P. Morgado, B. Colaço, V. Santos, G. Jackson, E.J.M. Filipe, Modelling the thermodynamic properties and fluid-phase equilibria of n-perfluoroalkanes and their binary mixtures with the SAFT- γ Mie group contribution equation of state, *Mol. Phys.* 118 (2020). <https://doi.org/10.1080/00268976.2020.1722270>.
- [155] V. Papaioannou, C.S. Adjiman, G. Jackson, A. Galindo, Simultaneous prediction of vapour–liquid and liquid–liquid equilibria (VLE and LLE) of aqueous mixtures with the SAFT- γ group contribution approach, *Fluid Phase Equilib.* 306 (2011) 82–96. <https://doi.org/10.1016/j.fluid.2011.02.016>.
- [156] V. Papaioannou, F. Calado, T. Lafitte, S. Dufal, M. Sadeqzadeh, Application of the SAFT- γ Mie group contribution equation of state to fluids of relevance to the oil and gas industry, *Fluid Phase Equilib.* 416 (2016) 104–119. <https://doi.org/10.1016/j.fluid.2015.12.041>.
- [157] N. Haarmann, R. Siewert, A.A. Samarov, S.P. Verevkin, C. Held, G. Sadowski, Thermodynamic Properties of Systems Comprising Esters: Experimental Data and Modeling with PC-SAFT and SAFT- γ Mie, *Ind. Eng. Chem. Res.* 58 (2019) 6841–6849. <https://doi.org/10.1021/acs.iecr.9b00714>.
- [158] Y. Peng, K.D. Goff, M.C. dos Ramos, C. McCabe, Predicting the Phase Behavior of Polymer Systems with the GC-SAFT-VR Approach, *Ind. Eng. Chem. Res.* 49 (2010) 1378–1394. <https://doi.org/10.1021/ie900795x>.
- [159] X.-S. Li, J.-F. Lu, Y.-G. Li, J.-C. Liu, Studies on UNIQUAC and SAFT equations for nonionic surfactant solutions, *Fluid Phase Equilib.* 153 (1998) 215–229. [https://doi.org/10.1016/S0378-3812\(98\)00411-7](https://doi.org/10.1016/S0378-3812(98)00411-7).
- [160] L. Wang, A. Haghmoradi, J. Liu, S. Xi, G.J. Hirasaki, C.A. Miller, W.G. Chapman, Modeling micelle formation and interfacial properties with iSAFT classical density functional theory, *J. Chem. Phys.* 146 (2017) 124705. <https://doi.org/10.1063/1.4978503>.
- [161] X. Mu, S. Xi, F.O. Alpak, W.G. Chapman, Modified Density Gradient Theory for Surfactant

- Molecules Applied to Oil/Water Interfaces, *Ind. Eng. Chem. Res.* 57 (2018) 7643–7654.
<https://doi.org/10.1021/acs.iecr.8b00164>.
- [162] P. Rehner, B. Bursik, J. Gross, Surfactant Modeling Using Classical Density Functional Theory and a Group Contribution PC-SAFT Approach, *Ind. Eng. Chem. Res.* (2021).
<https://doi.org/10.1021/acs.iecr.1c00169>.
- [163] N.M. Garrido, G.K. Folas, G.M. Kontogeorgis, Modelling of phase equilibria of glycol ethers mixtures using an association model, *Fluid Phase Equilib.* 273 (2008) 11–20.
<https://doi.org/10.1016/j.fluid.2008.08.006>.
- [164] A.S. Avlund, G.M. Kontogeorgis, M.L. Michelsen, Application of Simplified PC-SAFT to Glycol Ethers, *Ind. Eng. Chem. Res.* 51 (2012) 547–555. <https://doi.org/10.1021/ie2011406>.
- [165] M.N. García-Lisbona, A. Galindo, G. Jackson, A. Burgess, Predicting the high-pressure phase equilibria of binary aqueous solutions of 1-butanol, n-butoxyethanol and n-decylpentaoxyethylene ether (C10E5) using the SAFT-HS approach, *Mol. Phys.* 93 (1998) 57–72. <https://doi.org/10.1080/002689798169438>.
- [166] M.N. García-Lisbona, A. Galindo, G. Jackson, A.N. Burgess, An Examination of the Cloud Curves of Liquid–Liquid Immiscibility in Aqueous Solutions of Alkyl Polyoxyethylene Surfactants Using the SAFT-HS Approach with Transferable Parameters, *J. Am. Chem. Soc.* 120 (1998) 4191–4199. <https://doi.org/10.1021/ja9736525>.
- [167] G. Jackson, K.E. Gubbins, Mixtures of associating spherical and chain molecules, *Pure Appl. Chem.* 61 (1989) 1021. <https://doi.org/10.1351/pac198961061021>.
- [168] P. Hutacharoen, S. Dufal, V. Papaioannou, R.M. Shanker, C.S. Adjiman, G. Jackson, A. Galindo, Predicting the Solvation of Organic Compounds in Aqueous Environments: From Alkanes and Alcohols to Pharmaceuticals, *Ind. Eng. Chem. Res.* 56 (2017) 10856–10876.
<https://doi.org/10.1021/acs.iecr.7b00899>.
- [169] C. Tsonopoulos, G.M. Wilson, High-temperature mutual solubilities of hydrocarbons and water. Part I: Benzene, cyclohexane and n-hexane, *AIChE J.* 29 (1983) 990–999.
<https://doi.org/10.1002/aic.690290618>.
- [170] A. Maczynski, D.G. Shaw, M. Goral, B. Wisniewska-Gocłowska, A. Skrzecz, Z. Maczynska, I. Owczarek, K. Blazej, M.-C. Haulait-Pirson, F. Kapuku, G.T. Hefter, A.M. Szafranski, IUPAC-NIST Solubility Data Series. 81. Hydrocarbons with Water and Seawater—Revised and Updated Part 1. C5 Hydrocarbons with Water, *J. Phys. Chem. Ref. Data.* 34 (2005) 441.
<https://doi.org/10.1063/1.1790005>.
- [171] M. Goral, B. Wisniewska-Gocłowska, A. Skrzecz, I. Owczarek, K. Blazej, M.-C. Haulait-

- Pirson, G.T. Hefter, F. Kapuku, Z. Maczynska, A. Szafranski, C.L. Young, IUPAC-NIST Solubility Data Series. 81. Hydrocarbons with Water and Seawater-Revised and Updated. Part 5. C7 Hydrocarbons with Water and Heavy Water, *J. Phys. Chem. Ref. Data.* 34 (2005) 1399–1487. <https://doi.org/10.1063/1.1840737>.
- [172] M. Goral, B. Wisniewska-Gocłowska, A. Skrzecz, I. Owczarek, K. Blazej, M.-C. Haulait-Pirson, G.T. Hefter, F. Kapuku, Z. Maczynska, A. Szafranski, IUPAC-NIST Solubility Data Series. 81. Hydrocarbons with Water and Seawater Revised and Updated. Part 7. C8H12–C8H18 Hydrocarbons with Water, *J. Phys. Chem. Ref. Data.* 34 (2005) 2261–2298. <https://doi.org/10.1063/1.1842097>.
- [173] M. Goral, B. Wisniewska-Gocłowska, A. Skrzecz, I. Owczarek, K. Blazej, M.-C. Haulait-Pirson, G.T. Hefter, F. Kapuku, Z. Maczynska, A. Szafranski, IUPAC-NIST Solubility Data Series. 81. Hydrocarbons with Water and Seawater—Revised and Updated. Part 8. C9 Hydrocarbons with Water, *J. Phys. Chem. Ref. Data.* 34 (2005) 2299–2345. <https://doi.org/10.1063/1.1842098>.
- [174] D.G. Shaw, A. Maczynski, M. Goral, B. Wisniewska-Gocłowska, A. Skrzecz, I. Owczarek, K. Blazej, M.-C. Haulait-Pirson, G.T. Hefter, P.L. Huyskens, F. Kapuku, Z. Maczynska, A. Szafranski, IUPAC-NIST Solubility Data Series. 81. Hydrocarbons with Water and Seawater—Revised and Updated. Part 9. C10 Hydrocarbons with Water, *J. Phys. Chem. Ref. Data.* 35 (2006) 93–151. <https://doi.org/10.1063/1.2131103>.
- [175] A.G. Pradhan, V.R. Bhethanabotla, S.W. Campbell, Vapor-liquid equilibrium data for ethanol-n-heptane-1-propanol and ethanol-n-heptane-2-propanol and their interpretation by a simple association model, *Fluid Phase Equilib.* 84 (1993) 183–206. [https://doi.org/10.1016/0378-3812\(93\)85123-4](https://doi.org/10.1016/0378-3812(93)85123-4).
- [176] C.-B. Soo, E. El Ahmar, C. Coquelet, D. Ramjugernath, D. Richon, Vapor–liquid equilibrium measurements and modeling of the n-butane+ethanol system from 323 to 423K, *Fluid Phase Equilib.* 286 (2009) 79–87. <https://doi.org/10.1016/j.fluid.2009.08.007>.
- [177] K.S. Yuan, J.C.K. Ho, A.K. Koshpande, B.C.-Y. Lu, Vapor-Liquid Equilibria., *J. Chem. Eng. Data.* 8 (1963) 549–559. <https://doi.org/10.1021/je60019a024>.
- [178] J. Schmelzer, I. Lieberwirth, M. Krug, R. Pfestorf, Vapour-liquid equilibria and heats of mixing in alkane-alcohol(1) systems. I. Vapour-liquid equilibria in 1-alcohol-undecane systems, *Fluid Phase Equilib.* 11 (1983) 187–200. [https://doi.org/10.1016/0378-3812\(83\)80058-2](https://doi.org/10.1016/0378-3812(83)80058-2).
- [179] M.R.W. Maciel, A.Z. Francesconi, Excess Gibbs free energies of (n-hexane + propan-1-ol) at 338.15 and 348.15 K and of (n-hexane + propan-2-ol) at 323.15, 338.15, and 348.15 K, *J.*

- Chem. Thermodyn. 20 (1988) 539–544. [https://doi.org/10.1016/0021-9614\(88\)90081-X](https://doi.org/10.1016/0021-9614(88)90081-X).
- [180] R.J. McDougal, L. V Jasperson, G.M. Wilson, Vapor–Liquid Equilibrium for Several Compounds Relevant to the Biofuels Industry Modeled with the Wilson Equation, *J. Chem. Eng. Data*. 59 (2014) 1069–1085. <https://doi.org/10.1021/je400885z>.
- [181] A. Heintz, E. Dolch, R.N. Lichtenthaler, New experimental VLE-data for alkanol/alkane mixtures and their description by an extended real association (ERAS) model., *Fluid Phase Equilib.* 27 (1986) 61–79. [https://doi.org/10.1016/0378-3812\(86\)87041-8](https://doi.org/10.1016/0378-3812(86)87041-8).
- [182] A. Belabbaci, R.M. Villamañan, L. Negadi, C.M. Martin, A. Ait Kaci, M. a. Villamañan, Vapor–Liquid Equilibria of Binary Mixtures Containing 1-Butanol and Hydrocarbons at 313.15 K, *J. Chem. Eng. Data*. 57 (2012) 114–119. <https://doi.org/10.1021/je200840e>.
- [183] T. Hiaki, A. Taniguchi, T. Tsuji, M. Hongo, K. Kojima, Isobaric Vapor–Liquid Equilibria of Octane + 1-Butanol, +2-Butanol, and +2-Methyl-2-propanol at 101.3 kPa, *J. Chem. Eng. Data*. 41 (1996) 1087–1090. <https://doi.org/10.1021/je960112z>.
- [184] T. Hiaki, A. Taniguchi, T. Tsuji, M. Hongo, Isothermal vapor–liquid equilibria of octane with 1-butanol, 2-butanol, or 2-methyl-2-propanol, *Fluid Phase Equilib.* 144 (1998) 145–155. [https://doi.org/10.1016/S0378-3812\(97\)00253-7](https://doi.org/10.1016/S0378-3812(97)00253-7).
- [185] A. Hull, B. Kronberg, J. van Stam, I. Golubkov, J. Kristensson, Vapor–Liquid Equilibrium of Binary Mixtures. 1. Ethanol + 1-Butanol, Ethanol + Octane, 1-Butanol + Octane, *J. Chem. Eng. Data*. 51 (2006) 1996–2001. <https://doi.org/10.1021/je0600045>.
- [186] S. Bernatová, J. Linek, I. Wichterle, Vapour-liquid equilibrium in the butyl alcohol -n-decane system at 85, 100 and 115°C, *Fluid Phase Equilib.* 74 (1992) 127–132. [https://doi.org/10.1016/0378-3812\(92\)85057-F](https://doi.org/10.1016/0378-3812(92)85057-F).
- [187] M. Ronc, G.R. Ratcliff, Measurement of vapor-liquid equilibria using a semi-continuous total pressure static equilibrium still, *Can. J. Chem. Eng.* 54 (1976) 326–332. <https://doi.org/10.1002/cjce.5450540414>.
- [188] I. Máchová, J. Linek, I. Wichterle, Vapour—liquid equilibria in the heptane - 1-pentanol and heptane - 3-methyl-1-butanol systems at 75, 85 and 95 °C, *Fluid Phase Equilib.* 41 (1988) 257–267. [https://doi.org/10.1016/0378-3812\(88\)80010-4](https://doi.org/10.1016/0378-3812(88)80010-4).
- [189] H. Kirss, M. Kuus, E. Siimer, Isobaric Vapor–Liquid Equilibria of the Ternary System Dibutyl Ether + 1-Pentanol + Nonane, *J. Chem. Eng. Data*. 51 (2006) 1887–1891. <https://doi.org/10.1021/je060237w>.
- [190] P.R. Rao, C. Chiranjivi, C.J. Dasarao, VApour-liquid equilibria systems: Hexane-hexylalcohol and heptane-hexylalcohol, *J. Appl. Chem.* 18 (1968) 166–168.

- <https://doi.org/10.1002/jctb.5010180602>.
- [191] T.-H. Cho, K. Ochi, K. Kojima, Isobaric Vapor-Liquid Equilibria for Binary Systems with Limited Miscibility, Water - n-Amyl Alcohol and Water-Isoamyl Alcohol, KAGAKU KOGAKU RONBUNSHU. 10 (1984) 181–183. <https://doi.org/10.1252/kakoronbunshu.10.181>.
- [192] R. Stephenson, J. Stuart, M. Tabak, Mutual solubility of water and aliphatic alcohols, J. Chem. Eng. Data. 29 (1984) 287–290. <https://doi.org/10.1021/je00037a019>.
- [193] Y.-H. Pai, L.-J. Chen, Liquid–liquid equilibria of two binary systems: water+1-pentanol and water+2-methyl-2-butanol and two ternary systems: water+1-pentanol+2-butyloxyethanol and water+2-methyl-2-butanol+2-butyloxyethanol, Fluid Phase Equilib. 155 (1999) 95–105. [https://doi.org/10.1016/S0378-3812\(98\)00456-7](https://doi.org/10.1016/S0378-3812(98)00456-7).
- [194] M.J. Fernández, V. Gomis, M. Ramos, F. Ruíz, Influence of the Temperature on the Liquid–Liquid Equilibrium of the Ternary System 1-Pentanol + 1-Propanol + Water, J. Chem. Eng. Data. 45 (2000) 1053–1054. <https://doi.org/10.1021/je000073y>.
- [195] E.C. Voutsas, C. Pamouktsis, D. Argyris, G.D. Pappa, Measurements and thermodynamic modeling of the ethanol–water system with emphasis to the azeotropic region, Fluid Phase Equilib. 308 (2011) 135–141. <https://doi.org/10.1016/j.fluid.2011.06.009>.
- [196] C. Gabaldón, P. Marzal, J.B. Montón, M.A. Rodrigo, Isobaric Vapor–Liquid Equilibria of the Water + 1-Propanol System at 30, 60, and 100 kPa, J. Chem. Eng. Data. 41 (1996) 1176–1180. <https://doi.org/10.1021/je9601467>.
- [197] V. Orr, J. Coates, Versatile Vapor-Liquid Equilibrium Still, Ind. Eng. Chem. 52 (1960) 27–30. <https://doi.org/10.1021/ie50601a030>.
- [198] S. Tunik, T. Lesteva, V. Chernaya, Phase Equilibria in the Water-Alcohols-Formaldehyde Systems I. The Liquid-Vapor Equilibria in the Systems Water-C6 and C7 Alcohols, Russ. J. Phys. Chem. 51 (1977) 751.
- [199] A.E. Hill, W.M. Malisoff, The Mutual Solubility of Liquids. III. The Mutual Solubility of Phenol and Water IV. The Mutual Solubility of Normal Butyl Alcohol and Water, J. Am. Chem. Soc. 48 (1926) 918–927. <https://doi.org/10.1021/ja01415a011>.
- [200] D.C. Jones, CXI.—The systems n-butyl alcohol–water and n-butyl alcohol–acetone–water, J. Chem. Soc. (1929) 799–813. <https://doi.org/10.1039/JR9290000799>.
- [201] R. Stephenson, J. Stuart, Mutual binary solubilities: water-alcohols and water-esters, J. Chem. Eng. Data. 31 (1986) 56–70. <https://doi.org/10.1021/je00043a019>.
- [202] M. Schmitt, H. Hasse, Phase Equilibria for Hexyl Acetate Reactive Distillation, J. Chem. Eng. Data. 50 (2005) 1677–1683. <https://doi.org/10.1021/je050141m>.

- [203] A. Dallos, J. Liszi, (Liquid + liquid) equilibria of (octan-1-ol + water) at temperatures from 288.15 K to 323.15 K, *J. Chem. Thermodyn.* 27 (1995) 447–448.
<https://doi.org/10.1006/jcht.1995.0046>.
- [204] B.E. Lang, Solubility of Water in Octan-1-ol from (275 to 369) K, *J. Chem. Eng. Data.* 57 (2012) 2221–2226. <https://doi.org/10.1021/je3001427>.
- [205] S.O. Derawi, G.M. Kontogeorgis, E.H. Stenby, T. Haugum, A.O. Fredheim, Liquid–Liquid Equilibria for Glycols + Hydrocarbons: Data and Correlation, *J. Chem. Eng. Data.* 47 (2002) 169–173. <https://doi.org/10.1021/je010199a>.
- [206] F. Kruger, G.M. Kontogeorgis, N. von Solms, New association schemes for mono-ethylene glycol: Cubic-Plus-Association parameterization and uncertainty analysis, *Fluid Phase Equilib.* 458 (2018) 211–233. <https://doi.org/10.1016/j.fluid.2017.11.026>.
- [207] S. Saeki, N. Kuwahara, M. Nakata, M. Kaneko, Upper and lower critical solution temperatures in poly (ethylene glycol) solutions, *Polymer (Guildf).* 17 (1976) 685–689.
[https://doi.org/10.1016/0032-3861\(76\)90208-1](https://doi.org/10.1016/0032-3861(76)90208-1).
- [208] Y.C. Bae, S.M. Lambert, D.S. Soane, J.M. Prausnitz, Cloud-point curves of polymer solutions from thermo-optical measurements, *Macromolecules.* 24 (1991) 4403–4407.
<https://doi.org/10.1021/ma00015a024>.
- [209] J.C. Lang, R.D. Morgan, Nonionic surfactant mixtures. I. Phase equilibria in C10E4–H2O and closed-loop coexistence, *J. Chem. Phys.* 73 (1980) 5849–5861.
<https://doi.org/10.1063/1.440028>.
- [210] D.J. Mitchell, G.J.T. Tiddy, L. Waring, T. Bostock, M.P. McDonald, Phase behaviour of polyoxyethylene surfactants with water. Mesophase structures and partial miscibility (cloud points), *J. Chem. Soc. Faraday Trans. 1 Phys. Chem. Condens. Phases.* 79 (1983) 975–1000.
<https://doi.org/10.1039/F19837900975>.
- [211] K.-V. Schubert, R. Strey, M. Kahlweit, A new purification technique for alkyl polyglycol ethers and miscibility gaps for water-CiEj, *J. Colloid Interface Sci.* 141 (1991) 21–29.
[https://doi.org/10.1016/0021-9797\(91\)90298-M](https://doi.org/10.1016/0021-9797(91)90298-M).
- [212] A.G. Aizpiri, F. Monroy, C. del Campo, R.G. Rubio, M. Díaz Peña, Range of simple scaling and critical amplitudes near a LCST. The 2-butoxyethanol + water system, *Chem. Phys.* 165 (1992) 31–39. [https://doi.org/10.1016/0301-0104\(92\)80040-3](https://doi.org/10.1016/0301-0104(92)80040-3).
- [213] K.-H. Lim, J.S. Reckley, D.H. Smith, Liquid-Liquid Phase Equilibrium in Binary Mixtures of the Nonionic Amphiphile CH₃(CH₂)₅(OCH₂CH₂)₂OH and Water, *J. Colloid Interface Sci.* 161 (1993) 465–470. <https://doi.org/10.1006/jcis.1993.1490>.

- [214] S.A. Sanders, A.Z. Panagiotopoulos, Micellization behavior of coarse grained surfactant models, *J. Chem. Phys.* 132 (2010) 114902. <https://doi.org/10.1063/1.3358354>.
- [215] C. Cowan-Ellsberry, S. Belanger, P. Dorn, S. Dyer, D. McAvoy, H. Sanderson, D. Versteeg, D. Ferrer, K. Stanton, Environmental Safety of the Use of Major Surfactant Classes in North America, *Crit. Rev. Environ. Sci. Technol.* 44 (2014) 1893–1993. <https://doi.org/10.1080/10739149.2013.803777>.
- [216] T.M. Ferreira, D. Topgaard, O.H.S. Ollila, Molecular Conformation and Bilayer Pores in a Nonionic Surfactant Lamellar Phase Studied with ^1H – ^{13}C Solid-State NMR and Molecular Dynamics Simulations, *Langmuir*. 30 (2014) 461–469. <https://doi.org/10.1021/la404684r>.
- [217] J. Eastoe, R.F. Tabor, Surfactants and Nanoscience, in: D. Berti, G. Palazzo (Eds.), *Colloid. Found. Nanosci.*, Elsevier, Amsterdam (The Netherlands), 2014: pp. 135–157. <https://doi.org/10.1016/B978-0-444-59541-6.00006-0>.
- [218] K. Holmberg, B. Jonsson, B. Kronberg, B. Lindman, *Surfactants and Polymers in Aqueous Solutions*, 2nd ed., John Wiley & Sons, Hoboken, NJ, 2003.
- [219] J.-H. Ryu, S. Park, B. Kim, A. Klaukherd, T.P. Russell, S. Thayumanavan, Highly Ordered Gold Nanotubes Using Thiols at a Cleavable Block Copolymer Interface, *J. Am. Chem. Soc.* 131 (2009) 9870–9871. <https://doi.org/10.1021/ja902567p>.
- [220] S. Garde, L.U. Yang, J.S. Dordick, M.E. Paulaitis, Molecular dynamics simulation of C8E5 micelle in explicit water: structure and hydrophobic solvation thermodynamics, *Mol. Phys.* 100 (2002) 2299–2306. <https://doi.org/10.1080/00268970110118312>.
- [221] G.T. Dimitrova, T.F. Tadros, P.F. Luckham, Investigations of the Phase Changes of Nonionic Surfactants Using Microscopy, Differential Scanning Calorimetry, and Rheology. 1. Synperonic A7, a C13/C15 Alcohol with 7 mol of Ethylene Oxide, *Langmuir*. 11 (1995) 1101–1111. <https://doi.org/10.1021/la00004a012>.
- [222] M. Corti, V. Degiorgio, Critical Behavior of a Micellar Solution, *Phys. Rev. Lett.* 45 (1980) 1045–1048. <https://doi.org/10.1103/PhysRevLett.45.1045>.
- [223] M. Zulauf, J.P. Rosenbusch, Micelle clusters of octylhydroxyoligo(oxyethylenes), *J. Phys. Chem.* 87 (1983) 856–862. <https://doi.org/10.1021/j100228a032>.
- [224] R. Dong, J. Hao, Complex Fluids of Poly(oxyethylene) Monoalkyl Ether Nonionic Surfactants, *Chem. Rev.* 110 (2010) 4978–5022. <https://doi.org/10.1021/cr9003743>.
- [225] Y. Nibu, T. Inoue, Phase Behavior of Aqueous Mixtures of Some Polyethylene Glycol Decyl Ethers Revealed by DSC and FT-IR Measurements, *J. Colloid Interface Sci.* 205 (1998) 305–315. <https://doi.org/10.1006/jcis.1998.5621>.

- [226] B.A. Mulley, A.D. Metcalf, Nonionic surface-active agents. Part VI. Phase equilibria in binary and ternary systems containing nonionic surface-active agents, *J. Colloid Sci.* 19 (1964) 501–515. [https://doi.org/10.1016/0095-8522\(64\)90066-2](https://doi.org/10.1016/0095-8522(64)90066-2).
- [227] J.S. Clunie, J.M. Corkill, J.F. Goodman, P.C. Symons, J.R. Tate, Thermodynamics of non-ionic surface-active agent + water systems, *Trans. Faraday Soc.* 63 (1967) 2839–2845. <https://doi.org/10.1039/TF9676302839>.
- [228] S.S. Funari, G. Rapp, X-ray Studies on the C12EO2/Water System, *J. Phys. Chem. B.* 101 (1997) 732–739. <https://doi.org/10.1021/jp9629250>.
- [229] M.L. Lynch, K.A. Kochvar, J.L. Burns, R.G. Laughlin, Aqueous-Phase Behavior and Cubic Phase-Containing Emulsions in the C12E2–Water System, *Langmuir.* 16 (2000) 3537–3542. <https://doi.org/10.1021/la991366w>.
- [230] J.S. Clunie, J.F. Goodman, P.C. Symons, Phase equilibria of dodecylhexaoxyethylene glycol monoether in water, *Trans. Faraday Soc.* 65 (1969) 287–296. <https://doi.org/10.1039/TF9696500287>.
- [231] K. Shinoda, Thermodynamic aspects of nonionic surfactant—Water systems, *J. Colloid Interface Sci.* 34 (1970) 278–282. [https://doi.org/10.1016/0021-9797\(70\)90179-7](https://doi.org/10.1016/0021-9797(70)90179-7).
- [232] V. Degiorgio, R. Piazza, M. Corti, C. Minero, Critical properties of nonionic micellar solutions, *J. Chem. Phys.* 82 (1985) 1025–1031. <https://doi.org/10.1063/1.448570>.
- [233] E. Jahns, H. Finkelmann, Lyotropic liquid crystalline phase behavior of a polymeric amphiphile polymerized via their hydrophilic ends, *Colloid Polym. Sci.* 265 (1987) 304–311. <https://doi.org/10.1007/BF01417929>.
- [234] F. Sterpone, G. Briganti, C. Pierleoni, Molecular Dynamics Study of Spherical Aggregates of Chain Molecules at Different Degrees of Hydrophilicity in Water Solution, *Langmuir.* 17 (2001) 5103–5110. <https://doi.org/10.1021/la000750m>.
- [235] F. Sterpone, C. Pierleoni, G. Briganti, M. Marchi, Molecular Dynamics Study of Temperature Dehydration of a C12E6 Spherical Micelle, *Langmuir.* 20 (2004) 4311–4314. <https://doi.org/10.1021/la035964t>.
- [236] C. Senac, W. Urbach, E. Kurtisovski, P.H. Hünenberger, B.A.C. Horta, N. Taulier, P.F.J. Fuchs, Simulating Bilayers of Nonionic Surfactants with the GROMOS-Compatible 2016H66 Force Field, *Langmuir.* 33 (2017) 10225–10238. <https://doi.org/10.1021/acs.langmuir.7b01348>.
- [237] H. Lee, R.M. Venable, A.D. MacKerell, R.W. Pastor, Molecular Dynamics Studies of Polyethylene Oxide and Polyethylene Glycol: Hydrodynamic Radius and Shape Anisotropy, *Biophys. J.* 95 (2008) 1590–1599. <https://doi.org/10.1529/biophysj.108.133025>.

- [238] W. Shinoda, R. DeVane, M.L. Klein, Multi-property fitting and parameterization of a coarse grained model for aqueous surfactants, *Mol. Simul.* 33 (2007) 27–36. <https://doi.org/10.1080/08927020601054050>.
- [239] W. Shinoda, R. DeVane, M.L. Klein, Coarse-grained molecular modeling of non-ionic surfactant self-assembly, *Soft Matter*. 4 (2008) 2454–2462. <https://doi.org/10.1039/B808701F>.
- [240] M. Velinova, Y. Tsoneva, A. Ivanova, A. Tadjer, Estimation of the Mutual Orientation and Intermolecular Interaction of C12Ex from Molecular Dynamics Simulations, *J. Phys. Chem. B*. 116 (2012) 4879–4888. <https://doi.org/10.1021/jp212047r>.
- [241] G. Rossi, P.F.J. Fuchs, J. Barnoud, L. Monticelli, A Coarse-Grained MARTINI Model of Polyethylene Glycol and of Polyoxyethylene Alkyl Ether Surfactants, *J. Phys. Chem. B*. 116 (2012) 14353–14362. <https://doi.org/10.1021/jp3095165>.
- [242] M. Vuorte, J. Määttä, M. Sammalkorpi, Simulations Study of Single-Component and Mixed n-Alkyl-PEG Micelles, *J. Phys. Chem. B*. 122 (2018) 4851–4860. <https://doi.org/10.1021/acs.jpcc.8b00398>.
- [243] T. Taddese, P. Carbone, Effect of Chain Length on the Partition Properties of Poly(ethylene oxide): Comparison between MARTINI Coarse-Grained and Atomistic Models, *J. Phys. Chem. B*. 121 (2017) 1601–1609. <https://doi.org/10.1021/acs.jpcc.6b10858>.
- [244] V. Adrien, G. Rayan, M. Reffay, L. Porcar, A. Maldonado, A. Ducruix, W. Urbach, N. Taulier, Characterization of a Biomimetic Mesophase Composed of Nonionic Surfactants and an Aqueous Solvent, *Langmuir*. 32 (2016) 10268–10275. <https://doi.org/10.1021/acs.langmuir.6b02744>.
- [245] F. Grunewald, G. Rossi, A.H. de Vries, S.J. Marrink, L. Monticelli, Transferable MARTINI Model of Poly(ethylene Oxide), *J. Phys. Chem. B*. 122 (2018) 7436–7449. <https://doi.org/10.1021/acs.jpcc.8b04760>.
- [246] M. Bulacu, N. Goga, W. Zhao, G. Rossi, L. Monticelli, X. Periolo, D.P. Tieleman, S.J. Marrink, Improved Angle Potentials for Coarse-Grained Molecular Dynamics Simulations, *J. Chem. Theory Comput.* 9 (2013) 3282–3292. <https://doi.org/10.1021/ct400219n>.
- [247] G. Bussi, D. Donadio, M. Parrinello, Canonical sampling through velocity rescaling, *J. Chem. Phys.* 126 (2007) 14101. <https://doi.org/10.1063/1.2408420>.
- [248] M. Parrinello, A. Rahman, Polymorphic transitions in single crystals: A new molecular dynamics method, *J. Appl. Phys.* 52 (1981) 7182–7190. <https://doi.org/10.1063/1.328693>.
- [249] B. Hess, H. Bekker, H.J.C. Berendsen, J.G.E.M. Fraaije, LINCS: A linear constraint solver for molecular simulations, *J. Comput. Chem.* 18 (1997) 1463–1472.

- [https://doi.org/10.1002/\(SICI\)1096-987X\(199709\)18:12<1463::AID-JCC4>3.0.CO;2-H](https://doi.org/10.1002/(SICI)1096-987X(199709)18:12<1463::AID-JCC4>3.0.CO;2-H).
- [250] L. Martínez, R. Andrade, E.G. Birgin, J.M. Martínez, PACKMOL: A package for building initial configurations for molecular dynamics simulations, *J. Comput. Chem.* 30 (2009) 2157–2164. <https://doi.org/10.1002/jcc.21224>.
- [251] W. Humphrey, A. Dalke, K. Schulten, VMD: Visual molecular dynamics, *J. Mol. Graph.* 14 (1996) 33–38. [https://doi.org/10.1016/0263-7855\(96\)00018-5](https://doi.org/10.1016/0263-7855(96)00018-5).
- [252] J. Hoshen, R. Kopelman, Percolation and cluster distribution. I. Cluster multiple labeling technique and critical concentration algorithm, *Phys. Rev. B.* 14 (1976) 3438–3445. <https://doi.org/10.1103/PhysRevB.14.3438>.
- [253] W.C. Griffin, Calculation of HLB Values of Non-Ionic Surfactants, *J. Soc. Cosmetics Chem.* 5 (1954) 249–256.
- [254] H.N. Patrick, G.G. Warr, Self-assembly structures of nonionic surfactants at graphite–solution interfaces. 2. Effect of polydispersity and alkyl chain branching, *Colloids Surfaces A Physicochem. Eng. Asp.* 162 (2000) 149–157. [https://doi.org/10.1016/S0927-7757\(99\)00187-9](https://doi.org/10.1016/S0927-7757(99)00187-9).
- [255] P. Sakya, J.M. Seddon, R.H. Templer, R.J. Mirkin, G.J.T. Tiddy, Micellar Cubic Phases and Their Structural Relationships: The Nonionic Surfactant System C12EO12/Water, *Langmuir.* 13 (1997) 3706–3714. <https://doi.org/10.1021/la9701844>.
- [256] S.S. Funari, M.C. Holmes, G.J.T. Tiddy, Intermediate Lyotropic Liquid Crystal Phases in the C16EO6/Water System, *J. Phys. Chem.* 98 (1994) 3015–3023. <https://doi.org/10.1021/j100062a045>.
- [257] C.E. Fairhurst, M.C. Holmes, M.S. Leaver, Structure and Morphology of the Intermediate Phase Region in the Nonionic Surfactant C16EO6/Water System, *Langmuir.* 13 (1997) 4964–4975. <https://doi.org/10.1021/la970186o>.
- [258] S.P. Christensen, F.A. Donate, T.C. Frank, R.J. LaTulip, L.C. Wilson, Mutual Solubility and Lower Critical Solution Temperature for Water + Glycol Ether Systems, *J. Chem. Eng. Data.* 50 (2005) 869–877. <https://doi.org/10.1021/je049635u>.
- [259] W.H. Richtering, W. Burchard, E. Jahns, H. Finkelmann, Light scattering from aqueous solutions of a nonionic surfactant (C14E8) in a wide concentration range, *J. Phys. Chem.* 92 (1988) 6032–6040. <https://doi.org/10.1021/j100332a039>.
- [260] B. Lindman, H. Wennerstroem, Nonionic micelles grow with increasing temperature, *J. Phys. Chem.* 95 (1991) 6053–6054. <https://doi.org/10.1021/j100168a063>.
- [261] J.S. Marland, B.A. Mulley, A phase-rule study of multiple-phase formation in a model emulsion system containing water, n-octanol, n-dodecane and/a non-ionic surface-active agent at 10 and

- 25°, *J. Pharm. Pharmacol.* 23 (1971) 561–572. <https://doi.org/10.1111/j.2042-7158.1971.tb08718.x>.
- [262] D. Constantin, P. Oswald, Diffusion Coefficients in a Lamellar Lyotropic Phase: Evidence for Defects Connecting the Surfactant Structure, *Phys. Rev. Lett.* 85 (2000) 4297–4300. <https://doi.org/10.1103/PhysRevLett.85.4297>.
- [263] S.S. Funari, M.C. Holmes, G.J.T. Tiddy, Microscopy, x-ray diffraction, and NMR studies of lyotropic liquid crystal phases in the C22EO6/water system: a new intermediate phase, *J. Phys. Chem.* 96 (1992) 11029–11038. <https://doi.org/10.1021/j100205a076>.
- [264] J. Burgoyne, M.C. Holmes, G.J.T. Tiddy, An Extensive Mesh Phase Liquid Crystal in Aqueous Mixtures of a Long Chain Nonionic Surfactant, *J. Phys. Chem.* 99 (1995) 6054–6063. <https://doi.org/10.1021/j100016a048>.
- [265] K.L. Huang, K. Shigeta, H. Kunieda, Phase behavior of polyoxyethylene dodecyl ether-water systems, in: G.J.M. Koper, D. Bedeaux, C. Cavaco, W.F.C. Sager (Eds.), *Trends Colloid Interface Sci. XII, Progress in Colloid & Polymer Science*, vol. 110, 1998: pp. 171–174.
- [266] M.C. Holmes, Intermediate phases of surfactant-water mixtures, *Curr. Opin. Colloid Interface Sci.* 3 (1998) 485–492. [https://doi.org/10.1016/S1359-0294\(98\)80022-8](https://doi.org/10.1016/S1359-0294(98)80022-8).
- [267] S. Dutt, P.F. Siril, S. Remita, Swollen liquid crystals (SLCs): a versatile template for the synthesis of nano structured materials, *RSC Adv.* 7 (2017) 5733–5750. <https://doi.org/10.1039/C6RA26390A>.
- [268] W.L. Hinze, *Cloud Point Extraction and Preconcentration Procedures for Organic and Related Pollutants of State Concern*, Water Resources Research Institute of the University of North Carolina, 1992.
- [269] P. Levitz, Aggregative adsorption of nonionic surfactants onto hydrophilic solid/water interface. Relation with bulk micellization, *Langmuir.* 7 (1991) 1595–1608. <https://doi.org/10.1021/la00056a010>.
- [270] J.M. Corkill, J.F. Goodman, R.H. Ottewill, Micellization of homogeneous non-ionic detergents, *Trans. Faraday Soc.* 57 (1961) 1627–1636. <https://doi.org/10.1039/TF9615701627>.
- [271] C.-C. Chen, Molecular thermodynamic model for gibbs energy of mixing of nonionic surfactant solutions, *AIChE J.* 42 (1996) 3231–3240. <https://doi.org/10.1002/aic.690421124>.
- [272] J.S. Marland, B.A. Mulley, Effect of micelle formation and the nature of the oil-phase on the distribution of a non-ionic surfactant in three- and four-component emulsions, *J. Pharm. Pharmacol.* 24 (1972) 729–734. <https://doi.org/10.1111/j.2042-7158.1972.tb09098.x>.
- [273] F. Portet, P.L. Desbene, C. Treiner, Adsorption Isotherms at a Silica/Water Interface of the

- Oligomers of Polydispersed Nonionic Surfactants of the Alkylpolyoxyethylated Series., *J. Colloid Interface Sci.* 194 (1997) 379–391. <https://doi.org/10.1006/jcis.1997.5113>.
- [274] A. Gezae Daful, V.A. Baulin, J. Bonet Avalos, A.D. Mackie, Accurate Critical Micelle Concentrations from a Microscopic Surfactant Model, *J. Phys. Chem. B.* 115 (2011) 3434–3443. <https://doi.org/10.1021/jp1102302>.
- [275] F. Yuan, R.G. Larson, Multiscale Molecular Dynamics Simulations of Model Hydrophobically Modified Ethylene Oxide Urethane Micelles, *J. Phys. Chem. B.* 119 (2015) 12540–12551. <https://doi.org/10.1021/acs.jpcc.5b04895>.
- [276] S. Puvvada, D. Blankschtein, Molecular-thermodynamic approach to predict micellization, phase behavior and phase separation of micellar solutions. I. Application to nonionic surfactants, *J. Chem. Phys.* 92 (1990) 3710–3724. <https://doi.org/10.1063/1.457829>.
- [277] S.D. Anogiannakis, P.C. Petris, D.N. Theodorou, Promising Route for the Development of a Computational Framework for Self-Assembly and Phase Behavior Prediction of Ionic Surfactants Using MARTINI, *J. Phys. Chem. B.* 124 (2020) 556–567. <https://doi.org/10.1021/acs.jpcc.9b09915>.
- [278] A.P. Santos, A.Z. Panagiotopoulos, Determination of the critical micelle concentration in simulations of surfactant systems, *J. Chem. Phys.* 144 (2016) 44709. <https://doi.org/10.1063/1.4940687>.
- [279] C. Browarzik, D. Browarzik, J. Winkelmann, Calculation of the phase equilibrium for systems of the type water+nonionic surfactant+alkane, *Fluid Phase Equilib.* 261 (2007) 238–247. <https://doi.org/10.1016/j.fluid.2007.07.007>.
- [280] B.W. Ninham, S.J. Chen, D.F. Evans, Role of oils and other factors in microemulsion design, *J. Phys. Chem.* 88 (1984) 5855–5857. <https://doi.org/10.1021/j150668a023>.
- [281] Y. Wang, M.C. Holmes, M.S. Leaver, A. Fogden, Mesh Phases in a Ternary Nonionic Surfactant, Oil, and Water System, *Langmuir.* 22 (2006) 10951–10957. <https://doi.org/10.1021/la060840c>.
- [282] N. Denham, M.C. Holmes, A. V Zvelindovsky, The Phases in a Non-Ionic Surfactant (C12E6)–Water Ternary System: A Coarse-Grained Computer Simulation, *J. Phys. Chem. B.* 115 (2011) 1385–1393. <https://doi.org/10.1021/jp108980p>.
- [283] R.G. Laughlin, Aqueous Surfactant Phase Behavior, in: A.P. Inc (Ed.), *Aqueous Phase Behav. Surfactants*, 1st ed., Elsevier Science Publishing Co Inc, San Diego, United States, 1996: pp. 387–396.
- [284] J.J. Sheng, Optimum phase type and optimum salinity profile in surfactant flooding, *J. Pet. Sci.*

- Eng. 75 (2010) 143–153. <https://doi.org/10.1016/j.petro.2010.11.005>.
- [285] K. Mohan, R. Gupta, K.K. Mohanty, Wettability Altering Secondary Oil Recovery in Carbonate Rocks, *Energy & Fuels*. 25 (2011) 3966–3973. <https://doi.org/10.1021/ef200449y>.
- [286] R. Rostami Ravari, S. Strand, T. Austad, Combined Surfactant-Enhanced Gravity Drainage (SEGD) of Oil and the Wettability Alteration in Carbonates: The Effect of Rock Permeability and Interfacial Tension (IFT), *Energy & Fuels*. 25 (2011) 2083–2088. <https://doi.org/10.1021/ef200085t>.
- [287] W. Wu, J. Pan, M. Guo, Mechanisms of oil displacement by ASP-foam and its influencing factors, *Pet. Sci.* 7 (2010) 100–105. <https://doi.org/10.1007/s12182-010-0012-1>.
- [288] J. Tang, Z. Qu, J. Luo, L. He, P. Wang, P. Zhang, X. Tang, Y. Pei, B. Ding, B. Peng, Y. Huang, Molecular Dynamics Simulations of the Oil-Detachment from the Hydroxylated Silica Surface: Effects of Surfactants, Electrostatic Interactions, and Water Flows on the Water Molecular Channel Formation, *J. Phys. Chem. B*. 122 (2018) 1905–1918. <https://doi.org/10.1021/acs.jpcc.7b09716>.
- [289] L.S. de Lara, M.F. Michelon, C.R. Miranda, Molecular Dynamics Studies of Fluid/Oil Interfaces for Improved Oil Recovery Processes, *J. Phys. Chem. B*. 116 (2012) 14667–14676. <https://doi.org/10.1021/jp310172j>.
- [290] Q. Liu, S. Yuan, H. Yan, X. Zhao, Mechanism of Oil Detachment from a Silica Surface in Aqueous Surfactant Solutions: Molecular Dynamics Simulations, *J. Phys. Chem. B*. 116 (2012) 2867–2875. <https://doi.org/10.1021/jp2118482>.
- [291] S. Yuan, S. Wang, X. Wang, M. Guo, Y. Wang, D. Wang, Molecular dynamics simulation of oil detachment from calcite surface in aqueous surfactant solution, *Comput. Theor. Chem.* 1092 (2016) 82–89. <https://doi.org/10.1016/j.comptc.2016.08.003>.
- [292] E. Lowry, M. Sedghi, L. Goual, Molecular simulations of NAPL removal from mineral surfaces using microemulsions and surfactants, *Colloids Surfaces A Physicochem. Eng. Asp.* 506 (2016) 485–494. <https://doi.org/10.1016/j.colsurfa.2016.07.002>.
- [293] P.C.T. Souza, R. Alessandri, J. Barnoud, S. Thallmair, I. Faustino, F. Grünwald, I. Patmanidis, H. Abdizadeh, B.M.H. Bruininks, T.A. Wassenaar, P.C. Kroon, J. Melcr, V. Nieto, V. Corradi, H.M. Khan, J. Domański, M. Javanainen, H. Martinez-Seara, N. Reuter, R.B. Best, I. Vattulainen, L. Monticelli, X. Periole, D.P. Tieleman, A.H. de Vries, S.J. Marrink, Martini 3: a general purpose force field for coarse-grained molecular dynamics, *Nat. Methods*. 18 (2021) 382–388. <https://doi.org/10.1038/s41592-021-01098-3>.
- [294] E. Perrin, M. Schoen, F.-X. Coudert, A. Boutin, Structure and Dynamics of Solvated Polymers

- near a Silica Surface: On the Different Roles Played by Solvent, *J. Phys. Chem. B.* 122 (2018) 4573–4582. <https://doi.org/10.1021/acs.jpcc.7b11753>.
- [295] D. Sergi, G. Scocchi, A. Ortona, Coarse-graining MARTINI model for molecular-dynamics simulations of the wetting properties of graphitic surfaces with non-ionic, long-chain, and T-shaped surfactants, *J. Chem. Phys.* 137 (2012) 94904. <https://doi.org/10.1063/1.4747827>.
- [296] U. Nations, Transforming our world: The 2030 agenda for sustainable development, DESA. (2015). <https://sustainabledevelopment.un.org/post2015/transformingourworld> (accessed November 19, 2018).
- [297] P.J. Dunn, The importance of Green Chemistry in Process Research and Development, *Chem. Soc. Rev.* 41 (2012) 1452–1461. <https://doi.org/10.1039/C1CS15041C>.
- [298] C.J. Clarke, W.-C. Tu, O. Levers, A. Bröhl, J.P. Hallett, Green and Sustainable Solvents in Chemical Processes, *Chem. Rev.* 118 (2018) 747–800. <https://doi.org/10.1021/acs.chemrev.7b00571>.
- [299] E.L. Smith, A.P. Abbott, K.S. Ryder, Deep Eutectic Solvents (DESs) and Their Applications, *Chem. Rev.* 114 (2014) 11060–11082. <https://doi.org/10.1021/cr300162p>.
- [300] M.C. Kroon, D.T. Allen, J.F. Brennecke, P.E. Savage, G.C. Schatz, ACS Virtual Issue on Deep Eutectic Solvents, *J. Chem. Eng. Data.* 62 (2017) 1927–1928. <https://doi.org/10.1021/acs.jced.7b00545>.
- [301] M.A.R. Martins, S.P. Pinho, J.A.P. Coutinho, Insights into the Nature of Eutectic and Deep Eutectic Mixtures, *J. Solution Chem.* 48 (2019) 962–982. <https://doi.org/10.1007/s10953-018-0793-1>.
- [302] S.P. Verevkin, A.Y. Sazonova, A.K. Frolkova, D.H. Zaitsau, I. V. Prikhodko, C. Held, Separation Performance of BioRenewable Deep Eutectic Solvents, *Ind. Eng. Chem. Res.* 54 (2015) 3498–3504. <https://doi.org/10.1021/acs.iecr.5b00357>.
- [303] L.F. Zubeir, C. Held, G. Sadowski, M.C. Kroon, PC-SAFT Modeling of CO₂ Solubilities in Deep Eutectic Solvents, *J. Phys. Chem. B.* 120 (2016) 2300–2310. <https://doi.org/10.1021/acs.jpcc.5b07888>.
- [304] R. Haghbakhsh, S. Raeissi, Modeling the Phase Behavior of Carbon Dioxide Solubility in Deep Eutectic Solvents with the Cubic Plus Association Equation of State, *J. Chem. Eng. Data.* 63 (2018) 897–906. <https://doi.org/10.1021/acs.jced.7b00472>.
- [305] R. Haghbakhsh, S. Raeissi, K. Parvaneh, A. Shariati, The friction theory for modeling the viscosities of deep eutectic solvents using the CPA and PC-SAFT equations of state, *J. Mol. Liq.* 249 (2018) 554–561. <https://doi.org/10.1016/J.MOLLIQ.2017.11.054>.

- [306] S.E.E. Warrag, C. Pototzki, N.R. Rodriguez, M. van Sint Annaland, M.C. Kroon, C. Held, G. Sadowski, C.J. Peters, Oil desulfurization using deep eutectic solvents as sustainable and economical extractants via liquid-liquid extraction: Experimental and PC-SAFT predictions, *Fluid Phase Equilib.* 467 (2018) 33–44. <https://doi.org/10.1016/j.fluid.2018.03.018>.
- [307] C.H.J.T. Dietz, D.J.G.P. van Osch, M.C. Kroon, G. Sadowski, M. van Sint Annaland, F. Gallucci, L.F. Zubeir, C. Held, PC-SAFT modeling of CO₂ solubilities in hydrophobic deep eutectic solvents, *Fluid Phase Equilib.* 448 (2017) 94–98. <https://doi.org/10.1016/j.fluid.2017.03.028>.
- [308] P.V.A. Pontes, E.A. Crespo, M.A.R. Martins, L.P. Silva, C.M.S.S. Neves, G.J. Maximo, M.D. Hubinger, E.A.C. Batista, S.P. Pinho, J.A.P. Coutinho, G. Sadowski, C. Held, Measurement and PC-SAFT modeling of solid-liquid equilibrium of deep eutectic solvents of quaternary ammonium chlorides and carboxylic acids, *Fluid Phase Equilib.* 448 (2017) 69–80. <https://doi.org/10.1016/j.fluid.2017.04.007>.
- [309] E.A. Crespo, L.P. Silva, M.A.R. Martins, L. Fernandez, J. Ortega, O. Ferreira, G. Sadowski, C. Held, S.P. Pinho, J.A.P. Coutinho, Characterization and Modeling of the Liquid Phase of Deep Eutectic Solvents Based on Fatty Acids/Alcohols and Choline Chloride, *Ind. Eng. Chem. Res.* 56 (2017) 12192–12202. <https://doi.org/10.1021/acs.iecr.7b02382>.
- [310] E.A. Crespo, L.P. Silva, M.A.R. Martins, M. Bulow, O. Ferreira, G. Sadowski, C. Held, S.S.P.S. Pinho, J.A.P.J. Coutinho, M. Bülow, O. Ferreira, G. Sadowski, C. Held, S.S.P.S. Pinho, J.A.P.J. Coutinho, M. Bulow, O. Ferreira, G. Sadowski, C. Held, S.S.P.S. Pinho, J.A.P.J. Coutinho, The Role of Polyfunctionality in the Formation of [Ch]Cl-Carboxylic Acid-Based Deep Eutectic Solvents, *Ind. Eng. Chem. Res.* 57 (2018) 11195–11209. <https://doi.org/10.1021/acs.iecr.8b01249>.
- [311] J.O. Lloret, L.F. Vega, F. Llovel, Accurate description of thermophysical properties of Tetraalkylammonium Chloride Deep Eutectic Solvents with the soft-SAFT equation of state, *Fluid Phase Equilib.* 448 (2017) 81–93. <https://doi.org/10.1016/j.fluid.2017.04.013>.
- [312] R.M. Ojeda, F. Llovel, Soft-SAFT Transferable Molecular Models for the Description of Gas Solubility in Eutectic Ammonium Salt-Based Solvents, *J. Chem. Eng. Data.* (2018). <https://doi.org/10.1021/acs.jced.7b01103>.
- [313] L. Fernandez, L.P. Silva, M.A.R. Martins, O. Ferreira, J. Ortega, S.P. Pinho, J.A.P. Coutinho, Indirect assessment of the fusion properties of choline chloride from solid-liquid equilibria data, *Fluid Phase Equilib.* 448 (2017) 9–14. <https://doi.org/10.1016/j.fluid.2017.03.015>.
- [314] S.L. Perkins, P. Painter, C.M. Colina, Experimental and Computational Studies of Choline

- Chloride-Based Deep Eutectic Solvents, *J. Chem. Eng. Data.* 59 (2014) 3652–3662.
<https://doi.org/10.1021/je500520h>.
- [315] O.S. Hammond, D.T. Bowron, K.J. Edler, Liquid structure of the choline chloride-urea deep eutectic solvent (reline) from neutron diffraction and atomistic modelling, *Green Chem.* 18 (2016) 2736–2744. <https://doi.org/10.1039/C5GC02914G>.
- [316] C.R. Ashworth, R.P. Matthews, T. Welton, P.A. Hunt, Doubly ionic hydrogen bond interactions within the choline chloride-urea deep eutectic solvent, *Phys. Chem. Chem. Phys.* 18 (2016) 18145–18160. <https://doi.org/10.1039/C6CP02815B>.
- [317] C. Held, T. Neuhaus, G. Sadowski, Compatible solutes: Thermodynamic properties and biological impact of ectoines and prolines, *Biophys. Chem.* 152 (2010) 28–39.
<https://doi.org/10.1016/j.bpc.2010.07.003>.
- [318] C. Held, G. Sadowski, Compatible solutes: Thermodynamic properties relevant for effective protection against osmotic stress, *Fluid Phase Equilib.* 407 (2016) 224–235.
<https://doi.org/10.1016/j.fluid.2015.07.004>.
- [319] M. Atilhan, S. Aparicio, PpT measurements and derived properties of liquid 1,2-alkanediols, *J. Chem. Thermodyn.* 57 (2013) 137–144. <https://doi.org/10.1016/j.jct.2012.08.014>.
- [320] T. Reschke, C. Brandenbusch, G. Sadowski, Modeling aqueous two-phase systems: I. Polyethylene glycol and inorganic salts as ATPS former, *Fluid Phase Equilib.* 368 (2014) 91–103. <https://doi.org/10.1016/j.fluid.2014.02.016>.
- [321] X. Liang, W. Yan, K. Thomsen, G.M. Kontogeorgis, Modeling the liquid–liquid equilibrium of petroleum fluid and polar compounds containing systems with the PC-SAFT equation of state, *Fluid Phase Equilib.* 406 (2015) 147–155. <https://doi.org/10.1016/j.fluid.2015.07.042>.
- [322] E.A. Crespo, J.M.L. Costa, A.M. Palma, B. Soares, J.J. Segovia, P.J. Carvalho, J.A.P. Coutinho, Thermodynamic Characterization of Deep Eutectic Solvents at High Pressures, *Fluid Phase Equilib.* 500 (2019) 112249. <https://doi.org/10.1016/j.fluid.2019.112249>.
- [323] D.I. Sagdeev, M.G. Fomina, G.K. Mukhamedzyanov, I.M. Abdulagatov, Experimental study of the density and viscosity of polyethylene glycols and their mixtures at temperatures from 293K to 465K and at high pressures up to 245MPa, *Fluid Phase Equilib.* 315 (2012) 64–76.
<https://doi.org/10.1016/j.fluid.2011.11.022>.
- [324] H. Passos, I. Khan, F. Mutelet, M.B. Oliveira, P.J. Carvalho, L.M.N.B.F. Santos, C. Held, G. Sadowski, M.G. Freire, J.A.P. Coutinho, Vapor-liquid equilibria of water + alkylimidazolium-based ionic liquids: Measurements and perturbed-chain statistical associating fluid theory modeling, *Ind. Eng. Chem. Res.* 53 (2014) 3737–3748. <https://doi.org/10.1021/ie4041093>.

- [325] M.B. Oliveira, E.A. Crespo, F. Llovell, L.F. Vega, J.A.P. Coutinho, Modeling the vapor–liquid equilibria and water activity coefficients of alternative refrigerant-absorbent ionic liquid–water pairs for absorption systems, *Fluid Phase Equilib.* 426 (2016) 100–109. <https://doi.org/10.1016/j.fluid.2016.02.017>.
- [326] J.O. Lloret, L.F. Vega, F. Llovell, A consistent and transferable thermodynamic model to accurately describe CO₂ capture with monoethanolamine, *J. CO₂ Util.* 21 (2017) 521–533. <https://doi.org/10.1016/j.jcou.2017.08.018>.
- [327] L.M.C. Pereira, F. Llovell, L.F. Vega, Thermodynamic characterisation of aqueous alkanolamine and amine solutions for acid gas processing by transferable molecular models, *Appl. Energy.* 222 (2018) 687–703. <https://doi.org/10.1016/J.APENERGY.2018.04.021>.
- [328] G.K. Folas, G.M. Kontogeorgis, M.L. Michelsen, E.H. Stenby, Application of the Cubic-Plus-Association (CPA) Equation of State to Complex Mixtures with Aromatic Hydrocarbons, *Ind. Eng. Chem. Res.* 45 (2006) 1527–1538. <https://doi.org/10.1021/ie050976q>.
- [329] L.P. Silva, M.A.R. Martins, J.H.F. Conceição, S.P. Pinho, J.A.P. Coutinho, Eutectic Mixtures Based on Polyalcohols as Sustainable Solvents: Screening and Characterization, *ACS Sustain. Chem. Eng.* 8 (2020) 15317–15326. <https://doi.org/10.1021/acssuschemeng.0c05518>.
- [330] R.L. Collin, Polymorphism and Radiation Decomposition of Choline Chloride, *J. Am. Chem. Soc.* 79 (1957) 6086. <https://doi.org/10.1021/ja01579a064>.
- [331] P. Shanley, R.L. Collin, The crystal structure of the high temperature form of choline chloride, *Acta Crystallogr.* 14 (1961) 79–80. <https://doi.org/10.1107/S0365110X61000292>.
- [332] L.P. Silva, J.H.F. Conceição, M.A.R. Martins, S.P. Pinho, J.A.P. Coutinho, Unpublished data, (n.d.).
- [333] E.S. Domalski, E.D. Hearing, Heat Capacities and Entropies of Organic Compounds in the Condensed Phase. Volume III, *J. Phys. Chem. Ref. Data.* 25 (1996) 1–525. <https://doi.org/10.1063/1.555985>.
- [334] E.A. Crespo, L.P. Silva, J.O. Lloret, P.J. Carvalho, L.F. Vega, F. Llovell, J.A.P. Coutinho, A Methodology to Parameterize SAFT-type Equations of State for Solid Precursors of Deep Eutectic Solvents: The Example of Cholinium Chloride, *Phys. Chem. Chem. Phys.* 21 (2019) 15046–15061. <https://doi.org/10.1039/C9CP02548K>.
- [335] F.S. Mjalli, O. Ahmad, Density of aqueous choline chloride-based ionic liquids analogues, *Thermochim. Acta.* 647 (2017) 8–14. <https://doi.org/10.1016/j.tca.2016.11.008>.
- [336] W. Guo, Y. Hou, S. Ren, S. Tian, W. Wu, Formation of deep eutectic solvents by phenols and choline chloride and their physical properties, *J. Chem. Eng. Data.* 58 (2013) 866–872.

- <https://doi.org/10.1021/je300997v>.
- [337] A.P. Abbott, P.M. Cullis, M.J. Gibson, R.C. Harris, E. Raven, Extraction of glycerol from biodiesel into a eutectic based ionic liquid, *Green Chem.* 9 (2007) 868–872.
<https://doi.org/10.1039/B702833D>.
- [338] P.J. Carvalho, I. Khan, A. Morais, J.F.O. Granjo, N.M.C. Oliveira, L.M.N.B.F. Santos, J.A.P. Coutinho, A new microbulliometer for the measurement of the vapor-liquid equilibrium of ionic liquid systems, *Fluid Phase Equilib.* 354 (2013) 156–165.
<https://doi.org/10.1016/j.fluid.2013.06.015>.
- [339] M. Francisco, A.S.B. Gonzalez, S.L. Garcia de Dios, W. Weggemans, M.C. Kroon, Comparison of a low transition temperature mixture (LTTM) formed by lactic acid and choline chloride with choline lactate ionic liquid and the choline chloride salt: physical properties and vapour-liquid equilibria of mixtures containing water and ethanol, *RSC Adv.* 3 (2013) 23553–23561.
<https://doi.org/10.1039/C3RA40303C>.
- [340] I. Khan, K.A. Kurnia, T.E. Sintra, J.A. Saraiva, S.P. Pinho, J.A.P. Coutinho, Assessing the activity coefficients of water in cholinium-based ionic liquids: Experimental measurements and COSMO-RS modeling, *Fluid Phase Equilib.* 361 (2014) 16–22.
<https://doi.org/10.1016/j.fluid.2013.10.032>.
- [341] I. Polishuk, About the numerical pitfalls characteristic for SAFT EOS models, *Fluid Phase Equilib.* 298 (2010) 67–74. <https://doi.org/10.1016/j.fluid.2010.07.003>.
- [342] I. Polishuk, Addressing the issue of numerical pitfalls characteristic for SAFT EOS models, *Fluid Phase Equilib.* 301 (2011) 123–129. <https://doi.org/10.1016/j.fluid.2010.11.021>.
- [343] I. Polishuk, A. Mulero, The numerical challenges of SAFT EoS models, *Rev. Chem. Eng.* 27 (2011) 241–251. <https://doi.org/10.1515/revce.2011.009>.
- [344] X. Meng, K. Ballerat-Busserolles, P. Husson, J.-M. Andanson, Impact of water on the melting temperature of urea + choline chloride deep eutectic solvent, *New J. Chem.* 40 (2016) 4492–4499. <https://doi.org/10.1039/C5NJ02677F>.
- [345] O.S. Hammond, D.T. Bowron, K.J. Edler, The Effect of Water upon Deep Eutectic Solvent Nanostructure: An Unusual Transition from Ionic Mixture to Aqueous Solution, *Angew. Chemie Int. Ed.* 56 (2017) 9782–9785. <https://doi.org/10.1002/anie.201702486>.
- [346] R.B. Leron, A.N. Soriano, M.H. Li, Densities and refractive indices of the deep eutectic solvents (choline chloride+ethylene glycol or glycerol) and their aqueous mixtures at the temperature ranging from 298.15 to 333.15K, *J. Taiwan Inst. Chem. Eng.* 43 (2012) 551–557.
<https://doi.org/10.1016/j.jtice.2012.01.007>.

- [347] R.B. Leron, A. Caparanga, M.-H. Li, Carbon dioxide solubility in a deep eutectic solvent based on choline chloride and urea at $T = 303.15\text{--}343.15$ K and moderate pressures, *J. Taiwan Inst. Chem. Eng.* 44 (2013) 879–885. <https://doi.org/10.1016/j.jtice.2013.02.005>.
- [348] R.B. Leron, M.-H. Li, Solubility of carbon dioxide in a eutectic mixture of choline chloride and glycerol at moderate pressures, *J. Chem. Thermodyn.* 57 (2013) 131–136. <https://doi.org/10.1016/j.jct.2012.08.025>.
- [349] M. Francisco, A. van den Bruinhorst, L.F. Zubeir, C.J. Peters, M.C. Kroon, A new low transition temperature mixture (LTTM) formed by choline chloride+lactic acid: Characterization as solvent for CO₂ capture, *Fluid Phase Equilib.* 340 (2013) 77–84. <https://doi.org/10.1016/j.fluid.2012.12.001>.
- [350] T.L. Greaves, C.J. Drummond, Protic ionic liquids: Properties and applications, *Chem. Rev.* 108 (2008) 206–237. <https://doi.org/10.1021/cr068040u>.
- [351] T.L. Greaves, C.J. Drummond, Protic Ionic Liquids: Evolving Structure–Property Relationships and Expanding Applications, *Chem. Rev.* 115 (2015) 11379–11448. <https://doi.org/10.1021/acs.chemrev.5b00158>.
- [352] A. González de Castilla, J.P. Bittner, S. Müller, S. Jakobtorweihen, I. Smirnova, Thermodynamic and Transport Properties Modeling of Deep Eutectic Solvents: A Review on gE-Models, Equations of State, and Molecular Dynamics, *J. Chem. Eng. Data.* 65 (2020) 943–967. <https://doi.org/10.1021/acs.jced.9b00548>.
- [353] I.I.I. Alkhatib, D. Bahamon, F. Llovel, M.R.M. Abu-Zahra, L.F. Vega, Perspectives and guidelines on thermodynamic modelling of deep eutectic solvents, *J. Mol. Liq.* 298 (2020) 112183. <https://doi.org/10.1016/j.molliq.2019.112183>.
- [354] M. Yoshizawa, W. Xu, C.A. Angell, Ionic Liquids by Proton Transfer: Vapor Pressure, Conductivity, and the Relevance of ΔpK_a from Aqueous Solutions, *J. Am. Chem. Soc.* 125 (2003) 15411–15419. <https://doi.org/10.1021/ja035783d>.
- [355] M.L. Alcantara, M.L. de Carvalho, V.H. Álvarez, P.I.S. Ferreira, M.L.L. Paredes, L. Cardozo-Filho, A.K. Silva, L.M. Lião, C.A.M. Pires, S. Mattedi, High pressure vapor-liquid equilibria for binary carbon dioxide and protic ionic liquid based on ethanolamines + butanoic acid, *Fluid Phase Equilib.* 460 (2018) 162–174. <https://doi.org/10.1016/j.fluid.2017.12.018>.
- [356] M.L. Alcantara, J.P. Santos, M. Loreno, P.I.S. Ferreira, M.L.L. Paredes, L. Cardozo-Filho, A.K. Silva, L.M. Lião, C.A.M. Pires, S. Mattedi, Low viscosity protic ionic liquid for CO₂/CH₄ separation: Thermophysical and high-pressure phase equilibria for diethylammonium butanoate, *Fluid Phase Equilib.* 459 (2018) 30–43. <https://doi.org/10.1016/j.fluid.2017.12.001>.

- [357] A. Afsharpour, An RETM approach to model CO₂ and H₂S solubility in four protic ionic liquids using mSRK and CPA EoSs, *J. Mol. Liq.* 324 (2021) 114684. <https://doi.org/10.1016/j.molliq.2020.114684>.
- [358] Z.S. Baird, P. Uusi-Kyyny, A. Dahlberg, D. Cederkrantz, V. Alopaeus, Densities, Viscosities, and Thermal Conductivities of the Ionic Liquid 7-Methyl-1,5,7-triazabicyclo[4.4.0]dec-5-enium Acetate and Its Mixtures with Water, *Int. J. Thermophys.* 41 (2020) 160. <https://doi.org/10.1007/s10765-020-02742-4>.
- [359] Z.S. Baird, P. Uusi-Kyyny, J. Witos, A.H. Rantamäki, H. Sixta, S.K. Wiedmer, V. Alopaeus, Vapor–Liquid Equilibrium of Ionic Liquid 7-Methyl-1,5,7-triazabicyclo[4.4.0]dec-5-enium Acetate and Its Mixtures with Water, *J. Chem. Eng. Data.* 65 (2020) 2405–2421. <https://doi.org/10.1021/acs.jced.9b01039>.
- [360] C. Held, T. Reschke, S. Mohammad, A. Luza, G. Sadowski, ePC-SAFT revised, *Chem. Eng. Res. Des.* 92 (2014) 2884–2897. <https://doi.org/10.1016/j.cherd.2014.05.017>.
- [361] E.A. Crespo, L.P. Silva, C.I.P. Correia, M.A.R. Martins, R.L. Gardas, L.F. Vega, P.J. Carvalho, J.A.P. Coutinho, Development of a robust soft-SAFT model for protic ionic liquids using new high-pressure density data, *Fluid Phase Equilib.* 539 (2021) 113036. <https://doi.org/10.1016/j.fluid.2021.113036>.
- [362] L.P. Silva, E.A. Crespo, M.A.R. Martins, R.L. Gardas, L.F. Vega, J.A.P. Coutinho, P.J. Carvalho, Evaluating Sustainable Encapsulated Protic Ionic Liquids for CO₂ Capture and Separation, in preparation, (2021).
- [363] K.M. Johansson, E.I. Izgorodina, M. Forsyth, D.R. MacFarlane, K.R. Seddon, Protic ionic liquids based on the dimeric and oligomeric anions: [(AcO)_xHx–1][–], *Phys. Chem. Chem. Phys.* 10 (2008) 2972–2978. <https://doi.org/10.1039/B801405A>.
- [364] M.A.R. Martins, G. Sharma, S.P. Pinho, R.L. Gardas, J.A.P. Coutinho, P.J. Carvalho, Selection and characterization of non-ideal ionic liquids mixtures to be used in CO₂ capture, *Fluid Phase Equilib.* 518 (2020) 112621. <https://doi.org/10.1016/j.fluid.2020.112621>.
- [365] M.A.R. Martins, P.J. Carvalho, L.M.N.B.F. Santos, S.P. Pinho, J.A.P. Coutinho, The impact of oligomeric anions on the speciation of protic ionic liquids, *Fluid Phase Equilib.* 531 (2021) 112919. <https://doi.org/10.1016/j.fluid.2020.112919>.
- [366] F.M.S. Ribeiro, C.F.R.A.C. Lima, A.M.S. Silva, L.M.N.B.F. Santos, Experimental Evidence for Azeotrope Formation from Protic Ionic Liquids., *ChemPhysChem.* 19 (2018) 2364–2369. <https://doi.org/10.1002/cphc.201800335>.
- [367] K. Bica, R.D. Rogers, Confused ionic liquid ions—a “liquification” and dosage strategy for

- pharmaceutically active salts, *Chem. Commun.* 46 (2010) 1215–1217.
<https://doi.org/10.1039/B925147B>.
- [368] M.E. Easton, K. Li, H.M. Titi, S.P. Kelley, R.D. Rogers, Controlling the Interface between Salts, Solvates, Co-crystals, and Ionic Liquids with Non-stoichiometric Protic Azolium Azolates, *Cryst. Growth Des.* 20 (2020) 2608–2616. <https://doi.org/10.1021/acs.cgd.9b01733>.
- [369] J.L. Shamshina, H.B. Wineinger, H. Choudhary, T.P. Vaid, S.P. Kelley, R.D. Rogers, Confusing Ions on Purpose: How Many Parent Acid Molecules Can Be Incorporated in a Herbicidal Ionic Liquid?, *ACS Sustain. Chem. Eng.* 9 (2021) 1941–1948.
<https://doi.org/10.1021/acssuschemeng.0c08797>.
- [370] S. Fakouri Baygi, H. Pahlavanzadeh, Application of the perturbed chain-SAFT equation of state for modeling CO₂ solubility in aqueous monoethanolamine solutions, *Chem. Eng. Res. Des.* 93 (2015) 789–799. <https://doi.org/10.1016/j.cherd.2014.07.017>.
- [371] R. Mohammadkhani, A. Paknejad, H. Zarei, Thermodynamic Properties of Amines under High Temperature and Pressure: Experimental Results Correlating with a New Modified Tait-like Equation and PC-SAFT, *Ind. Eng. Chem. Res.* 57 (2018) 16978–16988.
<https://doi.org/10.1021/acs.iecr.8b04732>.
- [372] L.A. Román-Ramírez, G.A. Leeke, p–x Data of (Acetic Acid + Water) at T = (412.6, 443.2, 483.2) K, *J. Chem. Eng. Data.* 61 (2016) 2078–2082. <https://doi.org/10.1021/acs.jced.5b01104>.
- [373] L.A. Román-Ramírez, F. García-Sánchez, R.C.D. Santos, G.A. Leeke, Vapour–liquid equilibrium of propanoic acid+water at 423.2, 453.2 and 483.2K from 1.87 to 19.38bar. Experimental and modelling with PR, CPA, PC-SAFT and PCP-SAFT, *Fluid Phase Equilib.* 388 (2015) 151–159. <https://doi.org/10.1016/j.fluid.2015.01.004>.
- [374] L.A. Román-Ramírez, F. García-Sánchez, G.A. Leeke, Evaluation of association schemes in the CPA and PC-SAFT equations of state in modeling VLE of organic acids + water systems, *Chem. Eng. Commun.* (2020) 1–13. <https://doi.org/10.1080/00986445.2020.1771323>.
- [375] M. Kleiner, Thermodynamic modeling of complex systems: Polar and Associating Fluids and Mixtures, Ph.D. Thesis. Tech. Univ. Dortmund. (2008).
- [376] R.M. DiGuilio, R.J. Lee, S.T. Schaeffer, L.L. Brasher, A.S. Teja, Densities and viscosities of the ethanolamines, *J. Chem. Eng. Data.* 37 (1992) 239–242.
<https://doi.org/10.1021/je00006a028>.
- [377] W. V Steele, R.D. Chirico, S.E. Knipmeyer, A. Nguyen, Measurements of Vapor Pressure, Heat Capacity, and Density along the Saturation Line for Cyclopropane Carboxylic Acid, N,N-Diethylethanolamine, 2,3-Dihydrofuran, 5-Hexen-2-one, Perfluorobutanoic Acid, and 2-

- Phenylpropionaldehyde, *J. Chem. Eng. Data.* 47 (2002) 715–724.
<https://doi.org/10.1021/je010087j>.
- [378] L. Lebrette, Y. Maham, T.T. Teng, L.G. Hepler, A.E. Mather, Volumetric properties of aqueous solutions of mono, and diethylethanolamines at temperatures from 5 to 80 °C II, *Thermochim. Acta.* 386 (2002) 119–126. [https://doi.org/10.1016/S0040-6031\(01\)00813-9](https://doi.org/10.1016/S0040-6031(01)00813-9).
- [379] K. Klepáčová, P.J.G. Huttenhuis, P.W.J. Derks, G.F. Versteeg, Vapor Pressures of Several Commercially Used Alkanolamines, *J. Chem. Eng. Data.* 56 (2011) 2242–2248.
<https://doi.org/10.1021/je101259r>.
- [380] X. Wang, K. Kang, W. Wang, Y. Tian, Volumetric Properties of Binary Mixtures of 3-(Methylamino)propylamine with Water, N-Methyldiethanolamine, N,N-Dimethylethanolamine, and N,N-Diethylethanolamine from (283.15 to 363.15) K, *J. Chem. Eng. Data.* 58 (2013) 3430–3439. <https://doi.org/10.1021/je400679k>.
- [381] O. Noll, A. Valtz, D. Richon, T. Getachew-Sawaya, I. Mokbel, J. Jose, Vapor Pressures and liquid densities of N-methylethanolamine, diethanolamine, and N-methyldiethanolamine, *Int. Electron. J. Physico-Chemical Data.* 4 (1998) 105–120.
- [382] R.R. Pinto, S. Mattedi, M. Aznar, Synthesis and Physical Properties of Three Protic Ionic Liquids with the Ethylammonium Cation, *Chem. Eng. Trans.* 43 (2015) 1165–1170.
<https://doi.org/10.3303/CET1543195>.
- [383] J.A. Sarabando, P.J.M. Magano, A.G.M. Ferreira, J.B. Santos, P.J. Carvalho, S. Mattedi, I.M.A. Fonseca, Influence of temperature and pressure on the density and speed of sound of 2-hydroxyethylammonium propionate ionic liquid, *J. Chem. Thermodyn.* 122 (2018) 183–193.
<https://doi.org/10.1016/j.jct.2018.03.016>.
- [384] N.M.C. Talavera-Prieto, A.G.M. Ferreira, P.N. Simões, P.J. Carvalho, S. Mattedi, J.A.P. Coutinho, Thermophysical characterization of N-methyl-2-hydroxyethylammonium carboxylate ionic liquids, *J. Chem. Thermodyn.* 68 (2014) 221–234.
<https://doi.org/10.1016/j.jct.2013.09.010>.
- [385] N.H. Othman Zailani, N.M. Yunus, A.H. Ab Rahim, M.A. Bustam, Thermophysical Properties of Newly Synthesized Ammonium-Based Protic Ionic Liquids: Effect of Temperature, Anion and Alkyl Chain Length, *Process.* 8 (2020). <https://doi.org/10.3390/pr8060742>.
- [386] A.T. Nasrabadi, L.D. Gelb, How Proton Transfer Equilibria Influence Ionic Liquid Properties: Molecular Simulations of Alkylammonium Acetates, *J. Phys. Chem. B.* 122 (2018) 5961–5971.
<https://doi.org/10.1021/acs.jpcc.8b01631>.
- [387] X. Ji, C. Held, G. Sadowski, Modeling imidazolium-based ionic liquids with ePC-SAFT, *Fluid*

- Phase Equilib. 335 (2012) 64–73. <https://doi.org/10.1016/j.fluid.2012.05.029>.
- [388] X.-S. Li, P. Englezos, Vapor–Liquid Equilibrium of Systems Containing Alcohols Using the Statistical Associating Fluid Theory Equation of State, *Ind. Eng. Chem. Res.* 42 (2003) 4953–4961. <https://doi.org/10.1021/ie030256o>.
- [389] X.-S. Li, H.-J. Wu, P. Englezos, Prediction of Gas Hydrate Formation Conditions in the Presence of Methanol, Glycerol, Ethylene Glycol, and Triethylene Glycol with the Statistical Associating Fluid Theory Equation of State, *Ind. Eng. Chem. Res.* 45 (2006) 2131–2137. <https://doi.org/10.1021/ie051204x>.
- [390] S.O. Derawi, G.M. Kontogeorgis, M.L. Michelsen, E.H. Stenby, Extension of the Cubic-Plus-Association Equation of State to Glycol–Water Cross-Associating Systems, *Ind. Eng. Chem. Res.* 42 (2003) 1470–1477. <https://doi.org/10.1021/ie0206103>.
- [391] G.K. Folas, S.O. Derawi, M.L. Michelsen, E.H. Stenby, G.M. Kontogeorgis, Recent applications of the cubic-plus-association (CPA) equation of state to industrially important systems, *Fluid Phase Equilib.* 228–229 (2005) 121–126. <https://doi.org/10.1016/j.fluid.2004.08.013>.
- [392] G.K. Folas, G.M. Kontogeorgis, M.L. Michelsen, E.H. Stenby, E. Solbraa, Liquid–Liquid Equilibria for Binary and Ternary Systems Containing Glycols, Aromatic Hydrocarbons, and Water: Experimental Measurements and Modeling with the CPA EoS, *J. Chem. Eng. Data.* 51 (2006) 977–983. <https://doi.org/10.1021/je050485c>.
- [393] A. Grenner, G.M. Kontogeorgis, N. von Solms, M.L. Michelsen, Application of PC-SAFT to glycol containing systems – PC-SAFT towards a predictive approach, *Fluid Phase Equilib.* 261 (2007) 248–257. <https://doi.org/10.1016/j.fluid.2007.04.025>.
- [394] I. Tsvintzelis, A. Grenner, I.G. Economou, G.M. Kontogeorgis, Evaluation of the Nonrandom Hydrogen Bonding (NRHB) Theory and the Simplified Perturbed-Chain–Statistical Associating Fluid Theory (sPC-SAFT). 2. Liquid–Liquid Equilibria and Prediction of Monomer Fraction in Hydrogen Bonding Systems, *Ind. Eng. Chem. Res.* 47 (2008) 5651–5659. <https://doi.org/10.1021/ie071382l>.
- [395] G.N.I. Clark, A. Galindo, G. Jackson, S. Rogers, A.N. Burgess, Modeling and Understanding Closed-Loop Liquid–Liquid Immiscibility in Aqueous Solutions of Poly(ethylene glycol) Using the SAFT-VR Approach with Transferable Parameters, *Macromolecules.* 41 (2008) 6582–6595. <https://doi.org/10.1021/ma8007898>.
- [396] M.P. Breil, G.M. Kontogeorgis, Thermodynamics of Triethylene Glycol and Tetraethylene Glycol Containing Systems Described by the Cubic-Plus-Association Equation of State, *Ind.*

- Eng. Chem. Res. 48 (2009) 5472–5480. <https://doi.org/10.1021/ie801412y>.
- [397] W. Afzal, M.P. Breil, P. Théveneau, A.H. Mohammadi, G.M. Kontogeorgis, D. Richon, Phase Equilibria of Mixtures Containing Glycol and n-Alkane: Experimental Study of Infinite Dilution Activity Coefficients and Modeling Using the Cubic-Plus-Association Equation of State, *Ind. Eng. Chem. Res.* 48 (2009) 11202–11210. <https://doi.org/10.1021/ie900856q>.
- [398] I. Tsivintzelis, G.M. Kontogeorgis, M.L. Michelsen, E.H. Stenby, Modeling phase equilibria for acid gas mixtures using the CPA equation of state. Part II: Binary mixtures with CO₂, *Fluid Phase Equilib.* 306 (2011) 38–56. <https://doi.org/10.1016/j.fluid.2011.02.006>.
- [399] G.M. Kontogeorgis, I. Tsivintzelis, M.L. Michelsen, E.H. Stenby, Towards predictive association theories, *Fluid Phase Equilib.* 301 (2011) 244–256. <https://doi.org/10.1016/j.fluid.2010.11.025>.
- [400] I. Tsivintzelis, G.M. Kontogeorgis, Modelling phase equilibria for acid gas mixtures using the CPA equation of state. Part VI. Multicomponent mixtures with glycols relevant to oil and gas and to liquid or supercritical CO₂ transport applications, *J. Chem. Thermodyn.* 93 (2016) 305–319. <https://doi.org/10.1016/j.jct.2015.07.003>.
- [401] W. Afzal, M.P. Breil, I. Tsivintzelis, A.H. Mohammadi, G.M. Kontogeorgis, D. Richon, Experimental study and phase equilibrium modeling of systems containing acid gas and glycol, *Fluid Phase Equilib.* 318 (2012) 40–50. <https://doi.org/10.1016/j.fluid.2011.12.025>.
- [402] X. Liang, G. Aloupis, G.M. Kontogeorgis, Data Requirements and Modeling for Gas Hydrate-Related Mixtures and a Comparison of Two Association Models, *J. Chem. Eng. Data.* 62 (2017) 2592–2605. <https://doi.org/10.1021/acs.jced.7b00081>.
- [403] A.M. Palma, M.B. Oliveira, A.J. Queimada, J.A.P. Coutinho, Evaluating Cubic Plus Association Equation of State Predictive Capacities: A Study on the Transferability of the Hydroxyl Group Associative Parameters, *Ind. Eng. Chem. Res.* 56 (2017) 7086–7099. <https://doi.org/10.1021/acs.iecr.7b00760>.
- [404] R.R. Boesen, P.J. Herslund, H. Sørensen, Loss of Monoethylene Glycol to CO₂- and H₂S-Rich Fluids: Modeled Using Soave–Redlich–Kwong with the Huron and Vidal Mixing Rule and Cubic-Plus-Association Equations of State, *Energy & Fuels.* 31 (2017) 3417–3426. <https://doi.org/10.1021/acs.energyfuels.6b02365>.
- [405] E. Petropoulou, G.D. Pappa, E. Voutsas, Modelling of phase equilibrium of natural gas mixtures containing associating compounds, *Fluid Phase Equilib.* 433 (2017) 135–148. <https://doi.org/https://doi.org/10.1016/j.fluid.2016.10.028>.
- [406] T. Takagi, H. Teranishi, Ultrasonic speeds and thermodynamics for binary solutions of n-

- alkanes under high pressures, *Fluid Phase Equilib.* 20 (1985) 315–320.
[https://doi.org/10.1016/0378-3812\(85\)90050-0](https://doi.org/10.1016/0378-3812(85)90050-0).
- [407] A.J. Queimada, I.M. Marrucho, J.A.P. Coutinho, E.H. Stenby, Viscosity and Liquid Density of Asymmetric n-Alkane Mixtures: Measurement and Modeling, *Int. J. Thermophys.* 26 (2005) 47–61. <https://doi.org/10.1007/s10765-005-2352-4>.
- [408] H.H. Reamer, B.H. Sage, Phase Equilibria in Hydrocarbon Systems. Volumetric and Phase Behavior of the Ethane-n-Decane System., *J. Chem. Eng. Data.* 7 (1962) 161–168.
<https://doi.org/10.1021/je60013a001>.
- [409] P.C. Joyce, M.C. Thies, Vapor–Liquid Equilibria for the Hexane + Hexadecane and Hexane + 1-Hexadecanol Systems at Elevated Temperatures and Pressures, *J. Chem. Eng. Data.* 43 (1998) 819–822. <https://doi.org/10.1021/je980037n>.
- [410] E.A. Crespo, J.M.L.J.M.L.J.M.L. Costa, A.M.A.M.A.M. Palma, B. Soares, M.C. Martín, J.J.J.J.J. Segovia, P.J.P.J.P.J. Carvalho, J.A.P.J.A.P. Coutinho, Thermodynamic Characterization of Deep Eutectic Solvents at High Pressures, *Fluid Phase Equilib.* 500 (2019) 112249. <https://doi.org/10.1016/j.fluid.2019.112249>.
- [411] A. Allal, C. Boned, A. Baylaucq, Free-volume viscosity model for fluids in the dense and gaseous states, *Phys. Rev. E.* 64 (2001) 11203. <https://doi.org/10.1103/PhysRevE.64.011203>.
- [412] A. Allal, M. Moha-ouchane, C. Boned, A New Free Volume Model for Dynamic Viscosity and Density of Dense Fluids Versus Pressure and Temperature, *Phys. Chem. Liq.* 39 (2001) 1–30.
<https://doi.org/10.1080/00319100108030323>.
- [413] S.E. Quiñones-Cisneros, C.K. Zéberg-Mikkelsen, E.H. Stenby, The friction theory (f-theory) for viscosity modeling, *Fluid Phase Equilib.* 169 (2000) 249–276.
[https://doi.org/10.1016/S0378-3812\(00\)00310-1](https://doi.org/10.1016/S0378-3812(00)00310-1).
- [414] T.H. Chung, M. Ajlan, L.L. Lee, K.E. Starling, Generalized multiparameter correlation for nonpolar and polar fluid transport properties, *Ind. Eng. Chem. Res.* 27 (1988) 671–679.
<https://doi.org/10.1021/ie00076a024>.
- [415] P.D. Neufeld, A.R. Janzen, R.A. Aziz, Empirical Equations to Calculate 16 of the Transport Collision Integrals $\Omega(l, s)^*$ for the Lennard-Jones (12–6) Potential, *J. Chem. Phys.* 57 (1972) 1100–1102. <https://doi.org/10.1063/1.1678363>.
- [416] C.R. Wilke, A Viscosity Equation for Gas Mixtures, *J. Chem. Phys.* 18 (1950) 517–519.
<https://doi.org/10.1063/1.1747673>.
- [417] X. Canet, P. Daugé, A. Baylaucq, C. Boned, C.K. Zéberg-Mikkelsen, S.E. Quiñones-Cisneros, E.H. Stenby, Density and Viscosity of the 1-Methylnaphthalene+2,2,4,4,6,8,8-

- Heptamethylnonane System from 293.15 to 353.15 K at Pressures up to 100 MPa, *Int. J. Thermophys.* 22 (2001) 1669–1689. <https://doi.org/10.1023/A:1013182715406>.
- [418] C. Boned, C.K. Zéberg-Mikkelsen, A. Baylaucq, P. Daugé, High-pressure dynamic viscosity and density of two synthetic hydrocarbon mixtures representative of some heavy petroleum distillation cuts, *Fluid Phase Equilib.* 212 (2003) 143–164. [https://doi.org/10.1016/S0378-3812\(03\)00279-6](https://doi.org/10.1016/S0378-3812(03)00279-6).
- [419] A. Baylaucq, C. Boned, X. Canet, C.K. Zéberg-Mikkelsen, High-Pressure (up to 140 MPa) Dynamic Viscosity of the Methane and Toluene System: Measurements and Comparative Study of Some Representative Models, *Int. J. Thermophys.* 24 (2003) 621–638. <https://doi.org/10.1023/A:1024023913165>.
- [420] M.A. Monsalvo, A. Baylaucq, P. Reghem, S.E. Quiñones-Cisneros, C. Boned, Viscosity measurements and correlations of binary mixtures: 1,1,1,2-tetrafluoroethane (HFC-134a)+tetraethylene glycol dimethylether (TEGDME), *Fluid Phase Equilib.* 233 (2005) 1–8. <https://doi.org/10.1016/j.fluid.2005.03.030>.
- [421] A. Baylaucq, C. Boned, X. Canet, C.K. Zéberg-Mikkelsen, S.E. Quiñones-Cisneros, H. Zhou, Dynamic Viscosity Modeling of Methane + n-Decane and Methane + Toluene Mixtures : Comparative Study of Some Representative Models, *Pet. Sci. Technol.* 23 (2005) 143–157. <https://doi.org/10.1081/LFT-200028122>.
- [422] C.K. Zéberg-Mikkelsen, G. Watson, A. Baylaucq, G. Galliéro, C. Boned, Comparative experimental and modeling studies of the viscosity behavior of ethanol+C7 hydrocarbon mixtures versus pressure and temperature, *Fluid Phase Equilib.* 245 (2006) 6–19. <https://doi.org/10.1016/j.fluid.2006.01.030>.
- [423] N. Cain, G. Roberts, D. Kiserow, R. Carbonell, Modeling the thermodynamic and transport properties of decahydronaphthalene/propane mixtures: Phase equilibria, density, and viscosity, *Fluid Phase Equilib.* 305 (2011) 25–33. <https://doi.org/10.1016/j.fluid.2011.02.009>.
- [424] M.A.R. Martins, L.P. Silva, N. Schaeffer, D.O. Abranches, G.J. Maximo, S.P. Pinho, J.A.P. Coutinho, Greener Terpene–Terpene Eutectic Mixtures as Hydrophobic Solvents, *ACS Sustain. Chem. Eng.* 7 (2019) 17414–17423. <https://doi.org/10.1021/acssuschemeng.9b04614>.
- [425] N. Schaeffer, J.H.F. Conceição, M.A.R. Martins, M.C. Neves, G. Pérez-Sánchez, J.R.B. Gomes, N. Papaiconomou, J.A.P. Coutinho, Non-ionic hydrophobic eutectics – versatile solvents for tailored metal separation and valorisation, *Green Chem.* 22 (2020) 2810–2820. <https://doi.org/10.1039/D0GC00793E>.
- [426] E.A. Crespo, L.P. Silva, P.J. Carvalho, J.A.P. Coutinho, The Excess Molar Volumes of Protic

- Ionic Liquids and its Significance to their Thermodynamic Modelling, Fluid Phase Equilib. submitted (2021).
- [427] E.L. Byrne, R. O'Donnell, M. Gilmore, N. Artioli, J.D. Holbrey, M. Swadźba-Kwaśny, Hydrophobic functional liquids based on trioctylphosphine oxide (TOPO) and carboxylic acids, *Phys. Chem. Chem. Phys.* 22 (2020) 24744–24763. <https://doi.org/10.1039/D0CP02605K>.
- [428] M. Gilmore, É.N. McCourt, F. Connolly, P. Nockemann, M. Swadźba-Kwaśny, J.D. Holbrey, Hydrophobic Deep Eutectic Solvents Incorporating Trioctylphosphine Oxide: Advanced Liquid Extractants, *ACS Sustain. Chem. Eng.* 6 (2018) 17323–17332. <https://doi.org/10.1021/acssuschemeng.8b04843>.
- [429] E.J. González, L. Alonso, Á. Domínguez, Physical Properties of Binary Mixtures of the Ionic Liquid 1-Methyl-3-octylimidazolium Chloride with Methanol, Ethanol, and 1-Propanol at T = (298.15, 313.15, and 328.15) K and at P = 0.1 MPa, *J. Chem. Eng. Data.* 51 (2006) 1446–1452. <https://doi.org/10.1021/je060123k>.
- [430] T.L. Greaves, A. Weerawardena, C. Fong, I. Krodkiewska, C.J. Drummond, Protic Ionic Liquids: Solvents with Tunable Phase Behavior and Physicochemical Properties, *J. Phys. Chem. B.* 110 (2006) 22479–22487. <https://doi.org/10.1021/jp0634048>.
- [431] G.J. Maximo, R.J.B.N. Santos, J.A. Lopes-da-Silva, M.C. Costa, A.J.A. Meirelles, J.A.P. Coutinho, Lipidic Protic Ionic Liquid Crystals, *ACS Sustain. Chem. Eng.* 2 (2014) 672–682. <https://doi.org/10.1021/sc400365h>.
- [432] K. Huang, X.-M. Zhang, Y. Xu, Y.-T. Wu, X.-B. Hu, Y. Xu, Protic ionic liquids for the selective absorption of H₂S from CO₂: Thermodynamic analysis, *AIChE J.* 60 (2014) 4232–4240. <https://doi.org/10.1002/aic.14634>.
- [433] J.A. Sarabando, P.J.M. Magano, A.G.M. Ferreira, J.B. Santos, P.J. Carvalho, S. Mattedi, I.M.A. Fonseca, M. Santos, Influence of temperature and pressure on the density and speed of sound of N-ethyl-2-hydroxyethylammonium propionate ionic liquid, *J. Chem. Thermodyn.* 131 (2019) 303–313. <https://doi.org/10.1016/j.jct.2018.11.005>.
- [434] R.S. Pinheiro, F.M.R. Mesquita, F.X. Feitosa, H.B. de Sant Ana, R.S. de Santiago-Aguiar, Density, Viscosity and Excess Properties of Binary Mixtures of Protic Ionic Liquid (2-HDEAF, 2-HDEAA) + Water at Different Temperatures, *Brazilian J. Chem. Eng.* 35 (2018) 383–394.
- [435] G. Cai, S. Yang, Q. Zhou, L. Liu, X. Lu, J. Xu, S. Zhang, Physicochemical Properties of Various 2-Hydroxyethylammonium Sulfonate -Based Protic Ionic Liquids and Their Potential Application in Hydrodeoxygenation, *Front. Chem.* 7 (2019) 196. <https://doi.org/10.3389/fchem.2019.00196>.

Supplementary Material

A. Additional expressions for the mathematical description of the soft-SAFT EoS

Derivatives of the radial distribution function

$$\left(\frac{\partial g_{LJ}(\sigma_m)}{\partial \tilde{\rho}}\right)_{\tilde{T},x} = xm \times \sigma_m^3 \sum_{p=1}^5 p \sum_{q=1}^5 a_{pq} (\rho_c^*)^{p-1} (T^*)^{1-q} \quad (A.1)$$

$$\tilde{T} \left(\frac{\partial g_{LJ}(\sigma_m)}{\partial \tilde{T}}\right)_{\tilde{\rho},x} = T^* \left(\frac{\partial g_{LJ}(\sigma_m)}{\partial T^*}\right)_{\tilde{\rho},x} = (1-q) \sum_{p=1}^5 \sum_{q=1}^5 a_{pq} (\rho_c^*)^p (T^*)^{1-q} \quad (A.2)$$

$$\left(\frac{\partial g_{LJ}(\sigma_m)}{\partial x_i}\right)_{\tilde{\rho},\tilde{T},x_{k \neq i}} = \sum_{p=1}^5 \sum_{q=1}^5 a_{pq} (\rho_c^*)^p (T^*)^{1-q} \frac{m_i}{xm} \left[p \left(\frac{1}{\sigma_m^3} \frac{\partial \sigma_m^3}{\partial x_{c,i}} - 1 \right) - (1-q) \frac{1}{\varepsilon_m} \frac{\partial \varepsilon_m}{\partial x_{c,i}} \right] \quad (A.3)$$

Size parameter of the ‘hypothetical fluid’ and its derivatives in respect to molar and monomeric compositions.

The mixture segment diameter is given as a function of the molar compositions, by the following expression:

$$\sigma_m^3 = \frac{\sum_{i=1}^{NC} \sum_{j=1}^{NC} x_i m_i x_j m_j \tilde{\sigma}_{ij}^3}{\left(\sum_{i=1}^{NC} x_i m_i\right)^2} = \frac{1}{xm^2} \sum_{i=1}^{NC} \sum_{j=1}^{NC} x_i m_i x_j m_j \tilde{\sigma}_{ij}^3 \quad (A.4)$$

The derivative in respect to the molar fraction of component i is then expressed as:

$$\frac{\partial \sigma_m^3}{\partial x_i} = \frac{2m_i \times xm \left[xm \left(\sum_{j=1}^{NC} x_j m_j \tilde{\sigma}_{ij}^3 \right) - \sum_{i=1}^{NC} \sum_{j=1}^{NC} x_i m_i x_j m_j \tilde{\sigma}_{ij}^3 \right]}{xm^4} \quad (A.5)$$

which using the definition of monomeric compositions and that of σ_m^3 simplifies to:

$$\frac{\partial \sigma_m^3}{\partial x_i} = \frac{2m_i}{xm} \left[\left(\sum_{j=1}^{NC} x_{c,j} \tilde{\sigma}_{ij}^3 \right) - \sigma_m^3 \right] \quad (A.6)$$

Alternatively, if the average size parameter is expressed as a function of the monomeric compositions, one obtains:

$$\sigma_m^3 = \sum_{i=1}^{NC} \sum_{j=1}^{NC} x_{c,i} x_{c,j} \tilde{\sigma}_{ij}^3 \quad (A.7)$$

whose derivative in respect to the monomeric composition of segments type i is:

$$\frac{\partial \sigma_m^3}{\partial x_{c,i}} = 2 \sum_{j=1}^{NC} x_{c,j} \tilde{\sigma}_{ij}^3 \quad (\text{A.8})$$

Applying eq. A.8 in eq. A.6:

$$\frac{\partial \sigma_m^3}{\partial x_i} = \frac{m_i}{xm} \left(\frac{\partial \sigma_m^3}{\partial x_{c,i}} - 2\sigma_m^3 \right) \quad (\text{A.9})$$

Energy parameter of the ‘hypothetical fluid’ and its derivatives in respect to molar and monomeric compositions.

The ‘averaged’ dispersive energy for the mixture is given as a function of molar compositions by the following expression:

$$\varepsilon_m \sigma_m^3 = \frac{\sum_{i=1}^{NC} \sum_{j=1}^{NC} x_i m_i x_j m_j \tilde{\sigma}_{ij}^3 \varepsilon_m}{\left(\sum_{i=1}^{NC} x_i m_i \right)^2} \quad (\text{A.10})$$

or in terms of monomeric compositions by eq. A.11:

$$\varepsilon_m \sigma_m^3 = \sum_{i=1}^{NC} \sum_{j=1}^{NC} x_{c,i} x_{c,j} \tilde{\sigma}_{ij}^3 \tilde{\varepsilon}_{ij} \quad (\text{A.11})$$

Therefore, the derivative in respect to the molar composition of component i is given by:

$$\frac{\partial(\varepsilon_m \sigma_m^3)}{\partial x_i} = \frac{2m_i}{xm} \left[\left(\sum_{j=1}^{NC} x_{c,j} \tilde{\varepsilon}_{ij} \tilde{\sigma}_{ij}^3 \right) - \varepsilon_m \sigma_m^3 \right] \quad (\text{A.12})$$

or, alternatively, in terms of monomeric compositions:

$$\frac{\partial(\varepsilon_m \sigma_m^3)}{\partial x_{c,i}} = 2 \sum_{j=1}^{NC} x_{c,j} \tilde{\varepsilon}_{ij} \tilde{\sigma}_{ij}^3 \quad (\text{A.13})$$

Applying eq. A.13 in eq. A.12, the following expression is obtained:

$$\frac{\partial(\varepsilon_m \sigma_m^3)}{\partial x_i} = \frac{m_i}{xm} \left[\frac{\partial(\varepsilon_m \sigma_m^3)}{\partial x_{c,i}} - 2\varepsilon_m \sigma_m^3 \right] \quad (\text{A.14})$$

Using fundamental mathematics, A.14 yields the following expression:

$$\frac{\partial \varepsilon_m}{\partial x_i} = \frac{1}{\sigma_m^3} \left[\frac{\partial(\varepsilon_m \sigma_m^3)}{\partial x_i} - \varepsilon_m \frac{\partial \sigma_m^3}{\partial x_i} \right] \quad (\text{A.15})$$

Applying eqs. A.9, A.14 in A.15, one can obtain the following simpler and easier to implement expression:

$$\frac{\partial \varepsilon_m}{\partial x_i} = \frac{m_i}{xm} \left[\frac{1}{\sigma_m^3} \frac{\partial(\varepsilon_m \sigma_m^3)}{\partial x_{c,i}} - \frac{\varepsilon_m}{\sigma_m^3} \frac{\partial \sigma_m^3}{\partial x_{c,i}} \right] \quad (\text{A.16})$$

Derivation of eq.2.34

The derivation starts from **eq. A.8** of Chapman et al.[51]:

$$\begin{aligned} \frac{\tilde{\mu}_i^{seg}}{m_i \times xm} &= \frac{\tilde{A}^{seg}}{xm \times \varepsilon_m} + (\tilde{Z}^{seg+id} - 1) \left[\frac{2 \sum_{j=1}^{NC} x_j m_j \tilde{\sigma}_{ij}^3}{\sigma_m^3 \sum_{j=1}^{NC} x_j m_j} - 1 \right] \\ &+ \frac{\tilde{U}^{seg}}{xm \times \varepsilon_m} \left[\frac{2 \sum_{j=1}^{NC} x_j m_j \tilde{\varepsilon}_{ij} \tilde{\sigma}_{ij}^3}{\varepsilon_m \sigma_m^3 \sum_{j=1}^{NC} x_j m_j} - \frac{2 \sum_{j=1}^{NC} x_j m_j \tilde{\sigma}_{ij}^3}{\sigma_m^3 \sum_{j=1}^{NC} x_j m_j} \right] \end{aligned} \quad (A.4)$$

The following relationships are also known or deduced before:

$$\tilde{Z}^{seg+id} = \frac{\tilde{p}^{seg+id} \sigma_m^3}{\rho^* T^* \varepsilon_m} \quad (A.5)$$

$$\frac{\partial \sigma_m^3}{\partial x_{c,i}} = 2 \sum_{j=1}^{NC} x_{c,j} \tilde{\sigma}_{ij}^3 = \frac{2 \sum_{j=1}^{NC} x_j m_j \tilde{\sigma}_{ij}^3}{\sum_{j=1}^{NC} x_j m_j} \quad (A.6)$$

$$\frac{\partial (\varepsilon_m \sigma_m^3)}{\partial x_{c,i}} = 2 \sum_{j=1}^{NC} x_{c,j} \tilde{\varepsilon}_{ij} \tilde{\sigma}_{ij}^3 = \frac{2 \sum_{j=1}^{NC} x_j m_j \tilde{\varepsilon}_{ij} \tilde{\sigma}_{ij}^3}{\sum_{j=1}^{NC} x_j m_j} \quad (A.7)$$

$$\frac{\partial \varepsilon_m}{\partial x_{c,i}} = \frac{\frac{\partial (\varepsilon_m \sigma_m^3)}{\partial x_{c,i}} - \varepsilon_m \frac{\partial \sigma_m^3}{\partial x_{c,i}}}{\sigma_m^3} \quad (A.8)$$

Using **eqs. A.6** and **A.7** in **A.8** yields:

$$\frac{\partial \varepsilon_m}{\partial x_{c,i}} = \frac{1}{\sigma_m^3} \left[\frac{2 \sum_{j=1}^{NC} x_j m_j \tilde{\varepsilon}_{ij} \tilde{\sigma}_{ij}^3}{\sum_{j=1}^{NC} x_j m_j} - \frac{2 \varepsilon_m \sum_{j=1}^{NC} x_j m_j \tilde{\sigma}_{ij}^3}{\sum_{j=1}^{NC} x_j m_j} \right] \quad (A.9)$$

Then, using **eqs. A.5**, **A.6**, and **A.9** in **eq. A.4**, one can easily obtain the final form of **eq. 2.34**:

$$\frac{\tilde{\mu}_i^{seg}}{xm \times m_i} = \frac{\tilde{A}^{seg}}{xm \times \varepsilon_m} + \left(\frac{(\tilde{\rho} \tilde{T} + \tilde{p}^{seg}) \sigma_m^3}{\varepsilon_m \times \rho_c^*} - T^* \right) \left(\frac{\partial \sigma_m^3}{\partial x_{c,i}} \frac{1}{\sigma_m^3} - 1 \right) + \frac{\tilde{U}^{seg}}{xm \times \varepsilon_m} \frac{\partial \varepsilon_m}{\partial x_{c,i}} \frac{1}{\varepsilon_m}$$

B. SAFT modelling of glycols and glymes

Table. B.1. Literature survey on the modelling of glycols using SAFT-based EoSs.

Glycol component	Other components	EoS	Assoc. Scheme	Reference
PEG 200/1500/4000/8000	<i>n</i> -propane/N ₂ /CO ₂	CK-SAFT	2B	[111]
MEG/TEG TEG	water <i>n</i> -hexane / benzene	CK-SAFT	4C	[388]
MEG TEG	water + methane water + methane/ethane/ <i>n</i> -propane	CK-SAFT	4C	[389]
MEG/DEG/TEG/TeEG	<i>n</i> -hexane/ <i>n</i> -heptane, methylcyclohexane	CPA	2B/4C	[7]
MEG/DEG/TEG	water	CPA	4C	[390]
MEG	water	CPA	4C	[391]
MEG/DEG/TEG MEG/DEG MEG/TEG TEG	benzene/toluene water + benzene water + toluene toluene + <i>n</i> -heptane	CPA	4C	[328,392]
MEG DEG TEG TeEG	CO ₂ /N ₂ /methane/benzene CO ₂ <i>n</i> -hexane/benzene CO ₂ /benzene	soft-SAFT	2B	[75]
PEG 200/300/400/600/ 1000/1500/4000/6000/8000	N ₂ /CO ₂ / <i>n</i> -propane/water/methanol ethanol/2-propanol/benzene/toluene ethylbenzene/ <i>n</i> -propylbenzene/ <i>t</i> -butyl acetate	soft-SAFT	2B	[113]
MEG DEG TEG TeEG PG	CO ₂ /N ₂ /methane/water/ <i>n</i> -heptane/PG CO ₂ /water/ <i>n</i> -heptane/benzene benzene/toluene/ <i>n</i> -hexane/ <i>n</i> -heptane/water benzene/toluene/ <i>o</i> -xylene/ <i>n</i> -heptane water + MEG/ <i>n</i> -heptane	sPC-SAFT	4C	[393]

Table B.1. (Continued)

Glycol component	Other components	EoS	Assoc. Scheme	Reference
MEG/DEG/TEG/	<i>n</i> -heptane	sPC-SAFT	4C	[394]
PEG 2180-1.02·10 ⁶	water	SAFT-VR	other*	[395]
TEG	<i>n</i> -C _n (n=1, 6, ...10) / benzene/toluene/water	CPA	4C/6D	[396]
TeEG	<i>n</i> -heptane		4C/7D	
MEG/DEG/TEG/TeEG	<i>n</i> -alkanes up to C16	CPA	4C/6D/7D	[397]
MEG/DEG/TEG	CO ₂	CPA	4C	[398]
TEG	methane/CO ₂ /water	CPA	4C	[399]
MEG	water/ <i>n</i> -hexane/2,2,4-trimethylpentane			
MEG/DEG/TEG	CO ₂ /water/methane	CPA	4C	[400]
MEG/DEG/TEG	CO ₂ /COS/H ₂ S	CPA	4C/6D	[401]
PEG (different <i>M_w</i>)	water + inorganic acids (ATPS)	ePC-SAFT	4C	[320]
MEG	<i>n</i> -hexane/ <i>n</i> -heptane/condensates	sPC-SAFT	4C	[321]
MEG	H ₂ O/methane/ <i>n</i> - hexane/benzene/toluene	CPA sPC-SAFT	4C	[402]
MEG	methane/ethane/ <i>n</i> -propane/ <i>n</i> -hexane/ <i>n</i> - heptane methylcyclohexane/CO ₂ /COS/H ₂ S water/petroleum fluids	modified CPA	4C	[403]
MEG	water/methane/CO ₂ /H ₂ S	CPA	4C	[404]
MEG	water/methane	CPA-PR	4C	[405]
MEG	water/methane/ <i>n</i> -hexane/ <i>n</i> -heptane	CPA	3C/4C/4E/4F	[206]

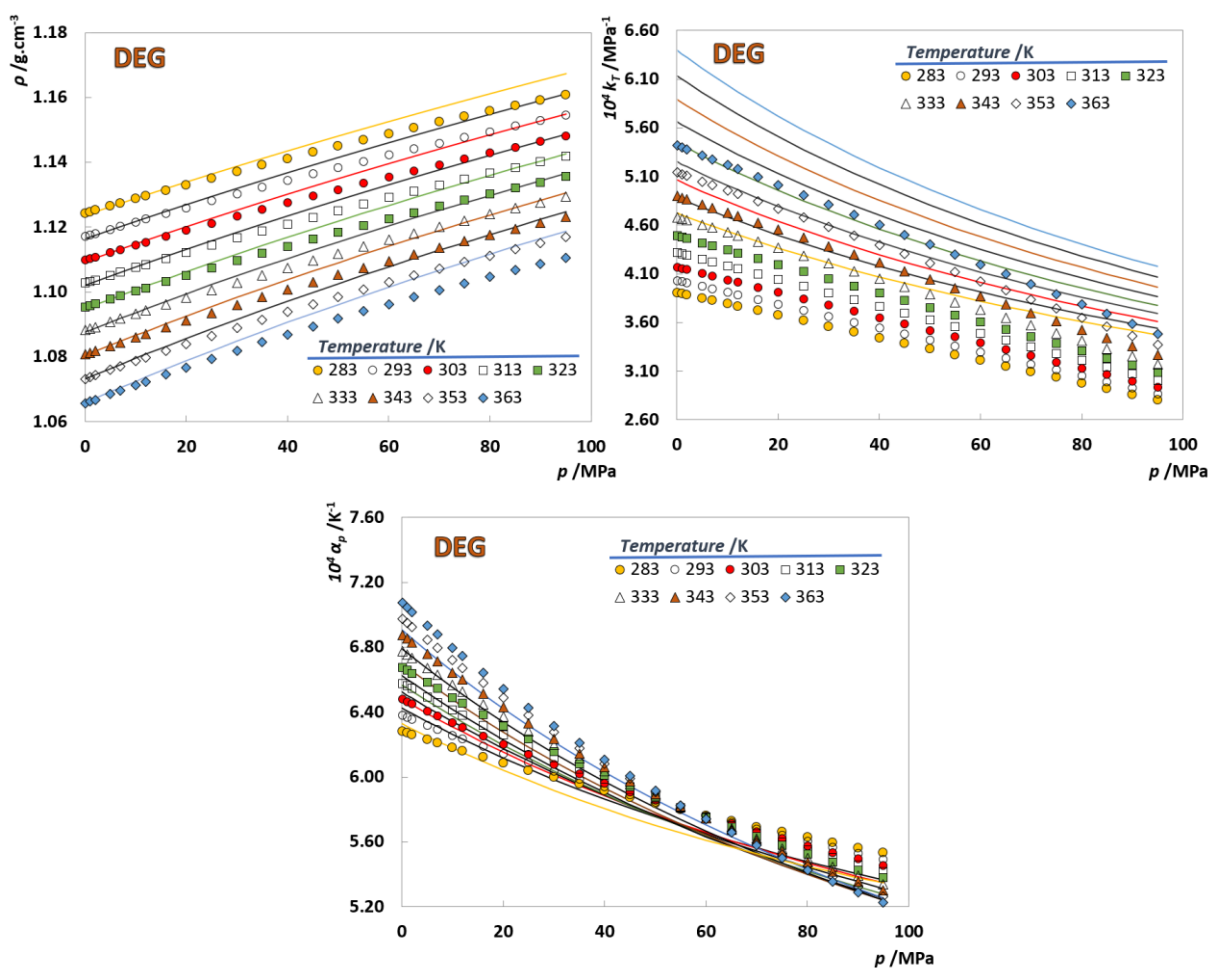


Figure. B.1. soft-SAFT modelling of the ppT data and second-order derivative properties of DEG. Symbols represent experimental data,[119] while the solid lines depict the soft-SAFT results using the parameters proposed by Pedrosa et al.[75]

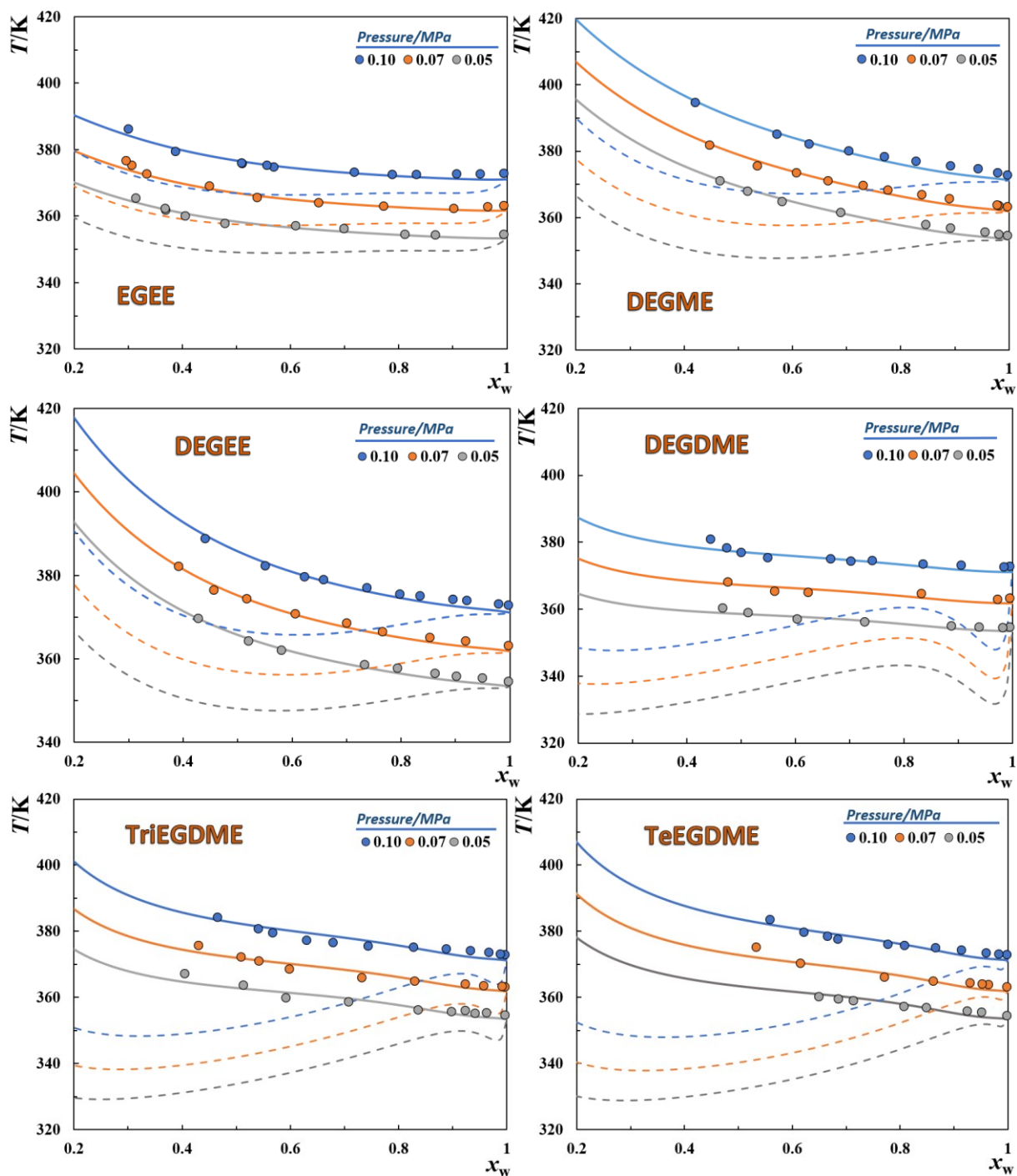


Figure. B.2. Isobaric temperature-composition phase diagrams of the binary glyme+ water mixtures. Symbols represent experimental data,[142] while the solid and dashed lines represent the soft-SAFT results, with and without using the binary interaction parameters from Table 3.11, respectively.

C. SAFT- γ -Mie EoS calculations

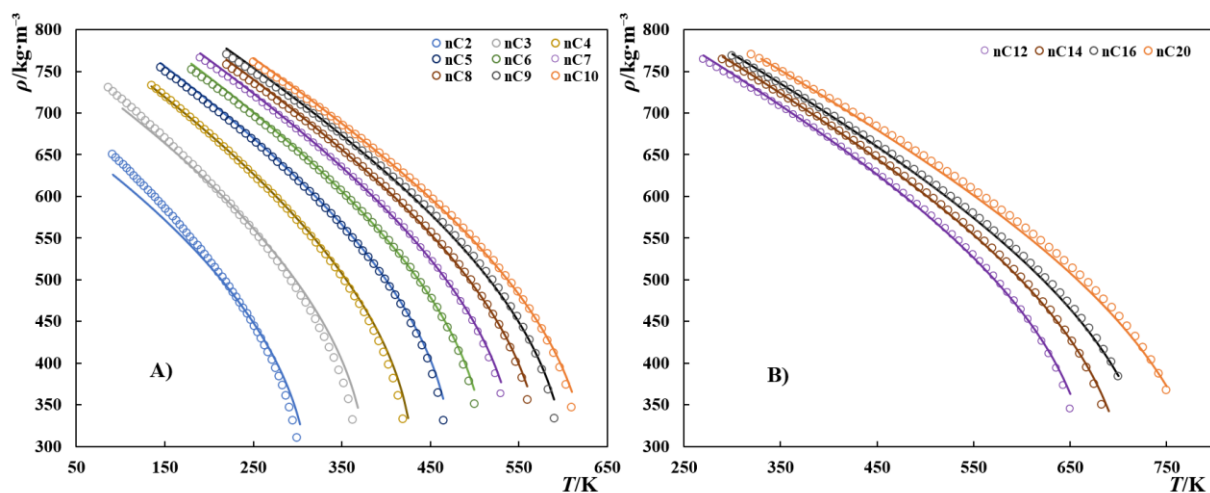


Figure. C.1. Saturated liquid density of linear alkanes. A) from ethane to n-decane (fitting) B) from n-dodecane to n-icosane (predicted). Symbols represent experimental data from the DIPPR database,[118] while the solid lines depict the SAFT- γ -Mie results.

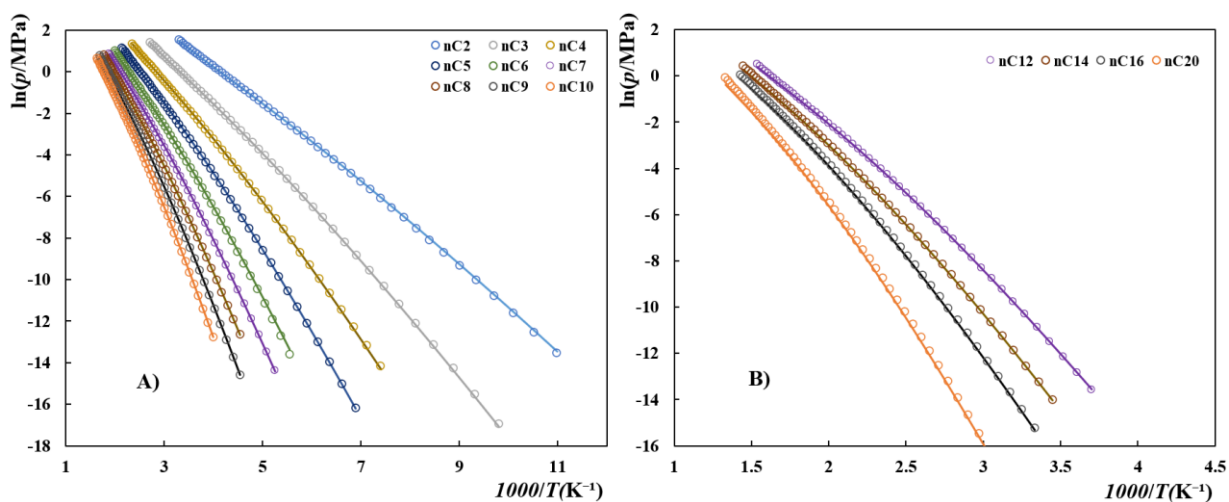


Figure. C.2. Vapor pressures of linear alkanes. A) from ethane to n-decane (fitting) B) from n-dodecane to n-icosane (predicted). Symbols represent experimental data from the DIPPR database,[118] while the solid lines depict the SAFT- γ -Mie results.

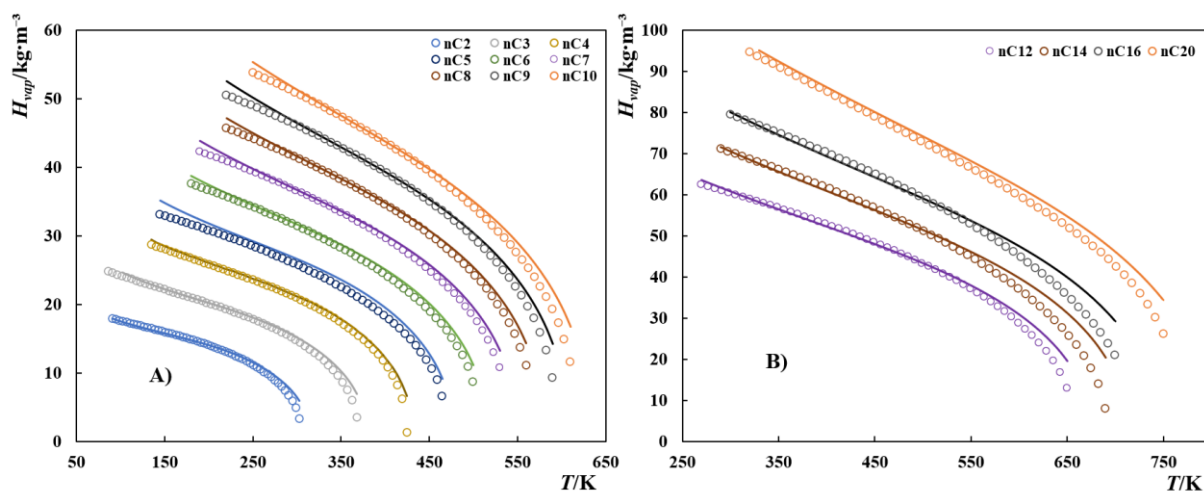


Figure. C.3. Vapor pressures of linear alkanes. A) from ethane to n-decane (fitting) B) from n-dodecane to n-icosane (predicted). Symbols represent experimental data from the DIPPR database,[117] while the solid lines depict the SAFT- γ -Mie results

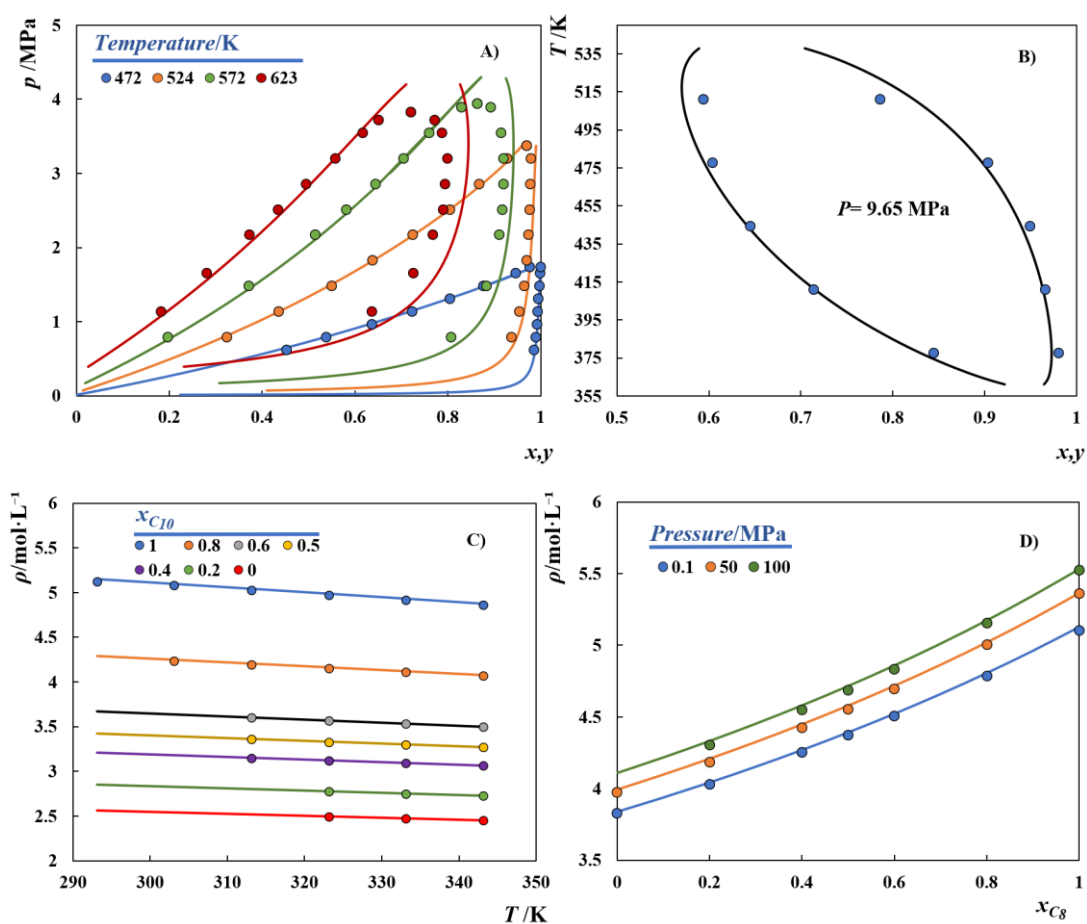


Figure. C.4. A) Isobaric VLE of n-hexane + n-hexadecane; B) Isothermal VLE of ethane + n-decane; C) atmospheric pressure liquid densities of n-decane + n-C22; D) high-pressure liquid densities of n-octane + n-

dodecane. Symbols represent the experimental data,[406–409] while the solid lines depict the SAFT- γ -Mie predictions.

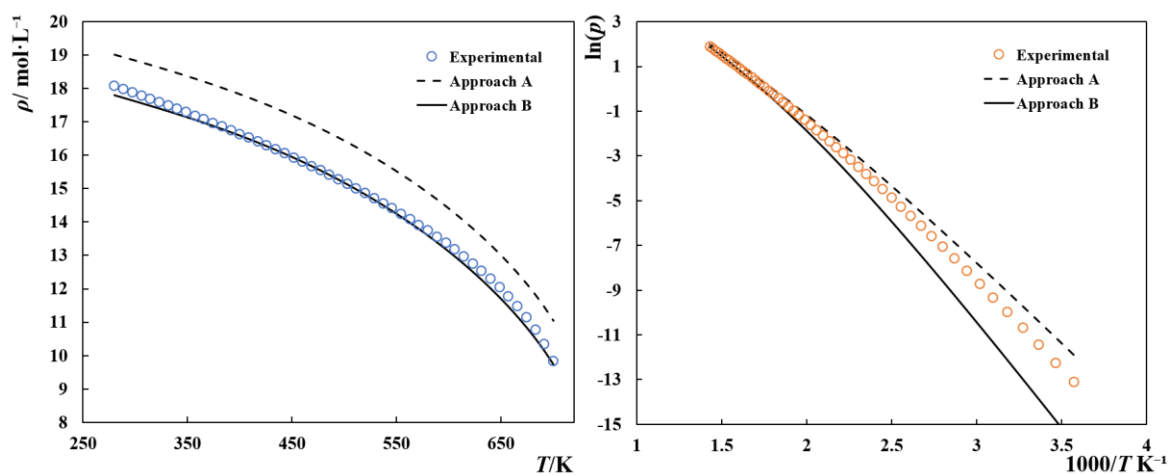


Figure. C.5. Saturation liquid densities and vapor pressures of pure EG. Symbols represent experimental data,[118] while the dashed and solid lines represent the SAFT- γ -Mie results following approach A and approach B, respectively.

Table. C.1. Deviations between the SAFT- γ -Mie results and the experimental data for the LLE of glycol (1) + n-heptane (2) systems [81] expressed in %ARD. x_1^{II} represents the molar fraction of glycol in the alkane-rich phase, while x_2^I represents the water mole fraction in the glycol rich-phase.

	Approach A		Approach B	
	x_1^{II}	x_2^I	x_1^{II}	x_2^I
DEG	16.34	85.50	60.07	16.27
TriEG	15.74	13.74	75.19	111.44
TeEG	55.20	266.8	91.34	178.20

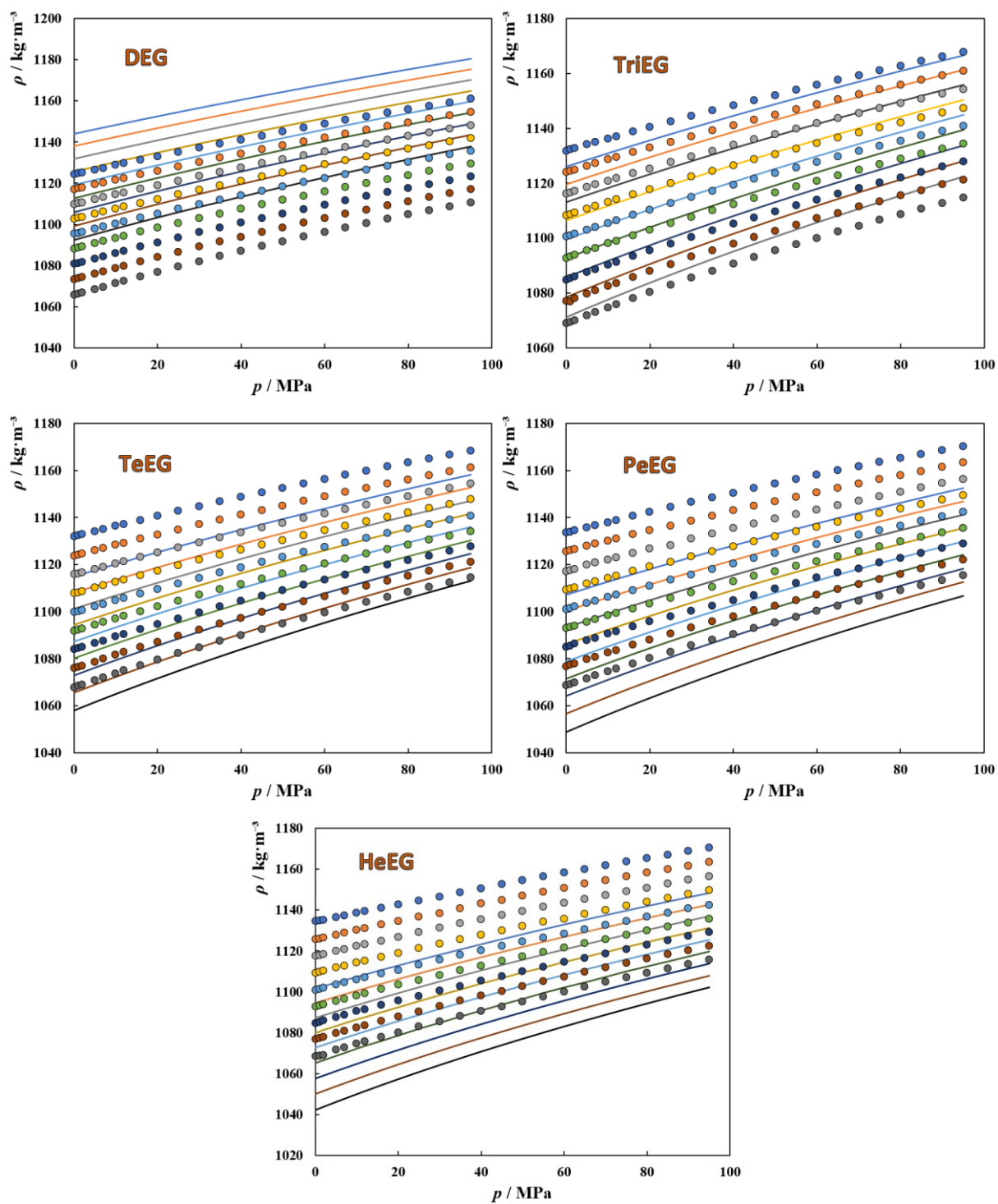
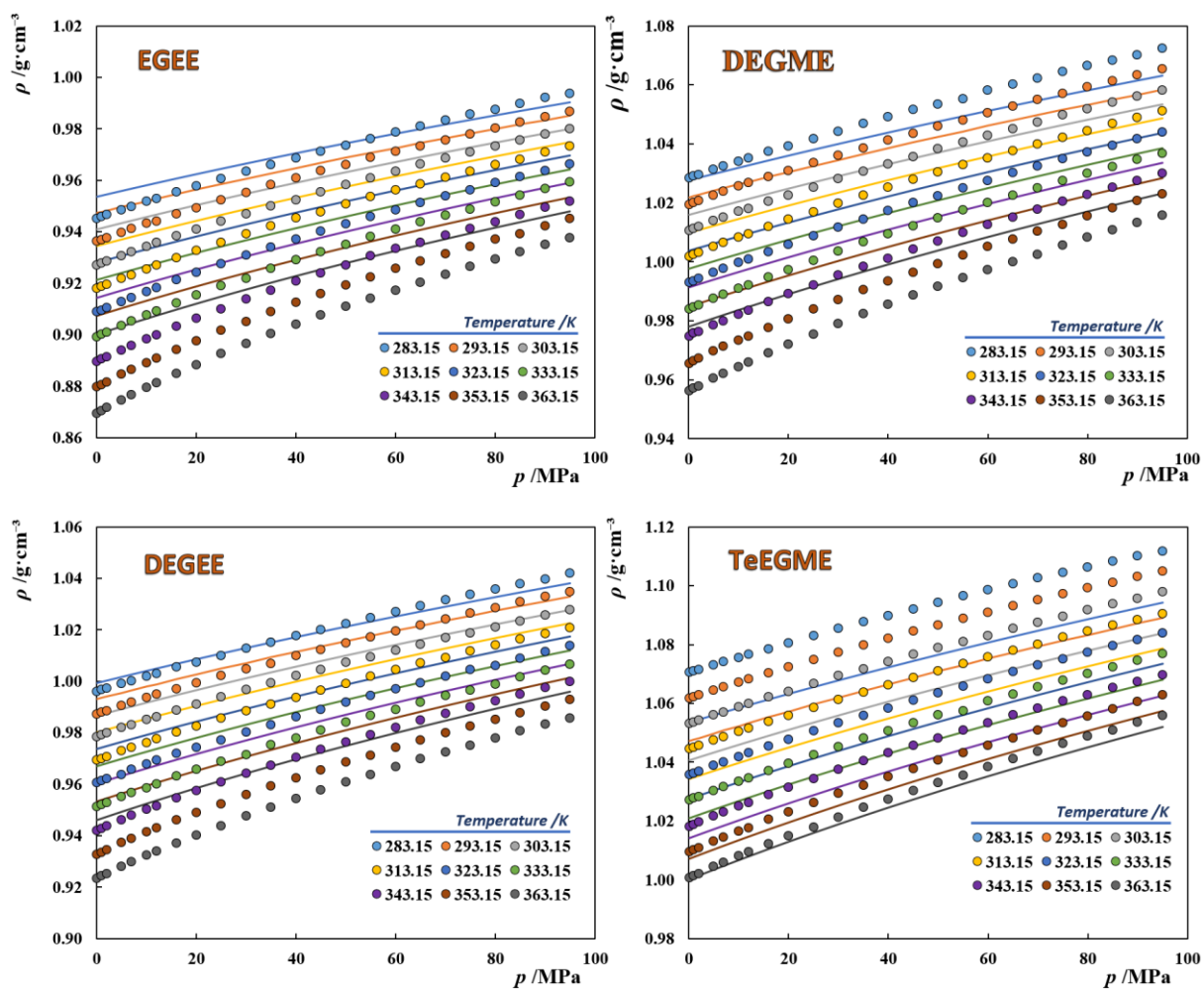


Figure. C.6. High-pressure liquid densities of pure glycols. Symbols represent the experimental data,[119] while the solid lines represent the SAFT- γ -Mie results following approach A.

Table. C.2. Deviations from the experimental VLE and $p\rho T$ data of pure glymes,[120] reported in %ARD.

	Approach A			Approach G		
	ρ_L	p^*	$p\rho T$	ρ_L	p^*	$p\rho T$
EGEE	3.87	91.79	1.25	0.67	39.20	1.04
DEGME	4.45	93.46	0.72	1.94	21.36	1.25
DEGEE	3.38	90.32	0.88	2.48	14.68	0.74
TeEGME	-	-	0.90	-	-	1.14
DEGDME	2.06	50.30	0.44	1.35	49.13	0.60
TriEGDME	1.21	38.74	1.18	1.36	36.08	0.41
TeEGDME	2.64	32.65	2.08	2.22	31.31	0.79



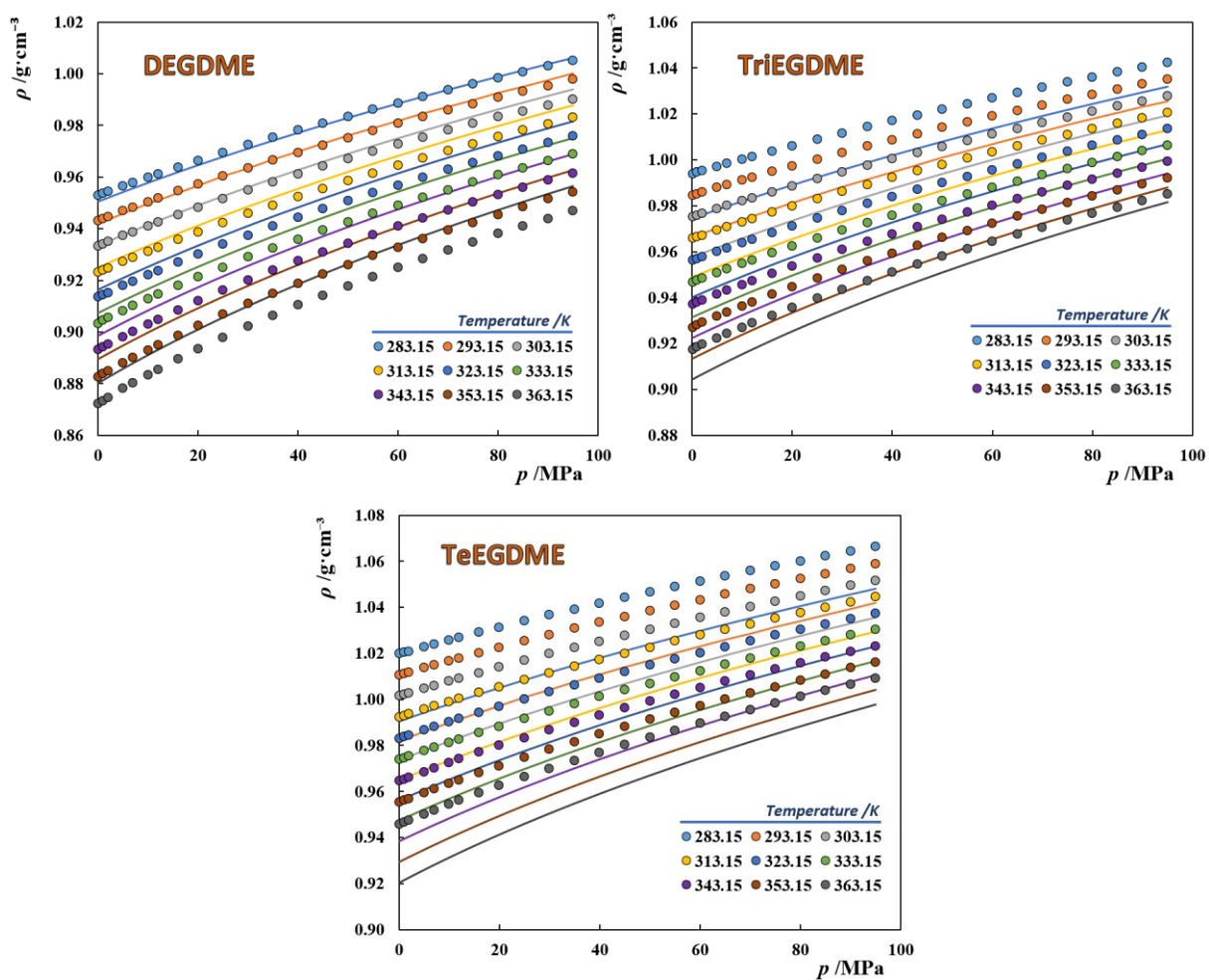
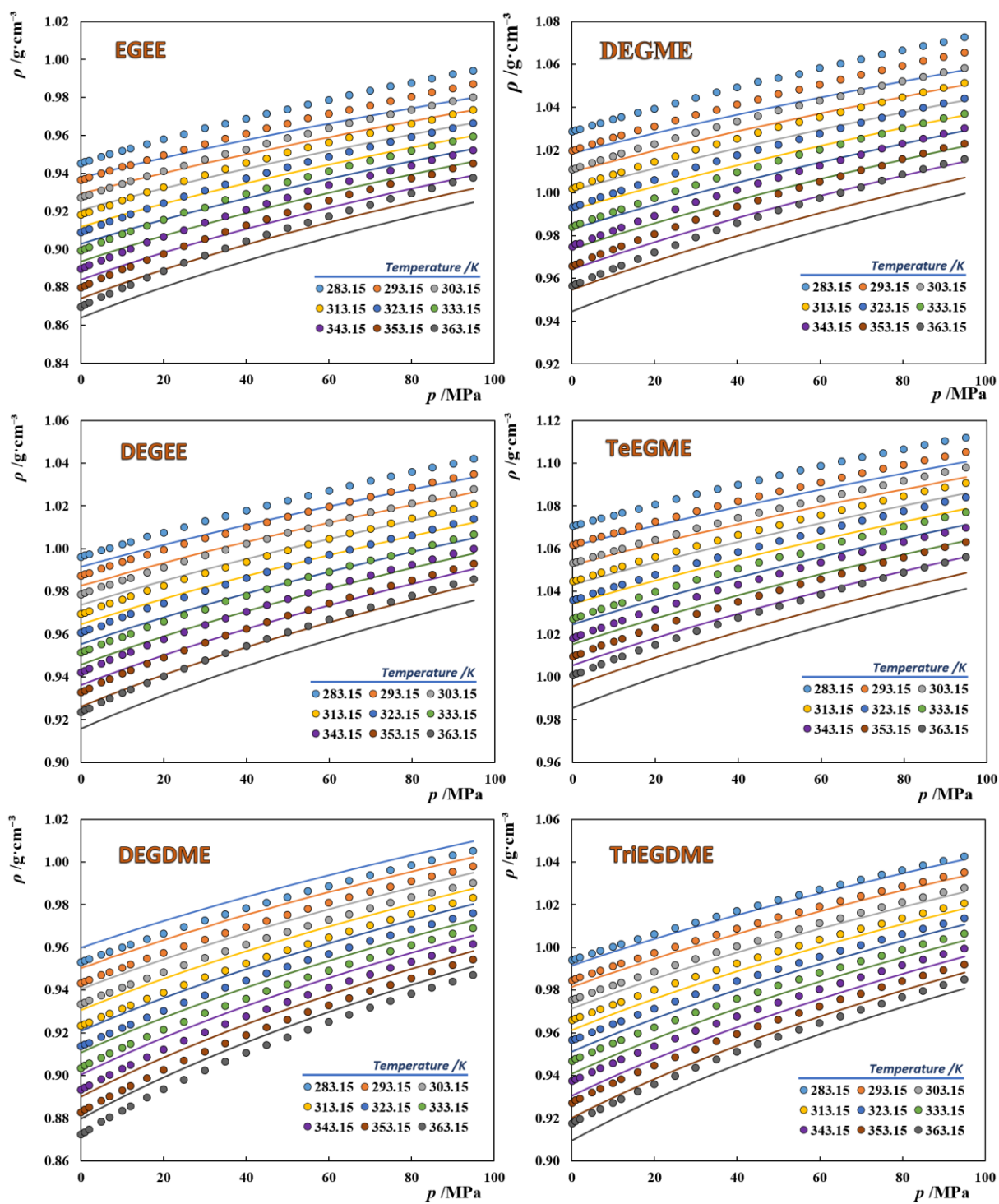


Figure. C.7. High-pressure liquid densities of pure glymes. Symbols represent experimental data,[120] while the solid lines depict the SAFT- γ -Mie results, following approach A.



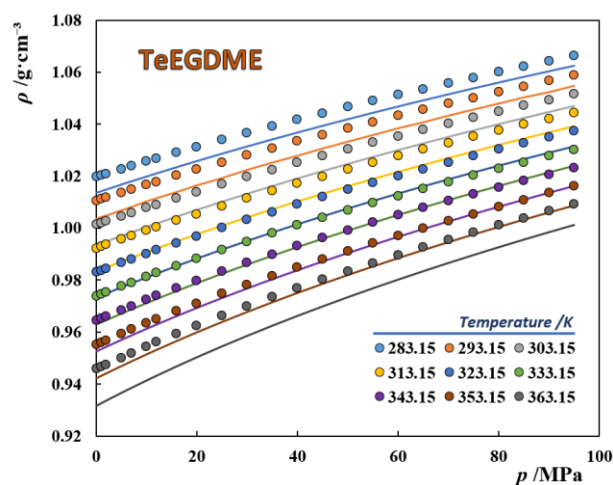


Figure. C.8. High-pressure liquid densities of pure glymes. Symbols represent experimental data,[120] while the solid lines depict the SAFT- γ -Mie results following approach G.

Table. C.3. Deviations between the SAFT- γ -Mie modelling results and the VLE experimental data for glyme + water systems.[138]

System	Approach A	Approach G
	AAD (T) /K	
EGEE + water	5.6	4.14
DEGME + water	1.38	0.49
DEGEE + water	1.11	0.55
DEGDME + water	0.63	2.08
TriEGDME + water	0.37	1.06
TeEGDME + water	0.64	1.90

D. CG-MD simulations of $C_iE_j + H_2O$ systems

60 wt% – Frontal View

60 wt% – Side View

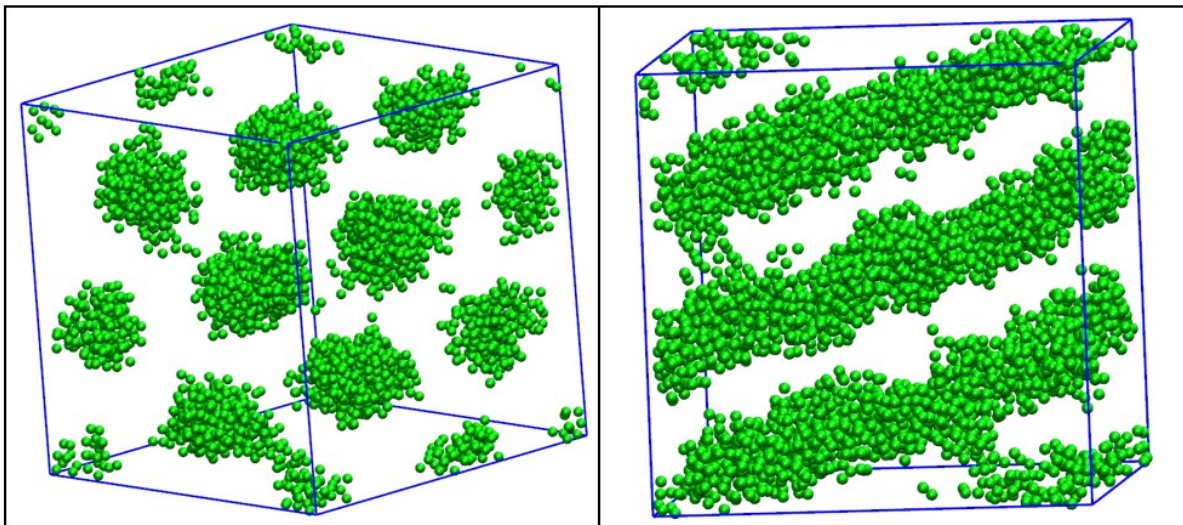


Figure. D.1. Final snapshot of the CG-MD simulation of C_8E_6/H_2O at 60 wt%, showing the alkyl tails disposition in the H_1 phase observed.

15 wt%

30 wt%

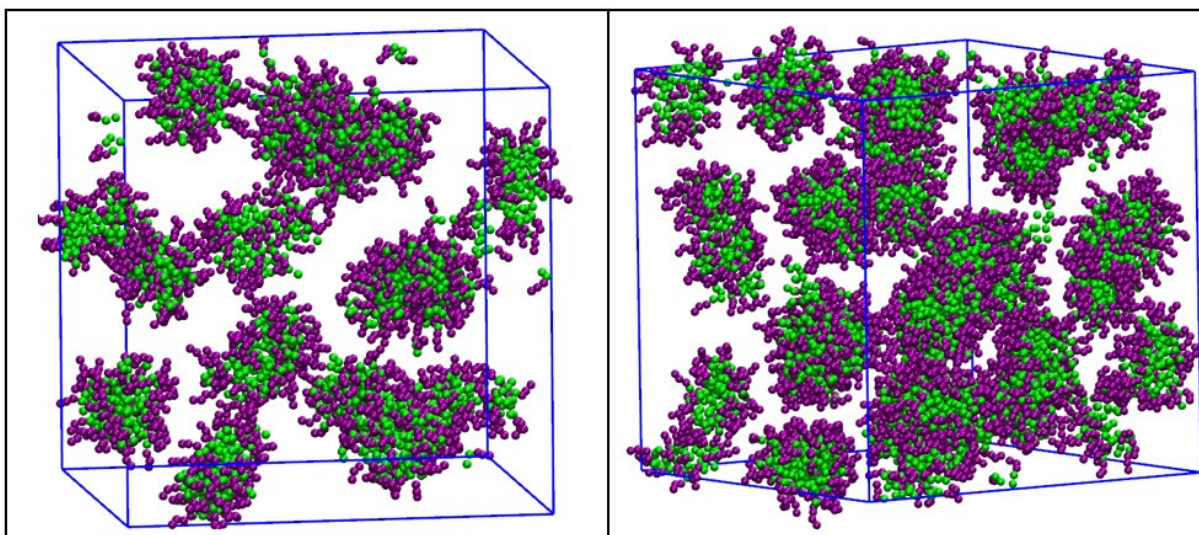
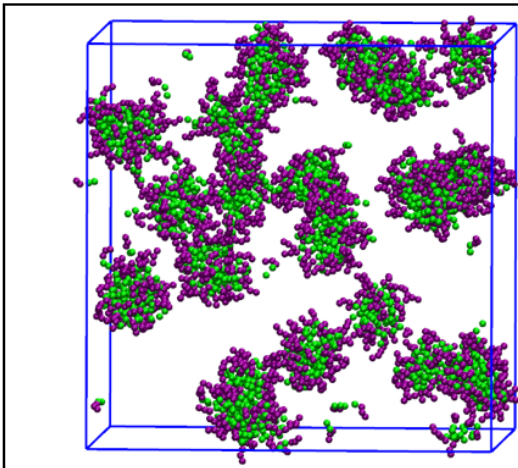
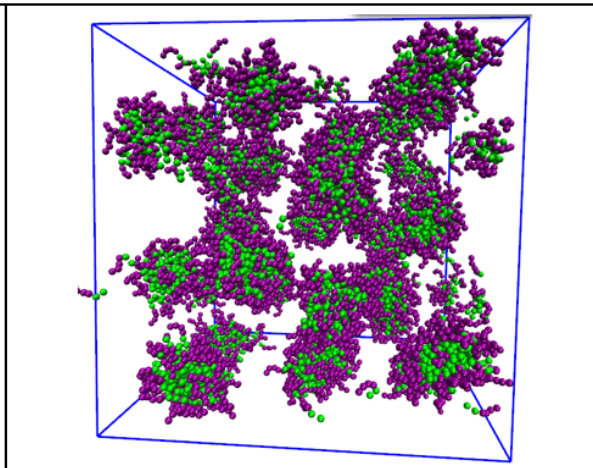


Figure. D.2. Final snapshots of the CG-MD simulations carried out for the system C_8E_6/H_2O at 15 and 30 wt%. Green is used to represent the alkyl tail beads, while purple represents the beads from the hydrophilic moiety. Water molecules are omitted to allow for an easier visualization.

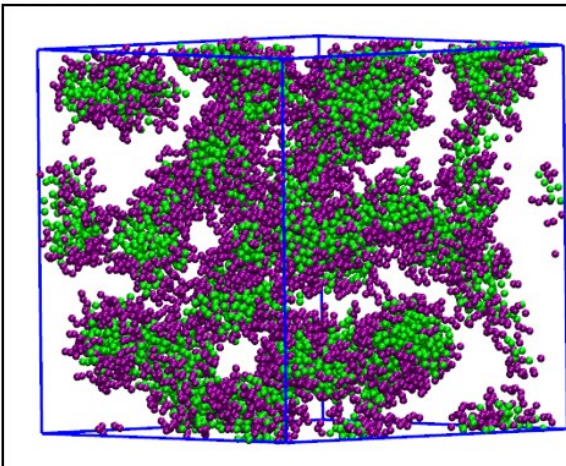
15 wt%



30 wt%



50 wt%



70 wt%

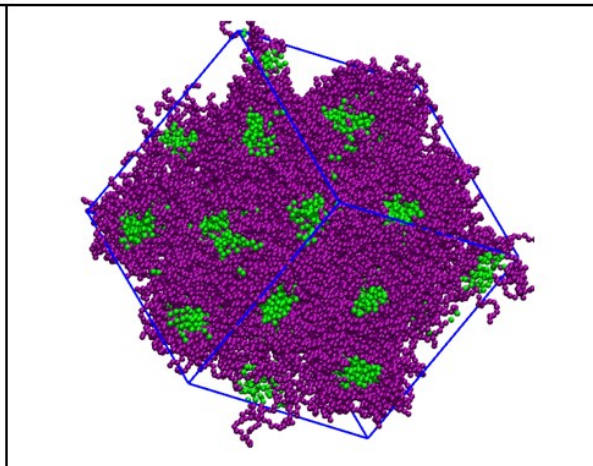


Figure. D.3. Final snapshots of the CG-MD simulations carried out for the system C_8E_{12}/H_2O at different concentrations. Colours as in **Figure D.2**.

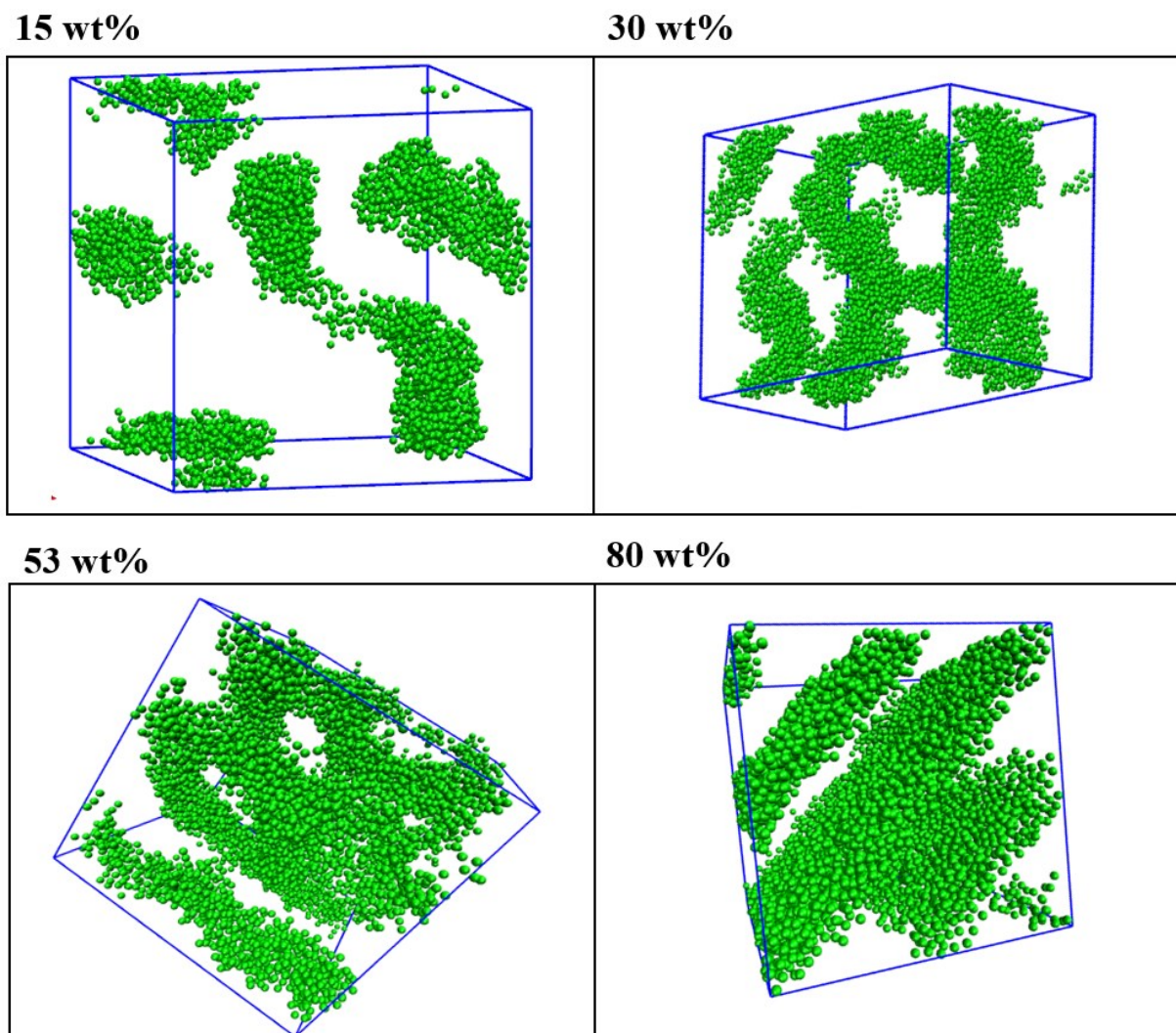
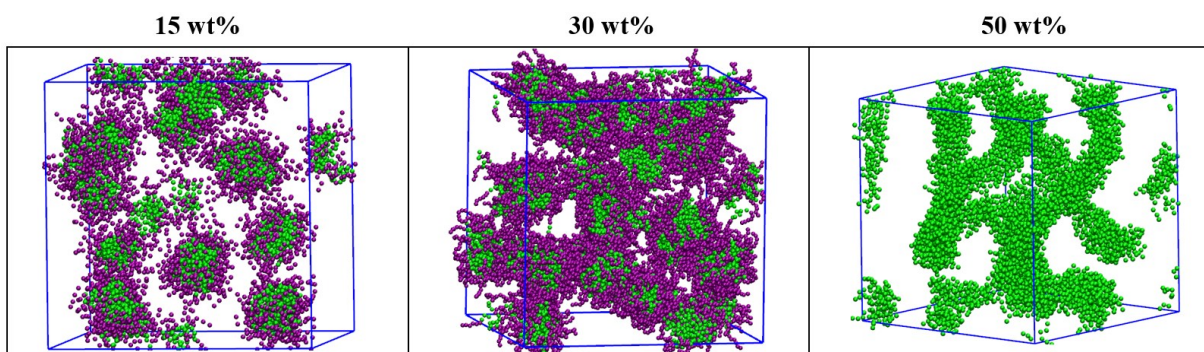


Figure. D.4. Final snapshots of the CG-MD simulations carried out for the system $C_{12}E_4/H_2O$ at different concentrations. For an easier visualization of the liquid structural organization only the alkyl chains are represented.



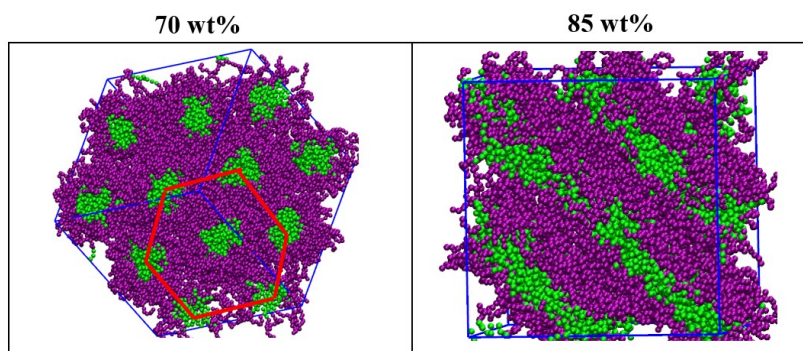


Figure. D.5. Final snapshots of the CG-MD simulations carried out for the system $C_{12}E_{10}/H_2O$ at different concentrations. Colours as in **Figure D.2**.

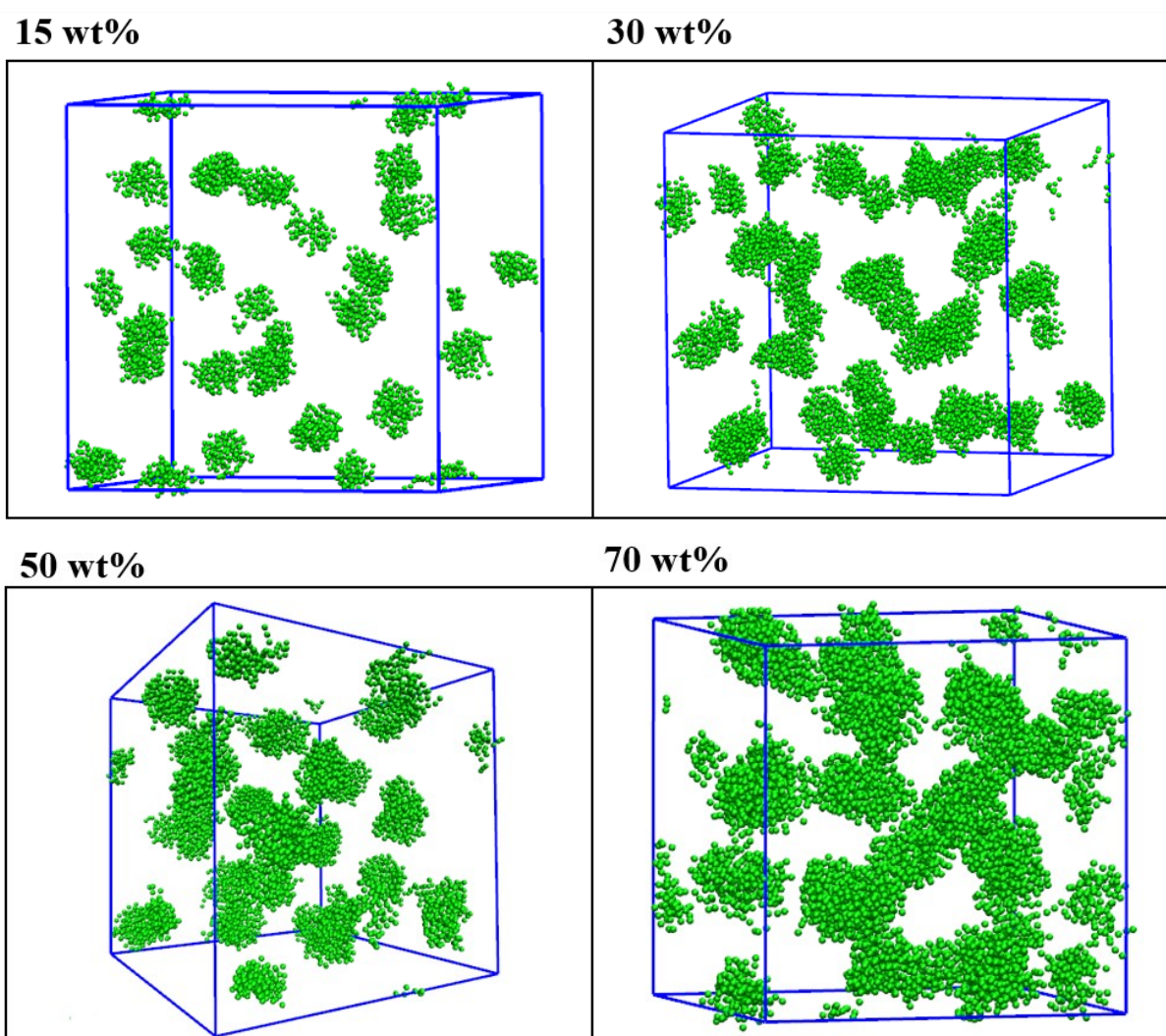


Figure. D.6. Final snapshots of the CG-MD simulations carried out for the system $C_{12}E_{23}/H_2O$ at different concentrations. For an easier visualization only the alkyl chains are represented.

70 wt%

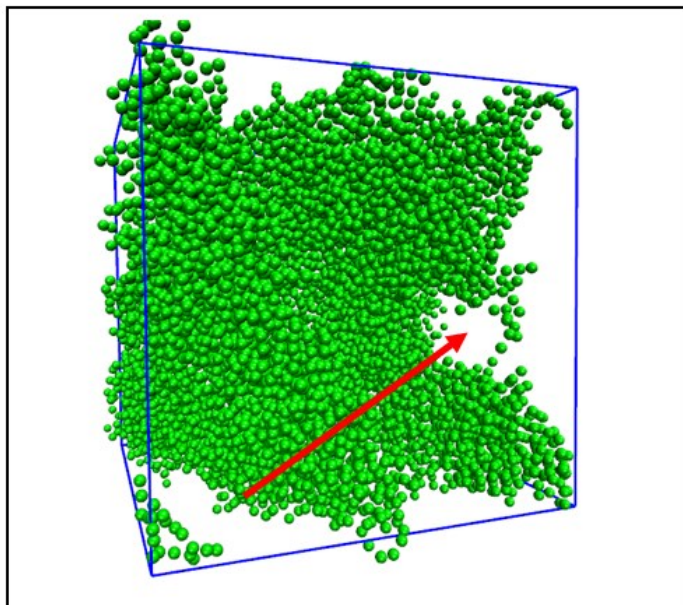


Figure. D.7. Pore defect in the $C_{16}E_6/H_2O$ system at 70 wt%.

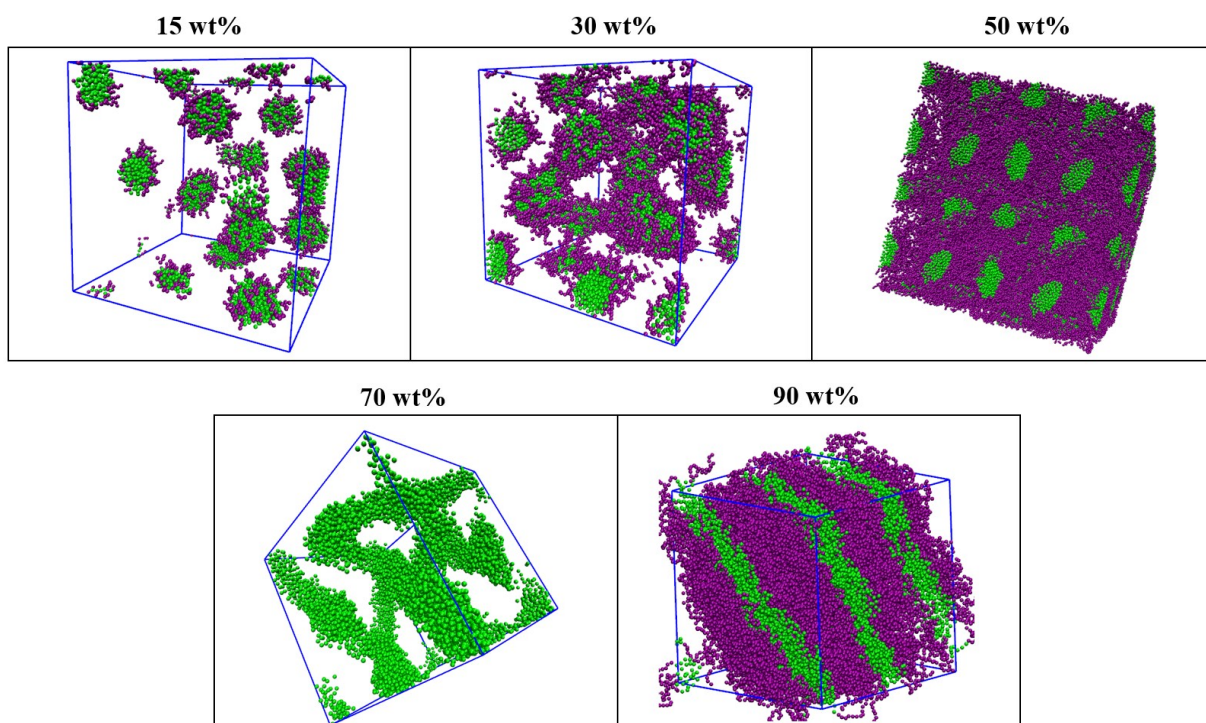


Figure. D.8. Final snapshots of the CG-MD simulations for the $C_{16}E_{12}/H_2O$ system at different concentrations. Colours as in Figure D.2.

E. CG-MD simulations of surfactant flooding processes

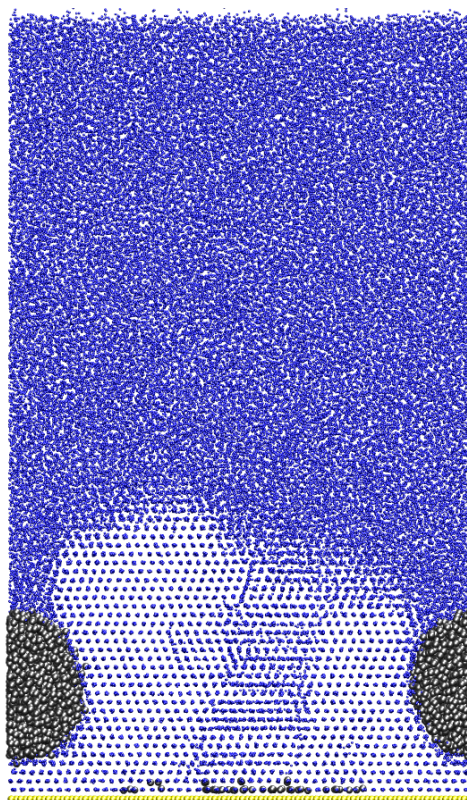


Figure. E.1. Final snapshot of the CG-MD simulation carried out for a simulation box containing a fixed silica surface (yellow), 1664 n-dodecane molecules (grey), and 400000 water molecules (blue).

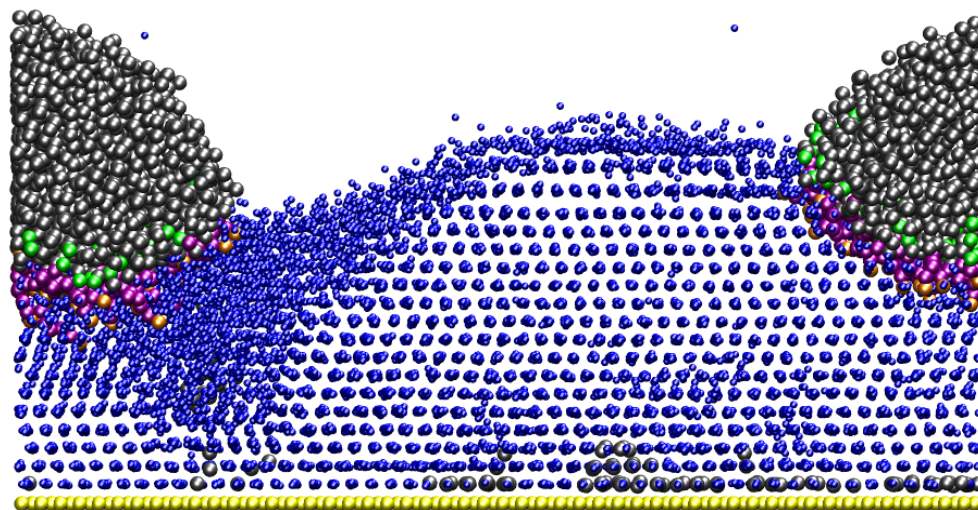


Figure. E.2. Final snapshot of the CG-MD simulation carried out for a simulation box containing a fixed silica surface (yellow), 1664 n-dodecane molecules (grey), and 100000 water molecules (blue) in the presence of 90 molecules of $C_{12}E_6$.

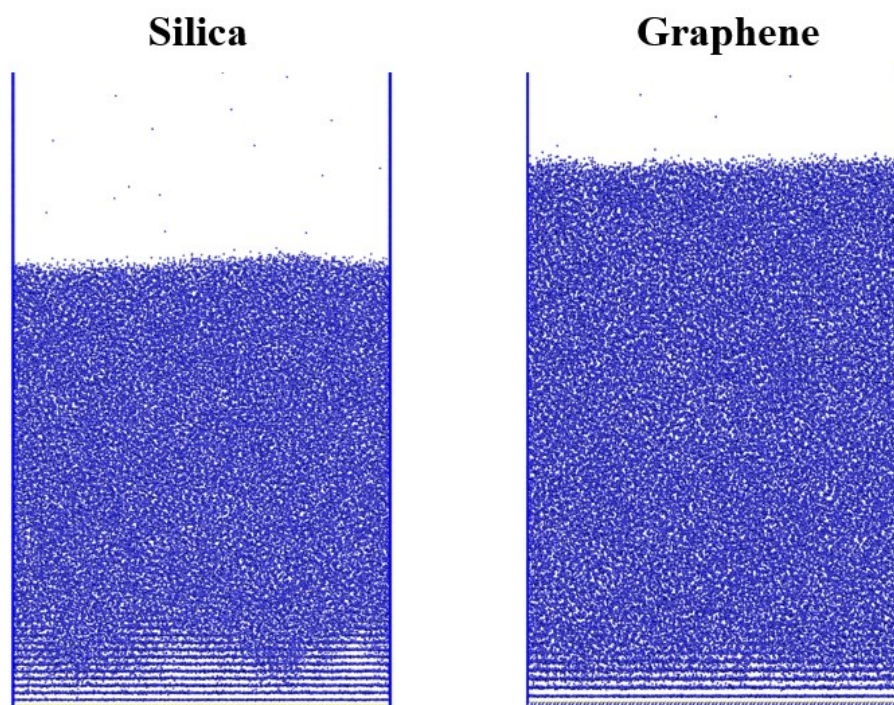


Figure. E.3. CG-MD simulations of water in contact with a silica or graphene surface using the MARTINI 2.0 FF.

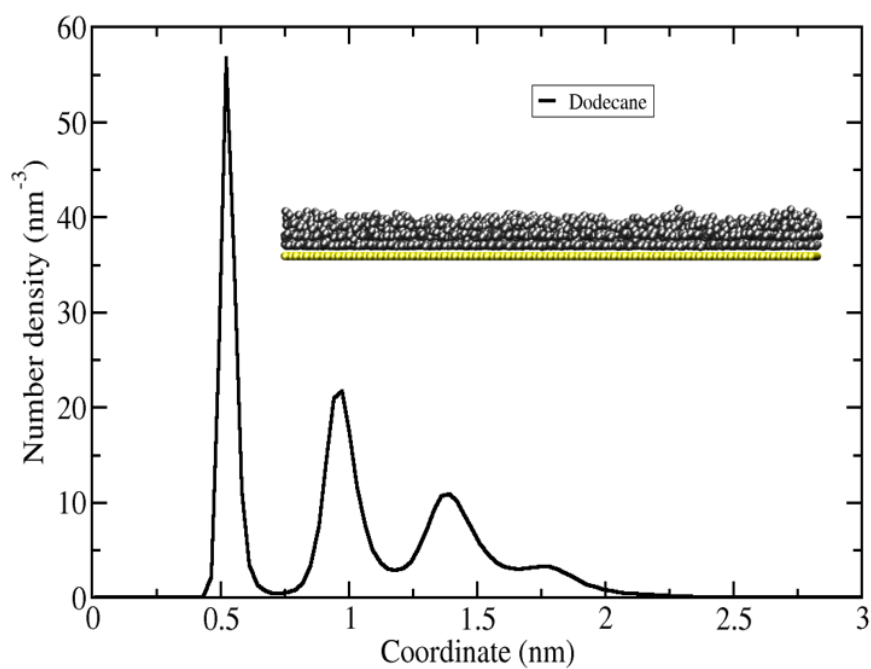


Figure. E.4. Number density of dodecane molecules as a function of the z-coordinate of the simulation box. The final snapshot of the CG-MD simulation of 1664 n-dodecane molecules (represented in grey) near a silica surface (yellow) using the MARTINI 3.0 FF is shown as an inset.

F. Thermodynamic Modelling of DESs

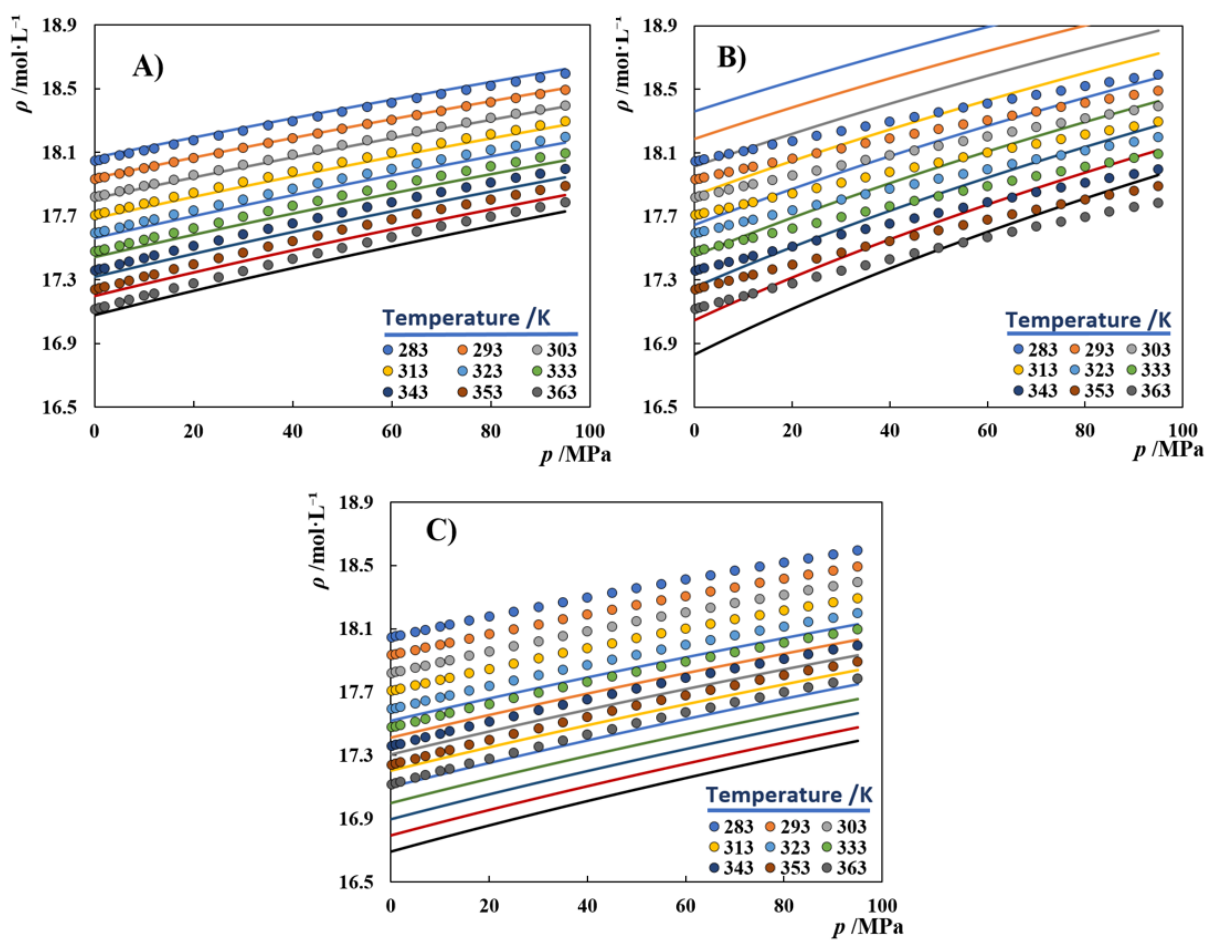


Figure. F.1. Prediction of high-pressure densities of pure ethylene glycol. Symbols represent experimental data from Crespo et al.[119] while the solid lines depict the PC-SAFT predictions using the parameters from: A) Atilhan et al.[319] B) Reschke et al.[320] C) Liang et al.[321]

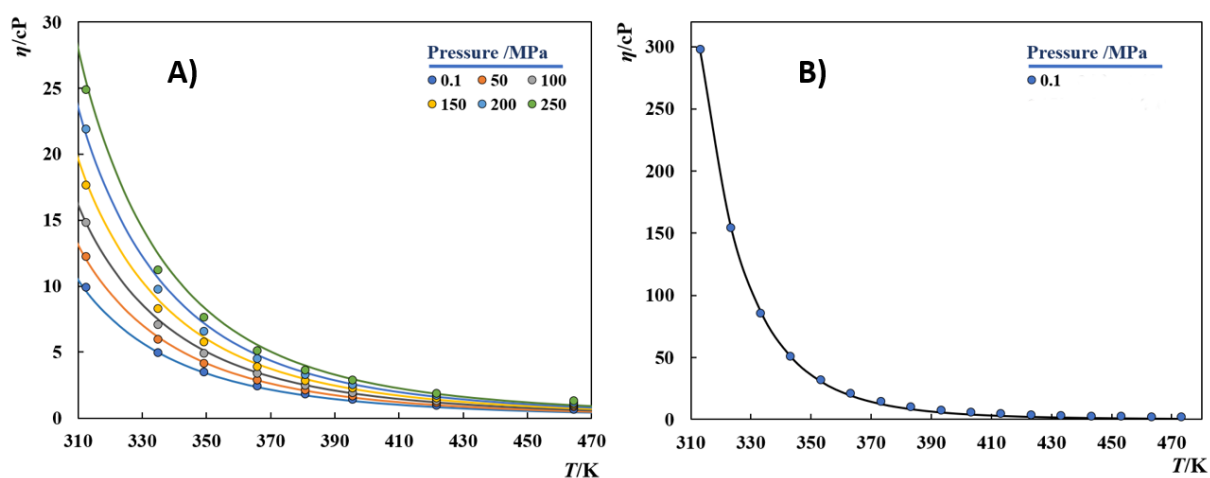


Figure. F.2. Viscosities of pure A) EG; B) glycerol. Symbols represent experimental data,[118,323] while the solid lines depict the FVT fitting to the experimental data.

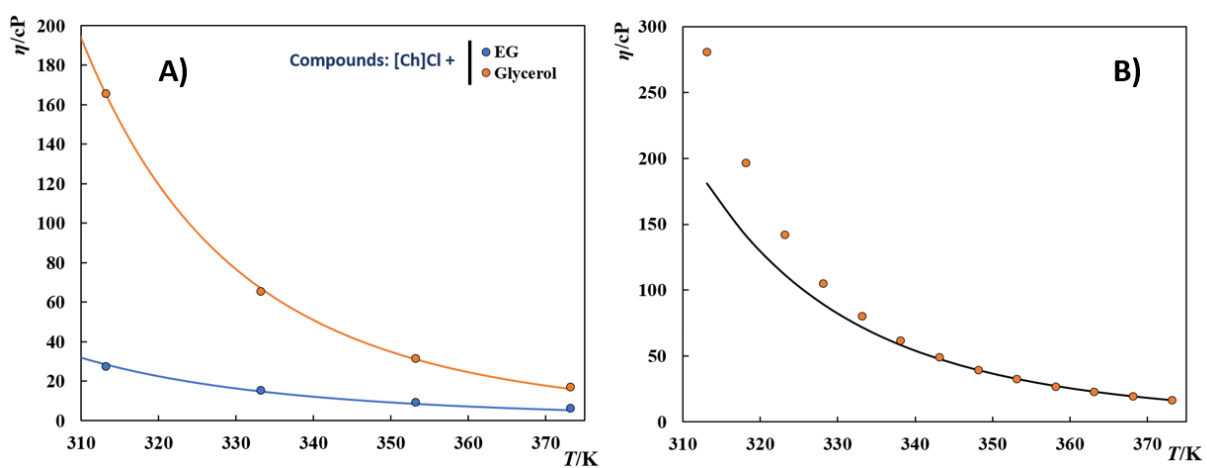


Figure. F.3. A) Viscosities of [Ch]Cl-based DESs at a 1:2 HBA:HBD ratio, at atmospheric pressure. B) Viscosities of [Ch]Cl + urea (1:2), at atmospheric pressure. Symbols represent the experimental data,[410] while the solid lines depict the PC-SAFT + FVT results.

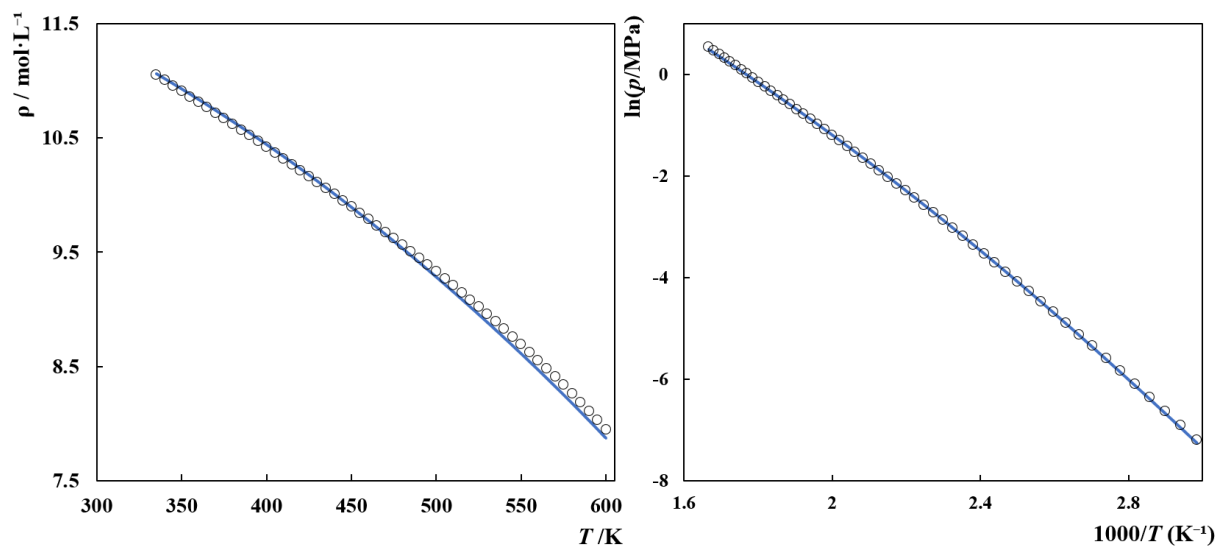


Figure. F.4. Saturated liquid densities and vapor pressures of phenol. Symbols represent experimental data from the DIPPR database,[118] while the solid lines depict the soft-SAFT fitting to the data.

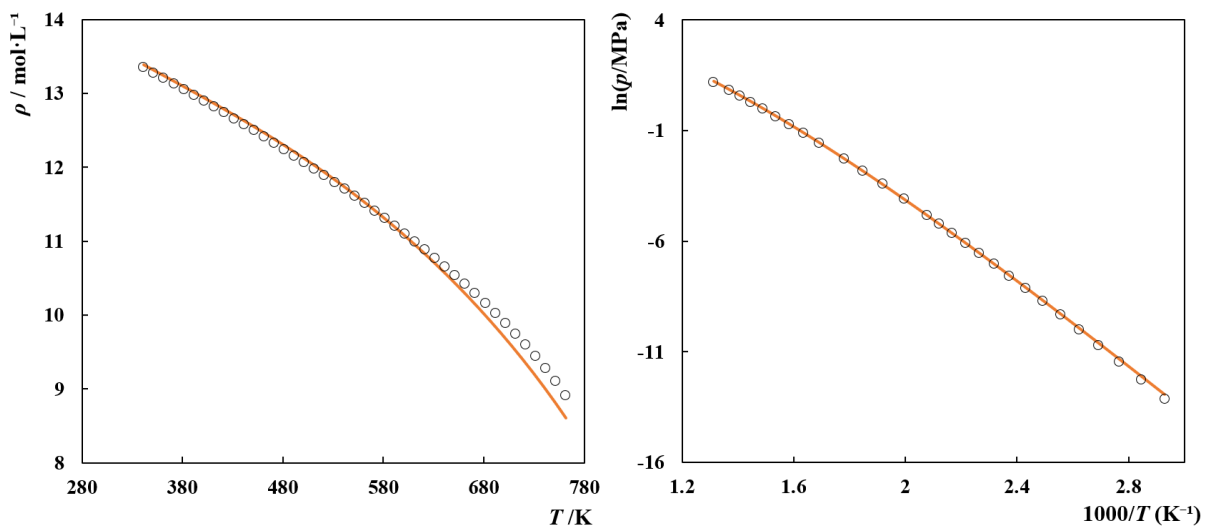


Figure. F.5. Saturated liquid densities and vapor pressures of glycerol. Symbols represent experimental data from the DIPPR database,[118] while the solid lines depict the soft-SAFT fitting to the data.

G. Free Volume Theory (FVT) - Description

One of the most popular approaches to model the viscosity of dense fluids is the Free Volume Theory (FVT) proposed by Allal et al.,[411,412] based in earlier concepts of free volume and diffusion. According to this theory, viscosity is given as a sum of two terms (**equation F.1**): the diluted gas term, η_0 , and the dense-state correction term, $\Delta\eta$, in an approach similar to that proposed by Quiñones-Cisneros et al.[413] for the friction theory, to isolate the purely kinematic physics of the diluted gas limit from the dense-state physics.

$$\eta = \eta_0 + \Delta\eta \quad (\text{F. 1})$$

The first term describes the viscosity of a fluid with a very low density using a modified version of the original Chapman-Enskog theory proposed by Chung et al.[414] in the following expression:

$$\eta_0 = 40.785 \times 10^{-4} \frac{\sqrt{M_w T}}{v_c^{2/3} \Omega^*(T^*)} F_c \quad (\text{F. 2})$$

where η_0 is the viscosity of the diluted gas in cP, T is the temperature in K, M_w is the molecular weight in g/mol and v_c is the critical volume in cm³/mol. $\Omega^*(T^*)$ is the reduced collision integral that is evaluated at a dimensionless temperature $T^* = 1.2593T/T_c$, from the Neufeld et al.,[415] F_c is a correction factor to include the effects of chain bonding, hydrogen bonding and polarity that was introduced by Chung et al.[414] as a function of the acentric factor, ω , a dimensionless dipole moment of the molecule, μ_r , and a parameter κ that accounts for hydrogen bonding:

$$F_c = 1 - 0.2756\omega - 0.059035\mu_r^4 - \kappa \quad (\text{F. 3})$$

In the case of mixtures, the contribution of each component to the diluted-gas term is first calculated independently and then a general equation for multi-component systems proposed by Wilke[416] is used to sum the different contributions:

$$\eta_0^{mix} = \sum_{i=1}^{NC} \frac{\eta_0^i}{1 + x_i \sum_{\substack{j=1 \\ j \neq i}}^{NC} x_j \phi_{ij}} \quad (\text{F. 4})$$

where ϕ_{ij} is given by the following expression:

$$\phi_{ij} = \frac{\left[1 + (\eta_0^i/\eta_0^j)^{0.5} (M_w^i/M_w^j)^{0.25}\right]^2}{(4/\sqrt{2})\left[1 + (M_w^i/M_w^j)\right]^{0.5}} \quad (\text{F. 5})$$

In this work the diluted-gas term is however neglected as the necessary critical properties are not available for [Ch]Cl. Nonetheless, the contribution of this term for the calculation of liquid viscosities is typically small, and may be neglected.[327]

The dense-state term is believed to be connected to the molecular structure of the fluid and exponentially dependent on the empty space (free volume) between molecules. The final expression is given by **equation F.6**.

$$\Delta\eta = L_v(0.1p + 10^{-4}\alpha\rho^2M_w) \sqrt{\frac{10^{-3}M_w}{3RT}} \exp\left[B\left(\frac{10^3p + \alpha\rho^2M_w}{\rho RT}\right)^{\frac{3}{2}}\right] \quad (\text{F.6})$$

where $\Delta\eta$ is the dense-term contribution to viscosity in cP, p is the pressure in MPa, ρ is the density in mol/L and R is the ideal gas constant in $\text{J}\cdot\text{K}^{-1}\cdot\text{mol}^{-1}$. **Equation F.6** includes three adjustable parameters: L_v which is a length parameter related to the molecule's structure and relaxation time, B the free-volume overlap, and α that is related to the energy barrier. These parameters must be fitted to the available experimental viscosity data and, whenever possible, related to the M_w if the compounds belong to the same chemical family.

The extension to mixtures requires the evaluation of the three parameters for the mixture through appropriate mixing rules. Given that there is still disagreement about the best mixing rule to be used with the FVT,[417–423], the simplest one is employed in this work, where the different parameters depend linearly on the mixture composition without any binary parameters in the viscosity treatment:

$$\alpha^{mix} = \sum_{i=1}^{NC} \alpha_i x_i \quad (\text{F.7})$$

$$B^{mix} = \sum_{i=1}^{NC} B_i x_i \quad (\text{F.8})$$

$$L_v^{mix} = \sum_{i=1}^{NC} L_{v,i} x_i \quad (\text{F.9})$$

The calculation of viscosity requires thus the previous calculation of some thermodynamic properties, namely the density and pressure/temperature of the system through an appropriate EoS. Therefore, the accuracy of the calculated viscosities may be greatly influenced by the accurate calculation of these properties by the chosen EoS.

H. Excess Molar Volumes of PILs and DES

Table. H.1. Average excess molar volumes of different DES calculated using experimental density data available in the literature.

Comp.1	Comp.2	x_1	T_{min} (K)	T_{max} (K)	Average V^E (cm^3/mol)	Density Ref.
thymol	Menthol	0.5	278.15	373.15	-0.802	[424]
thymol	TOPO	0.5	282.86	358.15	-1.033	[425]
thymol	decan-1-ol	0.5	303.15	373.15	-0.931	[426]
thymol	dodecan-1-ol	0.5	303.15	373.15	-0.592	[426]
thymol	tetradecane-1-ol	0.5	303.15	373.15	-0.538	[426]
TOPO	decanoic acid	0.5	287.91	373.1	-1.029	[425]
TOPO	dodecanoic acid	0.5	298.15	373.15	-1.047	[426]
TOPO	tetradecanoic acid	0.5	298.15	373.15	-0.131	[426]
TOPO	levulinic acid	1/3	293.15	323.15	-0.908	[427]
TOPO	levulinic acid	0.5	293.15	323.15	-1.431	[427]
TOPO	phenol	1/3	293.15	363.15	-0.649	[428]
TOPO	phenol	0.5	293.15	363.15	-0.440	[428]
TOPO	decan-1-ol	0.5	298.15	373.15	0.121	[426]
[Ch]Cl	ethylene glycol	1/3	283.15	363.15	-0.511	[322]
[Ch]Cl	glycerol	1/3	283.15	363.15	-0.304	[322]
[Ch]Cl	triethyleneglycol	1/3	303.15	353.15	-1.368	[335]
[Ch]Cl	phenol	1/3	293.2	318.2	-0.664	[336]
[C ₄ mim][Cl]	decan-1-ol	0.5	303.15	373.15	-0.569	[426]
[C ₄ mim][Cl]	dodecan-1-ol	0.5	303.15	373.15	-0.937	[426]
[C ₄ mim][Cl]	tetradecane-1-ol	0.5	303.15	373.15	-0.171	[426]
[C ₈ mim][Cl]	methanol	0.4411	298.15	328.15	-0.644	[429]
[C ₈ mim][Cl]	ethanol	0.3142	298.15	328.15	-0.661	[429]
[C ₈ mim][Cl]	propan-1-ol	0.3791	298.15	328.15	-0.413	[429]

Table. H.2. Average excess molar volumes of different PILs calculated using experimental density data available in the literature.

Base	Acid	x_I	T_{min} (K)	T_{max} (K)	Average V^E (cm^3/mol)	Density Ref.
ethylamine	nitric acid	0.5	300.15	300.15	-9.89	[430]
ethylamine	propanoic acid	0.5	300.15	300.15	-12.46	[430]
monoethanolamine	acetic acid	0.5	293.15	363.15	-6.90	[43]
monoethanolamine	nitric acid	0.5	300.15	300.15	--2.07	[430]
monoethanolamine	propanoic acid	0.5	298.15	343.15	-7.35	[383]
monoethanolamine	butanoic acid	0.5	293.15	363.15	-7.83	[43,382]
monoethanolamine	pentanoic acid	0.5	293.15	323.15	-6.94	[382]
monoethanolamine	hexanoic acid	0.5	293.15	323.15	-6.65	[382]
monoethanolamine	oleic acid	0.5	293.15	358.15	-7.96	[431]
diethylamine	pentanoic acid	0.5	293.15	363.15	-15.06831962	[385]
diethylamine	hexanoic acid	0.5	293.15	363.15	-16.02574726	[385]
diethylamine	heptanoic acid	0.5	293.15	363.15	-14.13922655	[385]
methylethanolamine	propanoic acid	0.5	298.15	358.15	-8.5968916	[384]
methylethanolamine	butanoic acid	0.5	298.15	358.15	-8.43093465	[384]
methylethanolamine	pentanoic acid	0.5	298.15	358.15	-7.91558621	[384]
dimethylethanolamine	formic acid	0.5	298.15	353.15	-8.87754063	[432]
dimethylethanolamine	acetic acid	0.5	298.15	353.15	-9.94402557	[432]
ethylethanolamine	propanoic acid	0.5	298.15	343.15	-8.68602087	[433]
diethanolamine	formic acid	0.5	293.15	343.15	-4.87324617	[434]
diethanolamine	acetic acid	0.5	293.15	343.15	-6.92483698	[434]
diethanolamine	methanesulfonic acid	0.5	293.15	353.15	-6.43307677	[435]
diethanolamine	oleic acid	0.5	298.15	378.15	-7.1257428	[431]
diethylethanolamine	acetic acid	0.5	283.15	363.15	-8.17877301	[361]
diethylethanolamine	propanoic acid	0.5	283.15	363.15	-8.75954169	[361]
diethylethanolamine	butanoic acid	0.5	283.15	363.15	-7.98628442	[361]
diethylethanolamine	pentanoic acid	0.5	283.15	363.15	-7.70775361	[361]
diethylethanolamine	hexanoic acid	0.5	283.15	363.15	-7.50633442	[361]
methyldiethanolamine	formic acid	0.5	298.15	353.15	-5.0738697	[432]
methyldiethanolamine	acetic acid	0.5	298.15	353.15	-5.77331682	[432]
methyldiethanolamine	methanesulfonic acid	0.5	293.15	353.15	-8.32877893	[435]
dibutylamine	pentanoic acid	0.5	293.15	363.15	-11.90162138	[385]

dibutylamine	hexanoic acid	0.5	293.15	363.15	-12.2887255	[385]
dibutylamine	heptanoic acid	0.5	293.15	363.15	-10.80150058	[385]
tributylamine	acetic acid	0.5	293.15	363.15	-13.66590274	[43]
tributylamine	butanoic acid	0.5	293.15	363.15	-6.11244414	[43]
